Mathematical Theory of Shells on Elastic Foundations:

An Analysis of Boundary Forms, Constraints, and Applications to Friction and Skin Abrasion

Dissertation of Doctor of Philosophy in Mathematics

Kavinda Jayawardana
zcahe58@ucl.ac.uk
Department of Mathematics
University College London
2016

I, Kavinda Jayawardana confirm that the work presented in this thesis is my own. Where information has been derived from other sources, I confirm that this has been indicated in the thesis.

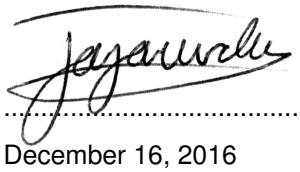

.....

December 16, 2016

Abstract

In this thesis we examine the behaviour of shells supported by elastic foundations. We begin by critically analysing the existing literature on the study of thin objects such as films, plates, membranes and shells, and we highlight their limitations, validity and present correct formulations when possible. We also do the same for various frictional laws, in particular, Coulomb's law of static friction. Then, we extend the capstan equation to noncircular geometries by modelling membranes supported by rigid foundations in presence of friction. We provide closed-form solutions and compare them to other similar existing models in the literature. Then, we begin the study of shells supported by elastic foundations. We treat the bonded case as a boundary form and prove the existence and the uniqueness of solutions, and thus, prove it is a mathematical theory and not merely a mathematical model. To conclude this case we conduct numerical experiments and compare the results against existing models in the literature. Finally, we introduce a constraint and assert that this condition is analogous to classical frictional laws. This constraint is then used to model shells supported by elastic foundations with friction. As with the previous case, we again prove the existence and the uniqueness of solutions, and conclude by conducting numerical experiments and comparing the results against existing models in the literature. Applications for our work can be found in cable drive electronic systems, curvilinear stretchable electronics and modelling skin abrasion.

Acknowledgments

I thank Dr Nick Ovenden (UCL) for his supervision, University College London for partly funding this project, The Sidney Perry Foundation [grant number 89], S. C. Witting Trust, Ms Helen Higgins (UCL) for securing funding for the last year of the project, Prof Alan M. Cottenden (UCL), Mr Clifford Ruff (UCLH) and Dr Sabrina Falloon (UCL) for their assistance with the experiments, and all the subjects for volunteering for the experiments. I also thank Dr Raul Sanchez Galan (UCL), Dr Andres A. Leon Baldelli (University of Oxford), Dr Christoph Ortner (University of Warwick), Prof Dmitri Vassiliev (UCL) and Prof Alan Sokal (UCL) for providing the essential research material, metalib-c.lib.ucl.ac.uk, scholar.google.co.uk and bookzz.org for making the necessary research material available, and Dr Robert Bowles (UCL), Prof Valery Smyshlyaev (UCL), Dr Edmund W. Judge (University of Kent), Sir John M. Ball (University of Oxford), Mr Phillip Harvey and Ms Camille London-Miyo for their assistance.

This work was supported by The Dunhill Medical Trust [grant number R204/0511].

I thank my mother Deepika, my brother Tharinda and my father Chithrasena Guruge for their support.

Supervisors

Dr Nick Ovenden (UCL) and Prof Alan M. Cottenden (UCL).

Examiners

Dr Christian G. Böhmer (UCL) and Dr Evgeniya Nolde (Brunel University).

Contents

1 Introduction

In this thesis we study the general behaviour of thin curvilinear static isotropic linearly elastic structures such as *shells* and *membranes* when supported by elastic bodies, and in this context such underlying bodies are commonly referred to as *foundations*. The significance of this research is that there exists no comprehensive mathematical theory to conclusively describe the behaviour of thin objects supported by elastic foundations. Thus, we attempt, with the best of our ability, to present a mathematical theory of shells supported by elastic foundations.

In Chapter 1 we introduce the critical definitions, fundamental theorems and most notable applications relating to the study of both shell and membrane theory, as well as contact conditions governing elastic bodies, in particular, friction. In Chapter 2 we examine behaviour of membranes supported by rigid foundations where the contact region is governed by the common friction-law. To be more precise, we extend the capstan equation to a general geometry. Then, we present explicit solutions and compare our results against other models, in particular, Coulomb's law of static friction [102]. In Chapter 3 we begin the study of shells supported by elastic foundations. Initially, we assume that the shell is bonded, and we derive the governing equations with the mathematical techniques for linear Koiter's shell theory that is put forward by Ciarlet [38] and a technique that is used in the derivation of surface Cauchy-Bourne model [89]. In this way, we treat the overlying shell as a boundary form of the elastic foundation, which is analogous to the work of Necas *et al.* [144], and use the mathematical techniques put forward by Ciarlet [38], and Badiale and Serra [13] to mathematically prove the existence and the uniqueness of solutions for the proposed model. Chapter 3 concludes by conducting numerical experiments: by comparing our bonded shell model against an existing model presented in the literature [16], but modified for our purposes by incorporating general elastic properties and extending it to curvilinear coordinates; by checking the numerical validity of our bonded shell model against the bonded two-body elastic problem. In Chapter 4 we conclude our study on shells by asserting that the contact region is governed by a displacement-based frictional-law that is analogous to Coulomb's law of static friction. We treat this displacement-based frictional-law as a constraint, which is analogous to the work of Kinderlehrer and Stampacchia [107], and with the mathematical techniques put forward by Evans [63], and Kinderlehrer and Stampacchia [107] we mathematically prove the existence and the uniqueness of solutions to the proposed model, and thus, concluding the mathematical theory of overlying shells on elastic foundations. Chapter 4 concludes by modifying the model for Coulomb's law of static friction, which is put forward by Kikuchi and Oden [102], to represent two-body elastic problem with friction in curvilinear coordinates, and we use this extended model to conduct numerical experiments against our shell model with friction. The reader must understand that, despite we may use other authors' work as comparisons, we never use authors' exact models. We adapt, extend and modify their work to an extent that they are not original authors' work, but they are our original work.

We consider Chapter 3 to be the most crucial and the most significant chapter of this thesis as it contains the most original and fundamental results. Chapter 3, and to a lesser extent Chapter

4, does not contain mere models: they are mathematical theories. By that what we mean is that, regardless if our models correctly describe a real life phenomenon or not, the models are mathematically valid as a unique solution exists with respect to an acceptable set of parameters. However, the work we present in this thesis is by no means complete, and thus, in Chapter 5 we extensively describe some remaining open questions and limitations of our work. Also, there we present possible extensions for future work. In Chapter 6 we extend the ideas that we present in Chapters 2, 4 and 5, and propose mathematical models to study the behaviour of in-vivo skin and fabrics in presence of friction. With real life experimental data gathered from human subjects and numerical experiment data from our models we attempt to extract some result that maybe implicated in reducing skin abrasion due to friction. Finally, we conclude our analysis, and thus, this thesis, in Chapter 7, where all our research findings and their significance are discussed.

The following chapter is a comprehensive introduction to the study of thin objects such as plates, shells, films and other relating subjects that are included in study of mathematical elasticity and friction. We begin, in Section 1.1, with a list of notations that we subsequently use in the latter chapters. Sections 1.2 and 1.3 contain all the necessary mathematical definitions and theorems that are vital for the rigorous mathematical analysis of the later chapters. Here, we are careful in the accuracy of our sources and our definitions. For example, the definition of hyperelasticity given by Kikuchi and Oden [102] (see section 5.1 of Kikuchi and Oden [102]) is 'hyperelastic means that there exists a differentiable *stored energy function* ... representing the strain energy per unit volume of material, which characterizes the mechanical behavior of the material of which the body is composed' [102]. Although, this is indeed a property of hyperelasticity, it does not merit as a definition as hyperelasticity is a fundamental concept in mathematical elasticity. For a more precise definition of hyperelasticity please consult Ball [17] or Ciarlet [38] (see chapter 7 of Ciarlet [38]). Note that, if having a differentiable energy functional (with respect to the strain tensor) constitutes as the material being hyperelastic, then any linear elastic material can be hyperelastic as any linear elastic material also have a differentiable energy functional with respect to the strain tensor. However, this is not the case as one can find a great example by Morassi and Paroni [139] (see section 2 subsection 7.7 of Morassi and Paroni [139] for the examples of convexity and policonvexity) where the linear elastic model failed to be physically realistic under a condition, while a hyperelastic model stayed perfectly physically realistic for the same condition. Also, in Sections 1.2 and 1.3 we only state the theorems and critical results. However, we correctly document the sources so that the reader may consult for the proofs and the justifications of the results. If the reader is unfamiliar with pure mathematics, then Sections 1.2 and 1.3 may seem unmotivated or even superfluous, but the significance of these results is revealed in the subsequent chapters.

Sections 1.4 and 1.5 are dedicated to the study of thin objects. We demonstrate to the reader the fundamental ideas behind the study of thin objects, the techniques used in deriving of such models and most notable results in the literature. Sections 1.6 and 1.7 are dedicated to literature of most notable and relevant commercial applications relating to this work. These sections also double as a thorough literature review.

Finally, Sections 1.8, 1.9, 1.10, 1.11 and 1.12 are dedicated to the critical study of vital publications that paved the way to our current work. Unfortunately, we reveal some authors' erroneous work that were responsible for significantly impeding the progress of this project. The reader must understand that we are not being iconoclastic, but we are merely being mathematically thorough. We urge the reader not to take our word, but actually review the given publications one's self as we gone to great lengths to be meticulous as possible when documenting the flaws (chapters, page numbers, equations, etc.). In fact, please consult the footnotes for URLs for the free copies of the publications, so that the reader can make an informative judgement on the matter.

1.1 Notations and Conventions

In this section we present common notations that we use throughout this thesis, but the strict definitions of the notations are defined in the subsequent sections. The given definitions stand unless it is strictly says otherwise.

- $n \in \mathbb{N}$ where $\mathbb{N}$ is the set of natural numbers.
- $\mathbb{R}$ is usually reserved for a curvilinear real-line.
- $\mathbf{E}$ is usually reserved for a Euclidean real-line.
- $\alpha, \beta, \gamma, \delta \in \{1, 2\}$ are usually reserved for the curvilinear indices.
- $i, j, k, l \in \{1, 2, 3\}$ are usually reserved for Euclidean indices.
- $\boldsymbol{\sigma} : \omega \subset \mathbb{R}^2 \to \boldsymbol{\sigma}(\omega) \subset \mathbf{E}^2$ describes the unstrained configuration of the shell.
- $\bar{\boldsymbol{X}} : \Omega \subset \mathbb{R}^3 \to \bar{\boldsymbol{X}}(\Omega) \subset \mathbf{E}^3$ describes the unstrained configuration of the foundation.
- $\partial_j = \dfrac{\partial}{\partial x^j}$ are usually describe the partial derivatives with respect to $\mathbb{R}^3$.
- $F_{[\mathrm{I}]\alpha\beta} = \partial_\alpha \sigma_k \partial_\beta \sigma^k$ is the covariant first fundamental form tensor induced by $\boldsymbol{\sigma}$ on $\mathbb{R}^2$.
- $g_{ij} = \partial_i \bar{X}_k \partial_j \bar{X}^k$ is the covariant metric tensor induced by $\bar{\boldsymbol{X}}$ on $\mathbb{R}^3$.
- $\boldsymbol{N} = \dfrac{\partial_1 \boldsymbol{\sigma} \times \partial_2 \boldsymbol{\sigma}}{||\partial_1 \boldsymbol{\sigma} \times \partial_2 \boldsymbol{\sigma}||}$ is the unit normal to the surface $\boldsymbol{\sigma}(\omega)$.
- $F_{[\mathrm{II}]\alpha\beta} = N^k \partial_{\alpha\beta} \sigma_k$ is the covariant second fundamental form tensor induced by $\boldsymbol{\sigma}$ on $\mathbb{R}^2$.
- $0 < -\dfrac{1}{2} F_{[\mathrm{II}]}{}^{\alpha}_{\alpha}$ signifies positive mean-curvature.
- $0 \leq F_{[\mathrm{II}]}{}^{\alpha}_{\alpha} F_{[\mathrm{II}]}{}^{\gamma}_{\gamma} - F_{[\mathrm{II}]}{}^{\gamma}_{\alpha} F_{[\mathrm{II}]}{}^{\alpha}_{\gamma}$ signifies nonnegative Gaussian-curvature, i.e. non-hyperbolic.
- ∇_β are the covariant derivatives in $\mathbb{R}^2$.
- $\bar{\nabla}_j$ are the covariant derivatives in $\mathbb{R}^3$.
- $\partial^\beta = F_{[\mathrm{I}]}^{\alpha\beta} \partial_\alpha$.
- $\partial^j = g^{ij} \partial_i$.
- h is the thickness of the shell or the membrane.
- H is the thickness of the foundation (special case only).
- E is Young's modulus of the shell or the membrane.
- $\bar{E}$ is Young's modulus of the foundation.
- ν is Poisson's ratio of the shell or the membrane.

- $\bar{\nu}$ is Poisson's ratio of the foundation.
- $\lambda = \dfrac{E}{(1+\nu)(1-2\nu)}$ is first Lamé's parameter of the shell or the membrane.
- $\bar{\lambda} = \dfrac{\bar{E}}{(1+\bar{\nu})(1-2\bar{\nu})}$ is first Lamé's parameter of the foundation.
- $\mu = \dfrac{1}{2}\dfrac{E}{(1+\nu)}$ is second Lamé's parameter of the shell or the membrane.
- $\bar{\mu} = \dfrac{1}{2}\dfrac{\bar{E}}{(1+\bar{\nu})}$ is second Lamé's parameter of the foundation.
- $B^{\alpha\beta\gamma\delta} = \mu\left(\dfrac{2\lambda}{\lambda+2\mu}F_{[\mathrm{I}]}^{\alpha\beta}F_{[\mathrm{I}]}^{\gamma\delta} + F_{[\mathrm{I}]}^{\alpha\gamma}F_{[\mathrm{I}]}^{\beta\delta} + F_{[\mathrm{I}]}^{\alpha\delta}F_{[\mathrm{I}]}^{\beta\gamma}\right)$ is the isotropic elasticity tensor of the shell or the membrane.
- $A^{ijkl} = \bar{\lambda}g^{ij}g^{kl} + \bar{\mu}\left(g^{ik}g^{jl} + g^{il}g^{jk}\right)$ is the isotropic elasticity tensor of the foundation.
- $\Lambda = 4\mu\dfrac{\lambda+\mu}{\lambda+2\mu}$.
- ϱ is the mass density with respect to the volume of the shell or the membrane.
- l is the width of the membrane.
- $\delta\tau = \tau_{\mathsf{max}}/\tau_0 = T_{\mathsf{max}}/T_0$ is the tension ratio.
- $g = 9.81$ is the acceleration due to gravity.
- μ_F is the capstan coefficient of friction.
- ν_F is Coulomb's coefficient of friction.
- a is the horizontal radius of the contact region.
- b is the vertical radius of the contact region.
- $\beta_\delta = \arctan\left(\dfrac{b}{a}\right)$ is the critical parametric-latitude.
- ε is the regularisation parameter.
- $|\boldsymbol{v}|_{\ell^2} = \left(\sum_i \left(\mathrm{norm}(v^i, 2)\right)^2\right)^{\frac{1}{2}}$, where $\mathrm{norm}(\cdot, 2)$ is Matlab 2-norm of matrix.
- R^2 is the coefficient of determination of linear regression.

Furthermore, the reader must note the following:

- We assume Einstein's summation notation unless it strictly says otherwise;
- In numerical modelling, whenever we say Young's modulus of the shell, we mean Young's modulus of the shell relative to Young's modulus of the foundation, i.e. $\delta E = E/\bar{E}$. Furthermore, if $\delta E \gg 1$, then we say the shell has a high stiffness;
- In numerical modelling, whenever we say Poisson's ratio of the shell, we mean Poisson's ratio of the shell relative to Poisson's ratio of the foundation, i.e. $\delta\nu = \nu/\bar{\nu}$. Furthermore, if $1 \ll \delta\nu < \frac{1}{2}\bar{\nu}^{-1}$, where $\bar{\nu} > 0$, then we say the shell is almost incompressible;
- In numerical modelling, whenever we say the thickness of the shell, we mean the thickness of the shell relative to the thickness of the foundation, i.e. $\delta h = h/H$. Furthermore, if $\delta h \ll 1$, then we say the shell is thin;

- In numerical modelling, whenever we say the vertical radius of the contact region, we mean the vertical radius of the contact region relative to the horizontal radius of the contact region, i.e. $\delta b = b/a$;
- When discussing numerical results, whenever we speak of a particular variable, we assume all other variables are fixed unless it is strictly says otherwise;
- All numerical results assume standard SI units unless it is strictly says otherwise;
- All of our numerical modelling is conducted using Matlab 2015b with *format long* and all numerical results are expressed in 3 significant figures: always rounded up.

1.2 Measure, Differential Geometry and Tensor Calculus

In this section we present the most important measure theory, differential geometry, and tensor calculus definitions and theorems that are required in this thesis. Almost all the results given in this section can be found in Ciarlet [38, 39][1], Kay [101] and Lipschutz [124].

Definition 1 (σ-algebra)**.** *A collection $\mathcal{M}(\mathbb{R}^n)$ of subsets of $\mathbb{R}^n$ is called a σ-algebra if*
(i) $\emptyset, \mathbb{R}^n \in \mathcal{M}(\mathbb{R}^n)$,
(ii) $U \in \mathcal{M}(\mathbb{R}^n) \Rightarrow \{\mathbb{R}^n \setminus U\} \in \mathcal{M}(\mathbb{R}^n)$,
(iii) if $\{U_k\}_{k\in\mathbb{N}} \subset \mathcal{M}(\mathbb{R}^n)$, *then* $\bigcup_{k\in\mathbb{N}} U_k, \bigcap_{k\in\mathbb{N}} U_k \in \mathcal{M}(\mathbb{R}^n)$.

Note that $n \in \mathbb{N}$ and $\emptyset$ is the empty set in $\mathbb{R}^n$.

Lemma 1 (Lebesgue Measure and Lebesgue Measurable Sets)**.** *There exists a σ-algebra $\mathcal{M}(\mathbb{R}^n)$ of subsets of $\mathbb{R}^n$ and a mapping $\mathrm{meas}(\cdot;\mathbb{R}^n) : \mathcal{M}(\mathbb{R}^n) \to [0, +\infty]$ such that:*
(i) Every open subset of $\mathbb{R}^n$ and every closed subsets of $\mathbb{R}^n$ are belong to $\mathcal{M}(\mathbb{R}^n)$;
(ii) If $\mathcal{B}$ is any ball in $\mathbb{R}^n$, then $\mathrm{meas}(\mathcal{B};\mathbb{R}^n)$ is the n-dimensional volume of $\mathcal{B}$;
(iii) If $\{U_k\}_{k\in\mathbb{N}} \subset \mathcal{M}(\mathbb{R}^n)$, where all U_k are pairwise disjoint, then $\mathrm{meas}(\bigsqcup_{k\in\mathbb{N}} U_k;\mathbb{R}^n) = \sum_{k\in\mathbb{N}} \mathrm{meas}(U_k;\mathbb{R}^n)$;
(iv) If $U \subseteq V$ such that $V \in \mathcal{M}(\mathbb{R}^n)$ and $\mathrm{meas}(V;\mathbb{R}^n) = 0$, then $U \in \mathcal{M}(\mathbb{R}^n)$ and $\mathrm{meas}(U;\mathbb{R}^n) = 0$.
Thus, for any $U \in \mathcal{M}(\mathbb{R}^n)$ we say U is a Lebesgue measurable set and we say $\mathrm{meas}(\cdot;\mathbb{R}^n)$ is the dimensional Lebesgue measure in $\mathbb{R}^n$.

Proof. Please consult chapter 6 of Schilling [175]. □

For an introduction on measure theory please consult chapter 1 of Kolmogorov *et al.* [111].

Definition 2 (Measurable Function)**.** *Let $f : \mathbb{R}^n \to \mathbb{R}$. Then we say f is a measurable function if $f^{-1}(U) \in \mathcal{M}(\mathbb{R}^n)$ for every open set $U \subset \mathbb{R}$.*

Note that $f^{-1}(\cdot)$ is the preimage of $f(\cdot)$ in this context.

Definition 3 (Essential Supremum $\mathrm{ess}-\sup(\cdot)$)**.** *Let $f : \mathbb{R}^n \to \mathbb{R}$ be a measurable function. Then the essential supremum of f is $\mathrm{ess}-\sup(f) = \inf\{a \in \mathbb{R} \mid \mathrm{meas}(\{\boldsymbol{x} \in \mathbb{R}^n : f(\boldsymbol{x}) > a\};\mathbb{R}^n) = 0\}$.*

[1] http://caos.fs.usb.ve/libros/Mechanics/Elasticity/An%20Introduction%20to%20Differential%20Geometry%20with%20Applications%20to%20Elasticity%20-%20Ciarlet.pdf

Definition 4 (Almost Everywhere a.e.). *Let $f, g : \mathbb{R}^n \to \mathbb{R}$ be a measurable functions. Then we say $f = g$ a.e. if $\int_U [f - g]\, d(\mathbb{R}^n) = 0$, for all $U \in \mathcal{M}(\mathbb{R}^n)$ with $\operatorname{meas}(U; \mathbb{R}^n) > 0$.*

For an introduction on measurable functions please consult chapter 2 of Spivak [184].

We say the map $\bar{\boldsymbol{X}} \in C^2(\bar{\Omega}; \mathbf{E}^3)$ is a diffeomorphism that describes the *reference configuration* of a Euclidean volume with respect to three-dimensional curvilinear coordinates (x^1, x^2, x^3), where $\Omega \subset \mathbb{R}^3$ is a three-dimensional bounded domain and $\mathbf{E}^3$ is the three-dimensional Euclidean space. By *diffeomorphism* we mean an invertible map that maps one differentiable manifold to another such that both the function and its inverse are sufficiently differentiable. Note that C^n is a space of continuous functions that has continuous first n partial derivatives in the underlying domain, where $n \in \mathbb{N}$. Bold symbols signify that we are dealing with vector and tensor fields and each must be understood in the context of the statement. Also, note that we usually reserve the vector brackets $(\,\cdot\,)_{\mathsf{E}}$ for vectors in the Euclidean space and $(\,\cdot\,)$ for vectors in the curvilinear space. Furthermore, the over-bar in the domain Ω implies the *closure* of the domain.

The covariant *metric tensor* of $\bar{\boldsymbol{X}}$ with respect to curvilinear coordinates is defined as

$$g_{ij} = \partial_i \bar{X}_k \partial_j \bar{X}^k \ , \ \forall\, i, j \in \{1, 2, 3\} \ .$$

Note that ∂_j is the partial derivative with respect to the coordinate x^j, and we assume *Einstein's summation notation*. Furthermore, $g_{ik} g^{kj} = \delta_i^j$, $\forall\, i, j \in \{1, 2, 3\}$ where δ_i^j is the Kronecker delta, and $\partial^j = g^{ji} \partial_i$. Einstein's summation notation is assumed herein unless it is strictly stays otherwise. Also, we regard the indices $i, j, k, l \in \{1, 2, 3\}$.

Here the metric tensor is a symmetric positive-definite $C^1(\bar{\Omega}; \mathbb{R}^9)$ function. By *positive definite* we mean that there exists a positive constant C that depends on $\bar{\Omega}$ and $\bar{\boldsymbol{X}}$ such that $C \delta_{ij} v^i v^j \leq g_{ij} v^i v^j$, $\forall\ \boldsymbol{v} \in \mathbb{R}^3$ (see section 6.1.1 of Evans [63]). The existence of such a constant can be guaranteed as all the three eigenvalues of $\boldsymbol{g}$ are positive in $\bar{\Omega}$ by construction, and thus, let $C = \inf_{(x^1, x^2, x^3) \in \bar{\Omega}} \{\lambda_1, \lambda_2, \lambda_3\}$ where λ_j are the eigenvalues of $\boldsymbol{g}$. Also, as $\boldsymbol{g} \in C^1(\bar{\Omega}; \mathbb{R}^9)$, there exists a finite positive constant M such that $M = \operatorname{ess-sup}(\det(\boldsymbol{g}))$.

We say $\bar{\boldsymbol{\nabla}}$ is the *covariant derivative* operator in the curvilinear space. For any $\boldsymbol{v} \in C^1(\bar{\Omega}; \mathbb{R}^3)$ we define its covariant derivative as

$$\bar{\nabla}_j v^k = \partial_j v^k + \bar{\Gamma}_{ij}^k v^i \ ,$$

where

$$\bar{\Gamma}_{ij}^k = \frac{1}{2} g^{kl} \left(-\partial_l g_{ij} + \partial_i g_{jl} + \partial_j g_{li} \right)$$

are *Christoffel symbols of the second kind*. Furthermore, $\bar{\nabla}_j x^i = \delta_j^i$, $\forall\, i, j \in \{1, 2, 3\}$, by definition. Note that here Christoffel symbols are $C^0(\bar{\Omega})$ functions with symmetry in their lower indices.

We say $\bar{\Delta}$ is the *vector Laplacian* operator in the curvilinear space. For any $\boldsymbol{v} \in C^2(\bar{\Omega}; \mathbb{R}^3)$ we define its vector Laplacian as

$$\bar{\Delta} v^j = \frac{1}{\sqrt{g}} \partial_i \left(\sqrt{g}\, g^{ik} \bar{\nabla}_k v^j \right) \ ,$$

where $g = \det(\boldsymbol{g})$ (see page 3 of Moon and Spencer [138]).

We further restrict the map $\bar{\boldsymbol{X}}$ by asserting that $\bar{\boldsymbol{X}}|_{x^3=0}$ describes a bounded portion of its boundary, i.e. given that $\partial\Omega$ is the boundary of the domain, there exists a plane $\omega \subset \partial\Omega$ with $\mathrm{meas}(\omega; \mathbb{R}^2) > 0$ such that $x^3 = 0$ in ω.

We say the map $\boldsymbol{\sigma} \in C^3(\bar{\omega}; \mathbf{E}^3)$ is an injective immersion that describes the *reference configuration* of an Euclidean surface with respect to two-dimensional curvilinear coordinates (x^1, x^2), where $\omega \subset \mathbb{R}^2$ is a two-dimensional bounded plane. By *immersion* we mean a differentiable map between differentiable manifolds whose derivative is everywhere injective.

The covariant *first fundamental form tensor* of $\boldsymbol{\sigma}$ with respect to curvilinear coordinates is defined as

$$F_{[\mathrm{I}]\alpha\beta} = \partial_\alpha \sigma_i \partial_\beta \sigma^i \ , \ \forall\ \alpha, \beta \in \{1, 2\} \ .$$

Also, we regard the indices $\alpha, \beta, \gamma, \delta \in \{1, 2\}$. Furthermore, $F_{[\mathrm{I}]\alpha\gamma} F^{\gamma\beta}_{[\mathrm{I}]} = \delta^\beta_\alpha$, $\forall\ \alpha, \beta \in \{1, 2\}$, by definition.

The covariant *second fundamental form tensor* of $\boldsymbol{\sigma}$ with respect to curvilinear coordinates is defined as

$$F_{[\mathrm{II}]\alpha\beta} = N_i \partial_{\alpha\beta} \sigma^i \ , \ \forall\ \alpha, \beta \in \{1, 2\} \ ,$$

where

$$\boldsymbol{N} = \frac{\partial_1 \boldsymbol{\sigma} \times \partial_2 \boldsymbol{\sigma}}{||\partial_1 \boldsymbol{\sigma} \times \partial_2 \boldsymbol{\sigma}||}$$

is the unit normal to the surface $\boldsymbol{\sigma}$, $\times$ is the Euclidean cross product and $||\cdot||$ is the Euclidean norm.

Here the first fundamental form tensor is a symmetric positive-definite $C^2(\bar{\omega}; \mathbb{R}^6)$ function. Thus, there exists a positive constant C that depends on $\bar{\omega}$ and $\boldsymbol{\sigma}$ such that $C\delta_{\alpha\beta} v^\alpha v^\beta \leq F_{[\mathrm{I}]\alpha\beta} v^\alpha v^\beta$, $\forall\ \boldsymbol{v} \in \mathbb{R}^2$. Also, as $\boldsymbol{F}_{[\mathrm{I}]} \in C^2(\bar{\omega}; \mathbb{R}^6)$, there exists a finite positive constant M such that $M = \mathrm{ess}-\sup(\det(\boldsymbol{F}_{[\mathrm{I}]}))$. Also, the second fundamental form tensor is a symmetric $C^1(\bar{\omega}; \mathbb{R}^6)$ function.

We say $\boldsymbol{\nabla}$ is the *covariant derivative* operator in the curvilinear plane. For any $\boldsymbol{u} \in C^1(\bar{\omega}; \mathbb{R}^2)$ we define its covariant derivative as

$$\nabla_\beta u^\gamma = \partial_\beta u^\gamma + \Gamma^\gamma_{\alpha\beta} u^\alpha \ ,$$

where

$$\Gamma^\gamma_{\alpha\beta} = \frac{1}{2} F^{\gamma\delta}_{[\mathrm{I}]} \left(-\partial_\delta F_{[\mathrm{I}]\alpha\beta} + \partial_\alpha F_{[\mathrm{I}]\beta\delta} + \partial_\beta F_{[\mathrm{I}]\delta\alpha} \right)$$

are *Christoffel symbols of the second kind* in the curvilinear plane. Furthermore, $\nabla_\beta x^\alpha = \delta^\alpha_\beta$, $\forall\ \alpha, \beta \in \{1, 2\}$. Note that here Christoffel symbols in the curvilinear plane are $C^1(\bar{\omega})$ functions with symmetry in their lower indices. Furthermore, as $\Gamma^\gamma_{\alpha\beta} \in C^1(\bar{\omega})$, there exists a finite positive constant M such that $\operatorname{ess}-\sup(\Gamma^\gamma_{\alpha\beta}) \leq M$, $\forall\ \alpha, \beta, \gamma \in \{1, 2\}$.

We say Δ is the *vector Laplacian* operator in the curvilinear plane. For any $\boldsymbol{v} \in C^2(\bar{\omega}; \mathbb{R}^2)$ we define its vector Laplacian as

$$\Delta v^\beta = \frac{1}{\sqrt{F_{[\mathrm{I}]}}} \partial_\alpha \left(\sqrt{F_{[\mathrm{I}]}}\, F^{\alpha\gamma}_{[\mathrm{I}]} \nabla_\gamma v^\beta \right) ,$$

where $F_{[\mathrm{I}]} = \det(\boldsymbol{F}_{[\mathrm{I}]})$ (see page 3 of Moon and Spencer [138]).

Lemma 2. *Let $\omega \subset \mathbb{R}^2$ be a plane and let $\boldsymbol{\sigma} \in C^3(\bar{\omega}; \boldsymbol{E}^3)$ be an injective immersion. Then there exists an $\varepsilon > 0$ such that the mapping $\boldsymbol{\Theta} : \bar{\omega} \times [-\varepsilon, \varepsilon] \to \boldsymbol{E}^3$ defined by*

$$\boldsymbol{\Theta} = \boldsymbol{\sigma} + x^3 \boldsymbol{N}$$

is a $C^2(\bar{\omega} \times [-\varepsilon, \varepsilon]; \boldsymbol{E}^3)$-diffeomorphism with $\det(\partial_1 \boldsymbol{\Theta}, \partial_2 \boldsymbol{\Theta}, \partial_3 \boldsymbol{\Theta}) > 0$, $\forall\ (x^1, x^2, x^3) \in \bar{\omega} \times [-\varepsilon, \varepsilon]$.

Proof. See the proof of theorem 4.1-1 of Ciarlet [39]. □

Note that $\times$ is the Cartesian product in this context.

Proposition 1. *Given that $(x^1, x^2, x^3) \in \{\omega \times (-\varepsilon, 0]\}$, for an $\varepsilon > 0$, the metric tensor, and the first and the second fundamental forms share the relation*

$$\begin{aligned} g_{\alpha\beta} &= F_{[\mathrm{I}]\alpha\beta} - 2x^3 F_{[\mathrm{II}]\alpha\beta} + \left(x^3\right)^2 F_{[\mathrm{III}]\alpha\gamma} F_{[\mathrm{III}]}{}^{\gamma}_{\beta} , \\ g_{3\beta} &= 0 , \\ g_{33} &= 1 . \end{aligned}$$

Proof. A trivial tensor calculus result that follows directly from the definition of $\bar{\boldsymbol{X}}$ and lemma 2. □

Proposition 2. *For a vector $\boldsymbol{v} \in C^1(\bar{\omega}; \mathbb{R}^3)$ the covariant derivative in the curvilinear space restricted to the plane ω is*

$$\begin{aligned} \bar{\nabla}_\beta v^\gamma &= \nabla_\beta v^\gamma - F_{[\mathrm{III}]}{}^{\gamma}_{\beta} v^3 , \\ \bar{\nabla}_\beta v^3 &= \partial_\beta v^3 + F_{[\mathrm{III}]\alpha\beta} v^\alpha . \end{aligned}$$

Proof. Note that $F_{[\mathrm{III}]\alpha\beta} = \bar{\Gamma}_{\alpha\beta 3}|_\omega = -\bar{\Gamma}_{3\alpha\beta}|_\omega = -\bar{\Gamma}_{\beta 3\alpha}|_\omega$ and the result follows directly from the definition of $\bar{\boldsymbol{\nabla}}$ and lemma 2. □

Proposition 3.

$$\nabla_\alpha F_{[\mathrm{III}]\beta\gamma} = \nabla_\beta F_{[\mathrm{III}]\gamma\alpha} .$$

Proof. See the proof of theorem 2.5-1 of Ciarlet [38]. □

Lemma 3 (Gauss' Theorema Egregium)**.** *The Gauss curvature is uniquely determined by the first fundamental form and is, therefore, preserved by isometries.*

Proof. See the proof of theorem 10.2.1 of Pressley [159]. □

By *isometry* we mean a distance-preserving injective map between metric spaces.

Lemma 4 (Fubini's theorem)**.** *Let $X, Y \subset \mathbb{R}$ be closed intervals and $f : X \times Y \to \mathbb{R}$. If f is measurable, then*

$$\int_Y \left[\int_X f(x,y)\, dX \right] dY = \int_X \left[\int_Y f(x,y)\, dY \right] dX \ .$$

Proof. See the proof of theorem 3-10 of Spivak [184]. □

Proposition 4. *As $\boldsymbol{g} \in C^2(\bar{\Omega}; \mathbb{R}^9)$ is positive definite, there exists a positive constant C that depends on $\bar{\Omega}$ and $\bar{\boldsymbol{X}}$ such that*

$$C \leq \int_\Omega d\Omega \ .$$

Proof. As $\boldsymbol{g}$ is positive definite, there exists a positive constant c such that $c \leq \det(\boldsymbol{g})$, $\forall\ (x^1, x^2, x^3) \in \bar{\Omega}$. Thus, we get $\int_\Omega d\Omega = \int_\Omega \det(\boldsymbol{g})^{\frac{1}{2}}\ dx^1 dx^2 dx^3 \geq c \int_\Omega dx^1 dx^2 dx^3 = C$. Note that Ω is a bounded domain in $\mathbb{R}^3$. □

Proposition 5. *As $\boldsymbol{F}_{[I]} \in C^2(\bar{\omega}; \mathbb{R}^6)$ is positive definite, there exists a positive constant C that depends on $\bar{\omega}$ and $\boldsymbol{\sigma}$ such that*

$$C \leq \int_\omega d\omega \ .$$

Proof. As $\boldsymbol{F}_{[\mathrm{I}]}$ is positive definite, there exists a positive constant c such that $c \leq \det(\boldsymbol{F}_{[\mathrm{I}]})$, $\forall\ (x^1, x^2) \in \bar{\omega}$. Thus, we get $\int_\omega d\omega = \int_\omega \det(\boldsymbol{F}_{[\mathrm{I}]})^{\frac{1}{2}}\ dx^1 dx^2 \geq c \int_\omega dx^1 dx^2 = C$. Note that ω is a bounded domain in $\mathbb{R}^2$. □

Lemma 5 (Positive Definiteness of the Elasticity Tensor)**.** *Let $\bar{E} > 0$ and $-1 < \bar{\nu} < \frac{1}{2}$. Then there exists a positive constant C that depends on $\bar{\Omega}$, $\bar{\boldsymbol{X}}$, $\bar{E}$ and $\bar{\nu}$ such that*

$$C\delta^{ik}\delta^{jl}M_{ij}M_{kl} \leq \left(\frac{\bar{\nu}\bar{E}}{(1+\bar{\nu})(1-2\bar{\nu})} g^{ij}g^{kl} + \frac{1}{2}\frac{\bar{E}}{(1+\bar{\nu})} \left(g^{ik}g^{jl} + g^{il}g^{jk} \right) \right) M_{ij}M_{kl} \ ,\ \forall\ \boldsymbol{M} \in \mathbb{S}_3 \ .$$

Proof. See the proof of theorem 3.9-1 of Ciarlet [39]. □

Note that $\mathbb{S}_n$ is the space of $n \times n$ real symmetric matrices.

Lemma 6 (Positive Definiteness of the Elasticity Tensor on a General Surface)**.** *Let $E > 0$ and $-1 < \nu < \frac{1}{2}$. Then there exists a positive constant C that depends on $\bar{\omega}$, $\boldsymbol{\sigma}$, E and ν such that*

$$C\delta^{\alpha\gamma}\delta^{\beta\delta}M_{\alpha\beta}M_{\gamma\delta} \leq \frac{1}{2}\frac{E}{(1+\nu)} \left(\frac{2\nu}{(1-\nu)} F^{\alpha\beta}_{[I]} F^{\gamma\delta}_{[I]} + F^{\alpha\gamma}_{[I]} F^{\beta\delta}_{[I]} + F^{\alpha\delta}_{[I]} F^{\beta\gamma}_{[I]} \right) M_{\alpha\beta}M_{\gamma\delta} \ ,\ \forall\ \boldsymbol{M} \in \mathbb{S}_2 \ .$$

Proof. See the proof of theorem 4.4-1 of Ciarlet [39]. □

Lemma 7 (Critical Angle of Deflection of a Semi-Ellipse)**.** *Consider the set* $\mathrm{Semi-Ellipse} = \{(a\sin(\theta), b\cos(\theta))_{\mathrm{E}} \mid a, b \in \mathbb{R}_{>0},\ \theta \in [-\frac{1}{2}\pi, \frac{1}{2}\pi]\}$*. Let δ be the acute angle that the radial vector $(a\sin(\theta), b\cos(\theta))_{\mathrm{E}}$ makes with the unit outward normal vector $(\varphi(\theta))^{-1}(b\sin(\theta), a\cos(\theta))_{\mathrm{E}}$, where $\varphi(\theta) = (b^2\sin^2(\theta) + a^2\cos^2(\theta))^{\frac{1}{2}}$, i.e.*

$$\tan(\delta) = \frac{(a^2 - b^2)}{2ab}\sin(2\theta) \ .$$

Then the critical value of δ over the set $\mathrm{Semi-Ellipse}$ *is given by*

$$\delta_{\textit{crit}} = \frac{1}{2}\pi - 2\arctan\left(\frac{b}{a}\right) .$$

Proof. Consider theorem 1 from chapter 8 of Kalman [98], which is proved for the set $\mathrm{Ellipse} = \{(a\sin(\theta), b\cos(\theta))_{\mathrm{E}} \mid 0 < b < a < \infty,\ \theta \in (-\pi, \pi]\}$ and for the angle $\delta > 0$. Now, notice that critical points occur at $\theta = \pm\frac{1}{4}\pi$, and thus, use a few elementary trigonometric identities to obtain the above lemma. □

Definition 5 (Parametric Latitude $\beta(\cdot)$)**.** *Consider the set* $\mathrm{Semi-Ellipse} = \{(a\sin(\theta), b\cos(\theta))_{\mathrm{E}} \mid a, b \in \mathbb{R}_{>0},\ \theta \in [-\frac{1}{2}\pi, \frac{1}{2}\pi]\}$*. Then the parametric latitude is define by* $\beta(\theta) = \arctan((b/a)\tan(\theta))$.

See section 5.5 of Osborne [145].

Consider a prism with an elliptical cross-section defined by the map $(x^1, a\sin(\theta), b\cos(\theta))_{\mathrm{E}}$, where $|x^1| < \infty$ and $\theta \in [-\frac{1}{2}\pi, \frac{1}{2}\pi]$, then we say $\beta_\delta = \arctan(b/a)$ is the *critical parametric-latitude*. To be more precise, β_δ is the parametric latitude with respect to the angle $\delta_{\textsf{crit}}$ implied by lemma 7, i.e. $\beta_\delta = \frac{1}{4}\pi - \frac{1}{2}\delta_{\textsf{crit}}$. Lemma 7 further implies that $\beta_\delta \propto b/a$ and we use this as a measure of the curvature of the contact region.

1.3 Functional Analysis

In this section we present the most important functional analysis definitions and theorems that are required in this thesis. Almost all the results given in this section can be found in Ciarlet [38], Evans [63], Adams and Fournier [3], and Badiale and Serra [13].

Definition 6 (Segment Condition)**.** *We say the domain $\Omega \subset \mathbb{R}^n$ satisfies the segment condition if for every $\boldsymbol{x} \in \partial\Omega$ there is a neighbourhood $U_{\boldsymbol{x}}$ and a nonzero vector $\boldsymbol{y}_{\boldsymbol{x}}$ such that, if $\boldsymbol{z} \in \bar{\Omega} \cap U_{\boldsymbol{x}}$, then $\boldsymbol{z} + t\boldsymbol{y}_{\boldsymbol{x}} \in \Omega$ for some $t \in (0, 1)$.*

Segment condition implies that, if the domain Ω is not empty, then the boundary must be $(n-1)$ dimensional and the domain cannot lie on both sides of any part of the boundary.

Definition 7 (Uniform-C^1 Regularity Condition)**.** *We say the boundary of the domain $\Omega \subset \mathbb{R}^n$ satisfies the uniform-$C^1(\mathbb{R}^n; \mathbb{R}^{n-1})$ condition, where $n \in \{2, 3\}$, if there exists a locally finite open cover $\{U_j\}$ of boundary $\partial\Omega$, a corresponding sequence $\{\boldsymbol{\Phi}_j\}$ of transformations with first-order continuous partial derivatives and with $\boldsymbol{\Phi}_j$ taking U_j into the ball $B = \{\boldsymbol{y} \in \mathbb{R}^n \mid ||\boldsymbol{y}|| < 1\}$, and having $\boldsymbol{\Psi}_j = \boldsymbol{\Phi}_j^{-1}$ such that:*
(i) For some finite R, every collection $R+1$ of the set U_j has empty intersection;
(ii) For some $\delta > 0, \Omega_\delta \subset \bigcup_{j=1}^{\infty} \boldsymbol{\Psi}_j(\{\boldsymbol{y} \in \mathbb{R}^n \mid ||\boldsymbol{y}|| < \frac{1}{2}\})$;
(iii) For each $j, \boldsymbol{\Phi}_j(U_j \cap \Omega) = \{\boldsymbol{y} \in B \mid \boldsymbol{y}_n > 0\}$;
(iv) There exists a finite constant M such that $|\partial_\alpha \Phi_j^\beta(\boldsymbol{x})| \leq M$, $\forall\ \boldsymbol{x} \in U_j$ and $|\partial_\alpha \Psi_j^\beta(\boldsymbol{y})| \leq M$, $\forall\ \boldsymbol{y} \in B,\ \forall\ \alpha, \beta \in [1, n]$.

Definition 8 (Lebesgue Space L^2)**.** *Let $\Omega \subset \mathbb{R}^n$ be a domain and let $v \in \mathbb{R}$. Then we say $v \in L^2(\Omega)$ if there exists a finite positive constant M such that*

$$||v||_{L^2(\Omega)} = \left(\int_\Omega |v|^2\, d\Omega\right)^{\frac{1}{2}} \leq M .$$

Furthermore, the space $(L^2(\Omega), ||\cdot||_{L^2(\Omega)})$ *is a Hilbert space, i.e. a complete normed space with the notion of an inner product.*

By *complete* we mean that every Cauchy sequence in the space converges with respect to the specified norm. Note that the *product space* $(\boldsymbol{L}^2(\Omega), ||\cdot||_{\boldsymbol{L}^2(\Omega)})$ must be understood in the context of the statement. For example, if the tensor $\boldsymbol{E} \in \mathbb{R}^2 \times \mathbb{R}^2$ is also $\boldsymbol{E} \in \boldsymbol{L}^2(\Omega)$, then we express the product space as $(\boldsymbol{L}^2(\Omega), ||\cdot||_{\boldsymbol{L}^2(\Omega)}) = (L^2(\Omega) \times L^2(\Omega) \times L^2(\Omega) \times L^2(\Omega), (||\cdot||^2_{L^2(\Omega)} + ||\cdot||^2_{L^2(\Omega)} + ||\cdot||^2_{L^2(\Omega)} + ||\cdot||^2_{L^2(\Omega)})^{\frac{1}{2}})$, i.e. $||\boldsymbol{E}||_{\boldsymbol{L}^2(\Omega)} = (\sum_{\alpha,\beta\in\{1,2\}} ||E_{\alpha\beta}||^2_{L^2(\Omega)})^{\frac{1}{2}} \leq M$ for a some finite positive constant M.

Definition 9 (Sobolev Space H^m)**.** *Let* $\Omega \subset \mathbb{R}^n$ *be a domain and let* $u \in \mathbb{R}$*. Then we say* $u \in H^1(\Omega)$ *if there exists a finite positive constant* M *such that*

$$||u||_{H^1(\Omega)} = \left(||u||^2_{L^2(\Omega)} + \sum_{j=1}^{n} ||\partial_j u||^2_{L^2(\Omega)} \right)^{\frac{1}{2}} \leq M \ ,$$

where $H^1(\Omega) = \{v \in L^2(\Omega) \mid \partial_j v \in L^2(\Omega) \ , \ \forall \ j \in [1, n]\}$*. Also, we say* $u \in H^2(\Omega)$ *if there exists a finite positive constant* M *such that*

$$||u||_{H^2(\Omega)} = \left(||u||^2_{L^2(\Omega)} + \sum_{j=1}^{n} ||\partial_j u||^2_{L^2(\Omega)} + \sum_{i,j=1}^{n} ||\partial_{ij} u||^2_{L^2(\Omega)} \right)^{\frac{1}{2}} \leq M \ ,$$

where $H^2(\Omega) = \{v \in H^1(\Omega) \mid \partial_{ij} v \in L^2(\Omega) \ , \ \forall \ i, j \in [1, n]\}$*. The space* $(H^m(\Omega), ||\cdot||_{H^m(\Omega)})$ *is a Hilbert space.*

Note that $\partial_i v$ and $\partial_{ij} v$ from above statements are *weak derivatives* and must be understood in a sense of distributions (see section 5.2.1 of Evans [63]). Also, note that $H^0 = L^2$ by definition.

Proposition 6 (Hölder Inequality)**.** *Let* $u, v \in L^2(\Omega)$*, then we have the inequity* $\int_\Omega |uv| \ d\Omega \leq ||u||_{L^2(\Omega)} ||v||_{L^2(\Omega)}$*. Also, let* $\operatorname{ess-sup}(\bar{u}) < \infty$ *and* $\int_\Omega |\bar{v}| \ d\Omega < \infty$*, then we have the inequality* $\int_\Omega |\bar{u}\bar{v}| \ d\Omega \leq \operatorname{ess-sup}(\bar{u}) \int_\Omega |\bar{v}| \ d\Omega$*.*

Proof. A simple extension of Cauchy-Schwarz inequality. See appendix B.2 of Evans [63]. □

Proposition 7 (Minkowski Inequality)**.** *Let* $u, v \in L^2(\omega)$*, then we have the inequality* $||u + v||_{L^2(\omega)} \leq ||u||_{L^2(\omega)} + ||v||_{L^2(\omega)}$*.*

Proof. A simple extension of the triangle inequality. See appendix B.2 of Evans [63]. □

Definition 10 (Support supp)**.** *Let* $\Omega \subset \mathbb{R}^n$ *and* $\phi : \Omega \to \mathbb{R}$*, then we say the support of the function* ϕ *is the set* $\operatorname{supp}(\phi) = \overline{\{\boldsymbol{x} \in \Omega \mid \phi(x) \neq 0\}}$*.*

Definition 11 (Space of smooth functions with compact supports C_0^∞)**.** *Let* $\Omega \subset \mathbb{R}^n$*, then the space of infinitely differentiable functions with compact support in the underlying domain is the set* $C_0^\infty(\Omega) = \{\phi \in C^\infty(\Omega) \mid \operatorname{supp}(\phi) \Subset \Omega\}$*, where* C^∞ *is the space of infinity differentiable functions.*

Note that $X \Subset \Omega \subset \mathbb{R}^n$ means that X is compact (closed and bounded) in $\mathbb{R}^n$ such that the closure of X is a proper subset of Ω.

Definition 12 (Space of test functions $\mathscr{D}$)**.** *Let $\Omega \subset \mathbb{R}^n$, then the space of test functions is the set $\mathscr{D}(\Omega) = \{\phi \in C_0^\infty(\Omega) \mid D^{\boldsymbol{\alpha}}\phi \in C_0^\infty(\Omega)\ ,\ \forall\ \boldsymbol{\alpha} \in \mathbb{N}^n\}$, where D is the differential operator and $\boldsymbol{\alpha}$ is a multi index.*

For more on distribution theory please consult chapter 2 of Demidov [53].

Definition 13 (Sobolev Space H_0^1)**.** *Let $\Omega \subset \mathbb{R}^n$, then $H_0^1(\Omega)$ is the closure of $C_0^\infty(\Omega)$ with respect to the norm in $H^1(\Omega)$.*

Lemma 8 (Fundamental Lemma of J. L. Lions)**.** *Let $\Omega \subset \mathbb{R}^n$ be a domain and v be a distribution on Ω. If $v \in H^{-1}(\Omega)$ and $\partial_j v \in H^{-1}(\Omega)$, $\forall\ j \in [1, n]$, then $v \in L^2(\Omega)$, where $H^{-1}(\Omega)$ is the dual space of $H_0^1(\Omega)$.*

Proof. See Magenes and Stampacchia [131]. □

Lemma 9 (Infinitesimal Rigid Displacement Lemma)**.** *Let $\Omega \subset \mathbb{R}^3$ be a domain, $\bar{\boldsymbol{X}} \in C^2(\bar{\Omega}; \boldsymbol{E}^3)$ be a diffeomorphism and $\boldsymbol{v} \in \boldsymbol{H}^1(\Omega)$. If*

$$\bar{\nabla}_i v_j + \bar{\nabla}_j v_i = 0\ ,\ \forall\ (x^1, x^2, x^3) \in \Omega\ ,\ \forall\ i, j \in \{1, 2, 3\}\ ,$$

then there exist two constant Euclidean vectors $\bar{\boldsymbol{a}}, \bar{\boldsymbol{b}} \in \boldsymbol{E}^3$ such that

$$v^i \partial_i \bar{\boldsymbol{X}} = \bar{\boldsymbol{a}} + \bar{\boldsymbol{b}} \times \bar{\boldsymbol{X}}\ ,\ \forall\ (x^1, x^2, x^3) \in \bar{\Omega}\ .$$

In particular, if $\boldsymbol{v}|_{\partial\Omega_0} = \boldsymbol{0}$, for some $\partial\Omega_0 \subseteq \partial\Omega$ with $\operatorname{meas}(\partial\Omega_0; \mathbb{R}^2) > 0$, then $\bar{\boldsymbol{a}} = \boldsymbol{0}$ and $\bar{\boldsymbol{b}} = \boldsymbol{0}$.

Proof. See the proof of theorem 1.7-3 of Ciarlet [38]. □

Lemma 10 (Infinitesimal Rigid Displacement Lemma on a General Surface)**.** *Let $\omega \subset \mathbb{R}^2$ be a plane, $\boldsymbol{\sigma} \in C^3(\bar{\omega}; \boldsymbol{E}^3)$ be an injective immersion and $\boldsymbol{v} \in H^1(\omega) \times H^1(\omega) \times H^2(\omega)$. If*

$$\bar{\nabla}_\alpha v_\beta + \bar{\nabla}_\beta v_\alpha = 0\ ,\ \forall\ (x^1, x^2) \in \omega\ ,\ \forall\ \alpha, \beta \in \{1, 2\}\ ,$$
$$\bar{\nabla}_\alpha \left(\bar{\nabla}_\beta v^3\right) + \bar{\nabla}_\beta \left(\bar{\nabla}_\alpha v^3\right) = 0\ ,\ \forall\ (x^1, x^2) \in \omega\ ,\ \forall\ \alpha, \beta \in \{1, 2\}\ ,$$

then there exist two constant Euclidean vectors $\boldsymbol{a}, \boldsymbol{b} \in \boldsymbol{E}^3$ such that

$$v^\alpha \partial_\alpha \boldsymbol{\sigma} + v^3 \boldsymbol{N} = \boldsymbol{a} + \boldsymbol{b} \times \boldsymbol{\sigma}\ ,\ \forall\ (x^1, x^2) \in \bar{\omega}\ .$$

In particular, if $\boldsymbol{v}|_{\partial\omega_0} = \boldsymbol{0}$ and $n^\alpha \partial_\alpha v^3|_{\partial\omega_0} = 0$, for some $\partial\omega_0 \subseteq \partial\omega$ with $\operatorname{meas}(\partial\omega_0; \mathbb{R}) > 0$, then $\boldsymbol{a} = \boldsymbol{0}$ and $\boldsymbol{b} = \boldsymbol{0}$, where $\boldsymbol{n}$ is the unit outward normal to the boundary $\partial\omega$.

Proof. See the proof of theorem 3.6-3 of Ciarlet [38]. □

By *unit* we mean $n_\alpha n^\alpha = F_{[\mathrm{I}]\alpha\beta} n^\alpha n^\beta = 1$.

Lemma 11 (Boundary Trace Embedding Theorem)**.** *Let $\Omega \subset \mathbb{R}^n$ be a domain with a uniform-$C^1(\mathbb{R}^n; \mathbb{R}^{n-1})$ boundary, where $n \in \{2, 3\}$, then the embedding $H^1(\Omega) \to L^2(\partial\Omega)$ is continuous.*

Proof. See the proof of theorem 5.36 of Adams and Fournier [3]. □

By *continuous* we mean that there exists a constant C that depends on Ω and $\partial\Omega$ such that $||v||_{L^2(\partial\Omega)} \leq C||v||_{H^1(\Omega)}$. Note that, if Ω is bounded, then there exists a bounded linear operator $\mathrm{Tr} : H^1(\Omega) \to L^2(\partial\Omega)$ such that $\mathrm{Tr}(v) = v|_{\partial\Omega}$ for $v \in H^1(\Omega) \cap C^0(\bar{\Omega})$, where $C^0(\bar{\Omega})$ is the space of uniformly continuous functions on Ω (see section 5.5 of Evans [63]). A word of caution: the trace theorem presented by Evans [63] does not seem to acknowledge the dimensions of the domain Ω. The reader must be aware that the dimensions of the domain play a significant role in the continuousness of the trace embedding into the specified Sobolev space. For a more accurate trace theorem please consult theorem 5.36 of Adams and Fournier [3] or section 2.6.2 of Necas *et al.* [144].

Lemma 12 (Trivial Traces)**.** *Let $\omega \subset \mathbb{R}^2$ be a domain with a uniform-$C^1(\mathbb{R}^2;\mathbb{R})$ boundary, then $v \in H_0^1(\omega)$ if and only if $v|_\omega = 0$, where $v \in H^1(\omega)$.*

Proof. See the proof theorem 5.37 of Adams and Fournier [3]. □

Lemma 13 (Rellich-Kondrachov Theorem)**.** *Let $\Omega \subset \mathbb{R}^3$ be a bounded domain with a uniform-$C^1(\mathbb{R}^3;\mathbb{R}^2)$ boundary, then the embedding $H^1(\Omega) \to L^2(\Omega)$ is compact. Also, let $\omega \subset \mathbb{R}^2$ be a bounded domain with a uniform-$C^1(\mathbb{R}^2;\mathbb{R})$ boundary, then the embeddings $H^1(\omega) \to L^2(\omega)$ and $H^2(\omega) \to H^1(\omega)$ are compact.*

Proof. See the proof of theorem 6.3 of Adams and Fournier [3]. □

Note that we say that the embedding $(X, ||\cdot||_X) \to (Y, ||\cdot||_Y)$ is *compact* if for every bounded sequence in $(X, ||\cdot||_X)$, under the given embedding, has a convergent subsequence in $(Y, ||\cdot||_Y)$. Note that Rellich-Kondrachov theorem (lemma 13) is proved for domains that satisfy the *cone condition* (see definition 4.10 of Adams [3]). As the uniform-C^1 boundary implies the cone condition, lemma 13 holds.

Definition 14 (Coercive)**.** *Let $(X, ||\cdot||_X)$ be a Banach space. We say the functional $J(\cdot) : X \to \mathbb{R}$ is coercive, if $||v_k||_X \to \infty$, then $J(v_k) \to \infty$, for any sequence $\{v_k\}_{k\in\mathbb{N}} \subseteq X$.*

By *Banach space* we mean a complete normed-space.

Definition 15 (Fréchet Differentiable)**.** *Let $(X, ||\cdot||_X)$ be a Banach space and let $U \subseteq X$ be an open set. Then we say the functional $J(\cdot) : U \to \mathbb{R}$ is Fréchet differentiable at $u \in U$ if there exists a unique linear map $J'(u) \in X'$ such that*

$$\lim_{||v||_X \to 0} \frac{J(u+v) - J(u) - J'(u)v}{||v||_X} = 0 \,,$$

where X' is the dual space of X.

By *linear* we mean that $J'(u)v$ is linear in v.

Definition 16 (Gâteaux Differentiable)**.** *Let $(X, ||\cdot||_X)$ be a Banach space and let $U \subseteq X$ be an open set. Then we say the functional $J(\cdot) : U \to \mathbb{R}$ is Gâteaux differentiable at $u \in U$ if there exists a linear map $J'_G(u) \in X'$ such that*

$$\lim_{t\to 0} \frac{J(u+tv) - J(u) - J'_G(u)tv}{t} = 0 \,.$$

Lemma 14. *Let $(X, ||\cdot||_X)$ be a Banach space and let $J(\cdot) : U \to \mathbb{R}$ be a Gâteaux differentiable functional in the open set $U \subseteq X$. If the Gâteaux differential is continuous at a point $u \in U$, then the functional is Fréchet differentiable at the point u, i.e. $J'_G(u) = J'(u)$.*

Proof. Simple extension of continuous partial-derivatives imply differentiability. See the proof of proposition 1.3.8 of Badiale and Serra [13]. □

Definition 17 (Local Minimum Point)**.** *Let $(X, ||\cdot||_X)$ be a normed space and let $U \subseteq X$ be an open set. Then we say $v \in U$ is a local minimum point of the functional $J(\cdot) : U \to \mathbb{R}$ if $J(u) = \min_{v \in U} J(v)$.*

Definition 18 (Critical Point)**.** *Let $(X, ||\cdot||_X)$ be a Banach space and let $U \subset X$ be an open set. Then we say $u \in U$ is the critical point of a Fréchet differentiable functional $J(\cdot) : U \to \mathbb{R}$ if $J'(u) = 0$.*

Lemma 15. *Let $(X, ||\cdot||_X)$ be a Banach space and let $J(\cdot) : X \to \mathbb{R}$ be a Fréchet differentiable functional, then any local minimum point is a critical point.*

Proof. See remark 1.5.1 of Badiale and Serra [13]. □

Definition 19 (Convex)**.** *Let $(X, ||\cdot||_X)$ be a Banach space. Then we say the functional $J(\cdot) : X \to \mathbb{R}$ is convex if $J(tu + (1-t)v) \leq tJ(u) + (1-t)J(v)$, $\forall\ t \in [0,1]$ and $\forall\ u, v \in X$.*

Definition 20 (Strictly Convex)**.** *Let $(X, ||\cdot||_X)$ be a Banach space. Then we say the functional $J(\cdot) : X \to \mathbb{R}$ is strictly convex if $J(tu + (1-t)v) < tJ(u) + (1-t)J(v)$, $\forall\ t \in (0,1)$ and $\forall\ u, v \in X$ where $u \neq v$.*

Lemma 16. *Let $(X, ||\cdot||_X)$ be a Banach space. Then the Fréchet differentiable functional $J(\cdot) : X \to \mathbb{R}$ is strictly convex if it satisfies the relation*

$$0 < \left(J'(u) - J'(v)\right)(u - v)\ ,\ \forall\ u, v \in X \text{ where } u \neq v.$$

In particular, if $J'(u)$ is linear in u, then there exist a positive constant C such that

$$C||u - v||_X^2 \leq \left(J'(u) - J'(v)\right)(u - v)\ ,\ \forall\ u, v \in X\ .$$

Proof. See the proof of proposition 1.5.10 of Badiale and Serra [13] and apply definition 20. □

Lemma 17 (Unique Global Minimum Point)**.** *Let $(X, ||\cdot||_X)$ be a Banach space and let $J(\cdot) : X \to \mathbb{R}$ be a continuous coercive strictly-convex functional. Then $J(\cdot)$ has a unique global minimum point.*

Proof. Combine the proofs of theorems 1.5.6 and 1.5.8 of Badiale and Serra [13]. □

Lemma 18 (Unique Critical Point)**.** *Let $(X, ||\cdot||_X)$ be a Banach space and let $J(\cdot) : X \to \mathbb{R}$ be a strictly-convex Fréchet-differentiable functional. Then $J(\cdot)$ has at most one critical point.*

Proof. See the proof of theorem 1.5.9 of Badiale and Serra [13]. □

Definition 21 (Closed Graph)**.** *Let (X, d_X) and (Y, d_Y) be metric spaces were is d_X and d_Y are metrics in respective spaces X and Y. Then we say the map $\iota : (X, d_X) \to (Y, d_Y)$ is a closed graph if the set $\operatorname{graph}(\iota) = \{(x, \iota(x)) \mid x \in X\}$ is a closed subset of the product space $(X, d_X) \times (Y, d_Y)$.*

Lemma 19 (Closed Graph Theorem)**.** *Let $(X, ||\cdot||_X)$ and $(Y, ||\cdot||_Y)$ be Banach spaces and let $\iota : (X, ||\cdot||_X) \to (Y, ||\cdot||_Y)$ be a be a linear map. Then ι is continuous if and only if it has a closed graph.*

Proof. See the proof of theorem 7.19 of Sokal [182]. □

Herein we assert that the set $\Omega \subset \mathbb{R}^3$ is an open bounded connected domain that satisfies the segment property with a uniform-$C^1(\mathbb{R}^3; \mathbb{R}^2)$ boundary, and we assert that the set $\omega \subset \mathbb{R}^2$ is an open bounded connected domain that satisfies the segment property with a uniform-$C^1(\mathbb{R}^2; \mathbb{R})$ boundary, unless it is strictly says otherwise. By *connected* we mean a set that cannot be represented as the union of two or more disjoint nonempty open subsets.

1.4 Beams, Plates and Shells

A *plate* is a structural element with planar dimensions that are large compared to its thickness. Thus, plate theories are derived from the three-dimensional elastic theory by making suitable assumptions concerning the kinematics of deformation or the state stress through the thickness of the lamina, thereby reducing three-dimensional elasticity problem into a two-dimensional one. In this section we only restrict our attention to displacement-based theories. Note that displacement-based theories such as Kirchhoff–Love plate theory, Mindlin–Reissner plate theory and Euler–Bernoulli beam theory are originally derived with the use of Newton's second law of motion and equilibrium considerations. However, in this work we review them as equations derived by *principle of virtual displacements*. For more on principle of virtual displacements please consult section 2.2.2 of Reddy [163].

For Kirchhoff–Love plate theory [126] the displacement field is defined as

$$\boldsymbol{u}(x, y, z) = \big(u^1(x, y) - z\partial_x u^3(x, y), u^2(x, y) - z\partial_y u^3(x, y), u^3(x, y)\big)_{\mathsf{E}} .$$

This is a first-order shear-deformation theory and it is only valid for thin plates and for very small deflections. The theory assumes that the order of the unknown functions are $\partial_\beta u^\alpha = \mathcal{O}(\varepsilon^2)$ and $\partial_\beta u^3 = \mathcal{O}(\varepsilon)$, and only the leading order terms are used to derive the governing equations. Furthermore, the following fundamental assumptions of classical plate theory (i.e. Kirchhoff–Love assumptions) are assumed, and they are: (i) straight lines normal to the mid-surface remain straight after deformation, (ii) straight lines normal to the mid-surface remain normal to the mid-surface after deformation, and (iii) the thickness of the plate does not change during a deformation [163]. Note that despite the prevalence Kirchhoff–Love assumptions, they are the subject of some scientific disputes [110].

Given that $q(x, y)$ is a traverse load and one is dealing with an isotropic plate, the governing equations reduce to the following form,

$$\frac{Eh^3}{12(1-\nu^2)}\Delta_{\mathsf{E}}^2 u^3 - q = 0 \,,$$

where Δ_{E} is the two-dimensional Euclidean Laplacian, E and ν are Young's modulus and Poisson's ratio of the plate respectively. Note that the term $\frac{1}{12}(1-\nu^2)^{-1}Eh^3$ is referred to as the bending stiffness and it signifies the magnitude of the force that is required to bend a plate in the transverse-direction per unit-volume.

As for the boundary conditions, one requires at least four boundary conditions per given plate theory. These boundary conditions include clamped, simply supported and free-end, and each condition varies from one plate-theory to another. To define each boundary condition in more detail is cumbersome, and thus, herein they are not reviewed.

For moderately thicker plates Mindlin–Reissner first-order shear-deformation plate theory is utilised. For Mindlin–Reissner plate theory [137] the displacement field is defined as

$$\boldsymbol{u}(x, y, z) = (u^1(x, y) - z\phi^1(x, y),\ u^2(x, y) - z\phi^2(x, y),\ u^3(x, y))_{\mathsf{E}} \,,$$

where $\boldsymbol{\phi}(x, y) = (\phi^1, \phi^2, 0)$ are defined as the angles that the normal to the mid-surface makes with the $z = 0$ axis. The theory assumes the plane-stress condition, i.e. there is a linear variation of the displacement across the plate thickness, but the plate thickness does not change during deformation. This theory is valid for thicker plates as it considers the shear deformations through the thickness of a plate. For this theory the transverse shear strains are represented as constant through lamina's thickness. Thus, it follows that the transverse shear-stress is also constant. It is known from the elementary theory of homogeneous beams (nonlinear Euler-Bernoulli beam theory [164]) that the transverse shear-stress variation is parabolic through the beam thickness. This discrepancy between the actual-stress state and the constant-stress state predicted by the first-order theory is often corrected by the introduction of the shear-correction factor (see chapter 10 of Reddy[166]). The theory assumes that the order of the unknown functions are $u^\alpha = \mathcal{O}(\varepsilon^2)$ and $\phi^\beta, \partial_\beta u^3 = \mathcal{O}(\varepsilon)$, and only the leading order terms are used to derive the governing equations. Thus, given that $q(x, y)$ is a traverse load and one is dealing with an isotropic plate, the governing equations take the form

$$\begin{aligned}
\frac{Eh^3}{12(1-\nu^2)}\Delta_{\mathsf{E}}(\boldsymbol{\nabla}_{\mathsf{E}} \cdot \boldsymbol{\phi}) + q = 0 \,, \\
\frac{Eh\kappa}{2(1+\nu)}(\Delta_{\mathsf{E}} w - \boldsymbol{\nabla}_{\mathsf{E}} \cdot \boldsymbol{\phi}) + q = 0 \,, \\
\frac{h^2}{12(1-\nu)}\Delta_{\mathsf{E}}(\boldsymbol{\nabla}_{\mathsf{E}} \times \boldsymbol{\phi}) + \kappa \boldsymbol{\nabla}_{\mathsf{E}} \times \boldsymbol{\phi} = 0 \,,
\end{aligned}$$

where κ is the shear-correction factor, $\boldsymbol{\nabla}_{\mathsf{E}}$ is the two-dimensional Euclidean differential operator and $\cdot$ is the Euclidean dot product operator. Furthermore, given that w^K is the vertical displacement function from Kirchhoff–Love plate theory and w^M is the vertical displacement function from Mindlin-Reissner plate theory, Wang and Alwis [205] show that the vertical displacement functions

are related by the relation $w^M = w^K + \frac{1}{6}(1-\nu)^{-1}h^2\Delta_{\mathsf{E}}w^K$.

For a second-order plate theory with transverse inextendibility the displacement field is defined as

$$\boldsymbol{u}(x,y,z) = \big(u^1(x,y) - z\phi^1(x,y) - z^2\psi^1(x,y),\ u^2(x,y) - z\phi^2(x,y) - z^2\psi^2(x,y),\ u^3(x,y)\big)_{\mathsf{E}}\ ,$$

where ψ^β are the curvatures at the mid-surface of the plate. The second-order shear deformation theories are rarely used as the theories incorrectly estimate the in-plane displacements of the points (x,y,z) and $(x,y,-z)$ to be the same, irrespective of the direction of bending [165].

Unlike Kirchhoff–Love plate theory for first-order deformations, there exists no standard third-order shear deformation theory. One theory proposed is Reddy plate theory [166]. For Reddy plate theory the displacement field is defined as

$$\boldsymbol{u}(x,y,z) = \big(u^1 + z\phi^1 - cz^3(\phi^1 + \partial_x u^3), u^2 + z\phi^2 - cz^3(\phi^2 + \partial_y u^3), u^3\big)_{\mathsf{E}},$$

where $c = \frac{4}{3}h^{-2}$. As a consequence of the term c, the displacement field accommodates quadratic variations of the transverse shear-strains, and thus, stress through the thickness, and vanishing of transverse shear-stress on the top and the bottom of the plate. Thus, Reddy plate theory requires no shear-correction factors. Just as in Mindlin–Reissner plate theory the order of the unknown displacement functions are given by $\partial_\beta u^\alpha = \mathcal{O}(\varepsilon^2)$ and $\phi^\beta, \partial_\beta u^3 = \mathcal{O}(\varepsilon)$. Assuming that $q(x,y)$ is a traverse load Reddy and Wang [166] provide a set of governing equations with boundary conditions. However, the format of the governing equations given in authors' publication is difficult to decipher. Thus, if one wishes to, an alternative format comparable with the publication can be formulated as

$$\begin{aligned}
\frac{1}{c}\left[\frac{1}{(1-2\nu)}\frac{\partial}{\partial x}\left(\frac{17}{128}\boldsymbol{\nabla}_{\mathsf{E}}\cdot\boldsymbol{\phi} - \frac{2}{65}\Delta_{\mathsf{E}}u^3\right) + \Delta_{\mathsf{E}}\left(\frac{17}{128}\phi^1 - \frac{2}{65}\frac{\partial u^3}{\partial x}\right)\right] &= \phi^1 + \frac{\partial u^3}{\partial x}\ ,\\
\frac{1}{c}\left[\frac{1}{(1-2\nu)}\frac{\partial}{\partial y}\left(\frac{17}{128}\boldsymbol{\nabla}_{\mathsf{E}}\cdot\boldsymbol{\phi} - \frac{2}{65}\Delta_{\mathsf{E}}u^3\right) + \Delta_{\mathsf{E}}\left(\frac{17}{128}\phi^2 - \frac{2}{65}\frac{\partial u^3}{\partial u^3}\right)\right] &= \phi^2 + \frac{\partial u^3}{\partial y}\ ,\\
\frac{Eh}{45c}\frac{(1-\nu)}{(1+\nu)(1-2\nu)}[4\Delta_{\mathsf{E}}\boldsymbol{\nabla}_{\mathsf{E}}\cdot\boldsymbol{\phi} - \Delta_{\mathsf{E}}^2 u^3] &= -q\ .
\end{aligned}$$

Now, suppose that w^K is the vertical displacement function from Kirchhoff–Love plate theory and w^R is the vertical displacement function from Reddy plate theory. Reddy and Wang [166] show that the displacement functions are related by $\Delta_{\mathsf{E}}w^R - \lambda^2 w^R = \lambda^2[\frac{17}{84}h^2\Delta_{\mathsf{E}}w^K - w^K]$, where $\lambda = 720h^{-2}(1-\nu)$. Note that the plate theory that Reddy and Wang[166] put forward is not a mathematical theory. It is derived purely in terms of mechanical considerations. The authors never paid any considerations to the existence of solutions or even variational analysis. Thus, given a specific problem, the plate theory that the authors proposed may not even have a solution. This implies that what the authors proposed is merely a mathematical model or a mathematical hypothesis. If the reader is interested in third-order plate models, Reddy's models in particular, please consult the sections 10.3 and 10.4 of [163], where reader can find many numerical results for various examples.

Suppose now that one of the degree of freedom is eliminated from the planer coordinates, and thus, reducing the two-dimensional plate theory problem into a one-dimensional problem. Such theories are known as *beam theories* and they provide methods of calculating the load-carrying

and deflection characteristics of beams. Thus, if one eliminates the y dependency of Kirchhoff–Love plate theory, then one obtains Euler–Bernoulli beam theory [195] (for zero-Poisson's ratio), where governing equations take the form

$$EI\frac{\partial^4 u^3}{\partial x^4} - q = 0\,, \tag{1}$$

and where I is the second moment of inertia of the beam.

Euler–Bernoulli beam theory is a good approximation for the case of small deflections of a beam that are subjected to lateral loads. However, if one also takes into account the shear deformation and the rotational inertia effects, making it suitable for describing the behaviour of thick beams, then the most acceptable beam theory to use is Timoshenko beam theory [194]. In fact, Euler–Bernoulli beam theory is a special case of Timoshenko beam theory. Note that the governing equations for Timoshenko beam theory maybe derived by eliminating the y dependency from Mindlin–Reissner plate theory.

Despite the fact that Euler-Bernoulli beam theory is valid only for infinitesimal strains and small rotations, the theory can be extended to problems involving moderately large rotations by the use of von Karman strains, provided that the strain remains small, which results in nonlinear Euler-Bernoulli beam theory [113]. However, in nonlinear Euler-Bernoulli beam theory the stress in the lateral direction is neglected, even though in large bending lateral stresses are considered to be significant [206]. Considering this and with the use of the fundamental hypotheses in the beam theory (i.e. the cross section of a beam, which is perpendicular to the centroid locus before bending, remain in plane and perpendicular to the deformed locus) Gao [71] modifies Timoshenko beam theory to model large deflections of beams. The author defines the displacement field as $(u(x) - y\partial_x w(x), w(x))_{\mathsf{E}}$, where the orders of the unknowns displacements are given as $\partial_x u = O(\varepsilon^2)$ and $\partial_x w = O(\varepsilon)$. Neglecting all $O(\varepsilon^5)$ terms the author derives the following governing equations,

$$\begin{aligned} \frac{Eh^3}{12}\frac{\partial^4 w}{\partial x^4} - \frac{3}{2}Eh\frac{\partial^2 w}{\partial x^2}\left(\frac{\partial w}{\partial x}\right)^2 + \lambda\frac{\partial^2 w}{\partial x^2} - (1-\nu^2)q = 0\,, \\ \frac{\partial u}{\partial x} + \frac{1}{2}(1+\nu)\left(\frac{\partial w}{\partial x}\right)^2 + \frac{\lambda}{2h(1+\nu)} = 0\,, \end{aligned} \tag{2}$$

where λ is an integral constant that depends on the x-directional external force on the boundary. A large part of author's publication is dedicated to proving the existence of solutions to a contact problem. For this contact problem the author considers a large deformed beam that is supported by a rigid obstacle, which is prescribed by a strictly concave function. The author shows that in the elastic buckling analysis of the beam problem, where $\lambda > 0$: the contact problem is a nonlinear unilateral bifurcation problem. Using a variational inequality approach the author shows that there exist numerical approaches that one can take to solve the contact problem. Furthermore, for the case $q = 0$ equation (2) may be treated as a nonlinear eigenvalue problem. For von Karman plates the author explore this case in an earlier publication [70].

In a further publication Gao [72] develops two dynamical nonlinear beam theories for precise modelling of post-buckling behaviour with finite deformation. The author shows that for both models that

the deformations in the thickness direction are proportional to $\partial_x w(x)$, which becomes significant when the beam is subjected to large rotations. The author utilises one of the models to study a frictional contact problem, and for this, unilateral post-buckling, problem an analytical solution is obtained. This publication is based on the finite deformation theory (very large deformations), which is beyond the scope of this thesis; hence, it is not reviewed in detail herein.

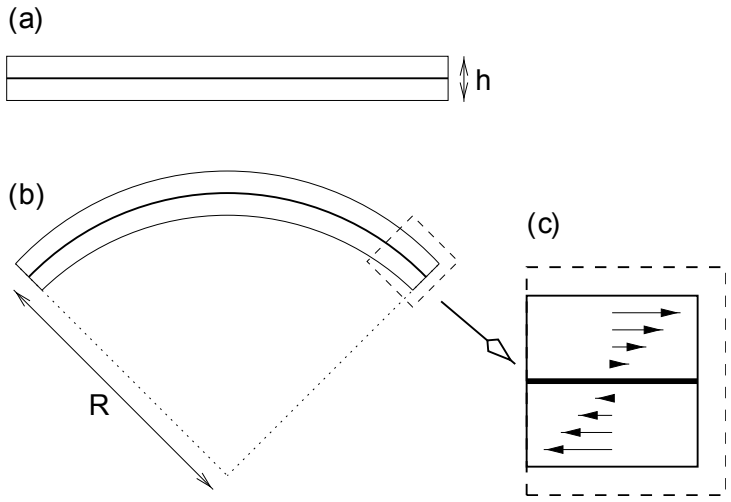

Figure 1: 'A beam (a) before bending and (b) after bending; (c) a close-up of the displacement field' [84], where h is the thickness of the beam and R is the radius of the curvature of deformation.

Howell *et al.* [84][2] propose another method for studying the behaviour of large defections of beams. Without considering any valid methods in the in the field of finite deformation theory or differential geometry, the authors derive their own version of the nonlinear Euler–Bernoulli beam equation (see section 4.9 of Howell *et al.* [84]), where governing equations take the form

$$EI\frac{d^2\theta}{ds^2} + N_0\cos\theta - T_0\sin\theta = 0\ , \tag{3}$$

where $\theta(s)$ and s are respectively the angle and the arc length between the centre-line of the beam (see figure 1), and T_0 and N_0 are the forces applied at the boundary which are parallel to the x and y axis respectively. The authors assume that the centre-line is *virtually unchanged*, and thus, large in-plane strains of the centre-line are ignored in the derivation of the equation (3). What the authors put forward is flawed and it does not depict a representation of the Euler–Bernoulli beam equation, nonlinear or otherwise. For a comprehensive study of the nonlinear Euler–Bernoulli beam equation please consult Reddy [164] or Hodges *et al.* [81].

To examine why equation (3) is flawed: consider the case where one is bending a beam into a shape with constant radius of curvature R, where $R^3 \gg I$, by applying appropriate boundary forces N_0 and T_0. Then equation (3) reduces to $EI\frac{d^2}{ds^2}(R^{-1}s) + N_0\cos\theta - T_0\sin\theta = 0$. As R is a constant, one finds that $N_0\cos\theta - T_0\sin\theta = 0$, $\forall\ \theta$, and thus, $N_0, T_0 = 0$. This implies that it takes no force to bend the beam with a constant radius of deformation, regardless of the magnitude of the deformation, which

[2] https://books.google.co.uk/books?isbn=0521671094

is not physically viable. Now, the reader can see that when the radius of curvature of deformation is constant, equation (3) is no longer valid. However, those who are familiar with the beam theory may argue that one cannot bend a beam so that the radius of the deformation is constant without an external forcing. However, if one considers equation 4.9.3 of the publication, then one can re-express equation (3) as $EI\frac{d^2}{ds^2}(R^{-1}s)+N(\theta)=0$, where $N(\theta)$ is an normal force acting on the beam. Again, bend the beam in to a constant radius of curvature R by applying a normal force of $N(\theta)$ to obtain $EI\frac{d^2}{ds^2}(R^{-1}s)+N(\theta)=0$. As the reader can see that authors' nonlinear beam equation is, again, no longer valid, regardless of the magnitude of the deformation, i.e. regardless of the limits of θ or the magnitude of the constant R. In contrast, consider, if one is to bending a beam into a shape with a constant radius R by a traverse load $q(x)$ below the x-axis with respect linear Euler–Bernoulli beam equation (1), then one finds that $EI(3(u+R)^{-3}+18x^2(u+R)^{-5}+15x^4(u+R)^{-7})+q=0$, where $u=\sqrt{R^2-x^2}-R$ and $x\ll R$. As the reader can see that Euler–Bernoulli equation stays perfectly valid under such deformations. Can the reader see now why Howell *et al.*'s [84] beam theory is flawed?

The flaws of equation (3) have arisen from the derivation of the equation (see section 4.9.1 of Howell *et al.* [84]) as the authors did not consider any valid mathematical techniques in study of the thin objects subjected to finite strains and mathematical techniques in study of coordinate transforms. The authors make a fundamental mistake by assuming that an arbitrary coordinate transform is the same as a deformation of an elastic body. For a model that is similar in nature, also happens to be flawed, please see Section 1.9, where we further examine in detail why aspects of Howell *et al.*'s [84] derivation of their model fails to work. Note that for a comprehensive mathematical study of thin bodies (plates and shells) subjected to finite strains please consult sections Bs of Ciarlet [37] and Ciarlet [38].

Over the recent years many important developments in the field of plate theory are made with the use of (and the mathematical techniques surrounding) Γ-convergence. Γ-convergence is used to rigorously justify the passage from three-dimensional to two-dimensional theories in elasticity theory. Friesecke *et al.* [69] show that the energy functional of nonlinear plate theory is a curvature functional for surfaces that arises from the Γ-limit of the three-dimensional nonlinear elasticity theory as the thickness of the plate goes to zero. In a separate publication the authors show that the low energy Γ-limit of the three-dimensional nonlinear elasticity theory gives rise to Foppl-von Karman theory [67]. In a further publication the authors present a hierarchy of plate models derived from nonlinear elasticity theory by Γ-convergence [68]. This is achieved by considering the asymptotic behaviour of minimisers of three-dimensional nonlinear elasticity theories for plates in the limit as thickness goes to zero. The authors demonstrate that three-dimensional minimisers converge, after suitable rescaling, to minimisers of a hierarchy of plate models. This implies that different limiting theories are distinguished by different scaling exponents of the energy as a function of the thickness. Furthermore, the scaling of the energy is, in turn, controlled by the scaling of the applied forces. Note that unlike classical derivations of plate theories, no 'priori' assumptions are made on the structure of the three-dimensional solutions. The different theories in the hierarchy are distin-

guished by the relation between the strength of the applied force and the thickness. If the reader is more interested in the subject, then an introduction to Γ-convergence methods for thin structures can be found in section 3 of Morassi and Paroni [139].

Mathematical *shells* are thin objects where the rest configuration exists in some curvilinear plane. To examine shells further, which we do in this thesis, let us derive linearised Koiter's shell equations presented by Ciarlet [38]. Before we proceed any further we inform the reader that the method in which we derive the equations is not the conventional method of derivation. Here, we derive the shell equations in a differential geometry fashion so that the reader may get a better understanding of the governing equations of thin elastic bodies in curvilinear coordinates. A more rigorous method of deriving the shell equations, in means of asymptotics, is found in Ciarlet [38] which the reader is urged to consult (for plates please consult Ciarlet [37]).

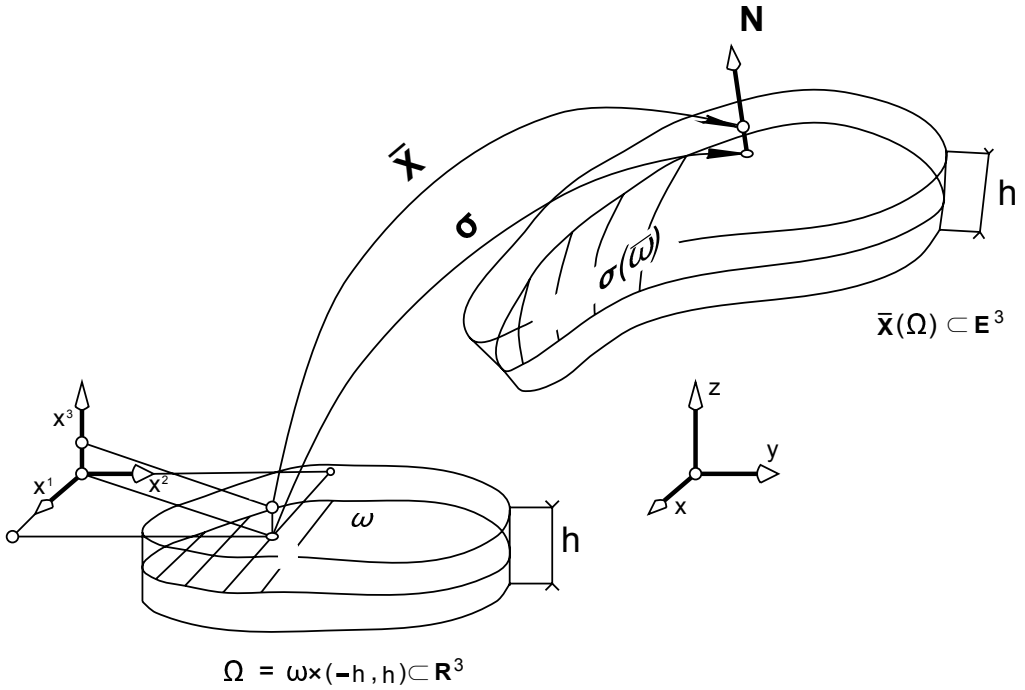

Figure 2: The reference configuration of an elastic shell (adapted from Ciarlet [39]).

Let $\omega \in \mathbb{R}^2$ be a connected open bounded domain with a sufficiently smooth boundary $\partial\omega$. Now, let $\boldsymbol{\sigma} : \omega \to \mathbf{E}^3$ be a smooth enough injective-immersion. Given that h is sufficiently small, $\boldsymbol{\Theta} : \omega \times (-\frac{1}{2}h, \frac{1}{2}h) \to \mathbf{E}^3$ describes a diffeomorphism where $\boldsymbol{\Theta} = \boldsymbol{\sigma}(x^1, x^2) + x^3 \boldsymbol{N}(x^1, x^2)$ (see figure 2). Now, consider the energy functional of an isotopic linearly elastic body in curvilinear coordinates described by the equation

$$J(\boldsymbol{v}) = \int\limits_{\omega\times(-\frac{1}{2}h,\frac{1}{2}h)} \left[\frac{1}{2}A^{ijkl}E_{ij}(\boldsymbol{v})E_{kl}(\boldsymbol{v}) - f^i v_i\right] d(\omega \times (-\frac{1}{2}h, \frac{1}{2}h)) \\ - \int\limits_{\partial\omega\times(-\frac{1}{2}h,\frac{1}{2}h)} \tau_0^i v_i \; d(\partial\omega \times (-\frac{1}{2}h, \frac{1}{2}h)) \; , \tag{4}$$

where $\boldsymbol{v} \in \boldsymbol{H}^1(\omega \times (-\frac{1}{2}h, \frac{1}{2}h))$ is the displacement field, $\boldsymbol{f} \in \boldsymbol{L}^2(\omega)$ is an external force density field and $\boldsymbol{\tau}_0 \in \boldsymbol{L}^2(\omega)$ is a traction field. Note that in equation (4) the isotropic *elasticity tensor* is defined

as

$$A^{ijkl} = \lambda g^{ij} g^{kl} + \mu \left(g^{ik} g^{jl} + g^{il} g^{jk} \right) \ ,$$

where $\lambda = (1 - \nu - 2\nu^2)^{-1} E\nu$ and $\mu = \frac{1}{2}(1+\nu)^{-1} E$ are first and second Lamé's parameters respectively with respective Young's modulus and Poisson's ratio E and ν. Also, *Green-St Venant stress tensor* is defined as

$$E_{ij}(\boldsymbol{v}) = \frac{1}{2}(g_{ik} \bar{\nabla}_j v^k + g_{jk} \bar{\nabla}_i v^k) \ ,$$

and finally *second Piola-Kirchhoff stress tensor* is defined as

$$T^{ij}(\boldsymbol{v}) = A^{ijkl} E_{kl}(\boldsymbol{v}) \ . \tag{5}$$

Now, assume that the boundaries of the body $\{\bar{\omega} \times \{-\frac{1}{2}h\}\} \cup \{\bar{\omega} \times \{\frac{1}{2}h\}\}$ are stress free. As the parameter h is small, i.e. the elastic body in question is very thin, assert that the stress in x^3 direction is constant. Thus, subject to the stress free boundary conditions one finds $T_3^j = 0$ in $\omega \times (-\frac{1}{2}h, \frac{1}{2}h)$, which in turn implies that

$$E_3^\beta(\boldsymbol{v}) = 0 \ , \tag{6}$$

$$E_3^3(\boldsymbol{v}) = -\frac{\lambda}{\lambda + 2\mu} E_\alpha^\alpha(\boldsymbol{v}) \ . \tag{7}$$

Substitute conditions (6) and (7) into equation (5) to obtain the following equation for the only nonzero terms of the stress tensor,

$$T^{\alpha\beta}(\boldsymbol{v}) = \mu \left(\frac{2\lambda}{\lambda + 2\mu} g^{\alpha\beta} g^{\gamma\delta} + g^{\alpha\gamma} g^{\beta\delta} + g^{\alpha\delta} g^{\beta\gamma} \right) E_{\gamma\delta}(\boldsymbol{v}) \ . \tag{8}$$

The true intention for what we are doing is to eliminate the x^3 dependency. However, the strain tensor in equation (8) is implicitly x^3 dependent. Can we re-express the stress tensor in such a way that it is an explicit function of x^3 and satisfies condition (6)?

To investigate this matter further one must analyse the strain tensor: linearised Green-St Venant strain tensor $\boldsymbol{E}$ to be exact. Let $\boldsymbol{g}$ be the metric of some unstrained body in curvilinear coordinates, and now deform the body with the use of an external loading. This process alters the metric of the body as the body is now deformed. Let the new metric be $\boldsymbol{g}_{\text{deformed}} = \boldsymbol{g} + \delta\boldsymbol{g} + \mathcal{O}(\delta^2)$. As the strain tensor is defined as the half of change in metric tensor, one finds $\boldsymbol{E} = \frac{1}{2}\delta\boldsymbol{g}$. Now, assume that one is dealing with a thin body with a constant thickness where the mid-surface of the unstrained body is described by the map $\boldsymbol{\sigma}$. After the given external loading the mid-surface deforms, and thus, attains the form $\boldsymbol{\sigma}_{\text{deformed}} = \boldsymbol{\sigma} + \delta\boldsymbol{\sigma} + \mathcal{O}(\delta^2)$ where $\delta\boldsymbol{\sigma} = \boldsymbol{\sigma}_{,\alpha} u^\alpha + \boldsymbol{N} u^3$. As a consequence of altering the mid-surface, the normal to the surface is also altered. Thus, the new normal of the deformed mid-surface is $\boldsymbol{N}_{\text{deformed}} = \boldsymbol{N} + \delta\boldsymbol{N} + \mathcal{O}(\delta^2)$ where $\delta\boldsymbol{N} = ||\boldsymbol{\sigma}_{,1} \times \boldsymbol{\sigma}_{,2}||^{-1}(\boldsymbol{\sigma}_{,1} \times \delta\boldsymbol{\sigma}_{,2} + \delta\boldsymbol{\sigma}_{,1} \times \boldsymbol{\sigma}_{,2}) - ||\boldsymbol{\sigma}_{,1} \times \boldsymbol{\sigma}_{,2}||^{-1} \boldsymbol{N} \cdot (\boldsymbol{\sigma}_{,1} \times \delta\boldsymbol{\sigma}_{,2} + \delta\boldsymbol{\sigma}_{,1} \times \boldsymbol{\sigma}_{,2}) \boldsymbol{N}$. Using some elementary differential geometry calculations one finds that the covariant components of the change in metric is $\delta g_{\alpha\beta} = (\boldsymbol{\sigma}_{,\alpha} \cdot \delta\boldsymbol{\sigma}_{,\beta} + \delta\boldsymbol{\sigma}_{,\alpha} \cdot \boldsymbol{\sigma}_{,\beta}) - 2x^3(\boldsymbol{\sigma}_{,\alpha\beta} \cdot \delta\boldsymbol{N} + \delta\boldsymbol{\sigma}_{,\alpha\beta} \cdot \boldsymbol{N}) + \mathcal{O}((x^3)^2)$. Thus, the nonzero components of the strain tensor can be expressed as $E_{\alpha\beta} = \epsilon_{\alpha\beta} - x^3 \rho_{\alpha\beta} + \mathcal{O}((x^3)^2)$, where $2\boldsymbol{\epsilon}$ is the change in

first fundamental form tensor and $\boldsymbol{\rho}$ is the change in the second fundamental form tensor.

In light of above analysis, consider the map of the deformed mid-surface

$$\boldsymbol{R}(\boldsymbol{u}) = \boldsymbol{\sigma} + \boldsymbol{\sigma}_{,\alpha} u^\alpha + \boldsymbol{N} u^3 \ ,$$

where $\boldsymbol{u} \in H^1(\omega) \times H^1(\omega) \times H^2(\omega)$ is the displacement field with respect to the mid surface. Assert that

$$\boldsymbol{\sigma}_{,\alpha} v^\alpha + \boldsymbol{N} v^3 + x^3(\boldsymbol{N} + \boldsymbol{N}_{,\alpha} v^\alpha) = \boldsymbol{\sigma}_{,\alpha} u^\alpha + \boldsymbol{N} u^3 + x^3 \frac{\boldsymbol{R}_{,1}(\boldsymbol{u}) \times \boldsymbol{R}_{,2}(\boldsymbol{u})}{||\boldsymbol{R}_{,1}(\boldsymbol{u}) \times \boldsymbol{R}_{,2}(\boldsymbol{u})||} \ .$$

Once the above relation is linearised in $\boldsymbol{u}$, one finds

$$v^\beta(\boldsymbol{u}) = u^\beta - x^3 \bar{\nabla}^\beta u_3 \ , \tag{9}$$

$$v^3(\boldsymbol{u}) = u^3 \ . \tag{10}$$

As a result of the new values of $v^j(\boldsymbol{u})$, one can re-express the strain tensor as an explicit function of x^3. Thus, with the use of equations (9) and (10), one can re-express the nonzero components of the strain tensor as

$$E_{\alpha\beta}(\boldsymbol{u}) = \epsilon_{\alpha\beta}(\boldsymbol{u}) - x^3 \rho_{\alpha\beta}(\boldsymbol{u}) + \mathcal{O}((x^3)^2) \ , \tag{11}$$

where

$$\epsilon_{\alpha\beta}(\boldsymbol{u}) = \frac{1}{2}\left(\bar{\nabla}_\alpha u_\beta + \bar{\nabla}_\beta u_\alpha\right)|_\omega \ ,$$
$$\rho_{\alpha\beta}(\boldsymbol{u}) = \frac{1}{2}\left(\bar{\nabla}_\alpha\left(\bar{\nabla}_\beta u^3\right) + \bar{\nabla}_\beta\left(\bar{\nabla}_\alpha u^3\right)\right)|_\omega \ .$$

Substituting equations (8) and (11) into equation (4), one obtains

$$J(\boldsymbol{u}) = \int_{-\frac{1}{2}h}^{\frac{1}{2}h} \int_\omega \left[\frac{1}{2} B^{\alpha\gamma}_{\beta\delta} E^\beta_\alpha(\boldsymbol{u}) E^\delta_\gamma(\boldsymbol{u}) - f^i\left(u_i + \mathcal{O}(x^3)\right)\right]\left(d\omega dx^3 + \mathcal{O}(x^3)\right)$$
$$- \int_{-\frac{1}{2}h}^{\frac{1}{2}h} \int_{\partial\omega} \left[\tau_0^i\left(u_i + \mathcal{O}(x^3)\right)\right]\left(d(\partial\omega) dx^3 + \mathcal{O}(x^3)\right) \ .$$

Ignoring any $\mathcal{O}(x^3)$ from both volume and the boundary elements from the above equation, integrating over the interval $[-\frac{1}{2}h, \frac{1}{2}h]$ to eliminate the x^3 dependency and finally ignoring all $\mathcal{O}(h^5)$ terms one obtains the *energy functional of a shell*,

$$J(\boldsymbol{u}) = \int_\omega \left[\frac{1}{2} B^{\alpha\beta\gamma\delta}\left(h\epsilon_{\alpha\beta}(\boldsymbol{u})\epsilon_{\gamma\delta}(\boldsymbol{u}) + \frac{1}{12}h^3 \rho_{\alpha\beta}(\boldsymbol{u})\rho_{\gamma\delta}(\boldsymbol{u})\right) - h f^i u_i\right] d\omega - \int_{\partial\omega} h\tau_0^j u_j \ d(\partial\omega) \ ,$$

where

$$B^{\alpha\beta\gamma\delta} = \mu\left(\frac{2\lambda}{\lambda + 2\mu} F^{\alpha\beta}_{[\mathrm{I}]} F^{\gamma\delta}_{[\mathrm{I}]} + F^{\alpha\gamma}_{[\mathrm{I}]} F^{\beta\delta}_{[\mathrm{I}]} + F^{\alpha\delta}_{[\mathrm{I}]} F^{\beta\gamma}_{[\mathrm{I}]}\right)$$

is the *isotropic elasticity tensor of a shell*,

$$\epsilon_{\alpha\beta}(\boldsymbol{u}) = \frac{1}{2}\left(F_{[\mathrm{I}]\alpha\gamma} \nabla_\beta u^\gamma + F_{[\mathrm{I}]\beta\gamma} \nabla_\alpha u^\gamma\right) - F_{[\mathrm{II}]\alpha\beta} u^3$$

is the *half of the change in first fundamental form tensor*, and

$$\rho_{\alpha\beta}(\boldsymbol{u}) = \nabla_\alpha \nabla_\beta u^3 - F_{[\mathrm{II}]\alpha\gamma} F_{[\mathrm{II}]}{}^\gamma_\beta u^3 + F_{[\mathrm{II}]\beta\gamma} \nabla_\alpha u^\gamma + F_{[\mathrm{II}]\alpha\gamma} \nabla_\beta u^\gamma + \left(\nabla_\alpha F_{[\mathrm{II}]\beta\gamma}\right) u^\gamma$$

is the *change in second fundamental form tensor*.

For future reference we define the *stress tensor of a shell* as $\tau^{\alpha\beta}(\boldsymbol{u}) = B^{\alpha\beta\gamma\delta}\epsilon_{\alpha\beta}(\boldsymbol{u})$ and the *negative of the moments density tensor of a shell* as $\eta^{\alpha\beta}(\boldsymbol{u}) = B^{\alpha\beta\gamma\delta}\rho_{\alpha\beta}(\boldsymbol{u})$.

1.5 Films and Membranes

A membrane is defined as a thin-walled body that can only transmit internal forces tangent to its deformed shape, and thus, the normal components of the stress tensor of the object may considered to be zero. The study of such materials is known as membrane theory. Membrane theory acknowledges two types of membranes: shell and true membranes. Shell-membranes are derived from suppressing stress couples and transverse shear in the shell equations compared with tangential force resultants. This suppression takes place in force equilibrium equations, force boundary conditions, energy and moment equilibrium around the normal of the shell. Shell-membranes are capable of modelling regions of the shell that cannot undergo inextensional bending and they are considered to support compressive stress without wrinkling until buckling take place [121]. True-membranes are derived by considering two-dimensional sheets (planar or curved) that are formally incapable of supporting any stress couples or transverse shears, and by assuming that they can only sustain tangential force resultants. They cannot sustain compressive stresses and they exhibit wrinkle fields to compensate for the nonexistence of compressive stresses. True-membranes can accept lines of angular discontinuity in the deformation pattern on the boundary or within the interior, while in shell-membranes the angular continuity is preserved. Also, unlike shell-membranes, true-membranes can sustain large inextensional deformations [26]. True-membranes are often used in modelling certain biological tissues, inflatables, soap bubbles and even shells subject to immense pressure and strain.

A grossly oversimplified definition of a true-membrane is a shell that is independent of any transverse effects. Thus, for our use, we eliminate the u^3 and the $\mathcal{O}(h^3)$ dependencies from linearised Koiter's shell equations to obtain the *energy functional of a true-membrane*,

$$J(\boldsymbol{u}) = h\int_\omega \left[\frac{1}{2}B^{\alpha\beta\gamma\delta}\epsilon_{\alpha\beta}(\boldsymbol{u})\epsilon_{\gamma\delta}(\boldsymbol{u}) - f^\alpha u_\alpha\right] d\omega - h\int_{\partial\omega} \tau_0^\alpha u_\alpha \; d(\partial\omega) \; , \tag{12}$$

where $\epsilon_{\alpha\beta}(\boldsymbol{u}) = \frac{1}{2}(\nabla_\alpha u_\beta + \nabla_\beta u_\alpha)$ is the strain tensor of the membrane.

A grossly oversimplified definition of the *energy functional of a shell-membrane* is, again, defined by equation (12), but with the exception that the strain tensor is now defined as $\epsilon_{\alpha\beta}(\boldsymbol{u}) = \frac{1}{2}(\bar{\nabla}_\alpha u_\beta + \bar{\nabla}_\beta u_\alpha)|_\omega$. Please consult chapters 4 and 5 of Ciarlet [38] for a comprehensive analysis on the theory of shell-membranes.

As for films, a grossly oversimplified definition of a film is a membrane whose reference domain is a subset of the two-dimensional Euclidean plane, i.e. the rest configuration is flat. For our purposes, we define the *energy functional of a film* as

$$J(\boldsymbol{u}) = h\int_\omega \left[\frac{\mu\lambda}{\lambda+2\mu}\epsilon_\alpha^\alpha(\boldsymbol{u})\epsilon_\beta^\beta(\boldsymbol{u}) + \mu\epsilon_\alpha^\beta(\boldsymbol{u})\epsilon_\beta^\alpha(\boldsymbol{u}) - f^\alpha u_\alpha\right] d\omega - h\int_{\partial\omega} \tau_0^\alpha u_\alpha \; d(\partial\omega) \; ,$$

where $\epsilon_{\alpha\beta}(\boldsymbol{u}) = \frac{1}{2}(\partial_\alpha u_\beta + \partial_\beta u_\alpha)$ is the strain tensor of the film, and $x^1 = x$ and $x^2 = y$.

If the reader is interested to find out more about this subject please consult chapter 7 of Libai and Simmonds [121], where the authors present a comprehensive study on the nonlinear membrane

theory. This publication includes topics such as aximembranes (membranes whose unstrained shapes are surfaces of revolution), cylindrical membranes (initially cylindrical membranes that are subject to pressure so that the membranes stretch to become non-cylindrical) and edge effects in a partially wrinkled aximembranes.

1.6 Capstan Equation and Applications in Cable Drive Systems

The capstan equation, otherwise known as Euler's equation of tension transmission, is the relationship governing the maximum applied-tension T_{max} with respect to the minimum applied-tension T_0 of an elastic string wound around a rough cylinder. Thus, the governing equation is given by

$$T_{\text{max}} = T_0 \exp(\mu_F \theta) \ , \tag{13}$$

where θ is the contact angle and μ_F is the coefficient of friction. By *string* we mean a one-dimensional elastic body, and *rough* is an engineering term that implies that the contact area exhibits friction. Note that the coefficient of friction is the physical ratio of the magnitude of the shear force and the normal force between two contacting bodies. The capstan equation is the most perfect example of a belt-friction model, which describes behaviour of a belt-like object moving over a rigid obstacle subjected to friction [162]. In engineering the capstan equation describes a body under a load equilibrium involving friction between a rope and a wheel like circular object, and thus, it is widely used to analyse the tension transmission behaviour of cable-like bodies in contact with circular profiled surfaces, such as in rope rescue systems, marine cable applications, computer storage devices (electro-optical tracking systems), clutch or brake systems in vehicles, belt-pulley machine systems and fibre-reinforced composites [97].

One of the largest applications of the capstan equation is in electronic cable drive systems, and notable devices include printers, photocopiers and tape recorders [19]. The most resent applications can be found in the field of robotics. Cable drive systems are fundamental in the design and manufacture of high-speed pick-and-place robots (DeltaBot, BetaBot and DashBot), wearable robot-assisted rehabilitation-devices (robotic prosthetics), biologically-inspired humanoid-robots (ASIMO by Honda [185]), and haptic devices. For high-speed pick-and-place robots high-speed, high-acceleration and low-inertia (ability to rapidly accelerate with minimum force) is required [21]. Wearable robot-assisted rehabilitation-devices and biologically-inspired humanoid-robots require to be light weight, have low inertia, have high stiffness (precise motion control and able to maintain its rigidity), and have backdrivable transmission with zero backlash [18, 143, 156]. Thus, cable drive systems are widely used in robot applications because of their low inertia, low backlash, high stiffness and simplicity. Further great advantage of using cable drive devices, especially in biomechanical robots, is that actuators (motors) do not need to be placed at each joint since the cables (or tendons) can transmit force from a distance. Also, complex designs can be realised due to the flexibility of the cables, which justifies the use of cable drive systems in portable robotic prosthetics devices [99]. Note that backdrivable is an engineering term given to a system where the system can be physically moved when the motor(s) governing the system is (are) not operational. Backlash is an engineering term given to the clearance or the lost motion in a mechanism caused by gaps

between the moving parts. A haptic device is an engineering term given to devices that use tactile feedback technology to recreate the sense of touch by applying forces, vibrations, or motions to the user.

Baser and Konukseven [19] present an analytical method developed for predicting the transmission-error of capstan drives due to cable slippage, as prior to the publication, the literature is devoid of both a common theory of capstan drive transmission-error, due to slippage, and its experimental validation. The authors develop a theory of wire capstan drive slippage for haptic device applications and verify the model in experimental tests. The theory based on the classic capstan equation which is then extended to include the capstan drive slip error. The authors assume that the bending stiffness of the cable is negligible and in the contact region, of the cable and the drum, the frictional relationship is linear. Experiments conducted on a thin rope with a 0.35mm diameter show that the slip of a capstan drive occurs, and results agree with the theory within 10% difference. The authors hope that the resulting analytical models provide a tool for the designers to predict the slip of capstan drives and allow the models to be utilised in the control algorithms.

Lu and Fan[130] present an analytical method to predict the transmission-backlash of precise-cable-drive systems. Authors' work is significant as transmission-backlash of precise-cable-drive systems is usually neglected as it is much smaller in magnitude than the backlash from gears, chains and other drives [29, 91, 189]. However, the existence of transmission backlash affects the precision and dynamic performance of the drive system, which cannot be neglected in high precision applications. The backlash also affects both the anti-resonance and resonance frequencies of a system, and the increase of the backlash magnitude [14, 135, 180]. Thus, the authors argue that it is necessary to develop both theoretical and experimental methods to predict the backlash transmission. Authors' analysis shows that as the load and centre distance increase, backlash also increases. Also, as the coefficient of friction and output drum radius increase, the backlash decreases. Increasing the preload force decreases the backlash, and the effect cause by decreasing the preload force is appears to be more significant relative to other parameters. The authors show that their experimental values fit well with the theoretical curve of transmission backlash. Also, they show experimentally that the transmission backlash of a precise cable drive is usually several sub-milli-radians and it is given to be significantly smaller than the backlash in gear, chains and belt drive, which is usually in tens of milli-radians. The authors hope that the theoretical method presented is to be used for design guidance and initial performance predictions.

Kang *et al.* [99] present a design of a passive break for a cable drive system, which is named by the authors as the capstan brake. Consider the following example of a robotic hand grabbing an object. As the actuating motor moves the finger, i.e. before the finger reaches the object, the robotic hand operates within the normal energy efficiency range (a real life example can be found in Kim *et al.* [103]). However, once in contact with the object, the motor still needs to apply torque to maintain in this position. Thus, as a result of backdrivability, energy dissipates even through the motor is not generating mechanical work [42]. To circumvent this problem Kang *et al.* [99] design a

non-backdrivable break with a cylinder (capstan) and two one-way clutches (see figure 3). Previous methods for non-backdrivable actuators, introduced by others, include worm gear pairs and lead-screws [32, 122], high reduction ratio transmissions [112, 157], and customised clutches [35, 42].

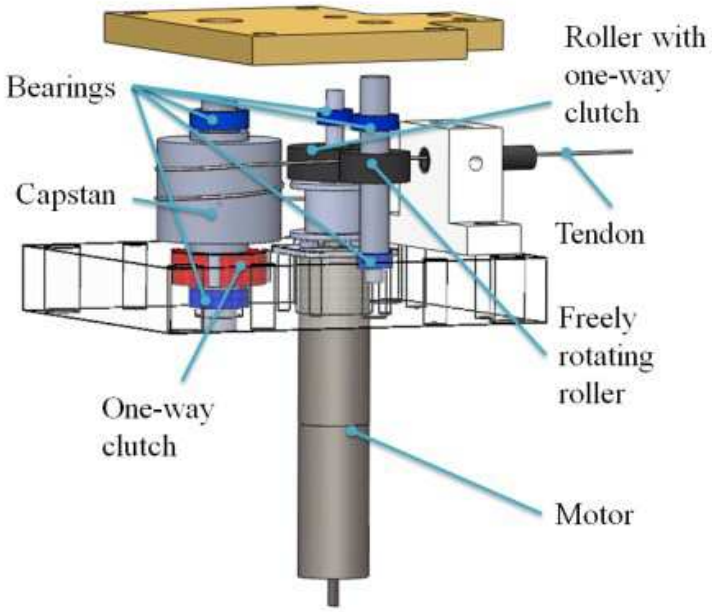

Figure 3: 'Design of the brake system' [87].

Kang *et al.* [99] state that their device it is capable of delivering enough brake force and its breaking force can be adjusted by simply changing the number of windings, and thus, making the device adaptable for various other devices. However, with each additional winding the external force required to release the cable increases, which results in a lower controllability of the device. The capstan does not reduce the maximum winding force and mechanical work. Experimental results show that lower than 2N is required to rotate the capstan. But, more importantly, releasing the cable is not an issue if the proper external force is present. The maximum brake force is approximately equal to 55N, which is suitable for a cable (tendon) driven wearable robotic arms [86], which is the intended application for the device.

Another application of the capstan equation can be found in the field of textiles, where tensioned fibres, yarns, or fabrics are frequently in contact with cylindrical bodies [95]. Doonmez and Marmarali [59] demonstrate the knitability of a yarn before knitting. The authors use a variation of the capstan equation with multiple regression analysis (analogous to hypothesis 4) and equations that depend on yarn's characteristics to predict yarn-needle and yarn-yarn friction values.

Many researchers report that the classical capstan equation does not hold in certain situations as it neglects bending stiffness. Thus, much research is devoted to incorporate bending stiffness into the capstan equation [34, 78]. Another limitation of the capstan equation is that it is based on an over-simplified friction theory, which stems from Amontons' laws. It is generally accepted in the field of polymers that the coefficient of friction, between fibres and other contacting surfaces, is not a

constant as Amontons' laws imply, but it is a variable that depends on the conditions such as the minimum applied-tension [97] (analogous to figure 9). Further evidence for this statement can be found in Martin an Mittelmann [134], where the authors find the coefficient of friction of wool fibres measured by experiments with the use of the classical capstan equation reduces by as much as 50% with an increase of the minimum applied-tension (analogous to figure 25). One of the attempts to include bending stiffness is given by Wei and Chen [207], where the authors give a theoretical model for the capstan equation for nonflexible fibres and yarns. Wei and Chen [207] consider the radius of the capstan and the yarn, and present two solutions for yarns (and fibres) with linear and nonlinear behaviours respectively. The authors conclude by saying that the theoretical model can be used to calculate the actual tension of cables with bending stiffness.

Jung *et al.* [95] present a mathematical model to incorporate bending stiffness into the capstan equation. The authors consider an inextensible beam and propose a mathematical model with an analytical solution. One numerical experiment suggests that the difference in the tension ratio (the ratio between the maximum and the minimum applied-tensions) between the classical and the modified results can be up to 71% for a mere 10° variation in the angle of inclination. In another publication, Jung *et al.* [97] present a capstan equation with bending stiffness and with nonlinear frictional behaviour. The authors consider a power-law friction model in place of Amontons' laws friction, which is adapted from the work of Howell [82, 83]. The authors criticise Howell's [82, 83] model, and assert that the coefficient of friction must not vary with the change of the beam radius and the capstan radius as Howell suggested, which is the basis for Jung *et al.*'s [97] power law. They show that using their power-law friction or including the rod bending stiffness can change the tension ratio. In a further publication the authors present a capstan equation with bending stiffness, nonlinear frictional behaviour and Poisson's ratio [96]. One of authors' findings show that presence of a nonzero Poisson's ratio tends to increase the tension ratio (analogous to figure 65). Unfortunately, Jung *et al.*'s [95, 97] mathematical work appear to be questionable as the authors assumptions and mathematical techniques are not consistent with nonlinear bending theories in study of thin objects (plates, beams etc.). A more precise analysis of the large deflection of beams over rigid obstacles can be found in the work of Gao [71, 72].

Kim *et al.* [105] present a finite-element solution for the capstan equation, where the authors model a three-dimensional aluminium-sheet deforming over a rigid cylinder. The friction is calculated by the friction model put forward by Swift [190]. The simulation shows non-uniform pressure distributions, both in the longitudinal and transverse directions of the contact surface, which include pressure peaks near the inlet and the outlet regions, and near the strip edges (see figure 4). This contradicts the results obtain by the simple capstan equation (13) and the work of Saha and Wilson [172], where one can observe a monotonic increase in pressure from the inlet region to the outlet region. Given an initial coefficient of friction $\mu_F = 0.1$ and the contact angle $\theta = 90^\circ$, Kim *et al.* [105] find the final coefficient of friction is $\mu_F = 0.093$ and the contact angle is $\theta = 74^\circ$. The loss of contact is clearly due to the bending stiffness of the aluminium-sheet as a portion of the applied force is expended on overcoming the bending stiffness; however, the reduction in the coefficient of

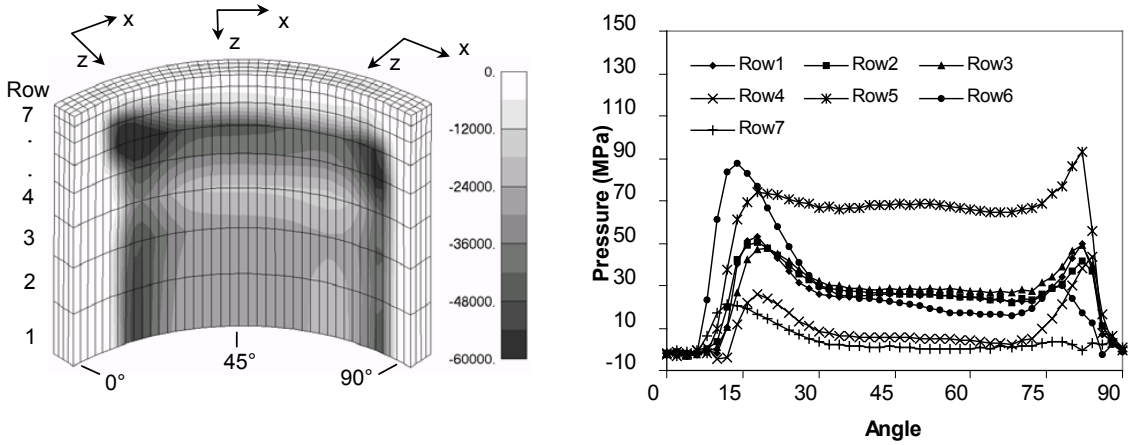

Figure 4: Contact pressure distribution at each row at time = 1.024s, where the contact angle is in degrees and contact pressure is in megapascals [87].

friction is not a factor of the final contact-angle. The author conclude that further investigation is needed with various geometries and test conditions.

In a rather older publication, Stuart [187] finds similar results to Kim *et al.* [105]. Stuart *et al.* [187] attempts to incorporate bending stiffness with the capstan equation, where the friction governed by Amontons' laws. Among other research findings, the author shows that a reduction in the contact angle and a variable coefficient of friction throughout the contact profile, which are two of the notable results that Kim *et al.* [105] discover in their finite-element experiments.

Due to the lack of time and resources we cannot verify the validity of the work of the authors discussed in this section. However, we analyse the mathematical aspects of this subject in great detail in Chapter 2, where we examine the theory and the behaviour of the capstan equation for non-cylindrical geometries.

1.7 Applications in Flexible and Stretchable Electronics

In recent years flexible and stretchable electronics become a common technology. Few notable commercially available devices that use this technology are the LG G Flex phone and the LG 77EG9900 4K Flexible OLed TV. Other than conformal displays, which can be folded or rolled [65], stretchable electronics have applications in thin film solar cells [33, 50, 117, 147], electronic skins for robots and humans [203], conformable electronic textiles [27] and complex curvilinear stretchable devices for biomedical applications [108]. For such applications the degree of the deformation of the electronic body can endure, before its basic functions (i.e. conductivity, transparency or light emission) are adversely affected, is immensely important. However, design and process engineers who are working on the implementation of flexible electronics often lack confidence due to a lack of understanding or a lack of input data for reliable modelling tools [125]. Thus, there is a tremendous amount research is conducted in the field of academia (Oxford Centre for Nonlinear Partial Differential Equations, Lu Research Group the University of Texas at Austin, Flexible Electronics

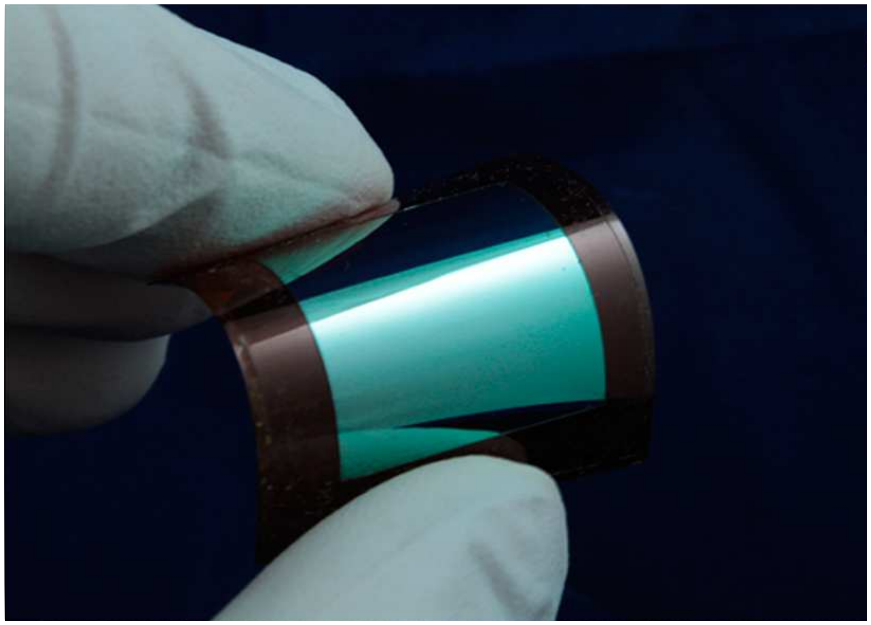

Figure 5: 'Transferred 2cm×2cm silicon nanomembrane on polyimide film' [213].

and Display Center Arizona State University) as well as in the commercial sector (LG Electronics [215, 183], Samsung Group [90, 104, 106]).

In a mathematical perspective modelling of such materials follows the following exact procedure. A thin film (often an inorganic conductor such as copper) is bonded to a thin elastic material, which in the literature defined as a substrate. In mathematical elasticity language: a film bonded to an elastic foundation. The problem can now be tackled with just the techniques of solid mechanics. The research mainly focuses on debonding between the film and the substrate, and the plastic deformation of the film due to stretching and the bending of the substrate.

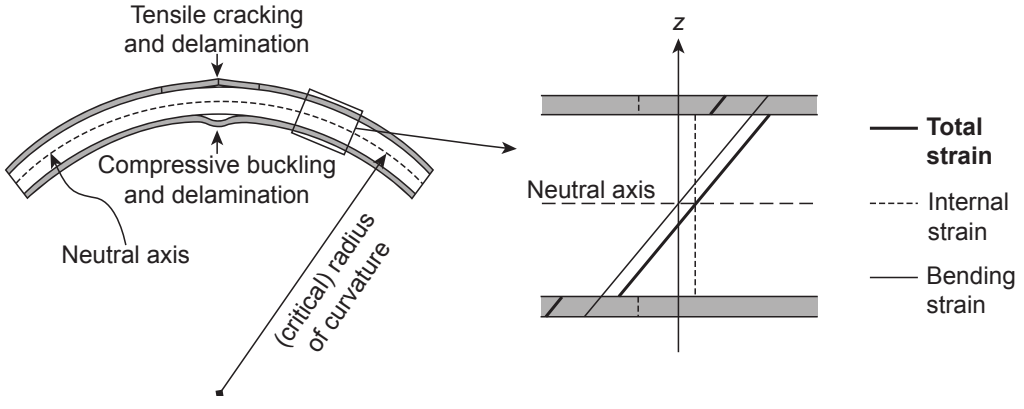

Figure 6: 'Summary sketch of damage events and strain state in a flexed substrate coated on both sides with thin films' [125].

Figure 6 is a simple visual representation, form Logothetidis [125], of the damage and the state of strain in an elastic substrate with thin brittle films bonded to both surfaces. Upon bending the body to some radius of curvature, the film located on the upper surface experiences tensile strain, and

may fracture and eventually debond. The film located beneath experiences compressive strain and may also debond, buckle and possibly fracture. The neutral axis is the plane where the strain is assumed to not change upon pure bending (this assumption is an erroneous for large deflections, for a comprehensive mathematical study of large deflections of plates please consult section B of Ciarlet [37]), and the total strain is the sum of the internal strain and the bending strain. The critical radius of curvature is among the key design parameters for flexible electronics. It is defined as the radius of curvature at which device failure occurs due to significant mechanical damage or functional failure. For such objects, applications can be found in the transfer-printing of nanomembranes with polymeric stamps, and annular rubbery gaskets and sealers under uniaxial compression during service [160].

Logothetidis [125] defines the classification of different branches of stretchable and flexible electronics as: (i) flexible electronics, which comprise films with $\epsilon_{\text{crit}} < 2\%$, which are based on substrate materials that are thin enough (100mm) to be safely bent to a minimum radius of curvature of 10mm, but cannot be stretched, (ii) compliant electronics, for which $2\% < \epsilon_{\text{crit}} < 10\%$, which can be flexed to radius of curvature of few millimetres to allow some in-plane loading and can be used with thicker substrates, and (iii) stretchable electronics, for which $\epsilon_{\text{crit}} > 10\%$, which can be conformed to a broad diversity of surfaces with two-dimensional curvatures and small radii below a few millimetres. Note that ϵ_{crit} is the critical strain, where strain exceeding this value results in irreversible mechanical failure. If the reader is interested more on this subject, especially on the applied mathematical and the engineering side of it, please consult Logothetidis [125].

Lu *et al.* [128] experimentally demonstrate that a microcrystalline copper film that is bonded to a Kapton (poly-oxydiphenylene-pyromellitimide) substrate can be stretched beyond 50% of its original length without being ruptured. However, at just below 60% debonding from the substrate and cracking are observed. When a chromium adhesion layer is introduced between the copper film and the Kapton substrate, to enhance adhesion, only a few micro-cracks in the film is observed. This implies that better adhering reduces the irreversible mechanical failure of the copper film. Also, in the chromium adhesion case the measured electrical resistance is shown to agree with the theoretical predictions. Micrographs (digital image taken through a microscope) show that the strain localisation and debonding coevolve, which are consistent with the existing finite-element models on the rupturing of plastically-deformable metal-films on polymer-substrates [118, 119]. Such finite-element models for strain-localisation analysis of strongly discontinuous fields are based on the standard Galerkin-approximation. Note that the strain localisation is a physically observed feature (such as the yield strength) of elastoplastic materials undergoing non-homogeneous deformation. The phenomenon is observed in the form of a shear band, which is a narrow zone of intense straining across, where some kinematical fields in a deforming body maybe discontinuous.

In another publication Lu *et al.* [129] show that strains to failure is lower, when stretched to approximately 10% over its unstrained length, for Kapton polymers when supporting nanocrystalline copper films. The microstructure (microscopic structure) of which is revealed to be inhomogeneous

and unstable under tensile loading compared to annealed (temperature sensitive) films (only stated as room temperature, but no specific temperature is given by the authors). The authors conclude by saying 'the films fail by ductile necking as a result of deformation-associated grain growth, strain localisation at large grains, and film debonding from the substrate' [129].

In a further publication Lu *et al.* [127] investigate polyimide-supported copper films with film thicknesses varying from 50 nanometres to 1 micromere and a (111) fibre texture, where $(\cdots)$ is the Taylor factor for a face-centered cubic film. The authors observe that the critical strains first rise with film thickness, reaching a maximum for the film thicknesses around 500nm, before decreasing again. The authors demonstrate that films with thicknesses less than 200nm fail at very low strains as a result of intergranular fracture (fractures that follow the grains of the material). For thicker films the failure mode switches to transgranular fracture (a fracture that follows the edges of lattices in a granular material) in a process that involves both strain localisation and debonding. As the yield strength decreases with increasing film thickness, it becomes increasingly difficult to debond the film from the substrate. Eventually a (100) texture component develop in the films leading to strain localisation and fracture at the softer (100) grains. The authors conclude by saying '[the critical strain of] a metal film on a polymer substrate can be maximised by ensuring good adhesion between film and substrate, a uniform crystallographic texture, and a large grain size to lower the yield strength' [127].

Qiao and Lu [160] derive solutions for an elastically compressible-layer bonded between two circular parallel-stiff-plates, similar to what is shown in figure 6. The authors give closed-form solutions for bonded elastic layers (i.e. disks, annuli, annuli with rigid shafts and infinitely long strips) under compression using separation of variables without any pre-assumed deformation profile. The authors demonstrate that the predicted stress, displacement and effective modulus of the solutions are in 'excellent' agreement with finite-element modelling results over a wide range of Poisson's ratios and aspect ratios, where the aspect ratio is the value of the radius of the plates divided by the length of two plate's separation. The solution that the authors derive is very sensitive to Poisson's ratio, in particular, when Poisson's ratio is approaching the value 0.5 (incompressibility condition). Also, as Poisson's ratio approaches 0.5, solutions reduces to classical solutions for incompressible elastic layers. The authors conclude by proposing that their analytical model is a viable means to simultaneously measure intrinsic Young's modulus and Poisson's ratio of elastically compressible layers without camera settings (mechanical experiment involved in measuring elastic properties).

The significance of Qiao and Lu's [160] work is that in previous cases 'for compressible materials, solutions obtained by the method of averaged equilibrium are sufficient for effective compression modulus, but inaccurate for the displacement or stress fields whereas solutions obtained by the method of series expansion are considerably complicated' [160]. Note that the effective compression modulus (also known as the apparent stiffness) is defined as the gradient of the stress-strain curve. It is observed that the effective compression modulus is often higher than Young's modulus of the elastic body, and this is due to the constraint of the parallel plates that are fully bonded to the elastic layer [74]. Unfortunately, Qiao and Lu [160] mathematical work appears to be questionable

due to their grossly oversimplified modelling assumptions.

Almost all the mathematical publications reviewed in this section are from the Lu Research Group the University of Texas at Austin. If the reader is interested in subject of flexible and stretchable electronics, then please visit their website[3] for a whole archive of free-to-view publications.

Due to the lack of time and resources we cannot verify the validity of the work of the authors discussed in this section. However, we analyse the mathematical aspects of this subject in great detail in Chapter 3, where we examine the theory and the behaviour of thin bodies bonded to elastic foundations in a curvilinear setting.

1.8 A Critical Study of the Work of Cottenden *et al.*

Cottenden *et al.* [48][4] (the principal author is D. J. Cottenden) attempt to derive a mathematical model to analyse a frictionally coupled membrane (defined as a nonwoven sheet) on an elastic foundation (defined as a substrate) based on the research findings of D. J. Cottenden [47][5] from his PhD thesis. It is assumed that friction (abrasion in the context of the publication) is the cause of some pressure ulcers in largely immobile patients (not necessarily true, for detailed cause of pressure ulcers see Maklebust and Sieggreen [132]), and abrasion due to friction contributes to the deterioration of skin health in incontinence pad users, especially in the presence of liquid. The current literature shows very little research in the area of frictional damage on skin due to fabrics, and thus, authors' goal is to present a mathematical model to investigate this phenomenon in a purely geometrical setting. Thus, the authors propose a model for a general class of frictional interfaces, which includes those that obey Amontons' laws.

In reality what Cottenden *et al.* [48] accomplished is the following: explicit solutions are derived for a membrane with a zero-Poisson's ratio and a zero-mass density on a rigid cylinder (ordinary capstan equation 13) and on a rigid right-circular cone. Finally limited experimental data is given to imply the trivial asymptotic nature of $\sin(\theta)$ near $\theta = 0$.

Cottenden *et al.*'s [48] method for calculating the kinetic frictional force induced on human skin due to nonwoven fabrics is as follows. The human body part in question is modelled as a homogeneous isotropic 'convex surface [*sic*]' [48] (the substrate) and the nonwoven fabric is modelled as an isotropic membrane (the nonwoven sheet). The goal is to find the stresses acting on the nonwoven sheet, including determining the friction acting on the substrate. The contact region between the fabric and the skin is defined as 'An *Instantaneous Isotropic Interface*, [which] is an interface composed of a pair of surfaces which have no intrinsically preferred directions and no directional memory effects, so that the frictional force acts in the opposite direction to the *current* relative velocity vector ... or to the sum of *current* applied forces acting to initiate motion ...' (see section 2.2

[3] http://lu.ae.utexas.edu/

[4] http://discovery.ucl.ac.uk/id/eprint/69944

[5] http://discovery.ucl.ac.uk/id/eprint/1301772

of Cottenden *et al.* [48]), this simply implies that the contact region is isotropic. Also, consider the contact body in question: it is modelled as a surface, i.e. a two-dimensional manifold. However, in reality it must be modelled as a three-dimensional object as a two-dimensional object cannot describe the elastic properties of a fully three-dimensional object such as a human body part, as a two-dimensional surface has measure zero in three-dimensional space (see Section 1.2 for more on measure): unless subtable assumptions are made as in shell theory (see Section 1.4 for more on shells), but this is not what the authors are considering. Now, consider authors' statement regarding the modelling assumptions carefully, particularly the term 'convex surface'. The authors definition of convexity is $\boldsymbol{\eta} \cdot \boldsymbol{\nabla}_{\mathsf{E}} \hat{\mathbf{N}} \cdot \boldsymbol{\eta} \geq 0$ (see section 3.1 of Cottenden *et al.* [48]), where $\hat{\mathbf{N}}$ and $\boldsymbol{\eta}$ are unit normal and tangential vectors surface respectively. However, authors' definition is erroneous. Convexity has a very precise mathematical definition, i.e. we say the functional $f : X \to \mathbb{R}$ is convex, if $f(tx + (1-t)y) \leq tf(x) + (1-t)f(y)$, $\forall\ t \in [0,1]$ and $\forall\ x, y \in X$ (see definition 19). Also, the very idea of a convex surface nonsensical as definition of convexity is only applicable to functionals. A simple example of a convex functional is $\exp(\cdot) : \mathbb{R} \to \mathbb{R}_{>0}$. One is left to assume that what the authors mean by convexity is surfaces (manifolds) of positive mean-curvature. For more on elementary differential geometry please consult do Carmo [58] or Lipschutz [124].

Now, consider a membrane with the following properties: (i) 'has no through thickness and can be represented as a two-dimensional object,' (ii) 'always drapes, following the substrate surface without tearing or puckering,' (iii) 'is of sufficiently low density that its weight makes a negligible contribution to the forces acting,' and (iv) 'does not resist bending in the sense that a beam does' [48]. Authors' statement (ii) is erroneous, as one cannot guarantee that the given property will hold for arbitrary curved surfaces. To illustrate the flaw, consider a flat elastic-membrane (i.e. a film) over a rigid sphere. The only way one can keep the membrane perfectly in contact with the sphere in a two-dimensional region with nonzero measure is by deforming the membrane by applying appropriate boundary stresses and or external loadings. Otherwise, the membrane only makes contact with the sphere at a single point or a line. Also, the authors do not specify whether the membrane is elastic or not. One is left to assume that the membrane is elastic as the proposed frame work does not acknowledge plastic deformations. Note that the authors never referred to their nonwoven sheet as a membrane, but a membrane (or a film) is the closest mathematical definition for modelling such objects.

To find the stresses acting on the membrane consider Cauchy's momentum equation in the Euclidean space, which the authors define as

$$\boldsymbol{\nabla}_{\mathsf{E}} \cdot \mathbf{T} + \mathbf{f} = \rho \ddot{\boldsymbol{\chi}} \,, \tag{14}$$

where $\mathbf{T}$ is Cauchy's stress tensor, $\mathbf{f} = \mathbf{f}(\mathbf{T}, \boldsymbol{\nabla}_{\mathsf{E}}\mathbf{T})$ is the force density field and ρ is the material mass density of the membrane, $\boldsymbol{\nabla}_{\mathsf{E}}$ is the Euclidean differential operator and $\boldsymbol{\chi}$ is given as a 'time-dependent deformation function mapping the positions of points in their undeformed *reference* configuration to their deformed positions and the superposed double dot denotes a double material description time derivative' [48]. It unclear what $\boldsymbol{\chi}$ represent from authors' definition, whether it is

the displacement field of the membrane or some time dependent mapping from one manifold to another. If the latter is true, then equation (14) has a very different meaning. It means that the space is dependent of time, and such problems are encountered in the field of cosmology. If the reader consults section 5.4 of Cottenden's [47] thesis, then it becomes evident that χ is a time dependent map. However, if one consults Cottenden *et al.* [45], Cottenden *et al.* [47] and Cottenden *et al.* [48], then one concludes that the authors do not put forward the framework to handle the 3+1 decomposition in general relativity, with any mathematical rigour. If the reader is interested in the 3+1 formalism in general relativity, then please consult the publications [77, 186, 204] or Dr J. A. V. Kroon (QMUL) on his LTCC lecture notes on *Problems of General Relativity*[6], where the reader can find an extraordinary solution for two merging black-holes (the Brill-Lindquist solution).

Assuming that the foundation is static and rigid, and the mass density of the membrane is negligible, i.e. $\rho \approx 0$, the authors state that Cauchy's momentum equation (14) can be expressed as

$$\mathbf{P}_s \cdot (\boldsymbol{\nabla}_{\mathsf{E}} \cdot \mathbf{T}) + \mathbf{P}_s \cdot \mathbf{f} = \mathbf{0} \,, \tag{15}$$

$$-(\boldsymbol{\nabla}_{\mathsf{E}} \hat{\mathbf{N}}) : \mathbf{T} + \hat{\mathbf{N}} \cdot \mathbf{f} = 0 \,, \tag{16}$$

where $\mathbf{P}_s$ projection matrix to the substrate (the explicit form is not defined by the authors), $\hat{\mathbf{N}}$ is the unit normal to the surface, and $\cdot$ and $:$ are a contraction and a double contraction in the Euclidean space respectively. Although it is not explicitly defined, one must assume that the authors use the fact that membranes cannot support any normal stresses, i.e. $\hat{\mathbf{N}} \cdot \mathbf{T} = \mathbf{0}$, to obtain equation (16). The authors give equations (15) and (16) as the state of the 'general case' of the problem. However, their assertion cannot hold as the system is underdetermined. Consider the vector $\mathbf{f}$ which consists of three unknowns. Also, consider the tensor $\mathbf{T}$ which is a symmetric tensor with six unknowns. Using the condition $\hat{\mathbf{N}} \cdot \mathbf{T} = \mathbf{0}$ the number of unknowns can be reduced by three: leaving six remaining unknowns. Now, direct one's attention to equations (15) and (16) which provide three additional equations. Thus, one comes to the conclusion that one has an underdetermined system, with three equations and six unknowns. Furthermore, there is no description of the boundary conditions for the 'general case', which are essential in obtaining a unique solution.

The derivation of authors' governing equations can be found on section 2.2 to 2.4 of the publication. In the risk of being pedantic we omit reviewing flaws of these sections. Instead, we refer reader to Kikuchi and Oden [102] to see how to model friction with mathematical precision and to show how incredibly difficult modelling such problems are. We further refer the reader to Ciarlet [38] to see how to model mathematical elasticity in a differential geometry setting with mathematical rigour.

To find explicit solutions the authors direct their attention to only 'surfaces that are isomorphic to the plane; that is, those which have the same first fundamental form as the plane; the identity matrix in the case of plane Cartesian coordinates. [*sic*]' [48]. Found in section 4.1 of Cottenden *et al.* [48], this is the basis for their entire publication (also Cottenden's [47] thesis). However, authors' statement is nonsensical. An *isomorphism* (perseveres form) is at least a homomorphism, i.e. there exists at

[6] http://www.maths.qmul.ac.uk/∼jav/LTCC.htm

least a continuous bijective mapping, whose inverse is also continuous, between the two manifolds in question [58, 124]. Thus, a surface that is isomorphic to the plane simply implies that there exits a continuous bijective map, with a continuous inverse, between the surface in question and the Euclidean plane, and it does not automatically guarantee that the surface have the same metric as the Euclidean plane under the given map. The latter part of authors' statement is clearly describing surfaces that are *isometric* (perseveres distance) to the Euclidean plane, i.e. surfaces of zero-Gaussian curvature. However, the statement is still erroneous as being a surface that is isometric to the Euclidean plane does not guarantee that the surface have the same metric as the Euclidean plane. Being isometric to the Euclidean plane simply implies that, if $f : U \subset \mathbb{R}^2 \to W \subset \mathbf{E}^3$ is a 2D manifold that is isometric to the Euclidean plane, then there exists a map $g : V \subset \mathbb{R}^2 \to U \subset \mathbb{R}^2$ such that the first fundamental form of the isometry $f \circ g : V \subset \mathbb{R}^2 \to W \subset \mathbf{E}^3$ is the 2×2 identity matrix [58, 124]. One is left to assume that the surfaces that are in question by the authors belongs a subgroup of surfaces of zero-Gaussian curvature that has the same metric as the Euclidean plane with respect to authors' coordinate system, i.e. cylinders of unit radius: as one later see that these are the only possible manifolds that generate any valid solutions. Note that Cottenden [47] accredits Pressley [159] for his differential geometry results. However, Pressley's [159] publication is a widely accepted and verified mathematical publication in the field of differential geometry. Apart from few typos Pressley's [159] publication does not contain such provably false statements as given by Cottenden [47].

Now, consider the equation

$$\mathbf{P}_s \cdot \mathbf{f} + \mu_d(\hat{\mathbf{N}} \cdot \mathbf{f})\dot{\boldsymbol{\chi}} = 0 \,, \tag{17}$$

which the authors define as Amontons' law friction, where μ_d is the coefficient of dynamic friction and $\dot{\boldsymbol{\chi}}$ is the relative velocity vector between the membrane and the foundation. The inclusion of the two equations implied by condition (17) still does not guarantee that the system is fully determined, as the system requires one more equation to be fully determined.

Now, assume that one is dealing with a rectangular membrane whose orthogonal axis defined by the coordinates (x, y), where y defines the longer dimension, that is placed over a surface defined by the regular map $\boldsymbol{\sigma}$. Also, assume that Poisson's ratio of the membrane is zero to prevent any lateral contractions due to positive tensile strain. To reduce the complexity the authors modify the problem by letting $\dot{\boldsymbol{\chi}}$ be parallel to $\boldsymbol{\sigma}_{,y}$. Also, by applying a boundary stress of T_0 at some point ϕ_1 whilst applying a even greater stress at ϕ_2 so that $T_{yy}(y)$ is an increasing function in y, where ϕ_α are angles of contact with $\phi_1 < \phi_2$. Due to zero-Poisson's ratio and the boundary conditions one finds $T_{xx} = 0$, $T_{xy} = 0$, where T_{ij} are stress tensor components. Thus, the governing equations finally reduce to a fully determined system. Therefore, one must understand that having zero-Gaussian curvature and zero-Poisson's ratio is a necessity for this model, and it is not some useful tool for deriving explicit equations as stated by by the authors. Upon integrating equation (17), under the specified boundary conditions, one finds solutions of the form,

$$T_{yy}(y) = T_0 \exp\left(-\mu_d \int^y F_{IIyy}(\eta)\, d\eta\right) \,, \tag{18}$$

where F_{IIyy} is the only nonzero component of the second fundamental form tensor. However, equation (18) (see equation 4.4 of Cottenden *et al.* [48]) is erroneous. This is because, whatever is inside the $\exp(\cdot)$ must be non-dimensional, but this is not the case with equation (18). To illustrate this flaw let L be an intrinsic Euclidean length scale and ℓ be an intrinsic length scale of the curvilinear coordinate y. Now, with the definition of F_{IIyy} (see equation 3.3 of Cottenden *et al.* [48]) one finds that the length scale inside the term $\exp(\cdot)$ in equation (18) is $(\ell/L)^3$. Given that $y = \theta$ (i.e. the contact angle, which is dimensionless), one finds that the length scale inside the term $\exp(\cdot)$ is L^{-3}, which is not mathematically viable.

To find the explicit solution for the general *prism* case the authors present the map

$$\boldsymbol{\sigma}(x, y) = \big(R(\phi)\cos(\phi), R(\phi)\sin(\phi), x\cos(\zeta) + y\sin(\zeta)\big)_{\mathsf{E}} \,, \tag{19}$$

where 'The angle ζ is defined as the angle between the flow vector and the prism's plane of cross section as measured on the surface' [48]. From authors' definition ζ appears to be the acute angle that the vector $\hat{\boldsymbol{\sigma}}_{,y}$ makes with the vector $\hat{\boldsymbol{\sigma}}_{,\phi}$, and R and ϕ appear to be the radius of curvature and the angle of the centre of rotation respectively. One can clearly see that map (19) is only valid for cylinders of unit radius as it must have the same metric as the Euclidean plane, i.e. $\boldsymbol{\sigma}_{,x} \cdot \boldsymbol{\sigma}_{,x} = 1$, $\boldsymbol{\sigma}_{,y} \cdot \boldsymbol{\sigma}_{,y} = 1$ and $\boldsymbol{\sigma}_{,x} \cdot \boldsymbol{\sigma}_{,y} = 0$, and thus, $R = 1$, $\phi = x$ and $\zeta = \frac{1}{2}\pi$ (or $\phi = y$ and $\zeta = \pm\pi$), if $\boldsymbol{\sigma}$ is positively oriented. Now, given that a solution exists in the interval $[\phi_1, \phi_2]$, the authors state that the solution is

$$T_{yy}(\phi_2) = T_0 \exp\left(\mu_d \cos(\zeta)\left[\phi - \arctan\left(\frac{R(\phi)_{,\phi}}{R(\phi)}\right)\right]\Big|_{\phi_1}^{\phi_2}\right) \,. \tag{20}$$

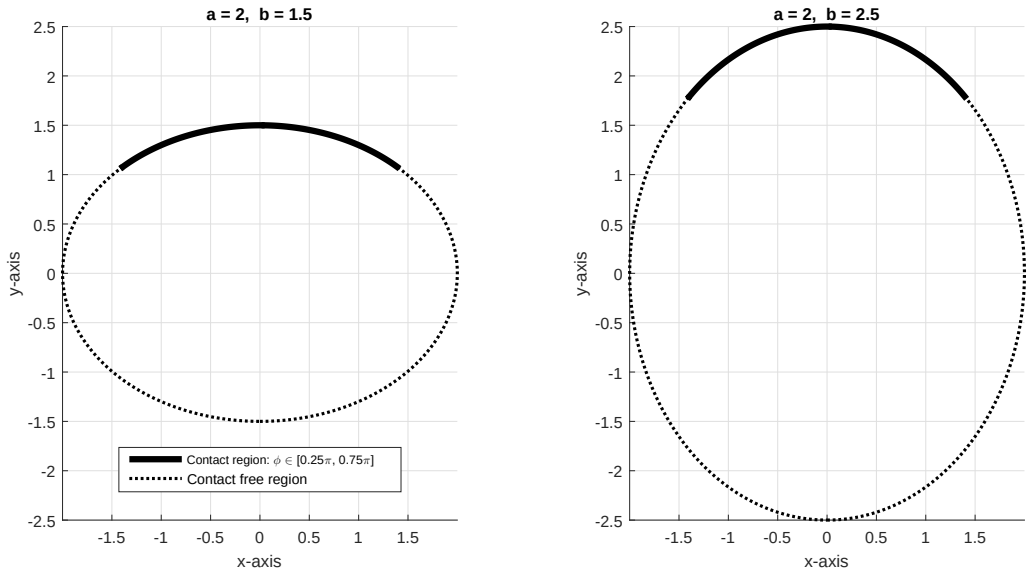

Figure 7: Cross sections of elliptical-prisms (and elliptical-cones for the $z = 1$ case).

Despite the fact that map (19) is only valid for cylinders of unit radius, solution (20) is valid for cylinders with constant radii, i.e. the capstan equation (13). But this is still an incorrect solution and it is a mere coincidence that it happens to be valid for the cylinder case. To see why equations (19) and (20) are incorrect one only needs to consider an example with noncircular cross section. If

the reader wishes to, then consider a positively-oriented elliptical-prism (for the $\zeta = 0$ case) that is defined by the map $\boldsymbol{\sigma}(\phi, z) = (a\cos(\phi), b\sin(\phi), z)_{\mathsf{E}}$ where $z \in \mathbb{R}$ and $a, b > 0$, and let $\phi \in [\frac{1}{4}\pi, \frac{3}{4}\pi]$ be the contact interval (see figure 7, and see Section 2.5.3 for the capstan equation on an elliptical-prism). Now, the reader can see that both map (19) and solution (20) are no longer valid.

To find the explicit solution for the *cone* case the authors present the map

$$\boldsymbol{\sigma}(x, y) = \frac{r}{\sqrt{1+R(\phi(\theta))^2}}(R(\phi(\theta))\cos(\phi(\theta)), R(\phi(\theta))\sin(\phi(\theta)), 1)_{\mathsf{E}} \,, \tag{21}$$

'where (r, θ) are plane polar coordinates ... derived from the Cartesian $(x, y)_{\mathsf{E}}$ coordinates by $r = \sqrt{x^2+y^2}$ and $\theta = [\arctan(\frac{y}{x}) - \zeta]$, where ζ is the angle between the direction of slip and the tangential direction when $\theta = \phi = 0$' [48]. From authors' definition ζ appears to be the acute angle that the vector $\hat{\boldsymbol{\sigma}}_{,y}$ makes with the vector $\hat{\boldsymbol{\sigma}}_{,\phi}$, R is given as a 'cylindrical polar function' and ϕ appears to be the angle of the centre of rotation. One can clearly see that map (21) is invalid as it cannot have the same metric as the Euclidean plane, i.e. if $\boldsymbol{\sigma}_{,x} \cdot \boldsymbol{\sigma}_{,x} = 1$, $\boldsymbol{\sigma}_{,y} \cdot \boldsymbol{\sigma}_{,y} = 1$ and $\boldsymbol{\sigma}_{,x} \cdot \boldsymbol{\sigma}_{,y} = 0$, then the conditions $\boldsymbol{\sigma}_{,x} \cdot \boldsymbol{\sigma}_{,x} = 1$ and $\boldsymbol{\sigma}_{,x} \cdot \boldsymbol{\sigma}_{,y} = 0$ (or $\boldsymbol{\sigma}_{,y} \cdot \boldsymbol{\sigma}_{,y} = 1$ and $\boldsymbol{\sigma}_{,x} \cdot \boldsymbol{\sigma}_{,y} = 0$) imply that $R = 0$, and this in turn implies that $\boldsymbol{\sigma}_{,x} \cdot \boldsymbol{\sigma}_{,x} = \boldsymbol{\sigma}_{,y} \cdot \boldsymbol{\sigma}_{,y} = 0$, which is a contradiction. Now, given that a solution exists in the interval $[\phi_1, \phi_2]$, the authors states that the solution is

$$T_{yy}(\phi_2) = T_0 \exp\left(\frac{\mu_d}{R(\phi)} \sin\left(\frac{R(\phi)\phi}{\sqrt{1+R(\phi)^2}}\right)\Big|_{\phi_1}^{\phi_2}\right) \,. \tag{22}$$

Despite the fact that map (21) is invalid, solution (22) is valid for right-circular cones, i.e. valid for $R = \tan(\alpha)$ where 2α is the (constant-) angle of aperture (see Section 2.5.4). But this is still an incorrect solution and it is a mere coincidence that it is valid for the arbitrary right-circular cones. To see why equation (22) is incorrect, one only needs to consider an example with noncircular cross section. If the reader wishes to, then consider a positively-oriented elliptical-cone (for the $\zeta = 0$ case) that is defined by the map $\boldsymbol{\sigma}(\phi, z) = (az\cos(\phi), bz\sin(\phi), z)_{\mathsf{E}}$ where $z \in \mathbb{R}_{>0}$ and $a, b > 0$, and let $\phi \in [\frac{1}{4}\pi, \frac{3}{4}\pi]$ be the contact interval (see figure 7 and consider the $z = 1$ case). Now, the reader can that solution (22) is no longer valid.

The authors conclude by saying that their experimental results agreed almost perfectly with equation (20) for the cylinder case. One expects that the solution to agree with experiment data for the cylinder case as the solution is only valid for the cylinder case. The authors further state 'Experimental data gathered on [right-circler] cones constructed from plaster of Paris and Neoprene ... with half-angles ranging up to 12° and contact angles in the range $[70^\circ, 120^\circ]$ show good agreement with the simple cylindrical model at their error level (around $\pm 10\%$ for most samples)' [48]. Again, one expects this be the case as solution (22) is only valid for right-circular cones. Also, it is given by the authors that in the limit $R \to 0$, the cone case is asymptotically equals to the cylinder case. This result is just a trivial mathematical result that follows directly from the Maclaurin series, i.e. $\sin(\theta) \approx \theta$, when $\theta \approx 0$.

In conclusion, no mathematical claim of Cottenden *et al.* [48] can be mathematically justified, and some fundamental and trivial results in mathematical elasticity and differential geometry are mis-

represented. Only the ordinary capstan equation, and a solution to a dynamic membrane with both a zero-Poisson's ratio and a zero-mass density on a right-circular cone are given. Finally limited experimental data is given to show the trivial asymptotic nature of $\sin(\theta)$ near $\theta = 0$.

In Cottenden *et al.*'s [48] publication the authors fails to demonstrate a sufficient knowledge in the subject of differential geometry, mathematical elasticity and contact mechanics to tackle this problem with any mathematical rigour, and this is evident in D. J. Cottenden's [47] thesis as the publication Cottenden *et al.* [48] is a summary of all the mathematical results from Cottenden's [47] thesis. For example, in section 2.15 of the thesis the compatibility conditions for left Cauchy-Green deformation tensor is given as a general condition (see page 8 of Cottenden [47]). However, there exists no general compatibility condition for left Cauchy-Green deformation tensor, and the given compatibility conditions exist for the two-dimensional case only [2]. Another example is that the entire section 5.4 of the thesis (see pages 132 to 137 of Cottenden [47]) is based on the assumption that one can invert a 3×2 matrix (see equation 5.15 of Cottenden [47]), i.e. given a sufficiently differentiable map $\boldsymbol{\lambda} : \mathbb{R}^2 \rightarrow \mathbf{E}^3$, the author asserts that the Jacobian matrix, $(\partial_\beta \lambda^j)_{3\times 2}$ where $\beta \in \{1, 2\}$ and $j \in \{1, 2, 3\}$, is invertible.

Despite the fact that Cottenden *et al.*'s [48] framework is only valid for two trivial cases, the very ideas and the very problems that the authors tried to model are important subjects of investigation in Chapters 2 and 6.

In a different publication, a precursor to the one we discussed, Cottenden *et al.* [45][7] give a mathematical model to calculate the coefficient of friction based on the experimental findings of S. E. S. Karavokyros [100] from his master's thesis. The authors state 'The model generalizes the common assumption of a cylindrical arm to any convex prism, and makes predictions for pressure and tension based on Amontons' law' [45]. Coefficients of friction are determined from experiments conducted on Neoprene-coated Plaster of Paris prisms of circular and elliptical cross-sections (defined as arm phantoms) and a nonwoven fabric. The authors state experimental results agreed within $\pm 8\%$, i.e. 16%. They also state that the coefficients of friction varied very little with the applied weight, geometry and contact angle. Thus, the authors conclude by asserting that accurate values of the coefficient of friction can be obtained by applying the cylindrical model (i.e. capstan model) to the experimental data on human arms. They further assert that the coefficient of friction is independent of the substrate geometry, applied weights and contact angles, and claims that both their mathematical model and experimental results are in complete agreement.

Unfortunately, none of Cottenden *et al.*'s [45] mathematical results can be mathematically justified, mostly for the reasons that we described before. For example, the reader may try to derive an arc-length of an ellipse with the use of the definition of an arc length from section 2.4 of the publication (see directly above equation 12 of Cottenden *et al.* [45]). Another example is the equation $1/\tan(0.5\pi) = 0$, which is from the latter part of section 4.1 of the publication (see directly below

[7] http://discovery.ucl.ac.uk/id/eprint/69867

equation 17 of Cottenden *et al.* [45]). Thus, in the risk of being pedantic, we omit reviewing the mathematics of publication in detail.

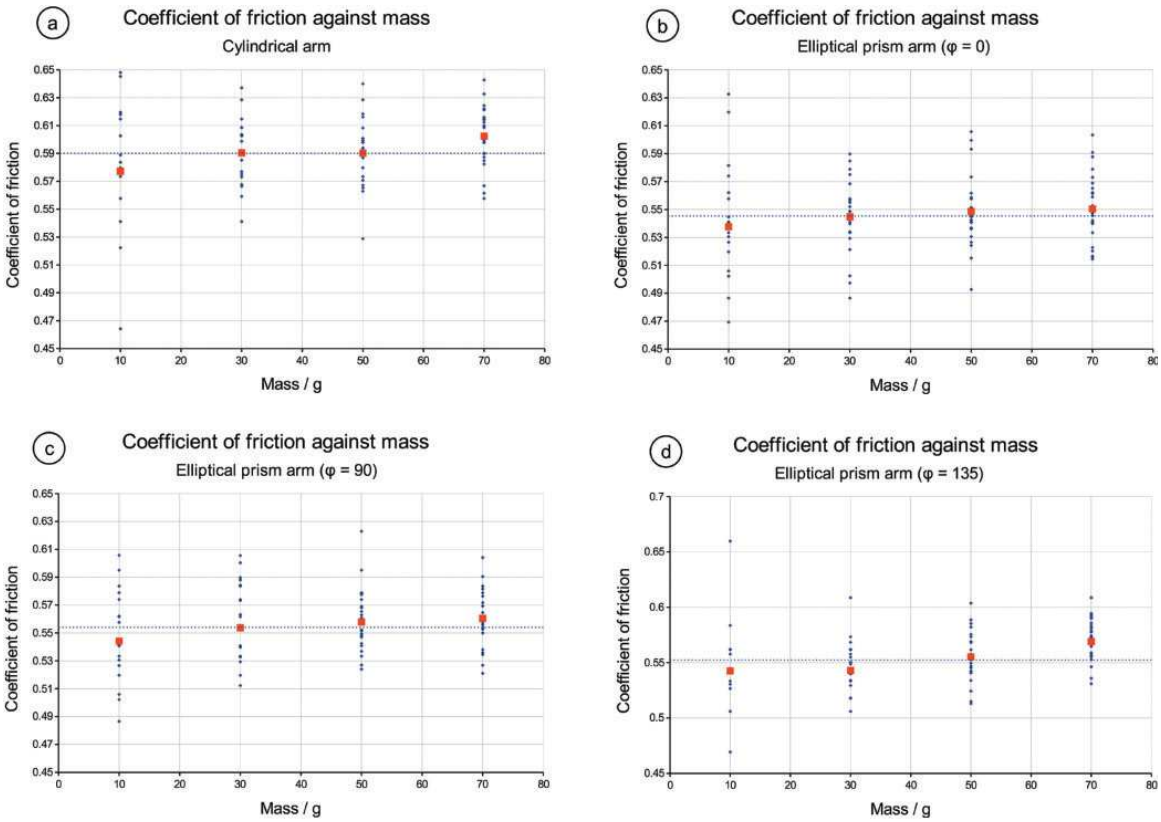

Figure 8: Coefficient of friction against applied mass in grams: (a) Cylindrical body; (b) Elliptical prism with horizontal major axis; (c) Elliptical prism with vertical major axis; (d) Elliptical prism with major axis making $+135^\circ$ to the horizontal [45].

As for the experimental results, consider figure 8 which shows the coefficients of friction in relation to different geometries, applied weights, and contact angles, where the figure is extracted directly from the publication (see figure 11 of Cottenden *et al.* [45]). One can see that there are clear discrepancies between each calculated coefficients of friction as the coefficients of friction vary between different geometries, weights, and contact angles. The authors only acknowledge the dependence of coefficient of friction relative to the applied weight (see section 4 of Cottenden *et al.* [48]), but dismiss this effect by asserting that '... the increase [coefficient of friction relative to the applied weight] is small compared to the scatter in the data, and moreover represents a variation in μ of less than 5 per cent across the experimental mass range. This is likely a result of changes in the interacting Neoprene and nonwoven surfaces as the pressure increases, and corresponds to a small departure from Amontons' law' [45].

If one consults Karavokyros [100] for the experimental data, then one finds the raw data of the cylinder for the $\frac{127}{360}\pi$ contact angle case (see table 2a of Karavokyros [100]), which is displayed in table 1. Now, using this data, if one plot the tension ratio, $\delta\tau = T_{\text{max}}/T_0$, against the applied mass, then one gets figure 9. Note that the capstan equation implies that the tension ratio is constant for

Mass g	Tension 10^{-3}N					
	1st	2nd	3rd	4th	5th	Mean
10	$16.0g$	$15.0g$	$15.0g$	$15.0g$	$16.0g$	$15.6g$
30	$51.0g$	$54.0g$	$51.0g$	$50.0g$	$51.0g$	$51.4g$
50	$88.0g$	$87.0g$	$89.0g$	$87.0g$	$90.0g$	$88.2g$
70	$125g$	$124g$	$128g$	$122g$	$124g$	$125g$

Table 1: Tensometer readings: Cylinder with $\frac{127}{360}\pi$ contact angle, where g is the acceleration due to gravity [100].

all applied mass, i.e. $\delta\tau = \exp(\mu_d\theta_0)$ is constant given that μ_d and θ_0 are constants. But this is not what the experimental results are implying, as the reader can clearly see from figure 9 that as the applied mass increases, tension ratio too increases, and this is documented phenomenon in the literature which cannot be simply dismissed [97]. Thus, this implies that, for the given experiments, it is unsuitable to use the standard capstan equation to find the coefficient of friction with a significant degree of accuracy. Now, this is direct evidence that shows the flaws in Cottenden *et al.* [48] data analysis methods and their interpretation of the experimental results.

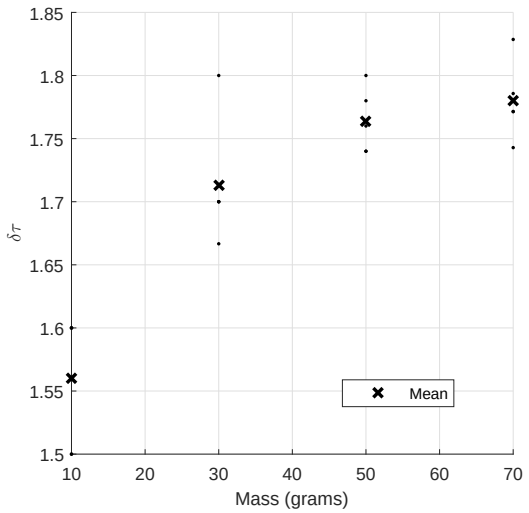

Figure 9: Tension ratio against applied mass.

Unfortunately no raw data is available for the other experiments in the theses of Karavokyros [100] or Cottenden [47] to conduct further rigorous analysis, as we did with the $\frac{127}{360}\pi$-cylinder case.

As a result of flawed mathematics and data analysis techniques, Cottenden *et al.* [45], Cottenden *et al.* [46] and Cottenden *et al.* [48] assert that the tension in the membrane is independent of the geometry and the elastic properties of the foundation, and thus, the stress profile at the contact region and the coefficient of friction can be calculated with the use of the ordinary capstan equation. They further assert that the experimental methodology for calculating the coefficient of

friction between fabrics and in-vivo (within the living) human skin is identical to the capstan model. However, we found no experimental evidence in the body of authors' publications to verify their assertion, i.e. no evidence is given for the assertion that foundation's elastic properties are irrelevant when calculating the coefficient friction between an elastic foundation and an overlying membrane. Thus, authors' experimental methodology is a subject of investigation in chapter 6.

1.9 A Critical Study of the Work of Efrati *et al.*

Efrati *et al.* [60][8] (the principal author is E. Sharon) present the mathematical model *non-Euclidean* plate theory for modelling deformation of thin objects. The main application of authors' work is in the study of natural growth of tissue such as growth of leaves and other natural slender bodies. The authors attempt to derive a thin plate theory, as a generalisation of existing elastic plate theories, that it is valid for large displacements and small strains in arbitrary intrinsic geometries. Some numerical results are present which is based on an example of a hemispherical plate, and they show the occurrence of buckling transition, from a stretching-dominated configuration to a bending-dominated configuration, under variation of the plate thickness. Note that by non-Euclidean the authors mean 'the internal geometry of the plate is not immersible in 3D Euclidean space' [60]. Also, the authors define 'a metric is immersible in $\mathbf{E}^3$' if Ricci curvature tensor with respect to the implicit coordinate system is identically zero, i.e. for a given immersion $\boldsymbol{\varphi} : \mathbb{R}^n \to \mathbf{E}^3$, where $1 \leq n \leq 3$, the metric $\bar{\boldsymbol{g}}$ on $\mathbb{R}^n$ induced by the immersion $\boldsymbol{\varphi}$ results in $\boldsymbol{Ric} = \mathbf{0}$ in $\mathbb{R}^n$.

Given that a growing leaf can be modelled by a plate, Efrati *et al.* [60] focus on the elastic response of the plate after its planar (i.e. rest) configuration is modified either by growth or by a plastic deformation. The authors ignore the thermodynamic limitations on plastic deformations as they are not relevant when modelling naturally growing tissue, and further assume that the reference configuration is a known quantity. Their main postulate is that a non-Euclidean plate cannot assume a rest configuration, i.e. no stress-free configuration can exist, and thus, one faces a nontrivial problem that always exhibits residual stress.

The authors define a plate as an elastic medium for which there exists a curvilinear set of coordinates $\boldsymbol{x} = (x^1, x^2, x^3)$, in which the 'reference metric', $\bar{g}_{ij} = \bar{g}_{ij}(x^1, x^2)$, takes the form $\bar{g}_{\alpha\beta} = \bar{g}_{\beta\alpha}$, $\bar{g}_{\alpha 3} = 0$, $\bar{g}_{33} = 1$. The reference metric is a symmetric positive-definite tensor and considered to be a known quantity. The plate is considered to be 'even', i.e. the domain $\mathscr{D} \subset \mathbb{R}^3$ of curvilinear coordinates can be decomposed into $\mathscr{D} = \mathscr{S} \times [-\frac{h}{2}, \frac{h}{2}]$, where $\mathscr{S} \subset \mathbb{R}^2$ and h is the thickness of the plate. Thus, it is given that an even plate is fully characterised by the metric of its mid-surface, at where $x^3 = 0$.

Although thin plates are three-dimensional bodies, the authors took advantage of the large aspect ratio by modelling the plates as two-dimensional surfaces, and thus, reducing the dimensionality of the problem. To achieve this the authors assume 'Kirchhoff–Love assumptions:' (i) 'the body is in a

[8] http://www.ma.huji.ac.il/∼razk/iWeb/My_Site/Publications_files/ESK08.pdf

state of plane-stress (the stress is parallel to the deformed mid-surface)', and (ii) 'points which are located in the undeformed configuration on the normal to the mid-surface at a point p, remain in the deformed state on the normal to the mid-surface at p, and their distance to p remains unchanged' [60].

Now, consider the deformed plate in the Euclidean space, which is defined as a compact domain $\Omega \subset \mathbb{R}^3$ endowed with a regular set of material curvilinear coordinates. Define the mapping $\boldsymbol{r} : \mathscr{D} \subset \mathbb{R}^3 \mapsto \Omega$, from the domain of parameterisation $\mathscr{D}$ into Ω, as the configuration of the body endowed with the metric tensor $\boldsymbol{g}$, which is defined as $g_{ij} = \partial_i \boldsymbol{r} \cdot \partial_j \boldsymbol{r}$. It is given that Kirchhoff–Love second assumption implies that $g_{\alpha 3} = 0$. Thus, when defined more precisely, one finds that $\boldsymbol{r}(x^1, x^2, x^3) = \boldsymbol{R}(x^1, x^2) + x^3 \hat{\boldsymbol{N}}(x^1, x^2)$, $g_{\alpha\beta} = a_{\alpha\beta} - 2x^3 b_{\alpha\beta} + (x^3)^2 c_{\alpha\beta}$, $g_{\alpha 3} = 0$ and $g_{33} = 1$, where $\boldsymbol{R}$ is the mid-surface, $\hat{\boldsymbol{N}}$ is the unit normal to the mid-surface, and $a_{\alpha\beta}$, $b_{\alpha\beta}$ and $c_{\alpha\beta}$ are the first, the second and the third fundamental form tensors respectively. With further inspection one finds that $a_{\alpha\beta} = \partial_\alpha \boldsymbol{R} \cdot \partial_\beta \boldsymbol{R}$, $b_{\alpha\beta} = (\partial_\alpha \partial_\beta \boldsymbol{R}) \cdot \hat{\boldsymbol{N}}$ and $c_{\alpha\beta} = (a^{-1})^{\gamma\delta} b_{\alpha\gamma} b_{\beta\delta}$. The ultimate goal is to find the metric tensor $\boldsymbol{g}$, and the authors state that the metric tensor $\boldsymbol{g}$ is immersed in $\mathbb{R}^3$, and thus, the metric tensor uniquely defines the physical configuration of a three-dimensional body. It is also the case that one needs to find equations to six unknowns which make up the metric tensor for the general case, where $\bar{\boldsymbol{g}}$ is not defined by $\boldsymbol{r}$. For the general case the authors describe one approach to this problem via the use of 'the modified version of the hyper-elasticity principle ... the elastic energy stored within a deformed elastic body can be written as a volume integral of a local elastic energy density, which depends only on (i) the local value of the metric tensor and (ii) local material properties that are independent of the configuration' [60]. It is unclear what the authors mean by this definition; thus, for a more precise definition of hyperelasticity we refer the reader to Ball [17] or Ciarlet [38].

The authors define the strain tensor by

$$\epsilon_{ij} = \frac{1}{2}(g_{ij} - \bar{g}_{ij}) \ , \tag{23}$$

and thus, the energy functional is expressed as

$$E(g) = \int_{\mathscr{D}} w(g) \sqrt{\bar{g}} \ dx^1 dx^2 dx^3 \ , \tag{24}$$

where $w = \frac{1}{2} A^{ijkl} \epsilon_{ij} \epsilon_{kl}$ is the energy density and $A^{ijkl} = \lambda \bar{g}^{ij} \bar{g}^{kl} + \mu(\bar{g}^{ik} \bar{g}^{jl} + \bar{g}^{il} \bar{g}^{jk})$ is the elasticity tensor. With the use of the energy functional (24) the configuration $\boldsymbol{r}$ is varied to find the three constraints that $g_{\alpha\beta}$ must satisfy, i.e. 'the fundamental model for three-dimensional elasticity' [60].

They also define symmetric Ricci curvature tensor of the metric $\boldsymbol{g}$ by

$$Ric_{li} = \frac{1}{2}(g^{-1})^{kj}(\partial_k \partial_i g_{lj} - \partial_k \partial_j g_{li} + \partial_j \partial_l g_{ki} - \partial_i \partial_l g_{kj}) + (g^{-1})^{kj} g_{pq}(\Gamma^p_{lj} \Gamma^q_{ki} - \Gamma^p_{kj} \Gamma^q_{li}) \ .$$

As the elastic body is immersed in $\mathbb{R}^3$, the variational principle implies that the six independent components of the symmetric Ricci curvature tensor must all vanish, i.e. $Ric_{ij} = 0$. However, $Ric_{ij} = 0$ and the three equations obtained by varying the configuration $\boldsymbol{r}$ in equation (24) imply that the system is over-determined. Thus, the authors postulate that there are two possible ways to resolve

this 'seemingly over-determination'. The first is by noticing that the six independent components of Ricci curvature tensor's derivatives are related through second Bianchi identity. The second way of resolving this issue is by identifying the immersion $\boldsymbol{r}$ as the three unknown functions (as defined previously), in which case the six equations that form Ricci tensor are the solvability conditions for the partial differential equation. However, as the equations in $\boldsymbol{r}$ are of higher order, one needs to supply additional conditions, namely to set the position and the orientation of the body, in order to obtain a unique solution for $\boldsymbol{r}$.

To find the reduced energy density the authors integrate the energy density (24) over the thin dimension as $w_{2D} = \int_{-\frac{h}{2}}^{\frac{h}{2}} w \, dx^3$ to obtain the equation

$$w_{2D} = h w_S + h^3 w_B \ ,$$

where

$$\begin{aligned} w_S &= \frac{Y}{8(1+\nu)} \left(\frac{\nu}{1-\nu} \bar{g}^{\alpha\beta} \bar{g}^{\gamma\delta} + \bar{g}^{\alpha\gamma} \bar{g}^{\beta\delta} \right) (a_{\alpha\beta} - \bar{g}_{\alpha\beta})(a_{\gamma\delta} - \bar{g}_{\gamma\delta}) \ , \\ w_B &= \frac{Y}{24(1+\nu)} \left(\frac{\nu}{1-\nu} \bar{g}^{\alpha\beta} \bar{g}^{\gamma\delta} + \bar{g}^{\alpha\gamma} \bar{g}^{\beta\delta} \right) b_{\alpha\beta} b_{\gamma\delta} \ , \end{aligned} \tag{25}$$

which are defined as stretching and bending densities respectively. Note that Y is Young's modulus and ν is Poisson's ratio of the plate.

It is stated that with the use of Cayley-Hamilton theorem the density of the bending content can be written in the following form,

$$w_B = \frac{Y}{8(1+\nu)} \big(\frac{1}{1-\nu} (\bar{g}^{\alpha\beta} b_{\alpha\beta})^2 - 2 \frac{|b|}{|\bar{g}|} \big) \ .$$

It is also stated that, if $a_{\alpha\beta} = \bar{g}_{\alpha\beta}$ (i.e. the two-dimensional configuration has zero-stretching energy), then the density of the bending content can be expressed as the density of Willmore functional [210],

$$w_W = \frac{Y}{24(1+\nu)} \left(\frac{4H^2}{1-\nu} - 2K \right) \ ,$$

where K and H are Gaussian and the mean curvatures of the mid-surface respectively.

With the vanishing of Ricci tensor the authors obtain Gaussian curvature and Gauss-Mainardi-Peterson-Codazzi equations, which are respectively defined as

$$K = \frac{|b|}{|a|} = \frac{1}{2} (a^{-1})^{\alpha\beta} (\partial_\gamma \Gamma^\gamma_{\alpha\beta} - \partial_\beta \Gamma^\gamma_{\alpha\gamma} + \Gamma^\gamma_{\gamma\delta} \Gamma^\delta_{\alpha\beta} - \Gamma^\gamma_{\beta\delta} \Gamma^\delta_{\alpha\gamma}) \ , \tag{26}$$

$$\partial_2 b_{\alpha 1} + \Gamma^\beta_{\alpha 1} b_{\beta 2} = \partial_1 b_{\alpha 2} + \Gamma^\beta_{\alpha 2} b_{\beta 1} \ , \tag{27}$$

where equations (26) and (27) given to provide sufficient conditions for immersiblility of the metric tensor $\boldsymbol{g}$ in $\mathbb{R}^3$.

It may appear to the uninitiated that Efrati *et al.*'s [60] publication is a coherent piece of work, but it is, in fact, flawed. To illustrate this matter in detail, we direct the reader's attention to section 3.4 of the publication. Upon examining the governing equations and the boundary conditions one can see

that the governing equations are defined for zero-external loadings, and the boundary conditions are defined for zero-tractions, zero-boundary moments and there are no descriptions of any Dirichlet conditions. Thus, it is mathematically impossible to obtain a non-zero solution (excluding any rigid motions). Furthermore, there is no evidence in authors' publication for proof of the existence of solutions, either via rigorous mathematics (Γ-limit or otherwise) or via numerical analysis.

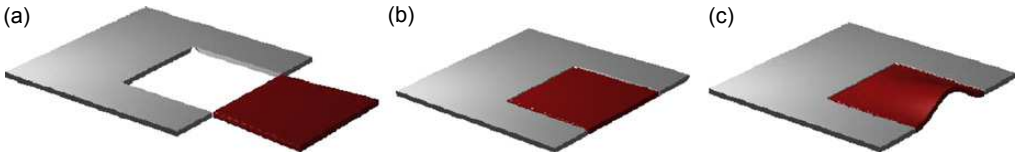

Figure 10: 'A schematic illustration of an unconstrained plate exhibiting residual stress. (a) The two elements composing the plate are shows side by side. (b) As the red trapezoid is too large to fit into the square opening, it is compressed. (c) For a plate sufficiently thin, the induced compression exceeds the buckling threshold, and the trapezoid buckles out of plane. Note that there are many shapes that preserve all lengths along the faces of the plate, yet they cannot be planar' [60].

Efrati *et al.*'s [60] erroneous work arises from not fully understanding how to model the given problem. Consider figure 10 (c), which extracted directly from the publication and considered by the authors as a simplified version of the problem: the very reason that the *red trapezoid* is deformed is because it is compressed at the boundary, i.e. it is deformed as it is subjected to a Dirichlet boundary condition. Thus, if one attempts to model this problem with mathematical rigour, then one can derive the actual energy functional for this problem. To do so, consider the map

$$\boldsymbol{r}(\boldsymbol{u}) = \boldsymbol{R}(\boldsymbol{u}) + z\frac{\partial_x \boldsymbol{R}(\boldsymbol{u}) \times \partial_y \boldsymbol{R}(\boldsymbol{u})}{||\partial_x \boldsymbol{R}(\boldsymbol{u}) \times \partial_y \boldsymbol{R}(\boldsymbol{u})||} \,, \tag{28}$$

which is assumed to be a sufficiently differentiable $\mathbf{E}^3 \to \mathbf{E}^3$ diffeomorphism for an appropriate $\boldsymbol{u} \in \mathbf{E}^3$, where $\boldsymbol{R}(\boldsymbol{u}) = (x, y, 0)_{\mathsf{E}} + (u^{\bar{1}}(x, y), u^{\bar{2}}(x, y), u^{\bar{3}}(x, y))_{\mathsf{E}}$ is the deformed mid-surface of the plate, and $\boldsymbol{u}$ is the displacement field that describes a vector displacement in the three-dimensional Euclidean space. The metric with respect to map (28) in the Euclidean space is $g_{\bar{\alpha}\bar{\beta}}(\boldsymbol{u}) = \partial_{\bar{\alpha}} r_{\bar{i}}(\boldsymbol{u}) \partial_{\bar{\beta}} r^{\bar{i}}(\boldsymbol{u})$, where the over-bar in the indices highlights the fact that one is using Euclidean coordinates. Now, the strain tensor of a plate can be expressed as

$$\epsilon_{\bar{\alpha}\bar{\beta}}(\boldsymbol{u}) = \frac{1}{2}\left(g_{\bar{\alpha}\bar{\beta}}(\boldsymbol{u}) - \delta_{\bar{\alpha}\bar{\beta}}\right) \,,$$

where $x^{\bar{1}} = x$ and $x^{\bar{2}} = y$. Thus, the energy functional can be expressed as

$$\begin{aligned} J(\boldsymbol{u}) = \int_{\mathscr{S}} \Bigg[& \frac{1}{8} h A^{\bar{\alpha}\bar{\beta}\bar{\gamma}\bar{\delta}} \left(\partial_{\bar{\alpha}} R_{\bar{i}}(\boldsymbol{u}) \partial_{\bar{\beta}} R^{\bar{i}}(\boldsymbol{u}) - \delta_{\bar{\alpha}\bar{\beta}}\right) \left(\partial_{\bar{\gamma}} R_{\bar{k}}(\boldsymbol{u}) \partial_{\bar{\delta}} R^{\bar{k}}(\boldsymbol{u}) - \delta_{\bar{\gamma}\bar{\delta}}\right) \\ & + \frac{1}{24} h^3 A^{\bar{\alpha}\bar{\beta}\bar{\gamma}\bar{\delta}} \left(\partial_{\bar{\alpha}\bar{\beta}} R_{\bar{i}}(\boldsymbol{u}) \frac{(\partial_x \boldsymbol{R}(\boldsymbol{u}) \times \partial_y \boldsymbol{R}(\boldsymbol{u}))^{\bar{i}}}{||\partial_x \boldsymbol{R}(\boldsymbol{u}) \times \partial_y \boldsymbol{R}(\boldsymbol{u})||}\right) \left(\partial_{\bar{\gamma}\bar{\delta}} R_{\bar{k}}(\boldsymbol{u}) \frac{(\partial_x \boldsymbol{R}(\boldsymbol{u}) \times \partial_y \boldsymbol{R}(\boldsymbol{u}))^{\bar{k}}}{||\partial_x \boldsymbol{R}(\boldsymbol{u}) \times \partial_y \boldsymbol{R}(\boldsymbol{u})||}\right) \Bigg] dxdy \,, \end{aligned} \tag{29}$$

$$\boldsymbol{u} \in \{\boldsymbol{v} \in \boldsymbol{W}(\mathscr{S}) \mid \boldsymbol{v}|_{\partial\mathscr{S}} = \boldsymbol{u}_0\} \,, \tag{30}$$

where $\mathscr{S} \subset \mathbf{E}^2$ is the mid-plane of the unstrained plate, $\boldsymbol{W}(\mathscr{S})$ is an appropriate Sobolev space, $\boldsymbol{u}_0 \in L^2(\partial\mathscr{S})$ is the Dirichlet boundary condition and $A^{\bar{\alpha}\beta\bar{\gamma}\bar{\delta}} = \frac{1}{2}(1+\nu)^{-1} Y (2(1-\nu)^{-1} \nu \delta^{\bar{\alpha}\bar{\beta}} \delta^{\bar{\gamma}\bar{\delta}} +$

$\delta^{\bar{\alpha}\bar{\gamma}}\delta^{\bar{\beta}\bar{\delta}} + \delta^{\bar{\alpha}\bar{\delta}}\delta^{\bar{\beta}\bar{\gamma}})$ is the elasticity tensor. As $\boldsymbol{R}(\boldsymbol{u})$ describes a surface, one may argue that with an appropriate coordinate transform one can express equation (29) in the same form as authors' energy functional (see equation 3.7 of Efrati *et al.* [60]), which is true if one is using an appropriate $(x, y)_{\mathsf{E}} : \mathbb{R}^2 \to \mathbf{E}^2$ coordinate transform (authors' erroneous coordinate transform leads to a reference metric of a shell at $x^3 = 0$; please see equation 4.1 and see the definition of $\Phi(r)$ from section 4.2 of Efrati *et al.* [60]). However, without the Dirichlet boundary condition from equation (30) or some other external loading, which is exactly what the authors are considering (see respectively equation 2.5 and section 3.2 of Efrati *et al.* [60]), one gets the trivial zero-displacement solution, i.e. $\boldsymbol{u} = \boldsymbol{0}$ in $\mathscr{S}$. The fact that the authors are claiming that nonzero solutions are possible without tractions, Dirichlet boundary conditions, external loadings and boundary moments imply that they are doing something fundamentally flawed.

Now, consider the sufficiently differentiable diffeomorphism $\boldsymbol{\varphi} : \omega \subset \mathbb{R}^2 \to \boldsymbol{\varphi}(\omega) \subset \mathbf{E}^2$ with the property $\det(\boldsymbol{J}) > 0$, where $(x, y)_{\mathsf{E}} = (\varphi^{\bar{1}}(x^1, x^2), \varphi^{\bar{2}}(x^1, x^2))_{\mathsf{E}}$ and $J^{\bar{\beta}}_{\alpha} = \partial_\alpha \varphi^{\bar{\beta}}$ is the Jacobian matrix of the map $\boldsymbol{\varphi}$. Now, consider the mapping $\boldsymbol{R}(\boldsymbol{u}) \circ \boldsymbol{\varphi} : \omega \subset \mathbb{R}^2 \to \boldsymbol{R}(\boldsymbol{u})(\mathscr{S}) \subset \mathbf{E}^3$. As $\boldsymbol{\varphi}$ is a diffeomorphism, $\boldsymbol{R}(\boldsymbol{u}) \circ \boldsymbol{\varphi}$ is a well defined surface for a suitable displacement field $\boldsymbol{u} \in \boldsymbol{W}(\mathscr{S})$, and as $\det(\boldsymbol{J}) > 0$, the unit normal to the surface $\boldsymbol{R}(\boldsymbol{u})$ is equal the unit normal to the surface $\boldsymbol{R}(\boldsymbol{u}) \circ \boldsymbol{\varphi}$ (see Section 2.4). Thus, with respect to $\boldsymbol{\varphi}$ equation (29) reduces to

$$J(\boldsymbol{u}) = \int\limits_{\omega} \frac{1}{2} A^{\alpha\beta\gamma\delta} \left(h a_{\alpha\beta}(\boldsymbol{u}) a_{\gamma\delta}(\boldsymbol{u}) + \frac{1}{12} h^3 b_{\alpha\beta}(\boldsymbol{u}) b_{\gamma\delta}(\boldsymbol{u}) \right) \sqrt{\det(\bar{g})}\, dx^1 dx^2 \,, \tag{31}$$
$$\boldsymbol{u} \in \{\boldsymbol{v} \in \boldsymbol{W}(\mathscr{S}) \mid \boldsymbol{v}|_{\partial\mathscr{S}} = \boldsymbol{u}_0\} \,,$$

where

$$\begin{aligned}
a_{\alpha\beta}(\boldsymbol{u}) &= \frac{1}{2}\left((\partial_\alpha R_{\bar{i}}(\boldsymbol{u}) \circ \boldsymbol{\varphi})(\partial_\beta R^{\bar{i}}(\boldsymbol{u}) \circ \boldsymbol{\varphi}) - \bar{g}_{\alpha\beta} \right) \,, \\
b_{\alpha\beta}(\boldsymbol{u}) &= (\partial_{\alpha\beta} R_{\bar{i}}(\boldsymbol{u}) \circ \boldsymbol{\varphi}) \frac{((\partial_1 \boldsymbol{R}(\boldsymbol{u}) \circ \boldsymbol{\varphi}) \times (\partial_2 \boldsymbol{R}(\boldsymbol{u}) \circ \boldsymbol{\varphi}))^{\bar{i}}}{||(\partial_1 \boldsymbol{R}(\boldsymbol{u}) \circ \boldsymbol{\varphi}) \times (\partial_2 \boldsymbol{R}(\boldsymbol{u}) \circ \boldsymbol{\varphi})||} \,, \\
\bar{g}_{\alpha\beta} &= \partial_\alpha \varphi^{\bar{\gamma}} \partial_\beta \varphi_{\bar{\gamma}} \,, \\
A^{\alpha\beta\gamma\delta} &= \frac{1}{2} \frac{Y}{1+\nu} \left(2 \frac{\nu}{1-\nu} \bar{g}^{\alpha\beta} \bar{g}^{\gamma\delta} + \bar{g}^{\alpha\gamma} \bar{g}^{\beta\delta} + \bar{g}^{\alpha\delta} \bar{g}^{\beta\gamma} \right) \,.
\end{aligned}$$

Now, equation (31) is exactly the same form as the nonlinear plates equations in curvilinear coordinators put forward by the authors, excluding the Dirichlet boundary condition. However, equation (31) is derived from the plate equations in Euclidean coordinates (29) with the use of the map $\boldsymbol{\varphi}$ which is a $\mathbb{R}^2 \to \mathbf{E}^2$ diffeomorphism, and thus, the reference metric $\bar{\boldsymbol{g}}$ is immersible in $\mathbf{E}^2$. To be more precise, consider Ricci curvature tensor in the two-dimensional Euclidean space, $Ric^{\mathsf{Euclidean}}_{\bar{\alpha}\bar{\beta}} = Ric_{\gamma\delta}(J^{-1})^{\gamma}_{\bar{\alpha}}(J^{-1})^{\delta}_{\bar{\beta}}$. As Ricci curvature tensor is identically zero in the Euclidean space (clearly!) and the map $\boldsymbol{\varphi}$ is a diffeomorphism, we have the vanishing of Ricci curvature tensor in $\omega \subset \mathbb{R}^2$, i.e. $\boldsymbol{Ric} = \boldsymbol{0}$. Now, consider the map $\boldsymbol{\varphi} \times (z)_{\mathsf{E}} : \{\omega \times [-\frac{1}{2}, \frac{1}{2}]\} \subset \mathbb{R}^2 \times \mathbf{E} \to \{\boldsymbol{\varphi}(\omega) \times [-\frac{1}{2}, \frac{1}{2}]\} \subset \mathbf{E}^3$. As $\boldsymbol{\varphi}$ is a diffeomorphism, the map $\boldsymbol{\varphi} \times (z)_{\mathsf{E}}$ is also a diffeomorphism, and thus, the metric generated by the map $\boldsymbol{\varphi} \times (z)_{\mathsf{E}}$ is immersible in $\mathbf{E}^3$. Furthermore, as $\boldsymbol{r}(\boldsymbol{u}) : \mathscr{S} \times [-\frac{1}{2}, \frac{1}{2}] \subset \mathbf{E}^3 \to \boldsymbol{r}(\boldsymbol{u})(\mathscr{S} \times [-\frac{1}{2}, \frac{1}{2}]) \subset \mathbf{E}^3$ is a diffeomorphism, the metric on $\mathbf{E}^3$ induced by $\boldsymbol{r}(\boldsymbol{u})$ (i.e. the metric of deformation) is immersible in $\mathbf{E}^3$. Thus, the metric on $\mathbb{R}^2 \times \mathbf{E}$ generated by the

map $r(\boldsymbol{u}) \circ (\boldsymbol{\varphi} \times (z)_{\mathsf{E}}) : \{\omega \times [-\frac{1}{2}, \frac{1}{2}]\} \subset \mathbb{R}^2 \times \mathbf{E} \to \boldsymbol{r}(\boldsymbol{u})(\mathscr{S} \times [-\frac{1}{2}, \frac{1}{2}]) \subset \mathbf{E}^3$ (i.e. the metric $\boldsymbol{g}$) is also immersible in $\mathbf{E}^3$. However, the authors assert that their reference metric is not immersible in $\mathbf{E}^3$. But it is mathematically impossible to derive equation (31) from equation (29) without the use of a sufficiently differentiable $\mathbb{R}^2 \to \mathbf{E}^2$ diffeomorphism; thus, the fact that the authors implying that their reference metric is not immersible in the three-dimensional Euclidean space (while their metric $\boldsymbol{g}$ is immersible in $\mathbf{E}^3$) means that the authors are attempting something fundamentally flawed.

Note that, if equation (29) linearised and along with the Dirichlet boundary condition, then one gets

$$J(\boldsymbol{u}) = \int\limits_{\mathscr{S}} \frac{1}{2} A^{\bar{\alpha}\bar{\beta}\bar{\gamma}\bar{\delta}} \left(h a_{\bar{\alpha}\bar{\beta}}(\boldsymbol{u}) a_{\bar{\gamma}\bar{\delta}}(\boldsymbol{u}) + \frac{1}{12} h^3 b_{\bar{\alpha}\bar{\beta}}(\boldsymbol{u}) b_{\bar{\gamma}\bar{\delta}}(\boldsymbol{u}) \right) dxdy \, ,$$

$$\boldsymbol{u} \in \{\boldsymbol{v} \in H^1(\mathscr{S}) \times H^1(\mathscr{S}) \times H^2(\mathscr{S}) \mid \boldsymbol{v}|_{\partial\mathscr{S}_0} = \boldsymbol{0},\ n^{\bar{\alpha}} \partial_{\bar{\alpha}} v^3|_{\partial\mathscr{S}_0} = 0,\ \boldsymbol{v}|_{\{\partial\mathscr{S} \setminus \partial\mathscr{S}_0\}} = \boldsymbol{u}_0\} \, ,$$

where $a_{\bar{\alpha}\bar{\beta}}(\boldsymbol{u}) = \frac{1}{2}(\partial_{\bar{\alpha}} u_{\bar{\beta}} + \partial_{\bar{\beta}} u_{\bar{\alpha}})$, $b_{\bar{\alpha}\bar{\beta}}(\boldsymbol{u}) = \partial_{\bar{\alpha}\bar{\beta}} u^{\bar{3}}$, $\boldsymbol{n}$ is the unit outward normal to the boundary $\partial\mathscr{S}$ and $\partial\mathscr{S}_0 \subset \partial\mathscr{S}$ with $\mathrm{meas}(\partial\mathscr{S}_0; \mathbb{R}) > 0$. Such problems can be solved by consulting the literature that is specialised in the study of linear plate theory (see Ciarlet [37] and Reddy [163]).

For numerical results, instead of finding the unknown metric tensor $\boldsymbol{g}$ which is the goal of the publication, the authors attempt to analyse the respective stretching and bending densities w_s and w_b for a predetermined reference metric $\bar{\boldsymbol{g}}$ and a predetermined deformed mid-surface $\boldsymbol{R}$, and thus, a predetermined metric $\boldsymbol{g}$ (see section 4 of Efrati *et al.* [60]). The authors give numerical results for an 'annular hemispherical plate', i.e. annular plate deformed in to a hemispherical shape, and state that numerical results demonstrate that in the general case there is no 'equipartition' between bending and stretching energies. The authors conclude by saying their numerical findings support treating very thin bodies as inextensible, and 'it also shows that not only in the equilibrium 3D configuration dominated by the minimisation of the bending energy term, but the total elastic energy is dominated by it also' [60]. The reader must understand that authors' numerical results do not imply the existence of a solutions, i.e. the existence of the deformation metric $\boldsymbol{g}$, as the numerical results are obtained for a predetermined metric $\boldsymbol{g}$.

Authors' numerical analysis implies that a thin object can be stretched substantially with very little force. To examine this in more detail consider the following simple example in accordance with authors' numerical analysis. Consider two circular plates: plate c and plate s, with same Young's modulus Y, Poisson's ratio ν, thickness h and radius r, and further assert that $h/r = \varepsilon \ll 1$. Now, take plate c and deform it into the shape of a semi-cylinder with a radius $\frac{2}{\pi} r$ (an area preserving deformation). Following authors' publication one finds that the mid-surface is $\boldsymbol{R}(x^1, x^2) = (x^1, \frac{2}{\pi} r \sin(x^2), \frac{2}{\pi} r \cos(x^2))_{\mathsf{E}}$, and as one knows the deformed configuration in advance, one finds that the reference metric is $\bar{\boldsymbol{g}}(x^1, x^2) = \mathrm{diag}(1, (\frac{2}{\pi} r)^2, 1)$. Thus, the stored energy of a circular plate that is being deformed into a semi-cylindrical shape is

$$\begin{aligned} E_c &= \frac{1}{2} \frac{Y}{1-\nu^2} \int_{-\frac{1}{2}h}^{\frac{1}{2}h} \iint_{\{(x^1)^2 + (\frac{2r}{\pi} x^2)^2 \leq r^2\}} \left(\frac{\pi x^3}{2r} \right)^2 \left(\frac{2r}{\pi} \right) dx^1 dx^2 dx^3 \\ &= \frac{1}{96} \pi^3 \frac{Y}{1-\nu^2} h^3 \, . \end{aligned} \tag{32}$$

Now, take plate s and deform it into a shape of a hemisphere with a radius $\frac{1}{2}\sqrt{2}r$ (an area preserving deformation). Following authors' publication, one finds that the mid-surface is $\boldsymbol{R}(x^1, x^2) = \frac{1}{2}\sqrt{2}r(\sin(x^1)\cos(x^2), \sin(x^1)\sin(x^2), \cos(x^1))_{\mathsf{E}}$ (see the definition of $\boldsymbol{R}(r, \theta)$ from section 4.1 of Efrati *et al.* [60]), and as one knows the deformed configuration in advance, one finds that the reference metric is $\bar{\boldsymbol{g}}(x^1, x^2) = \mathrm{diag}(\frac{1}{2}r^2, \frac{1}{2}r^2\sin^2(x^1), 1)$ (see equation 4.1 and the definition of $\Phi(r)$ from section 4.2 of Efrati *et al.* [60]), where this configuration is defined as the 'stretch-free configuration' (see section 4.1 of Efrati *et al.* [60]). Thus, the stored energy of a circular plate that is being deformed into a hemisphere is

$$\begin{aligned} E_s &= \frac{Y}{1-\nu}\int_{-\frac{1}{2}h}^{\frac{1}{2}h}\int_{0}^{\frac{1}{2}\pi}\int_{-\pi}^{\pi}\left(\frac{\sqrt{2}\,x^3}{r}\right)^2\left(\frac{\sqrt{2}\,r}{2}\right)\sin(x^2)\,dx^1dx^2dx^3 \\ &= \frac{1}{3}\pi\frac{Y}{1-\nu}h^3\,. \end{aligned} \tag{33}$$

Equations (32) and (33), therefore, imply that, if one deforms a circular plate into a semi-cylinder with a radius $\frac{2}{\pi}r$ and deform a circular plate into a hemisphere with radius $\frac{1}{2}\sqrt{2}r$, then one gets the very similar respective energy densities $\frac{1}{96}\pi^2(1-\nu^2)^{-1}Y\varepsilon^2\mathsf{Jm}^{-3}$ and $\frac{1}{3}Y(1-\nu)^{-1}\varepsilon^2\mathsf{Jm}^{-3}$, i.e. both deformations' internal energies are of $\mathcal{O}(\varepsilon^2)\mathsf{Jm}^{-3}$. Which in turn implies that both deformations require force of $\mathcal{O}(\varepsilon)\mathsf{N}$, given that one is applying the forces to the boundaries of the each respective plates. Thus, authors' work asserts that it take approximately the same amount of force to bend a plate into a semi-cylindrical shape or stretch a plate into a hemispherical shape with a similar radius. The reader may try this one's self: find a piece of aluminium foil (i.e. kitchen foil) and try to bend it over one's water bottle. This is a very simple process and the reader will able to accomplish this with a minimum of effort. In fact, the force of gravity is alone may even be sufficient to deform the piece of aluminium foil over the bottle without much interference. Now, try to stretch that same piece of aluminium foil smoothly over a rigid sphere with a similar radius, e.g. over a cricket ball. Can the reader do this without tearing or crumpling and with the same force as one applied in the previous case?

To attempt this problem with mathematical precision consider the set $\mathscr{S} = \{(x, y, 0)_{\mathsf{E}} \in \mathbf{E}^3 \mid x^2 + y^2 \leq r^2\}$, which describes the mid-plane of the unstrained plates c and s. Now, if one deforms plate c is into a semi-cylindrical shape with a radius $\frac{2}{\pi}r$, then one finds that the map of the deformed mid-surface is $\boldsymbol{R}(x, y) = (x, \frac{2}{\pi}r\sin(\frac{1}{2}r^{-1}\pi y), \frac{2}{\pi}r\cos(\frac{1}{2}r^{-1}\pi y))_{\mathsf{E}}$, and thus, the total stored energy of a circular plate of radius r that is being deformed into a semi-cylindrical shape with a radius $\frac{2}{\pi}r$ is

$$\begin{aligned} E_c &= \frac{1}{2}\frac{Y}{1-\nu^2}r\int_{-\frac{1}{2}h}^{\frac{1}{2}h}\iint_{\mathscr{S}}\left(\frac{\pi z}{2r}\right)^2 dxdydz \\ &= \frac{1}{96}\pi^3\frac{Y}{1-\nu^2}h^3\,. \end{aligned} \tag{34}$$

Now, if one deforms plate s is in to a hemisphere with a radius $\frac{1}{2}\sqrt{2}r$, then one finds that the map of the deformed mid-surface is $\boldsymbol{R}(x, y) = \frac{1}{2}\sqrt{2}(x\sin(\frac{1}{2}r^{-1}\pi\sqrt{x^2+y^2}), y\sin(\frac{1}{2}r^{-1}\pi\sqrt{x^2+y^2}),$ $r\cos(\frac{1}{2}r^{-1}\pi\sqrt{x^2+y^2}))_{\mathsf{E}}$, and thus, the total stored energy of a circular plate with a radius r that is being deformed into a hemisphere with a radius $\frac{1}{2}\sqrt{2}r$ is

$$E_s = \frac{1}{2}\int_{-\frac{1}{2}h}^{\frac{1}{2}h}\iint_{\mathscr{S}} A^{\alpha\beta\gamma\delta}\epsilon_{\alpha\beta}(x, y)\epsilon_{\gamma\delta}(x, y)\,dxdydz + \mathcal{O}(h^3)$$

$$= ChYr^2 + \mathcal{O}(h^3)\ , \tag{35}$$

where C is an order-one positive constant that is independent of h, Y and r, and

$$\boldsymbol{\epsilon}(x,y) = \left(\frac{r}{2}\right)^2 \frac{\sin^2\left(\frac{\pi}{2r}\sqrt{x^2+y^2}\right)}{(x^2+y^2)^2}\begin{pmatrix} y^2 & -xy \\ -xy & x^2 \end{pmatrix} + \left(\frac{\pi}{4}\right)^2 \frac{1}{x^2+y^2}\begin{pmatrix} x^2 & xy \\ xy & y^2 \end{pmatrix} - \frac{1}{2}\begin{pmatrix} 1 & 0 \\ 0 & 1 \end{pmatrix}\ ,$$

is the strain tensor of the plate at $z = 0$. As the reader can see from equations (34) and (35) that, if one deforms a circular plate into a semi-cylinder with a radius $\frac{2}{\pi}r$ and deform a circular plate into a hemisphere with a radius $\frac{1}{2}\sqrt{2}r$, then one get the respective energy densities $\mathcal{O}(\varepsilon^2)\text{Jm}^{-3}$ and $\mathcal{O}(1)\text{Jm}^{-3}$. Thus, one can see that it takes significantly higher amount of energy to deform plate in to a hemisphere than to simply bend it in to a semi-cylinder, as the former deformation requires a significant amount of stretching and compression, while the latter requires no such in-plane deformations, which is far more realistic than results obtained by Efrati *et al.*'s [60] approach. Note that the both deformations conserve area.

As further analysis consider the deformed plate s in curvilinear coordinate coordinates (x^1, x^2), where $0 \leq x^1 \leq \frac{1}{2}\pi$ and $|x^2| \leq \pi$. Now, the first and the second fundamental form tensors of the deformed configuration can be expressed respectively as $\boldsymbol{F}_{[\text{I}]}(x^1,x^2) = \frac{1}{2}r^2\text{diag}(1,\sin^2(x^1))$ and $\boldsymbol{F}_{[\text{II}]}(x^1,x^2) = -\frac{1}{2}\sqrt{2}r\text{diag}(1,\sin^2(x^1))$. If one follows authors' publication, then one finds that the reference metric tensor is $\bar{\boldsymbol{g}}(x^1,x^2) = \text{diag}(\frac{1}{2}r^2, \frac{1}{2}r^2\sin^2(x^1), 1)$. This can only be derived by $\bar{g}_{ij}(x^1,x^2) = \partial_i r_{\bar{k}}(x^1,x^2,x^3)\partial_j r^{\bar{k}}(x^1,x^2,x^3)|_{x^3=0}$, where $\boldsymbol{r}(x^1,x^2) = (\frac{1}{2}\sqrt{2}r + x^3)(\sin(x^1)\cos(x^2), \sin(x^1)\sin(x^2), \cos(x^1))_{\mathsf{E}}$. This implies that $\bar{\boldsymbol{g}}$ is the reference metric of a shell at $x^3 = 0$, and thus, $\bar{\boldsymbol{g}}$ is clearly not immersible in $\mathbf{E}^3$ as Ricci tensor is not identically zero, i.e. $\boldsymbol{Ric} = \frac{1}{2}r^2\text{diag}(1,\sin^2(x^1))$. Thus, authors' erroneous reference metric implies that $a_{\alpha\beta} - \bar{g}_{\alpha\beta} = 0$, $\forall\ \alpha,\beta \in \{1,2\}$, i.e. zero-planar strain, which in turn implies the existence of a 'stretch-free configuration' for a substantially deformed plate. Now, if one attempts this same problem with mathematical precession, then one finds that the reference metric tensor is $\bar{\boldsymbol{g}}(x^1,x^2) = 4\pi^{-2}r^2\text{diag}(1,(x^1)^2)$, where $\bar{g}_{\alpha\beta}(x^1,x^2) = \partial_\alpha x\partial_\beta x + \partial_\alpha y\partial_\beta y$ with $x^1 = \frac{1}{2}r^{-1}\pi\sqrt{x^2+y^2}$ and $x^2 = \arctan(y/x)$. The coordinate transform $(x(x^1,x^2), y(x^1,x^2))_{\mathsf{E}} : \mathbb{R}^2 \to \mathbf{E}^2$ is a diffeomorphism (except at $x^1 = x^2 = 0$) and Ricci tensor is identically zero, i.e. $\boldsymbol{Ric} = \boldsymbol{0}$. Furthermore, $\det(\partial_1 x, \partial_2 x; \partial_1 y, \partial_2 y) > 0$, and thus, the definition of the unit normal to the deformed surface is not violated (again, except at $x^1 = x^2 = 0$). Thus, the change in first fundamental form tensor (i.e. planer strain) can be expressed as $2\boldsymbol{a}(x^1,x^2) = \frac{1}{2}r^2\text{diag}(1-8\pi^{-2}, \sin^2(x^1) - 8\pi^{-2}(x^1)^2)$ and the change in second fundamental form tensor (i.e. bending) can be expressed as $\boldsymbol{b}(x^1,x^2) = -\frac{1}{2}\sqrt{2}r\text{diag}(1,\sin^2(x^1))$. Now, with this coordinate transform no such 'stretch-free configuration' can exist for a plate with a radius r that is being deformed into a hemisphere with a $\frac{1}{2}\sqrt{2}r$, unless the radius of the plate is zero.

Above analysis shows that Efrati *et al.* [60] are not studying plates, but they are studying nonlinear Koiter shells with an erroneous strain tensor. This definition of the strain tensor leads to an incorrect change in second fundamental form tensor, and thus, an overestimation of the bending energy density of the shell per h^3 (see equation (25)). To attempt this problem with mathematical precision, let $\tilde{g}_{ij}(\boldsymbol{x}) = \partial_i X_{\bar{k}}\partial_j X^{\bar{k}}$ be the metric of the reference configuration $\boldsymbol{X}(\boldsymbol{x}) = \boldsymbol{\sigma}(x^1,x^2) +$

$x^3||\boldsymbol{\sigma}_{,1} \times \boldsymbol{\sigma}_{,2}||^{-1}(\boldsymbol{\sigma}_{,1} \times \boldsymbol{\sigma}_{,2})$ with respect to the curvilinear coordinate system $\boldsymbol{x} = (x^1, x^2, x^3)$, where $\boldsymbol{\sigma} : \mathbb{R}^2 \to \mathbf{E}^3$ is a sufficiently differentiable immersion (Efrati *et al.*'s [60] reference metric is derived by $\bar{\boldsymbol{g}} = \tilde{\boldsymbol{g}}|_{x^3=0}$). Thus, in nonlinear shell theory one defines the strain tensor as $\epsilon_{\alpha\beta}(\boldsymbol{u}) = \frac{1}{2}(g_{\alpha\beta}(\boldsymbol{u}) - \tilde{g}_{\alpha\beta})$, where $g_{\alpha\beta}(\boldsymbol{u}) = \partial_\alpha r_{\bar{i}}(\boldsymbol{u})\partial_\beta r^{\bar{i}}(\boldsymbol{u})$, $\boldsymbol{r}(\boldsymbol{u}) = \boldsymbol{R}(\boldsymbol{u}) + x^3||\partial_1\boldsymbol{R}(\boldsymbol{u}) \times \partial_2\boldsymbol{R}(\boldsymbol{u})||^{-1}(\partial_1\boldsymbol{R}(\boldsymbol{u}) \times \partial_2\boldsymbol{R}(\boldsymbol{u}))$, $\boldsymbol{R}(\boldsymbol{u}) = \boldsymbol{\sigma} + u^\alpha\partial_\alpha\boldsymbol{\sigma} + u^3\boldsymbol{N}$ and $\boldsymbol{u}(\boldsymbol{x})$ is the displacement field in curvilinear coordinates (see Section 1.4). For more on nonlinear Koiter's shells please consult Ciarlet [38], Koiter [109], and Libai and Simmonds [121].

Even if Efrati *et al.* [60] obtain the correct form of the strain tensor for shells they are still unjustified in using the shell strain tensor to model plates. To explain this matter with mathematical rigour let $\mathscr{S}$ be a two-dimensional plane and let $\mathscr{S}'$ be a two-dimensional surface. What the authors fail to grasp is that an arbitrary mapping from $\mathscr{S}$ to $\mathscr{S}'$ (i.e. $\boldsymbol{\sigma} : \mathscr{S} \subset \mathbb{R}^2 \to \mathscr{S}' \subset \mathbf{E}^3$) is not same as deforming the plane $\mathscr{S}$ into the surface $\mathscr{S}'$ (i.e. $\{\mathscr{S} \cup \{\boldsymbol{u} \in \mathbf{E}^3\} \subset \mathbf{E}^3\} = \{\mathscr{S}' \subset \mathbf{E}^3\}$). The former is a simple coordinate transform (which may or may not be related to deforming the body), while the latter is a unique vector displacement (unique up to a rigid motion). This is one of the concepts that both Cottenden [47] (see section 5.2.1 of Cottenden [47]) and Howell *et al.* [84] (see section 4.9.1 of Howell *et al.* [84]) also failed to grasp, which in turn contributed to their erroneous work. To understand the distinction between a coordinate transform and a vector displacement please consult section 1 and section 2 of Morassi and Paroni [139].

In conclusion, Efrati *et al.*'s [60] publication is not on plate theory: it is on shell theory with an incorrect strain tensor. Thus, the authors numerical results imply that a thin object can be stretched substantially with very little force, which is physically unrealistic and mathematically disprovable. All the theoretical work of the authors, i.e. nonlinear plate equations in curvilinear coordinates, can easily be rectified with the inclusion of both a sufficiently differentiable $\mathbb{R}^2 \to \mathbf{E}^2$ diffeomorphism and some external loadings, such as an external strain field.

1.10 A Critical Study of the Work of Baldelli and and Bourdin

Baldelli and Bourdin [16][9] (the principal author is A. A. L. Baldelli) analyses the asymptotic behaviour of bonded thin elastic structures (i.e. films and plates) on elastic foundations. The work is presented as the first attempt at providing a rigorous derivation of these heuristic models from three-dimensional elasticity. The authors perform an asymptotic study to explore the different asymptotic regimes reached in the limit as the thickness of the overlying thin body goes to zero: for varying thickness of the foundation and stiffness ratios. They give a two-dimensional phase diagram to visualise the asymptotically reduced dimension models as a function of two relevant parameters. Two of the major presented results are the identification of the regime of films over in-plane elastic foundations and the identification of the regime of plates over out-of-plane elastic foundations.

Elastic foundation models are used in the study of many mechanical concepts such as the buckling

[9] http://arxiv.org/pdf/1410.0629.pdf

of stiff films bound to compliant substrates under compression [10, 11, 12] (which are considered to be important in designing of structural sandwich panels [7]) and in the study of crack patterns in thin films subjected to equi-biaxial residual tensile stress [211] (which are considered to be important in the study of spiral cracks, in thin brittle adhesive layers bonding glass plates together, due to environment stress [56]).

Baldelli and Bourdin [16] begin by classifying the study of thin objects on elastic foundations as Winkler foundations and asserting that the derivation of the Winkler foundations equations must be done by rigorous asymptotic analysis. However, authors' assertion is false. Winkler foundation is a very specific mathematical problem: where an elastic body is supported unilaterally on a bed of continuously distributed springs with a foundation modulus $\mathscr{K}_0$ and where the surface of the foundation is lubricated so that no tangential forces can develop (see section 5.5 of Kikuchi and Oden [102] and section 10.4.1 of Ding *et al.* [57] or Section 1.11). Winkler foundation type problem is a boundary condition that exists regardless of the elastic properties of the elastic body or the bed of springs (see equation 5.111 of Kikuchi and Oden [102] or equation (47)). Often in the engineering community Winkler foundation equations are used to describe the behaviour of beams and plates on elastic foundations of infinite depth [80], with complete disregard to understanding why the Winkler foundation equations are applicable to modelling such problems. Thus, the work of the authors may have intended to be used in justifying the use of Winkler foundation equations in modelling such problems.

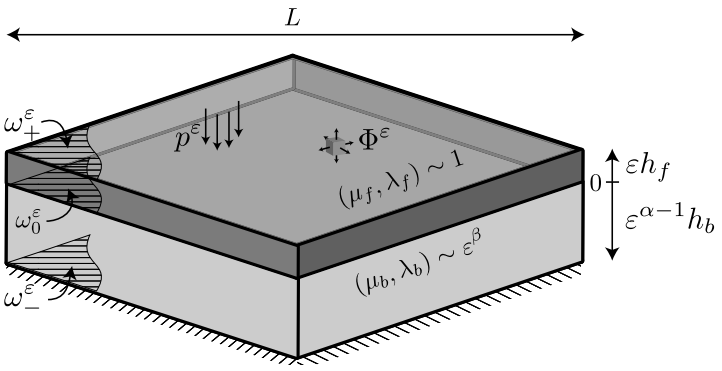

Figure 11: 'Film on the bonding layer' [16].

The core idea behind Baldelli and Bourdin [16] is as follows. Consider a thin overlying elastic body (which the authors called the film/membrane) with a constant thickness εh_f bonded to an elastic foundation (which the authors called the bonding layer) with a constant thickness $\varepsilon^{\alpha-1} h_b$, where the displacement of the bottom of the bonding layer is zero, i.e. displacement field of the bonding layer satisfies zero-Dirichlet boundary condition at its lowest boundary (see figure 11). The parameter ε is consider to be a small constant and α is yet to be determined. In their analysis the authors assume that there exists a common asymptotic behaviour between the elastic properties (Young's modulus and Poisson's ratio) of the overlying body and the bonding layer. To be more precise, the authors assume that both first and second Lamé's parameters of the overlying body are the same order, i.e. $\lambda_f \sim \mu_f$, both first and the second Lamé's parameters of the bonding layer are the same

order, i.e. $\lambda_b \sim \mu_b$ (see figure 11 or figure 1 of Baldelli and Bourdin [16]), both Poisson's ratios of the overlying body and the bonding layer are the same order, i.e. $\nu_f \sim \nu_b$ (see hypothesis 2 of Baldelli and Bourdin [16]), and both Poisson's ratios of the overlying body and the bonding layer are the same sign, i.e. $\nu_b/\nu_f > 0$ (see remark 2 of Baldelli and Bourdin [16]). Now, these conditions result in $-1 < \nu_f \approx \nu_b < 0$ or $0 < \nu_f \approx \nu_b < \frac{1}{2}$, given that both Poisson's ratios are sufficiently away from 0 and $\frac{1}{2}$. To be more precise, the conditions $\lambda_f \sim \mu_f$ and $\lambda_b \sim \mu_b$ imply that $\lambda_f = c_f\mu_f$ and $\lambda_b = c_b\mu_b$ for some $c_f, c_b \sim 1$ constants, and thus, $\nu_f = \frac{1}{2}(1+c_f)^{-1}c_f$ and $\nu_b = \frac{1}{2}(1+c_b)^{-1}c_b$. Furthermore, the conditions $\nu_f \sim \nu_b$ and $\nu_b/\nu_f > 0$ imply that $-\frac{1}{2}(1-|c_f|)^{-1}|c_f| = \nu_f \approx \nu_b = -\frac{1}{2}(1-|c_b|)^{-1}|c_b|$ or $\frac{1}{2}(1+|c_f|)^{-1}|c_f| = \nu_f \approx \nu_b = \frac{1}{2}(1+|c_b|)^{-1}|c_b|$. Thus, one gets the condition $-1 < \nu_f \approx \nu_b < 0$, sufficiently away from 0, or the antithetical condition $0 < \nu_f \approx \nu_b < \frac{1}{2}$, sufficiently away from 0 and $\frac{1}{2}$. However, Poisson's ratio of an object can vary strictly between -1 and $\frac{1}{2}$ [84] and different materials have different Poisson's ratios, and thus, Baldelli and Bourdin's [16] assertion cannot hold in general. For example, assume that the bonding layer's Poisson's ratio is $\frac{1}{4}$ and the overlying body's Poisson's ratio is infinitesimally small, i.e. ε, and thus, one finds $\nu_b/\nu_f \sim \varepsilon^{-1}$, which violates authors' assumption.

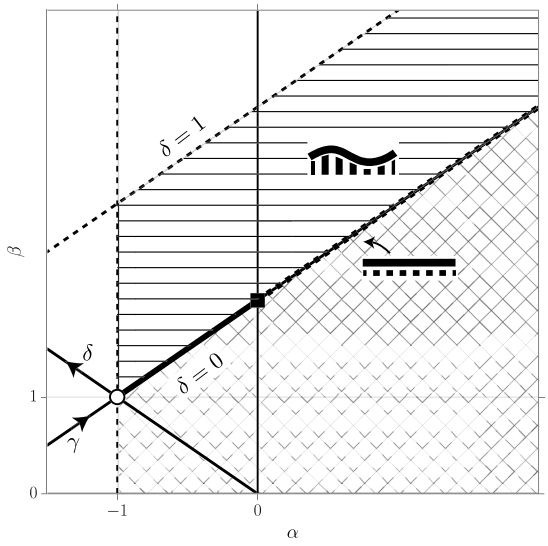

Figure 12: The phase plane: 'The square-hatched region represents systems behaving as "rigid" bodies, under the assumed scaling hypotheses on the loads. Along the open half line (displayed with a thick solid and dashed stroke) $(\delta, 0)$, $\delta > 0$ lay systems whose limit for vanishing thickness leads to a "membrane over in-plane elastic foundation" mode ... The solid segment $0 < \gamma < 1$ (resp. *dashed open line* $\gamma > 1$) is related to systems in which bonding layer is thinner (resp. *thicker*) than the film, for $\gamma = 1$ (*black square*) their thickness is of the same order of magnitude. All systems within the horizontally hatched region $\gamma > 0$, $0 < \delta \leq 1$, $\delta > \gamma$ behave, in the vanishing thickness limit, as "plates over out-of-plane elastic foundation".' [16]. Note that $\gamma = \frac{1}{2}(1+q-\alpha)$, $\delta = \frac{1}{2}(\alpha+q-3)$ and $E_b/E_f \sim \varepsilon^q$.

As a result of the restrictive nature of Poisson's ratios of authors' analysis, they assert that all asymptotic behaviour of the overlying bonded body on an elastic bonding layer can be expressed

on a two-dimensional phase diagram (see figure 12). However, this cannot hold in general as the phase diagram is four-dimensional due to the four asymptotic scalings ($\varepsilon^{\alpha-2}h_b/h_f, \lambda_b/\mu_f, \mu_b/\mu_f, 2\nu_f/(1-2\nu_f)$), for all Poisson's ratios. The only way one may collapse the dimensionality of the phase diagram is by assuming that one is only considering Poisson's ratios with the very specific values $-1 < \nu_f \approx \nu_b < 0$ or $0 < \nu_f \approx \nu_b < \frac{1}{2}$, given that both Poisson's ratios are sufficiently away from 0 and $\frac{1}{2}$.

While describing the rigorous asymptotic analysis, the authors asymptotically rescale the displacement field as $u_\varepsilon = (\varepsilon u^1_\varepsilon, \varepsilon u^2_\varepsilon, u^3_\varepsilon)_{\mathsf{E}}$ (see equation 9 of Baldelli and Bourdin [16]), which is implied by hypothesis 1 of the publication. If one defines the displacement filed as described, then the only physical interpretation is that the planar displacement field $(\varepsilon u^1, \varepsilon u^1, 0)_{\mathsf{E}}$ is infinitesimally small relative to the normal displacement field $(0, 0, u^3)_{\mathsf{E}}$, and such scaling results in only plate like problems.

As an example of their analysis, the authors put forward a model for an overlying film (defined as a membrane) with a very high Young's modulus (i.e. stiff) bonded to an elastic foundation (see theorem 1 of Baldelli and Bourdin [16]). With rigorous mathematics the authors show that there exists a unique solution in $\boldsymbol{H}^1(\omega)$, where ω is the contact surface between the film and the bonding layer (see section 3.2 of Baldelli and Bourdin [16]). Beneath authors' analysis the method in which the authors use to derive the governing equations is simple. Below, we describe in detail the method used by authors to derive the energy functional of a film bonded to an elastic foundation. However, we omit authors' restrictive scalings of the displacement field (see equation 9 of Baldelli and Bourdin [16]) and Poisson's ratios (see figure 1 of Baldelli and Bourdin [16]), and the insufficient asymptotic condition $E_f h_f \gg E_b h_b$, where E_f and E_b are respective Young's moduli of the film and the bonding layer (see definition of δ of Baldelli and Bourdin [16]).

Consider an overlying film with Poisson ratio ν_f, Young's modulus E_f and thickness h_f, and a bonding layer (i.e. foundation) with Poisson ratio ν_b, Young's modulus E_b and thickness h_b. Now, define the displacement field of the film by $\boldsymbol{u} = (u^1(x^1, x^2), u^2(x^1, x^2), 0)_{\mathsf{E}}$ and the displacement field of the foundation by $\boldsymbol{w} = (1 + x^3 h_b^{-1})(u^1(x^1, x^2), u^2(x^1, x^2), 0)_{\mathsf{E}}$, where $x^3 \in (0, -h_b)$. One can see that the displacement field of the foundation satisfies the boundary conditions i.e. when $x^3 = -h_b$, $\boldsymbol{w}$ satisfies zero-Dirichlet boundary condition (i.e. $\boldsymbol{w}|_{x^3=-h_b} = \boldsymbol{0}$), and when $x^3 = 0$, $\boldsymbol{w}$ is same as the displacement field of the film (i.e. $\boldsymbol{w}|_{x^3=0} = \boldsymbol{u}$). Now, the energy functional of the system can be expressed as

$$J(\boldsymbol{u}) = \int_0^{h_f} \int_\omega \left[\frac{1}{2} B^{\alpha\beta\gamma\sigma} \epsilon_{\alpha\beta}(\boldsymbol{u}) \epsilon_{\gamma\delta}(\boldsymbol{u}) - f^\alpha u_\alpha \right] d\omega dx^3 + \int_{-h_b}^0 \int_\omega \frac{1}{2} A^{ijkl} \epsilon_{ij}(\boldsymbol{w}) \epsilon_{kl}(\boldsymbol{w}) \, d\omega dx^3 \, ,$$

where $B^{\alpha\beta\gamma\delta} = \mu_f(2(\lambda_f + 2\mu_f)^{-1}\lambda_f \delta^{\alpha\beta}\delta^{\gamma\delta} + \delta^{\alpha\gamma}\delta^{\beta\delta} + \delta^{\alpha\delta}\delta^{\beta\gamma})$ is the elasticity tensor of the film and $A^{ijkl} = (\lambda_b \delta^{ij}\delta^{kl} + \mu_b \delta^{ik}\delta^{jl} + \mu_b \delta^{il}\delta^{jk})$ is the elasticity tensor of the foundation. Due to Poisson's ratio dependence one comes to the conclusion that $\{\Lambda_f h_f \sim h_b^{-1}\mu_b \mathrm{meas}(\omega; \mathbf{E}^2), \Lambda_f h_f \gg (\lambda_b + 2\mu_b)h_b\}$ is the only possible asymptotic scaling that allows any valid governing equations (i.e. problems that allow traction), where $\Lambda_f = 4(\lambda_f + 2\mu_f)^{-1}\mu_f(\lambda_f + \mu_f)$, and where $\lambda_f = (1 - \nu_f - 2\nu_f^2)^{-1} E_f \nu_f$ and $\mu_f = \frac{1}{2}(1 + \nu_f)^{-1} E_f$ are first and second Lamé's parameters of the film respectively, and

$\lambda_b = (1-\nu_b-2\nu_b^2)^{-1}E_b\nu_b$ and $\mu_b = \frac{1}{2}(1+\nu_b)^{-1}E_b$ are first and second Lamé's parameters of the foundation respectively. To be more precise, above is the asymptotic scaling that allows

$$\int_0^{h_f}\int_\omega \frac{1}{2}B^{\alpha\beta\gamma\delta}\epsilon_{\alpha\beta}(\boldsymbol{u})\epsilon_{\gamma\delta}(\boldsymbol{u})\,d\omega dx^3 \approx \int_{-h_b}^0\int_\omega A^{\alpha 3\beta 3}\epsilon_{\alpha 3}(\boldsymbol{w})\epsilon_{\beta 3}(\boldsymbol{w})\,d\omega dx^3\,,$$
$$\int_0^{h_f}\int_\omega \frac{1}{2}B^{\alpha\beta\gamma\delta}\epsilon_{\alpha\beta}(\boldsymbol{u})\epsilon_{\gamma\delta}(\boldsymbol{u})\,d\omega dx^3 \gg \int_{-h_b}^0\int_\omega \frac{1}{2}A^{\alpha\beta\gamma\sigma}\epsilon_{\alpha\beta}(\boldsymbol{w})\epsilon_{\gamma\delta}(\boldsymbol{w})\,d\omega dx^3\,. \tag{36}$$

To see why relation (36) implies the condition $\Lambda_f h_f \gg (\lambda_b+2\mu_b)h_b$ please consult the proof of theorems 3.9-1 and theorem 4.4-1of Ciarlet [39].

Now, with a little more asymptotic analysis, one can express the leading-order terms of the energy functional of a film bonded to an elastic pseudo-foundation as

$$J(\boldsymbol{u}) = \frac{1}{2}h_f\int_\omega\left[\frac{2\mu_f\lambda_f}{(\lambda_f+2\mu_f)}\epsilon^\alpha_\alpha(\boldsymbol{u})\epsilon^\beta_\beta(\boldsymbol{u}) + 2\mu_f\epsilon^\beta_\alpha(\boldsymbol{u})\epsilon^\alpha_\beta(\boldsymbol{u}) + \left(\frac{\mu_b}{h_f h_b}\right)u_\alpha u^\alpha - 2f^\alpha u_\alpha\right]d\omega\,, \tag{37}$$

where $\epsilon_{\alpha\beta}(\boldsymbol{u}) = \frac{1}{2}(\partial_\alpha u_\beta + \partial_\beta u_\alpha)$, $\forall\ \alpha,\beta\in\{1,2\}$, is the strain tensor, $(f^1,f^2,0)_{\mathsf{E}}$ is an external force density field and ω is the two-dimensional Euclidean domain representing the contact surface. If $\omega\subset\mathbf{E}^2$ is a connected bounded plane with a Lipchitz-continuous boundary $\partial\omega$, and $f^\alpha\in L^1(\omega)$, then there exist a unique minimiser $(u^1,u^2)\in\boldsymbol{H}^1(\omega)$ to equation (37) (see section 1.5 of Ciarlet [37], in particular Korn's inequality on a surface without boundary conditions, but with $u^3=0$). In particular, this unique minimiser is also a critical point in $\boldsymbol{H}^1(\omega)$ (see section 1.5 of Badiale and Serra [13]).

The authors go further with this approach to derive a set of governing equations to describe the behaviour of a bonded overlying stiff plate on an elastic foundation, where now only the normal component of the displacement field of the foundation satisfies zero-Dirichlet boundary condition at foundation's lower boundary (see theorem 2 of Baldelli and Bourdin [16]). The authors define the energy functional to this problem as

$$\begin{aligned}J(\boldsymbol{u}) = &\int_0^{h_f}\int_\omega\left[\frac{1}{2}B^{\alpha\beta\gamma\sigma}\epsilon_{\alpha\beta}(\bar{\boldsymbol{u}})\epsilon_{\gamma\delta}(\bar{\boldsymbol{u}}) - f^\alpha u_\alpha\right]d\omega dx^3\\ &+\int_{-h_b}^0\int_\omega\frac{2\mu_f(\lambda_b+\mu_b)}{\lambda_b+2\mu_b}\epsilon^3_3(\boldsymbol{w})\epsilon^3_3(\boldsymbol{w})\,d\omega dx^3\,,\end{aligned} \tag{38}$$

where

$$\bar{\boldsymbol{u}} = \big(u^1(x^1,x^2)-(x^3-\frac{1}{2}h_f)\partial^1u_3(x^1,x^2), u^2(x^1,x^2)-(x^3-\frac{1}{2}h_f)\partial^2u_3(x^1,x^2), u^3(x^1,x^2)\big)_{\mathsf{E}}\,,$$
$$\boldsymbol{w} = \big(u^1(x^1,x^2), u^2(x^1,x^2), (h_b+x^3)u^3(x^1,x^2)\big)_{\mathsf{E}}\,,$$

are the respective displacement fields of the plate and the foundation.

Unfortunately, authors' theorem 2 is erroneous (see equation 18-22 of Baldelli and Bourdin [16]) and the proof (see section 3.3 of Baldelli and Bourdin [16]) is inapplicable to authors' theorem. For example, one can clearly see that the displacement field is not continuous at the contact region, i.e. $\bar{\boldsymbol{u}}(x^1,x^2,0)\neq\boldsymbol{w}(x^1,w^2,0)$. Authors' proof of theorem 2 is cumbersome and consists of many errors, and thus, in the risk of being pedantic we omit reviewing the proof. Instead, we derive a

solution for a plate bonded to an elastic foundation in accordance with the techniques implied by the proof of theorem 2, but with mathematical precision. Just as before, we omit authors' restrictive scalings of the displacement field (see equation 9 of Baldelli and Bourdin [16]) and Poisson's ratios (see figure 1 of Baldelli and Bourdin [16]), and the insufficient asymptotic condition $E_f h_f \gg E_b h_b$ (see definition of δ of Baldelli and Bourdin [16]).

Let $T^i_j(\boldsymbol{v})$ be the stress tensor and let $\boldsymbol{v}$ be the displacement field of the foundation. Now, consider a situation where the planer stresses are zero, i.e. $T^\alpha_\beta(\boldsymbol{v}) = 0$, $\forall\ \alpha, \beta \in \{1, 2\}$, and use these conditions to modify the elasticity tensor and the displacement field of the foundation, i.e. use the conditions $\epsilon^\alpha_\beta(\boldsymbol{v}) = 0$, $\forall\ \alpha, \beta \in \{1, 2\}$ and $\epsilon^\alpha_\alpha(\boldsymbol{v}) = -(\lambda_b + \mu_b)^{-1}\lambda_b \epsilon^3_3(\boldsymbol{v})$ to obtain $T^j_3(\boldsymbol{v}(\boldsymbol{w})) = (\lambda_b + \mu_b)^{-1}\lambda_b\mu_b\epsilon^3_3(\boldsymbol{v}(\boldsymbol{w}))\delta^j_3 + 2\mu_b\epsilon^j_3(\boldsymbol{v}(\boldsymbol{w}))$, and thus, one gets $T^{j3}(\boldsymbol{w}) = A^{j3kl}_{\text{new}}\epsilon_{kl}(\boldsymbol{w})$, where $A^{j3kl}_{\text{new}} = (\lambda_b + \mu_b)^{-1}\lambda_b\mu_b\delta^{j3}\delta^{kl} + \mu_b\delta^{jk}\delta^{3l} + \mu_b\delta^{jl}\delta^{3k}$ is the new elasticity tensor and $\boldsymbol{w}$ is the new the displacement field of the foundation that satisfies the conditions $\epsilon^\alpha_\beta(\boldsymbol{w}) = 0$, $\forall\ \alpha, \beta \in \{1, 2\}$. Now, seek a displacement field $\boldsymbol{w}$ of the form such that $\epsilon^\alpha_\beta(\boldsymbol{w}) = 0$, $\epsilon^j_3(\boldsymbol{w}) \neq 0$ and $w^3(x^1, x^2, -h_b) = 0$, and thus, one finds $\boldsymbol{w} = (1 + h_b^{-1}x^3)(0, 0, u^3(x^1, x^2))_{\mathsf{E}}$, where $x^3 \in (0, -h_b)$. Now, assume that there is an overlying plate bonded to the foundation. As the displacement filed at the contact region must be continuous, one finds that the displacement field of the plate is $\bar{\boldsymbol{u}} = (-x^3\partial^1 u_3(x^1, x^2), -x^3\partial^2 u_3(x^1, x^2), u^3(x^1, x^2))_{\mathsf{E}}$, where $x^3 \in [0, h_f)$. Due to Poisson's ratio dependence, one comes to the conclusion that $\{\Lambda_f h_f^3 \sim h_b^{-1}\mu_b(\lambda_b + \mu_b)^{-1}(3\lambda_b + 2\mu_b)(\text{meas}(\omega; \mathbf{E}^2))^2, \Lambda_f h_f^3 \gg h_b\mu_b\text{meas}(\omega; \mathbf{E}^2)\}$ is the only possible asymptotic scaling that allows any valid governing equations (i.e. that allows Winkler foundation type problems), i.e. the asymptotic scaling that allows

$$\begin{aligned}
&\int_0^{h_f}\int_\omega \frac{1}{2}B^{\alpha\beta\gamma\delta}\epsilon_{\alpha\beta}(\bar{\boldsymbol{u}})\epsilon_{\gamma\delta}(\bar{\boldsymbol{u}})\ d\omega dx^3 \approx \int_{-h_b}^0\int_\omega \frac{1}{2}A^{3333}_{\text{new}}\epsilon_{33}(\boldsymbol{w})\epsilon_{33}(\boldsymbol{w})\ d\omega dx^3\ , \\
&\int_0^{h_f}\int_\omega \frac{1}{2}B^{\alpha\beta\gamma\delta}\epsilon_{\alpha\beta}(\bar{\boldsymbol{u}})\epsilon_{\gamma\delta}(\bar{\boldsymbol{u}})\ d\omega dx^3 \gg \int_{-h_b}^0\int_\omega A^{\alpha3\beta3}_{\text{new}}\epsilon_{\alpha3}(\boldsymbol{w})\epsilon_{\beta3}(\boldsymbol{w})\ d\omega dx^3\ .
\end{aligned} \tag{39}$$

To see why relation (39) implies the condition $\Lambda_f h_f^3 \sim h_b^{-1}\mu_b(\lambda_b + \mu_b)^{-1}(3\lambda_b + 2\mu_b)(\text{meas}(\omega; \mathbf{E}^2))^2$ please consult the proof of theorems 3.9-1 and theorem 4.4-1of Ciarlet [39].

Now, with a little more asymptotic analysis one can express the leading-order terms of the energy functional of an overlying plate on an elastic pseudo-foundation as

$$J(\boldsymbol{u}) = \frac{1}{2}h_f\int_\omega \left[\frac{1}{3}\Lambda_f h_f^2\Delta u_3\Delta u^3 + \frac{\mu_b}{h_f h_b}\left(\frac{3\lambda_b + 2\mu_b}{\lambda_b + \mu_b}\right)u_3u^3 - 2f^3u_3\right]d\omega\ , \tag{40}$$

where Δ is the scalar Laplacian in the Euclidean plane and f^3 is a force density. As the reader can clearly see that equation 38 is different to equation 40, i.e. there exist clear discrepancies between what Baldelli and Bourdin's [16] theorem 2 and the method implied by the proof of theorem 2. Note that we used the condition $\partial_\beta u^3|_{\partial\omega} = 0$, $\forall\ \beta \in \{1, 2\}$, to obtain equation (40), where $\boldsymbol{n}$ is the unit outward normal to the boundary of the plate $\partial\omega$.

Equation (40) is a Winkler foundation type problem for a plate that is supported by a continuous bed of springs with a foundation modulus of $h_b^{-1}\mu_b(\lambda_b + \mu_b)^{-1}(3\lambda_b + 2\mu_b)$. Furthermore, if $\omega \subset \mathbf{E}^2$ is an connected bounded plane with a Lipchitz-continuous boundary $\partial\omega$, $f^3 \in L^1(\omega)$, and $\partial_\beta u^3|_{\partial\omega} = 0$,

$\forall\ \beta \in \{1,2\}$, in a trace sense, then there exists a unique minimiser $u^3 \in H^2(\omega)$ to equation (40) (see section 1.5 of Ciarlet [37], in particular Korn's inequality on a surface without boundary conditions, but with $(u^1, u^2)_{\mathsf{E}} = \mathbf{0}$). In particular, this unique minimiser is also a critical point in $H^2(\omega)$ (see section 1.5 of Badiale and Serra [13]).

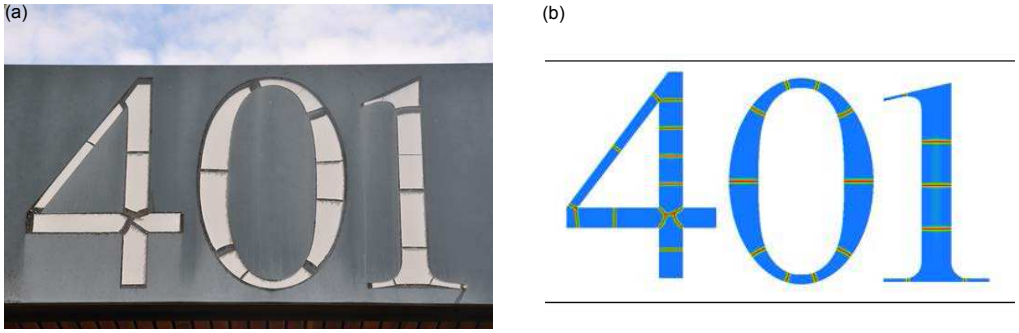

Figure 13: (a) 'Cracked lettering at Ecole Polytechnique, Palaiseau, France. A vinyl sticker is bonded to an aluminium substrate and exposed to the sun which causes tensile stresses and subsequent cracking.' (b) 'Numerical experiment: nucleation at weak singularities, multiple cracking in the smooth domain, periodic fissuration of slender segments' [15].

Despite above highlighted flaws, the strength of Baldelli and Bourdin's [16] work appears lies in the study of overlying bonded films on elastic foundations, where A. A. L. Baldelli [15][10] uses the bonded film model to examine the crack patterns that occurs in thin structures, which is the subject of his PhD thesis (see page 147 of Baldelli [15]). Baldelli [15] numerically shows that, without any priori assumptions on the crack geometry, one can capture complex evolving crack patterns in different asymptotic regimes: parallel, sequential, periodic cracking and possible debonding in a uni-axial traction test as well as the appearance of polygonal crack patterns in a two-dimensional equi-biaxial load, and cracking in a geometrically complex domain. One of the perfect examples of author's work is a comparison against a real life crack pattern and author's numerical model, which the reader can see in figure 13: author's numerical result in figure 13 (b) is almost identical to the real crack pattern observed in figure 13 (a). Note that we cannot comment on the validity of author's numerical results with any degree of certainty as author's asymptotic method only utilises linear elasticity, while the study plastic deformations, such as factures and cracks, is conducted with nonlinear elasticity in the existing literature. For more on the numerical study of crack formation please consult Sumi [188].

In conclusion, Baldelli and Bourdin's [16] work is flawed and valid only when describing the behaviour of overlying bonded films on elastic pseudo-foundations (note that authors' foundation is not an actual elastic foundation as the displacement field of the foundation is grossly over simplified), where Poisson's ratios of the both bodies are in between -1 and 0 or in between 0 and $\frac{1}{2}$ (where both Poisson's ratios are sufficiently away from 0 and $\frac{1}{2}$), and with the asymptotic condition $\{E_f h_f \sim h_b^{-1} E_b \mathrm{meas}(\omega; \mathbb{R}^2), E_f h_f \gg E_b h_b\}$. The authors assert that their method is the

[10] http://citeseerx.ist.psu.edu/viewdoc/download?doi=10.1.1.402.3946&rep=rep1&type=pdf

correct method of derivation of Winkler foundations equations, but this is false statement as Winkler foundation is a very specific mathematical problem (see chapter 5 of Kikuchi and Oden [102]) and different to what the authors put forward. The authors further assert that their asymptotic approach is valid for all elastic properties. However, we mathematically proved that the asymptotic approach is only valid if both Poisson's ratios are in between -1 and 0 or in between 0 and $\frac{1}{2}$ (where both Poisson's ratios are sufficiently away from 0 and $\frac{1}{2}$). For all Poisson's ratios authors' phase diagram is four-dimensional and not two-dimensional as the authors present. Also, due to the Poisson's ratio dependence the only scalings that can yield any valid asymptotic solutions are $\{\Lambda_f h_f \sim h_b^{-1}\mu_b \mathrm{meas}(\omega;\mathbb{R}^2), \Lambda_f h_f \gg (\lambda_b + 2\mu_b)h_b\}$ for a film that is bonded to an elastic foundation, and $\{\Lambda_f h_f^3 \sim h_b^{-1}\mu_b(\lambda_b + \mu_b)^{-1}(3\lambda_b + 2\mu_b)(\mathrm{meas}(\omega;\mathbb{R}^2))^2, \Lambda_f h_f^3 \gg h_b\mu_b\mathrm{meas}(\omega;\mathbb{R}^2)\}$ for a plate that is supported by an elastic foundation, but not $E_f h_f \gg E_b h_b$ as the authors present. Authors' scaling of the displacement field implies that the method cannot be applicable to films (or strings) with planar loading, unless u^3 is zero. Finally, authors' method cannot be applied to plates due to the structure of the overlying body (i.e. limits of integration of the plate) and the foundation (i.e. planer-stress free condition of the foundation), unless field $(u^1, u^2)_{\mathsf{E}}$ is identically zero.

In chapter 3, we extend Baldelli and Bourdin's [16] model for bonded films on elastic foundations to curvilinear coordinates with mathematical rigour (original work) and conduct numerical experiments to see its effectiveness.

1.11 A Critical Study of the Work of Kikuchi and Oden

Kikuchi and Oden [102][11] present a comprehensive analysis of the Signorini's problem, Coulomb's law of static friction and non-classical friction laws. The work includes meticulous documentation of the existence, the uniqueness and the regularity results for the given mathematical problems with finite-element modelling techniques, where the numerical analysis techniques are treated with a significant degree of mathematical rigour. Also, each method consists of peer-reviewed numerical examples and real life data. As far as we, and the authors, are aware that this is the most comprehensive documentation and analysis of the problem of unilateral contact that attempts to unify physical problems of contact with the mathematical modelling and numerical implementation of the mathematical models, as well as their applications to real-world problems.

Signorini's problem [178, 179] is a class of contact problems that study the deformation of a body that is unilaterally supported by a frictionless (lubricated) rigid foundation. The study of this problem is unusually complicated as the actual surface on which the body comes into contact with the foundation is unknown prior to the problem. Thus, the range and the geometry of the actual contact region are calculated as a part of the solution. Furthermore, the variational formulation is an inequality, an thus, the process of finding numerical solutions is far more complicated than with ordinary variational-problems. We discuss this problem in more detail in Section 5.4.

[11] https://books.google.co.uk/books?isbn=0898714680

Kikuchi and Oden [102] analyse the problem by considering equilibrium of a linearly elastic body in contact with a frictionless rigid foundation and derive a variational inequality to represent the given problem. In chapter 6 of the publication the authors show results on the existence and the uniqueness of solutions, and the approximation of solutions of such problems by means of penalty methods. They present the formulation and the analysis of rigid punch problems and provide a solution-method based on Uzawa's iterative scheme for solving saddle point problems. The authors give many examples of the rigid punch problem modelled by Q2-elements and Simpson's rule. They conclude the chapter with the formulation and the analysis of two-body contact problems as an extensions of Signorini's problem, and further propose a numerical scheme for two-body contact problems. Unfortunately, no numerical examples are given for the two-body case.

The latter part of the publication is dedicated to the study of dry-friction (see chapter 10 of Kikuchi and Oden [102]), Coulomb's law of static friction in particular. Given that ν_F is the coefficient of friction, $\boldsymbol{\sigma}_T(\mathbf{u})$ is the tangential stress tensor and $\sigma_n(\mathbf{u}) < 0$ is the normal stress at the contact boundary, Coulomb's law can be expressed as

$$\begin{aligned}
&\text{if } \ |\boldsymbol{\sigma}_T(\mathbf{u})| < \nu_F|\sigma_n(\mathbf{u})| \ , \text{ then } \mathbf{u}_T = \mathbf{0} \ , \text{ or} \\
&\text{if } \ |\boldsymbol{\sigma}_T(\mathbf{u})| = \nu_F|\sigma_n(\mathbf{u})| \ , \text{ then } \ \exists\lambda \geq 0 \ \text{ such that } \ \mathbf{u}_T = -\lambda\boldsymbol{\sigma}_T(\mathbf{u}) \ ,
\end{aligned}$$

where $\mathbf{u}$ is the displacement field and $\mathbf{u}_T$ is the tangential displacement field of the contact boundary. It is shown by Demkowicz and Oden [54] that these conditions can alternatively be expressed as

$$\begin{aligned}
&\text{if } \ |\boldsymbol{\sigma}_T(\mathbf{u})| < \nu_F|\sigma_n(\mathbf{u})| \ , \text{ then } \ (\nu_F|\sigma_n(\mathbf{u})| - |\boldsymbol{\sigma}_T(\mathbf{u})|)\mathbf{u}_T = \mathbf{0} \ , \text{ or} \\
&\text{if } \ |\boldsymbol{\sigma}_T(\mathbf{u})| = \nu_F|\sigma_n(\mathbf{u})| \ , \text{ then } \ \boldsymbol{\sigma}_T(\mathbf{u}) \cdot \mathbf{u}_T + \nu_F|\sigma_n(\mathbf{u})||\mathbf{u}_T| = 0 \ .
\end{aligned}$$

Given that one is considering Signorini's problem, one may express the variational formulation for Coulomb's law as

$$\mathbf{u} \in \mathbf{V} : a(\mathbf{u}, \mathbf{v} - \mathbf{u}) + j(\mathbf{v}) - j(\mathbf{u}) \geq f(\mathbf{v} - \mathbf{u}) \ , \ \forall \ \mathbf{v} \in \mathbf{V} \ , \tag{41}$$

where

$$\begin{aligned}
\mathbf{V} &= \{\mathbf{v} \in \mathbf{H}^1 \mid \mathbf{v}_T = \mathbf{0}\} \ , \\
j(\mathbf{u}, \mathbf{v}) &= \int_\Gamma \nu_F|\sigma_n(\mathbf{u})||\mathbf{v}_T| \ ds \ , \ \mathbf{u}, \mathbf{v} \in \mathbf{V} \ , \\
a(\mathbf{u}, \mathbf{v}) &= \int_\Omega \sigma_{ij}(\mathbf{u})\epsilon_{ij}(\mathbf{v}) \ dx \ , \ \mathbf{u}, \mathbf{v} \in \mathbf{V} \ , \\
f(\mathbf{v}) &= \int_\Omega \mathbf{f} \cdot \mathbf{v} \ dx + \int_{\Gamma_F} \mathbf{t} \cdot \mathbf{v} \ ds \ , \ \mathbf{v} \in \mathbf{V} \ ,
\end{aligned} \tag{42}$$

and where $\mathbf{f}$ is an external force density field, $\mathbf{t}$ is a external traction applied at some boundary Γ_F, and Γ is the contact boundary.

Equation (41) is non-convex and non-differentiable, and therefore, cannot be analysed by the conventional mathematical methods; thus, the question of existence of solutions remains open. The culprit is equation (42), because it is non-convex, non-differentiable, and, coupled with formulation of Signorini's problem, it makes the problem almost impossible to mathematically analyse. To

simplify this problem Kikuchi and Oden [102] disregard Signorini's problem by assuming that the contact region of the body is fixed and prescribed, and attempt to approximate equation (42).

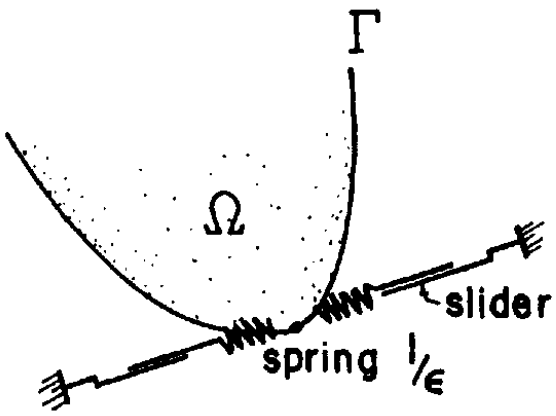

Figure 14: System of springs and sliders attached to an elastic boundary [102].

Consider a uniformly distributed system of springs and sliders attached to the boundary of an elastic body in such a way as to resist tangential motions (see figure 14), which can be formulated as

$$j_\varepsilon(\mathbf{u}) = \begin{cases} \displaystyle\int_\Gamma \left[\mathscr{K}|\mathbf{u}_T| - \frac{1}{2}\varepsilon \right] ds \ , \text{ if } |\mathbf{u}_T| \geq \varepsilon \ , \\ \displaystyle\int_\Gamma \frac{1}{2}\mathscr{K}\frac{|\mathbf{u}_T|^2}{\varepsilon}\, ds \qquad , \text{ if } |\mathbf{u}_T| < \varepsilon \ , \end{cases} \tag{43}$$

where $\mathscr{K}$ (units: Nm^{-2}) is the spring modulus of the springs and ε is the *regularisation parameter*. If one assumes that the purely normal stress σ_n (pressure) is no longer an unknown, but it is prescribed, and further assumes that $\mathscr{K} = -\nu_F \sigma_n$, then one sees that the boundary condition $j_\varepsilon(\cdot)$ satisfies Coulomb's law of static friction in the limit $\varepsilon \to 0$. This is even more evident if one takes the Gâteaux derivative of $j(\cdot)$ and rearranging it before taking the $\varepsilon \to 0$ limit to find

$$\sigma_T(\mathbf{u}) = \begin{cases} \nu_F \sigma_n \dfrac{\mathbf{u}_T}{|\mathbf{u}_T|} \ , \text{ if } |\mathbf{u}_T| \geq \varepsilon \ , \\ \nu_F \sigma_n \dfrac{\mathbf{u}_T}{\varepsilon} \quad , \text{ if } |\mathbf{u}_T| < \varepsilon \ . \end{cases} \tag{44}$$

The authors prove that $j_\varepsilon(\cdot)$ (43) is convex and Gâteaux differentiable, and thus, weakly lower semi-continuous on all of $\mathbf{V}$, $\forall\ \varepsilon > 0$ (see Lemma 10.1 of Kikuchi and Oden [102]).

With the use of $j_\varepsilon(\cdot)$ the pseudo-variational form for an elastic body subject to Coulomb's law of static friction with a prescribed pressure can be written as a perturbed potential energy functional, which can be expresses as

$$F_\varepsilon(\mathbf{u}) = \frac{1}{2}a(\mathbf{u},\mathbf{u}) - f(\mathbf{u}) + j_\varepsilon(\mathbf{u}) \ . \tag{45}$$

The authors prove that the perturbed potential energy functional (45) has a unique solution $\mathbf{u}_\varepsilon$, $\forall\ \varepsilon$ (see theorem 10.3 of Kikuchi and Oden [102]). Furthermore, they prove that the solution $\mathbf{u}_\varepsilon$ strongly converge to a solution $\mathbf{u}$ as $\varepsilon \to 0$ (see theorem 10.3 of Kikuchi and Oden [102]).

The implication of this approach is that one has a mathematically proven theory to model a real-life phenomenon, and the theory is simple enough to be numerically modelled. If $|\mathbf{u}_T| < \varepsilon$, then it means the body is sticking, i.e. *bonded* to the boundary as the shear acting on the body at the boundary (in that given region) is not great enough to yield any displacements. If $|\mathbf{u}_T| \geq \varepsilon$, then the authors define that the body is sliding. However, this terminology is ambiguous as this is a static problem. Thus, $|\mathbf{u}_T| \geq \varepsilon$ must imply that the body has debonded but still stationary, i.e. it must imply that the shear acting on the body (in that given region) is great enough to break contact and now the body is at the *static equilibrium* state (at the point of slipping).

Note that the $j_\varepsilon(\cdot)$ is a nonlinear function of $\mathbf{u}$, even though the authors only consider linear elasticity. However, numerical solutions can still be obtained via the use of methods such as Newton-Raphson method for nonlinear PDEs. Thus, the authors meticulously describe a finite-element algorithm for solving equation (45) (see chapter 10.6 of Kikuchi and Oden [102]).

It is important to note that the authors only consider very simple problems where the pressure is known a quantity prior. Now, consider the initial problem of Coulomb's law of static friction where the pressure is an unknown. For this, the authors go further (see chapter 10.7 of Kikuchi and Oden [102]) and give a sketch proof to the problem by claiming that, if one prescribes an appropriate initial guess for the pressure to the reduced problem (45), then one can use the numerical solution to calculate an updated pressure, and thus, feeding this new value of the pressure back in to the reduce problem (45) should provide one an iteratively converging method to obtain a solution for Coulomb's law of static friction. However, this approach is not handled with the same mathematical rigour as previous sections, and thus, the mathematical viability of this approach remains as an open question. Fortunately, this method does work, numerically at least, as the authors conclude the chapter with an abundance of numerical examples.

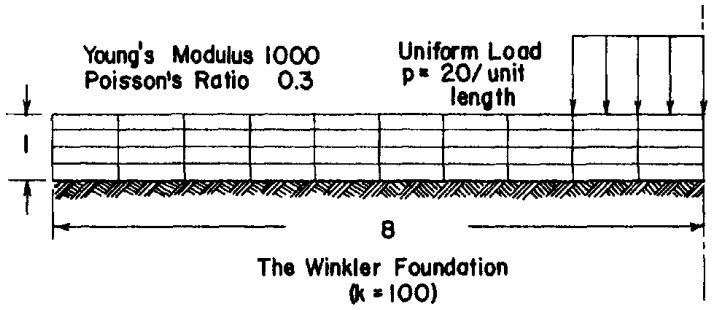

Figure 15: 'finite-element model of an elastic slab resting on a Winkler foundation' [31].

One example that the authors present is a numerical solution of a thick elastic slab resting on a Winkler foundation, between which Coulomb's law holds. Four-node bilinear elements and the regular mesh are used to discretise a slab of unit width, length B and thickness I. The foundation is assumed to have a spring constant of 100Pa, and a regularisation parameter of 10^{-5} is used. A pressure of 20Pa is applied as indicated in figure 15, and numerical solutions are calculated for no friction case (i.e. $\nu_F = 0$) and friction case with a coefficient of friction of 0.5. Numerical results

show that in the non-friction case the contact area is smaller and the magnitude of the deformation is smaller owing to the absence of frictional forces, with respect to the to the friction case. The results also demonstrate that the classical Kirchhoff hypothesis of beam theory is not valid when frictional forces are present. This is due to the fact that plane and normal sections to slab's axis before deformation are not plane and normal (respectively) to slab's axis after deformation.

Note that similar work for Coulomb's law of static friction is attempted by Panagiotopoulos [148, 149]. One approach author present is the numerical scheme for solving Signorini's problem with friction based on stochastic optimisation concepts. Such work is beyond the scope of our understanding, and thus, it is not discussed any further.

A very important section of Kikuchi and Oden [102] is Chapter 5, where variational formulations of contact problems in elasticity are present: trace theorems, Green's formulas and Korn's inequalities which are crucial for showing the existence of solutions of contact problems. But, more importantly, the authors supply precise mathematical formulations for various contact problems, which include Dirichlet conditions (i.e. constrained displacements), Neumann conditions (i.e. applied traction), elastic springs are attached normally and tangentially to the boundary (i.e. bonded to an elastic foundation), on a bed of continuously distributed springs (i.e. Winkler foundation), uniformly distributed system of springs and sliders (i.e. Coulomb's law of static friction as we already discussed) and many more.

By authors' analysis, elastic springs that are attached normally and tangentially to the boundary can approximately simulate the bonding to an elastic foundation. Note that this is the same form of the formulation is proposed by Baldelli and Bourdin's [16] (consider the boundary condition at the contact region) before the asymptotic analysis.

Kikuchi and Oden [102] define the formulation of Winkler foundation as

$$F_w(\mathbf{u}) = \frac{1}{2}a(\mathbf{u},\mathbf{u}) - f(\mathbf{u}) + j(\mathbf{u})_w \ , \tag{46}$$

where

$$j_w(\mathbf{u}) = \begin{cases} \displaystyle\int_\Gamma \frac{1}{2}\mathscr{K}_0(u_n - g)^2 \, ds \ , \text{ if } (u_n - g) \geq 0 \ , \\ 0 \qquad\qquad\qquad\qquad\quad , \text{ if } (u_n - g) < 0 \ , \end{cases}$$

and where $\mathscr{K}_0$ (units: Nm^{-3}) is the foundation modulus [57] (erroneously defined as the spring modulus by Kikuchi and Oden [102]), u_n is the normal component of the displacement field at the contact boundary and g is the gap function between the contact boundary of the body and the foundation. Thus, the equation describing an elastic body resting on bed of continuously distributed springs, i.e. the Winkler foundation, is given by the equation

$$(u_n - g)^+ = -\frac{1}{\mathscr{K}_0}\sigma_n(\mathbf{u}) \ \text{ in } \ L^2(\Gamma) \ , \tag{47}$$

where $\sigma_n \leq 0$ and $(\cdot)^+ = \max(\cdot, 0)$. Note how equation (47) is different to what Baldelli and Bourdin's [16] present as Winkler foundation equations.

From chapter 11 and beyond the authors examine a more general class of contact problems with friction. These problems are non-classical and nonlinear with a vast number of models to model applications in static, quasi-static, and dynamic contact problems. Problems of large deformation, rolling contact, inelastic materials, phenomena such as stick and slip behaviour, and the mechanics of dry-friction between metallic bodies are all analysed. As the latter sections contain work still very much in development, the authors do not treat these chapters with the same mathematical or numerical rigour as they do with the previous chapters.

Regarding commercial applications, in the introductory section, the authors comment 'The large treatise of Bowden and Tabor [28], for example, represents a classical treatment of the physics of friction; while the National Bureau of Standards Monograph on the Mechanics of Pneumatic Tires edited by Clark [41] is a frequently referenced source on practical solutions for contact and friction problems encountered in tire design' [102].

If the reader is interested in historical notes on Signorini's problem and Coulomb's law of static friction or friction laws in general please consult chapter 1 of Kikuchi and Oden [102], where the reader can find a richly detailed mathematical history of the subject.

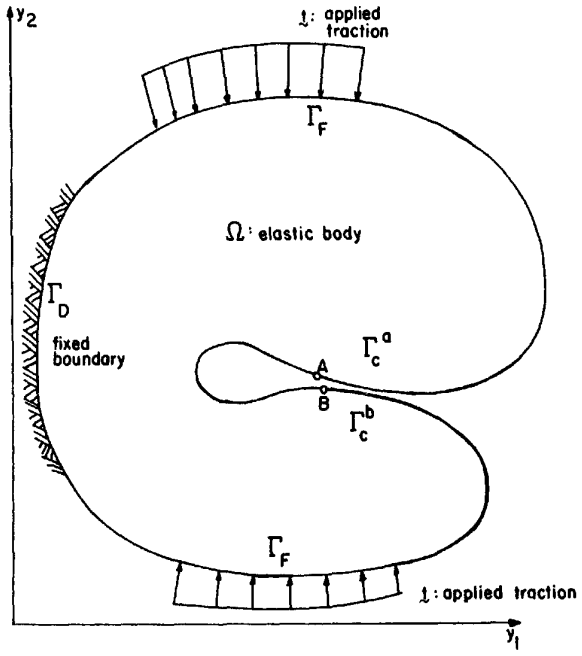

Figure 16: 'Contact of two surfaces.' [102] (Kikuchi and Oden's [102] pseudo-two-body contact problem).

Kikuchi and Oden's [102] work is the basis for most of our work from Chapters 2, 5, 6 and Chapter 4 in particular. Note that some of the work present in this publication remains incomplete. One of the limitations of authors' work is that they only consider the Euclidean geometry. Another is that the authors never attempt a full two-body friction problem. The two-body problem the authors consider is a single elastic body that is being folded in on itself so one only needs to consider a single displacement field (see figure 16 or see section 6.8 of Kikuchi and Oden's [102]). Thus, in

latter chapters of our thesis we extend Kikuchi and Oden's [102] model for Coulomb's law of static friction to the curvilinear space and then to model the full two-body contact problem, and use the numerical solutions to compare against our own models. Most importantly, we treat the our models with the same mathematical rigour as seen in Kikuchi and Oden [102].

1.12 A Critical Study of the Work of Jayawardana *et al.*

Jayawardana *et al.* [89][12] (the principal author is C. Ortner) analyse the validity of the surface Cauchy-Bourne model relative to the Cauchy-Bourne model, when approximating the atomistic model for large stiffness parameters. The authors show numerically that, if the mean strain between the atomistic solution and Cauchy-Bourne solution is order 1, then the mean strain between the atomistic solution and surface Cauchy-Bourne solution is order $\exp(-\alpha)$ for a chain of semi-infinite atoms, where α is the stiffness parameter.

Consider an atomic lattice. Relative to the atoms that lie within the material bulk, the surface atoms have fewer bonding neighbouring atoms. Now, this results in the elastic properties of surfaces atoms being different from elastic properties of the atoms that occupy the interior, which is an affect not observed in continuum mechanics, and such properties are observed in real life and documented in the literature. For example, Cuenot *et al.* [52] observe that the elastic modulus of the silver and lead nano-wires on polypyrrole nano-tubes with smaller diameters is significantly higher than elastic modulus of ones with larger diameters. They conclude that the increase in the apparent elastic-modulus for the smaller diameter ones is a result of surface tension effects. Study of objects with large surface area to volume ratio, such as nano-wires, is an area of focus in the recent years for their applications in next generation electronics, opto-electronics and sensor systems [151].

When studying the behaviour of a particular body below the length scale of 100 nanometres (nm = 10^{-9}m), it is experimentally observed that such bodies stop behaving as a continuum as the interaction between individual particles becomes more significant [120]. Thus, if one wishes to observe a solid at this scale, often referred to as the nanoscopic scale in the literature, then one must depart from conventional continuum mechanics of elasticity. One of the common ways of modelling a nanoscale body is by taking account of each atom and its interaction with its neighbouring atoms. This is often referred to as the atomistic model. For a one-dimensional semi-infinite chain of atoms with the deformed configuration y the total energy maybe written as

$$E^a(y) = \sum_{j=0}^{\infty} \left(\phi(y_{j+1} - y_j) + \phi(y_{j+2} - y_j)\right) \ ,$$

where ϕ is shifted Morse potential, which is defined as $\phi(r) = \exp(-2\alpha(r - r_0)) - 2\exp(-\alpha(r - r_0)) - \phi_0$ [140]. Morse potential is a map that represents the interaction between an atom and its first and second neighbour, and α is the stiffness between these interactions, i.e. the molecular bond. For authors' purposes, they only consider large values of α, in particular, $\alpha \geq 1 + \sqrt{3}$. This ensures that $\phi''(2) \leq 0$ which is vital for the error analysis.

[12] http://wrap.warwick.ac.uk/56730/1/WRAP_2013-M2AN-ac.scb.1d.pdf

Now, introduce the potential $W(r) = \phi(r)+\phi(2r)$, which is defined as Cauchy-Bourne stored energy density. Now, choose ϕ_0 such that $W(1) = 0$ to ensures that $E^a(id)$ is finite, where id is the zero-Deformation configuration of the chain of atoms. Also, choose r_0 such that $W'(1) = 0$, which can be explicitly expressed as

$$r_0 = 1 + \frac{1}{\alpha}\log\left(\frac{1+2\exp(-\alpha)}{1+2\exp(-2\alpha)}\right) . \tag{48}$$

The drawback of using an atomistic model to model nanoscale materials is that it is computationally expensive. The equations are nonlinear and it is given that a fully atomistic simulation of a nano-structure object on the scale of 100 nanometres requires a model consisting of order 10^8 atoms. Thus, it motivates one to seek alternative methods to model bulk behaviour of the body: perhaps by approximating the atomistic model. One such model is Cauchy-Bourne model. This is a mathematical approximation to model the bulk behaviour of stiff material such as crystals. Cauchy-Bourne model assumes that the configuration of the atoms is uniform throughout the medium, and thus, the stored energy density is chosen such that 'Cauchy-Bourne energy is exact under homogeneous deformations in the absence of defects' [89]. As a consequence, any contributions made to the energy functional by the surface, cracks or point forces are completely ignored.

For a one-dimensional semi-infinite chain of atoms the total Cauchy-Bourne energy can be defined as

$$E^{cb}(y) = \sum_{j=0}^{\infty} h_j W(y'_j) , \tag{49}$$

where h_j are the atomic spacing and y' is the forward finite-difference operator, which is defined as $y'_j = y_{j+1} - y_j$ with $y_0 = 0$. Note that Cauchy-Bourne model is derived from the atomistic model by replacing the second-order interaction by localised quantities, i.e. $\phi(y'_j + y'_{j+1}) \approx \frac{1}{2}(\phi(2y_j) + \phi(2y_{j+1}))$.

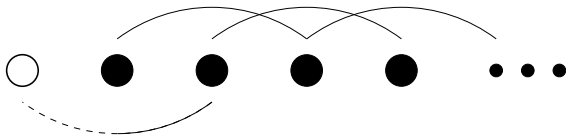

Figure 17: Graphical representation of an over-counted left-hand bond by Cauchy–Born model [89].

Note that in Cauchy-Bourne model one counts the second-neighbour interaction at the edge too often (see figure 17). Thus, surface Cauchy-Bourne model is derived by removing this over counted quantity $\frac{1}{2}\phi(2y'(0))$ from the boundary. Thus, for a one-dimensional semi-infinite chain of atoms total surface Cauchy-Bourne energy can be defined as

$$E^{scb}(y) = \sum_{j=0}^{\infty} h_j W(y'_j) - \frac{1}{2}\phi(2y'(0)) .$$

Surface Cauchy-Borne model is a recently developed mathematical model by Park *et al.* [153, 154, 155] to study surface-dominated nanoscale structures. It is successfully applied to various nano-mechanical boundary value problems such as surface stress effects due to thermo-mechanical

coupling [216], the resonant properties of silicon nano-wires [154, 150], surface stress effects on the bending of face-centred cubic metal nano-wires [217] and the electromechanical coupling in surface-dominated nanostructures to externally applied electric fields [152].

The choice of r_0 implies that the value 1 is the minimiser of Cauchy-Bourne stored energy function. This implies that the solution to equation (49) is given by the equation $(u_j^{cb})_{j=0}^{\infty} = \mathbf{0}$, which is defined as Cauchy-Bourne ground state. Notice that at Cauchy-Bourne ground state the distance between each atom is 1. However, consider the boundary of the chain of atom (described by both atomistic model and surface Cauchy-Bourne model): the distance between the boundary atom and its neighbouring atom maybe greater as a result of the relaxation of the atom at the boundary. Define this distance as h_0. Now, the error analysis can be split into two cases: case $h_0 = 1$ and case $h_0 > 1$. Note that $h_0 > 1$ is the physically realistic result.

To conduct error analysis define the relative error as

$$Err_p = \frac{||u^{scb} - u^a||_{\ell^p}}{||u^a||_{\ell^p}} \,, \tag{50}$$

where u^{scb}, u^a are respectively the solutions of surface Cauchy-Bourne model and the atomistic model with respect to Cauchy-Bourne ground state. With asymptotic analysis the authors show that the relative error is between the values $\frac{1}{2}$ and 2 for $h_0 > 1$, and the error is $2^{1/p}\exp(-\alpha)$ for $h_0 = 1$. This implies that the discrete (i.e. point wise) positioning of the atoms described by surface Cauchy-Bourne model is closer to the atomistic model than described by the regular Cauchy-Bourne model, for the $h_0 > 1$ case. Unfortunately, if $h_0 > 1$, then the accuracy gained by using surface Cauchy-Bourne model over Cauchy-Bourne model is negligible.

However, the goal of Cauchy-Bourne and surface Cauchy-Bourne models are to describe the bulk behaviour of the body: the chain of atoms in this case. Thus, introduce the notion of mean strain by the error metric

$$\bar{E}rr = \left| \frac{\sum_{j=0}^{\infty}(u_j^{scb} - u_j^a)}{\sum_{j=0}^{\infty} u_j^a} \right| \,. \tag{51}$$

With asymptotic analysis the authors show that the mean-stain error is $2(1 - h_0^{-1})\exp(-\alpha) + \mathcal{O}(\exp(-2\alpha))$. This is the most crucial result of this publication. It shows that surface Cauchy-Bourne model substantially improve the accuracy of Cauchy-Bourne model at a small additional computational cost when approximation the atomistic model in the study of bulk behaviour. The relevance of this publication is that, as far as the authors aware, this work presents the first error analysis of surface Cauchy-Bourne method.

The authors go further by numerically calculating the relative error and mean-strain error for a chain consisting of 31 atoms with the stiffness parameter ranging between 3 and 7, and for the first atomic spacing $h_0 = 1$ and $h_0 = 5$. Note that the authors chose to let $r_0 = 1$ in their numerical error-analysis and it unclear why they do so as $r_0 > 1$, $\forall \alpha \in \mathbb{R}$ (see equation (48)).

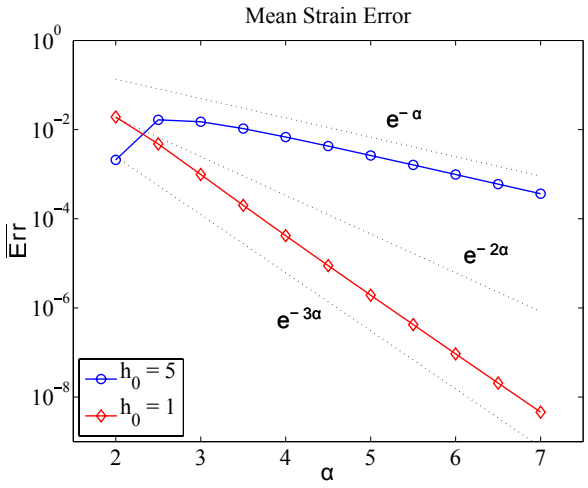

Figure 18: Relative error in the $W^{1,2}$-seminorm of the 1D nonlinear SCB model for varying stiffness parameter α [89].

Jayawardana *et al.* [89] numerically find that the relative error for $p = 2$ is again is order 1 for the $h_0 = 5$ case and order $\exp(-\alpha)$ for the $h_0 = 1$ case. Authors' mean-strain error is order $\exp(-3\alpha)$ for the $h_0 = 5$ case, and order $\exp(-\alpha)$ for the $h_0 = 1$ case (see figures 18). The authors do not speculate on the discrepancy between the asymptotic mean stain error and the numerical mean stain error for the $h_0 = 5$ case. But note that the asymptotic results are obtained for a semi-infinite chain of atoms whilst the numerical results are obtained for a finite chain of atoms. Perhaps difference in the length of the chain of atoms may lead to the discrepancy. Either way, the numerical results further justify the use of surface Cauchy-Bourne model over ordinary Cauchy-Bourne model.

The latter part of the publication extends the error analysis to a two-dimensional lattice of atoms. However, our knowledge in this area is very limited, and thus, we refrain from examining this section in detail. In this latter part of the publication, authors' numerical results for domains with corners are inconclusive. This is due to the coupling between the normal stress and tangential stress of adjacent edges, which creates additional elastic fields. The authors conclude by proposing that a finer analysis is needed to estimate the corrections to the energy at corners, similar to what is attempted by Rosakis [169].

Despite the fact that surface Cauchy-Bourne model belongs to discrete mechanics, the presented work is relevant to our work as the process in which we derive our overlying shell model in Chapter 3 utilises the same logical process that is used in the derivation of surface Cauchy-Bourne model. Also, our numerical analysis from chapter 3 follows the basic structure of this publication, and our work too has applications in the field of flexible and stretchable electronics.

2 Membranes Supported by Rigid Foundations with Friction

Abstract

In this chapter we extend the capstan equation to more general geometries. We show that for a general prism defined by the map $(x^1, f(x^2), g(x^2))_{\mathsf{E}}$, where the limits of x^2 are chosen such that $g'f'' - f'g'' > 0, \forall\, x^2$, and an external stress field in the curvilinear space defined by $(0, g_{r2}, g_{r3})$, the capstan equation can be generalised as

$$T(\theta) = \exp\left(-\mu_F \arctan\left(\frac{g'(\theta)}{f'(\theta)}\right)\right)\left(C - \int_{\theta_0}^{\theta}\left(g_{r2} + \mu_F (F_{[\mathsf{l}]22})^{\frac{1}{2}} g_{r3}\right)\exp\left(\mu_F \arctan\left(\frac{g'}{f'}\right)\right) dx^2\right) ,$$

where $F_{[\mathsf{l}]22} = (f')^2 + (g')^2$, $C = T_0 \exp(\mu_F \arctan(g'/f'))|_{x^2=\theta_0}$, T_0 is the minimum applied-tension at $x^2 = \theta_0$. Also, we show that for a general cone defined by the map $(x^1, x^1\bar{f}(x^2), x^1\bar{g}(x^2))_{\mathsf{E}}$, where the limits of x^2 are chosen such that $\bar{g}'\bar{f}'' - \bar{f}'\bar{g}'' > 0, \forall\, x^2$, the capstan equation can be generalised as

$$T(\theta) = T_0 \exp\left(\mu_F \int_{\theta_0}^{\theta} \frac{\left(1 + \bar{f}^2 + \bar{g}^2\right)^{\frac{1}{2}} (\bar{g}'\bar{f}'' - \bar{f}'\bar{g}'')}{(\bar{f}')^2 + (\bar{g}')^2 + (\bar{g}\bar{f}' - \bar{f}\bar{g}')^2} \cos(\phi)\, dx^2\right) ,$$

where

$$\phi(x^2) = \int_0^{x^2} \frac{\sqrt{\left(\bar{f}'\right)^2 + \left(\bar{g}'\right)^2 + \left(\bar{g}\bar{f}' - \bar{f}\bar{g}'\right)^2}}{1 + \bar{f}^2 + \bar{g}^2}\, d\theta .$$

2.1 Introduction

Friction is the force resisting the relative motion of solid surfaces, fluid layers (viscosity) and material elements sliding against each other. It is caused by molecular adhesion, surface roughness and the ploughing effect (deformations of the objects). Note that adhesion is the molecular force resulting when two materials are brought into close contact, and separating the objects requires breaking these adhesive bonds. Also, friction leads to energy dissipation, and in micro-contacts, where extreme stresses are present, friction leads to micro-fractures and surface wear [146]. There are several types of friction: fluid friction, lubricated friction, skin friction and internal friction. However, in this thesis we only focus on one type: dry-friction. Dry-friction resists relative lateral motion of two surfaces that are in contact. Dry-friction is subdivided into static friction between relatively non-moving surfaces and kinetic friction between relatively moving surfaces. In this chapter, also mainly in this thesis, we only focus on the static case. For a comprehensive historical and scientific study on dry-friction please consult chapter 11 of Kikuchi and Oden [102].

Consider a membrane (i.e. two-dimensional elastic body) with a zero-Poisson's ratio or a *string* (i.e. one-dimensional elastic body with a zero or a nonzero Poisson's ratio) over a *rough* rigid cylinder subject to appropriate boundary conditions such that the body in question is at *limiting equilibrium*, i.e. at the point of slipping. This is a simple belt-friction problem and its properties can be described by the capstan equation (13). We ask that what if the rigid contact body is no longer a cylinder, but some arbitrary geometry? If one extends the capstan equation to these geometries, then what form of solutions can one expects? Such questions are the main focus of this chapter. Note that by *rough* we mean that the contact area of the two bodies exhibits friction [161, 92].

2.2 Derivation

Consider an elastic body on a rough rigid surface subjected to external loadings and boundary conditions such that the body is at limiting equilibrium. The governing equation for friction at the contact region can be expressed as

$$F = \mu_F R \,, \tag{52}$$

where R is the normal reaction force and F is the frictional force experienced on the body, and μ_F is the coefficient of friction between the rough rigid surface and the body at the contact region [92, 161]. Equation (52) is simply known as the *friction law*. A word of caution: some authors erroneously refer to equation (52) as Amontons' law of friction [45, 48]. However, Amontons only postulated three nonmathematical frictional laws [146]. Equation (52) may have been derived from Amontons' laws, but in the in the literature it is commonly referred to as the friction law [92].

To mathematically investigate the behaviour of an elastic body at the boundary one must know its stress at the boundary, which is analogous to the boundary force divided by the contact area. Now, let F^α be the frictional forces and F^3 be the normal reaction force at the contact region, where the contact region described by the surface $x^3 = 0$ in curvilinear coordinates (x^1, x^2, x^3). Then, the friction law (52) can be expressed in the curvilinear space as $F_\alpha F^\alpha = \mu_F^2 F_3 F^3$. Dividing this equation by the contact area twice is analogous to $\tau_3^\alpha \tau_\alpha^3 = \mu_F^2 \tau_3^3 \tau_3^3$, where τ_3^j are normal stresses at the contact surface. If one assumes that one is dealing with a very thin structure (i.e. a membrane), then the notion of normal stress is meaningless. However, note that the stress tensor is constant throughout the normal direction for such thin objects, and thus, dividing the above equation further by the thickness of the object twice enable us to obtain a relation that is analogous in terms of force densities, i.e. $f_\alpha f^\alpha = \mu_F^2 f_3 f^3$. This leads to our first hypothesis:

Hypothesis 1. *For a membrane over a rigid foundation, where the contact area is described by $(x^1, x^2, 0)$, at limiting equilibrium the contact region is governed by the equation*

$$\sqrt{f_{r\alpha} f_r^\alpha} = \mu_F \sqrt{f_{r3} f_r^3} \,, \tag{53}$$

where f_r^α are the frictional force densities and f_r^3 is the normal reaction force density of the membrane in the curvilinear space, and μ_F is the coefficient of friction at the contact region.

2.3 General Prism Case

Now, consider a general prism parameterised by the map

$$\boldsymbol{\sigma}(x^1, x^2) = \big(x^1, f(x^2), g(x^2)\big)_{\mathsf{E}} \,, \ \forall \ (x^1, x^2) \in \omega \,,$$

where $\omega \subset \mathbb{R}^2$ and $f(\cdot)$ and $g(\cdot)$ are $C^1(\omega)$ 2π-periodic functions. Note that ω is a simply-connected bounded two-dimensional domain with a positively-oriented piecewise-smooth closed boundary $\partial\omega$ such that $\boldsymbol{\sigma}$ forms an injection. Prism's first fundamental form tensor can be expressed as $\boldsymbol{F}_{[\mathsf{I}]} = \operatorname{diag}(1, (f')^2 + (g')^2)$ and the only nonzero component of its second fundamental form tensor can

be expressed as

$$F_{[\mathrm{II}]22} = -\frac{(g'f'' - f'g'')}{\sqrt{(f')^2 + (g')^2}} \,.$$

Note that this is a surface of zero-Gaussian curvature, i.e. $\det(\boldsymbol{F}_{[\mathrm{II}]}) = 0$.

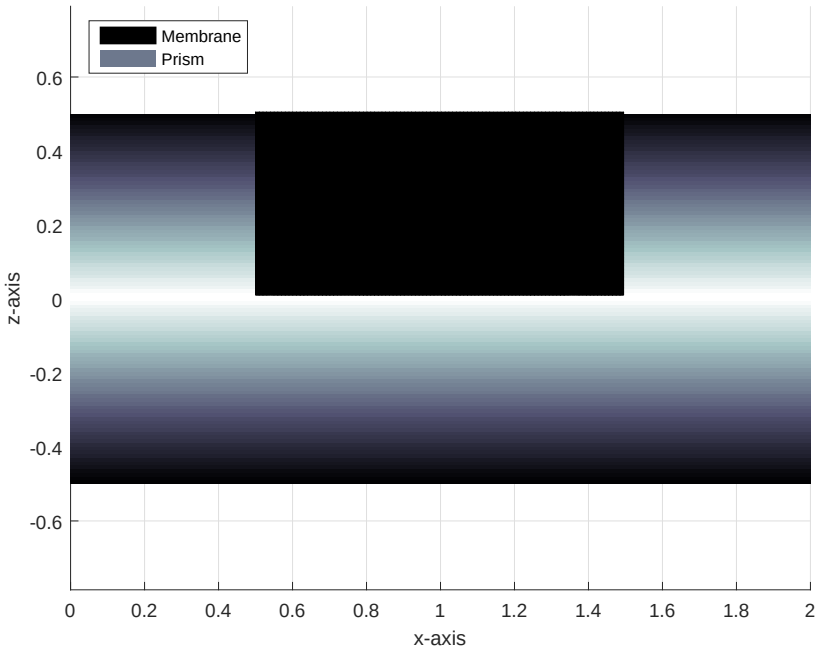

Figure 19: Two-Dimensional schematic representation of a rectangular membrane on a rigid prism.

Now, consider a rectangular membrane with a zero-Poisson's ratio (or a string) and with a thickness h that is in contact with the prism (see figure 19) and at limiting equilibrium such that the boundary of this membrane has the form

$$\partial\omega = \partial\omega_f \cup \partial\omega_{T_0} \cup \partial\omega_{T_{\text{max}}} \,,$$

where

$$\begin{aligned}
\partial\omega_f &= \{(x^1, x^2) \mid x^1 \in \{0, l\} \text{ and } \theta_0 < x^2 < \theta_{\text{max}}\} \,, \\
\partial\omega_{T_0} &= \{(x^1, x^2) \mid 0 \leq x^1 \leq l \text{ and } x^2 = \theta_0\} \,, \\
\partial\omega_{T_{\text{max}}} &= \{(x^1, x^2) \mid 0 \leq x^1 \leq l \text{ and } x^2 = \theta_{\text{max}}\} \,.
\end{aligned}$$

Now, assert that the limits of x^2, i.e. limits of the contact interval, is chosen such that $F_{[\mathrm{II}]2}^{\,2} < 0$ in ω, i.e. the contact region is a surface of positive mean-curvature.

Consider the diffeomorphism $\boldsymbol{\Theta} = \boldsymbol{\sigma}(x^1, x^2) + x^3 \boldsymbol{N}(x^1, x^2)$ with respect to the map $\boldsymbol{\sigma}$, where $\boldsymbol{N}$ is the unit outward normal to the surface and $x^3 \in (-\varepsilon, \varepsilon)$, for some $\varepsilon > 0$ (see lemma 2). Now, with respect to the diffeomorphism $\boldsymbol{\Theta}$ full three-dimensional Cauchy's momentum equation in the curvilinear space can be expressed as $\bar{\nabla}_i T^i_j + f_j = 0$, where is $\boldsymbol{f}$ is a force density field. By definition, $\boldsymbol{f}$ is the sum of all the force densities, and thus, one can re-express it as $\boldsymbol{f} = \boldsymbol{f}_r + \boldsymbol{g}_r$ where $\boldsymbol{g}_r$ is

some external loading (e.g. effects due to gravity).

Now, assert that $f^1 = 0$ and the membrane is subjected to the boundary conditions

$$T^1_\beta\big|_{\partial\omega} = 0 \,,$$
$$T^2_2\big|_{\partial\omega_{T0}} = \frac{T_0}{hl} \,, \tag{54}$$
$$T^2_2\big|_{\partial\omega_{T\max}} = \frac{T_{\max}\left(\mu_F, \boldsymbol{\sigma}(\omega), \boldsymbol{g}_r, T_0\right)}{hl} \,, \tag{55}$$

where $\theta_0 < \theta_{\max}$, and T_0 and $T_{\max}(\mu_F, \boldsymbol{\sigma}(\omega), \boldsymbol{g}_r, T_0)$ are forces applied at the boundary such that $T_0 < T_{\max}(\mu_F, \boldsymbol{\sigma}(\omega), \boldsymbol{g}_r, T_0)$. Note that $T_{\max}(\mu_F, \boldsymbol{\sigma}(\omega), \boldsymbol{g}_r, T_0)$ is not arbitrary. For the membrane to remain at limiting equilibrium $T_{\max}(\mu_F, \boldsymbol{\sigma}(\omega), \boldsymbol{g}_r, T_0)$ must have a very specific value that depends on T_0, the contact angle, curvature, external loadings and most importantly the coefficient of friction, μ_F.

Due to conditions which include zero-Gaussian curvature, zero-Poisson's ratio (i.e. $\nu = 0$) and $f^1 = 0$, and the construction of the boundary conditions (i.e. x^1 independence) one finds that the only nonzero component of the stress tensor is $T^2_2 = T^2_2(x^2)$. This result can be further justified as, if one attempts this as a displacement-based problem, then one finds that the only nonzero component of the strain tensor is $\epsilon^2_2(u^2(x^2))$. Thus, Cauchy's momentum equation at $x^3 = 0$ reduce to

$$\partial_2 T^2_2 + f_{r2} + g_{r2} = 0 \,,$$
$$F_{[\mathrm{II}]}{}^2_2 T^2_2 + f_{r3} + g_{r3} = 0 \,.$$

As friction opposes potential motion i.e. $f^2_r < 0$ (f^2_r is decreasing as x^2 is increases for our case) and the normal reaction force is positive i.e. $f^3_r > 0$ (as we are considering a unit outward normal the surface), hypothesis 1 implies that

$$\partial_2 T^2_2 + \mu_F (F_{[\mathrm{I}]22})^{\frac{1}{2}} F_{[\mathrm{II}]}{}^2_2 T^2_2 + g_{r2} + \mu_F (F_{[\mathrm{I}]22})^{\frac{1}{2}} g_{r3} = 0 \,,$$

i.e.

$$\partial_2 T^2_2 - \mu_F \frac{(g'f'' - f'g'')}{(f')^2 + (g')^2} T^2_2 + g_{r2} + \mu_F (F_{[\mathrm{I}]22})^{\frac{1}{2}} g_{r3} = 0 \,. \tag{56}$$

Finally, integrate equation (56) with respect to boundary condition (54) and multiply the resulting solution by lh to arrive at our first theorem:

Theorem 1. *The tension $T(\cdot)$ of a membrane with a zero-Poisson's ratio (or a string) on a prism parameterised by the map $(x^1, f(x^2), g(x^2))_E$, subjected to an external stress field $(0, g^2_r, g^3_r)$ in the curvilinear space, at limiting equilibrium is*

$$T(\theta) = \exp\left(-\mu_F \arctan\left(\frac{g'(\theta)}{f'(\theta)}\right)\right)\left[C - \int_{\theta_0}^{\theta}\left(g_{r2} + \mu_F (F_{[\mathrm{I}]22})^{\frac{1}{2}} g_{r3}\right)\exp\left(\mu_F \arctan\left(\frac{g'}{f'}\right)\right)dx^2\right] \,,$$

where $C = T_0 \exp(\mu_F \arctan(g'/f'))|_{x^2=\theta_0}$, T_0 is the minimum applied-tension at $x^2 = \theta_0$, $f(\cdot)$ and $g(\cdot)$ are $C^1([\theta_0, \theta_{max}])$ 2π-periodic functions and the interval $[\theta_0, \theta_{max}]$ is chosen such that $g'f'' - f'g'' > 0$, $\forall\, x^2 \in [\theta_0, \theta_{max}]$.

Proof. Please see above for the derivation. □

Yes, we do see the irony of calling a result a *theorem* which is in fact based on a *hypothesis*. But hypothesis 1 is based on the standard friction law (52) and there is no way of avoiding it. Thus, given that hypothesis 1 holds, theorem 1 holds mathematically. In fact, for the cylindrical case with no external loadings theorem 1 implies that the tension is described by the standard capstan equation (13). We show this explicitly in Section 2.5.1.

Note that theorem 1 is not valid when f' and g' are either singular or zero between the limits θ_0 and θ_{max}. However, one can still evaluate such problems with some thought as $\arctan(x)$ remains finite in the limit $x \to \infty$. Such a problem is analysed in Section 2.5.3.

Corollary 1. *The tensile stress $\tau(\cdot)$ of an infinitely long membrane with a nonzero (or zero) Poisson's ratio on a prism parameterised by the map $(x^1, f(x^2), g(x^2))_E$, where $|x^1| \leq \infty$, subjected to an external force density field $(0, g_r^2, g_r^3)$ in the curvilinear space, at limiting equilibrium is*

$$\tau(\theta) = \exp\left(-\mu_F \arctan\left(\frac{g'(\theta)}{f'(\theta)}\right)\right)\left[C - \int_{\theta_0}^{\theta}\left(g_{r2} + \mu_F(F_{[II]22})^{\frac{1}{2}} g_{r3}\right)\exp\left(\mu_F \arctan\left(\frac{g'}{f'}\right)\right)dx^2\right] ,$$

where $C = \tau_0 \exp\left(\mu_F \arctan(g'/f')\right)|_{x^2=\theta_0}$, τ_0 is the minimum applied tensile stress applied at $x^2 = \theta_0$, $f(\cdot)$ and $g(\cdot)$ are $C^1([\theta_0, \theta_{max}])$ 2π-periodic functions and the interval $[\theta_0, \theta_{max}]$ is chosen such that $g'f'' - f'g'' > 0$, $\forall\ x^2 \in [\theta_0, \theta_{max}]$.

Proof. Simple case of noting that the solution in theorem 1 is invariant in the x^1 direction for all Poisson's ratios given that the membrane is infinitely long in the x^1 direction. This result is even more evident if one is to use a displacement-based method to derive the solution. □

A word of caution: the field $\boldsymbol{g}_r$ from theorem 1 is dimensionally different to one from corollary 1, and thus, do not be confused by the apparent same notation.

2.4 General Cone Case

Now, consider a general cone parameterised by the map

$$\boldsymbol{\sigma}(x^1, x^2) = \left(x^1, x^1\bar{f}(x^2), x^1\bar{g}(x^2)\right)_{\mathsf{E}} ,\ \forall\ (x^1, x^2) \in \omega ,$$

where $\omega \subset \mathbb{R}_{>0} \times \mathbb{R}$, and $\bar{f}(\cdot)$ and $\bar{g}(\cdot)$ are $C^2(\omega)$ 2π-periodic functions. Note that ω is a simply-connected bounded two-dimension domain with a positively-oriented piecewise-smooth closed boundary $\partial\omega$ such that $\boldsymbol{\sigma}$ forms an injection. Thus, cone's first fundamental form can be expressed as

$$\boldsymbol{F}_{[\mathrm{I}]} = \begin{pmatrix} 1 + \bar{f}^2 + \bar{g}^2 & x^1\bar{f}\bar{f}' + x^1\bar{g}\bar{g}' \\ x^1\bar{f}\bar{f}' + x^1\bar{g}\bar{g}' & \left(x^1\bar{f}'\right)^2 + \left(x^1\bar{g}'\right)^2 \end{pmatrix} .$$

Also, only nonzero component of cone's second fundamental form can be expressed as

$$F_{[\mathrm{II}]22} = -x^1 \frac{\left(\bar{g}'\bar{f}'' - \bar{f}'\bar{g}''\right)}{\sqrt{\left(\bar{f}'\right)^2 + \left(\bar{g}'\right)^2 + \left(\bar{g}\bar{f}' - \bar{f}\bar{g}'\right)^2}} .$$

Due to the non-diagonal nature of the first fundamental form of the cone it is difficult to find a simple friction law as with the prism case. But note that this is a surface of zero-Gaussian curvature, i.e. $\det(\boldsymbol{F}_{[\mathrm{II}]}) = 0$. Thus, Gauss' *Theorema Egregium* (lemma 3) implies that there exists map $\boldsymbol{\varphi} : (\chi^1, \chi^2) \mapsto \omega$ such that the first fundamental form tensor with respect to the isometry $\boldsymbol{\sigma} \circ \boldsymbol{\varphi}$ is the 2×2 identity matrix. With some calculations, one can define the properties of this map $\boldsymbol{\varphi}$ as

$$\begin{aligned}
\chi^1 &= x^1 \sqrt{1 + \bar{f}^2 + \bar{g}^2}\ \cos(\phi), \\
\chi^2 &= x^1 \sqrt{1 + \bar{f}^2 + \bar{g}^2}\ \sin(\phi)\ , \\
\phi(x^2) &= \int_0^{x^2} \frac{\sqrt{\left(\bar{f}'\right)^2 + \left(\bar{g}'\right)^2 + \left(\bar{g}\bar{f}' - \bar{f}\bar{g}'\right)^2}}{1 + \bar{f}^2 + \bar{g}^2}\, d\theta\ .
\end{aligned}$$

Also,

$$\boldsymbol{J} = \begin{pmatrix}
\sqrt{1 + \bar{f}^2 + \bar{g}^2}\ \cos(\phi) & x^1 \frac{\bar{f}\bar{f}' + \bar{g}\bar{g}'}{\sqrt{1+\bar{f}^2+\bar{g}^2}} \cos(\phi) - x^1 \frac{\sqrt{\left(\bar{f}'\right)^2 + (\bar{g}')^2 + \left(\bar{g}\bar{f}' - \bar{f}\bar{g}'\right)^2}}{\sqrt{1+\bar{f}^2+\bar{g}^2}} \sin(\phi) \\
\sqrt{1 + \bar{f}^2 + \bar{g}^2}\ \sin(\phi) & x^1 \frac{\bar{f}\bar{f}' + \bar{g}\bar{g}'}{\sqrt{1+\bar{f}^2+\bar{g}^2}} \sin(\phi) + x^1 \frac{\sqrt{\left(\bar{f}'\right)^2 + (\bar{g}')^2 + \left(\bar{g}\bar{f}' - \bar{f}\bar{g}'\right)^2}}{\sqrt{1+\bar{f}^2+\bar{g}^2}} \cos(\phi)
\end{pmatrix}.$$

is the Jacobian matrix of the map $\boldsymbol{\varphi}$. Furthermore, by the construction of $\boldsymbol{\varphi}$ implies that $\det(\boldsymbol{J}) > 0$. With further calculations one finds that the first fundamental form tensor of the cone with respect to the isometry $\boldsymbol{\sigma} \circ \boldsymbol{\varphi}$ is $F^{\boldsymbol{\varphi}}_{[\mathrm{I}]\alpha\beta} = \delta_{\alpha\beta}$ and the second fundamental form tensor is

$$\boldsymbol{F}^{\boldsymbol{\varphi}}_{[\mathrm{II}]} = -\frac{\left(1 + \bar{f}^2 + \bar{g}^2\right)\left(\bar{g}'\bar{f}'' - \bar{f}'\bar{g}''\right)}{x^1 \left(\left(\bar{f}'\right)^2 + \left(\bar{g}'\right)^2 + \left(\bar{g}\bar{f}' - \bar{f}\bar{g}'\right)^2\right)^{\frac{3}{2}}} \begin{pmatrix} \sin^2(\phi) & -\sin(\phi)\cos(\phi) \\ -\sin(\phi)\cos(\phi) & \cos^2(\phi) \end{pmatrix}.$$

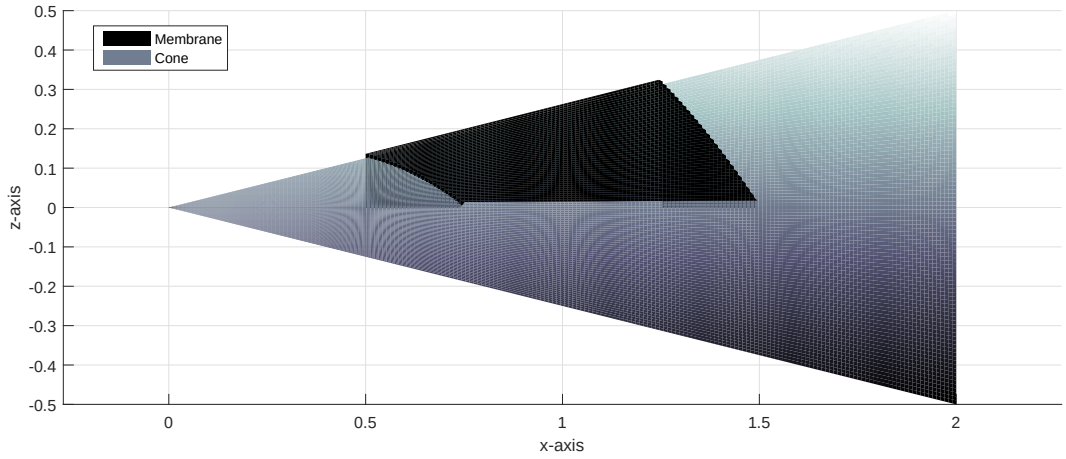

Figure 20: Two-Dimensional schematic representation of a isosceles-trapezium membrane on a rigid cone.

Now, consider an isosceles-trapezium membrane with a zero-Poisson's ratio (or a string), with a thickness h and a length l separating its parallel sides that is in contact with the cone such that it is at limiting equilibrium (see figure 20). The boundary of this membrane has the form

$$\partial\omega = \partial\omega_f \cup \partial\omega_{T_0} \cup \partial\omega_{T_{\max}}\ ,$$

where

$$\partial\omega_f = \{(\chi^1, x^2) \mid \chi^1 \in \{d, d + l\} \text{ and } \theta_0 < x^2 < \theta_{\max}\}\ ,$$

$$\partial\omega_{T_0} = \{(\chi^1, x^2) \mid d \leq \chi^1 \leq d + l \text{ and } x^2 = \theta_0\} \ ,$$
$$\partial\omega_{T_{\mathsf{max}}} = \{(\chi^1, x^2) \mid d \leq \chi^1 \leq d + l \text{ and } x^2 = \theta_{\mathsf{max}}\} \ ,$$

and d is the distance between the membrane and the apex of the cone at $x^2 = 0$. Note that d must always be a positive constant, and, just as it is in Section 2.3, assert that the limits of x^2, i.e. limits of the contact interval, is chosen such that $F^{\varphi 2}_{[\mathrm{II}]2} < 0$ in ω, i.e. the contact area is surface of positive mean-curvature.

Now, consider the diffeomorphism $\boldsymbol{\Theta} = \boldsymbol{\sigma} \circ \boldsymbol{\varphi}(\chi^1, \chi^2) + x^3 \boldsymbol{N}^{\varphi}(\chi^1, \chi^2)$ with respect to the map $\boldsymbol{\sigma} \circ \boldsymbol{\varphi}$, where $\boldsymbol{N}^{\varphi}$ is the unit outward normal to the surface and $x^3 \in (-\varepsilon, \varepsilon)$, for some $\varepsilon > 0$ (see lemma 2). Note that $\boldsymbol{N}(x^1, x^2) = \boldsymbol{N}^{\varphi}(\chi^1, \chi^2)$, i.e. unit normal to the surface is unchanged under the mapping $\boldsymbol{\sigma} \circ \boldsymbol{\varphi}$. To prove this assertion consider following calculation,

$$\begin{aligned}
\boldsymbol{N}^{\varphi} &= \frac{(\boldsymbol{\sigma} \circ \boldsymbol{\varphi})_{,\chi^1} \times (\boldsymbol{\sigma} \circ \boldsymbol{\varphi})_{,\chi^2}}{||(\boldsymbol{\sigma} \circ \boldsymbol{\varphi})_{,\chi^1} \times (\boldsymbol{\sigma} \circ \boldsymbol{\varphi})_{,\chi^2}||} \\
&= \frac{\boldsymbol{\sigma}_{,\alpha} J^{\alpha}_{\chi^1} \times \boldsymbol{\sigma}_{,\beta} J^{\beta}_{\chi^2}}{||\boldsymbol{\sigma}_{,\gamma} J^{\gamma}_{\chi^1} \times \boldsymbol{\sigma}_{,\delta} J^{\delta}_{\chi^2}||} \\
&= \frac{\det(\boldsymbol{J})\,(\boldsymbol{\sigma}_{,1} \times \boldsymbol{\sigma}_{,2})}{||\det(\boldsymbol{J})\,(\boldsymbol{\sigma}_{,1} \times \boldsymbol{\sigma}_{,2})\,||} \\
&= \frac{\boldsymbol{\sigma}_{,1} \times \boldsymbol{\sigma}_{,2}}{||\boldsymbol{\sigma}_{,1} \times \boldsymbol{\sigma}_{,2}||} \ .
\end{aligned}$$

Above result guarantees that the normal reaction force density remains unchanged under the new coordinate system. Now, with respect to the diffeomorphism $\boldsymbol{\Theta}$ full three-dimensional Cauchy's momentum equation in the curvilinear space can be expressed as $\bar{\nabla}_i T^i_j + f_j = 0$ where is $\boldsymbol{f}$ is a force density field. Unfortunately, due to the geometry of the cone one cannot impose a simple physically-realistic external-loading as one did with the prism case, and thus, omit the external loading field $\boldsymbol{g}_r$ form the calculations, i.e. now $f^j = f^j_r$.

Now, assert that $f^1 = 0$ and the membrane is subjected to the boundary conditions

$$\begin{aligned}
T^1_{\beta}\big|_{\partial\omega} &= 0 \ , \ \forall\ \beta \in \{1, 2\} \ , \\
\cos(\phi) T^2_2\big|_{\partial\omega_{T0}} &= \frac{T_0}{hl} \ , \\
\cos(\phi) T^2_2\big|_{\partial\omega_{T\mathsf{max}}} &= \frac{T_{\mathsf{max}}\,(\mu_F, \boldsymbol{\sigma}(\omega), T_0)}{hl} \ ,
\end{aligned} \tag{57}$$

where $\theta_0 < \theta_{\mathsf{max}}$, and T_0 and $T_{\mathsf{max}}(\mu_F, \boldsymbol{\sigma}(\omega), T_0)$ are forces applied at the boundary such that $T_0 < T_{\mathsf{max}}(\mu_F, \boldsymbol{\sigma}(\omega), T_0)$. Comments that we made regarding $T_{\mathsf{max}}(\mu_F, \boldsymbol{\sigma}(\omega), T_0)$ in Section 2.3 still stand, with exception of the external loadings.

Due to conditions which include zero-Gaussian curvature, zero-Poisson's ratio (i.e $\nu = 0$) and $f^1 = 0$, and the construction of the boundary conditions, one finds that the only nonzero component of the stress tensor is $T^2_2 = T^2_2(\chi^2)$. This result can be further justified as, if one attempts this as a displacement-based problem, then one finds that the only nonzero component of the strain tensor is $\epsilon^2_2(u^2(\chi^2))$. Thus, Cauchy's momentum equation at $x^3 = 0$ reduces to

$$\partial_2 T^2_2 + f_{r2} = 0 \ ,$$

$$F^{\varphi 2}_{[\mathrm{II}]_2} T_2^2 + f_{r3} = 0 \, .$$

As friction opposes potential motion i.e. $f_r^2 < 0$ (f_r^2 is decreasing as χ^2 is increases for our case) and the normal reaction force is positive i.e. $f_r^3 > 0$ (as we are considering a unit outward normal to the surface), hypothesis 1 implies that

$$\partial_2 T_2^2 + \mu_F F^{\varphi 2}_{[\mathrm{II}]_2} T_2^2 = 0 \, . \tag{58}$$

Despite the fact that equation (58) provides one with a simple relation for friction, it is near impossible to integrate with respect to χ^1. But notice that χ^1 is related to χ^2 by the equation

$$\chi^2 = \chi^1 \tan(\phi) \, . \tag{59}$$

In accordance with Fubini's theorem (lemma 4) one may keep χ^1 fixed. Thus, take the differential of equation (59) to find

$$d\chi^2 = \chi^1 \frac{\sqrt{\left(\bar{f}'\right)^2 + \left(\bar{g}'\right)^2 + \left(\bar{g}\bar{f}' - \bar{f}\bar{g}'\right)^2}}{1 + \bar{f}^2 + \bar{g}^2} \sec^2(\phi) \, dx^2 \, ,$$

i.e.

$$d\chi^2 = x^1 \frac{\sqrt{\left(\bar{f}'\right)^2 + \left(\bar{g}'\right)^2 + \left(\bar{g}\bar{f}' - \bar{f}\bar{g}'\right)^2}}{\sqrt{1 + \bar{f}^2 + \bar{g}^2}} \sec(\phi) \, dx^2 \, . \tag{60}$$

Now, with the use of equation (60) one can express equation (58) purely in terms of x^2 as

$$\frac{\partial}{\partial x^2} \log(T_2^2) - \mu_F \frac{\sqrt{1 + \bar{f}^2 + \bar{g}^2} \, \left(\bar{g}'\bar{f}'' - \bar{f}'\bar{g}''\right)}{\left(\bar{f}'\right)^2 + \left(\bar{g}'\right)^2 + \left(\bar{g}\bar{f}' - \bar{f}\bar{g}'\right)^2} \cos(\phi) = 0 \, . \tag{61}$$

Finally, integrate equation (61) with respect to boundary condition (57) and multiply the result by $hl\cos(\phi(\theta_0))$ to arrive at our second theorem:

Theorem 2. *The tension $T(\cdot)$ of a membrane with a zero-Poisson's ratio (or a string) on a cone parameterised by the map $(x^1, x^1\bar{f}(x^2), x^1\bar{g}(x^2))_E$ at limiting equilibrium is*

$$T(\theta) = T_0 \exp\left(\mu_F \int_{\theta_0}^{\theta} \frac{\left(1 + \bar{f}^2 + \bar{g}^2\right)^{\frac{1}{2}} \left(\bar{g}'\bar{f}'' - \bar{f}'\bar{g}''\right)}{\left(\bar{f}'\right)^2 + \left(\bar{g}'\right)^2 + \left(\bar{g}\bar{f}' - \bar{f}\bar{g}'\right)^2} \cos(\phi) \, dx^2 \right) \, ,$$

where

$$\phi(x^2) = \int_0^{x^2} \frac{\sqrt{\left(\bar{f}'\right)^2 + \left(\bar{g}'\right)^2 + \left(\bar{g}\bar{f}' - \bar{f}\bar{g}'\right)^2}}{1 + \bar{f}^2 + \bar{g}^2} \, d\theta \, ,$$

and where T_0 is the minimum applied-tension at $x^2 = \theta_0$, $\bar{f}(\cdot)$ and $\bar{g}(\cdot)$ are $C^2([\theta_0, \theta_{max}])$ 2π-periodic functions, and the interval $[\theta_0, \theta_{max}]$ is chosen such that $\bar{g}'\bar{f}'' - \bar{f}'\bar{g}'' > 0$, $\forall \; x^2 \in [\theta_0, \theta_{max}]$.

Proof. Please see above for the derivation. □

Note that, if one expresses the map of the cone as $x^1\boldsymbol{\vartheta}(x^2) = (x^1, x^1\bar{f}(x^2), x^1\bar{g}(x^2))_{\mathsf{E}}$, then one can alternatively express the above theorem as:

Corollary 2. *The tension $T(\cdot)$ of a membrane with a zero-Poisson's ratio (or a string) on a cone parameterised by the map $x^1\boldsymbol{\vartheta}(x^2)$, where $\boldsymbol{\vartheta}'' \cdot (\boldsymbol{\vartheta}' \times \boldsymbol{\vartheta}) > 0$, $\forall\ x^2 \in [\theta_0, \theta]$, at limiting equilibrium is*

$$T(\theta) = T_0 \exp\left(\mu_F \int_{\theta_0}^{\theta} ||\boldsymbol{\vartheta}|| \frac{\boldsymbol{\vartheta}'' \cdot (\boldsymbol{\vartheta}' \times \boldsymbol{\vartheta})}{||\boldsymbol{\vartheta}' \times \boldsymbol{\vartheta}||^2} \cos(\phi)\ dx^2 \right) ,$$

where

$$\phi(x^2) = \int_0^{x^2} \frac{||\boldsymbol{\vartheta}' \times \boldsymbol{\vartheta}||}{||\boldsymbol{\vartheta}||^2}\ d\theta ,$$

and where T_0 is the minimum applied-tension at $x^2 = \theta_0$.

Proof. Let $\boldsymbol{\vartheta}(x^2) = (1, \bar{f}(x^2), \bar{g}(x^2))_{\mathsf{E}}$, then the result follows form theorem 2. □

Perhaps the reader may wonder why one requires Poisson's ratio of the membrane to be zero. Well, Poisson's ratio is the negative ratio of the transverse strain to the axial strain. Thus, if one wish to reduce the two-dimensional problem into an one-dimensional problem, then one must assert a zero-Poisson's ratio, as one does not want the strain of the body to be altered in one direction due to the strains of its perpendicular direction. Similar reasoning is necessary for asserting that the contact region is isometric to the Euclidean plane (prisms, cones). As, if the contact region has two principal curvatures, then any change in strain in one principal direction alters the strain in the other principal direction. However, this effect can be avoided if one asserts that one of the principal curvatures is zero. Therefore, membranes of zero-Poisson's ratio and contact surfaces of zero-Gaussian curvature are both vital for deriving theorems 1 and 2.

2.5 Explicit Solutions

Let us devote this section to find some explicit solutions, which are subsequently used in Sections 2.6, 6.3 and 6.4.

2.5.1 Capstan Equation

Consider a cylinder with a radius a. The cylinder can easily be parameterised by the map $\boldsymbol{\sigma}(x^1, \theta) = (x^1, a\sin(\theta), a\cos(\theta))_{\mathsf{E}}$. Now, consider a membrane with a zero-Poisson's ratio (or a string) over the cylinder at limiting equilibrium. Given that one is applying a minimum tension T_0 at $\theta_0 = 0$ and the membrane is not subject to an external loading, in accordance with theorem 1 one finds

$$T(\theta) = T_0 \exp(\mu_F \theta) , \tag{62}$$

which is just the ordinary capstan equation (13).

2.5.2 Capstan Equation with Gravity

Consider a membrane with a zero-Poisson's ratio (or a string) over a cylinder at limiting equilibrium subjected to the force of gravity $\boldsymbol{g} = (0, 0, -g)_{\mathsf{E}}$, where g is the acceleration due to gravity. Note that the negative sign in the field $\boldsymbol{g}$ implies that acceleration is towards the ground (i.e. towards the centre of the earth). To transform $\boldsymbol{g}$ into the curvilinear space, consider the Jacobian matrix

between standard Euclidean coordinates $(x,y,z)_{\mathsf{E}}$ and the diffeomorphism $\boldsymbol{\Theta}(x^1,\theta,x^3)=(x^1,(a+x^3)\sin(\theta),(a+x^3)\cos(\theta))_{\mathsf{E}}$, at $x^3=0$. This can be used to transform the field $\boldsymbol{g}$ into contravariant curvilinear coordinates, and thus, one finds

$$\begin{bmatrix} 0 \\ \frac{g}{a}\sin(\theta) \\ -g\cos(\theta) \end{bmatrix} = \begin{bmatrix} 1 & 0 & 0 \\ 0 & \frac{1}{a}\cos(\theta) & -\frac{1}{a}\sin(\theta) \\ 0 & \sin(\theta) & \cos(\theta) \end{bmatrix} \begin{bmatrix} 0 \\ 0 \\ -g \end{bmatrix} ,$$

where θ is the acute angle that the vector $(0,0,1)_{\mathsf{E}}$ makes with the vector $(0,a,0)$. Given that ϱ is the mass density of the membrane (with respect to the volume), one finds that the covariant force density due to gravity in the curvilinear space with respect to the map $\boldsymbol{\sigma}$ is $\boldsymbol{g}_r=(0,a\varrho g\sin(\theta),-\varrho g\cos(\theta))$. Thus, given that one is applying an minimum tension T_0 at $\theta_0=0$, in accordance with theorem 1 one finds

$$T(\theta)=\left(T_0-ahl\varrho g\frac{1-\mu_F^2}{1+\mu_F^2}\right)\exp(\mu_F\theta)+ahl\varrho g\left(\frac{1-\mu_F^2}{1+\mu_F^2}\cos(\theta)+\frac{2\mu_F}{1+\mu_F^2}\sin(\theta)\right) .$$

2.5.3 Elliptical-Prism Case

Consider prism with an elliptical cross section where the horizontal diameter is $2a$ and the vertical diameter is $2b$. The prism can easily be parameterised by the map $\boldsymbol{\sigma}(x^1,\theta)=(x^1,a\sin(\theta),b\cos(\theta))_{\mathsf{E}}$. Note that θ is the acute angle that the vector $(0,0,1)_{\mathsf{E}}$ makes with the vector $(0,\varphi(\theta),0)$, where $\varphi(\theta)=(b^2\sin^2(\theta)+a^2\cos^2(\theta))^{\frac{1}{2}}$. Now, consider a membrane with a zero-Poisson's ratio over the cylinder at limiting equilibrium. Given that one is applying a minimum tension T_0 at $\theta_0=0$ and the membrane is not subject to an external loading, in accordance with theorem 1 one finds

$$T(\theta)=T_0\exp\left(\mu_F\arctan\left(\frac{b}{a}\tan(\theta)\right)\right) . \tag{63}$$

Note that θ must not exceed the value $\frac{1}{2}\pi$, as at $\frac{1}{2}\pi$, $\tan(\cdot)$ is singular. However, this is still not a problem for the final solution as $\arctan((b/a)\tan(\cdot))$ remain finite at $\frac{1}{2}\pi$, i.e. $\arctan x\to\pm\frac{1}{2}\pi$ as $x\to\pm\infty$. For example, assume that the contact angle is $\frac{1}{2}\pi+\alpha$ where $0<\alpha<\frac{1}{2}\pi$. Thus, by considering the finiteness of $\arctan(\cdot)$ and some elementary trigonometric identities, one finds that the solution to this problem is

$$T\left(\frac{1}{2}\pi+\alpha\right)=T_0\exp\left(\mu_F\left[\frac{1}{2}\pi+\arctan\left(\frac{b}{a}\tan(\alpha)\right)\right]\right) .$$

On a different note equation (63) implies that the maximum applied-tension, T_{max}, is dependent of the mean curvature of the rigid prism. To investigate this matter further consider a membrane (infinitely long in x^1 direction or otherwise) on a rough elliptical prism at limiting equilibrium between the contact angles $\theta_0=-\frac{1}{4}\pi$ and $\theta_{\mathsf{max}}=\frac{1}{4}\pi$. Thus, theorem 1 (and corollary 1) implies that

$$\delta\tau=\frac{\tau_{\mathsf{max}}}{\tau_0}=\frac{T_{\mathsf{max}}}{T_0}=\exp\left(2\mu_F\arctan\left(\frac{b}{a}\right)\right) . \tag{64}$$

As the reader can see that for a fixed contact interval and a fixed coefficient friction, equation 64 implies a non-constant tension ratio, $\delta\tau$, for varying $\delta b=b/a$. As the mean curvature of the prism is $\bar{H}(\theta)=\frac{1}{2}ab\varphi(\theta)^{-3}$, one can see that the tension ratio is related to the mean curvature by

$$\delta\tau=\exp\left(2\mu_F\arctan\left[\max(2a\bar{H},1)+\min(2a\bar{H},1)-1\right]\right) .$$

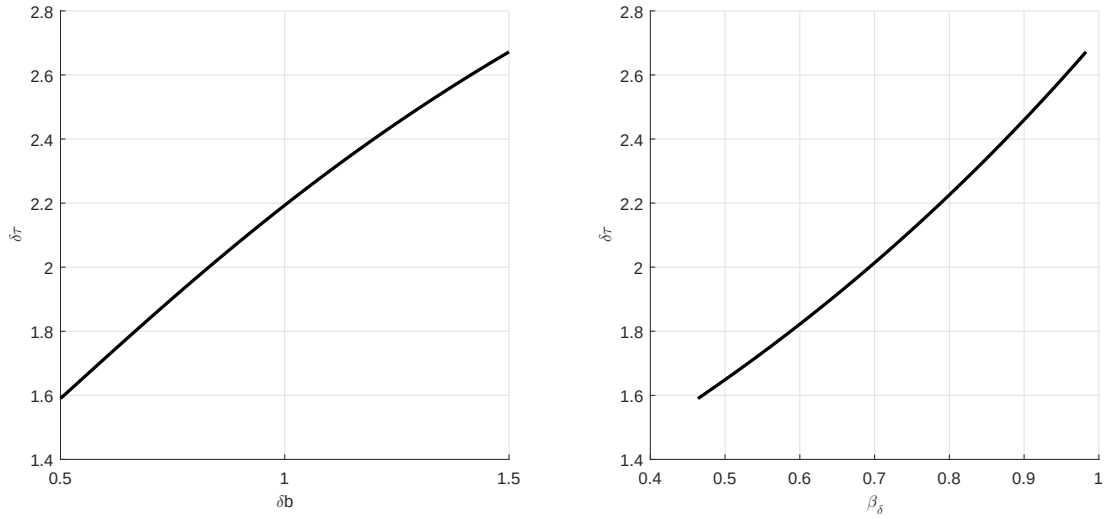

Figure 21: Tension ratio against δb and β_δ.

To investigate this matter further plot the tension ratio, $\delta\tau$, against δb, and, as the mean curvature is not constant at the contact region, plot the tension ratio against the critical parametric-latitude, β_δ. Figure 21 is calculated with $\mu_F = \frac{1}{2}$ and $\frac{1}{2} \leq \delta b \leq \frac{3}{2}$. It shows that, for a fixed contact interval, as δb and the critical parametric-latitude increases, i.e. as the mean curvature of the contact region increases, the tension ratio also increases. This is an intuitive result as the curvature of the contact region increases, the normal reaction force on the membrane also increases, which intern leads to higher frictional force, and thus, a higher tension ratio. Now, this is a fascinating result as this effect cannot be observed with the ordinary capstan equation.

2.5.4 Right-Circular Cone Case

Consider a right-circular cone with a 2α-aperture (i.e. angle between two generatrix lines). The cone can easily be parameterised by the map $\boldsymbol{\sigma}(x^1, \theta) = (x^1, x^1 \tan(\alpha) \sin(\theta), x^1 \tan(\alpha) \cos(\theta))_{\mathsf{E}}$. Now, consider a membrane with a zero-Poisson's ratio over the cone, which resides in sufficiently away from the apex, at limiting equilibrium. Given that one is applying a minimum tension T_0 at $\theta_0 = 0$, in accordance with theorem 2 one finds

$$T(\theta) = T_0 \exp\left(\mu_F \cot[\alpha] \sin\left(\sin[\alpha]\theta\right)\right) \ . \tag{65}$$

As the aperture becomes infinitesimally small, i.e. $2\alpha \approx 0$, one expects the cone to resemble a cylinder with an infinitesimally small radius. Thus, in the limit $\alpha \to 0$, equation 65 reduces to

$$T(\theta) = T_0 \exp\left(\mu_F \theta\right) \ ,$$

which is just the ordinary capstan equation 62. Also, when the aperture is π, one gets a (flat-) Euclidean plane, i.e. $(c, y, z)_{\mathsf{E}}$ where $c > 0$. Thus, in the limit $\alpha \to \frac{1}{2}\pi$, equation 65 reduces to

$$T(\theta) = T_0 \ ,$$

which is a logical result as this represent a membrane on a flat surface being pulled tangentially and independent of any transverse effects. To visualise consider a straight rope under tension, i.e. $T_{\mathsf{max}} = T_0$.

2.6 Comparison Against the Works of Kikuchi and Oden

In this section, we extend Kikuchi and Oden's [102] model for Coulomb's law of static friction to curvilinear coordinates, and we conduct several numerical examples to compare the results against our generalised capstan equation.

Let $\Omega \subset \mathbb{R}^3$ be a simply connected open bounded domain and let $\partial\Omega = \partial\Omega_0 \cup \partial\Omega_f \cup \partial\Omega_T$ be the sufficiently smooth boundary of the domain, where all $\operatorname{meas}(\partial\Omega_0;\mathbb{R}^2)$, $\operatorname{meas}(\partial\Omega_f;\mathbb{R}^2)$, $\operatorname{meas}(\partial\Omega_T;\mathbb{R}^2) > 0$. Now, let $\bar{\boldsymbol{X}} : \Omega \to \mathbf{E}^3$ be a diffeomorphism where $\bar{\boldsymbol{X}}(x^1,x^2,x^3) = \boldsymbol{\sigma}(x^1,x^2) + x^3\boldsymbol{N}(x^1,x^2)$ and $\boldsymbol{\sigma} \in C^2(\partial\Omega_0;\mathbb{R}^2)$ is an injective immersion.

Now, assume that Ω describes the domain of an elastic body such that $\partial\Omega_0$ describes the region where the body is in contact with a rough rigid surface, $\partial\Omega_f$ describes the stress free boundary and $\partial\Omega_T$ describes the boundary with traction. Let $\boldsymbol{v} \in C^2(\Omega;\mathbb{R}^3)$ be the displacement field of the body. Given that $\boldsymbol{f} \in C^0(\Omega;\mathbb{R}^3)$ is an external force density field and $\boldsymbol{\tau}_0 \in C^0(\partial\Omega_0;\mathbb{R}^3)$ is a traction field (i.e. applied boundary stress) at $\partial\Omega_T$, one can express the equations of equilibrium in curvilinear coordinates as $\bar{\nabla}_i T^i_j(\boldsymbol{v}) + f_j = 0$, where $T^{ij}(\boldsymbol{v}) = A^{ijkl}E_{kl}(\boldsymbol{v})$ is second Piola-Kirchhoff stress tensor, $E_{kl}(\boldsymbol{v}) = \frac{1}{2}(\bar{\nabla}_i v_j + \bar{\nabla}_j v_i)$ is linearised Green-St Venant strain tensor and $A^{ijkl} = \lambda g^{ij}g^{kl} + \mu(g^{ik}g^{jl} + g^{il}g^{jk})$ is the isotropic elasticity tensor in curvilinear coordinates. The trivial boundary conditions are $\bar{n}_i T^i_j(\boldsymbol{v}) = 0$ on $\partial\Omega_f$ and $\bar{n}_i T^i_j(\boldsymbol{v}) = \tau_{0j}$ on $\partial\Omega_T$, where $\bar{\boldsymbol{n}}$ is the unit outward normal to $\partial\Omega$.

But what about the boundary conditions at the boundary $\partial\Omega_0$? To investigate this matter further recall Kikuchi and Oden's [102] model for Coulomb's law of static friction from Section 1.11. Now, assume that $\bar{\boldsymbol{X}}$ is constructed such that v^3 describes the normal displacement and v^β describe the tangential displacements at the boundary $\partial\Omega_0$. Noticing that $T^3_3(\boldsymbol{v})|_{\partial\Omega_0} = -\sigma_n(\boldsymbol{v})$ simply re-express the friction equation (44) in curvilinear coordinates to obtain

$$
\begin{gathered}
u^3|_{\partial\Omega_0^+} = 0\,, \\
T^\beta_3(\boldsymbol{v})|_{\partial\Omega_0^+} = \begin{cases} -\dfrac{\nu_F\,(g_{33})^{\frac{1}{2}}\,v^\beta}{(v_\alpha v^\alpha)^{\frac{1}{2}}} T^3_3(\boldsymbol{v})|_{\partial\Omega_0^+}\,, \text{ if } (v_\alpha v^\alpha)^{\frac{1}{2}}|_{\partial\Omega_0^+} \geq \varepsilon\,, \\ -\dfrac{\nu_F\,(g_{33})^{\frac{1}{2}}\,v^\beta}{\varepsilon} T^3_3(\boldsymbol{v})|_{\partial\Omega_0^+}\,, \text{ if } (v_\alpha v^\alpha)^{\frac{1}{2}}|_{\partial\Omega_0^+} < \varepsilon\,, \end{cases}
\end{gathered}
\tag{66}
$$

where $\partial\Omega_0^+ = \lim_{x^3\to 0^+}\Omega$, ν_F is the coefficient of friction with respect to Coulomb's law of static friction, $T^3_3(\boldsymbol{v})|_{\partial\Omega_0^+}$ is the purely normal stress, $T^\beta_3(\boldsymbol{v})|_{\partial\Omega_0^+}$ are the shear stresses and $\varepsilon > 0$ is the regularisation parameter. Note that in this framework one has $g_{33} = 1$. Despite the fact that one is working with linear elasticity, the above equations makes this problem inherently nonlinear. Thus, to find numerical solutions, employ Newton's method for nonlinear systems (see chapter 10 of Burden *et al.* [30]).

Note that the above set of equations depends on the physical properties of the elastic body. Now, recall the standard friction law (52). This is a very simple law that does not depend on any mechanical and geometrical properties of the body in question. Thus, under what conditions does

Coulomb's law satisfy the standard friction law?

To investigate this matter further consider the map of a rigid semi-prism $(x^1, a\sin(x^2), b\cos(x^2))_{\mathsf{E}}$, where $x^2 \in [-\frac{1}{2}\pi, \frac{1}{2}\pi]$, a is the horizontal radius and b is the vertical radius. Now, assume that an elastic body is over this prism and one is applying a traction τ_0 at $x^2 = -\frac{1}{2}\pi$ and a traction τ_{max} at $x^2 = \frac{1}{2}\pi$. Also, assume that the cylinder is rough and the coefficient of friction between the prism and the body in question is $\frac{1}{2}$. Assume further that the body in question is of thickness h, infinitely long and in contact with an infinitely long semi-prism. This leads to the following map of the unstrained configuration,

$$\bar{\boldsymbol{X}}(x^1, x^2, x^3) = (x^1, a\sin(x^2), b\cos(x^2))_{\mathsf{E}} + x^3(\varphi(x^2))^{-1}(0, b\sin(x^2), a\cos(x^2))_{\mathsf{E}} \ ,$$

where $\varphi(x^2) = (b^2\sin^2(x^2) + a^2\cos^2(x^2))^{\frac{1}{2}}$, $x^1 \in (-\infty, \infty)$, $x^2 \in (-\frac{1}{2}\pi, \frac{1}{2}\pi)$ and $x^3 \in (0, h)$. With some calculations, one finds that the covariant metric tensor is $(g_{ij}) = \mathrm{diag}(1, (\bar{\psi}_2)^2, 1)$ and Christoffel symbols of the second kind are

$$\begin{aligned}
\bar{\Gamma}^2_{22} &= (\bar{\psi}_2)^{-1}\partial_2\bar{\psi}_2 \ , \\
\bar{\Gamma}^2_{23} &= (\bar{\psi}_2)^{-1}\partial_3\bar{\psi}_2 \ ,
\end{aligned}$$

where $\bar{\psi}_2 = \varphi(x^2) + x^3 ab(\varphi(x^2))^{-2}$. Now, let $\boldsymbol{v} = (0, v^2(x^2, x^3), v^3(x^2, x^3))$ be the displacement field of the elastic body and let $\delta\boldsymbol{v} = (0, \delta v^2(x^2, x^3), \delta v^3(x^2, x^3))$ be a perturbation of the displacement field. Thus, with some calculations, one finds that covariant derivatives are

$$\begin{aligned}
\bar{\nabla}_2 v^2 &= \partial_2 v^2 + \bar{\Gamma}^2_{22} v^2 + \bar{\Gamma}^2_{23} v^3 \ , \\
\bar{\nabla}_2 v^3 &= \partial_2 v^3 - (\bar{\psi}_2)^2 \bar{\Gamma}^2_{23} v^2 \ , \\
\bar{\nabla}_3 v^2 &= \partial_3 v^2 + \bar{\Gamma}^2_{23} v^2 \ , \\
\bar{\nabla}_3 v^3 &= \partial_3 v^3 \ .
\end{aligned}$$

Now, with relative ease, one can express the governing equations as

$$\begin{aligned}
(\lambda + \mu)\partial^2\left(\bar{\nabla}_i v^i\right) + \mu\bar{\Delta} v^2 &= 0 \ , \\
(\lambda + \mu)\partial^3\left(\bar{\nabla}_i v^i\right) + \mu\bar{\Delta} v^3 &= 0 \ , \\
(\lambda + \mu)\partial^2\left(\bar{\nabla}_i \delta v^i\right) + \mu\bar{\Delta}\delta v^2 &= 0 \ , \\
(\lambda + \mu)\partial^3\left(\bar{\nabla}_i \delta v^i\right) + \mu\bar{\Delta}\delta v^3 &= 0 \ .
\end{aligned}$$

Eliminating x^1 dependency one can express the remaining boundaries as

$$\partial\Omega^{\mathsf{New}} = \partial\Omega^{\mathsf{New}}_0 \cup \partial\Omega^{\mathsf{New}}_f \cup \overline{\partial\Omega}^{\mathsf{New}}_{T_0} \cup \overline{\partial\Omega}^{\mathsf{New}}_{T_{\mathsf{max}}} \ ,$$

where

$$\begin{aligned}
\partial\Omega^{\mathsf{New}}_0 &= \{(-\frac{1}{2}\pi, \frac{1}{2}\pi) \times \{0\}\} \ , \\
\partial\Omega^{\mathsf{New}}_f &= \{(-\frac{1}{2}\pi, \frac{1}{2}\pi) \times \{h\}\} \ , \\
\partial\Omega^{\mathsf{New}}_{T_0} &= \{\{-\frac{1}{2}\pi\} \times (0, h)\} \ ,
\end{aligned}$$

$$\partial\Omega^{\text{New}}_{T_{\text{max}}} = \{\{\frac{1}{2}\pi\} \times (0, h)\} \ .$$

Thus, the boundary conditions reduce to

$$\begin{aligned}
v^3|_{\overline{\partial\Omega}^{\text{New}}_0} &= 0 \text{ (zero-Dirichlet)} \ , \qquad (67)\\
\left[(\lambda+2\mu)\left(\partial_2 v^2 + \bar{\Gamma}^2_{22}v^2 + \bar{\Gamma}^2_{23}v^3\right) + \lambda\partial_3 v^3\right]|_{\overline{\partial\Omega}^{\text{New}}_{T_0}} &= \tau_0 \text{ (traction)} \ ,\\
\left[(\lambda+2\mu)\left(\partial_2 v^2 + \bar{\Gamma}^2_{22}v^2 + \bar{\Gamma}^2_{23}v^3\right) + \lambda\partial_3 v^3\right]|_{\overline{\partial\Omega}^{\text{New}}_{T_{\text{max}}}} &= \tau_{\text{max}} \text{ (traction)} \ ,\\
\left[(\bar{\psi}_2)^2\partial_3 v^2 + \partial_2 v^3\right]|_{\partial\Omega^{\text{New}}_f \cup \partial\Omega^{\text{New}}_{T_0} \cup \partial\Omega^{\text{New}}_{T_{\text{max}}}} &= 0 \text{ (zero-Robin)} \ ,\\
\left[\lambda\left(\partial_2 v^2 + \bar{\Gamma}^2_{22}v^2 + \bar{\Gamma}^2_{23}v^3\right) + (\lambda+2\mu)\partial_3 v^3\right]|_{\overline{\partial\Omega}^{\text{New}}_f} &= 0 \text{ (zero-Robin)} \ ,\\
\delta v^2|_{\overline{\partial\Omega^{\text{New}}_f \cup \partial\Omega^{\text{New}}_{T_0} \cup \partial\Omega^{\text{New}}_{T_{\text{max}}}}} &= 0 \ ,\\
\delta v^3|_{\partial\Omega^{\text{New}}} &= 0 \ .
\end{aligned}$$

Note that condition (67) arises due to the fact that the body is in contact with a rigid boundary. In chapter 4 we examine a more complicated example where this condition is no longer true.

Now, with some more calculations, one can find the fiction laws governing the boundary conditions at the boundary $\overline{\partial\Omega}^{\text{New}}_0$, which are:

If $\bar{\psi}_2|v^2||_{\partial\Omega^{\text{New}}_0} \geq \epsilon$, then

$$\left[\mu\bar{\psi}_2\partial_3 v^2 + \nu_F \text{sign}(v^2)T^3_3(\boldsymbol{v})\right]|_{\partial\Omega^{\text{New}}_0} = 0 \ ;$$

If $\bar{\psi}_2|v^2||_{\partial\Omega^{\text{New}}_0} < \epsilon$, then

$$\left[\mu\bar{\psi}_2\partial_3\delta v^2 + \nu_F\epsilon^{-1}\bar{\psi}_2 v^2 T^3_3(\delta\boldsymbol{v}) + \nu_F\epsilon^{-1}\bar{\psi}_2\delta v^2 T^3_3(\boldsymbol{v}) + \mu\bar{\psi}_2\partial_3 v^2 + \nu_F\epsilon^{-1}\bar{\psi}_2 v^2 T^3_3(\boldsymbol{v})\right]|_{\partial\Omega^{\text{New}}_0} = 0 \ ,$$

where $T^3_3(\boldsymbol{v}) = \lambda(\partial_2 v^2 + \bar{\Gamma}^2_{22}v^2 + \bar{\Gamma}^2_{23}v^3) + (\lambda+2\mu)\partial_3 v^3$.

Despite the fact that the original problem is three-dimensional, as a result of problem's invariance in the x^1 direction, it is now to a two-dimensional problem. Now, the domain resides in the set $\{(x^2, x^3) \mid (x^2, x^3) \in [-\frac{1}{2}\pi, \frac{1}{2}\pi] \times [0, h]\}$. We are fully aware that Kikuchi and Oden's [102] model is only defend for bounded domains; however, we later show that the reduced two-dimensional problem is numerically sound.

To conduct numerical experiments we use the second-order-accurate finite-difference method in conjunction with Newton's method for nonlinear systems, i.e. given that $\boldsymbol{v}_m$ and $\delta\boldsymbol{v}_m$ are m^{th} iterative solutions of the problem obtained by the finite-difference method, we assert that $\boldsymbol{v}_{m+1} = \boldsymbol{v}_m + \delta\boldsymbol{v}_m$ is the updated solution, and we follow this iterative scheme such that $\delta\boldsymbol{v}_m$ converges to zero in the limit $m \to \infty$. Another issue we must tackle is the discretisation of the (reduced two-dimensional) domain. As we are dealing with curvilinear coordinates, there is an inherit grid dependence. To be precise, it is approximately $\psi_0\Delta x^2 \leq \Delta x^3$, $\forall\ \psi_0 \in \{\bar{\psi}_2(x^2, x^3) \mid x^2 \in [-\frac{1}{2}\pi, \frac{1}{2}\pi] \text{ and } x^3 \in [0, h]\}$, where Δx^j is a small increment in x^j direction. For our purposes we use $\Delta x^2 = \frac{1}{N-1}$ and $\psi_0 = \bar{\psi}_2(\frac{1}{4}\pi, h)$, where $N = 250$. Finally, we must define a terminating condition. For this we terminate our iterating

process given that the condition $|1 - (||\boldsymbol{v}_m||_{\ell^2} + ||\delta\boldsymbol{v}_m||_{\ell^2})^{-1}(||\boldsymbol{v}_{m+1}||_{\ell^2} + ||\delta\boldsymbol{v}_{m+1}||_{\ell^2})| < 10^{-10}$ is satisfied, where $|\boldsymbol{v}|_{\ell^2} = ([\mathrm{norm}(v^2, 2)]^2 + [\mathrm{norm}(v^3, 2)]^2)^{\frac{1}{2}}$ and $\mathrm{norm}(\cdot, 2)$ is Matlab 2-norm of matrix [201]. Note that for all our examples we fix the values $\nu_F = \frac{1}{2}$, $\tau_0 = 1$ and $a = 2$.

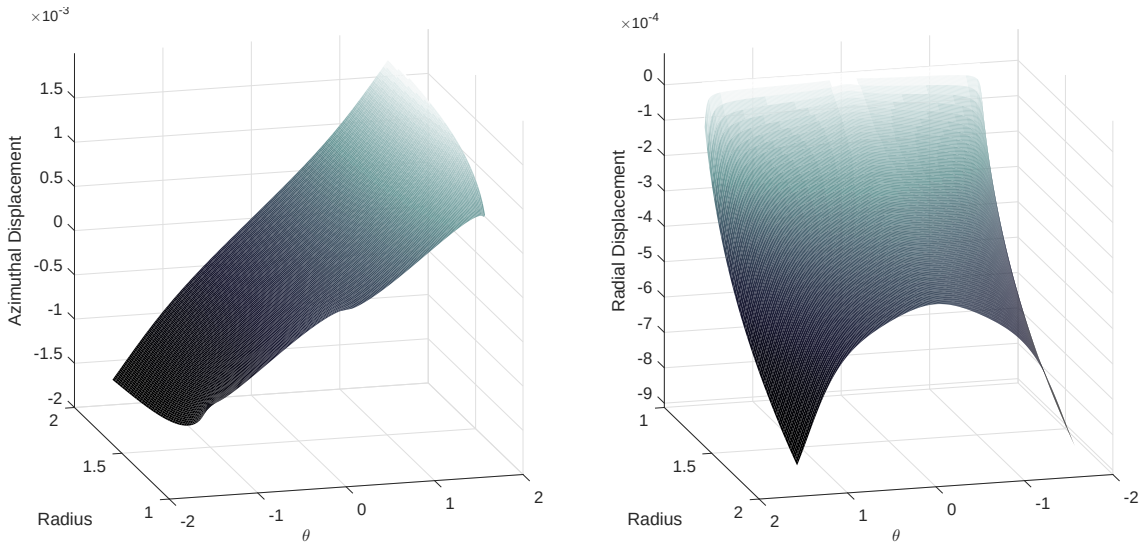

Figure 22: Displacement field of the modified Kikuchi and Oden's model.

Figures 22 and 23 are calculated with the values of $\tau_{\text{max}} = 1$, $b = 2$, $h = 1$, $E = 10^3$, $\nu = \frac{1}{4}$, $\varepsilon = 10^{-5}$ and with a grid of 250×41 points. Figure 22 shows the azimuthal (i.e v^2) and the radial (i.e v^3) displacements. The maximum azimuthal displacements are observed at $x^2 = \pm\frac{1}{2}\pi$, with respective azimuthal displacements of $v^2 = \pm 1.72 \times 10^{-3}$. The maximum radial displacement is observed at $x^2 = \pm\frac{1}{2}\pi$, with a radial displacement of $v^3 = -8.24 \times 10^{-4}$.

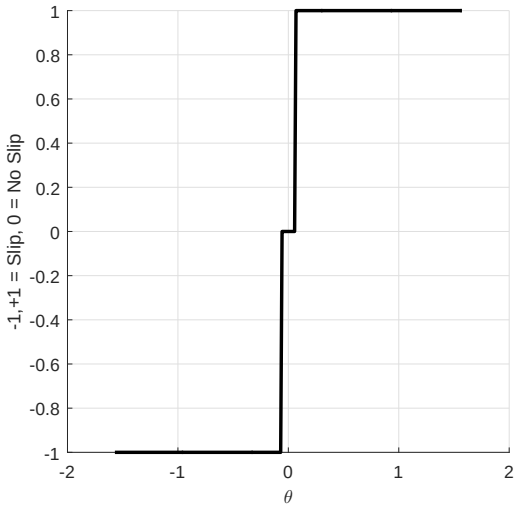

Figure 23: Slip and stick regions of the modified Kikuchi and Oden's model.

Figure 23 shows the behaviour of the elastic body at the boundary $\overline{\partial\Omega_0}^{\text{New}}$. It shows that in the region $[-\frac{1}{2}\pi, -0.0694]$ the body slid in the negative (i.e. decreasing) azimuthal direction, and in the region $[0.0694, \frac{1}{2}\pi]$ the body slid in the positive (i.e. increasing) azimuthal direction. The region

$(-0.0201, 0.0201)$ describes the azimuthal region of the body that lies below the threshold of sliding determined by the Coulomb's friction condition, i.e. $|v^2| < 10^{-5}$ for our case. This does not imply the displacement inside this region is identically zero (see figure 23), but it implies that the displacement in this region infinitesimal, i.e. the body is unable to overcome the force of friction or in other words the body is *bonded*. This bonded region is determined by the regularisation parameter ε which is not a physical parameter as it has no real life significance. It is merely introduced make Coulomb's friction law regular when displacements are zero, i.e. to avoid singularities in the numerical solutions. Note that, if the applied traction at $x^2 = \frac{1}{2}\pi$ is larger than the traction at $x^2 = -\frac{1}{2}\pi$, then figure 23 will no longer be symmetric in the azimuthal direction, and for this case the right side (i.e. where slip $= 1$) will be much greater than the left side (i.e. where slip $= -1$). Thus, if one increases the traction at $x^2 = \frac{1}{2}\pi$ enough, then the entire body will slip in the positive azimuthal direction, i.e. slip $= 1$, $\forall\, \theta$. The subject of this section to investigate how this slip region behaves for a given set of variables.

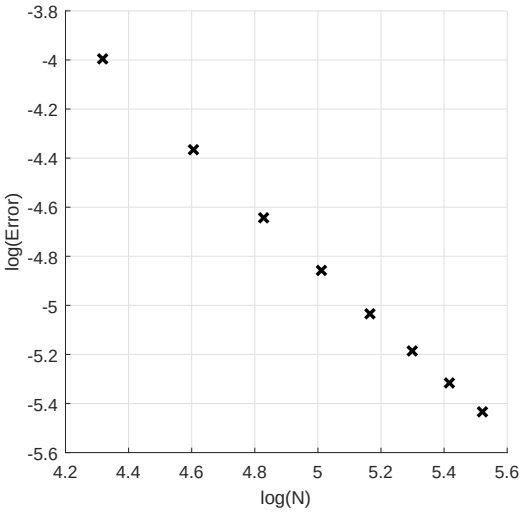

Figure 24: Grid dependence of the modified Kikuchi and Oden's model.

Prior to our investigation we must perform is the grid dependence analysis for the numerical solution. For this, we examine how the solution behave as we vary number of grid points N. To conduct this experiment let us define the error between two solutions with azimuthal grid points $N-1$ and N as $\text{Error} = |1 - ||\boldsymbol{u}_{N-1}||_{\ell^2}^{-1}||\boldsymbol{u}_N||_{\ell^2}|$. As the reader can see from figure 24 as N increases, the difference between the numerical solution N and $N+1$ decreases. For our experiments we found that the azimuthal grid points and the error share the relation $N \propto \text{Error}^{-0.840}$. Note that figure 24 is calculated with the values of $\tau_{\text{max}} = 2$, $b = 2$, $h = 1$, $E = 10^3$, $\nu = \frac{1}{4}$ and $\varepsilon = 10^{-5}$.

Another input parameter we must determine is our choice in the regularisation parameter, ε. For these experiments we use the values $\tau_{\text{max}} = 2$, $b = 2$, $h = 1$, $E = 10^3$, $\nu = \frac{1}{4}$ and $10^{-5} \leq \varepsilon \leq 10^{-10}$. For all our experiments we find that the slip region remains at a constant value of 71.2% for all ε, except for the value $\varepsilon = 10^{-10}$. For this particular value we find the slip region to reduce to 69.6%. This may be caused by the terminating error condition as it is also 10^{-10}. Thus, for all our experiments we continue to use the value $\varepsilon = 10^{-5}$.

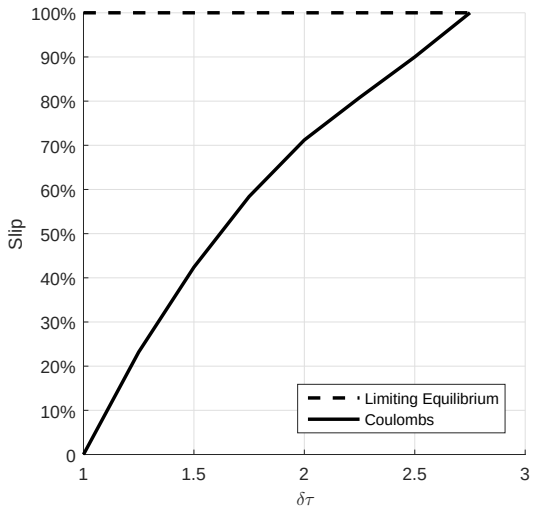

Figure 25: Slip for $\delta\tau = \tau_{\max}/\tau_0$.

Figure 25 shows how close the elastic body is to limiting equilibrium for varying tension ratio, $\delta\tau$. For these experiments we assert that $\delta\tau \in \{1, \frac{5}{4}, \frac{6}{4}, \frac{7}{4}, 2, \frac{9}{4}, \frac{10}{4}, \frac{11}{4}\}$, $\delta b = 1$, $h = 1$, $E = 10^3$ and $\nu = \frac{1}{4}$. In figure 25 we see that as the tension ratio increases, the elastic body gets closer and closer to fully debonding. In fact, when $\delta\tau = \frac{11}{4}$, our elastic body is fully debonded from the rigid foundation and sliding in the positive x^2 direction. To compare it against the capstan equation we invoke corollary 1 with $\delta\tau = \frac{11}{4}$, which implies that the capstan coefficient of friction is $\mu_F = 0.322$, regardless of the Poisson's ratio of the body. This result implies that the capstan coefficient of friction is an underestimate of Coulomb's coefficient of friction, i.e. $\mu_F \leq \nu_F$. Note that capstan equation underestimating the actual coefficient of friction is a documented phenomenon in the literature [134].

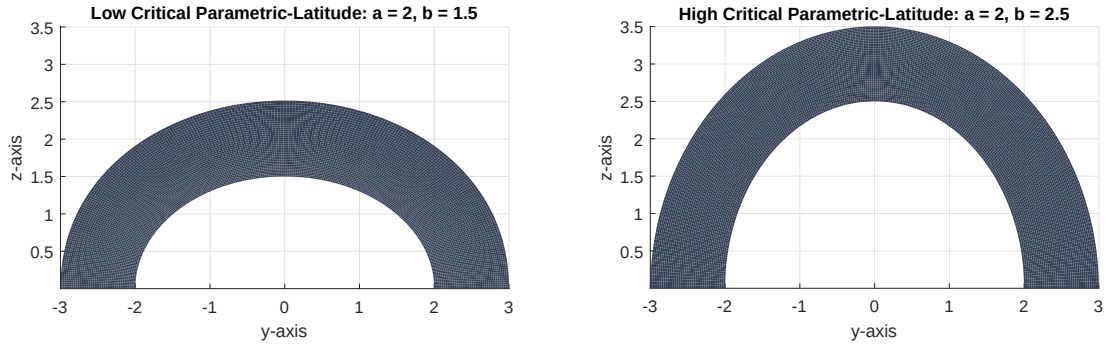

Figure 26: Schematic representations of the reduced two-dimensional domain for the $h = 1$, $a = 2$, and $b = \frac{3}{2}$ and $b = \frac{5}{2}$ cases.

Figure 27 shows how close the elastic body is to limiting equilibrium for a set of vertical radii of the contact region, $\delta b = b/a$. For these experiments we assert that $\delta\tau = 2$, $\delta b \in \{\frac{5}{10}, \frac{6}{10}, \frac{7}{10}, \frac{8}{10}, \frac{9}{10}, 1, \frac{11}{10}, \frac{12}{10}, \frac{13}{10}, \frac{14}{10}, \frac{15}{10}\}$ (see figure 26), $h = 1$, $E = 10^3$ and $\nu = \frac{1}{4}$. Figure 27 implies that as δb increases, the modified Kikuchi and Oden's model moves away from limiting equilibrium, i.e. as the critical parametric-latitude increases, the normal reaction force of the body increases, which intern leads to

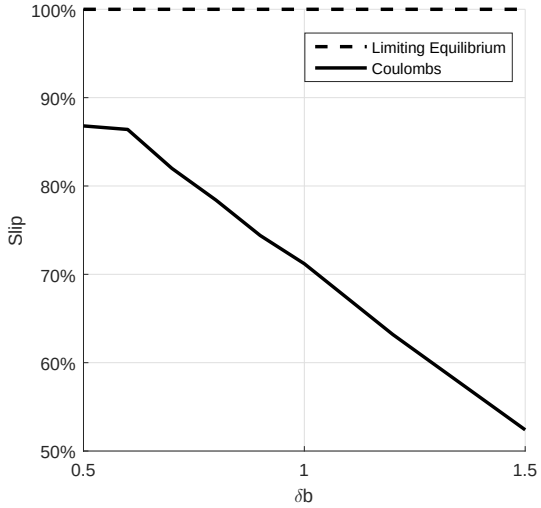

Figure 27: Slip for $\delta b = b/a$.

greater frictional force. This is an intuitive result, and analogous results are found in Section 2.5.3 for the modified capstan equation.

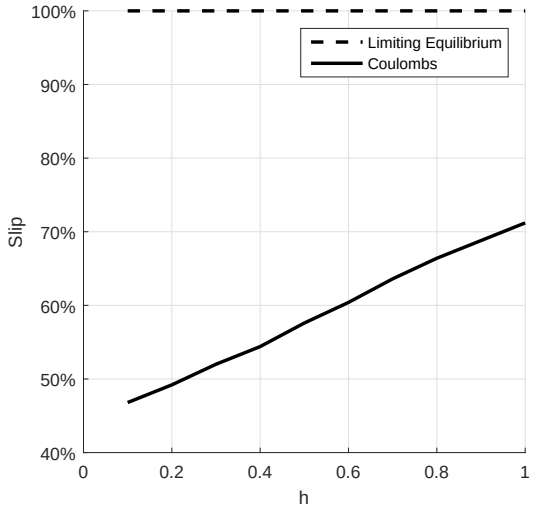

Figure 28: Slip for h.

Figure 28 shows how close the elastic body is to limiting equilibrium for varying thickness of the overlying body, h. For these experiments we assert that $\delta\tau = 2$, $\delta b = 1$, $h \in \{\frac{1}{10}, \frac{2}{10}, \frac{3}{10}, \frac{4}{10}, \frac{5}{10}, \frac{6}{10}, \frac{7}{10}, \frac{8}{10}, \frac{9}{10}, 1\}$, $E = 10^3$ and $\nu = \frac{1}{4}$. Figure 28 implies that as h decreases, the modified Kikuchi and Oden's model moves away from limiting equilibrium, i.e. as the thickness decreases, Coulomb's law of static friction behaves more like the standard friction law.

Another numerical experiment that we conduct is to examine the behaviour of the body under variable Young's modulus, E. For these experiments we assert that $\tau_{\text{max}} = 2$, $b = 2$, $h = 1$, $500 \leq E \leq 1500$ and $\nu = \frac{1}{4}$. We find that the body has a constant slip of 71.2% in the positive x^2 direction for all values of Young's modulus. This is intuitive as, whatever the value of Young's mod-

ulus is (given that it is not zero or infinite), one can always rescale the displacement field without affecting the final form of the solution. This result also tends to coincide with the capstan equation as the capstan equation is also invariant with respect to Young's modulus of the elastic body. Note that for values above $E = 10^{10}$ we observe total bonding. We hypothesise that this is due to the magnitude of ε and not to do with any physical realistic properties as the displacement field can be rescaled for any given value of Young's modulus. Our hypothesis is further justified as when the magnitude of the regularisation parameter is reduced further, we did not observe total bonding for the case $E = 10^{10}$.

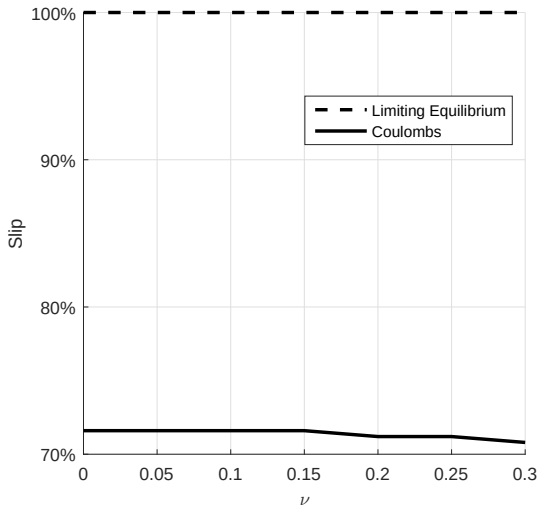

Figure 29: Slip for ν.

Figure 29 shows how close to the elastic body is to limiting equilibrium for varying Poisson's ratio, ν. For these experiments we assert that $\delta\tau = 2$, $\delta b = 2$, $h = 1$, $E = 10^3$ and $\nu \in \{0, \frac{1}{20}, \frac{2}{20}, \frac{3}{20}, \frac{4}{20}, \frac{5}{20}, \frac{6}{20}\}$. Figure 29 implies that as ν increases, the modified Kikuchi and Oden's model moves away from the limiting equilibrium, i.e. as the body becomes incompressible, one needs to apply more force to debonded the body from the rigid surface. This is a surprising result as this tends to contradict the capstan equation, as the modified capstan equation for the infinite width case (see corollary 1) is invariant with respect to Poisson's ratio of the elastic body. This effect is incredibly small, but it is still noticeable. Note that at the value $\nu = \frac{7}{20}$ the terminating error of the solution failed to fall below the value 10^{-10}.

2.7 Conclusions

In this chapter we taken the standard friction law (52) and extend it to model thin objects on rough rigid surfaces in an attempt to extend the capstan equation (13) to more general geometries. In Section 2.3 we derived a closed from solutions for a membrane with a zero-Poisson's ratio (or a string) supported by a rigid prism at limiting equilibrium. Then, in Section 2.4, we derived a closed from solution for a membrane with a zero-Poisson's ratio (or a string) over a rigid cone at limiting equilibrium.

Then, in Section 2.6, we extended Kikuchi and Oden's [102] model for Coulomb's law of static friction to curvilinear coordinates. There, we conducted numerical experiments to see how close Coulomb's law of static friction is to the ordinary friction law (52) is, in curvilinear coordinates. To do this we modelled an elastic body over a rigid rough prism with an elliptical cross section. Our numerical results indicate the following (for a fixed coefficient of friction): (i) capstan coefficient of friction is an underestimate of Coulomb's coefficient of friction, i.e. $\mu_F \leq \nu_F$, (ii) as the critical parametric-latitude of the contact region increases, one require a larger force to debond the body, a result that coincides with the modified capstan equation, (iii) as the thickness of the body decreases, one require a larger force to debond the body, yet this force is still an underestimate to what is predicted by the modified capstan equitation, (iv) Young's modulus of the body does not affect the governing equation of the contact region, a result that coincides with the ordinary capstan equation, and (v) as Poisson's ratio of the body increases, one requires a larger force to debond the body. The last result implies that incompressible elastic bodies such as rubber tend to be more difficult to debond from a rigid surface relative to a compressible object (e.g. piece of marshmallow) with the same coefficient of friction acting on the contact region. Now, this is a surprising result as this behaviour is not predicted by the modified capstan equation as the modified capstan equation is invariant with respect to Poisson's ratio of the body, for the given problem.

Our analysis shows that modelling friction is not a well understood problem. This is due to the fact that for the same value of coefficient of friction different models predict vastly different results, such as different limiting equilibriums. This further implies that, if one's goal is to find the coefficient of friction for a given set of input values, then different models predict a different coefficient of friction for the same set of input values, i.e. coefficient of fiction is dependent on the friction model that is being used to calculate it.

Note that the work we presented in Sections 2.3 and 2.4 has real life significance as it can be easily be applied to cable drive devices (see Section 1.6). Consider an electronic robotic hand, where precision is significant, and consider a tendon running over outer part of a joint. Given that the joint has a noncircular crosses section, hypothetically assume it is elliptical, one can easily calculate the force required to overcome friction with the use of equation (63), or using theorem 1 for a more complicated geometry.

3 Shells Supported by Elastic foundations: Boundary Forms to Model the Bonded Case

Abstract

In this chapter we derive a theory for bonded shells on elastic foundations. We show that, if the diffeomorphism $\bar{\boldsymbol{X}} \in C^2(\bar{\Omega}; \mathbf{E}^3)$ describes the unstrained configuration of the foundation and the injective immersion $\boldsymbol{\sigma} \in C^3(\bar{\omega}; \mathbf{E}^3)$ describes the unstrained configuration of the overlying shell, where $\Omega \subset \mathbb{R}^3$ is a connected open bounded domain that satisfies the segment condition with a uniform-$C^1(\mathbb{R}^3; \mathbb{R}^2)$ boundary $\partial\Omega$ such that $\omega, \partial\Omega_0 \subset \partial\Omega$, $\bar{\omega} \cap \partial\bar{\Omega}_0 = \emptyset$, $\mathrm{meas}(\partial\Omega_0; \mathbb{R}^2) > 0$, and $\omega \subset \mathbb{R}^2$ is a connected open bounded plane that satisfies the segment condition with a uniform-$C^1(\mathbb{R}^2; \mathbb{R})$ boundary $\partial\omega$, with $\boldsymbol{f} \in \boldsymbol{L}^2(\Omega)$, $\boldsymbol{f}_0 \in \boldsymbol{L}^2(\omega)$ and $\boldsymbol{\tau}_0 \in \boldsymbol{L}^2(\partial\omega)$, then there exists a unique field $\boldsymbol{u} \in \boldsymbol{V}_{\mathscr{S}}(\omega, \Omega)$ such that $\boldsymbol{u}$ is the solution to the minimisation problem

$$J(\boldsymbol{u}) = \min_{\boldsymbol{v} \in \boldsymbol{V}_{\mathscr{S}}(\omega,\Omega)} J(\boldsymbol{v}) \, ,$$

where

$$\boldsymbol{V}_{\mathscr{S}}(\omega, \Omega) = \{\boldsymbol{v} \in \boldsymbol{H}^1(\Omega) \mid \boldsymbol{v}|_\omega \in H^1(\omega) \times H^1(\omega) \times H^2(\omega), \ \boldsymbol{v}|_{\partial\Omega_0} = \boldsymbol{0}, \ \partial_\beta(v^3|_\omega)|_{\partial\omega} = 0 \ \forall \beta \in \{1, 2\}\} \, ,$$

$$\begin{aligned} J(\boldsymbol{u}) = &\int_\Omega \left[\frac{1}{2} A^{ijkl} E_{ij}(\boldsymbol{u}) E_{kl}(\boldsymbol{u}) - f^i u_i\right] d\Omega \\ &+ \int_\omega \left[\frac{1}{2} B^{\alpha\beta\gamma\delta} \left(h \epsilon_{\alpha\beta}(\boldsymbol{u}) \epsilon_{\gamma\delta}(\boldsymbol{u}) + \frac{1}{3} h^3 \rho_{\alpha\beta}(\boldsymbol{u}) \rho_{\gamma\delta}(\boldsymbol{u})\right) - h f_0^i u_i\right] d\omega - \int_{\partial\omega} h \pi_0^i u_i \, d(\partial\omega) \, , \end{aligned}$$

and where $\boldsymbol{A}$ is the elasticity tensor and $\boldsymbol{E}(\cdot)$ is the stain tensor of the foundation, and $\boldsymbol{B}$ is the elasticity tensor, $\boldsymbol{\epsilon}(\cdot)$ is half of the change in first fundamental form tensor, $\boldsymbol{\rho}(\cdot)$ is the change in second fundamental form tensor and h is the thickness of the shell. In particular, the unique minimiser $\boldsymbol{u}$ is also a critical point in $(\boldsymbol{V}_{\mathscr{S}}(\omega, \Omega), J(\cdot))$.

3.1 Introduction

In this chapter we develop a theory for elastic shells that are bonded to elastic foundations (see figure 30). In the current literature there exists a limited number of publications on the study of plates and films that are bonded to elastic foundations (see sections 1.7 and 1.10), yet there exists no comprehensive theory to describe the behaviour of shells that are supported by elastic foundations. In Section 3.2, we begin by modifying the linear Koiter's shell equations to describe the behaviour of a shell if it is in contact with a three-dimensional elastic body by considering a technique that is used in the derivation of surface Cauchy-Bourne model [89]. Then, in Section 3.3, we explicitly derive the governing equations and the boundary conditions for the general case. In Section 3.4 we treat the bonded shell as a boundary form of the elastic foundation, which is analogous to the work of Necas *et al.* [144]. Then, we use a combination of Ciarlet's [38], and Badiale and Serra's [13] work to prove the existence and the uniqueness of solutions, and then conduct some numerical experiments in Section 3.5. In Section 3.6 we extend Baldelli and Bourdin's [16] model for bonded films on elastic foundations to curvilinear coordinates and show how numerical solutions fair against our numerical model, with respect to the bonded two-body elastic problem. To conclude our numerical analysis, in Section 3.7, we analyse how effective our model is at approximating the bonded two-body problem. Finally, in Section 3.8, we conclude this chapter with our findings and some notable applications.

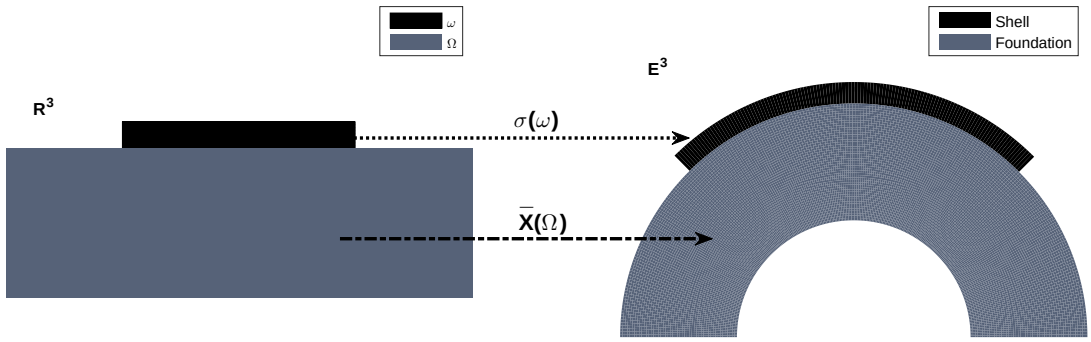

Figure 30: Two-Dimensional schematic representation of the reference configuration of an overlying shell bonded to an elastic foundation.

3.2 Derivation

Consider an unstrained static three-dimensional elastic body described by the diffeomorphism $\bar{\boldsymbol{X}} \in C^2(\bar{\Omega}; \mathbf{E}^3)$, where $\Omega \subset \mathbb{R}^3$ is a connected open bounded domain that satisfies the segment condition with a uniform-$C^1(\mathbb{R}^3; \mathbb{R}^2)$ boundary. Now, assume that on a part of body's boundary, with a positive mean-curvature with respect to the unit outward normal and described by the injection $\boldsymbol{\sigma} \in C^3(\bar{\omega}; \mathbf{E}^2)$ where $\omega \subset \mathbb{R}^2$ is a connected open bounded plane that satisfies the segment condition with a uniform-$C^1(\mathbb{R}^2; \mathbb{R})$ boundary, lies an elastic shell with the same curvature and the same physical form as the given surface, which is also bonded to the surface. Now, recalling the shell equations form from Section 1.4 it is clear that one cannot directly apply the shell equations to describe the behaviour of an overlying shell for the following reasons: (i) if one applies the shell equations as it stands, they imply that both the shell and the elastic body occupy the region $\bar{\omega} \times [0, -\frac{1}{2}h]$, which is not physically viable, and (ii) one may displace the map $\boldsymbol{\sigma}$ by $\frac{1}{2}h\boldsymbol{N}$ amount, where $\boldsymbol{N}$ unit outward normal at the contact region, but this violates the condition that the lower (and the upper) surface of the shell is stress free. Also, the latter condition is problematic as when trying to prove the existence and the uniqueness of the solutions as one will not be able to express the governing equations of shell as a boundary form. Thus, one must consider an alternative way of tackling this problem.

To do so, consider the following: assume an overlying shell whose lower-surface is parameterised by the sufficiently smooth injection $\boldsymbol{\sigma}(x^1, x^2)$. Thus, any surface of the shell can be parameterised by the map $\boldsymbol{\varphi}(x^1, x^2) = \boldsymbol{\sigma} + \xi \boldsymbol{N}(x^1, x^2)$, $\forall\, \xi \in [0, h]$, where h is the thickness of the shell. Now, consider the normal (not the unit normal) of the map $\boldsymbol{\varphi}(x^1, x^2)$, which can be expressed as

$$\partial_1\boldsymbol{\varphi} \times \partial_2\boldsymbol{\varphi} = (\partial_1\boldsymbol{\sigma} \times \partial_2\boldsymbol{\sigma}) \left(1 - \xi F_{[\mathrm{II}]}{}^{\alpha}_{\alpha} + \xi^2 \left(F_{[\mathrm{II}]}{}^{1}_{1} F_{[\mathrm{II}]}{}^{2}_{2} - F_{[\mathrm{II}]}{}^{2}_{1} F_{[\mathrm{II}]}{}^{1}_{2}\right)\right) \ , \ \forall\, \xi \in [0, h] \ .$$

For our analysis we require the normal to any surface of the overlying shell, $\partial_1\boldsymbol{\varphi} \times \partial_2\boldsymbol{\varphi}$, to be the same sign as the normal to the lower-surface, $\partial_1\boldsymbol{\sigma} \times \partial_2\boldsymbol{\sigma}$, and to be almost the same magnitude as the normal to the lower-surface, for all ξ. Now, this can be achieved by asserting the following:

Assertion 1. *Let the map $\boldsymbol{\sigma} \in C^3(\bar{\omega}; \boldsymbol{E}^2)$ describes the lower-surface of an unstrained shell, where $\omega \subset \mathbb{R}^2$ is a connected open bounded plane that satisfies the segment condition with*

a uniform-$C^1(\mathbb{R}^2;\mathbb{R})$ boundary. Given that the thickness of the shell is h, we assert that

$$0 \leq h^2 \left(F_{[II]}{}^1_1 F_{[II]}{}^2_2 - F_{[II]}{}^2_1 F_{[II]}{}^1_2 \right) < -\frac{1}{2} h F_{[II]}{}^\alpha_\alpha \ll 1 \ , \forall \ (x^1, x^2) \in \bar{\omega} \ ,$$

i.e. the lower-surface of the shell is not hyperbolic and it is a surface of positive mean curvature, and the thickness of the shell is sufficiently small .

Note that positive mean-curvature (i.e. $\frac{1}{2} F_{[II]}{}^\alpha_\alpha < 0$) is essential in our numerical modeling in Section 3.5, 3.6 and 3.7. Also, assertion 1 is essential in chapter 4, where we no longer assert that the shell is bonded to the elastic body.

Now, assume that one is dealing with shell with a thickness $2h$, i.e. the energy functional is $J_{2h}(\boldsymbol{w}) = J(\boldsymbol{w}, 2h, \frac{2}{3}h^3)$, where $\boldsymbol{w}$ describes the displacement field with respect to the mid-surface. Given that this shell satisfies the conditions described by assertion 1, its upper and lower half maybe approximated by dividing energy functional of the shell by 2. To be more precise, if $J_{2h}(\boldsymbol{w}) = J_{\text{upper}}(\boldsymbol{w}) + J_{\text{lower}}(\boldsymbol{w})$, then assume that $\frac{1}{2} J_{2h}(\boldsymbol{w}) \approx J_{\text{upper}}(\boldsymbol{w}) \approx J_{\text{lower}}(\boldsymbol{w})$. This is due to the fact that we asserted that the lower-surface of the shell is not hyperbolic and it is a surface of positive mean curvature, and the thickness of the shell is sufficiently small, and thus, these conditions imply that the change in the second fundamental form tensor is small for infinitesimal deformations, i.e. $h^2 F_{[II]}{}^\gamma_\alpha F_{[II]}{}^\alpha_\gamma \approx 0 \implies h^2 \rho^\alpha_\gamma(\boldsymbol{w}) \rho^\gamma_\alpha(\boldsymbol{w}) \approx 0$. Thus, one can expect $J_{2h}(\boldsymbol{w})$ to behave approximately linear in h, despite its cubic h dependence. Now, take the upper half and assert that this is the form of an overlying shell equation: this is a similar logical process that is used in the derivation of surface Cauchy-Bourne model [89]. Thus, we come to our second hypothesis of this thesis:

Hypothesis 2. *The energy functional of an overlying shell with a thickness h is*

$$J(\boldsymbol{u})_{\text{shell}} = \int_\omega \left[\frac{1}{2} B^{\alpha\beta\gamma\delta} \left(h \epsilon_{\alpha\beta}(\boldsymbol{u}) \epsilon_{\gamma\delta}(\boldsymbol{u}) + \frac{1}{3} h^3 \rho_{\alpha\beta}(\boldsymbol{u}) \rho_{\gamma\delta}(\boldsymbol{u}) \right) - h f^i u_i \right] d\omega - \int_{\partial\omega} h \tau^i_0 u_i \ d(\partial\omega) \ ,$$

given that the shell satisfies the conditions from assertion 1, where $\boldsymbol{u}$ describes the displacement field with respect to the lower-surface, the map $\boldsymbol{\sigma} \in C^3(\bar{\omega}; \boldsymbol{E}^2)$ describes the lower-surface of an unstrained shell, and $\omega \subset \mathbb{R}^2$ is a connected open bounded plane that satisfies the segment condition with a uniform-$C^1(\mathbb{R}^2;\mathbb{R})$ boundary.

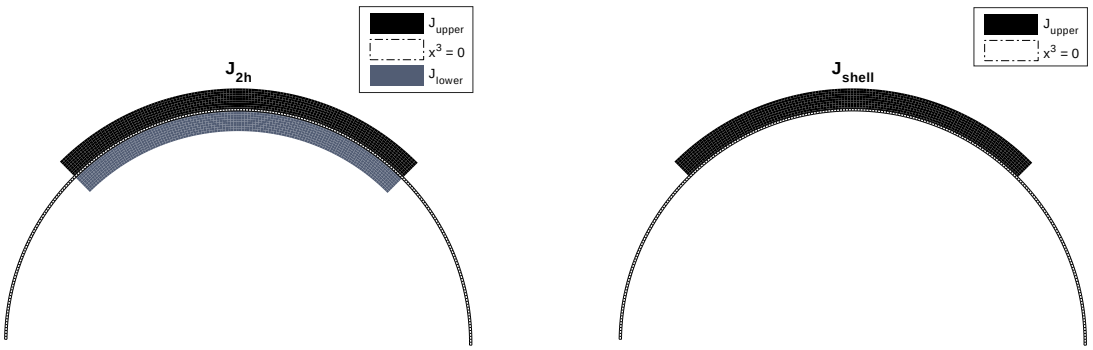

Figure 31: Two-Dimensional schematic representation of hypothesis 2.

Note that there are two things differ from the ordinary shell equations and our overlying shell equations: the choice in the displacement field and the fraction that proceeding the h^3 term. In the

ordinary shell equations the displacement field describes the displacement from the mid-surface and, for a shell with a thickness h, fraction that proceeding the h^3 term is $\frac{1}{12}$. But, in our overlying shell equations the displacement field describes the displacement from the lower-surface and, for a shell with a thickness h, fraction that proceeding the h^3 term is $\frac{1}{3}$. Why does this make sense? Well, consider a thin overlying body. Let the diffeomorphism $\boldsymbol{\Theta} = \boldsymbol{\sigma} + x^3\boldsymbol{N} \in C^2(\bar{\omega} \times [0,h]; \mathbb{R}^3)$ describes the unstrained configuration of this body and let $\boldsymbol{u}(x^1, x^2)$ be the displacement field with respect to the lower-surface, i.e. $\boldsymbol{u}$ is the displacement field with respect to the contact surface. Now, consider the *pure-stretching* case with the displacement field $(u^1, u^2, 0)$, an external force density field $(f^1, f^2, 0)$ and a traction field $(\tau_0^1, \tau_0^2, 0)$. For this case one can express the energy functional as

$$\begin{aligned} J(\boldsymbol{u}) &= \int_\omega \left[\frac{1}{2} h B^{\alpha\beta\gamma\delta} \epsilon_{\alpha\beta}(\boldsymbol{u}) \epsilon_{\gamma\delta}(\boldsymbol{u}) - h f^\alpha u_\alpha\right] d\omega - \int_{\partial\omega} h\tau_0^\alpha u_\alpha \, d(\partial\omega) \\ &= \lim_{u^3, \boldsymbol{\rho}(\boldsymbol{u}) \to 0} J(\boldsymbol{u})_{\text{shell}} \, . \end{aligned}$$

Now, consider the *pure-bending* case with the displacement field $(-x^3\partial^1 u_3, -x^3\partial^2 u_3, 0)$, an external force density field $(f^1, f^2, 0)$ and a traction field $(\tau_0^1, \tau_0^2, 0)$. For this case one can express the energy functional as

$$\begin{aligned} J(\boldsymbol{u}) &= \int_\omega \left[\frac{1}{2}\left(\frac{1}{3}h^3\right) B^{\alpha\beta\gamma\delta} \rho_{\alpha\beta}(\boldsymbol{u}) \rho_{\gamma\delta}(\boldsymbol{u}) - h f^3 u_3\right] d\omega - \int_{\partial\omega} h\tau_0^3 u_3 \, d(\partial\omega) \\ &= \lim_{u^1, u^2, \boldsymbol{\epsilon}(\boldsymbol{u}) \to 0} J(\boldsymbol{u})_{\text{shell}} \, , \end{aligned}$$

where $f^3 = \frac{1}{2} h \nabla_\alpha f^\alpha$ and $\tau_0^3 = \frac{1}{2} h \nabla_\alpha \tau_0^\alpha$. Thus, if one considers the pure-stretching and the pure-bending case separately for a thin overlying body where the displacement field is approximated by the displacement with respect to the contact region, then hypothesis 2 perfectly coincides with the each respective energy functionals. Can the reader now see why hypothesis 2 makes sense?

Now, with hypothesis 2 one can finally express the equations for a bonded shell on an elastic foundation, which leads to the following theorem:

Theorem 3. *Let $\Omega \subset \mathbb{R}^3$ be a connected open bounded domain that satisfies the segment condition with a uniform-$C^1(\mathbb{R}^3; \mathbb{R}^2)$ boundary $\partial\Omega$ such that $\omega, \partial\Omega_0 \subset \partial\Omega$, where $\bar{\omega} \cap \partial\bar{\Omega}_0 = \emptyset$ with $\operatorname{meas}(\partial\Omega_0; \mathbb{R}^2) > 0$, and let $\omega \subset \mathbb{R}^2$ be a connected open bounded plane that satisfies the segment condition with a uniform-$C^1(\mathbb{R}^2; \mathbb{R})$ boundary $\partial\omega$. Let $\bar{\boldsymbol{X}} \in C^2(\bar{\Omega}; \boldsymbol{E}^3)$ be a diffeomorphism and $\boldsymbol{\sigma} \in C^3(\bar{\omega}; \boldsymbol{E}^3)$ be an injective immersion. Let $\boldsymbol{f} \in \boldsymbol{L}^2(\Omega)$, $\boldsymbol{f}_0 \in \boldsymbol{L}^2(\omega)$ and $\boldsymbol{\tau}_0 \in \boldsymbol{L}^2(\partial\omega)$. Then there exists a unique field $\boldsymbol{u} \in \boldsymbol{V}_{\mathscr{I}}(\omega, \Omega)$ such that $\boldsymbol{u}$ is the solution to the minimisation problem*

$$J(\boldsymbol{u}) = \min_{\boldsymbol{v} \in \boldsymbol{V}_{\mathscr{I}}(\omega,\Omega)} J(\boldsymbol{v}) \, ,$$

where

$$\boldsymbol{V}_{\mathscr{I}}(\omega, \Omega) = \{\boldsymbol{v} \in \boldsymbol{H}^1(\Omega) \mid \boldsymbol{v}|_\omega \in H^1(\omega) \times H^1(\omega) \times H^2(\omega), \ \boldsymbol{v}|_{\partial\Omega_0} = \boldsymbol{0}, \ \partial_\beta(v^3|_\omega)|_{\partial\omega} = 0 \ \forall \beta \in \{1, 2\}\} \, ,$$

$$\begin{aligned} J(\boldsymbol{u}) = &\int_\Omega \left[\frac{1}{2} A^{ijkl} E_{ij}(\boldsymbol{u}) E_{kl}(\boldsymbol{u}) - f^i u_i\right] d\Omega \\ &+ \int_\omega \left[\frac{1}{2} B^{\alpha\beta\gamma\delta}\left(h\epsilon_{\alpha\beta}(\boldsymbol{u})\epsilon_{\gamma\delta}(\boldsymbol{u}) + \frac{1}{3}h^3 \rho_{\alpha\beta}(\boldsymbol{u})\rho_{\gamma\delta}(\boldsymbol{u})\right) - h f_0^i u_i\right] d\omega - \int_{\partial\omega} h\tau_0^i u_i \, d(\partial\omega) \, . \end{aligned}$$

In particular, the unique minimiser $\boldsymbol{u}$ is also a critical point in $(\boldsymbol{V}_{\mathscr{I}}(\omega, \Omega), J(\cdot))$.

Proof. See Section 3.4. □

Note that by $\boldsymbol{v}|_{\partial\Omega_0}$ and $\boldsymbol{v}|_{\omega}$ we mean in a trace sense.

What does theorem 3 mean? Well, it means that for some well-posed normal and tangential forcings, and tractions acting on a shell with a thickness h that is bonded to an elastic foundation, $J(\cdot)$ has a unique weak solution in the set $\boldsymbol{V}_{\mathscr{S}}(\omega, \Omega)$. This weak solution is sufficient for finding finite-element solutions. For a comprehensive study of finite-element modelling of similar problems please consult chapter 4 of Kikuchi and Oden [102]. However, one requires higher regularity results to prove the existence of classical solutions. This problem is a subject of discussion in Section 5.3. Also, note that due to the conditions $\partial_\beta(u^3|_\omega)|_{\partial\omega} = 0, \forall\ \beta \in \{1, 2\}$, external moments cannot be applied to the boundary of the shell.

Theorem 3 is also valid for the weaker conditions $\boldsymbol{f} \in \boldsymbol{L}^{\frac{6}{5}}(\Omega)$ (see theorem 3.9-2 of Ciarlet [39]), $f_0^\alpha \in L^r(\omega)\ \forall\ \alpha \in \{1, 2\}$ and $f_0^3 \in L^1(\omega)$, where $r > 1$ (see theorem 4.4-2 of Ciarlet [39]). However, we are unfamiliar with the proof, and thus, we refrain from asserting these weaker conditions herein.

Note that the displacement $\boldsymbol{u}$ restricted to the boundary ω should be understood in the context of the statement. For example, by $\int_\omega \boldsymbol{u}\ d\omega$ we mean that $\int_\omega \boldsymbol{u}|_\omega\ d\omega$, where $u|_\omega$ in a trace sense. We often neglect the term $|_\omega$ for convenience.

3.3 Equations of Equilibrium

For this section we assume that $\boldsymbol{u} \in C^2(\Omega; \mathbb{R}^3)$ with $u^\alpha|_\omega \in C^3(\omega)$ and $u^3|_\omega \in C^4(\omega)$, and use theorem 3 to derive a set of governing equations and boundary conditions for our problem.

3.3.1 Governing Equations of the Elastic Foundation

$$\bar{\nabla}_i T^i_j(\boldsymbol{u}) + f_j = 0\ ,\ \forall\ j \in \{1, 2, 3\}\ ,$$

where $T^{ij}(\boldsymbol{u}) = A^{ijkl}E_{kl}(\boldsymbol{u})$ is second Piola-Kirchhoff stress tensor, $E_{ij}(\boldsymbol{u}) = \frac{1}{2}(g_{ik}\bar{\nabla}_j u^k + g_{jk}\bar{\nabla}_i u^k)$ is linearised Green-St Venant stress tensor, $A^{ijkl} = \bar{\lambda}g^{ij}g^{kl} + \bar{\mu}(g^{ik}g^{jl} + g^{il}g^{jk})$ is the isotropic elasticity tensor, $\bar{\lambda} = (1 - \bar{\nu} - 2\bar{\nu}^2)^{-1}\bar{\nu}\bar{E}$ is first Lamé's parameter, $\bar{\mu} = \frac{1}{2}(1 + \bar{\nu})^{-1}\bar{E}$ is second Lamé's parameter, $\bar{E}$ is Young's modulus and $\bar{\nu}$ is Poisson's ratio of the elastic foundation, and $\boldsymbol{f}$ is an external force density field acting on the elastic foundation.

3.3.2 Boundary Conditions of the Elastic Foundation

$$\boldsymbol{u}|_{\partial\Omega_0} = \boldsymbol{0}\ , \tag{68}$$

$$\bar{n}_i T^i_j(\boldsymbol{u})|_{\{\partial\Omega\setminus\{\omega\cup\partial\Omega_0\}\}} = 0\ ,\ \forall\ j \in \{1, 2, 3\}\ , \tag{69}$$

where $\bar{\boldsymbol{n}}$ is the unit outward normal to the boundary $\partial\Omega$ in curvilinear coordinates. Dirichlet boundary condition (68) is often referred to as the *zero-displacement* boundary condition and Robin boundary condition (69) is often referred to as the *stress free* boundary condition.

3.3.3 Governing Equations of the Overlying Shell

$$\nabla_\alpha \tau^\alpha_\beta(\boldsymbol{u}) + \frac{2}{3}h^2 F_{[\mathrm{II}]\beta}^{\ \alpha} \nabla_\gamma \eta^\gamma_\alpha(\boldsymbol{u}) + \frac{1}{3}h^2 \left(\nabla_\gamma F_{[\mathrm{II}]\beta}^{\ \alpha}\right) \eta^\gamma_\alpha(\boldsymbol{u}) - \frac{1}{h}\mathrm{Tr}(T^3_\beta(\boldsymbol{u})) + f_{0\beta} = 0 \ , \ \forall\, \beta \in \{1,2\} \ ,$$
$$F_{[\mathrm{II}]\alpha}^{\ \ \gamma} \tau^\alpha_\gamma(\boldsymbol{u}) - \frac{1}{3}h^2 \nabla_\alpha \left(\nabla_\gamma \eta^{\alpha\gamma}(\boldsymbol{u})\right) + \frac{1}{3}h^2 F_{[\mathrm{II}]\alpha}^{\ \ \delta} F_{[\mathrm{II}]\gamma}^{\ \ \alpha} \eta^\gamma_\delta(\boldsymbol{u}) - \frac{1}{h}\mathrm{Tr}(T^3_3(\boldsymbol{u})) + f_{03} = 0 \ ,$$

where $\tau^{\alpha\beta}(\boldsymbol{u}) = B^{\alpha\beta\gamma\delta}\epsilon_{\gamma\delta}(\boldsymbol{u})$ is the stress tensor, $\eta^{\alpha\beta}(\boldsymbol{u}) = B^{\alpha\beta\gamma\delta}\rho_{\gamma\delta}(\boldsymbol{u})$ negative of the change in moments density tensor,

$$\epsilon_{\alpha\beta}(\boldsymbol{u}) = \frac{1}{2}\left(\nabla_\alpha(u_\beta|_\omega) + \nabla_\beta(u_\alpha|_\omega)\right) - F_{[\mathrm{II}]\alpha\beta}(u^3|_\omega)$$

is half of the change in first fundamental form tensor,

$$\rho_{\alpha\beta}(\boldsymbol{u}) = \nabla_\alpha\nabla_\beta(u^3|_\omega) - F_{[\mathrm{II}]\alpha\gamma}F_{[\mathrm{II}]\beta}^{\ \ \gamma}(u^3|_\omega) + F_{[\mathrm{II}]\beta\gamma}\nabla_\alpha(u^\gamma|_\omega) + F_{[\mathrm{II}]\alpha\gamma}\nabla_\beta(u^\gamma|_\omega) + \left(\nabla_\alpha F_{[\mathrm{II}]\beta\gamma}\right)(u^\gamma|_\omega)$$

the change in second fundamental form tensor,

$$B^{\alpha\beta\gamma\delta} = \frac{2\lambda\mu}{\lambda+2\mu}F_{[\mathrm{I}]}^{\alpha\beta}F_{[\mathrm{I}]}^{\gamma\delta} + \mu(F_{[\mathrm{I}]}^{\alpha\gamma}F_{[\mathrm{I}]}^{\beta\delta} + F_{[\mathrm{I}]}^{\alpha\delta}F_{[\mathrm{I}]}^{\beta\gamma})$$

is the isotropic elasticity tensor, $\lambda = (1-\nu-2\nu^2)^{-1}\nu E$ is first Lamé's parameter, $\mu = \frac{1}{2}(1+\nu)^{-1}E$ is second Lamé's parameter, E is Young's modulus and ν is Poisson's ratio of the overlying bonded shell, $\mathrm{Tr}(T^3_j(\boldsymbol{u})) = T^3_j(\boldsymbol{u})|_\omega$ is the normal stresses of the foundation at the contact region and $\boldsymbol{f}_0$ is an external force density field action on the overlying bonded shell.

3.3.4 Boundary Conditions of the Overlying Shell

$$\begin{aligned}
\left[n_\alpha \tau^\alpha_\beta(\boldsymbol{u}) + \frac{2}{3}h^2 n_\gamma F_{[\mathrm{II}]\beta}^{\ \ \alpha}\eta^\gamma_\alpha(\boldsymbol{u})\right]|_{\partial\omega} &= \tau_{0\beta} \ , \ \forall\, \beta \in \{1,2\} \ , \\
-\frac{1}{3}h^2 n_\gamma \nabla_\alpha \eta^{\alpha\gamma}(\boldsymbol{u})|_{\partial\omega} &= \tau_{03} \ , \\
\partial_\beta(u^3|_\omega)|_{\partial\omega} &= 0 \ , \ \forall\, \beta \in \{1,2\} \ ,
\end{aligned} \tag{70}$$

where $\boldsymbol{n}$ is the unit outward normal vector to the boundary $\partial\omega$ in curvilinear coordinates and $\boldsymbol{\tau}_0$ is an external traction field acting on the boundary of the overlying bonded shell. Neumann boundary condition (70) is often referred to as the *zero-slope* boundary condition. Due the zero-slope boundary conditions one cannot apply external moments to the boundary of the shell. If one requires to apply boundary moments to the shell, then one must assume that $\partial_\beta(u^3|_\omega)|_{\partial\omega}$ are unknowns. The reason that we insist upon the zero-slope boundary conditions is described in Section 5.2.

3.4 Existence and Uniqueness of Solutions

In this section we prove theorem 3, and thus, finally concluding that the model derived in this chapter is a mathematical theory. As we consider the equations of the overlying shell as a boundary form of the foundation, one may think that we may easily prove the existence and the uniqueness of solutions of our problem with the use of mathematical techniques for boundary forms put forward by Necas *et al.* [144] (see chapter 4 of Necas *et al.* [144]). However, this is not the case. This is due to the fact that $\boldsymbol{u}$ requires higher regularity at the boundary than in the interior of the foundation. Thus, we need to prove the existence and the uniqueness results from scratch. However, we still

retain the mathematical techniques introduced by Necas *et al.* [144] in our proof.

Step 1 : Reflexive

The space

$$\boldsymbol{W}(\omega,\Omega) = \{\boldsymbol{v} \in \boldsymbol{H}^1(\Omega) \mid \boldsymbol{v}|_\omega \in H^1(\omega)\times H^1(\omega)\times H^2(\omega)\} \ ,$$

equipped with the norm

$$||\boldsymbol{v}||_{\boldsymbol{W}(\omega,\Omega)} = \left(||v^1||^2_{H^1(\Omega)}+||v^2||^2_{H^1(\Omega)}+||v^3||^2_{H^1(\Omega)}+||v^1|_\omega||^2_{H^1(\omega)}+||v^2|_\omega||^2_{H^1(\omega)}+||v^3|_\omega||^2_{H^2(\omega)}\right)^{\frac{1}{2}} \ ,$$

is a Hilbert space, and thus, it is reflexive. This is due to the fact that $\boldsymbol{W}(\omega,\Omega)$ is a finite Cartesian product of Hilbert spaces equipped with a product norm consists of a finite collection of the norms of each respective spaces. This is a trivial result. For comments on the subject please see the proof of theorem 7.19 of Sokal [182].

Step 2 : Coercive

$J(\boldsymbol{u})$ is coercive in the set $\boldsymbol{V}_{\mathscr{S}}(\omega,\Omega)$ with respect to the norm $||\cdot||_{\boldsymbol{W}(\omega,\Omega)}$. To show this we introduce *Korn's inequity*, which states that there exists a constant C that depends on Ω, $\partial\Omega_0$, $\bar{\boldsymbol{X}}$, ω, $\partial\omega$ and $\boldsymbol{\sigma}$ such that

$$||\boldsymbol{u}||_{\boldsymbol{W}(\omega,\Omega)} \leq C\left(||\boldsymbol{E}(\boldsymbol{u})||^2_{\boldsymbol{L}^2(\Omega)} + ||\boldsymbol{\epsilon}(\boldsymbol{u})||^2_{\boldsymbol{L}^2(\omega)} + ||\boldsymbol{\rho}(\boldsymbol{u})||^2_{\boldsymbol{L}^2(\omega)}\right)^{\frac{1}{2}} \ , \ \forall \ \boldsymbol{u} \in \boldsymbol{V}_{\mathscr{S}}(\omega,\Omega) \ . \tag{71}$$

This implies that $\boldsymbol{V}_{\mathscr{S}}(\omega,\Omega)$ is a closed subspace of the complete space $\boldsymbol{W}(\omega,\Omega)$, closed under the norm $||\cdot||_{\boldsymbol{W}(\omega,\Omega)}$. The given Korn's inequality (71) can be proved by combining and modifying the proofs of theorems 1.7-2, 1.7-4, 2.6-1 and 2.6-4 of Ciarlet [38]. For an explicit proof please see Section 3.4.1.

Now, recall the energy functional from theorem 3 and consider that

$$\begin{aligned}
J(\boldsymbol{u}) &= \int_\Omega \left[\frac{1}{2}A^{ijkl}E_{ij}(\boldsymbol{u})E_{kl}(\boldsymbol{u}) - f^i u_i\right] d\Omega \\
&\quad + \int_\omega \left[\frac{1}{2}B^{\alpha\beta\gamma\delta}\left(h\epsilon_{\alpha\beta}(\boldsymbol{u})\epsilon_{\gamma\delta}(\boldsymbol{u}) + \frac{1}{3}h^3\rho_{\alpha\beta}(\boldsymbol{u})\rho_{\gamma\delta}(\boldsymbol{u})\right) - hf^i_0 u_i\right] d\omega - \int_{\partial\omega} h\tau^i_0 u_i \ d(\partial\omega) \\
&\geq C_1||\boldsymbol{E}(\boldsymbol{u})||^2_{\boldsymbol{L}^2(\Omega)} + C_2\left(h||\boldsymbol{\epsilon}(\boldsymbol{u})||^2_{\boldsymbol{L}^2(\omega)} + \frac{1}{3}h^3||\boldsymbol{\rho}(\boldsymbol{u})||^2_{\boldsymbol{L}^2(\omega)}\right) \\
&\quad - C_3||\boldsymbol{f}||_{\boldsymbol{L}^2(\Omega)}||\boldsymbol{u}||_{\boldsymbol{L}^2(\Omega)} - hC_3||\boldsymbol{f}_0||_{\boldsymbol{L}^2(\omega)}||\boldsymbol{u}||_{\boldsymbol{L}^2(\omega)} - hC_4||\boldsymbol{\tau}_0||_{\boldsymbol{L}^2(\partial\omega)}||\boldsymbol{u}||_{\boldsymbol{L}^2(\partial\omega)} \\
&\geq C_5||\boldsymbol{u}||^2_{\boldsymbol{W}(\omega,\Omega)} - C_3||\boldsymbol{f}||_{\boldsymbol{L}^2(\Omega)}||\boldsymbol{u}||_{\boldsymbol{L}^2(\Omega)} - hC_3||\boldsymbol{f}_0||_{\boldsymbol{L}^2(\omega)}||\boldsymbol{u}||_{\boldsymbol{L}^2(\omega)} - C_6||\boldsymbol{u}||_{\boldsymbol{H}^1(\omega)} \\
&\geq C_5||\boldsymbol{u}||^2_{\boldsymbol{W}(\omega,\Omega)} - C_7||\boldsymbol{u}||_{\boldsymbol{W}(\omega,\Omega)} - C_8||\boldsymbol{u}||_{\boldsymbol{H}^1(\omega)} \\
&\geq C_5||\boldsymbol{u}||^2_{\boldsymbol{W}(\omega,\Omega)} - C_9||\boldsymbol{u}||_{\boldsymbol{W}(\omega,\Omega)} \ , \ \forall \ \boldsymbol{u} \in \boldsymbol{V}_{\mathscr{S}}(\omega,\Omega) \ .
\end{aligned}$$

This implies that there exist positive constants c_1 and c_2 that depends on Ω, $\partial\Omega_0$, $\bar{\boldsymbol{X}}$, ω, $\partial\omega$ and $\boldsymbol{\sigma}$ such that $J(\boldsymbol{u}) \geq c_1||\boldsymbol{u}||^2_{\boldsymbol{W}(\omega,\Omega)} - c_2||\boldsymbol{u}||_{\boldsymbol{W}(\omega,\Omega)}, \ \forall \ \boldsymbol{u} \in \boldsymbol{V}_{\mathscr{S}}(\omega,\Omega)$, i.e. $J(\boldsymbol{u})$ is coercive. Note that the constant C_1 follows from positive definiteness of the elasticity tensor (lemma 5) and proposition 4, C_2 follows form the positive definiteness of the elasticity tensor on a general surface (lemma 6) and proposition 5. Furthermore, C_3 and C_4 follow from Hölder inequality (proposition 6), C_5 follow

from Korn's inequality (71), and C_6 follows from the boundary trace embedding theorem (lemma 11).

Step 3 : Differentiable

$J(\boldsymbol{u})$ is Fréchet differentiable. To show this, let $\boldsymbol{u} \in \boldsymbol{W}(\omega, \Omega)$ and consider the Gâteaux derivative of the functional $J(\boldsymbol{u})$,

$$
\begin{aligned}
J'(\boldsymbol{u})\boldsymbol{v} &= \int_\Omega \left[A^{ijkl} E_{ij}(\boldsymbol{u}) E_{kl}(\boldsymbol{v}) - f^i v_i\right] d\Omega \\
&\quad + \int_\omega \left[B^{\alpha\beta\gamma\delta}\left(h\epsilon_{\alpha\beta}(\boldsymbol{u})\epsilon_{\gamma\delta}(\boldsymbol{v}) + \frac{1}{3}h^3 \rho_{\alpha\beta}(\boldsymbol{u})\rho_{\gamma\delta}(\boldsymbol{v})\right) - h f_0^i v_i\right] d\omega - \int_{\partial\omega} h\tau_0^i v_i \, d(\partial\omega) \\
&\leq C_1 ||\boldsymbol{E}(\boldsymbol{u})||_{\boldsymbol{L}^2(\Omega)} ||\boldsymbol{E}(\boldsymbol{v})||_{\boldsymbol{L}^2(\Omega)} \\
&\quad + C_2\left(||\boldsymbol{\epsilon}(\boldsymbol{u})||_{\boldsymbol{L}^2(\omega)} ||\boldsymbol{\epsilon}(\boldsymbol{v})||_{\boldsymbol{L}^2(\omega)} + \frac{1}{3}h^3 ||\boldsymbol{\rho}(\boldsymbol{u})||_{\boldsymbol{L}^2(\omega)} ||\boldsymbol{\rho}(\boldsymbol{v})||_{\boldsymbol{L}^2(\omega)}\right) \\
&\quad + C_3 ||\boldsymbol{f}||_{\boldsymbol{L}^2(\Omega)} ||\boldsymbol{v}||_{\boldsymbol{L}^2(\Omega)} + hC_3 ||\boldsymbol{f}_0||_{\boldsymbol{L}^2(\omega)} ||\boldsymbol{v}||_{\boldsymbol{L}^2(\omega)} + hC_4 ||\boldsymbol{\tau}_0||_{\boldsymbol{L}^2(\partial\omega)} ||\boldsymbol{v}||_{\boldsymbol{L}^2(\partial\omega)} \\
&\leq C_5 ||\boldsymbol{u}||_{\boldsymbol{W}(\omega,\Omega)} ||\boldsymbol{v}||_{\boldsymbol{W}(\omega,\Omega)} \\
&\quad + C_3 ||\boldsymbol{f}||_{\boldsymbol{L}^2(\Omega)} ||\boldsymbol{v}||_{\boldsymbol{L}^2(\Omega)} + hC_3 ||\boldsymbol{f}_0||_{\boldsymbol{L}^2(\omega)} ||\boldsymbol{v}||_{\boldsymbol{L}^2(\omega)} + C_6 ||\boldsymbol{v}||_{\boldsymbol{H}^1(\omega)} \\
&\leq C_5 ||\boldsymbol{u}||_{\boldsymbol{W}(\omega,\Omega)} ||\boldsymbol{v}||_{\boldsymbol{W}(\omega,\Omega)} + C_7 ||\boldsymbol{v}||_{\boldsymbol{W}(\omega,\Omega)} + C_8 ||\boldsymbol{v}||_{\boldsymbol{H}^1(\omega)} \\
&\leq C_5 ||\boldsymbol{u}||_{\boldsymbol{W}(\omega,\Omega)} ||\boldsymbol{v}||_{\boldsymbol{W}(\omega,\Omega)} + C_9 ||\boldsymbol{v}||_{\boldsymbol{W}(\omega,\Omega)} \\
&\leq C\left(||\boldsymbol{u}||_{\boldsymbol{W}(\omega,\Omega)} + 1\right) ||\boldsymbol{v}||_{\boldsymbol{W}(\omega,\Omega)} \ , \ \forall \ \boldsymbol{v} \in \boldsymbol{W}(\omega, \Omega) \ .
\end{aligned}
$$

This implies that there exists a positive constant C that depends on Ω, $\partial\Omega_0$, $\bar{\boldsymbol{X}}$, ω, $\partial\omega$ and $\boldsymbol{\sigma}$ such that $|J'(\boldsymbol{u})| \leq C(||\boldsymbol{u}||_{\boldsymbol{W}(\omega,\Omega)} + 1)$, $\forall \ \boldsymbol{u} \in \boldsymbol{W}(\omega, \Omega)$. Now, this implies that $J'(\boldsymbol{u})$ is continuous in $\boldsymbol{W}'(\omega, \Omega)$, which is the topological dual space of $\boldsymbol{W}(\omega, \Omega)$. By lemma 14, $J(\boldsymbol{u})$ is Fréchet differentiable. Note that the constant C_6 follows from the boundary trace embedding theorem (lemma 11).

Step 4 : Strictly Convex

$J(\boldsymbol{u})$ is strictly convex. To show this consider the following relation,

$$
\begin{aligned}
\left(J'(\boldsymbol{u}) - J'(\boldsymbol{v})\right)(\boldsymbol{u} - \boldsymbol{v}) &= \int_\Omega A^{ijkl}\left(E_{ij}(\boldsymbol{u}) - E_{ij}(\boldsymbol{v})\right)\left(E_{kl}(\boldsymbol{u}) - E_{kl}(\boldsymbol{v})\right) \, d\Omega \\
&\quad + h\int_\omega B^{\alpha\beta\gamma\delta}\left(\epsilon_{\alpha\beta}(\boldsymbol{u}) - \epsilon_{\alpha\beta}(\boldsymbol{v})\right)\left(\epsilon_{\gamma\delta}(\boldsymbol{u}) - \epsilon_{\gamma\delta}(\boldsymbol{v})\right) \, d\omega \\
&\quad + \frac{1}{3}h^3\int_\omega B^{\alpha\beta\gamma\delta}\left(\rho_{\alpha\beta}(\boldsymbol{u}) - \rho_{\alpha\beta}(\boldsymbol{v})\right)\left(\rho_{\gamma\delta}(\boldsymbol{u}) - \rho_{\gamma\delta}(\boldsymbol{v})\right) \, d\omega \\
&\geq C_1 ||\boldsymbol{E}(\boldsymbol{u}) - \boldsymbol{E}(\boldsymbol{v})||^2_{\boldsymbol{L}^2(\Omega)} \\
&\quad + C_2\left(h||\boldsymbol{\epsilon}(\boldsymbol{u}) - \boldsymbol{\epsilon}(\boldsymbol{v})||^2_{\boldsymbol{L}^2(\omega)} + \frac{1}{3}h^3 ||\boldsymbol{\rho}(\boldsymbol{u}) - \boldsymbol{\rho}(\boldsymbol{v})||^2_{\boldsymbol{L}^2(\omega)}\right) \\
&\geq C||\boldsymbol{u} - \boldsymbol{v}||^2_{\boldsymbol{W}(\omega,\Omega)} \ , \ \forall \ \boldsymbol{u}, \boldsymbol{v} \in \boldsymbol{W}(\omega, \Omega) \ .
\end{aligned}
$$

This implies that there exists a positive constant C that depends on Ω, $\partial\Omega_0$, $\bar{\boldsymbol{X}}$, ω, $\partial\omega$ and $\boldsymbol{\sigma}$ such that $\left(J'(\boldsymbol{u}) - J'(\boldsymbol{v})\right)(\boldsymbol{u} - \boldsymbol{v}) \geq C||\boldsymbol{u} - \boldsymbol{v}||^2_{\boldsymbol{W}(\omega,\Omega)}$, $\forall \ \boldsymbol{u}, \boldsymbol{v} \in \boldsymbol{W}(\omega, \Omega)$. By lemma 16, $J(\boldsymbol{u})$ is strictly convex. Note that the constant C_1 follows from positive definiteness of the elasticity tensor (lemma 5) and proposition 4, and C_2 follows from the positive definiteness of the elasticity tensor on a general surface (lemma 6) and proposition 5.

The above analyses imply that $J(\cdot) : \boldsymbol{V}_{\mathscr{S}}(\omega,\Omega) \subset \boldsymbol{W}(\omega,\Omega) \to \mathbb{R}$ is a coercive differentiable strictly-convex functional, where $\boldsymbol{V}_{\mathscr{S}}(\omega,\Omega)$ is complete as subspace of the reflexive Banach space $\boldsymbol{W}(\omega,\Omega)$ under the norm $||\cdot||_{\boldsymbol{W}(\omega,\Omega)}$. Thus, lemmas 17 and 18 imply that there exists a unique field $\boldsymbol{u} \in \boldsymbol{V}_{\mathscr{S}}(\omega,\Omega)$ such that $\boldsymbol{u}$ is the solution to the minimisation problem $J(\boldsymbol{u}) = \min_{\boldsymbol{v}\in\boldsymbol{V}_{\mathscr{S}}(\omega,\Omega)} J(\boldsymbol{v})$. In particular, this unique minimiser $\boldsymbol{u}$ is also a critical point in $(\boldsymbol{V}_{\mathscr{S}}(\omega,\Omega), J(\cdot))$.

As a result of the symmetry (in indices $\{\{1^{\text{st}}, 2^{\text{nd}}\}, \{3^{\text{rd}}, 4^{\text{th}}\}\}$) of the elasticity tensors $\boldsymbol{A}$ and $\boldsymbol{B}$, one can also use *Lax-Milgram Theorem* (see section 6.2.1 of Evans [63]) to prove the existence and the uniqueness of solutions. Although, we do not explicitly use the *segment condition* (definition 6), it is used in some fundamental theorems that are necessary for our proof to work, as the segment condition ensures that the boundary of an n-dimensional domain is an $(n-1)$-dimensional and that the boundary remains on one side of the domain.

3.4.1 Korn's Inequality

In this section we prove Korn's inequality that we introduced, i.e. equation (71). The following proof is a combination of the modified versions of Ciarlet's [38] proofs of theorems 1.7-2, 1.7-4, 2.6-1 and 2.6-4.

Step 1 : Korn's Inequality Without Boundary Conditions

Consider the space

$$\boldsymbol{K}(\omega,\Omega) = \{\boldsymbol{v} \in \boldsymbol{L}^2(\Omega) \mid \boldsymbol{v}|_\omega \in L^2(\omega)\times L^2(\omega)\times H^1(\omega),\ \boldsymbol{E}(\boldsymbol{v}) \in \boldsymbol{L}^2(\Omega),\ \boldsymbol{\epsilon}(\boldsymbol{v}) \in \boldsymbol{L}^2(\omega),\ \boldsymbol{\rho}(\boldsymbol{v}) \in \boldsymbol{L}^2(\omega)\}\ ,$$

equipped with the norm

$$||\boldsymbol{v}||_{\boldsymbol{K}(\omega,\Omega)} = \Big(||\boldsymbol{v}||^2_{\boldsymbol{L}^2(\Omega)} + ||v^1||^2_{L^2(\omega)} + ||v^2||^2_{L^2(\omega)} + ||v^3||^2_{H^1(\omega)} + ||\boldsymbol{E}(\boldsymbol{v})||^2_{\boldsymbol{L}^2(\Omega)} + ||\boldsymbol{\epsilon}(\boldsymbol{v})||^2_{\boldsymbol{L}^2(\omega)} + ||\boldsymbol{\rho}(\boldsymbol{v})||^2_{\boldsymbol{L}^2(\omega)}\Big)^{\frac{1}{2}},$$

where $\boldsymbol{E}(\boldsymbol{u}) \in \boldsymbol{L}^2(\Omega)$, $\boldsymbol{\epsilon}(\boldsymbol{u}) \in \boldsymbol{L}^2(\omega)$ and $\boldsymbol{\rho}(\boldsymbol{u}) \in \boldsymbol{L}^2(\omega)$ in a sense of distributions. We assert that there exists a positive constant C that depends on Ω, $\partial\Omega_0$, $\bar{\boldsymbol{X}}$, ω, $\partial\omega$ and $\boldsymbol{\sigma}$ such that

$$||\boldsymbol{u}||_{\boldsymbol{W}(\omega,\Omega)} \leq C||\boldsymbol{u}||_{\boldsymbol{K}(\omega,\Omega)}\ ,\ \forall\ \boldsymbol{u} \in \boldsymbol{W}(\omega,\Omega)\ , \tag{72}$$

i.e. *Korn's inequality without boundary conditions*.

First we must show that the space $(\boldsymbol{K}(\omega,\Omega), ||\cdot||_{\boldsymbol{K}(\omega,\Omega)})$ is a complete space. To prove this, let $\{\boldsymbol{u}_m\}_{m\in\mathbb{N}} \subset \boldsymbol{K}(\omega,\Omega)$ be a Cauchy sequence. As $L^2(\Omega)$, $L^2(\omega)$ and $H^1(\omega)$ are complete and the fact that $||\cdot||_{\boldsymbol{K}(\omega,\Omega)}$ is a product norm with a finite collection of the standard norms in $L^2(\Omega)$, $H^1(\omega)$ and $L^2(\omega)$, there exist unique fields $\boldsymbol{u} \in \{\boldsymbol{v} \in \boldsymbol{L}^2(\Omega) \mid \boldsymbol{v}|_\omega \in L^2(\omega)\times L^2(\omega)\times H^1(\omega)\}$, $\boldsymbol{E} \in \boldsymbol{L}^2(\Omega)$, $\boldsymbol{\epsilon} \in \boldsymbol{L}^2(\omega)$ and $\boldsymbol{\rho} \in \boldsymbol{L}^2(\omega)$ such that $\boldsymbol{u}_m \to \boldsymbol{u}$ in $\{\boldsymbol{v} \in \boldsymbol{L}^2(\Omega) \mid \boldsymbol{v}|_\omega \in L^2(\omega)\times L^2(\omega)\times H^1(\omega)\}$, $\boldsymbol{E}(\boldsymbol{u}_m) \to \boldsymbol{E}$ in $\boldsymbol{L}^2(\Omega)$, $\boldsymbol{\epsilon}(\boldsymbol{u}_m) \to \boldsymbol{\epsilon}$ in $\boldsymbol{L}^2(\omega)$ and $\boldsymbol{\rho}(\boldsymbol{u}_m) \to \boldsymbol{\rho}$ in $\boldsymbol{L}^2(\omega)$. Note that $\boldsymbol{g} \in C^1(\bar{\Omega};\mathbb{R}^9)$, $\bar{\Gamma}^k_{ij} \in C^0(\bar{\Omega})$, $\boldsymbol{F}_{[\text{I}]} \in C^2(\bar{\omega};\mathbb{R}^6)$, $\boldsymbol{F}_{[\text{II}]} \in C^1(\bar{\omega},\mathbb{R}^6)$ and $\Gamma^\gamma_{\alpha\beta} \in C^1(\bar{\omega})$ from our definitions of $\bar{\boldsymbol{X}}$ and $\boldsymbol{\sigma}$. Thus, given any test functions $\phi \in \mathscr{D}(\Omega)$ and $\varphi \in \mathscr{D}(\omega)$, we get

$$\int_\Omega E_{ij}(\boldsymbol{u}_m)\phi\ dx^1dx^2dx^3 = -\int_\Omega \left(\frac{1}{2}g_{ik}\partial_j\phi + \frac{1}{2}g_{jk}\partial_i\phi + \bar{\Gamma}_{ijk}\phi\right) u^k_m\ dx^1dx^2dx^3$$

$$
\begin{aligned}
&\to -\int_\Omega \left(\frac{1}{2}g_{ik}\partial_j\phi + \frac{1}{2}g_{jk}\partial_i\phi + \bar{\Gamma}_{ijk}\phi\right) u^k \; dx^1dx^2dx^3 \\
&= \int_\Omega E_{ij}(\boldsymbol{u})\phi \; dx^1dx^2dx^3 \; , \\
\int_\omega \epsilon_{\alpha\beta}(\boldsymbol{u}_m)\varphi \; dx^1dx^2 &= -\int_\omega \left[\left(\frac{1}{2}F_{[\mathrm{I}]\alpha\gamma}\partial_\beta\varphi + \frac{1}{2}F_{[\mathrm{I}]\beta\gamma}\partial_\alpha\varphi + \Gamma_{\alpha\beta\gamma}\varphi\right) u^\gamma_m + \varphi F_{[\mathrm{II}]\alpha\beta}u^3_m\right] dx^1dx^2 \\
&\to -\int_\omega \left[\left(\frac{1}{2}F_{[\mathrm{I}]\alpha\gamma}\partial_\beta\varphi + \frac{1}{2}F_{[\mathrm{I}]\beta\gamma}\partial_\alpha\varphi + \Gamma_{\alpha\beta\gamma}\varphi\right) u^\gamma + \varphi F_{[\mathrm{II}]\alpha\beta}u^3\right] dx^1dx^2 \\
&= \int_\omega \epsilon_{\alpha\beta}(\boldsymbol{u})\varphi \; dx^1dx^2 \; , \\
\int_\omega \rho_{\alpha\beta}(\boldsymbol{u}_m)\varphi \; dx^1dx^2 &= -\int_\omega \Big[\partial_\alpha\varphi\partial_\beta u^3_m + \Gamma^\delta_{\alpha\beta}\varphi\partial_\delta u^3_m + F_{[\mathrm{II}]\alpha\delta}F_{[\mathrm{II}]}{}^\delta_\beta\varphi u^3_m \\
&\qquad + \left(\partial_\alpha(F_{[\mathrm{II}]\beta\gamma}\varphi) + \partial_\beta(F_{[\mathrm{II}]\alpha\gamma}\varphi)\right) u^\gamma_m \\
&\qquad - \left(\partial_\alpha F_{[\mathrm{II}]\beta\gamma} - \Gamma^\delta_{\alpha\beta}F_{[\mathrm{II}]\delta\gamma} - \Gamma^\delta_{\alpha\gamma}F_{[\mathrm{II}]\beta\delta}\right)\varphi u^\gamma_m\Big] dx^1dx^2 \\
&\to -\int_\omega \Big[\partial_\alpha\varphi\partial_\beta u^3 + \Gamma^\delta_{\alpha\beta}\varphi\partial_\delta u^3 + F_{[\mathrm{II}]\alpha\delta}F_{[\mathrm{II}]}{}^\delta_\beta\varphi u^3 \\
&\qquad + \left(\partial_\alpha(F_{[\mathrm{II}]\beta\gamma}\varphi) + \partial_\beta(F_{[\mathrm{II}]\alpha\gamma}\varphi)\right) u^\gamma \\
&\qquad - \left(\partial_\alpha F_{[\mathrm{II}]\beta\gamma} - \Gamma^\delta_{\alpha\beta}F_{[\mathrm{II}]\gamma\delta} - \Gamma^\delta_{\alpha\gamma}F_{[\mathrm{II}]\beta\delta}\right)\varphi u^\gamma\Big] dx^1dx^2 \\
&= \int_\omega \rho_{\alpha\beta}(\boldsymbol{u})\varphi \; dx^1dx^2 \; ,
\end{aligned}
$$

$\forall\; i,j,k \in \{1,2,3\}$, $\forall\; \alpha,\beta,\gamma,\delta \in \{1,2\}$ and for the unique field $\boldsymbol{u} \in \{\boldsymbol{v} \in \boldsymbol{L}^2(\Omega) \mid \boldsymbol{v}|_\omega \in L^2(\omega)\times L^2(\omega)\times H^1(\omega)\}$. The weak limits are obtained by using integration by parts, and to see why these results follow please consult section 1.2 of Gelfand and Shilov [73]. The above results imply that $\boldsymbol{E} = \boldsymbol{E}(\boldsymbol{u})$, $\boldsymbol{\epsilon} = \boldsymbol{\epsilon}(\boldsymbol{u})$ and $\boldsymbol{\rho} = \boldsymbol{\rho}(\boldsymbol{u})$ in a weak sense, i.e. $(\boldsymbol{K}(\omega,\Omega), ||\cdot||_{\boldsymbol{K}(\omega,\Omega)})$ is complete.

Now, we must show that the spaces $(\boldsymbol{K}(\omega,\Omega), ||\cdot||_{\boldsymbol{K}(\omega,\Omega)})$ and $(\boldsymbol{W}(\omega,\Omega), ||\cdot||_{\boldsymbol{W}(\omega,\Omega)})$ coincide. Due to the construction of the space $\boldsymbol{K}(\omega,\Omega)$, one can see that it is larger than the space $\boldsymbol{W}(\omega,\Omega)$, i.e. $(\boldsymbol{W}(\omega,\Omega), ||\cdot||_{\boldsymbol{W}(\omega,\Omega)}) \subseteq (\boldsymbol{K}(\omega,\Omega), ||\cdot||_{\boldsymbol{K}(\omega,\Omega)})$. This is due to the fact that the space $(\boldsymbol{K}(\omega,\Omega), ||\cdot||_{\boldsymbol{K}(\omega,\Omega)})$ allows more functions than the space $(\boldsymbol{W}(\omega,\Omega), ||\cdot||_{\boldsymbol{W}(\omega,\Omega)})$. One can clearly see this by observing the norms of each respective spaces.

To prove the other inclusion first we must show that, if $\partial^j u^k + \partial^k u^j$ is in $L^2(\Omega)$, then $\partial_j u^k$ is in $L^2(\Omega)$. To do so, consider the covariant displacement field components $u_j = g_{ij}u^i$. As $\boldsymbol{u} \in \boldsymbol{L}^2(\Omega)$ and $\boldsymbol{g} \in C^1(\bar{\Omega};\mathbb{R}^9)$, we get $u_j \in L^2(\Omega)$, $\forall\; j \in \{1,2,3\}$. Now, let $\bar{s}_{ij}(\boldsymbol{u}) = \frac{1}{2}(\partial_i u_j + \partial_j u_i)$ and let $\bar{t}_{ij}(\boldsymbol{u}) = -\bar{\Gamma}^k_{ij}u_k$, and thus, by construction, we get $E_{ij}(\boldsymbol{u}) = \bar{s}_{ij}(\boldsymbol{u}) + \bar{t}_{ij}(\boldsymbol{u})$, $\forall\; i,j \in \{1,2,3\}$. As $u_j \in L^2(\Omega)$ and $\bar{\Gamma}^k_{ij} \in C^0(\bar{\Omega})$, we get $\bar{\boldsymbol{t}}(\boldsymbol{u}) \in \boldsymbol{L}^2(\Omega)$. Now, as $\boldsymbol{E}(\boldsymbol{u}), \bar{\boldsymbol{t}}(\boldsymbol{u}) \in \boldsymbol{L}^2(\Omega)$, we get $\bar{\boldsymbol{s}}(\boldsymbol{u}) \in \boldsymbol{L}^2(\Omega)$, and this implies that $\partial_k\bar{s}_{ij}(\boldsymbol{u}) \in H^{-1}(\Omega)$, $\forall\; i,j,k \in \{1,2,3\}$. By rearranging a linear combination of $\partial_k\bar{s}_{ij}(\boldsymbol{u})$, we obtain the relation

$$
\partial_{ij}u_k = -\partial_k\bar{s}_{ij}(\boldsymbol{u}) + \partial_i\bar{s}_{jk}(\boldsymbol{u}) + \partial_j\bar{s}_{ki}(\boldsymbol{u}) \; .
$$

Thus, the fact $\partial_k\bar{s}_{ij}(\boldsymbol{u}) \in H^{-1}(\Omega)$ implies that $\partial_{ij}u_k \in H^{-1}(\Omega)$, $\forall\; i,j,k \in \{1,2,3\}$. Note that $u_k \in L^2(\Omega)$ implies that $\partial_j u_k \in H^{-1}(\Omega)$, and thus, along with the condition $\partial_{ij}u_k \in H^{-1}(\Omega)$ fundamental Lemma of J. L. Lions (lemma 8) implies that $u_k \in H^1(\Omega)$, $\forall\; k \in \{1,2,3\}$. Now, recall the contravariant displacement field components $u^j = g^{ij}u_i$. As $u_i \in H^1(\Omega)$ and $\boldsymbol{g} \in C^1(\bar{\Omega};\mathbb{R}^9)$, we find

$\boldsymbol{u} \in \boldsymbol{H}^1(\Omega)$.

Now, we must do the same process on the plane ω. To do so, consider the covariant displacement field components $v_\beta = F_{[\mathrm{I}]\alpha\beta}u^\alpha|_\omega$ and $v_3 = u^3|_\omega$. As $\boldsymbol{u}|_\omega \in L^2(\omega)\times L^2(\omega)\times H^1(\omega)$ and $\boldsymbol{F}_{[\mathrm{I}]} \in C^2(\bar{\omega};\mathbb{R}^4)$, we get $v_\beta \in L^2(\omega)$, $\forall\ \beta \in \{1,2\}$. Now, let $s_{\alpha\beta}(\boldsymbol{v}) = \frac{1}{2}(\partial_\alpha v_\beta + \partial_\beta v_\alpha)$ and $t_{\alpha\beta}(\boldsymbol{v}) = -\Gamma^\gamma_{\alpha\beta}v_\gamma - F_{[\mathrm{II}]\alpha\beta}v^3$, and thus, by construction, we get $\epsilon_{\alpha\beta}(\boldsymbol{v}) = s_{\alpha\beta}(\boldsymbol{v}) + t_{\alpha\beta}(\boldsymbol{v})$, $\forall\ \alpha,\beta \in \{1,2\}$. As $v_\beta \in L^2(\omega)$, $v_3 \in H^1(\omega)$, $\Gamma^\gamma_{\alpha\beta} \in C^1(\bar{\omega})$ and $\boldsymbol{F}_{[\mathrm{II}]} \in C^1(\bar{\omega};\mathbb{R}^4)$, we get $\boldsymbol{t}(\boldsymbol{v}) \in \boldsymbol{L}^2(\omega)$. Now, as $\boldsymbol{\epsilon}(\boldsymbol{v}), \boldsymbol{t}(\boldsymbol{v}) \in \boldsymbol{L}^2(\omega)$, we get $\boldsymbol{s}(\boldsymbol{v}) \in \boldsymbol{L}^2(\omega)$, and this implies that $\partial_\gamma s_{\alpha\beta}(\boldsymbol{v}) \in H^{-1}(\omega)$, $\forall\ \alpha,\beta \in \{1,2\}$. By rearranging a linear combination of $\partial_\gamma s_{\alpha\beta}(\boldsymbol{v})$, we obtain the relation

$$\partial_{\alpha\beta}v_k = -\partial_\gamma s_{\alpha\beta}(\boldsymbol{v}) + \partial_\alpha s_{\beta\gamma}(\boldsymbol{v}) + \partial_\beta s_{\gamma\alpha}(\boldsymbol{v})\ .$$

Thus, the fact $\partial_\gamma s_{\alpha\beta}(\boldsymbol{v}) \in H^{-1}(\omega)$ implies that $\partial_{\alpha\beta}v_\gamma \in H^{-1}(\omega)$, $\forall\ \alpha,\beta,\gamma \in \{1,2\}$. Note that $v_\gamma \in L^2(\omega)$ implies that $\partial_\beta v_\gamma \in L^2(\Omega)$, and thus, along with the condition $\partial_{\alpha\beta}v_\gamma \in H^{-1}(\omega)$ fundamental Lemma of J. L. Lions (lemma 8) implies that $v_\gamma \in H^1(\Omega)$, $\forall\ \gamma \in \{1,2\}$. Now, recall the contravariant displacement field components $u^\beta|_\omega = F^{\alpha\beta}_{[\mathrm{I}]}v_\alpha$ and $u^3|_\omega = v_3$. As $v_\alpha \in H^1(\omega)$, $v_3 \in H^1(\omega)$ and $\boldsymbol{F}_{[\mathrm{I}]} \in C^2(\bar{\omega};\mathbb{R}^4)$, we find $\boldsymbol{u}|_\omega \in \boldsymbol{H}^1(\omega)$.

Finally, recall the change in the second fundamental form tensor $\boldsymbol{\rho}_{\alpha\beta}(\boldsymbol{v})$ and rearrange it as

$$\begin{aligned}\partial_{\alpha\beta}v_3 = -\rho_{\alpha\beta}(\boldsymbol{v}) + \Gamma^\delta_{\alpha\beta}\partial_\delta v_3 + F_{[\mathrm{II}]\alpha\delta}F^{\ \delta}_{[\mathrm{II}]\beta}v_3 + F_{[\mathrm{II}]\alpha}^{\ \ \gamma}\partial_\beta v_\gamma + F_{[\mathrm{II}]\beta}^{\ \ \gamma}\partial_\alpha v_\gamma \\ - \left(\partial_\alpha F^{\ \gamma}_{[\mathrm{II}]\beta} + \Gamma^\gamma_{\alpha\delta}F^{\ \delta}_{[\mathrm{II}]\beta} - \Gamma^\delta_{\alpha\beta}F^{\ \gamma}_{[\mathrm{II}]\delta}\right)v_\gamma\ .\end{aligned}$$

As $\boldsymbol{\rho}(\boldsymbol{v}) \in \boldsymbol{L}^2(\omega)$, $\boldsymbol{v} \in \boldsymbol{H}^1(\omega)$, $\boldsymbol{F}_{[\mathrm{I}]} \in C^2(\bar{\omega};\mathbb{R}^4)$, $\boldsymbol{F}_{[\mathrm{II}]} \in C^1(\bar{\omega};\mathbb{R}^4)$ and $\Gamma^\gamma_{\alpha\beta} \in C^1(\bar{\omega})$, we get $\partial_{\alpha\beta}v_3 \in L^2(\omega)$, $\forall\ \alpha,\beta \in \{1,2\}$. Now, as $v_3 \in H^2(\omega)$ and along with the fact $\boldsymbol{u}|_\omega \in \boldsymbol{H}^1(\omega)$, we get $\boldsymbol{u}|_\omega \in H^1(\omega)\times H^1(\omega)\times H^2(\omega)$.

Above analyses imply that, if $\boldsymbol{u} \in \boldsymbol{K}(\omega,\Omega)$, then we get $\boldsymbol{u} \in \boldsymbol{W}(\omega,\Omega)$, i.e. $(\boldsymbol{K}(\omega,\Omega),\ ||\cdot||_{\boldsymbol{K}(\omega,\Omega)}) \subseteq (\boldsymbol{W}(\omega,\Omega), ||\cdot||_{\boldsymbol{W}(\omega,\Omega)})$. Thus, the two spaces $(\boldsymbol{K}(\omega,\Omega), ||\cdot||_{\boldsymbol{K}(\omega,\Omega)})$ and $(\boldsymbol{W}(\omega,\Omega),\ ||\cdot||_{\boldsymbol{W}(\omega,\Omega)})$ coincide.

Above results show that the identity mapping $\iota : (\boldsymbol{K}(\omega,\Omega), ||\cdot||_{\boldsymbol{K}(\omega,\Omega)}) \to (\boldsymbol{W}(\omega,\Omega), ||\cdot||_{\boldsymbol{W}(\omega,\Omega)})$ is a injective, surjective and continuous. Thus, by the closed graph theorem (lemma 19), ι is a continuous bijection. Thus, Korn's inequality without boundary conditions (72) holds.

Our proof of Korn's inequality without boundary derived from Ciarlet's [38] proof of Korn's inequality without boundary conditions. The required inequality can also be obtained by applying the triangle inequity to Ciarlet's [38] Korn's inequality without boundary conditions (theorem 1.7-2 of Ciarlet [38]) and Korn's inequality on a surface without boundary conditions (theorem 2.6-1 of Ciarlet [38]).

Step 2 : The Rigid Displacement Result

Consider the space

$$\boldsymbol{V}(\omega,\Omega) = \{\boldsymbol{v} \in \boldsymbol{H}^1(\Omega) \mid \boldsymbol{v}|_\omega \in H^1(\omega)\times H^1(\omega)\times H^2(\omega),\ \boldsymbol{v}|_{\partial\Omega_0} = \boldsymbol{0}\}\ .$$

We assert that, if for any $\boldsymbol{u} \in \boldsymbol{V}(\omega, \Omega)$, if $\boldsymbol{E}(\boldsymbol{u}) = \boldsymbol{0}$ in Ω, and $\boldsymbol{\epsilon}(\boldsymbol{u}) = \boldsymbol{0}$ and $\boldsymbol{\rho}(\boldsymbol{u}) = \boldsymbol{0}$ in ω, then $\boldsymbol{u} = \boldsymbol{0}$ in $\bar{\Omega}$.

To show this recall the infinitesimal rigid displacement lemma (lemma 9), which states that for $\boldsymbol{v} \in \boldsymbol{H}^1(\Omega)$, if $\boldsymbol{E}(\boldsymbol{v}) = \boldsymbol{0}$ in Ω, then there exist constant Euclidean vectors $\bar{\boldsymbol{a}}, \bar{\boldsymbol{b}} \in \mathbf{E}^3$ such that $v^i \partial_i \bar{\boldsymbol{X}} = \bar{\boldsymbol{a}} + \bar{\boldsymbol{b}} \times \bar{\boldsymbol{X}}$ in $\bar{\Omega}$. Also, if $\boldsymbol{v}|_{\partial\Omega_0} = \boldsymbol{0}$, then lemma 9 further implies that $\bar{\boldsymbol{a}} = \boldsymbol{0}$ and $\bar{\boldsymbol{b}} = \boldsymbol{0}$. Now, recall the infinitesimal rigid displacement lemma on a general surface (lemma 10), which states that for $\boldsymbol{w} \in H^1(\omega) \times H^1(\omega) \times H^2(\omega)$, if $\boldsymbol{\epsilon}(\boldsymbol{w}) = \boldsymbol{0}$ and $\boldsymbol{\rho}(\boldsymbol{w}) = \boldsymbol{0}$ in ω, then there exist constant Euclidean vectors $\boldsymbol{a}, \boldsymbol{b} \in \mathbf{E}^3$ such that $w^\alpha \partial_\alpha \boldsymbol{\sigma} + w^3 \boldsymbol{N} = \boldsymbol{a} + \boldsymbol{b} \times \boldsymbol{\sigma}$ in $\bar{\omega}$. By construction, we have $\bar{\boldsymbol{X}}|_\omega = \boldsymbol{\sigma}$, and thus, for any $\boldsymbol{u} \in \boldsymbol{V}(\omega, \Omega)$, if $\boldsymbol{E}(\boldsymbol{u}) = \boldsymbol{0}$ in Ω, and $\boldsymbol{\epsilon}(\boldsymbol{u}) = \boldsymbol{0}$ and $\boldsymbol{\rho}(\boldsymbol{u}) = \boldsymbol{0}$ in ω, then boundary trace embedding theorem (lemma 11) implies that $\bar{\boldsymbol{a}} + \bar{\boldsymbol{b}} \times \bar{\boldsymbol{X}}|_\omega = \boldsymbol{a} + \boldsymbol{b} \times \boldsymbol{\sigma}$ in $\boldsymbol{L}^2(\omega)$. This implies that $\boldsymbol{a} = \bar{\boldsymbol{a}} = \boldsymbol{0}$ and $\boldsymbol{b} = \bar{\boldsymbol{b}} = \boldsymbol{0}$, i.e. $\boldsymbol{u} = \boldsymbol{0}$ in $\bar{\Omega}$.

As our shell is bonded to the elastic foundation, it is possible to omit the assertions $\boldsymbol{u}|_{\partial\omega_0} = \boldsymbol{0}$ and $n^\alpha \partial_\alpha u^3|_{\partial\omega_0} = 0$ from the infinitesimal rigid displacement lemma on a general surface (lemma 10).

Step 3 : Korn's Inequality With Boundary Conditions

Consider the space $\boldsymbol{V}(\omega, \Omega)$ equipped with the norm

$$||\boldsymbol{v}||_{\boldsymbol{S}(\omega,\Omega)} = \left(||\boldsymbol{E}(\boldsymbol{v})||^2_{\boldsymbol{L}^2(\Omega)} + ||\boldsymbol{\epsilon}(\boldsymbol{v})||^2_{\boldsymbol{L}^2(\omega)} + ||\boldsymbol{\rho}(\boldsymbol{v})||^2_{\boldsymbol{L}^2(\omega)} \right)^{\frac{1}{2}} ,$$

where $\boldsymbol{E}(\boldsymbol{u}) \in \boldsymbol{L}^2(\Omega)$, $\boldsymbol{\epsilon}(\boldsymbol{u}) \in \boldsymbol{L}^2(\omega)$ and $\boldsymbol{\rho}(\boldsymbol{u}) \in \boldsymbol{L}^2(\omega)$ in a sense of distributions. We assert that there exists a positive constant C that depends on Ω, $\partial\Omega_0$, $\bar{\boldsymbol{X}}$, ω, $\partial\omega$ and $\boldsymbol{\sigma}$ such that

$$||\boldsymbol{u}||_{\boldsymbol{W}(\omega,\Omega)} \leq C||\boldsymbol{u}||_{\boldsymbol{S}(\omega,\Omega)} \ , \ \forall \ \boldsymbol{u} \in \boldsymbol{V}(\omega, \Omega) \ ,$$

i.e. *Korn's inequity with boundary condition*.

To prove this assertion consider the converse, i.e. consider the claim that $\exists \ C > 0$ such that $||\boldsymbol{u}||_{\boldsymbol{W}(\omega,\Omega)} > C||\boldsymbol{u}||_{\boldsymbol{S}(\omega,\Omega)}$, $\forall \ \boldsymbol{u} \in \boldsymbol{V}(\omega, \Omega)$. If this is indeed the case, then we can find a sequence $\{\boldsymbol{u}_m\}_{m\in\mathbb{N}} \subset \boldsymbol{V}(\omega, \Omega)$ such that $||\boldsymbol{u}_m||_{\boldsymbol{W}(\omega,\Omega)} = 1$, $\forall \ m > 0$, and $||\boldsymbol{u}_m||_{\boldsymbol{S}(\omega,\Omega)} \to 0$. As $C||\boldsymbol{u}_m||_{\boldsymbol{S}(\omega,\Omega)} < 1$, $\forall \ m > 0$, the sequence is $\{\boldsymbol{u}_m\}_{m\in\mathbb{N}}$ is bounded in $\boldsymbol{V}(\omega, \Omega)$, and thus, by Rellich-Kondrasov theorem (lemma 13) there exists a convergent subsequence $\{\boldsymbol{u}_{m_n}\}_{m_n\in\mathbb{N}}$ in $\{\boldsymbol{v} \in \boldsymbol{L}^2(\Omega) \mid \boldsymbol{v}|_\omega \in L^2(\omega) \times L^2(\omega) \times H^1(\omega)\}$. As the subsequence $\{\boldsymbol{u}_{m_n}\}_{m_n\in\mathbb{N}}$ is convergent in $\{\boldsymbol{v} \in \boldsymbol{L}^2(\Omega) \mid \boldsymbol{v}|_\omega \in L^2(\omega) \times L^2(\omega) \times H^1(\omega)\}$, the condition $||\boldsymbol{u}_{m_n}||_{\boldsymbol{S}(\omega,\Omega)} \to 0$ implies that the subsequence $\{\boldsymbol{u}_{m_n}\}_{m_n\in\mathbb{N}}$ is a Cauchy sequence with respect to the norm $||\cdot||_{\boldsymbol{K}(\omega,\Omega)}$. As the subsequence $\{\boldsymbol{u}_{m_n}\}_{m_n\in\mathbb{N}}$ is a Cauchy sequence with respect to the norm $||\cdot||_{\boldsymbol{K}(\omega,\Omega)}$, Korn's inequity without boundary conditions implies that the subsequence $\{\boldsymbol{u}_{m_n}\}_{m_n\in\mathbb{N}}$ is Cauchy sequence with respect to the norm $||\cdot||_{\boldsymbol{W}(\omega,\Omega)}$. By construction, the space $(\boldsymbol{V}(\omega, \Omega), ||\cdot||_{\boldsymbol{W}(\omega,\Omega)})$ is complete as a closed subspace of $(\boldsymbol{W}(\omega, \Omega), ||\cdot||_{\boldsymbol{W}(\omega,\Omega)})$, and thus, there exists a unique field $\boldsymbol{u} \in \boldsymbol{W}(\omega, \Omega)$ such that $||\boldsymbol{u}_{m_n}||_{\boldsymbol{W}(\omega,\Omega)} \to ||\boldsymbol{u}||_{\boldsymbol{W}(\omega,\Omega)} = 1$, in particular, $||\boldsymbol{E}(\boldsymbol{u}_{m_n})||^2_{\boldsymbol{L}^2(\Omega)} \to ||\boldsymbol{E}(\boldsymbol{u})||^2_{\boldsymbol{L}^2(\Omega)} = 0$, $||\boldsymbol{\epsilon}(\boldsymbol{u}_{m_n})||^2_{\boldsymbol{L}^2(\omega)} \to ||\boldsymbol{\epsilon}(\boldsymbol{u})||^2_{\boldsymbol{L}^2(\omega)} = 0$ and $||\boldsymbol{\rho}(\boldsymbol{u}_{m_n})||^2_{\boldsymbol{L}^2(\omega)} \to ||\boldsymbol{\rho}(\boldsymbol{u})||^2_{\boldsymbol{L}^2(\omega)} = 0$, and this is due to the fact that $||\boldsymbol{u}_{m_n}||_{\boldsymbol{S}(\omega,\Omega)} \to 0$. But recall that for any $\boldsymbol{u} \in \boldsymbol{V}(\omega, \Omega)$, we have $\boldsymbol{u}|_{\partial\Omega_0} = \boldsymbol{0}$.

Thus, our rigid displacement result implies that the limit is identically zero, i.e. $\boldsymbol{u} = \boldsymbol{0}$, but this contradicts our assumption $||\boldsymbol{u}_m||_{\boldsymbol{W}(\omega,\Omega)} = 1,\ \forall\ m > 0$. This implies that our initial assumption $||\boldsymbol{u}||_{\boldsymbol{W}(\omega,\Omega)} > C||\boldsymbol{u}||_{\boldsymbol{S}(\omega,\Omega)}, \forall\ \boldsymbol{u} \in \boldsymbol{V}(\omega,\Omega)$, cannot hold, and thus, we conclude the proof by confirming that exists a positive constant C that is independent of $\boldsymbol{u}$, such that $||\boldsymbol{u}||_{\boldsymbol{W}(\omega,\Omega)} \leq C||\boldsymbol{u}||_{\boldsymbol{S}(\omega,\Omega)}$, $\forall\ \boldsymbol{u} \in \boldsymbol{V}(\omega,\Omega)$.

Our proof of Korn's inequality is not too dissimilar to Ciarlet's [38] proof of Korn's inequalities for the displacement-traction case. The only difference is that Ciarlet's [38] Korn's inequity for a general surface is proved for the $\boldsymbol{u}|_{\partial\omega_0} = \boldsymbol{0}$ and $n^\alpha \partial_\alpha u^3|_{\partial\omega_0} = 0$ case, while our Korn's equality is proved for the $\boldsymbol{u}|_{\Omega_0} = \boldsymbol{0}$ case, as it was possible to omit the conditions $\boldsymbol{u}|_{\partial\omega_0} = \boldsymbol{0}$ and $n^\alpha \partial_\alpha u^3|_{\partial\omega_0} = 0$ due to the fact that we treated the shell as a boundary form of the foundation (please see step 2 for more detail).

Step 4 : Zero-Slope Boundary Conditions
Now, we must show that the space $\boldsymbol{V}_{\mathscr{S}}(\omega,\Omega)$ is a proper subset of the space $\boldsymbol{V}(\omega,\Omega)$ that is closed under the norm $||\cdot||_{\boldsymbol{W}(\omega,\Omega)}$.

The rigid displacement result (see step 2) implies that for any $\boldsymbol{u} \in \boldsymbol{V}(\omega,\Omega)$, if $\boldsymbol{E}(\boldsymbol{u}) = \boldsymbol{0}$ in Ω, and $\boldsymbol{\epsilon}(\boldsymbol{u}) = \boldsymbol{0}$ and $\boldsymbol{\rho}(\boldsymbol{u}) = \boldsymbol{0}$ in ω, then $\boldsymbol{u} = \boldsymbol{0}$ in $\bar{\Omega}$. Thus, if $\boldsymbol{u} = \boldsymbol{0}$ in $\bar{\Omega}$, then clearly we get $\boldsymbol{\nabla}(u^3|_\omega) = \boldsymbol{0}$, in particular $\partial_\beta(u^3|_\omega)|_{\partial\omega} = 0, \forall\ \beta \in \{1,2\}$. This implies that the conditions $\partial_\beta(u^3|_\omega)|_{\partial\omega} = 0, \forall\ \beta \in \{1,2\}$ does not violate the rigid displacement result. Thus, for any $\boldsymbol{u} \in \boldsymbol{V}_{\mathscr{S}}(\omega,\Omega)$, we get $\boldsymbol{u} \in \boldsymbol{V}(\omega,\Omega)$, i.e. $\boldsymbol{V}_{\mathscr{S}}(\omega,\Omega) \subset \boldsymbol{V}(\omega,\Omega)$.

By definition, for any $v \in H^2(\omega)$, we have $\partial_\beta v \in H^1(\omega),\ \forall\ \beta \in \{1,2\}$. Also, as $\partial\omega$ is a uniform-$C^1(\mathbb{R}^2;\mathbb{R})$ boundary, trivial traces (lemma 12) implies that the space $H^1_0(\omega)$ is a proper subset of the Hilbert space $H^1(\omega)$ that is closed under the norm $||\cdot||_{H^1(\omega)}$, i.e. the space $(H^1_0(\omega), ||\cdot||_{H^1(\omega)}) \subset (H^1(\omega), ||\cdot||_{H^1(\omega)})$ is closed. Note that for any $\boldsymbol{u} \in \boldsymbol{V}_{\mathscr{S}}(\omega,\Omega)$, we get $\partial_\beta(u^3|_\omega)|_{\partial\omega} = 0, \forall\ \beta \in \{1,2\}$, and thus, we get $\partial_\beta(u^3|_\omega) \in H^1_0(\omega), \forall\ \beta \in \{1,2\}$, by trivial traces (lemma 12). Now, this implies that the space $(\boldsymbol{V}_{\mathscr{S}}(\omega,\Omega), ||\cdot||_{\boldsymbol{W}(\omega,\Omega)}) \subset (\boldsymbol{V}(\omega,\Omega), ||\cdot||_{\boldsymbol{W}(\omega,\Omega)})$ is closed.

Above analyses imply that the space $\boldsymbol{V}_{\mathscr{S}}(\omega,\Omega)$ is a proper subset of the space $\boldsymbol{V}(\omega,\Omega)$ that is closed under the norm $||\cdot||_{\boldsymbol{W}(\omega,\Omega)}$. Thus, we can conclude our proof of *Korn's inequality* by confirming that $||\boldsymbol{u}||_{\boldsymbol{W}(\omega,\Omega)} \leq C||\boldsymbol{u}||_{\boldsymbol{S}(\omega,\Omega)}, \forall\ \boldsymbol{u} \in \boldsymbol{V}_{\mathscr{S}}(\omega,\Omega)$, where C is a positive constant that is independent of $\boldsymbol{u}$.

3.5 Numerical Example

To conduct numerical experiments assume that one is dealing with overlying shell with a thickness h that is bonded to an elastic foundation, where the unstrained configuration of the foundation is an infinitely long annular semi-prism characterised by the diffeomorphism $\bar{\boldsymbol{X}}(x^1,x^2,x^3) = (x^1, a\sin(x^2), b\cos(x^2))_{\mathsf{E}} + x^3(\varphi(x^2))^{-1}(0, b\sin(x^2), a\cos(x^2))_{\mathsf{E}}$, where $\varphi(x^2) = (b^2\sin^2(x^2) + a^2\cos^2(x^2))^{\frac{1}{2}}$, $x^1 \in (-\infty,\infty)$, $x^2 \in (-\frac{1}{2}\pi, \frac{1}{2}\pi)$, $x^3 \in (-H, 0)$, and a is the horizontal radius and b is the ver-

tical radius of the upper surface. With some calculations, one finds that the metric tensor is $\boldsymbol{g} = \mathrm{diag}(1, (\bar{\psi}_2)^2, 1)$, where $\bar{\psi}_2 = \varphi(x^2) + x^3 ab(\varphi(x^2))^{-2}$, and Christoffel symbols are

$$\bar{\Gamma}^2_{22} = (\bar{\psi}_2)^{-1}\partial_2\bar{\psi}_2 \ ,$$
$$\bar{\Gamma}^2_{23} = (\bar{\psi}_2)^{-1}\partial_3\bar{\psi}_2 \ .$$

With few more calculations one finds

$$\bar{\nabla}_2 u^2 = \partial_2 u^2 + \bar{\Gamma}^2_{22}u^2 + \bar{\Gamma}^2_{23}u^3 \ ,$$
$$\bar{\nabla}_2 u^3 = \partial_2 u^3 - (\bar{\psi}_2)^2\bar{\Gamma}^2_{23}u^2 \ ,$$
$$\bar{\nabla}_3 u^2 = \partial_3 u^2 + \bar{\Gamma}^2_{23}u^2 \ ,$$
$$\bar{\nabla}_3 u^3 = \partial_3 u^3 \ ,$$

where $\boldsymbol{u} = (0, u^2(x^2, x^3), u^3(x^2, x^3))$ is the displacement field. Armed with this knowledge, one can express the governing equations of the foundation as

$$(\bar{\lambda} + \bar{\mu})\partial^2\left(\bar{\nabla}_i u^i\right) + \bar{\mu}\bar{\Delta}u^2 = 0 \ ,$$
$$(\bar{\lambda} + \bar{\mu})\partial^3\left(\bar{\nabla}_i u^i\right) + \bar{\mu}\bar{\Delta}u^3 = 0 \ .$$

Now, eliminating x^1 dependency one can express the remaining boundaries as

$$\partial\Omega^{\mathsf{New}} = \bar{\omega}^{\mathsf{New}} \cup \partial\Omega_0^{\mathsf{New}} \cup \partial\Omega_f^{\mathsf{New}} \ ,$$
$$\omega^{\mathsf{New}} = \{(-\frac{1}{2}\pi, \frac{1}{2}\pi) \times \{-0\}\} \ ,$$
$$\partial\Omega_0^{\mathsf{New}} = \{(-\frac{1}{2}\pi, \frac{1}{2}\pi) \times \{-H\}\} \ ,$$
$$\partial\Omega_f^{\mathsf{New}} = \{\{-\frac{1}{2}\pi\} \times (-H, 0)\} \cup \{\{\frac{1}{2}\pi\} \times (-H, 0)\} \ .$$

Thus, the boundary conditions one imposes on the foundation reduce to

$$u^2|_{\overline{\partial\Omega_0^{\mathsf{New}}}} = 0 \text{ (zero-Dirichlet)} \ ,$$
$$u^3|_{\overline{\partial\Omega_0^{\mathsf{New}}}} = 0 \text{ (zero-Dirichlet)} \ ,$$
$$\left[(\bar{\psi}_2)^2\partial_3 u^2 + \partial_2 u^3\right]|_{\partial\Omega_f^{\mathsf{New}}} = 0 \text{ (zero-Robin)} \ ,$$
$$\left[(\bar{\lambda} + 2\bar{\mu})\partial_2 u^2 + \bar{\lambda}\left(\partial_3 u^3 + \bar{\Gamma}^2_{22}u^2 + \bar{\Gamma}^2_{23}u^3\right)\right]|_{\partial\Omega_f^{\mathsf{New}}} = 0 \text{ (zero-Robin)} \ .$$

Now, consider overlying shell's unstrained configuration, which is described by the injective immersion $\boldsymbol{\sigma}(x^1, x^2) = (x^1, a\sin(x^2), b\cos(x^2))_{\mathsf{E}}$, where $x^1 \in (-\infty, \infty)$ and $x^2 \in (-\frac{1}{2}\pi, \frac{1}{2}\pi)$. With some calculations one finds that the first fundamental form tensor is $\boldsymbol{F}_{[\mathrm{I}]} = \mathrm{diag}(1, (\psi_2)^2)$, the second fundamental form tensor is $\boldsymbol{F}_{[\mathrm{II}]} = \mathrm{diag}(0, -ab(\varphi(x^2))^{-1})$ and only nonzero Christoffel symbol is $\Gamma^2_{22} = \psi_2^{-1}\partial_2\psi_2$, where $\psi_2 = \varphi(x^2)$. With few more calculations one further finds

$$\nabla_2 u^2 = \partial_2 u^2 + \Gamma^2_{22}u^2 \ ,$$
$$\epsilon^2_2(\boldsymbol{u}) = \nabla_2 u^2 - {F_{[\mathrm{II}]}}^2_2 u^3 \ ,$$
$$\rho^2_2(\boldsymbol{u}) = \Delta u^3 - {F_{[\mathrm{II}]}}^2_2 {F_{[\mathrm{II}]}}^2_2 u^3 + 2{F_{[\mathrm{II}]}}^2_2\nabla_2 u^2 + \partial_2 {F_{[\mathrm{II}]}}^2_2 u^2 \ ,$$

where $\boldsymbol{u}|_{\bar{\omega}^{\text{New}}} = (0, u^2(x^2, 0), u^3(x^2, 0))$ is the displacement field of the shell. Thus, one may express the governing equations of the shell as

$$h\Lambda\partial_2\epsilon_2^2(\boldsymbol{u}) + \frac{1}{3}h^3\Lambda(2F_{[\text{II}]^2}^2\partial_2\rho_2^2(\boldsymbol{u}) + \partial_2 F_{[\text{II}]^2}^2\rho_2^2(\boldsymbol{u})) - \text{Tr}(T_2^3(\boldsymbol{u})) = 0 \,, \tag{73}$$

$$-h\Lambda F_{[\text{II}]^2}^2\epsilon_2^2(\boldsymbol{u}) + \frac{1}{3}h^3\Lambda(\Delta\rho_2^2(\boldsymbol{u}) - F_{[\text{II}]^2}^2 F_{[\text{II}]^2}^2\rho_2^2(\boldsymbol{u})) + \text{Tr}(T_3^3(\boldsymbol{u})) = 0 \,, \tag{74}$$

where

$$\text{Tr}(T_2^3(\boldsymbol{u})) = \bar{\mu}\left((\bar{\psi}_2)^2\partial_3 u^2 + \partial_2 u^3\right)|_{\omega^{\text{New}}} \,,$$
$$\text{Tr}(T_3^3(\boldsymbol{u})) = \left[\bar{\lambda}\left(\partial_2 u^2 + \bar{\Gamma}_{22}^2 u^2 + \bar{\Gamma}_{23}^2 u^3\right) + (\bar{\lambda} + 2\bar{\mu})\partial_3 u^3\right]|_{\omega^{\text{New}}} \,,$$

and

$$\Lambda = 4\mu\frac{\lambda + \mu}{\lambda + 2\mu} \,.$$

Now, eliminating x^1 dependency one can express the remaining boundaries as

$$\partial\omega^{\text{New}} = \partial\omega_{T_0}^{\text{New}} \cup \partial\omega_{T_{\text{max}}}^{\text{New}} \,,$$
$$\partial\omega_{T_0}^{\text{New}} = \{0\} \,,$$
$$\partial\omega_{T_{\text{max}}}^{\text{New}} = \{\pi\} \,.$$

Thus, the boundary conditions of the shell reduce to

$$\left[\Lambda\epsilon_2^2(\boldsymbol{u}) + \frac{2}{3}h^2\Lambda F_{[\text{II}]^2}^2\rho_2^2(\boldsymbol{u})\right]|_{\partial\omega_{T_0}^{\text{New}}} = \tau_0 \text{ (traction)} \,,$$
$$\left[\Lambda\epsilon_2^2(\boldsymbol{u}) + \frac{2}{3}h^2\Lambda F_{[\text{II}]^2}^2\rho_2^2(\boldsymbol{u})\right]|_{\partial\omega_{T_{\text{max}}}^{\text{New}}} = \tau_{\text{max}} \text{ (traction)} \,,$$
$$\partial_2\rho_2^2(\boldsymbol{u})|_{\partial\omega^{\text{New}}} = 0 \text{ (zero-pressure)} \,,$$
$$\partial_2 u^3|_{\partial\omega^{\text{New}}} = 0 \text{ (zero-Neumann)} \,.$$

Despite the fact that the original problem is three-dimensional, as a result of problem's invariance in the x^1 direction, it is now to a two-dimensional problem. Now, the domain merely resides in the set $\{(x^2, x^3) \mid (x^2, x^3) \in [-\frac{1}{2}\pi, \frac{1}{4}\pi] \times [-H, 0]\}$. Despite the fact that theorem 3 is only valid for bounded domains, we show later that the reduced two-dimensional problem is numerically sound.

To conduct numerical experiments we use the second-order-accurate finite-difference method, but one issue we must tackle prior is the discretisation of the (reduced two-dimensional) domain. As we are dealing with curvilinear coordinates, there is an inherit grid dependence. To be precise, it is approximately $\psi_0\Delta x^2 \leq \Delta x^3$, $\forall\ \psi_0 \in \{\bar{\psi}_2(x^2, x^3) \mid x^2 \in [-\frac{1}{2}\pi, \frac{1}{2}\pi]$ and $x^3 \in [-H, 0]\}$, where Δx^j is a small increment in x^j direction. For our purposes we use $\Delta x^2 = \frac{1}{N-1}$ and $\psi_0 = \bar{\psi}_2(\frac{1}{4}\pi, 0)$, where $N = 250$ (see figure 32). We also keep the values $a = 2$, $H = 1$, $\bar{E} = 10^3$, $\bar{\nu} = \frac{1}{4}$, $\tau_0 = 1$ and $\tau_{\text{max}} = 1$ fixed for all experiments. Finally, we must define a terminating condition. For this, we choose to terminate our iterating process once the condition $|1 - ||\boldsymbol{u}_m||_{\ell^2}^{-1}||\boldsymbol{u}_{m+1}||_{\ell^2}| < 10^{-10}$ is satisfied, where $\boldsymbol{u}_m$ is the m^{th} iterative solution.

Figure 33 is calculated with the values $b = 2$, $h = \frac{1}{4}$, $E = 6000$ and $\nu = \frac{1}{4}$. Figure 33 shows the azimuthal (i.e. u^2) and the radial (i.e. u^3) displacements at the contact region ω^{New}. The maximum

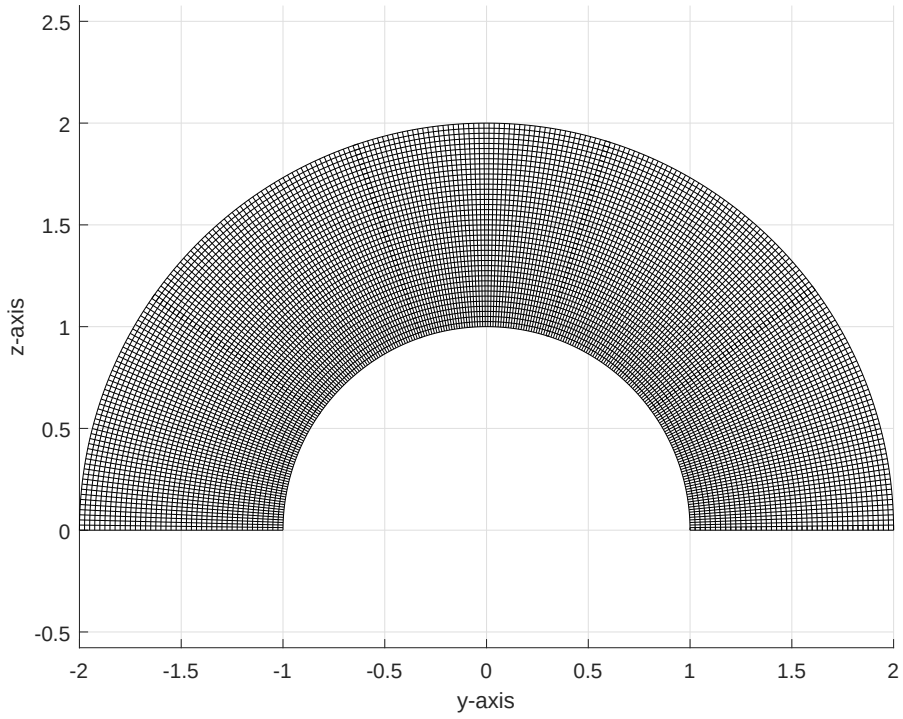

Figure 32: Discretised reduced two-dimensional domain for the $a = 2$, $b = 2$, $H = 1$ and $N = 250$ case.

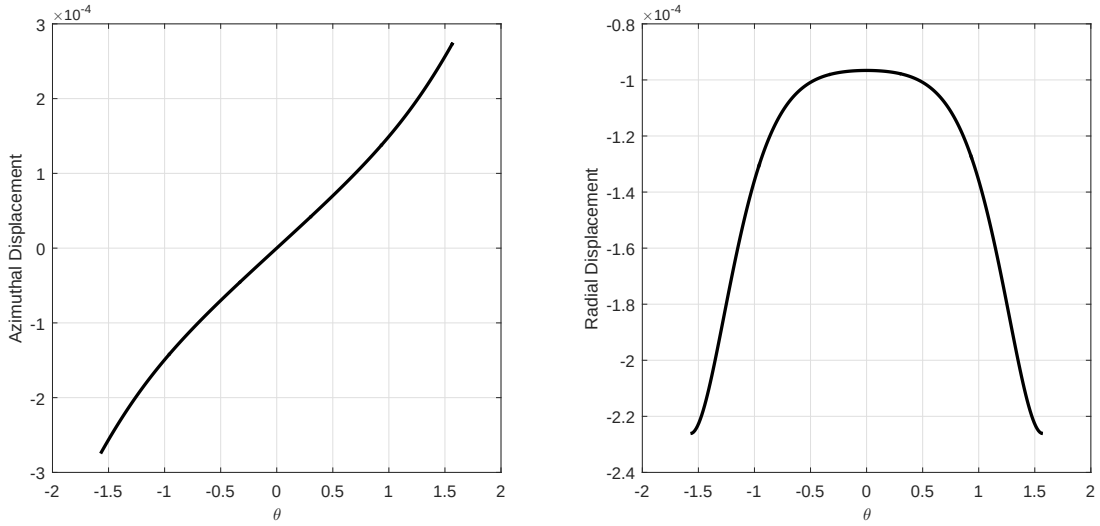

Figure 33: Displacement field of the bonded shell model at the contact region.

azimuthal displacements are observed at $x^2 = \pm\frac{1}{2}\pi$, with respective azimuthal displacements of $u^2 = \pm 2.75 \times 10^{-4}$. The maximum radial displacement is observed at $x^2 = \pm\frac{1}{2}\pi$, with a radial displacement $u^3 = -2.26 \times 10^{-4}$. As the displacement field experiences maximum displacements at the boundary of the shell (i.e. at $\partial\omega^{\text{New}}$), one may expect that this is the region where the shell is most likely to debond from the elastic foundation, in this scenario of course.

To confirm our numerical scheme we must perform a grid dependence analysis for the numerical solution. As the reader can see from figure 34, as N increases, the difference between the numer-

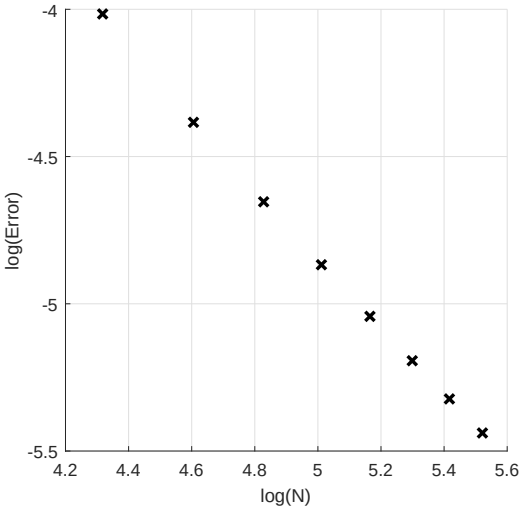

Figure 34: Grid dependence of the bonded shell model.

ical solution N and $N+1$ decreases. For our experiments we found that the azimuthal grid points and the error share the relation $N \propto \text{Error}^{-0.851}$, where $\text{Error} = |1 - ||\boldsymbol{u}_{N-1}||_{\ell^2}^{-1}||\boldsymbol{u}_N||_{\ell^2}|$. Note that figure 33 is calculated with the values $b = 2$, $h = \frac{1}{4}$, $E = 6000$ and $\nu = \frac{1}{4}$. Also, we use UCL DPS machines (operating-system: Centos 7, CPU: 8 core Intel Xeon, memory: 64GB) to run the numerical simulations.

While the above numerical results seem interesting, without something tangible to compare it against any conclusions deduced from above results are merely speculative. Thus, we dedicate the next section to numerical comparison against another, but a similar, model that is described by the work of Baldelli and Bourdin [16].

3.6 Comparison Against the Works of Baldelli and and Bourdin

In this section we extend Baldelli and Bourdin's [16] model for bonded films on elastic pseudo-foundations into curvilinear coordinates. To extend Baldelli and Bourdin's [16] model to curvilinear coordinates consider the following: consider a thin overlying body with constant thickness h whose unstrained configuration is described by the diffeomorphism $\bar{\boldsymbol{X}} \in C^1(\bar{\omega} \times (0,h); \mathbf{E}^3)$, where $\bar{\boldsymbol{X}} = (x^1, x^2, x^3) = \boldsymbol{\sigma}(x^1, x^2) + x^3 \boldsymbol{N}(x^1, x^2)$, $\boldsymbol{\sigma} \in C^2(\bar{\omega}; \mathbf{E}^3)$ is an injective immersion and $\omega \subset \mathbb{R}^2$ is a domain of concern, and with the displacement field of the lower-surface $(w^1 - x^3 \bar{\nabla}^1 w_3, w^2 - x^3 \bar{\nabla}^2 w_3, w^3)$, where $\boldsymbol{w} \in H^1(\omega) \times H^1(\omega) \times H^2(\omega)$. Now, assume that this overlying body is bonded to an elastic foundation with a constant thickness H whose unstrained configuration is described by the diffeomorphism $\bar{\boldsymbol{X}} \in C^1(\omega \times (-H, 0]; \mathbf{E}^3)$ such that at $x^3 = -H$ the displacement field of the foundation satisfies zero-Dirichlet boundary condition. Thus, in accordance with Baldelli and Bourdin [16], we may approximate the displacement field of the foundation as $\boldsymbol{u} = (1 + H^{-1} x^3)\boldsymbol{w}$. However, unlike Baldelli and Bourdin [16], we make no prior assumptions regarding the asymptotic nature of Young's moduli or Poisson's ratios or the displacement fields. Now, with some asymptotic analysis one finds that the condition $\{\Lambda h \sim H^{-1} \bar{\mu} \text{meas}(\boldsymbol{\sigma}(\omega); \mathbf{E}^2), h B^{\alpha\beta\gamma\delta} F_{[\text{II}]\alpha\beta} F_{[\text{II}]\gamma\delta} \sim H^{-1}(\bar{\lambda} + 2\bar{\mu})\}$

is the only asymptotic scaling possible that yields any valid leading order solutions, i.e the scaling that allows

$$\int_0^h \int_\omega \frac{1}{2} B^{\alpha\beta\gamma\delta} \epsilon_{\alpha\beta}(w^1, w^2) \epsilon_{\gamma\delta}(w^1, w^2) \, d\omega dx^3 \approx \int_{-H}^0 \int_\omega A^{\alpha 3 \beta 3} E_{\alpha 3}(u^1, u^2) E_{\beta 3}(u^1, u^2) \, d\omega dx^3 \, ,$$
$$\int_0^h \int_\omega \frac{1}{2} B^{\alpha\beta\gamma\delta} \epsilon_{\alpha\beta}(w^3) \epsilon_{\gamma\delta}(w^3) \, d\omega dx^3 \approx \int_{-H}^0 \int_\omega \frac{1}{2} A^{3333} E_{33}(u^3) E_{33}(u^3) \, d\omega dx^3 \, .$$

Thus, collect all the leading order terms to find:

Corollary 3. *Let $\omega \subset \mathbb{R}^2$ be a connected open bounded plane that satisfies the segment condition with a uniform-$C^1(\mathbb{R}^2; \mathbb{R})$ boundary $\partial\omega$. Let $\boldsymbol{\sigma} \in C^2(\bar{\omega}; \boldsymbol{E}^3)$ be an injective immersion. Let $\boldsymbol{f}_0 \in \boldsymbol{L}^2(\omega)$ and $\boldsymbol{\tau}_0 \in \boldsymbol{L}^2(\partial\omega)$. If $\{\Lambda h \sim H^{-1}\bar{\mu}\text{meas}(\boldsymbol{\sigma}(\omega); \boldsymbol{E}^2), hB^{\alpha\beta\gamma\delta} F_{[\text{III}]\alpha\beta} F_{[\text{III}]\gamma\delta} \sim H^{-1}(\bar{\lambda} + 2\bar{\mu})\}$, then exists a unique field $\boldsymbol{w} = (w^1, w^2) \in \boldsymbol{H}^1(\omega)$ such that $\boldsymbol{w}$ is the solution to the minimisation problem*

$$J(\boldsymbol{w})_{\textit{Baldelli}} = \min_{\boldsymbol{v} \in \boldsymbol{H}^1(\omega)} J(\boldsymbol{v}) \, ,$$

where

$$J(\boldsymbol{w})_{\textit{Baldelli}} = \int_\omega \left[\frac{1}{2} h B^{\alpha\beta\gamma\delta} \epsilon^M_{\alpha\beta}(\boldsymbol{w}) \epsilon^M_{\gamma\delta}(\boldsymbol{w}) + \frac{1}{2} \frac{\bar{\mu}}{H} w_\alpha w^\alpha - h f_0^\alpha w_\alpha \right] d\omega - \int_{\partial\omega} h \tau_0^\alpha w_\alpha \, d(\partial\omega) \, ,$$

and where $\Lambda = 4(\lambda + 2\mu)^{-1}\mu(\lambda + \mu)$, λ and μ are respectively first and second Lamé's parameters, h is the thickness, $\epsilon^M_{\alpha\beta}(\boldsymbol{w}) = \frac{1}{2}(\nabla_\alpha w_\beta + \nabla_\beta w_\alpha)$ is the strain tensor and $\boldsymbol{B}$ is the isotropic elasticity tensor of the membrane, and $\bar{\lambda}$ and $\bar{\mu}$ are respectively first and second Lamé's parameters and H is the thickness of the foundation. In particular, the unique minimiser $\boldsymbol{w}$ is also a critical point in $(\boldsymbol{H}^1(\omega), J(\cdot)_{\textit{Baldelli}})$.

Proof. **Coersive**: $J(\boldsymbol{w})_{\text{Baldelli}} \geq C_1 ||\boldsymbol{\epsilon}^M(\boldsymbol{w})||^2_{\boldsymbol{L}^2(\omega)} + C_2 ||\boldsymbol{w}||^2_{\boldsymbol{L}^2(\omega)} - C_3 ||\boldsymbol{w}||_{\boldsymbol{L}^2(\omega)} - C_4 ||\boldsymbol{w}||_{\boldsymbol{L}^2(\partial\omega)} \geq c_1 ||\boldsymbol{w}||^2_{\boldsymbol{H}^1(\omega)} - c_2 ||\boldsymbol{w}||_{\boldsymbol{H}^1(\omega)}$, $\forall \, \boldsymbol{w} \in \boldsymbol{H}^1(\omega)$. Note that we use the condition $||\boldsymbol{w}||_{\boldsymbol{H}^1(\omega)} \leq C(||\boldsymbol{\epsilon}^M(\boldsymbol{w})||^2_{\boldsymbol{L}^2(\omega)} + ||\boldsymbol{w}||^2_{\boldsymbol{L}^2(\omega)})^{\frac{1}{2}}$, which is Korn's inequality without boundary conditions for a membrane (see chapter 4 and 5 of Ciarlet [38] with $w^3 = 0$). **Fréchet Differentiable**: $J'(\boldsymbol{w})_{\text{Baldelli}} \boldsymbol{v} \leq C_1 ||\boldsymbol{\epsilon}^M(\boldsymbol{w})||_{\boldsymbol{L}^2(\omega)} ||\boldsymbol{\epsilon}^M(\boldsymbol{v})||_{\boldsymbol{L}^2(\omega)} + C_2 ||\boldsymbol{w}||_{\boldsymbol{L}^2(\omega)} ||\boldsymbol{v}||_{\boldsymbol{L}^2(\omega)} + C_3 ||\boldsymbol{v}||_{\boldsymbol{L}^2(\omega)} + C_4 ||\boldsymbol{v}||_{\boldsymbol{L}^2(\partial\omega)} \leq C(||\boldsymbol{w}||_{\boldsymbol{H}^1(\omega)} + 1) ||\boldsymbol{v}||_{\boldsymbol{H}^1(\omega)}$, $\forall \, \boldsymbol{v}, \boldsymbol{w} \in \boldsymbol{H}^1(\omega)$. **Strictly convex**: $(J'(\boldsymbol{w})_{\text{Baldelli}} - J'(\boldsymbol{v})_{\text{Baldelli}})(\boldsymbol{w} - \boldsymbol{v}) \geq C_1 ||\boldsymbol{\epsilon}^M(\boldsymbol{w}) - \boldsymbol{\epsilon}^M(\boldsymbol{v})||^2_{\boldsymbol{L}^2(\omega)} + C_2 ||\boldsymbol{w} - \boldsymbol{v}||^2_{\boldsymbol{L}^2(\omega)} \geq C ||\boldsymbol{w} - \boldsymbol{v}||^2_{\boldsymbol{H}^1(\omega)}$, $\forall \, \boldsymbol{v}, \boldsymbol{w} \in \boldsymbol{H}^1(\omega)$. Thus, lemmas 17 and 18 imply that there exists a unique field $\boldsymbol{w} \in \boldsymbol{H}^1(\omega)$ such that $\boldsymbol{w}$ is the unique solution to the minimisation problem $J(\boldsymbol{w})_{\text{Baldelli}} = \min_{\boldsymbol{v} \in \boldsymbol{H}^1(\omega)} J(\boldsymbol{v})_{\text{Baldelli}}$. In particular, this unique minimiser $\boldsymbol{w}$ is also a critical point in $(\boldsymbol{H}^1(\omega), J(\cdot)_{\text{Baldelli}})$.

Alternatively, proof follows from theorem 3 in the leading order case when the foundation takes the form $\Omega = \omega \times (-H, 0)$ and for the asymptotic condition $\{\Lambda h \sim H^{-1}\bar{\mu}\text{meas}(\boldsymbol{\sigma}(\omega); \mathbf{E}^2), hB^{\alpha\beta\gamma\delta} F_{[\text{III}]\alpha\beta} F_{[\text{III}]\gamma\delta} \sim H^{-1}(\bar{\lambda} + 2\bar{\mu})\}$, given that the displacement field of the foundation is approximated by $\boldsymbol{u} = (1 + H^{-1}x^3)\boldsymbol{w}$. □

To conduct numerical experiments we remain with the framework that we introduced in Section 3.5. Thus, given that $\boldsymbol{w} = (0, w^2(x^2), 0)$ is the displacement field of extended Baldelli and Bourdin's model for a membrane supported by an elastic foundation, one finds

$$\nabla_2 w^2 = \partial_2 w^2 + \Gamma^2_{22} w^2 \, ,$$

$$\epsilon_2^2(\boldsymbol{w}) = \nabla_2 w^2 \ .$$

Thus, one can express the governing equations as

$$\Lambda \partial_2 \epsilon(w)_2^2 - \bar{\mu}(hH)^{-1}(\psi_2)^2 w^2 = 0 \ ,$$

and the boundary conditions as

$$\Lambda \epsilon_2^2(\boldsymbol{w})|_{\partial\omega_{T_0}^{\text{New}}} = \tau_0 \text{ (traction)} \ ,$$
$$\Lambda \epsilon_2^2(\boldsymbol{w})|_{\partial\omega_{T_{\text{max}}}^{\text{New}}} = \tau_{\text{max}} \text{ (traction)} \ .$$

With a little more effort, one can solve this problem explicitly. For example, given that $\tau_0, \tau_{\text{max}} = 1$, the explicit solution is

$$w^2(x^2) = \frac{\sinh\left(a\alpha E(x^2, e)\right)}{\alpha\Lambda\varphi(x^2)\cosh\left(a\alpha E(e)\right)} \ , \tag{75}$$

where $E(x^2, e) = \int_0^{x^2}(1 - e^2\sin^2(\theta))^{\frac{1}{2}} \ d\theta$ is the incomplete elliptic integral of the second kind, $E(e) = E(\frac{1}{2}\pi, e)$ is the complete elliptic integral of the second kind, $e = (1 - (b/a)^2)^{\frac{1}{2}}$ is the elliptical modulus (see chapter 17 of Abramowitz *et al.* [1]) and $\alpha = (\bar{\mu}/(hH\Lambda))^{\frac{1}{2}}$.

Let $\phi_b = (2a\alpha E(e))^2$. As a result of the asymptotic condition $\{h\Lambda \sim H^{-1}\bar{\mu}(\text{meas}(\boldsymbol{\sigma}(\omega^{\text{New}}); \mathbf{E}))^2$, $hB_{22}^{22}F_{[\text{II}]2}^2F_{[\text{II}]2}^2 \sim H^{-1}(\bar{\lambda} + 2\bar{\mu})\}$ (modified as ω is now no longer bounded), one finds that $\phi_b \approx 1$ is the condition that equation (75) is mostly accurate for when approximating the contact region. Thus, we use this fact in our numerical analysis.

Now, recall equations (73) and (74), and non-dimensionalise them by substituting in the transformations $(x^2, x^3) \to (\bar{x}^2, H\bar{x}^3)$ and $(u^2, u^3) \to (\bar{u}^2, H\bar{u}^3)$. Collecting all the leading order $\bar{u}^2$ terms for the $\phi_b \approx 1$ case, and with a little intuition, one finds that the only asymptotic scaling is of significance is $a\alpha E(x^2, e) \sim \frac{1}{2}\pi$, and thus, let $\phi_s = \pi^{-2}(2a\alpha E(e))^2$. This is another asymptotic scaling we examine with the numerical experiments.

Figure 35 is calculated with the values $b = 2$, $h = \frac{1}{4}$, $E = 6000$ and $\nu = \frac{1}{4}$. Figure 35 shows the azimuthal (i.e. w^2) and the radial (i.e. w^3) displacements at the contact region ω^{New}. The maximum azimuthal displacements are observed at $x^2 = \pm\frac{1}{2}\pi$, with respective azimuthal displacements of $w^2 = \pm 1.43 \times 10^{-4}$. This is a significantly lower result than what is predicted by our bonded shell model. Also, extended Baldelli and Bourdin's model predicts the radial displacement to be identically zero, while our shell model gives nonzero radial displacement. Now, this raises an important question: which model accurately depicts the displacement field at the contact region?

To investigate this matter further, we numerically model the overlying body as a three-dimensional body and we do not approximate this body as a shell or otherwise. Thus, the displacement at the contact region with this approach is the displacement field at the contact region of the bonded two-body elastic problem, whose solution is obtained by the use of the stranded equilibrium equations in the liner elasticity theory.

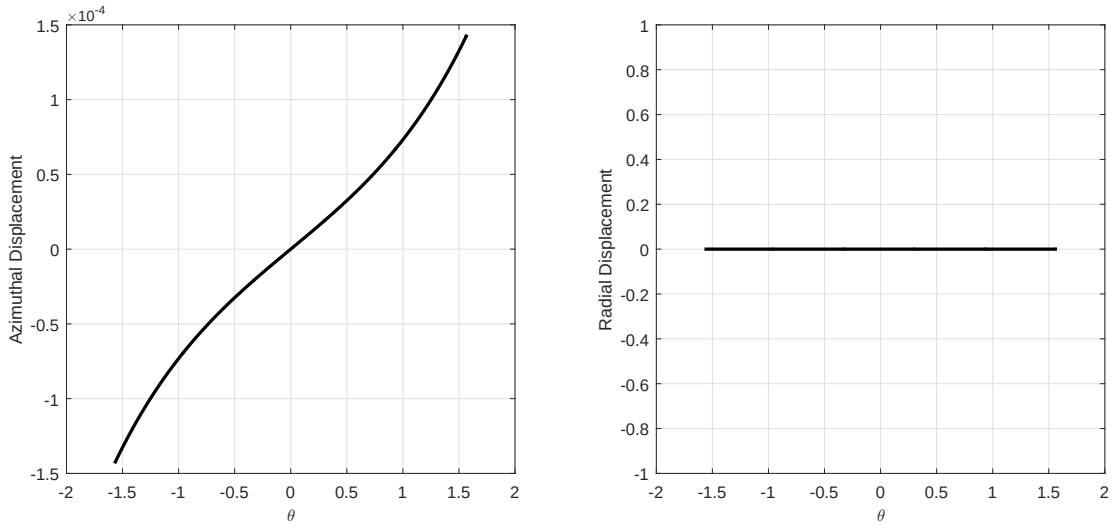

Figure 35: Displacement field of extended Baldelli and Bourdin's model at the contact region.

In accordance with the framework that is introduced in Section 3.5, the overlying body is restricted to the region $x^3 \in (0, h)$. Thus, with some calculations one finds

$$\begin{aligned}
\bar{\nabla}_2 v^2 &= \partial_2 v^2 + \bar{\Gamma}^2_{22} v^2 + \bar{\Gamma}^2_{23} v^3 \,, \\
\bar{\nabla}_2 v^3 &= \partial_2 v^3 - (\bar{\psi}_2)^2 \bar{\Gamma}^2_{23} v^2 \,, \\
\bar{\nabla}_3 v^2 &= \partial_3 v^2 + \bar{\Gamma}^2_{23} v^2 \,, \\
\bar{\nabla}_3 v^3 &= \partial_3 v^3 \,,
\end{aligned}$$

where $\boldsymbol{v} = (0, v^2(x^2, x^3), v^3(x^2, x^3))$ is the displacement field of the overlying body. With relative ease, one can express the governing equations of the overlying body as

$$\begin{aligned}
(\lambda + \mu)\partial^2 \left(\bar{\nabla}_i v^i\right) + \mu \bar{\Delta} v^2 = 0 \,, \\
(\lambda + \mu)\partial^3 \left(\bar{\nabla}_i v^i\right) + \mu \bar{\Delta} v^3 = 0 \,,
\end{aligned}$$

and the boundary conditions of the overlying body as

$$\begin{aligned}
\left[(\lambda + 2\mu)\partial_2 v^2 + \lambda \left(\partial_3 v^3 + \bar{\Gamma}^2_{22} v^2 + \bar{\Gamma}^2_{23} v^3\right)\right]|_{\{\partial \omega^{\text{New}}_{T_0} \times [0,h]\}} &= \tau_0 \text{ (traction)} \,, \\
\left[(\lambda + 2\mu)\partial_2 v^2 + \lambda \left(\partial_3 v^3 + \bar{\Gamma}^2_{22} v^2 + \bar{\Gamma}^2_{23} v^3\right)\right]|_{\{\partial \omega^{\text{New}}_{T_{\max}} \times [0,h]\}} &= \tau_{\max} \text{ (traction)} \,, \\
\left[\lambda \left(\partial_2 v^2 + \bar{\Gamma}^2_{22} v^2 + \bar{\Gamma}^2_{23} v^3\right) + (\lambda + 2\mu)\partial_3 v^3\right]|_{\{(-\frac{1}{2}\pi, \frac{1}{2}\pi) \times \{h\}\}} &= 0 \text{ (zero-Robin)} \,, \\
\left[(\bar{\psi}_2)^2 \partial_3 v^2 + \partial_2 v^3\right]|_{\{\partial \omega^{\text{New}} \times [0,h]\} \cup \{(-\frac{1}{2}\pi, \frac{1}{2}\pi) \times \{h\}\}} &= 0 \text{ (zero-Robin)} \,,
\end{aligned}$$

with following equations characterising the bonding of the overlying body to the foundation

$$\begin{aligned}
\left[u^2 - v^2\right]|_{\omega^{\text{New}}} &= 0 \text{ (continuous azimuthal displacement)} \,, \\
\left[u^3 - v^3\right]|_{\omega^{\text{New}}} &= 0 \text{ (continuous radial displacement)} \,, \\
\text{Tr}(T^2_3(\boldsymbol{u})) - \mu \left((\bar{\psi}_2)^2 \partial_3 v^2 + \partial_2 v^3\right)|_{\omega^{\text{New}}} &= 0 \text{ (continuous azimuthal stress)} \,, \\
\text{Tr}(T^3_3(\boldsymbol{u})) - \left[\lambda \left(\partial_2 v^2 + \bar{\Gamma}^2_{22} v^2 + \bar{\Gamma}^2_{23} v^3\right) + (\lambda + 2\mu)\partial_3 v^3\right]|_{\omega^{\text{New}}} &= 0 \text{ (continuous radial stress)} \,.
\end{aligned}$$

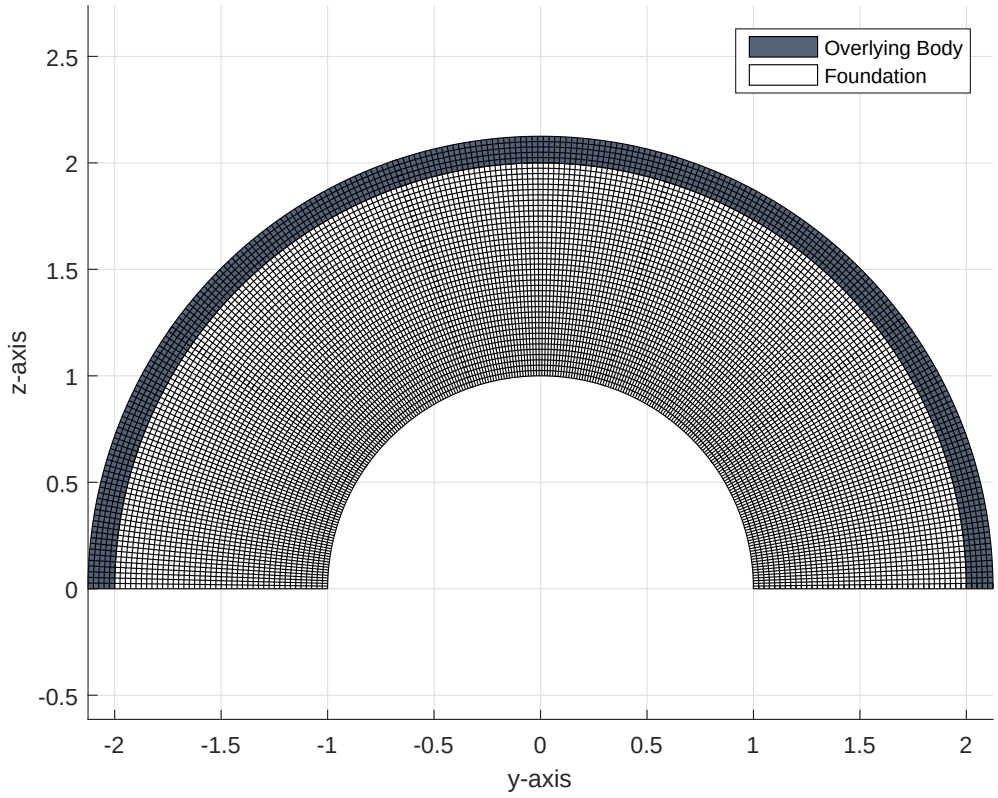

Figure 36: Discretised reduced two-dimensional domain of the two-body elastic problem for the $a = 2$, $b = 2$, $h = \frac{1}{8}$, $H = 1$ and $N = 250$ case.

Note that the grid dependence of the overlying body is approximately $\psi_0 \Delta x^2 \leq \Delta x^3$, $\forall\ \psi_0 \in \{\bar{\psi}_2(x^2, x^3) \mid x^2 \in [-\frac{1}{2}\pi, \frac{1}{2}\pi]$ and $x^3 \in [0, h]\}$, where Δx^j is a small increment in x^j direction. For our purposes, we use $\Delta x^2 = \frac{1}{N-1}$ and $\psi_0 = \bar{\psi}_2(\frac{1}{4}\pi, h)$, where $N = 250$ (see figure 36). Furthermore, we choose to terminate our iterating process once the condition $|1 - (||\boldsymbol{u}_m||_{\ell^2} + ||\boldsymbol{v}_m||_{\ell^2})^{-1}(||\boldsymbol{u}_{m+1}||_{\ell^2} + ||\boldsymbol{v}_{m+1}||_{\ell^2})| < 10^{-10}$ is satisfied, where $\boldsymbol{u}_m$ and $\boldsymbol{v}_m$ are the m^{th} iterative solutions of the bonded two-body model.

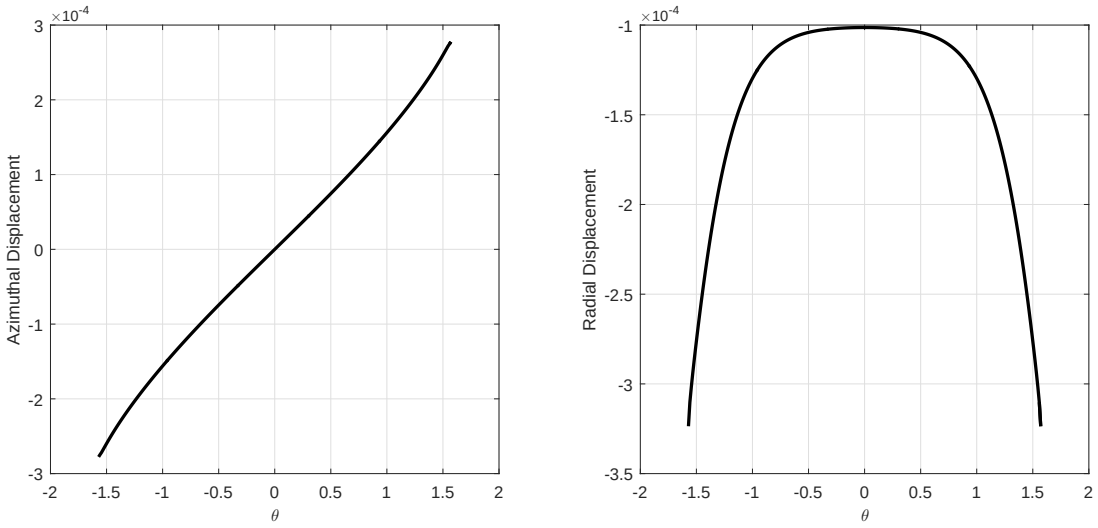

Figure 37: Displacement field of the bonded two-body model at the contact region.

Figure 37 is calculated with the values of $b = 2$, $h = \frac{1}{4}$, $E = 6000$ and $\nu = \frac{1}{4}$. Figure 37 shows the azimuthal (i.e. v^2) and the radial (i.e. v^3) displacements at the contact region ω^{New}. The maximum azimuthal displacements are observed at $x^2 = \pm\frac{1}{2}\pi$, with respective azimuthal displacements of $v^2 = \pm 2.78 \times 10^{-4}$. The maximum radial displacement is observed at $x^2 = \pm\frac{1}{2}\pi$, with a radial displacement of $v^3 = -3.24 \times 10^{-4}$. This implies that our overlying shell model's prediction is closer to bonded two-body's displacement field at the contact region relative to extended Baldelli and Bourdin's model's prediction, for this case of course.

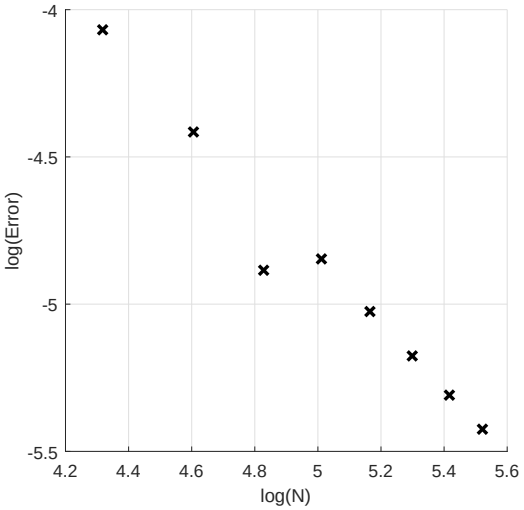

Figure 38: Grid dependence of the bonded two-body model.

As for the analysis on grid dependence, the reader can see from figure 38, as N increases, the difference between the numerical solution N and $N + 1$ decreases. For our experiments we found that the azimuthal grid points and the error share the relation $N \propto \text{Error}^{-0.894}$, where $\text{Error} = |1 - (||\boldsymbol{u}_{N-1}||_{\ell^2} + ||\boldsymbol{v}_{N-1}||_{\ell^2})^{-1}(||\boldsymbol{u}_N||_{\ell^2} + ||\boldsymbol{v}_N||_{\ell^2})|$. Note that figure 37 is calculated with the values of $b = 2$, $h = \frac{1}{4}$, $E = 6000$ and $\nu = \frac{1}{4}$.

But this is still not sufficient analysis, and thus, our goal in this section is to investigate how our bonded shell model approximates bonded two-body model's displacement field at the contact region relative to extended Baldelli and Bourdin's model for the variables $\delta b = b/a$, $\delta h = h/H$, $\delta E = E/\bar{E}$ and $\delta\nu = \nu/\bar{\nu}$. To proceed with this investigation we calculate the error in the energy-norm (see Jayawardana *et al.* [89]) as

$$Err_2(u^i) = \frac{\left(\sum_{\{\Delta x^2\}} ||u^i_{\text{shell}}(\Delta x^2, 0) - u^i_{\text{two-body}}(\Delta x^2, 0)||^2\right)^{\frac{1}{2}}}{\left(\sum_{\{\Delta x^2\}} ||u^i_{\text{two-body}}(\Delta x^2, 0)||^2\right)^{\frac{1}{2}}},$$

$$Err_2(w^i) = \frac{\left(\sum_{\{\Delta x^2\}} ||w^i_{\text{Baldelli}}(\Delta x^2) - u^i_{\text{two-body}}(\Delta x^2, 0)||^2\right)^{\frac{1}{2}}}{\left(\sum_{\{\Delta x^2\}} ||u^i_{\text{two-body}}(\Delta x^2, 0)||^2\right)^{\frac{1}{2}}},$$

to calculate the relative error between the bonded two-body displacement field and the approximated displacement fields at the contact region.

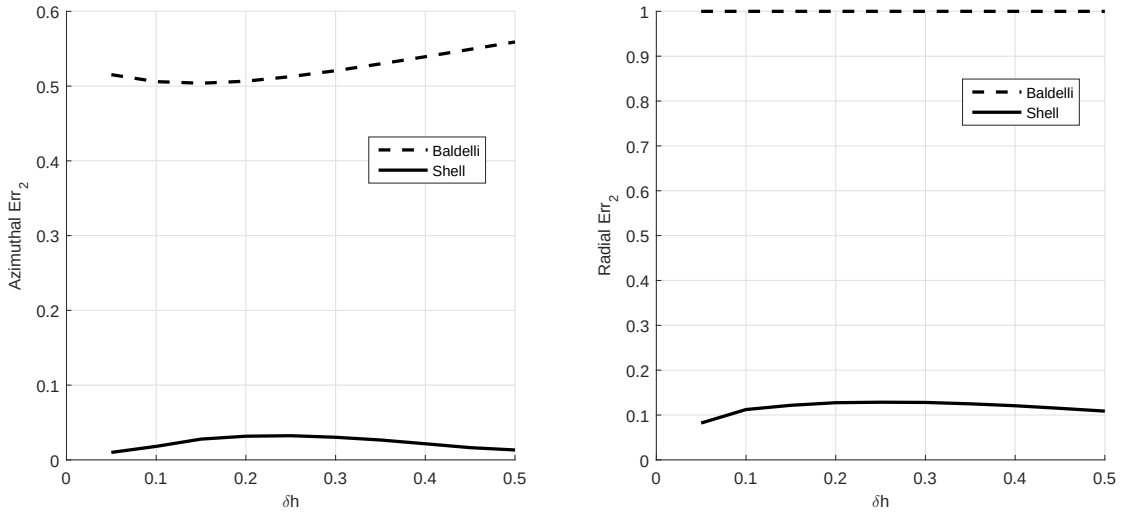

Figure 39: Shell model error v extended Baldelli and Bourdin's model error for $\delta h = h/H$.

Figure 39 is calculated with the values $\delta b = 1$, $\delta h \in \{\frac{1}{20}, \frac{2}{20}, \frac{3}{20}, \frac{4}{20}, \frac{5}{20}, \frac{6}{20}, \frac{7}{20}, \frac{8}{20}, \frac{9}{20}, \frac{10}{20}\}$, $\delta E = 6$ and $\delta \nu = 1$. From figure 39 one can see that the azimuthal error of the extended Baldelli and Bourdin's model attains a minimum at $\delta h = \frac{3}{20}$ with an azimuthal error of 50.4%. This coincides with the asymptotic condition ϕ_b, as when $\phi_b \approx 1$, one observes this minimum in the azimuthal error. Notice how extended Baldelli and Bourdin's azimuthal error increases as the thickness of the overlying body decreases. Now, this raises an important issue regarding Baldelli and Bourdin's work [16] as the authors present their model to be valid for analysing overlying thin objects, yet the asymptotic condition ϕ_b implies that their assertion cannot be valid, i.e. authors' model is mostly accurate for overlying bodies with a very specific thickness. Now, consider the azimuthal error of our bonded shell model, and it is significantly smaller than the error of extended Baldelli and Bourdin's model. For our bonded shell model the maximum azimuthal error is observed at $\delta h = \frac{1}{4}$ with an error of 3.32%, and it rapidly decreases as δh decreases or increases. This maximum in azimuthal error of the bonded shell model is observed for the asymptotic condition $\phi_s = 1$. The radial error of extended Baldelli and Bourdin's model is 100% and this is the case for all values of δh. This is due to the fact that with extended Baldelli and Bourdin's model the only value the normal displacement can obtain is zero, and this is case for all variables. In contrast, the radial error of our bonded shell model is, again, significantly smaller. For the shell model, the highest radial error is, again, observed at $\delta h = \frac{1}{4}$, with an error of 12.9%. This maximum in radial error of the shell model is observed again for the asymptotic condition $\phi_s = 1$.

Figure 40 is calculated with the values $\delta b = 1$, $\delta h = \frac{1}{4}$, $\delta E \in \{1, 2, 3, 4, 5, 6, 7, 8, 9, 10\}$ and $\delta \nu = 1$. From figure 40 one can see that the azimuthal error of extended Baldelli and Bourdin's model attains a minimum at $\delta E = 4$ with an azimuthal error of 50.8%. This, again, coincides with the asymptotic condition ϕ_b, as when $\phi_b \approx 1$, we observe this minimum in the azimuthal error. Notice how extended Baldelli and Bourdin's azimuthal error increases as Young's modulus of the overlying body increases. Now, this raises an important issue regarding Baldelli and Bourdin's work [16] as the au-

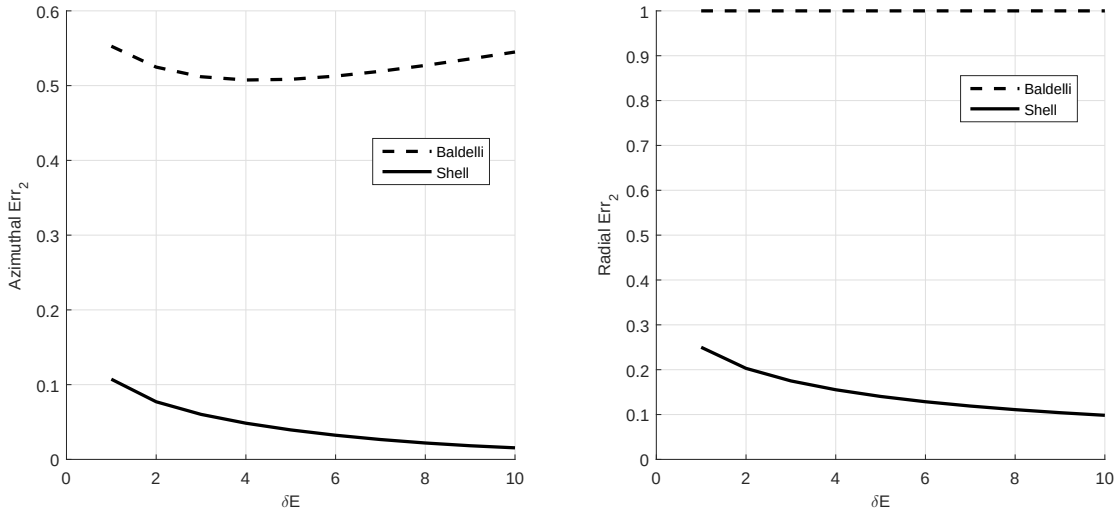

Figure 40: Shell model error v extended Baldelli and Bourdin's model error for $\delta E = E/\bar{E}$.

thors present their model to be valid for analysing overlying stiff objects, yet the asymptotic condition ϕ_b implies that their assertion cannot be valid, i.e. authors' model is mostly accurate for overlying bodies with a very specific Young's modulus. Now, consider the azimuthal error of our overlying shell model, again, it is significantly smaller than the error of extended Baldelli and Bourdin's model. For our bonded shell model the lowest azimuthal error is observed at $\delta E = 10$ with an error of 1.55%, and it increases as δE decreases. For our bonded shell model the radial error decreases monotonically, from 25.0% to 9.83%, as δE of the overlying body increases, from 1 to 10. This implies that for a stiff overlying body on an elastic foundation, our bonded shell model can approximate the normal displacement with a much higher degree of accuracy.

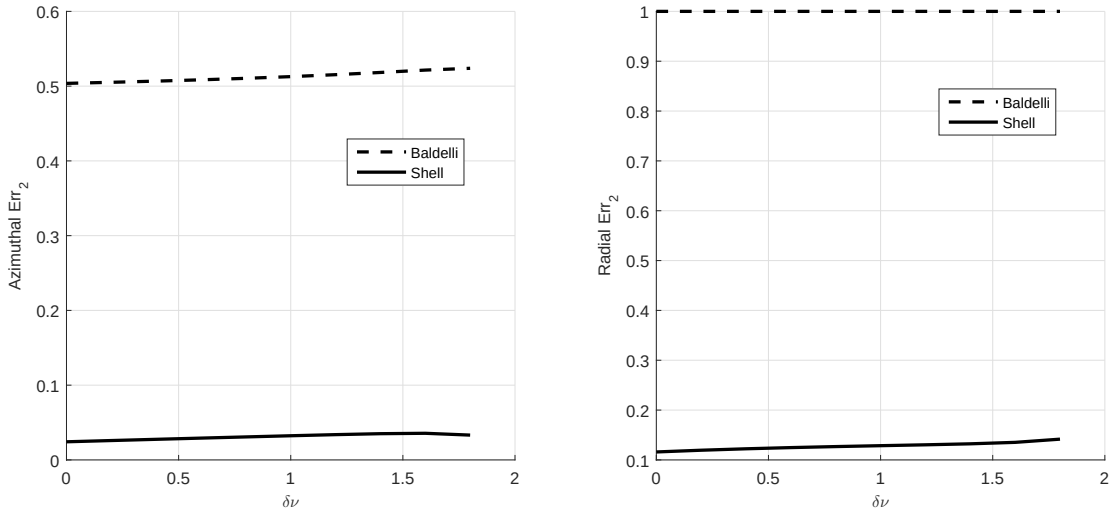

Figure 41: Shell model error v extended Baldelli and Bourdin's model error for $\delta\nu = \nu/\bar{\nu}$.

Figure 41 is calculated with the values $\delta b = 1$, $\delta h = \frac{1}{4}$, $\delta E = 6$ and $\delta\nu \in \{0, \frac{1}{5}, \frac{2}{5}, \frac{3}{5}, \frac{4}{5}, 1, \frac{6}{5}, \frac{7}{5}, \frac{8}{5}, \frac{9}{5}\}$. From figure 41, one can see that the azimuthal error of extended Baldelli and Bourdin's model at-

tains a minimum at $\delta\nu = 0$, with an azimuthal error of 50.4%. This, once again, coincides with the asymptotic condition ϕ_b, as when $\phi_b \approx 1$, we observe this minimum in the azimuthal error. Now, this raises an important issue regarding Baldelli and Bourdin's work [16] as the authors present their model to be valid for overlying bodies with nonzero Poisson's ratios, yet the asymptotic condition ϕ_b implies that their assertion cannot be valid, i.e. authors' model is mostly accurate for overlying bodies with zero-Poisson's ratio. Now, consider azimuthal error from our bonded shell model, it is, again, significantly smaller than the error of extended Baldelli and Bourdin's model. For our bonded shell model the highest azimuthal error is observed at $\delta\nu = \frac{8}{5}$ with an error of 3.56%. Also, for our bonded shell model the radial error increases monotonically, from 11.6% to 14.2%, as $\delta\nu$ of the overlying body increases, from 0 to $\frac{9}{5}$.

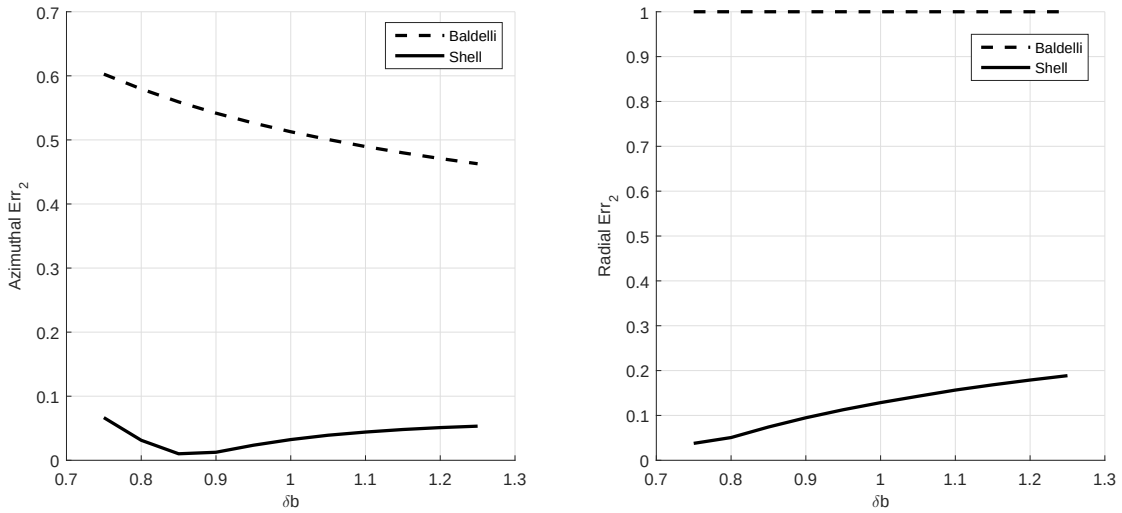

Figure 42: Shell model error v extended Baldelli and Bourdin's model error for $\delta b = b/a$.

Figure 42 and calculated with the values $\delta b \in \{\frac{15}{20}, \frac{16}{20}, \frac{17}{20}, \frac{18}{20}, \frac{19}{20}, 1, \frac{21}{20}, \frac{22}{20}, \frac{23}{20}, \frac{24}{20}, \frac{25}{20}\}$, $\delta h = \frac{1}{4}$, $\delta E = 6$ and $\delta\nu = 1$. From figure 42, one can see that the azimuthal error of extended Baldelli and Bourdin's model decreases monotonically with increasing δb, and at $\delta b = \frac{5}{4}$, the azimuthal error is 46.3%. This, however, is not predicted by the asymptotic condition ϕ_b as in accordance with the condition $\phi_b \approx 1$ we expect to observe this minimum in the azimuthal error at $\delta b = 1$ i.e. when the mean curvature of the system is constant. Now, consider the azimuthal error of our bonded shell model, once more, it is significantly smaller than the error of extended Baldelli and Bourdin's model. The lowest azimuthal error of our bonded shell model is observed at $\delta b = \frac{17}{20}$ with an error of 1.02% and this error increases as δb increases or decreases. These results imply that there exists a critical parametric-latitude where the azimuthal error of our shell model is a minimum. For the bonded shell model the radial error increases monotonically, from 3.78% to 18.9% as δb increases, from $\frac{3}{4}$ to $\frac{5}{4}$.

The above analysis appears show that our bonded shell on an elastic foundation model is far superior to extended Baldelli and Bourdin's model with respect to the bonded two-body model, as extended Baldelli and Bourdin's model's error failed to fall below or even come close to our bonded shell model's error, even a for set of variables which extended Baldelli and Bourdin's model is mostly

accurate for. Also, extended Baldelli and Bourdin's model asserts that the normal displacement is always zero, while our bonded shell model can predict a nonzero normal displacement, often differing from two-body problem's solution by 10%. Another disadvantage of extended Baldelli and Bourdin's model is that, for the model to be valid, the foundation must have a very specific form (i.e. constant thickness H, planer dimension cannot exceed the contact region ω, the lower boundary must satisfy zero-Dirichlet boundary condition and the remaining boundaries must be stress free), while for our bonded shell model the foundation may take arbitrary form, as long as in a proper subset of the boundary of the foundation the displacement field of the foundation satisfies zero-Dirichlet boundary condition. However, there are some advantages of extended Baldelli and Bourdin's model over our bonded shell model. For example, extended Baldelli and Bourdin's model is extremely simple to numerically model as it approximates the foundation. Thus, often a closed-form of a solution can be found, while our bonded shell model requires lengthy computations to calculate solutions, even for a simple problem such as the one investigated in this section.

The numerical results raise fundamental questions regarding extended Baldelli and Bourdin's model. As δh decreases beyond a certain threshold, extended Baldelli and Bourdin's solution diverge away from two-body model's azimuthal solution, implying that extended Baldelli and Bourdin's model is mostly accurate for overlying bodies with a very specific thickness. However, Baldelli and Bourdin [16] assert that their model is to be used for overlying thin bodies, such as thin films and membranes. Clearly our numerical experiments (see figure 39) contradict their assertion about the model must be used for modelling very thin overlying bodies. Another peculiar behaviour we observed is that as δE of the overlying body increases above a certain threshold, extended Baldelli and Bourdin's azimuthal error diverge away from two-body model's azimuthal solution. This, again, contradicts authors' asymptotic assertion, which states that the stiffer the overlying body is, then more accurate their model is. Furthermore, we observed that then the Poisson's ratio of the overlying body is zero Baldelli and Bourdin's azimuthal error attains a minimum. This, further, contradicts authors' asymptotic assertion, which states that the Poisson's ratio of the overlying body must be sufficiently away from zero for the model to be mostly accurate. Note that we do not find any numerical evidence in authors' publications (or Baldelli [15]) to support theirs asymptotic assertions.

On a last note: we remind the reader again that the model we present in this section is not a model derived by Baldelli and Bourdin [16]. We merely called it the extended Baldelli and Bourdin's model for convenience. The main thing we used from the authors is that their approximate for the displacement field of the foundation, which is $\boldsymbol{u} = (1 + H^{-1}x^3)\boldsymbol{w}$ where $\boldsymbol{w}$ is the displacement filed of the overlying body at the contact region. Please see Section 1.10 for a comprehensive review of authors' work.

3.7 Error analysis

It is documented in the literature that given a thin overlying body on an elastic foundation, the thin body must only be approximated by a shell (a plate, a membrane or a film), if the thin overlying body

has a significantly higher Young's modulus relative to Young's modulus of the foundation[4]. In light of this information we dedicate this section to see how physically valid our bonded shell model is with respect to varying elastic and geometrical properties.

To proceed with this investigation we calculate the relative error between the displacement field of the foundation predicted by our bonded shell model and the displacement field of the foundation predicted by the bonded two-body elastic model by

$$\text{Relative Error}(u^i) = \frac{\left(\sum_{\{\Delta x^2, \Delta x^3\}} ||u^i_{\text{shell}}(\Delta x^2, \Delta x^3) - u^i_{\text{two-body}}(\Delta x^2, \Delta x^3)||^2\right)^{\frac{1}{2}}}{\left(\sum_{\{\Delta x^2, \Delta x^3\}} ||u^i_{\text{shell}}(\Delta x^2, \Delta x^3) + u^i_{\text{two-body}}(\Delta x^2, \Delta x^3)||^2\right)^{\frac{1}{2}}} .$$

We retain the same numerical procedure that we introduced in Sections 3.5 and 3.6, and see how the relative error behaves for various values of $\delta E = E/\bar{E}$, $\delta\nu = \nu/\bar{\nu}$, $\delta h = h/H$, and $\delta b = b/a$.

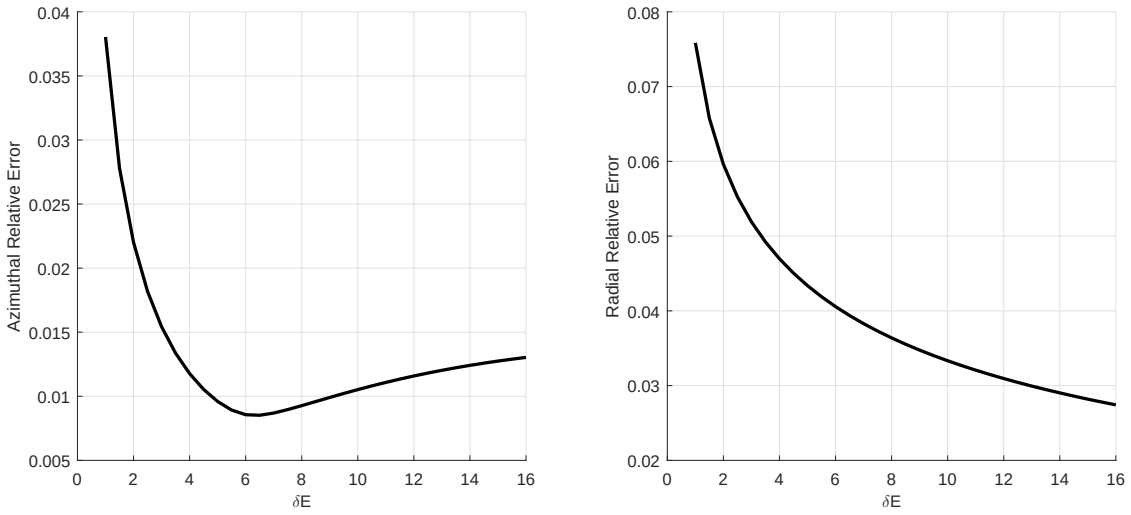

Figure 43: Relative error for $\delta E = E/\bar{E}$.

Figure 43 is calculated with the values $\delta b = 1$, $\delta h = \frac{1}{8}$, $\delta E \in \{1, \frac{3}{2}, 2, \frac{5}{2}, 3, \frac{7}{2}, 4, \frac{9}{2}, 5, \frac{11}{2}, 6, \frac{13}{2}, 7, \frac{15}{2}, 8, \frac{17}{2}, 9, \frac{19}{2}, 10, \frac{21}{2}, 11, \frac{22}{2}, 12, \frac{25}{2}, 13, \frac{27}{2}, 14, \frac{29}{2}, 15, \frac{31}{2}, 16\}$ and $\delta\nu = 1$. From figure 43 one can see that the azimuthal relative error attains a minimum at $\delta E = \frac{13}{2}$ with a relative error of 0.852%. Now, this implies that, despite the fact that a higher Young's modulus of the shell results in more accurate solutions, increasing Young's modulus of the shell indefinitely may not result in the most accurate solutions. We observe a similar effect in Section 3.6, where the model presented assumed to be valid for membranes with high Young's moduli, yet we observed that there exists an optimum Young's modulus where the error is a minimum. As for the relative radial error, one can see that as δE of shell increases, from 1 to 16, the relative error decreases, from 7.59% to 2.74%. Now, to reduce the radial error, it appears to be a sound choice to increase Young's modulus of the shell to extremely high values.

Figure 44 is calculated with the values $\delta b = 1$, $\delta h \in \{\frac{2}{32}, \frac{3}{32}, \frac{4}{32}, \frac{5}{32}, \frac{6}{32}, \frac{7}{32}, \frac{8}{32}, \frac{9}{32}, \frac{10}{32}, \frac{11}{32}, \frac{12}{32}\}$, $\delta E = 8$ and $\delta\nu = 1$. From figure 44 one can see that the azimuthal relative error attains a minimum at

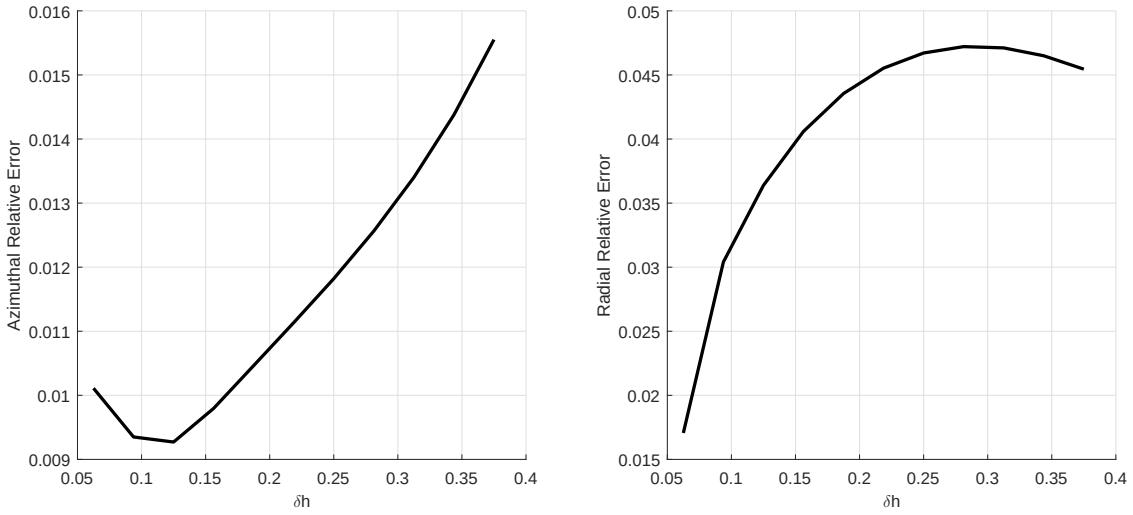

Figure 44: Relative error for $\delta h = h/H$.

$\delta h = \frac{1}{8}$ with a relative error of 0.927%. Now, this implies that there exists an optimum shell thickness where the azimuthal relative error is a minimum. We observe a similar effect in Section 3.6, where the model presented assumed to be valid for thin membranes, yet we observed that there exists an optimum thickness where the error is a minimum. As for the relative radial error, one can see that it attains a maximum at $\delta h = \frac{1}{4}$ with a relative error of 4.67%.

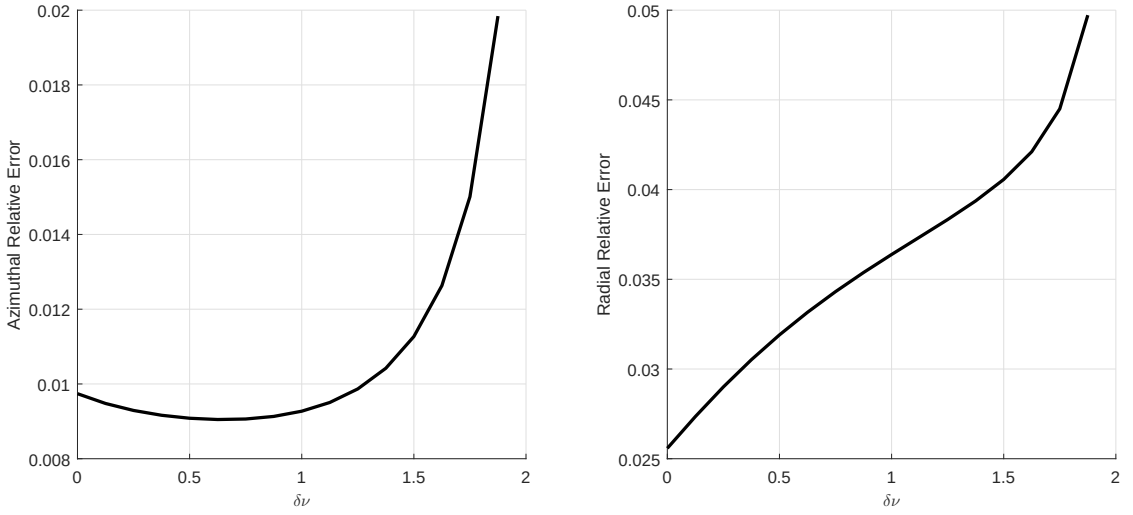

Figure 45: Relative error for $\delta\nu = \nu/\bar{\nu}$.

Figure 45 is calculated with the values $\delta b = 1$, $\delta h = \frac{1}{8}$, $\delta E = 8$ and $\delta\nu \in \{\frac{2}{8}, \frac{3}{8}, \frac{4}{8}, \frac{5}{8}, \frac{6}{8}, \frac{7}{8}, 1, \frac{9}{8}, \frac{10}{8}, \frac{11}{8}, \frac{12}{8}, \frac{13}{8}, \frac{14}{8}, \frac{15}{8}\}$. From figure 45 one can see that the azimuthal relative error attains a minimum at $\delta\nu = \frac{5}{8}$ with a relative error of 0.905%. Now, this implies that there exists an optimum Poisson's ratio of the shell where the azimuthal relative error is a minimum. As for the relative radial error, one can see that as $\delta\nu$ of shell increases, from 0 to $\frac{15}{8}$, the relative error also increases, from 2.56% to 4.97%.

Figure 46 and calculated with the values $\delta b \in \{\frac{32}{40}, \frac{33}{40}, \frac{34}{40}, \frac{35}{40}, \frac{36}{40}, \frac{37}{40}, \frac{38}{40}, \frac{39}{40}, 1, \frac{41}{40}, \frac{42}{40}, \frac{43}{40}, \frac{44}{40}, \frac{45}{40}, \frac{46}{40}, \frac{47}{40},$

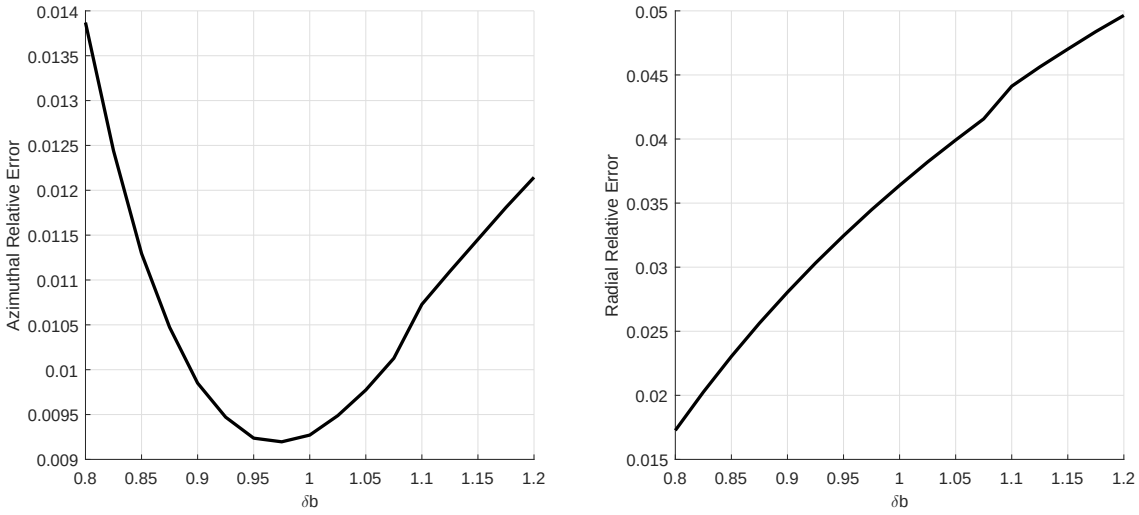

Figure 46: Relative error for $\delta b = b/a$.

$\frac{48}{40}\}$, $\delta h = \frac{1}{8}$, $\delta E = 8$ and $\delta\nu = 1$. From figure 46, one can see that the azimuthal relative error attains a minimum at $\delta b = \frac{39}{40}$ with a relative error of 0.920%. Now, this implies that when the mean curvature of the contact region is almost constant, the azimuthal relative error attains a minimum. As for the relative radial error, one can see that as δb increases, from $\frac{4}{5}$ to $\frac{6}{5}$, the relative error increases, from 1.72% to 4.96%.

Above analyses show that our bonded shell on an elastic foundation can predict the displacement field of foundation of the bonded two-body elastic model, with a significant degree of accuracy, given that Young's modulus of the shell is significantly high. Now, this result coincides with what is documented in the literature [4]. However, we also observe that arbitrary increasing Young's modulus of the shell may not result in the most accurate solutions as for the azimuthal relative error, we observed an optimum Young's modulus where the error is a minimum. We also observe that other factors can equally improve the accuracy of our bonded shell model, such as the magnitude of Poisson's ratio of the shell, the thickness of the shell and the critical parametric-latitude of the contact region, i.e. all elastic properties and geometric properties affect the accuracy of the solution. However, one cannot arbitrarily increase or decrease the thickness, Poisson's ratio or critical parametric-latitude, as we often observe optimal values for elastic and geometric properties where the error is a minimum. To to obtain the exact conditions where our bonded shell model is asymptotically justifiable require further analysis.

3.8 Conclusions

In this chapter we studied bonded shells on elastic foundations. In Section 3.2 we derived a mathematical model for a bonded shell on an elastic foundation, by modifying Koiter's linear shell equations presented by Ciarlet [38] and by considering a similar logical process that is used in the derivation of surface Cauchy-Bourne model [89], to describe the behaviour of a shell if it is bonded to a three-dimensional elastic body, by treating the shell as a boundary form of the foundation,

which is analogous to the work of Necas *et al.* [144]. Then, in Section 3.3, we explicitly derived the governing equations and the boundary conditions for the general case for bonded shells on elastic foundations. In Section 3.4 we used a combination of Ciarlet's [38], and Badiale and Serra's [13] work to prove the existence and the uniqueness of the solutions, and thus, proving that what we derived is a mathematical theory and not a hypothetical model.

In Section 3.5 we presented framework to conduct a set of numerical solutions. As a comparison, in Section 3.6, we extended Baldelli and Bourdin's [16] model for bonded films on elastic pseudo-foundations to curvilinear coordinates and showed how numerical solutions fair against our bonded shell model. The method of numerical analysis is simple: we numerically model the bonded two-body problem and compare the solution against our bonded shell model and extended Baldelli and Bourdin's model, for a set of variables which extended Baldelli and Bourdin's model is mostly accurate for, i.e. for $\phi_b \approx 1$. The numerical solutions shows that our bonded shell model is far superior when it comes to approximating displacement filed at the contact region than extended Baldelli and Bourdin's model, as often our azimuthal shell solution only differs from bonded two-body model's solution by $1-5\%$, while extended Baldelli and Bourdin's azimuthal solution can differ from the from bonded two-body model's solution by 50%. For an extreme example, for the case $\delta h = \frac{1}{20}$ we see that the azimuthal error of the shell solution is 0.998%, while azimuthal error of extended Baldelli and Bourdin's solution is 51.5% (see figure 39). Also, extended Baldelli and Bourdin's model assumes that the normal displacement is always zero, while our shell model predicts a normal displacement closer to the bonded two-body model's normal displacement, often with 10% difference.

We also saw that the asymptotic scaling ϕ_b is a great indicator for judging how accurate extended Baldelli and Bourdin's model is, as for a given thickness, Young's modulus, Poisson's ratio of the overlying body, the condition $\phi_b \approx 1$ yield the solutions with the minimum error. However, the scaling ϕ_b failed to predict the validity of the solution with respect to the critical parametric-latitude of the contact region. In contrast, we observe that the asymptotic scaling ϕ_s is a good indicator of judging how invalid our bonded shell model is for a given thickness, as for a given δh, the condition $\phi_s = 1$ yield the solutions with the maximum error. However, even for this case our shell model solution is still several magnitudes closer to the bonded two-body solution than extended Baldelli and Bourdin's solution (see figure 39).

To conclude our numerical analysis, in Section 3.7, we conducted further error analysis to see how our bonded shell on an elastic foundation can approximate the displacement field of the foundation of the two-body elastic model. Our analyses how that our bonded shell model can approximate the displacement field of foundation with a significant degree of accuracy given that Young's modulus of the shell is significantly high. Now, this result coincides with what is documented in the literature [4]. We further the found that, if the thickness the shell, Poisson's ratio of the shell and the critical parametric-latitude of the contact region are very low, then the relative error is very small. However, one cannot arbitrarily increase Young's modulus of the shell or decrease the thickness the shell, Poisson's ratio of the shell and the critical parametric-latitude of the contact region, as we often

observe optimal values for elastic and geometric properties where the relative error is a minimum.

With our analyses we shown that our theory for bonded shells on elastic foundations is mathematically valid via the existence of unique solutions, numerically superior to an existing model that model the same problem, and under which elastic and geometrical properties can one obtains the most accurate solutions. These types of models are largely used in the field of flexible and stretchable electronics. The reader can find a rich literature review regarding this subject matter in Section 1.7. For example, consider a curved flexible display screen. One may model the flexible organic layer as an elastic foundation and the thin conductive layer as a thin shell. Thus, by using our theory for bonded shells on elastic foundations, one may derive an accurate depiction of the displacement field and the stress profiles for the body in question, with respect to an appropriate set of variables.

3.8.1 Remark

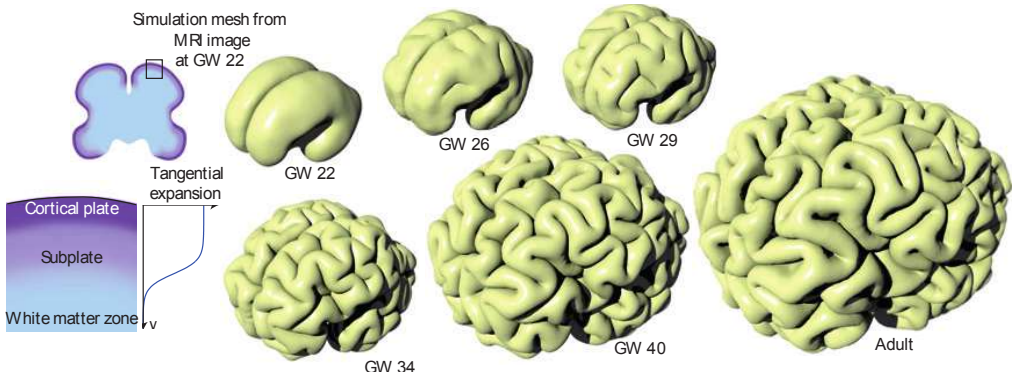

Figure 47: 'A simulation starting from a smooth fetal brain shows gyrification as a result of uniform tangential expansion of the cortical layer. The brain is modelled as a soft elastic solid and a relative tangential expansion is imposed on the cortical layer as shows at left, and the system allowed to relax to its elastic equilibrium' [192].

A further possible area of application for our theory for bonded shells on elastic foundations can be in modelling gyrification. Gyrification is the formation of folds in the cerebral cortex during the development of the brain. Tallinen *et al.* [191] numerically shows that gyrification is the result of mechanical buckling of the cortical plate due to rapid tangential expansion of gray matter zone constrained by the white matter zone (see figure 47). The authors model the human brain as a thin elastic body that is bonded to a thicker elastic body (spherical and ellipsoidal for the three-dimensional case) with zero-Dirichlet boundary condition imposed on the lowest of its boundary (see figure 48). The thin elastic body is assumed to be only 10% of the thickness of the elastic foundation. Both two-dimensional and three-dimensional numerical solutions are constructed with the finite-element method with an explicit solver for quasistatic equilibration of the system. Two-dimensional solutions are based on constant strain triangle with 60 layers of elements through its thickness to model the cortical plate, and three-dimensional solutions are based on irregular tetrahedron or curved cube mesh (for large brain simulations) with 8 layers of elements through its thickness to model the cortical plate.

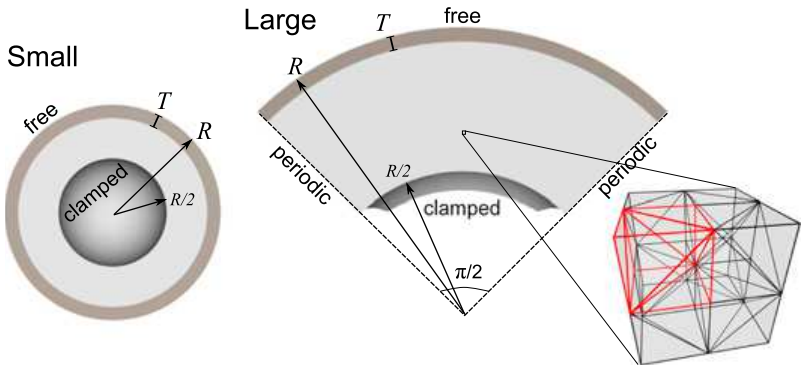

Figure 48: 'Cross-section views of 3D simulation geometries for small and large brains in their initial undeformed states. The gray-matter thickness T, brain radius R, and boundary conditions are indicated. A detailed image of the regular mesh structure of the large brain domain shows the reflection symmetry between every pair of elementary cubes that share a face' [191].

A word of caution: Tallinen *et al.* [191] referrer to the overlying elastic layer as a shell, but it is not a shell in the sense of mathematical shells as we investigate here in this thesis.

But what if such a fine mesh is not possible due to computational restraints or what if one wishes to model brain with a high gyrencephalic index where the gray matter layer is significantly thinner than white matter zone, i.e. the brains of Cetaceans (whales and dolphins) [198, 133]. For such scenarios we propose that one may use our theory for bonded shells on elastic foundations. This proposal is further justified, considering that Tallinen *et al.*'s [191] model (see figure 48) is schematically identical to the numerical model that we analysed in this chapter (see figure 36) with the exceptions of that Tallinen *et al.* [191] did not approximate the thin layer, they are considering quasistatic case and they are using finite strains. For more on nonlinear elasticity and the dynamic case please consult chapter 5.

4 Shells Supported by Elastic Foundations: Constraints to Model the Frictionally Coupled Case

Abstract

In this chapter we derive a theory for frictionally coupled shells on elastic foundations. We show that, if the diffeomorphism $\bar{\boldsymbol{X}} \in C^2(\bar{\Omega}; \mathbf{E}^3)$ describes the unstrained configuration of the foundation and the injective immersion $\boldsymbol{\sigma} \in C^3(\bar{\omega}; \mathbf{E}^3)$ describes the unstrained configuration of the overlying frictionally coupled shell, where $\Omega \subset \mathbb{R}^3$ is a connected open bounded domain that satisfies the segment condition with a uniform-$C^1(\mathbb{R}^3; \mathbb{R}^2)$ boundary $\partial\Omega$ such that $\omega, \partial\Omega_0 \subset \partial\Omega$, $\bar{\omega} \cap \partial\bar{\Omega}_0 = \emptyset$, $\text{meas}(\partial\Omega_0; \mathbb{R}^2) > 0$, and $\omega \subset \mathbb{R}^2$ is a connected open bounded plane that satisfies the segment condition with a uniform-$C^1(\mathbb{R}^2; \mathbb{R})$ boundary $\partial\omega$, with $\boldsymbol{f} \in \boldsymbol{L}^2(\Omega)$, $\boldsymbol{f}_0 \in \boldsymbol{L}^2(\omega)$ and $\boldsymbol{\tau}_0 \in \boldsymbol{L}^2(\partial\omega)$, then there exists a unique field $\boldsymbol{u} \in \boldsymbol{V}_{\mathscr{F}}(\omega, \Omega)$ such that $\boldsymbol{u}$ is the solution to the minimisation problem

$$J(\boldsymbol{u}) = \min_{\boldsymbol{v} \in \boldsymbol{V}_{\mathscr{F}}(\omega,\Omega)} J(\boldsymbol{v}) \ ,$$

where

$$\boldsymbol{V}_{\mathscr{F}}(\omega, \Omega) = \{\boldsymbol{v} \in \boldsymbol{V}_{\mathscr{I}}(\omega, \Omega) \mid \left[2\nu_F v^3 + (v_\alpha v^\alpha)^{\frac{1}{2}}\right]|_\omega \leq 0 \text{ a.e.}\} \ ,$$

$$\begin{aligned} J(\boldsymbol{u}) = &\int_\Omega \left[\frac{1}{2} A^{ijkl} E_{ij}(\boldsymbol{u}) E_{kl}(\boldsymbol{u}) - f^i u_i\right] d\Omega \\ &+ \int_\omega \left[\frac{1}{2} B^{\alpha\beta\gamma\delta} \left(h\epsilon_{\alpha\beta}(\boldsymbol{u})\epsilon_{\gamma\delta}(\boldsymbol{u}) + \frac{1}{3}h^3 \rho_{\alpha\beta}(\boldsymbol{u})\rho_{\gamma\delta}(\boldsymbol{u})\right) - h f_0^i u_i\right] d\omega - \int_{\partial\omega} h\tau_0^i u_i \, d(\partial\omega) \ , \end{aligned}$$

and where $\boldsymbol{A}$ is the elasticity tensor and $\boldsymbol{E}(\cdot)$ is the stain tensor of the foundation, $\boldsymbol{B}$ is the elasticity tensor, $\boldsymbol{\epsilon}(\cdot)$ is half of the change in first fundamental form tensor, $\boldsymbol{\rho}(\cdot)$ is the change in second fundamental form tensor and h is the thickness of the shell, and ν_F is the coefficient of friction between the foundation and the shell.

4.1 Introduction

In this chapter we examine the behaviour of shells supported by elastic foundations when subjected to a friction condition. In Section 4.2 we use Kikuchi and Oden's [102] model for Coulomb's law of static friction to derive a displacement-based static friction condition. Then, we take the overlying shell theory that we derived in chapter 3, but now, we assert that the shell is no longer bonded to the foundation and we use the displacement-based friction condition to transform the model into a constrained type problem. Then, in Section 4.3, we explicitly derive the governing equations and the boundary condition for the general case. In Section 4.4 we prove the existence and the uniqueness of solutions of the derived model, and conclusively proving what we derived is a mathematical theory. In Section 4.5 we present numerical examples to examine the properties for the given theory. Then, in Section 4.6, we extend Kikuchi and Oden's model for Coulomb's law of static friction in the curvilinear space that we derived in Section 2.6 to model a two-body contact problem, i.e. an elastic two-body contact problem subjected to Coulomb's law of static friction in curvilinear coordinates. We use this extended Kikuchi and Oden's model to numerically simulate an overlying thin, but still three-dimensional, body on an elastic foundation and compare the results with our shell model with friction to see how the both models predict the displacement field of the foundation, for a given set of variables.

4.2 Derivation

Recall Kikuchi and Oden's model for Coulomb's law of static friction that we extended to curvilinear coordinates, i.e. equation (66). By eliminating the regularisation parameter, ε, from the equations one may express it in the following form,

$$T_3^\beta(\boldsymbol{u}) + \nu_F \left(g_{33}\right)^{\frac{1}{2}} \left(u_\alpha u^\alpha\right)^{-\frac{1}{2}} T_3^3(\boldsymbol{u}) u^\beta \leq 0 \ .$$

Now, assume that $u^\beta \geq 0$ and contract the above equation with u^β. Noting that in this framework $g_{33} = 1$, and thus, one finds

$$\mu \left(u^\alpha \bar{\nabla}_\alpha u^3 + \frac{1}{2} \bar{\nabla}_3 (u_\alpha u^\alpha) \right) + \nu_F (u_\alpha u^\alpha)^{\frac{1}{2}} \left(\lambda \bar{\nabla}_\alpha u^\alpha + (\lambda + 2\mu) \bar{\nabla}_3 u^3 \right) \leq 0 \ .$$

Now, assume that this body is in contact with an elastic foundation, and thus, it permits normal displacements at the contact region, so assume that only the normal derivatives are of any consequence. Thus, one may approximate the above relation as

$$\mu \bar{\nabla}_3 (u_\alpha u^\alpha)^{\frac{1}{2}} + \nu_F (\lambda + 2\mu) \bar{\nabla}_3 u^3 \leq 0 \ .$$

To simplify the matters further assume that the above condition is independent of any elastic properties of the overlying body. This may be achieved by assuming $\lambda = 0$, and thus, one finds

$$\bar{\nabla}_3 \left((u_\alpha u^\alpha)^{\frac{1}{2}} + 2\nu_F u^3 \right) \leq 0 \ .$$

By approximating the above condition even further we arrive at the third hypothesis of our thesis:

Hypothesis 3. *A shell supported by an elastic foundation with a rough contact area that is compliant with assertion 1 satisfies the following displacement-based friction condition*

$$u^3 \leq -\frac{1}{2\nu_F} (u_\alpha u^\alpha)^{\frac{1}{2}} \ ,$$

where ν_F is the coefficient of friction between the shell and the foundation, and $\boldsymbol{u}$ is the displacement field of the shell with respect to the contact region. If $2\nu_F u^3 + (u_\alpha u^\alpha)^{\frac{1}{2}} < 0$, then we say that the shell is bonded to the foundation, and, if $2\nu_F u^3 + (u_\alpha u^\alpha)^{\frac{1}{2}} = 0$, then we say that the shell is at limiting equilibrium.

The justifications for introducing the hypothesis 3 is as follows. Recall equation (42): which asserts that the variational form of a linear elastic body subjected to Coulomb's law of static friction is non-convex and non-differentiable. Thus, the existence of a (unique or otherwise) solution is an open question that cannot be proven with conventional means. But, we show that the variational form, i.e. the energy functional of a linear elastic body subjected to the displacement-based friction condition from hypothesis 3, is convex, coercive and differentiable, and thus, proving the existence of solutions is perfectly possible. Also, unlike Kikuchi and Oden's [102] model, hypothesis 3 is independent of the regularisation parameter, ε, and it is well defined for all finite values of $\boldsymbol{u}$. Furthermore, we show that our problem can be numerically modelled without an initial guess of the purely normal stress, which is something Kikuchi and Oden's [102] model is incapable of. Note that we can guarantee that the condition from hypothesis 3 holds as we already asserted that the lower-surface of the shell is not hyperbolic and it is a surface of positive mean curvature (see assertion 1). Thus, for

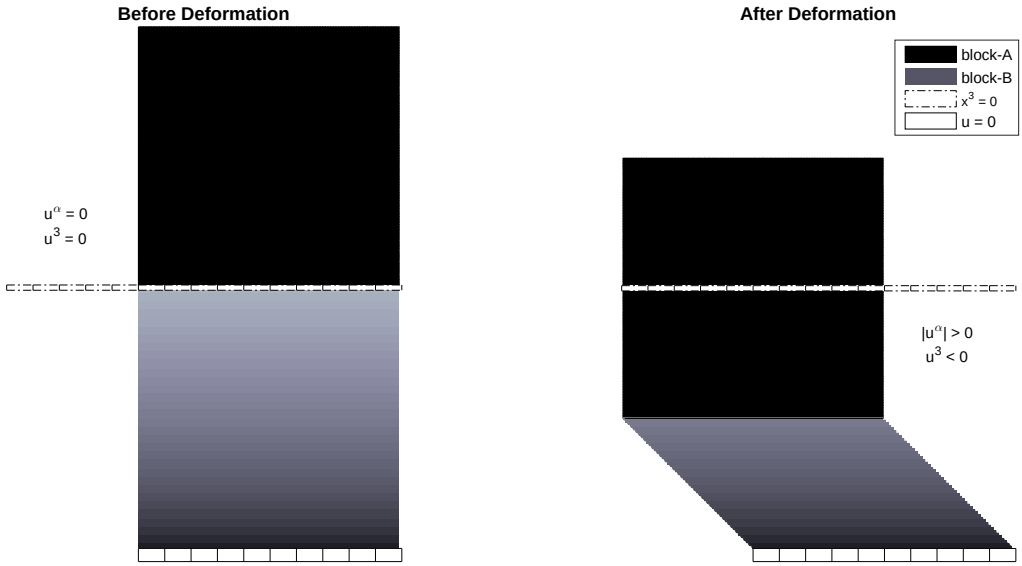

Figure 49: Two-Dimensional schematic representation of block-A and block-B, before and after deformation.

sensible boundary conditions we can always expect the normal displacement to be non-positive.

Why does hypothesis 3 make sense? Well, consider two elastic blocks in a zero-gravity scenario: block-A is at the top and block-B is at the bottom, where the lowest part of the block-B satisfies zero-Dirichlet boundary condition. Now, assume that the contact region, between the both blocks, is rough. Now, assume that one is applying forces to both the top and to a side of the block-A to mimic respectively compression and shear at the contact region. Higher the compression, then higher the normal displacement is towards the bottom, i.e. $u^3 < 0$, and higher the shear, then higher the tangential displacement is in the direction of the applied tangential force (see figure 49). Just as for Coulomb's friction case, where the bodies are in relative equilibrium given that the magnitude of the normal stress is above a certain factor of the magnitude of the tangential stress, i.e. $|T^3_3(\boldsymbol{u})| > \nu_F^{-1}|T^\alpha_3(\boldsymbol{u})T^3_\alpha(\boldsymbol{u})|^{\frac{1}{2}}$, we assert that the bodies are in relative equilibrium given that the normal displacement is a below a certain factor of the magnitude of the tangential displacement, i.e. $u^3 < -\frac{1}{2}\nu_F^{-1}(u_\alpha u^\alpha)^{\frac{1}{2}}$, if $u^3 < 0$. Note that this factor may or may not be $\frac{1}{2}\nu_F^{-1}$, but this is the most mathematically logical factor we derived. With this knowledge we obtain the following theorem:

Theorem 4. *Let $\Omega \subset \mathbb{R}^3$ be a connected open bounded domain that satisfies the segment condition with a uniform-$C^1(\mathbb{R}^3;\mathbb{R}^2)$ boundary $\partial\Omega$ such that $\omega, \partial\Omega_0 \subset \partial\Omega$ with $\bar{\omega} \cap \partial\bar{\Omega}_0 = \emptyset$ and $\mathrm{meas}(\partial\Omega_0;\mathbb{R}^2) > 0$, and let $\omega \subset \mathbb{R}^2$ be a connected open bounded plane that satisfies the segment condition with a uniform-$C^1(\mathbb{R}^2;\mathbb{R})$ boundary $\partial\omega$. Let $\bar{\boldsymbol{X}} \in C^2(\bar{\Omega};\boldsymbol{E}^3)$ be a diffeomorphism and $\boldsymbol{\sigma} \in C^3(\bar{\omega};\boldsymbol{E}^3)$ be an injective immersion. Let $\boldsymbol{f} \in \boldsymbol{L}^2(\Omega)$, $\boldsymbol{f}_0 \in \boldsymbol{L}^2(\omega)$ and $\boldsymbol{\tau}_0 \in \boldsymbol{L}^2(\partial\omega)$. Then there exists a unique field $\boldsymbol{u} \in \boldsymbol{V}_{\mathscr{F}}(\omega,\Omega)$ such that $\boldsymbol{u}$ is the solution to the minimisation problem*

$$J(\boldsymbol{u}) = \min_{\boldsymbol{v}\in\boldsymbol{V}_{\mathscr{F}}(\omega,\Omega)} J(\boldsymbol{v}) \ ,$$

where

$$\boldsymbol{V}_{\mathscr{F}}(\omega,\Omega)=\{\boldsymbol{v}\in\boldsymbol{V}_{\mathscr{S}}(\omega,\Omega)\mid\left[2\nu_F v^3+(v_\alpha v^\alpha)^{\frac{1}{2}}\right]|_\omega\leq 0\text{ a.e.}\}\ ,$$

$$\begin{aligned}J(\boldsymbol{u})=&\int_\Omega\left[\frac{1}{2}A^{ijkl}E_{ij}(\boldsymbol{u})E_{kl}(\boldsymbol{u})-f^iu_i\right]d\Omega\\&+\int_\omega\left[\frac{1}{2}B^{\alpha\beta\gamma\delta}\left(h\epsilon_{\alpha\beta}(\boldsymbol{u})\epsilon_{\gamma\delta}(\boldsymbol{u})+\frac{1}{3}h^3\rho_{\alpha\beta}(\boldsymbol{u})\rho_{\gamma\delta}(\boldsymbol{u})\right)-hf_0^iu_i\right]d\omega-\int_{\partial\omega}h\tau_0^iu_i\ d(\partial\omega)\ ,\end{aligned}$$

and ν_F is the coefficient of friction between the foundation and the shell.

Proof. See Section 4.4. □

What does theorem 4 mean? Well, it means that given some well-posed normal and tangential forcings, and tractions acting on a shell with a thickness h that is frictionally coupled to an elastic foundation has a unique weak solution. This weak solution is sufficient for finding finite-element solutions. However, due to the constraint $[2\nu_F u^3+(u_\alpha u^\alpha)^{\frac{1}{2}}]|_\omega\leq 0$ a.e. the unique minimiser $\boldsymbol{u}$ may fail be a critical point in $(\boldsymbol{V}_{\mathscr{F}}(\omega,\Omega),J(\cdot))$. Thus, to model finite-element solutions competently one requires the following:

Corollary 4. *Let $\boldsymbol{u}\in\boldsymbol{V}_{\mathscr{F}}(\omega,\Omega)$ be the unique solution to the minimisation problem $J(\boldsymbol{u})=\min_{\boldsymbol{v}\in\boldsymbol{V}_{\mathscr{F}}(\omega,\Omega)}J(\boldsymbol{v})$, then we get the following variational inequity*

$$0\leq J'(\boldsymbol{u})(\boldsymbol{v}-\boldsymbol{u})\ ,\ \forall\ \boldsymbol{v}\in\boldsymbol{V}_{\mathscr{F}}(\omega,\Omega)\ .$$

Proof. As $(\boldsymbol{V}_{\mathscr{F}}(\omega,\Omega),J(\cdot))$ is a convex space (see Section 4.4), for any $\boldsymbol{u},\boldsymbol{v}\in\boldsymbol{V}_{\mathscr{F}}(\omega,\Omega)$ we have $(1-t)\boldsymbol{u}+t\boldsymbol{v}\in\boldsymbol{V}_{\mathscr{F}}(\omega,\Omega)$, $\forall\ t\in[0,1]$ (see definition 19). Now, let $\boldsymbol{u}$ be the unique minimiser, then we have relation $J(\boldsymbol{u})\leq J((1-t)\boldsymbol{u}+t\boldsymbol{v})$, $\forall\ t\in[0,1]$. This implies that, as a function of t, $J((1-t)\boldsymbol{u}+t\boldsymbol{v})$ has a global minimum at $t=0$ in the set $[0,1]$. As $J(\cdot)$ is a convex functional in the set $\boldsymbol{V}_{\mathscr{F}}(\omega,\Omega)$, we get $\partial_tJ((1-t)\boldsymbol{u}+t\boldsymbol{v})|_{t=0}\geq 0$, i.e. $0\leq J'(\boldsymbol{u})(\boldsymbol{v}-\boldsymbol{u})$, $\forall\ \boldsymbol{v}\in\boldsymbol{V}_{\mathscr{F}}(\omega,\Omega)$. See section 8.4.2 of Evans [63] for the original proof. □

For a comprehensive study of finite-element modelling of similar problems, please consult chapter 4 of Kikuchi and Oden [102]. Also, one requires higher regularity results to prove the existence of classical solutions. This problem is a subject of discussion in Section 5.3.

4.3 Equations of Equilibrium

For this section we assume that $\boldsymbol{u}\in C^2(\Omega;\mathbb{R}^3)$, $u^\alpha|_\omega\in C^3(\omega)$, $u^3|_\omega\in C^4(\omega)$ and $2\nu_F u^3+(u_\alpha u^\alpha)^{\frac{1}{2}}\leq 0$ everywhere in ω, and we use theorem 4 and corollary 4 to derive a set of governing equations and boundary conditions to our problem.

4.3.1 Governing Equations of the Elastic Foundation

$$\bar{\nabla}_iT^i_j(\boldsymbol{u})+f_j=0\ ,\ \forall\ j\in\{1,2,3\}\ ,$$

where $T^{ij}(\boldsymbol{u})=A^{ijkl}E_{kl}(\boldsymbol{u})$ is second Piola-Kirchhoff stress tensor, $E_{ij}(\boldsymbol{u})=\frac{1}{2}(g_{ik}\bar{\nabla}_ju^k+g_{jk}\bar{\nabla}_iu^k)$ is linearised Green-St Venant stress tensor, $A^{ijkl}=\bar{\lambda}g^{ij}g^{kl}+\bar{\mu}(g^{ik}g^{jl}+g^{il}g^{jk})$ is the isotropic

elasticity tensor, $\bar{\lambda} = (1-\bar{\nu}-2\bar{\nu}^2)^{-1}\bar{\nu}\bar{E}$ is first Lamé's parameter, $\bar{\mu} = \frac{1}{2}(1+\bar{\nu})^{-1}\bar{E}$ is second Lamé's parameter, $\bar{E}$ is Young's modulus and $\bar{\nu}$ is Poisson's ratio of the elastic foundation and $\boldsymbol{f}$ is an external force density field acting on the elastic foundation.

4.3.2 Boundary Conditions of the Elastic Foundation

$$\boldsymbol{u}|_{\partial\Omega_0} = \boldsymbol{0}\ ,$$
$$\bar{n}_i T_j^i(\boldsymbol{u})|_{\{\partial\Omega\setminus\{\omega\cup\partial\Omega_0\}\}} = 0\ ,\ \forall\, j\in\{1,2,3\}\ ,$$

where $\bar{\boldsymbol{n}}$ is the unit outward normal to the boundary $\partial\Omega$ in curvilinear coordinates.

4.3.3 Governing Equations of the Overlying Shell

The set $\boldsymbol{V}_{\mathscr{F}}(\omega,\Omega)$ is not a linear set as it violates the homogeneity property. Thus, to proceed in finding governing equations of the shell consider the fields $\boldsymbol{w},\boldsymbol{v}\in\boldsymbol{V}_{\mathscr{F}}(\omega,\Omega)$. By definition, we have $\int_U[2\nu_F v^3+(v_\alpha v^\alpha)^{\frac{1}{2}}]\,dx^1dx^2\le 0$ and $\int_U[2\nu_F w^3+(w_\alpha w^\alpha)^{\frac{1}{2}}]\,dx^1dx^2\le 0$, $\forall\, U\in\mathcal{M}(\omega)$ with $\mathrm{meas}(U;\omega)>0$, and thus, we get $\int_U[2\nu_F(v^3+sw^3)+(v_\alpha v^\alpha)^{\frac{1}{2}}+|s|(w_\alpha w^\alpha)^{\frac{1}{2}}]\,dx^1dx^2\le 0, \forall\, U\in\mathcal{M}(\omega)$ with $\mathrm{meas}(U;\omega)>0$ and $\forall\, s\in(-\varepsilon,1]$ for a sufficiently small $\varepsilon\ge 0$. Now, the triangle inequity (see Section 4.4, step 1) implies that $\int_U[2\nu_F(v^3+sw^3)+|(v_\alpha+sw_\alpha)(v^\alpha+sw^\alpha)|^{\frac{1}{2}}]\,dx^1dx^2\le 0, \forall\, U\in\mathcal{M}(\omega)$ with $\mathrm{meas}(U;\omega)>0$, and thus, we get $\boldsymbol{v}+s\boldsymbol{w}\in\boldsymbol{V}_{\mathscr{F}}(\omega,\Omega)$, $\forall\, s\in(-\varepsilon,1]$ for a sufficiently small $\varepsilon\ge 0$.

To find the governing equations for the $[2\nu_F u^3+(u_\alpha u^\alpha)^{\frac{1}{2}}]|_\omega<0$ case considerer the unique minimiser $\boldsymbol{u}\in\{\boldsymbol{v}\in\boldsymbol{V}_{\mathscr{F}}(\omega,\Omega)\mid[2\nu_F v^3+(v_\alpha v^\alpha)^{\frac{1}{2}}]|_V<0\ \text{a.e.}\}$ where $V\subseteq\omega$. Now, we get $\boldsymbol{u}+s\boldsymbol{w}\in\boldsymbol{V}_{\mathscr{F}}(\omega,\Omega)$, $\forall\, s\in(-\varepsilon(\boldsymbol{w}),\varepsilon(\boldsymbol{w}))$ where $\varepsilon(\boldsymbol{w})<\min(1,||\boldsymbol{w}||^{-1}_{L^2(\omega)}||\boldsymbol{u}||_{L^2(\omega)})$, $\forall\, \boldsymbol{w}\in\boldsymbol{V}_{\mathscr{F}}(\omega,\Omega)$. Now, simply let $\boldsymbol{v}=\boldsymbol{u}+s\boldsymbol{w}$ in corollary 4 to obtain $0\le J'(\boldsymbol{u})(s\boldsymbol{w})$, $\forall\, s\in(-\varepsilon(\boldsymbol{w}),\varepsilon(\boldsymbol{w}))$, $\forall\, \boldsymbol{w}\in\boldsymbol{V}_{\mathscr{F}}(\omega,\Omega)$. Finally, noticing that $0\le J'(\boldsymbol{u})(\mathrm{sign}(s)|s|\boldsymbol{w})$, $\forall\, \boldsymbol{w}\in\boldsymbol{V}_{\mathscr{F}}(\omega,\Omega)$, we get the following governing equations for the *bonded* case:

If $\left[2\nu_F u^3+(u_\alpha u^\alpha)^{\frac{1}{2}}\right]|_\omega<0$, **then**

$$\nabla_\alpha\tau^\alpha_\beta(\boldsymbol{u})+\frac{2}{3}h^2F^\alpha_{[\mathrm{II}]\beta}\nabla_\gamma\eta^\gamma_\alpha(\boldsymbol{u})+\frac{1}{3}h^2\left(\nabla_\gamma F^\alpha_{[\mathrm{II}]\beta}\right)\eta^\gamma_\alpha(\boldsymbol{u})-\frac{1}{h}\mathrm{Tr}(T^3_\beta(\boldsymbol{u}))+f_{0\beta}=0\ ,\ \forall\,\beta\in\{1,2\}\ ,$$
$$F^\gamma_{[\mathrm{II}]\alpha}\tau^\alpha_\gamma(\boldsymbol{u})-\frac{1}{3}h^2\nabla_\alpha\left(\nabla_\gamma\eta^{\alpha\gamma}(\boldsymbol{u})\right)+\frac{1}{3}h^2F^\delta_{[\mathrm{II}]\alpha}F^\alpha_{[\mathrm{II}]\gamma}\eta^\gamma_\delta(\boldsymbol{u})-\frac{1}{h}\mathrm{Tr}(T^3_3(\boldsymbol{u}))+f_{03}=0\ .$$

To find the governing equations for the $[2\nu_F u^3+(u_\alpha u^\alpha)^{\frac{1}{2}}]|_\omega=0$ case consider the unique minimiser $\boldsymbol{u}\in\{\boldsymbol{v}\in\boldsymbol{V}_{\mathscr{F}}(\omega,\Omega)\mid[2\nu_F v^3+(v_\alpha v^\alpha)^{\frac{1}{2}}]|_V=0\ \text{a.e.}\}$ where $V\subseteq\omega$. Now, we get $\boldsymbol{u}+s\boldsymbol{w}\in\boldsymbol{V}_{\mathscr{F}}(\omega,\Omega)$, $\forall\, \boldsymbol{w}\in\boldsymbol{V}_{\mathscr{F}}(\omega,\Omega)$ and $\forall\, s\in(0,1]$. Now, simply let $\boldsymbol{v}=\boldsymbol{u}+s\boldsymbol{w}$ in corollary 4 to obtain $0\le J'(\boldsymbol{u})(\boldsymbol{w})$, $\forall\, \boldsymbol{w}\in\boldsymbol{V}_{\mathscr{F}}(\omega,\Omega)$. Noticing that $w^j|_\omega$ are not independent, but related by $w^3|_\omega\le-\frac{1}{2}\nu_F^{-1}(w_\alpha w^\alpha)^{\frac{1}{2}}|_\omega$, we get $0\le J'(\boldsymbol{u})(\delta\boldsymbol{w}|_\Omega+(\delta w^1,\delta w^2,-\frac{1}{2}\nu_F^{-1}(u_\alpha u^\alpha)^{-\frac{1}{2}}u_\gamma\delta w^\gamma)|_\omega)$, $\forall\, \boldsymbol{w}\in\boldsymbol{V}_{\mathscr{F}}(\omega,\Omega)$. Further noticing that the above inequality results in $0\le J'(\boldsymbol{u})(\delta\boldsymbol{w}|_\Omega+(\mathrm{sign}(w^1)|\delta w^1|,\mathrm{sign}(w^2)|\delta w^2|,-\frac{1}{2}\nu_F^{-1}(u_\alpha u^\alpha)^{-\frac{1}{2}}(u_1\mathrm{sign}(w^1)|\delta w^1|+u_2\mathrm{sign}(w^2)|\delta w^2|))|_\omega)$, $\forall\, \boldsymbol{w}\in\boldsymbol{V}_{\mathscr{F}}(\omega,\Omega)$, we get the following governing equations for the *limiting equilibrium* case (see section 8.4.2 of Evans [63] for the original proof):

If $\left[2\nu_F u^3 + (u_\alpha u^\alpha)^{\frac{1}{2}}\right]|_\omega = 0$, **then**

$$\begin{aligned}
\nu_F \nabla_\alpha \tau^\alpha_\beta(\bar{\boldsymbol{u}}) &- \frac{1}{2}\frac{u_\beta}{(u_\alpha u^\alpha)^{\frac{1}{2}}} F_{[\mathrm{II}]\alpha}{}^{\gamma} \tau^\alpha_\gamma(\bar{\boldsymbol{u}}) \\
&+ \frac{2}{3}\nu_F h^2 F_{[\mathrm{II}]\beta}{}^{\alpha} \nabla_\gamma \eta^\gamma_\alpha(\bar{\boldsymbol{u}}) + \frac{1}{6} h^2 \frac{u_\beta}{(u_\alpha u^\alpha)^{\frac{1}{2}}} \nabla_\alpha \nabla_\gamma \eta^{\alpha\gamma}(\bar{\boldsymbol{u}}) \\
&+ \frac{1}{3}\nu_F h^2 \left(\nabla_\gamma F_{[\mathrm{II}]\beta}{}^{\alpha}\right) \eta^\gamma_\alpha(\bar{\boldsymbol{u}}) - \frac{1}{6} h^2 \frac{u_\beta}{(u_\alpha u^\alpha)^{\frac{1}{2}}} F_{[\mathrm{II}]\alpha}{}^{\delta} F_{[\mathrm{II}]\gamma}{}^{\alpha} \eta^\gamma_\delta(\bar{\boldsymbol{u}}) \\
&- \frac{\nu_F}{h}\mathrm{Tr}(T^3_\beta(\bar{\boldsymbol{u}})) + \frac{1}{2h}\frac{u_\beta}{(u_\alpha u^\alpha)^{\frac{1}{2}}}\mathrm{Tr}(T^3_3(\bar{\boldsymbol{u}})) \\
&+ \nu_F f_{0\beta} - \frac{1}{2}\frac{u_\beta}{(u_\alpha u^\alpha)^{\frac{1}{2}}} f_{03} = 0 \,, \qquad\qquad \forall\ \beta \in \{1,2\} \,,
\end{aligned}$$

where $\bar{\boldsymbol{u}}|_\omega = (u^1, u^2, -\frac{1}{2}\nu_F^{-1}(u_\alpha u^\alpha)^{\frac{1}{2}})|_\omega$ and $(\partial_3 \bar{u}^1, \partial_3 \bar{u}^2, \partial_3 \bar{u}^3)|_\omega = (\partial_3 u^1, \partial_3 u^2, \partial_3 u^3)|_\omega$.

Note that $\tau^{\alpha\beta}(\boldsymbol{u}) = B^{\alpha\beta\gamma\delta}\epsilon_{\gamma\delta}(\boldsymbol{u})$ is the stress tensor, $\eta^{\alpha\beta}(\boldsymbol{u}) = B^{\alpha\beta\gamma\delta}\rho_{\gamma\delta}(\boldsymbol{u})$ negative of the change in moments density tensor,

$$\epsilon_{\alpha\beta}(\boldsymbol{u}) = \frac{1}{2}\left(\nabla_\alpha(u_\beta|_\omega) + \nabla_\beta(u_\alpha|_\omega)\right) - F_{[\mathrm{II}]\alpha\beta}(u^3|_\omega)$$

is half of the change in first fundamental form tensor,

$$\rho_{\alpha\beta}(\boldsymbol{u}) = \nabla_\alpha\nabla_\beta(u^3|_\omega) - F_{[\mathrm{II}]\alpha\gamma}F_{[\mathrm{II}]\beta}{}^{\gamma}(u^3|_\omega) + F_{[\mathrm{II}]\beta\gamma}\nabla_\alpha(u^\gamma|_\omega) + F_{[\mathrm{II}]\alpha\gamma}\nabla_\beta(u^\gamma|_\omega) + \left(\nabla_\alpha F_{[\mathrm{II}]\beta\gamma}\right)(u^\gamma|_\omega)$$

the change in second fundamental form tensor,

$$B^{\alpha\beta\gamma\delta} = \frac{2\lambda\mu}{\lambda+2\mu}F^{\alpha\beta}_{[\mathrm{I}]}F^{\gamma\delta}_{[\mathrm{I}]} + \mu(F^{\alpha\gamma}_{[\mathrm{I}]}F^{\beta\delta}_{[\mathrm{I}]} + F^{\alpha\delta}_{[\mathrm{I}]}F^{\beta\gamma}_{[\mathrm{I}]})$$

is the isotropic elasticity tensor, $\lambda = (1-\nu-2\nu^2)^{-1}\nu E$ is first Lamé's parameter, $\mu = \frac{1}{2}(1+\nu)^{-1}E$ is second Lamé's parameter, E is Young's modulus and ν is Poisson's ratio of the frictionally coupled shell, $\mathrm{Tr}(T^3_j(\boldsymbol{u})) = T^3_j(\boldsymbol{u})|_\omega$ is the normal stress of the foundation at the contact region, $\boldsymbol{f}_0$ is an external force density field action on the overlying shell.

Due to the condition $[2\nu_F u^3 + (u_\alpha u^\alpha)^{\frac{1}{2}}]|_\omega \leq 0$ a.e., the region in which the shell is attains limiting equilibrium is unknown prior to the problem. In the literature these types of problems are often referred to as *free-boundary* type problems. If the reader is more interested in this subject, then a rich study of such problems can be found in chapter 2 of Kinderlehrer and Stampacchia [107].

4.3.4 Boundary Conditions of the Overlying Shell

$$\begin{aligned}
\left[n_\alpha \tau^\alpha_\beta(\boldsymbol{u}) + \frac{2}{3}h^2 n_\gamma F_{[\mathrm{II}]\beta}{}^{\alpha}\eta^\gamma_\alpha(\boldsymbol{u})\right]|_{\partial\omega} &= \tau_{0\beta} \,,\ \forall\ \beta \in \{1,2\} \,, \\
-\frac{1}{3}h^2 n_\gamma \nabla_\alpha \eta^{\alpha\gamma}(\boldsymbol{u})|_{\partial\omega} &= \tau_{03} \,, \\
\partial_\beta(u^3|_\omega)|_{\partial\omega} &= 0 \,,\ \forall\ \beta \in \{1,2\} \,,
\end{aligned}$$

where $\boldsymbol{n}$ is the unit outward normal vector to the boundary $\partial\omega$ in curvilinear coordinates and $\boldsymbol{\tau}_0$ is an external traction field acting on the boundary of the overlying shell.

4.4 Existence and Uniqueness of Solutions

In this section we prove theorem 4, and thus, finally concluding that the model derived in this chapter it is a mathematical theory. As we already proved the existence and the uniqueness of solutions for an overlying bonded shell on an elastic foundation, in chapter 3, it is now a relatively straight forward task to prove theorem 4. We treat the displacement-based friction condition from hypothesis 3 as a constraint and use the mathematical techniques put forward by Kinderlehrer and Stampacchia [107], and Evans [63] to prove theorem 4.

Step 1: Convex

As $(\boldsymbol{V}_{\mathscr{F}}(\omega,\Omega), J(\cdot)) \subset (\boldsymbol{V}_{\mathscr{S}}(\omega,\Omega), J(\cdot))$ by construction, it is sufficient to show that $2\nu_F u^3 + (u_\alpha u^\alpha)^{\frac{1}{2}} \leq 0$ a.e. in ω is a convex functional. To proceed, let $\boldsymbol{v}_{\mathsf{E}} = \boldsymbol{\sigma}_{,\alpha} v^\alpha$ be a Euclidean vector, i.e. $\boldsymbol{v}_{\mathsf{E}} \in \mathbf{E}^3$, where $\boldsymbol{v} \in \mathbb{R}^2$. Thus, for any two vectors $\boldsymbol{v}, \boldsymbol{w} \in \mathbb{R}^2$ we get

$$\begin{aligned} |(v_\alpha + w_\alpha)(v^\alpha + w^\alpha)|^{\frac{1}{2}} &= ||\boldsymbol{v}_{\mathsf{E}} + \boldsymbol{w}_{\mathsf{E}}|| \\ &\leq ||\boldsymbol{v}_{\mathsf{E}}|| + ||\boldsymbol{w}_{\mathsf{E}}|| \\ &= (v_\alpha v^\alpha)^{\frac{1}{2}} + (w_\alpha w^\alpha)^{\frac{1}{2}} \ , \end{aligned}$$

where the above inequality follows from the triangle inequality. We can guarantee that the above condition will hold due to the positive definiteness of $\boldsymbol{F}_{[\mathrm{I}]}$ in $\bar{\omega}$.

Now, let $I(\boldsymbol{u}; U) = \int_U [2\nu_F u^3 + (u_\alpha u^\alpha)^{\frac{1}{2}}]\, dx^1 dx^2$. By construction $I(\boldsymbol{u}; U) \leq 0$, $\forall\ U \in \mathcal{M}(\omega)$ with $\mathrm{meas}(U;\omega) > 0$. We claim that $I(\cdot; U)$ is a convex functional for all $U \in \mathcal{M}(\omega)$ with $\mathrm{meas}(U;\omega) > 0$. Thus, $\forall\ t \in [0,1]$, $\forall\ \boldsymbol{u}, \boldsymbol{v} \in \boldsymbol{V}_{\mathscr{S}}(\omega,\Omega)$ and with the above triangle inequality we get

$$\begin{aligned} I(t\boldsymbol{u} + (1-t)\boldsymbol{v}; U) &= \int_U \left[2\nu_F(tu^3 + (1-t)v^3) + |(tu_\alpha + (1-t)v_\alpha)(tu^\alpha + (1-t)v^\alpha)|^{\frac{1}{2}}\right] dx^1 dx^2 \\ &\leq \int_U \left[t2\nu_F u^3 + (1-t)2\nu_F v^3 + t(u_\alpha u^\alpha)^{\frac{1}{2}} + (1-t)(v_\alpha v^\alpha)^{\frac{1}{2}}\right] dx^1 dx^2 \\ &= tI(\boldsymbol{u}; U) + (1-t)I(\boldsymbol{v}; U) \ , \end{aligned}$$

$\forall\ U \in \mathcal{M}(\omega)$ with $\mathrm{meas}(U;\omega) > 0$. Furthermore $I(t\boldsymbol{u} + (1-t)\boldsymbol{v}; U) \leq tI(\boldsymbol{u}; U) + (1-t)I(\boldsymbol{v}; U) \leq 0$, $\forall\ U \in \mathcal{M}(\omega)$ with $\mathrm{meas}(U;\omega) > 0$, and thus, our convexity result does not violate the definition of the functional $I(\cdot; U)$, i.e. the condition $2\nu_F u^3 + (u_\alpha u^\alpha)^{\frac{1}{2}} \leq 0$ a.e. in ω is not violated. By definition 19, we see that $I(\cdot; U)$ is a convex functional, and thus, $(\boldsymbol{V}_{\mathscr{F}}(\omega,\Omega), J(\cdot))$ is a convex space.

Step 2: Existence

First, we must to show that, if $\boldsymbol{u}|_\omega \in L^2(\omega)$, then $2\nu_F u^3 + (u_\alpha u^\alpha)^{\frac{1}{2}} \leq 0$ a.e. in ω is bounded below by $-||\boldsymbol{u}||_{\boldsymbol{L}^2(\omega)}$. To do so, consider the field $\boldsymbol{u} \in \boldsymbol{V}_{\mathscr{S}}(\omega,\Omega)$, and thus, the condition $2\nu_F u^3 + (u_\alpha u^\alpha)^{\frac{1}{2}} \leq 0$ a.e. in ω implies that

$$\begin{aligned} 0 \ &\leq \int_U \left[-2\nu_F u^3 - (u_\alpha u^\alpha)^{\frac{1}{2}}\right] dx^1 dx^2 \\ &\leq C_1 \int_\omega \left[-2\nu_F u^3 - (u_\alpha u^\alpha)^{\frac{1}{2}}\right]\, dx^1 dx^2 \\ &\leq C_2 ||2\nu_F u^3 + (u_\alpha u^\alpha)^{\frac{1}{2}}||_{L^2(\omega)} \end{aligned}$$

$$
\begin{aligned}
&\leq 2\nu_F C_2||u^3||_{L^2(\omega)} + C_2||u_\alpha u^\alpha||^{\frac{1}{2}}_{L^1(\omega)} \\
&\leq 2\nu_F C_2||u^3||_{L^2(\omega)} + C_2\left(C_3||u^1||^2_{L^2(\omega)} + C_4||u^1u^2||_{L^1(\omega)} + C_5||u^2||^2_{L^2(\omega)}\right)^{\frac{1}{2}} \\
&\leq 2\nu_F C_2||u^3||_{L^2(\omega)} + C_2\left(C_3||u^1||^2_{L^2(\omega)} + C_4||u^1||_{L^2(\omega)}||u^2||_{L^2(\omega)} + C_5||u^2||^2_{L^2(\omega)}\right)^{\frac{1}{2}} \\
&\leq 2\nu_F C_2||u^3||_{L^2(\omega)} + C_6||u^1||_{L^2(\omega)} + C_7||u^2||_{L^2(\omega)} \\
&\leq C_8\left(||u^3||_{L^2(\omega)} + ||u^1||_{L^2(\omega)} + ||u^2||_{L^2(\omega)}\right) \\
&\leq \sqrt{3}\,C_8\left(||u^1||^2_{L^2(\omega)} + ||u^2||^2_{L^2(\omega)} + ||u^3||^2_{L^2(\omega)}\right)^{\frac{1}{2}},
\end{aligned}
$$

$\forall\, U \in \mathcal{M}(\omega)$ with $\mathrm{meas}(U;\omega) > 0$. This implies that, if $\boldsymbol{u} \in \boldsymbol{V}_{\mathscr{F}}(\omega,\Omega)$, then there exists a positive constant C that depends on ω and $\boldsymbol{\sigma}$ such that $0 \leq \int_U[-2\nu_F u^3 - (u_\alpha u^\alpha)^{\frac{1}{2}}]\; dx^1dx^2 \leq C||\boldsymbol{u}||_{\boldsymbol{L}^2(\omega)}$, $\forall\, U \in \mathcal{M}(\omega)$ with $\mathrm{meas}(U;\omega) > 0$. Note that throughout the derivation of the above result we used Hölder inequality (lemma 6) and Minkowski inequality (lemma 7).

Now, we must show that for any sequence $\{\boldsymbol{u}_m|_\omega\}_{m\in\mathbb{N}} \subset \boldsymbol{L}^2(\omega)$ that converges to $\boldsymbol{u}$ in $\boldsymbol{L}^2(\omega)$, if $2\nu_F u^3_m + (u_{m\alpha}u^\alpha_m)^{\frac{1}{2}} \leq 0$ a.e. in ω, then we can expect the limit to satisfy the relation $2\nu_F u^3 + (u_\alpha u^\alpha)^{\frac{1}{2}} \leq 0$ a.e. in ω. To do so, consider a minimising sequence $\{\boldsymbol{u}_m\}_{m\in\mathbb{N}} \subset \boldsymbol{V}_{\mathscr{F}}(\omega,\Omega)$. This sequence converges weakly to $\boldsymbol{u}$ in the space $\boldsymbol{W}(\omega,\Omega)$, in particular, $\boldsymbol{u} \in \boldsymbol{V}_{\mathscr{S}}(\omega,\Omega)$ by theorem 3. By Rellich-Kondrachov theorem (lemma 13), there exists a subsequence $\{\boldsymbol{u}_{m_n}\}_{m_n\in\mathbb{N}}$ that converges strongly in $\{\boldsymbol{v} \in \boldsymbol{L}^2(\Omega) \mid \boldsymbol{v}|_\omega \in \boldsymbol{L}^2(\omega)\}$, in particular, $\boldsymbol{u}_{m_n}|_\omega \to \boldsymbol{u}|_\omega$ in $\boldsymbol{L}^2(\omega)$. Thus, for any minimising sequence $\{\boldsymbol{u}_m\}_{m\in\mathbb{N}} \subset \boldsymbol{V}_{\mathscr{F}}(\omega,\Omega)$, the limit satisfies the relation $2\nu_F u^3 + (u_\alpha u^\alpha)^{\frac{1}{2}} \leq 0$ a.e. in ω as $0 \leq \int_U[-2\nu_F u^3 - (u_\alpha u^\alpha)^{\frac{1}{2}}]\; dx^1dx^2 \leq C||\boldsymbol{u}||_{\boldsymbol{L}^2(\omega)}$, $\forall\, U \in \mathcal{M}(\omega)$ with $\mathrm{meas}(U;\omega) > 0$, and this implies that $\boldsymbol{u} \in \boldsymbol{V}_{\mathscr{F}}(\omega,\Omega)$. Thus, we confirm that there exists a field $\boldsymbol{u} \in \boldsymbol{V}_{\mathscr{F}}(\omega,\Omega)$ such that $\boldsymbol{u}$ is the solution to the minimisation problem $J(\boldsymbol{u}) = \min_{\boldsymbol{v}\in\boldsymbol{V}_{\mathscr{F}}(\omega,\Omega)} J(\boldsymbol{v})$.

Step 3: Uniqueness

We prove the uniqueness of the minimiser by a contradiction. Let the fields $\boldsymbol{u}, \tilde{\boldsymbol{u}} \in \boldsymbol{V}_{\mathscr{F}}(\omega,\Omega)$ be two distinct minimisers, i.e. $\boldsymbol{u} \neq \tilde{\boldsymbol{u}}$. Let $\boldsymbol{w} = \frac{1}{2}(\boldsymbol{u} + \tilde{\boldsymbol{u}})$. As $(\boldsymbol{V}_{\mathscr{F}}(\omega,\Omega), J(\cdot))$ is a convex space, we have $\boldsymbol{w} \in \boldsymbol{V}_{\mathscr{F}}(\omega,\Omega)$. Thus,

$$
\begin{aligned}
J(\boldsymbol{w}) &= \int_\Omega \left[\frac{1}{2}A^{ijkl}E_{ij}(\boldsymbol{w})E_{kl}(\boldsymbol{w}) - f^i w_i\right] d\Omega \\
&\quad + \int_\omega \left[\frac{1}{2}B^{\alpha\beta\gamma\delta}\left(h\epsilon_{\alpha\beta}(\boldsymbol{w})\epsilon_{\gamma\delta}(\boldsymbol{w}) + \frac{1}{3}h^3\rho_{\alpha\beta}(\boldsymbol{w})\rho_{\gamma\delta}(\boldsymbol{w})\right) - hf^i_0 w_i\right] d\omega - \int_{\partial\omega} h\tau^i_0 w_i\; d(\partial\omega) \\
&= \frac{1}{4}\int_\Omega \left[\frac{1}{2}A^{ijkl}E_{ij}(\boldsymbol{u})E_{kl}(\boldsymbol{u}) - f^i u_i\right] d\Omega \\
&\quad + \frac{1}{4}\int_\omega \left[\frac{1}{2}B^{\alpha\beta\gamma\delta}\left(h\epsilon_{\alpha\beta}(\boldsymbol{u})\epsilon_{\gamma\delta}(\boldsymbol{u}) + \frac{1}{3}h^3\rho_{\alpha\beta}(\boldsymbol{u})\rho_{\gamma\delta}(\boldsymbol{u})\right) - hf^i_0 u_i\right] d\omega - \frac{1}{4}\int_{\partial\omega} h\tau^i_0 u_i\; d(\partial\omega) \\
&\quad + \frac{1}{4}\int_\Omega \left[\frac{1}{2}A^{ijkl}E_{ij}(\tilde{\boldsymbol{u}})E_{kl}(\tilde{\boldsymbol{u}}) - f^i \tilde{u}_i\right] d\Omega \\
&\quad + \frac{1}{4}\int_\omega \left[\frac{1}{2}B^{\alpha\beta\gamma\delta}\left(h\epsilon_{\alpha\beta}(\tilde{\boldsymbol{u}})\epsilon_{\gamma\delta}(\tilde{\boldsymbol{u}}) + \frac{1}{3}h^3\rho_{\alpha\beta}(\tilde{\boldsymbol{u}})\rho_{\gamma\delta}(\tilde{\boldsymbol{u}})\right) - hf^i_0 \tilde{u}_i\right] d\omega - \frac{1}{4}\int_{\partial\omega} h\tau^i_0 \tilde{u}_i\; d(\partial\omega) \\
&\quad + \frac{1}{2}\int_\Omega \frac{1}{2}A^{ijkl}E_{ij}(\tilde{\boldsymbol{u}})E_{kl}(\boldsymbol{u})\; d\Omega \\
&\quad + \frac{1}{2}\int_\omega \frac{1}{2}B^{\alpha\beta\gamma\delta}\left(h\epsilon_{\alpha\beta}(\tilde{\boldsymbol{u}})\epsilon_{\gamma\delta}(\boldsymbol{u}) + \frac{1}{3}h^3\rho_{\alpha\beta}(\tilde{\boldsymbol{u}})\rho_{\gamma\delta}(\boldsymbol{u})\right) d\omega
\end{aligned}
$$

$$
\begin{aligned}
&= \frac{1}{2}J(\boldsymbol{u}) + \frac{1}{2}J(\tilde{\boldsymbol{u}}) \\
&\quad - \frac{1}{4}\int_\Omega \frac{1}{2}A^{ijkl}E_{ij}(\boldsymbol{u}-\tilde{\boldsymbol{u}})E_{kl}(\boldsymbol{u}-\tilde{\boldsymbol{u}})\, d\Omega \\
&\quad - \frac{1}{4}\int_\omega \frac{1}{2}B^{\alpha\beta\gamma\delta}\left(h\epsilon_{\alpha\beta}(\boldsymbol{u}-\tilde{\boldsymbol{u}})\epsilon_{\gamma\delta}(\boldsymbol{u}-\tilde{\boldsymbol{u}}) + \frac{1}{3}h^3\rho_{\alpha\beta}(\boldsymbol{u}-\tilde{\boldsymbol{u}})\rho_{\gamma\delta}(\boldsymbol{u}-\tilde{\boldsymbol{u}})\right) d\omega \\
&\leq \frac{1}{2}J(\boldsymbol{u}) + \frac{1}{2}J(\tilde{\boldsymbol{u}}) \\
&\quad - C_1\int_\Omega E_{ij}(\boldsymbol{u}-\tilde{\boldsymbol{u}})E_{ij}(\boldsymbol{u}-\tilde{\boldsymbol{u}})\, d\Omega \\
&\quad - C_2\int_\omega \left(h\epsilon_{\alpha\beta}(\boldsymbol{u}-\tilde{\boldsymbol{u}})\epsilon_{\alpha\beta}(\boldsymbol{u}-\tilde{\boldsymbol{u}}) + \frac{1}{3}h^3\rho_{\alpha\beta}(\boldsymbol{u}-\tilde{\boldsymbol{u}})\rho_{\alpha\beta}(\boldsymbol{u}-\tilde{\boldsymbol{u}})\right) d\omega \\
&< \frac{1}{2}J(\boldsymbol{u}) + \frac{1}{2}J(\tilde{\boldsymbol{u}})\ .
\end{aligned}
$$

This implies that for the given two distinct minimises $\boldsymbol{u}$ and $\tilde{\boldsymbol{u}}$, there exists a field $\boldsymbol{w}$ such that $J(\boldsymbol{w}) < \frac{1}{2}J(\boldsymbol{u}) + \frac{1}{2}J(\tilde{\boldsymbol{u}})$. However, by the very definition of a minimiser, we must have $J(\boldsymbol{u}), J(\tilde{\boldsymbol{u}}) \leq J(\boldsymbol{w})$, and this implies that $\frac{1}{2}J(\boldsymbol{u}) + \frac{1}{2}J(\tilde{\boldsymbol{u}}) \leq J(\boldsymbol{w})$. This is a contradiction, i.e. the assertion of the existence of multiple distinct minimisers is false. Note that the constant C_1 follows from the positive definiteness of the elasticity tensor (lemma 5) and the constant C_2 follows from the positive definiteness of the elasticity tensor on a general surface (lemma 6).

Thus, we conclude this proof by confirming that there exists a unique field $\boldsymbol{u} \in \boldsymbol{V}_{\mathscr{F}}(\omega, \Omega)$ such that $\boldsymbol{u}$ is the solution to the minimisation problem $J(\boldsymbol{u}) = \min_{\boldsymbol{v}\in\boldsymbol{V}_{\mathscr{F}}(\omega,\Omega)} J(\boldsymbol{v})$.

Please consult section 2.6 of Kinderlehrer and Stampacchia [107] or section of 8.4.2 Evans [63] to see similar proofs for elliptic problems with obstacles.

4.5 Numerical Example

To conduct numerical experiments we remain with the framework that we introduced in Chapter 3 (see Section 3.5). Now, assume that the sufficiently smooth field $\boldsymbol{u}$ is a unique minimiser to the problem that we introduced in theorem 4. Thus, we may express the governing equations of the shell as:

If $[2\nu_F u^3 + \psi_2|u^2|]|_{\omega^{\text{New}}} < 0$, then

$$
\begin{aligned}
h\Lambda\partial_2\epsilon_2^2(\boldsymbol{u}) + \frac{1}{3}h^3\Lambda(2F_{[\text{II}]^2}^2\partial_2\rho_2^2(\boldsymbol{u}) + \partial_2 F_{[\text{II}]^2}^2\rho_2^2(\boldsymbol{u})) - \text{Tr}(T_2^3(\boldsymbol{u})) = 0\ , \\
-h\Lambda F_{[\text{II}]^2}^2\epsilon_2^2(\boldsymbol{u}) + \frac{1}{3}h^3\Lambda(\Delta\rho_2^2(\boldsymbol{u}) - F_{[\text{II}]^2}^2 F_{[\text{II}]^2}^2\rho_2^2(\boldsymbol{u})) + \text{Tr}(T_3^3(\boldsymbol{u})) = 0\ ;
\end{aligned}
$$

If $[2\nu_F u^3 + \psi_2|u^2|]|_{\omega^{\text{New}}} = 0$, then

$$
\begin{aligned}
\nu_F h\Lambda\partial_2\epsilon_2^2(\bar{\boldsymbol{u}}) &- \frac{1}{2}h\Lambda\psi_2\text{sign}(u^2)F_{[\text{II}]^2}^2\epsilon_2^2(\bar{\boldsymbol{u}}) \\
&+ \frac{1}{3}\nu_F h^3\Lambda(2F_{[\text{II}]^2}^2\partial_2\rho_2^2(\bar{\boldsymbol{u}}) + \partial_2 F_{[\text{II}]^2}^2\rho_2^2(\bar{\boldsymbol{u}})) \\
&+ \frac{1}{6}h^3\Lambda\psi_2\text{sign}(u^2)(\Delta\rho_2^2(\bar{\boldsymbol{u}}) - F_{[\text{II}]^2}^2 F_{[\text{II}]^2}^2\rho_2^2(\bar{\boldsymbol{u}})) \\
&- \nu_F\text{Tr}(T_2^3(\bar{\boldsymbol{u}})) + \frac{1}{2}\psi_2\text{sign}(u^2)\text{Tr}(T_3^3(\bar{\boldsymbol{u}})) = 0\ ,
\end{aligned}
$$

where $\bar{\boldsymbol{u}}|_{\omega^{\text{New}}} = (0, u^2, -\frac{1}{2}\nu_F^{-1}\psi_2|u^2|)|_{\omega^{\text{New}}}$ and $(0, \partial_3\bar{u}^2, \partial_3\bar{u}^3)|_{\omega^{\text{New}}} = (0, \partial_3 u^2, \partial_3 u^3)|_{\omega^{\text{New}}}$. Note that

$$\begin{aligned}
\mathrm{Tr}(T_2^3(\boldsymbol{u})) &= \bar{\mu}\left((\bar{\psi}_2)^2\partial_3 u^2 + \partial_2 u^3\right)|_{\omega^{\text{New}}}\,, \\
\mathrm{Tr}(T_3^3(\boldsymbol{u})) &= \left[\bar{\lambda}\left(\partial_2 u^2 + \bar{\Gamma}_{22}^2 u^2 + \bar{\Gamma}_{23}^2 u^3\right) + (\bar{\lambda}+2\bar{\mu})\partial_3 u^3\right]|_{\omega^{\text{New}}}\,.
\end{aligned}$$

To conduct numerical experiment we use the second-order-accurate finite-difference method. Also, we keep the values $\tau_0 = 1$, $a = 2$, $H = 1$, $\bar{E} = 10^3$ and $\bar{\nu} = \frac{1}{4}$ fixed for all experiments.

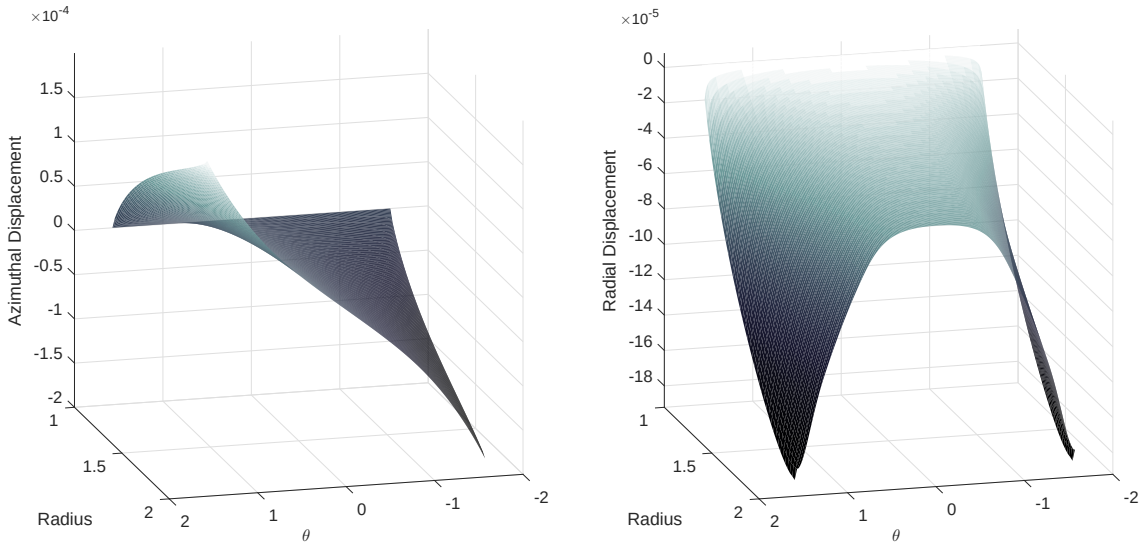

Figure 50: Displacement field of the foundation predicted by the shell model with friction.

Figure 50 is calculated with the values of $\tau_{\text{max}} = 1$, $b = 2$, $h = \frac{1}{8}$, $E = 8000$, $\nu = \frac{1}{4}$, $\nu_F = 1$ and with a grid of 250×41 points. Figure 50 shows the azimuthal (i.e u^2) and the radial (i.e. u^3) displacements. The maximum azimuthal displacements are observed at $x^2 = \pm\frac{1}{2}\pi$, with respective azimuthal displacements of $u^2 = \pm 1.79 \times 10^{-4}$. The maximum radial displacement is observed at $x^2 = \pm\frac{1}{2}\pi$, with a radial displacement of $u^3 = -1.84 \times 10^{-4}$. Furthermore, in the intervals $x^2 \in (-1.26, -0.788)$ and $x^2 \in (0.788, 1.26)$ we see that the shell is at limiting equilibrium.

To confirm our numerical scheme we must perform a grid dependence analysis for the numerical solution. As the reader can see from figure 51, as N increases, the difference between the numerical solution N and $N+1$ decreases. For our experiments we found that the azimuthal grid points and the error share the relation $N \propto \text{Error}^{-0.969}$, where $\text{Error} = |1 - ||\boldsymbol{u}_{N-1}||_{\ell^2}^{-1}||\boldsymbol{u}_N||_{\ell^2}|$. Note that figure 51 is calculated with the values of $\tau_{\text{max}} = 1$, $b = 2$, $h = \frac{1}{8}$, $E = 8000$, $\nu = \frac{1}{4}$ and $\nu_F = 1$.

We dedicate the next section for the numerical comparison against another, but a similar model, extended Kikuchi and Oden's model for Coulomb's law of static friction. However, unlike in chapter 3, there exists no definitive friction model that we can compare our model against. Thus, instead, we compare how similar our friction model is to extended Kikuchi and Oden's model.

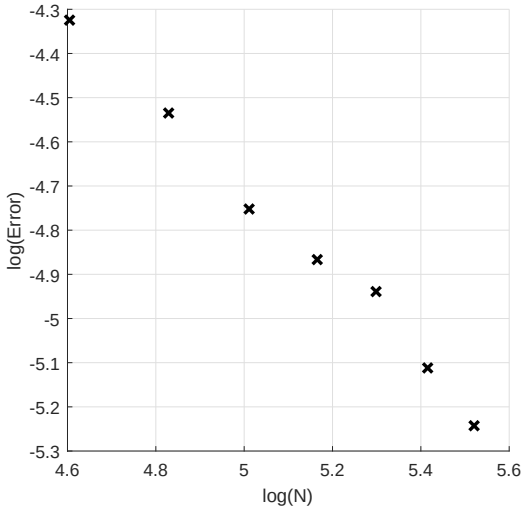

Figure 51: Grid dependence of the shell model with friction.

4.6 Comparison against the works of Kikuchi and Oden

To extend Kikuchi and Oden [102] model, to model two-body contact problem with friction, one must modify equation (43) (see section 5.5 (v) of Kikuchi and Oden [102]). Now, assume an elastic body on a rough rigid surface where the fiction is governed by Coulomb's law of static friction. Given that one is using curvilinear coordinates, fix the purely normal stress at the contact boundary as a constant, i.e. $\nu_F T_3^3(\boldsymbol{v})|_\omega = \mathscr{K}$, where $\mathscr{K}$ is the spring modulus. Then, equation (43) and the analysis that is conducted in section 2.6 imply that $j'_\varepsilon(\boldsymbol{v})\delta\boldsymbol{v} = -\int_\omega (g_{33})^{\frac{1}{2}} T_\alpha^3(\boldsymbol{v})\delta v^\alpha \, d\omega$, where $\boldsymbol{v}$ is the displacement field of the elastic body. Note that $\boldsymbol{v}|_\omega$ describes the relative displacement between the elastic body and the boundary ω, and thus, if the elastic body is in contact with another rough elastic body, then the displacement field one must consider is the relative displacement, due to the fact that friction apposes relative potential motion. Now, consider a two-body contact problem where the contact area is rough and the friction is governed by Coulomb's law of static friction. Now, let the displacement fields of the overlying body be $\boldsymbol{v}$ and the foundation be $\boldsymbol{u}$. As normal stress is continuous at the boundary, just as before, fix the purely normal stress as $\nu_F T_3^3(\boldsymbol{u})|_\omega = \nu_F T_3^3(\boldsymbol{v})|_\omega = \mathscr{K}$ and make the transformation $v^\beta \to v^\beta - u^\beta$ in the functional $j_\varepsilon(\cdot)$ to signify the relative displacement field. Now, collecting all the tangential terms from the contact boundary (i.e. $u^\beta|_\omega$ and $v^\beta|_\omega$ terms) one finds $j'_\varepsilon(\boldsymbol{v}-\boldsymbol{u})(\delta\boldsymbol{v}-\delta\boldsymbol{u}) = -\int_\omega (g_{33})^{\frac{1}{2}} (T_\alpha^3(\boldsymbol{v})\delta v^\alpha|_{\omega^-} - T_\alpha^3(\boldsymbol{u})\delta u^\alpha|_{\omega^+}) \, d\omega$, where

$$j_\varepsilon(\boldsymbol{v}-\boldsymbol{u}) = \begin{cases} \displaystyle\int_\omega (\mathscr{K}\Phi(\boldsymbol{v}-\boldsymbol{u}) - \frac{1}{2}\varepsilon) \, d\omega \ , \text{ if } \Phi(\boldsymbol{v}-\boldsymbol{u})|_\omega \geq \varepsilon \ , \\ \displaystyle\int_\omega \frac{1}{2}\mathscr{K}\varepsilon^{-1}\Phi(\boldsymbol{v}-\boldsymbol{u})^2 \, d\omega \ , \text{ if } \Phi(\boldsymbol{v}-\boldsymbol{u})|_\omega < \varepsilon \ , \end{cases}$$

and where $\Phi(\boldsymbol{v}-\boldsymbol{u}) = |(v_\alpha - u_\alpha)(v^\alpha - u^\alpha)|^{\frac{1}{2}}$, $\omega^+ = \lim_{x^3\to 0^+}\{\omega \times [0,h)\}$, $\omega^- = \lim_{x^3\to 0^-}\Omega$ and $\varepsilon > 0$ is the regularisation parameter.

In accordance with our previous work we keep $\boldsymbol{v}$ as the displacement field of the overlying body and $\boldsymbol{u}$ as the displacement field of the foundation. As the two bodies are in contact, the normal displacement, of the both bodies, is identical. Thus, one obtain the extended Kikuchi and Oden's

model for Coulomb's law of static friction for a two-body problem in curvilinear coordinates, which is described by the equations

$$v^3|_{\omega^+} - u^3|_{\omega^-} = 0 \ ,$$
$$T_3^3(\boldsymbol{v})|_{\omega^+} - T_3^3(\boldsymbol{u})|_{\omega^-} = 0 \ ,$$

$$T_3^\beta(\boldsymbol{v})|_{\omega^+} = \begin{cases} -\dfrac{\nu_F (g_{33})^{\frac{1}{2}}(v^\beta - u^\beta)}{\Phi(\boldsymbol{v}-\boldsymbol{u})} T_3^3(\boldsymbol{v})|_{\omega^+} \ , \text{ if } \Phi(\boldsymbol{v}-\boldsymbol{u})|_{\omega^+} \geq \varepsilon \ , \\ -\dfrac{\nu_F (g_{33})^{\frac{1}{2}}(v^\beta - u^\beta)}{\varepsilon} T_3^3(\boldsymbol{v})|_{\omega^+} \ , \text{ if } \Phi(\boldsymbol{v}-\boldsymbol{u})|_{\omega^+} < \varepsilon \ , \end{cases}$$

$$T_3^\beta(\boldsymbol{u})|_{\omega^-} = \begin{cases} -\dfrac{\nu_F (g_{33})^{\frac{1}{2}}(v^\beta - u^\beta)}{\Phi(\boldsymbol{v}-\boldsymbol{u})} T_3^3(\boldsymbol{u})|_{\omega^-} \ , \text{ if } \Phi(\boldsymbol{v}-\boldsymbol{u})|_{\omega^-} \geq \varepsilon \ , \\ -\dfrac{\nu_F (g_{33})^{\frac{1}{2}}(v^\beta - u^\beta)}{\varepsilon} T_3^3(\boldsymbol{u})|_{\omega^-} \ , \text{ if } \Phi(\boldsymbol{v}-\boldsymbol{u})|_{\omega^-} < \varepsilon \ , \end{cases}$$

where

$$T_3^\beta(\boldsymbol{v}) = \mu \left(\bar{\nabla}^\beta v_3 + \bar{\nabla}_3 v^\beta \right) \ ,$$
$$T_3^3(\boldsymbol{v}) = \lambda \bar{\nabla}_\alpha v^\alpha + (\lambda + 2\mu) \bar{\nabla}_3 v^3 \ ,$$
$$T_3^\beta(\boldsymbol{u}) = \bar{\mu} \left(\bar{\nabla}^\beta u_3 + \bar{\nabla}_3 u^\beta \right) \ ,$$
$$T_3^3(\boldsymbol{u}) = \bar{\lambda} \bar{\nabla}_\alpha u^\alpha + \left(\bar{\lambda} + 2\bar{\mu} \right) \bar{\nabla}_3 u^3 \ ,$$

and where λ and μ are respectively first and second Lame' parameters of the overlying body, $\bar{\lambda}$ and $\bar{\mu}$ are respectively first and second Lame' parameters of the foundation, and ν_F is the coefficient of friction. Note that in this framework one has $g_{33} = 1$. Also, given that $T_3^3(\boldsymbol{u})|_{\omega^-}$ is fixed as a positive constant and one is considering Euclidean coordinates, one can see that the above problem simply reduces to Kikuchi and Oden's [102] model for Coulomb's law of static friction in the limit $\boldsymbol{u} \to 0$.

Despite the fact that we are working in linear elasticity, the above equations make our problem inherently nonlinear. Thus, to find numerical solutions we employ the Newton's method for nonlinear systems (see chapter 10 of Burden *et al.* [30]).

To conduct numerical experiments consider the following. In accordance with the framework that is introduced in section 3.5, the overlying body is restricted to the region $x^3 \in (0, h)$. Thus, with some calculations, one finds that the perturbed governing equations of the overlying body are

$$(\lambda + \mu) \partial^2 \left(\bar{\nabla}_i \delta v^i \right) + \mu \bar{\Delta} \delta v^2 = 0 \ ,$$
$$(\lambda + \mu) \partial^3 \left(\bar{\nabla}_i \delta v^i \right) + \mu \bar{\Delta} \delta v^3 = 0 \ ,$$

where

$$\bar{\nabla}_2 \delta v^2 = \partial_2 \delta v^2 + \bar{\Gamma}_{22}^2 \delta v^2 + \bar{\Gamma}_{23}^2 \delta v^3 \ ,$$
$$\bar{\nabla}_2 \delta v^3 = \partial_2 \delta v^3 - (\bar{\psi}_2)^2 \bar{\Gamma}_{23}^2 \delta v^2 \ ,$$
$$\bar{\nabla}_3 \delta v^2 = \partial_3 \delta v^2 + \bar{\Gamma}_{23}^2 \delta v^2 \ ,$$
$$\bar{\nabla}_3 \delta v^3 = \partial_3 \delta v^3 \ ,$$

and $\delta\boldsymbol{v} = (0, \delta v^2(x^2, x^3), \delta v^3(x^2, x^3))$ is a small perturbation of the displacement field of the overlying body. With relative ease, one finds that the perturbed governing equations of the foundation are

$$(\bar{\lambda} + \bar{\mu})\partial^2 \left(\bar{\nabla}_i \delta u^i\right) + \bar{\mu}\bar{\Delta}\delta u^2 = 0 \,,$$
$$(\bar{\lambda} + \bar{\mu})\partial^3 \left(\bar{\nabla}_i \delta u^i\right) + \bar{\mu}\bar{\Delta}\delta u^3 = 0 \,,$$

where $\delta\boldsymbol{u} = (0, \delta u^2(x^2, x^3), \delta u^3(x^2, x^3))$ is the perturbation of the displacement field of the foundation. With some more calculations, one finds the following boundary conditions to the displacement fields,

$$\left[v^3 - u^3\right]|_{\omega^{\text{New}}} = 0 \text{ (continuous radial displacement)} \,,$$
$$\left[T_3^3(\boldsymbol{v}) - T_3^3(\boldsymbol{u})\right]|_{\omega^{\text{New}}} = 0 \text{ (continuous radial stress)} \,,$$

and the boundary conditions for the perturbations

$$\delta u^2|_{\partial\Omega_0^{\text{New}} \cup \overline{\partial\Omega}_f^{\text{New}}} = 0 \,,$$
$$\delta u^3|_{\overline{\partial\Omega}^{\text{New}}} = 0 \,,$$
$$\delta v^2|_{\{\partial\omega^{\text{New}} \times (0,h)\} \cup \{[-\frac{1}{2}\pi, \frac{1}{2}\pi] \times \{h\}\}} = 0 \,,$$
$$\delta v^3|_{\bar{\omega}^{\text{New}} \cup \{\partial\omega^{\text{New}} \times (0,h)\} \cup \{[-\frac{1}{2}\pi, \frac{1}{2}\pi] \times \{h\}\}} = 0 \,.$$

Thus, the equations characterising the frictionally coupling of the overlying body to the foundation can be expressed as:

If $\bar{\psi}_2|v^2 - u^2||_{\omega^{\text{New}}} \geq \epsilon$, then

$$\left[\mu\left(\bar{\psi}_2\partial_3 v^2 + (\bar{\psi}_2)^{-1}\partial_2 v^3\right) + \nu_F \text{sign}(v^2 - u^2)T_3^3(\boldsymbol{v})\right]|_{\omega^{\text{New}}} = 0 \,,$$
$$\left[\bar{\mu}\left(\bar{\psi}_2\partial_3 u^2 + (\bar{\psi}_2)^{-1}\partial_2 u^3\right) + \nu_F \text{sign}(v^2 - u^2)T_3^3(\boldsymbol{u})\right]|_{\omega^{\text{New}}} = 0 \,;$$

If $\bar{\psi}_2|v^2 - u^2||_{\omega^{\text{New}}} < \epsilon$, then

$$\begin{aligned}
&\left[\mu\left(\bar{\psi}_2\partial_3\delta v^2\right) + \nu_F\epsilon^{-1}\bar{\psi}_2(v^2 - u^2)T_3^3(\delta\boldsymbol{v}) + \nu_F\epsilon^{-1}\bar{\psi}_2(\delta v^2 - \delta u^2)T_3^3(\boldsymbol{v})\right. \\
&\qquad \left. + \mu\left(\bar{\psi}_2\partial_3 v^2 + (\bar{\psi}_2)^{-1}\partial_2 v^3\right) + \nu_F\epsilon^{-1}\bar{\psi}_2(v^2 - u^2)T_3^3(\boldsymbol{v})\right]|_{\omega^{\text{New}}} = 0 \,, \\
&\left[\bar{\mu}\left(\bar{\psi}_2\partial_3\delta u^2\right) + \nu_F\epsilon^{-1}\bar{\psi}_2(v^2 - u^2)T_3^3(\delta\boldsymbol{u}) + \nu_F\epsilon^{-1}\bar{\psi}_2(\delta v^2 - \delta u^2)T_3^3(\boldsymbol{u})\right. \\
&\qquad \left. + \bar{\mu}\left(\bar{\psi}_2\partial_3 u^2 + (\bar{\psi}_2)^{-1}\partial_2 u^3\right) + \nu_F\epsilon^{-1}\bar{\psi}_2(v^2 - u^2)T_3^3(\boldsymbol{u})\right]|_{\omega^{\text{New}}} = 0 \,,
\end{aligned}$$

where

$$T_3^3(\boldsymbol{v}) = \lambda\left(\partial_2 v^2 + \bar{\Gamma}_{22}^2 v^2 + \bar{\Gamma}_{23}^2 v^3\right) + (\lambda + 2\mu)\partial_3 v^3 \,,$$
$$T_3^3(\boldsymbol{u}) = \bar{\lambda}\left(\partial_2 u^2 + \bar{\Gamma}_{22}^2 u^2 + \bar{\Gamma}_{23}^2 u^3\right) + (\bar{\lambda} + 2\bar{\mu})\partial_3 u^3 \,.$$

To conduct numerical experiments we use the second-order-accurate finite-difference method in conjunction with Newton's method for nonlinear systems, as in section 2.6. Also, we keep the values $\tau_0 = 1$, $a = 2$, $H = 1$, $\bar{E} = 10^3$ and $\bar{\nu} = \frac{1}{4}$ fixed for all experiments. Furthermore, we choose to terminate our iterating process once the condition $|1 - (||\boldsymbol{u}_m||_{\ell^2} + ||\boldsymbol{v}_m||_{\ell^2} + ||\delta\boldsymbol{u}_m||_{\ell^2} + ||\delta\boldsymbol{v}_m||_{\ell^2})^{-1}(||\boldsymbol{u}_{m+1}||_{\ell^2} + ||\boldsymbol{v}_{m+1}||_{\ell^2} + ||\delta\boldsymbol{u}_{m+1}||_{\ell^2} + ||\delta\boldsymbol{v}_{m+1}||_{\ell^2})| < 10^{-10}$ is satisfied, where $\boldsymbol{u}_m$, $\boldsymbol{v}_m$,

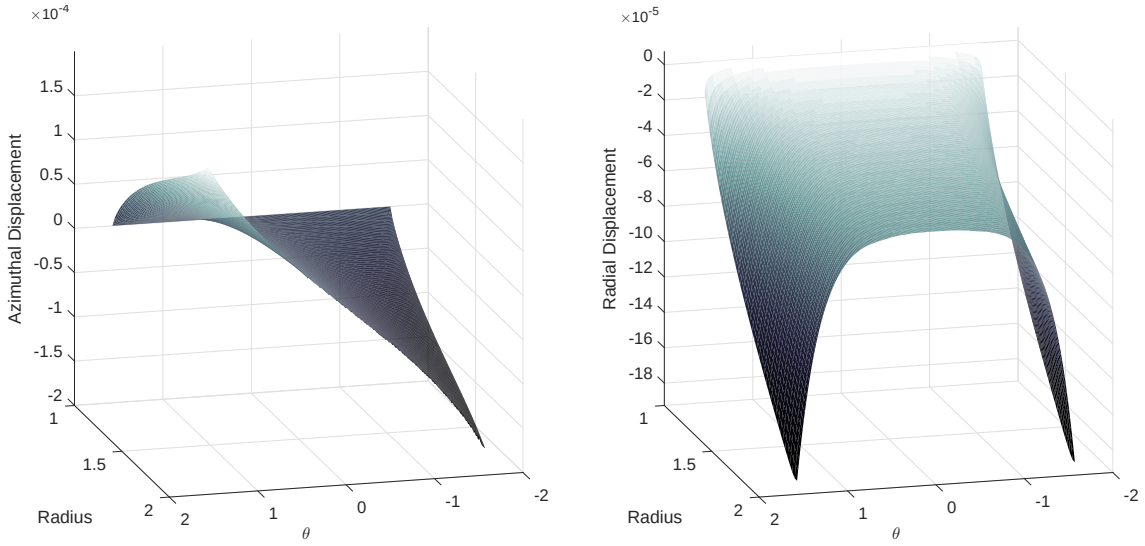

Figure 52: Displacement field of the foundation of the extended Kikuchi and Oden's model.

$\delta \boldsymbol{u}_m$ and $\delta \boldsymbol{v}_m$ are the m^{th} iterative solutions of extended Kikuchi and Oden's model model.

Figure 52 is calculated with the values of $\tau_{\text{max}} = 1$, $b = 2$, $h = \frac{1}{8}$, $E = 8000$, $\nu = \frac{1}{4}$, $\varepsilon = 10^{-10}$, $\nu_F = 1$ and with a grid of 250×41 points. Figure 50 shows the azimuthal (i.e. u^2) and the radial (i.e. u^3) displacements of the foundation. The maximum azimuthal displacements are observed at $x^2 = \pm\frac{1}{2}\pi$ with respective azimuthal displacements of $u^2 = \pm 1.70 \times 10^{-4}$. The maximum radial displacement is observed at $x^2 = \pm\frac{1}{2}\pi$ with a radial displacement of $u^3 = -1.85 \times 10^{-4}$. Also, in the interval $x^2 \in (-\frac{1}{2}\pi, \frac{1}{2}\pi)$, i.e. the entire contact region ω, we see that the overlying body is at limiting equilibrium. For more on bonding and limiting equilibrium please see Section 2.6.

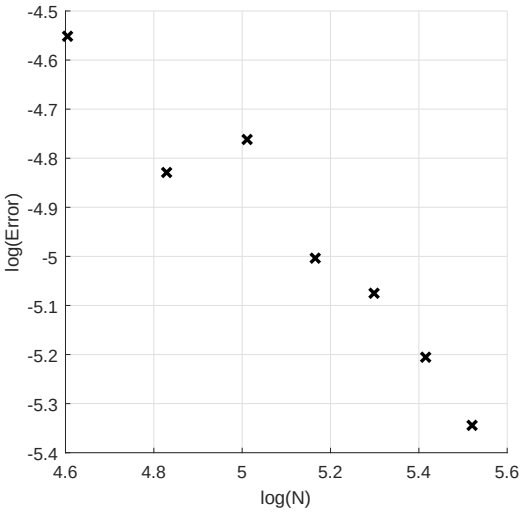

Figure 53: Grid dependence of the extended Kikuchi and Oden's model.

Another numerical analysis we must perform is the grid dependence analysis for the numerical solution. As the reader can see from figure 53, as N increases, the difference between the numerical solution N and $N + 1$ decreases. For our experiments we found that the azimuthal grid points and

the error share the relation $N \propto \text{Error}^{-0.806}$, where $\text{Error} = |1-(||\boldsymbol{u}_{N-1}||_{\ell^2}+||\boldsymbol{v}_{N-1}||_{\ell^2})^{-1}(||\boldsymbol{u}_N||_{\ell^2}+||\boldsymbol{v}_N||_{\ell^2})|$. Note that figure 53 is calculated with the values of $\tau_{\text{max}} = 1$, $b = 2$, $h = \frac{1}{8}$, $E = 8000$, $\nu = \frac{1}{4}$, $\varepsilon = 10^{-10}$ and $\nu_F = 1$.

But this is still not sufficient analysis, and thus, our goal in this section is to investigate how our shell model with friction predicts the displacement field of the foundation relative to extended Kikuchi and Oden's model for the given variables ν_F, $\delta\tau = \tau_{\text{max}}/\tau_0$, $\delta b = b/a$, $\delta h = h/H$, $\delta E = E/\bar{E}$ and $\delta\nu = \nu/\bar{\nu}$. To proceed with this investigation we calculate the relative error between the displacement field of the foundation predicted by shell model with friction and extended Kikuchi and Oden's model by

$$\text{Relative Error}(u^i) = \frac{\left(\sum_{\Delta x^2,\Delta x^3} ||u^i_{\text{Shell}}(\Delta x^2,\Delta x^3) - u^i_{\text{Kikuchi}}(\Delta x^2,\Delta x^3)||^2\right)^{\frac{1}{2}}}{\left(\sum_{\Delta x^2,\Delta x^3} ||u^i_{\text{Shell}}(\Delta x^2,\Delta x^3) + u^i_{\text{Kikuchi}}(\Delta x^2,\Delta x^3)||^2\right)^{\frac{1}{2}}}.$$

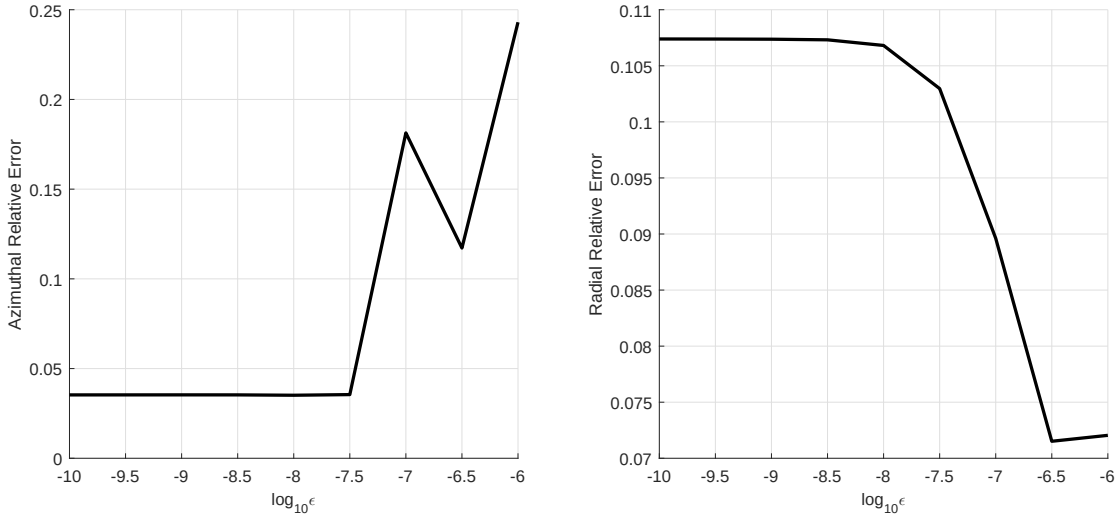

Figure 54: Relative error for ε.

Before we proceed any further, we must determine an appropriate value for the regularisation parameter, ε. Figure 54 is calculated with the values $\delta\tau = 1$, $\delta b = 1$, $\delta h = \frac{1}{8}$, $\delta E = 8$, $\delta\nu = 1$, $\varepsilon \in \{10^{-6}, 10^{-6.5}, 10^{-7}, 10^{-7.5}, 10^{-8}, 10^{-8.5}, 10^{-9}, 10^{-9.5}, 10^{-10}\}$ and $\nu_F = 1$. From figure 54 one can see that both relative errors remain constant (up to 3 significant figures) for the values $10^{-8.5} \leq \varepsilon \leq 10^{-10}$, implying that as ε tends to zero, extended Kikuchi and Oden's solution converges to a specific solution. Thus, for all our experiments we continue to use the value $\varepsilon = 10^{-10}$.

Figure 55 shows the relative error between our shell model with friction and extended Kikuchi and Oden's model for varying coefficient of friction between the shell and the foundation. For these experiments we assert that $\delta\tau = 1$, $\delta b = 1$, $\delta h = \frac{1}{8}$, $\delta E = 8$, $\delta\nu = 1$ and $\nu_F \in \{\frac{3}{10}, \frac{4}{10}, \frac{5}{10}, \frac{6}{10}, \frac{7}{10}, \frac{8}{10}, \frac{9}{10}, 1\}$. From figure 55 one can see that as the coefficient of friction at the contact surface increases, the relative error reduces, and this a significant reduction in the error. At $\nu_F = 1$ we observe respective azimuthal and radial relative errors of 3.53% and 10.7%. This implies that rougher the contact surface is, then closer our shell model with friction resembles extended Kikuchi and Oden's model. This is an intuitive result as the coefficient of friction increases, both models resemble the bonded

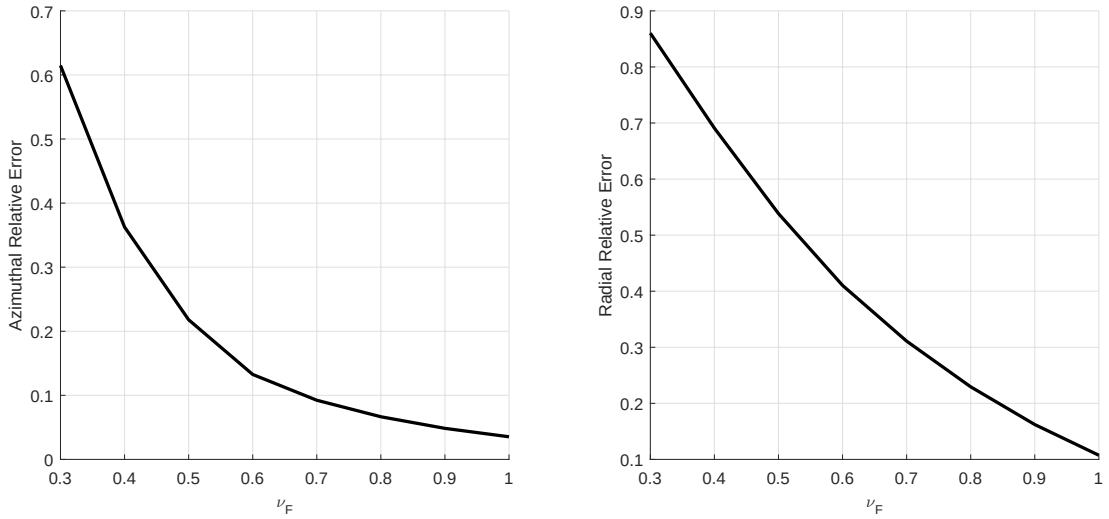

Figure 55: Relative error for ν_F.

case, and in Sections 3.6 and 3.7 we concluded that our overlying shell model is a good approximation of the two-body problem for the bonded case.

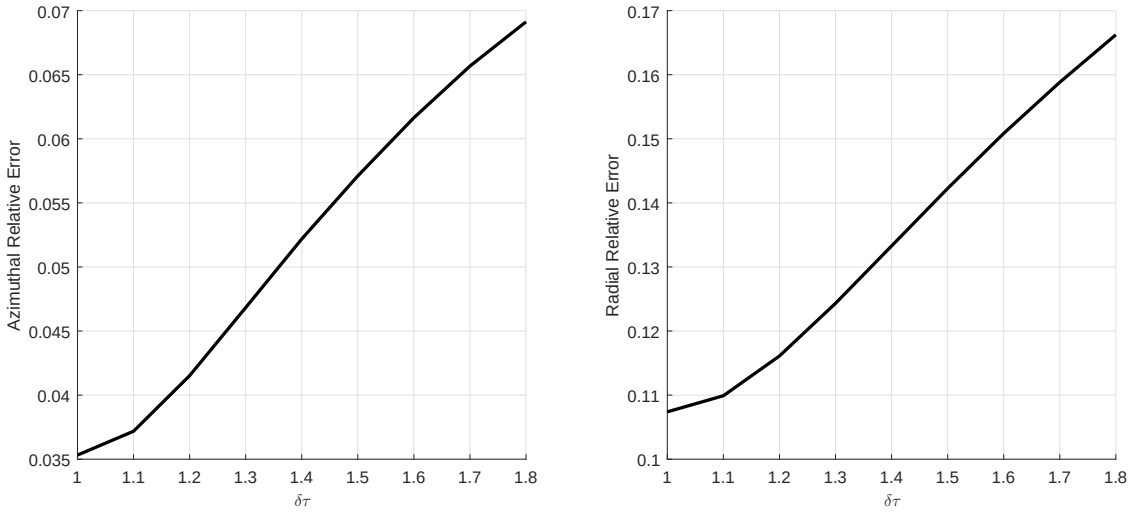

Figure 56: Relative error for $\delta\tau = \tau_{\max}/\tau_0$.

Figure 56 shows the relative error between our shell model with friction and extended Kikuchi and Oden's model for varying maximum applied traction at the boundary. For these experiments we assert that $\delta\tau \in \{1, \frac{11}{10}, \frac{12}{10}, \frac{13}{10}, \frac{14}{10}, \frac{15}{10}, \frac{16}{10}, \frac{17}{10}, \frac{18}{10}\}$, $\delta b = 1$, $\delta h = \frac{1}{8}$, $\delta E = 8$, $\delta\nu = 1$ and $\nu_F = 1$. From figure 56 one can see that as the maximum applied traction increases, both azimuthal and radial relative errors too increases. The minimum azimuthal and radial relative errors are 3.53% and 10.7%, and they are both observed for $\delta\tau = 1$. Also, we notice that the radial relative error is significantly higher than azimuthal error, and this is analogous to the results of error analyses from Sections 3.6 and 3.7.

Figure 57 shows the relative error between our shell model with friction and extended Kikuchi and

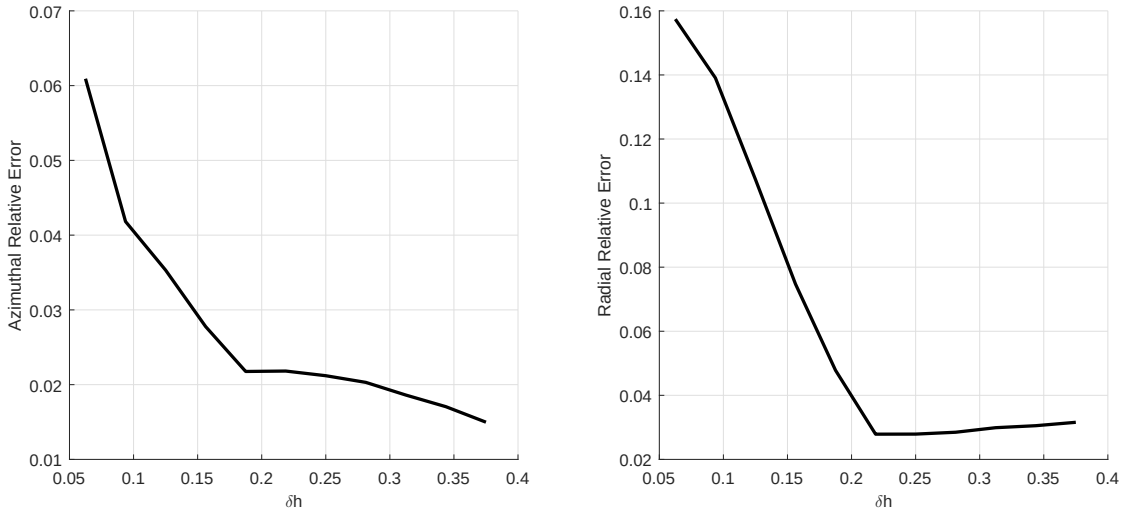

Figure 57: Relative error for $\delta h = h/H$.

Oden's model for for varying thicknesses of the shell. For these experiments we asserted that $\delta\tau = 1$, $\delta b = 1$, $\delta h \in \{\frac{2}{32}, \frac{3}{32}, \frac{4}{32}, \frac{5}{32}, \frac{6}{32}, \frac{7}{32}, \frac{8}{32}, \frac{9}{32}, \frac{10}{32}, \frac{11}{32}, \frac{12}{32}\}$, $\delta E = 8$, $\delta\nu = 1$ and $\nu_F = 1$. From figure 57 one can see that as δh increases, azimuthal relative error between our shell model with friction and extended Kikuchi and Oden's model decreases. At $\delta h = \frac{3}{8}$ we observe an azimuthal relative error of 1.50%. As for the radial relative error, one can see that it attains a minimum at $\delta h = \frac{7}{20}$ with a relative error of 2.79%. This implies that there exits an optimum thickness of the shell where the radial error between or shell model with friction and extended Kikuchi and Oden's model is a minimum.

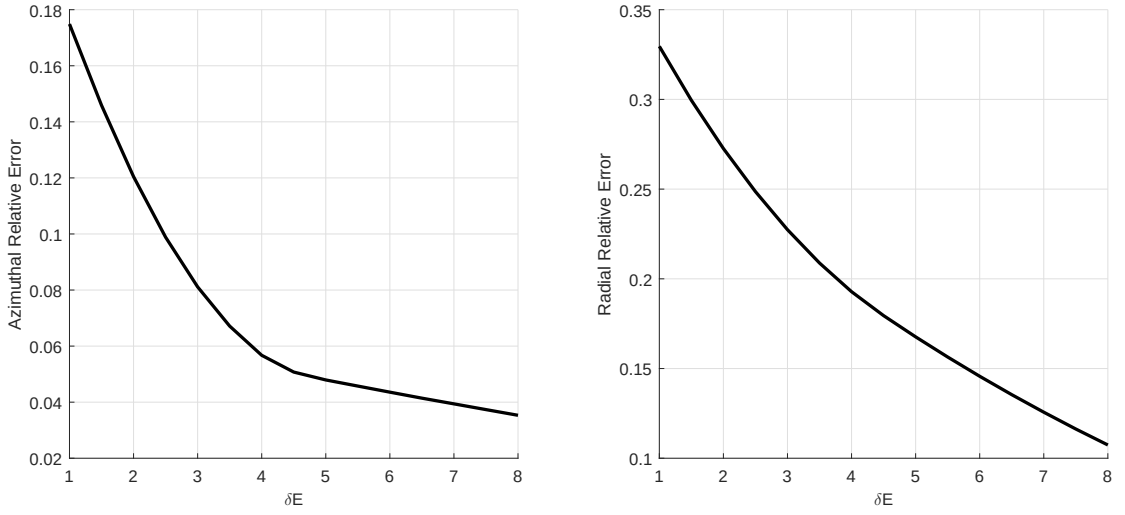

Figure 58: Relative error for $\delta E = E/\bar{E}$.

Figure 58 shows the relative error between our shell model with friction and extended Kikuchi and Oden's model for for varying Young's modulus of the shell. For these experiments we assert that $\delta\tau = 1$, $\delta b = 1$, $\delta h = \frac{1}{8}$, $\delta E \in \{1, \frac{3}{2}, 2, \frac{5}{2}, 3, \frac{7}{2}, 4, \frac{9}{2}, 5, \frac{11}{2}, 6, \frac{13}{2}, 7, \frac{15}{2}, 8\}$, $\delta\nu = 1$ and $\nu_F = 1$. From figure 58 one can see that as Young's modulus of the shell increases, the relative error decreases.

At $\delta E = 8$ we observe respective azimuthal and radial relative errors of 3.53% and 10.7%. This implies that stiffer the shell is, closer the shell model with friction resembles extended Kikuchi and Oden's model. Furthermore, this result analogous to our numerical results from Section 3.7.

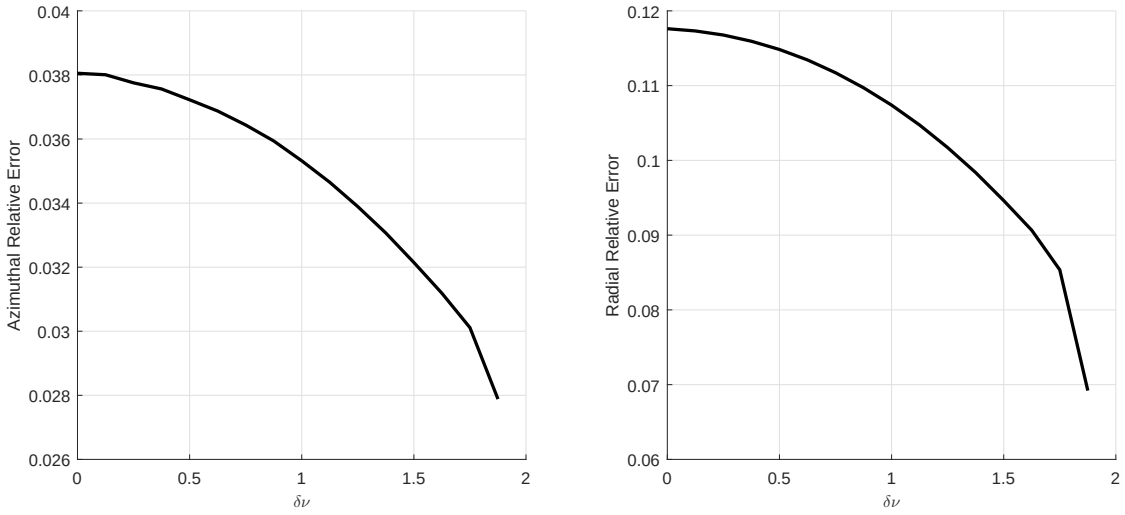

Figure 59: Relative error for $\delta\nu = \nu/\bar{\nu}$.

Figure 59 shows the relative error between our shell model with friction and extended Kikuchi and Oden's model for varying Poisson's ratio of the shell. For these experiments we assert that $\delta\tau = 1$, $\delta b = 1$, $\delta h = \frac{1}{8}$, $\delta E = 8$, $\delta\nu \in \{\frac{2}{8}, \frac{3}{8}, \frac{4}{8}, \frac{5}{8}, \frac{6}{8}, \frac{7}{8}, 1, \frac{9}{8}, \frac{10}{8}, \frac{11}{8}, \frac{12}{8}, \frac{13}{8}, \frac{14}{8}, \frac{15}{8}\}$. From figure 59 one can see that as Poisson's ratio of the shell increases, the relative error decreases. At $\delta\nu = \frac{15}{8}$ we observe respective azimuthal and radial relative errors of 2.79% and 6.92%. This implies that as the shell becomes incompressible, closer the shell model with friction resembles extended Kikuchi and Oden's model. However, unlike for Young's modulus case, one cannot indefinitely reduce the relative error by increasing Poisson's ratio as Poisson's ratio cannot neither attain nor exceed the value $\frac{1}{2}$.

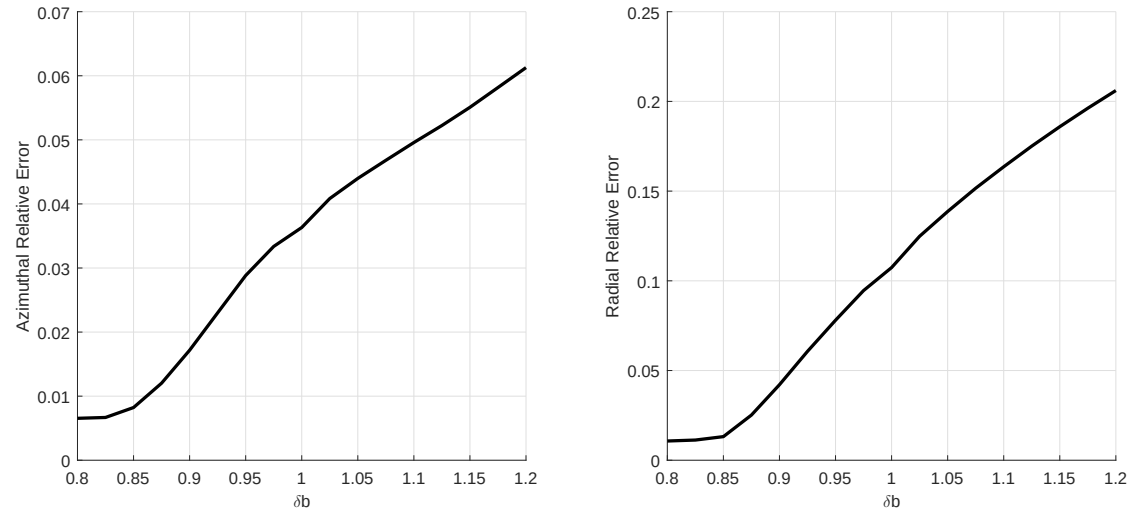

Figure 60: Relative error for $\delta b = b/a$.

Figure 60 shows the relative error between our shell model with friction and extended Kikuchi and Oden's model for varying vertical radii of the contact region. For these experiments we asserted that $\delta\tau = 1$, $\delta b \in \{\frac{32}{40}, \frac{33}{40}, \frac{34}{40}, \frac{35}{40}, \frac{36}{40}, \frac{37}{40}, \frac{38}{40}, \frac{39}{40}, 1, \frac{41}{40}, \frac{42}{40}, \frac{43}{40}, \frac{44}{40}, \frac{45}{40}, \frac{46}{40}, \frac{47}{40}, \frac{48}{40}\}$, $\delta h = \frac{1}{8}$, $\delta E = 8$, $\delta\nu = 1$ and $\nu_F = 1$. From figure 60 one can see that as the critical parametric-latitude increases, both azimuthal and radial relative error also increases. At $\delta b = \frac{4}{5}$, we observe respective azimuthal and radial relative errors of 0.654% and 1.07%. This implies that lower the critical parametric-latitude of the contact region is, closer the shell model with friction resembles extended Kikuchi and Oden's model.

The above analyses show how the displacement field of an elastic foundation modelled with our overlying shell, on an elastic foundation subjected to the hypothetical displacement-based friction condition, model relative to Kikuchi and Oden's [102] model, extended to model fully two-body contact problem in curvilinear coordinates. However, unlike in chapter 3, there exists no definitive two-body friction theorem (or at least a model) that we can compare our results against. Hence, the reason we investigated the relative errors between the two solutions to see how they fair against a set of variables.

The disadvantage of extended Kikuchi and Oden's model is that it is unsuitable for modelling thin overlying bodies, as the thickness of overlying body becomes infinitesimally small relative to the thickness of the foundation, it is numerically impractical to model the overlying body as a three-dimensional object. Thus, in this scenario extended Kikuchi and Oden's model breaks down. This justifies the existence of our overlying shell model with friction as this model is numerically valid for such cases.

We again remind the reader that the physical validity of each model is still an open question as there exits no definitive friction model that we can compare our results against. We further remind the reader that the model we presented in this section is not a model that is derived by Kikuchi and Oden [102]. We taken the model for Coulomb's law of static friction from Kikuchi and Oden [102] (see Section 1.11) and extended to curvilinear coordinates (see Section 2.6) which is then extended to model a full two-body problem in this section. We merely called it extended Kikuchi and Oden's model for convenience.

4.7 Conclusions

In this chapter we studied frictionally coupled overlying shells supported by elastic foundations. In Section 4.2 we used Kikuchi and Oden's [102] model for Coulomb's law of static friction to derive a displacement-based static friction condition. By construction this displacement-based hypothetical friction condition is more mathematically sound than Coulomb's law, but its physical validity still remains an open question. Then, in Section 4.3, we explicitly derived the governing equations and the boundary conditions for the general case for overlying shells on elastic foundations when subjected to a displacement-based friction condition. In Section 4.4 we used the work of Evans [63]

and, Kinderlehrer and Stampacchia [107] to prove the existence and the uniqueness of the solutions, and thus, proving that what we derived is a mathematical theory and not a hypothetical model.

In chapter 4.5 we presented framework to conduct a set of numerical solutions. For numerical analysis, in Section 4.6, we extended Kikuchi and Oden's [102] model for Coulomb's law of static friction to model a full two-body contact problem in curvilinear coordinates and shown how numerical solutions fair against our shell model with friction. The method of numerical analysis is to ascertain how the displacement field of the foundation behave when the overlying body is modelled by our shell model with friction relative to extended Kikuchi and Oden's model. The numerical analysis shows that, if the shell is thick, the shell is stiff, the shell is close to incompressible, contact region has a very high coefficient of friction or contact region has a low critical parametric-latitude, then the displacement field of the foundation predicted by both models be in better agreement.

From our numerical analysis the greatest reduction in the error is observed for higher coefficients of friction, i.e. as the coefficient of friction increases, the bodies behaves as if they are bonded, and thus, the greater agreement between the solutions of extended Kikuchi and Oden's model and our shell model with friction. This is an expected result as we initially derived our overlying shell model to approximate bonded thin bodies on elastic foundations, and the efficacy of our initial model is numerically modelled in Sections 3.6 and 3.7. The second greatest reduction in the error is observed for higher Young's moduli of the shell. This is also an expected result as we observed in Section 3.7 that the overlying shell models are mostly accurate for shells with relatively high Young's moduli.

5 Open Questions

Abstract

In this chapter we discuss a question regarding the well-posedness of our shell model, higher regularity that is vital for finding finite-difference solutions, Signorini's problem and how to extend it to our problem with friction, how to extend our results to model semi-linear problems and then fully nonlinear problems, and finally how to extend our results to the dynamic case.

5.1 Introduction

In this section we discuss few interesting areas that still remain open for investigation. We begin, in Section 5.2, by discussing a fundamental question concerning the well-posedness of our overlying shell model. In Section 5.3 we discuss about the higher regularity that is vital for finding finite-difference solutions. In Section 5.4 we discuss Signorini's problem and how to extend it to our shell model with friction. There, we assert that the contact region of the elastic foundation is unknown and for any proper subset of the boundary of the foundation need not have the same physical form (same curvature and same shape) as the shell, i.e. the shell can no longer be expressed as a boundary form of the foundation, and we put forward a model for a shell supported by an elastic foundation as a full two-body contact problem. In Section 5.5 we describe how to extend our results to model semi-linear problems and then to model fully nonlinear problems. Finally, in Section 5.6, we describe how to extend our results to the dynamic case.

The reader must be aware that everything in this chapter is hypothetical. Due to time constrains everything we present is this chapter are areas that we do not consider in depth and not prove with mathematical rigour. But, we meticulously present the necessary publications so that the reader may consult for constructing possible proofs. We present this chapter as possible future work or at least as open questions that worthy of some discussion.

5.2 Well-Posedness of the Boundary Conditions

Recall the zero-slope boundary conditions, i.e. $\partial_\beta(u^3|_\omega)|_{\partial\omega} = 0 \ , \ \forall \ \beta \in \{1,2\}$, from theorem 3. The proof of theorem 3 (see Section 3.4) implies that a unique solution can be found even if one omit the zero-slope conditions, i.e. given that $\partial_\beta(u^3|_\omega)|_{\partial\omega}$ are unknowns. This implies that one can apply boundary moments to the shell, i.e. $n_\alpha \eta^\alpha_\beta(\boldsymbol{u})|_{\partial\omega} = \eta_{0\beta}$, $\forall \ \beta \in \{1,2\}$, where $\boldsymbol{\eta}_0 \in \boldsymbol{L}^2(\partial\omega)$ is an external moments density field. However, from our numerical analysis we found that omitting the zero-slope boundary conditions leads to an ill-posed fourth-order finite-difference problem.

To illustrate this problem in more detail consider a simple example of an infinity long plate with a zero-Poisson's ratio that is bonded to an infinitely long foundation with a zero-Poisson's ratio. Given that $(u^1, 0, u^3)_{\mathsf{E}}$ is the displacement filed, one can exploit the invariance in the y direction and express the energy functional per unit y as

$$J(u) = \frac{1}{2}\bar{E}\int_{-H}^{0}\int_{-x_0}^{x_0}\left[(\partial_x u^1)^2 + (\partial_z u^3)^2 + \frac{1}{2}(\partial_x u^2 + \partial_z u^3)^2\right] dxdz$$

$$+\frac{1}{2}E\int_{-x_0}^{x_0}\left[h(\partial_x u^1)^2+\frac{1}{3}h^3(\partial_{xx}u^3)^2\right]dx$$
$$+h(\tau_0^1u^1+\tau_0^3u^3)|_{(x,z)=(-x_0,0)}-h(\tau_0^1u^1+\tau_0^3u^3)|_{(x,z)=(x_0,0)}\ ,\ \forall\ (v^1,v^3)\in \boldsymbol{V}_{\mathscr{P}}(\omega,\Omega)\ ,$$

where

$$\boldsymbol{V}_{\mathscr{P}}(\omega,\Omega)=\{(v^1,v^3)\in \boldsymbol{H}^1(\Omega)\mid (v^1,v^3)\in H^1(\omega)\times H^2(\omega)|_\omega,\ (v^1,v^3)|_{z=-H}=\mathbf{0},\ \partial_x u^3|_{(x,z)=(\pm x_0,0)}=0\}\ ,$$

and where $\bar{E}$ is Young's modulus and H is the thickness of the foundation, E is Young's modulus and h is the thickness of the plate, $\tau_0^1,\tau_0^3\in\mathbb{R}$ are constant tractions, $\Omega=(-x_0,x_0)\times(-H,0)$ and $\omega=(-x_0,x_0)$. It can be shown that the above problem has a unique minimiser, which is also a critical point. Thus, assuming that $u^1\in C^2(\Omega)$, $u^3\in C^2(\Omega)$, $u^1|_\omega\in C^2(\omega)$, and $u^3|_\omega\in C^4(\omega)$ one can express the governing equations of the problems as

$$\begin{aligned}
\left[\partial_{xx}u^1+\frac{1}{2}\partial_{zz}u^1+\frac{1}{2}\partial_{xz}u^3\right]|_\Omega&=0\ ,\\
\left[\frac{1}{2}\partial_{xz}u^1+\frac{1}{2}\partial_{xx}u^3+\partial_{zz}u^3\right]|_\Omega&=0\ ,\\
\left[\partial_{xx}u^1-\frac{\bar{E}}{hE}(\partial_z u^1+\partial_x u^3)\right]|_\omega&=0\ ,\\
\left[\partial_{xxxx}u^3+3\frac{\bar{E}}{h^3E}\partial_z u^3\right]|_\omega&=0\ ,
\end{aligned}$$

and the boundary conditions of the problems as

$$\begin{aligned}
(u^1,u^3)_{\mathsf{E}}|_{(x,z)\in\{[-x_0,x_0]\times\{-H\}\}}&=\mathbf{0}\ , & \partial_x u^3|_{(x,z)=(\pm x_0,0)}&=0\ ,\\
\partial_x u^1|_{(x,z)\in\{\{\pm x_0\}\times(-H,0)\}}&=0\ , & \partial_x u^1|_{(x,z)=(\pm x_0,0)}&=2\frac{\tau_0^1}{E},\\
\partial_z u^1+\partial_x u^3|_{(x,z)\in\{\{\pm x_0\}\times(-H,0)\}}&=0\ , & \partial_{xxx}u^3|_{(x,z)=(\pm x_0,0)}&=-6\frac{\tau_0^3}{h^2E}\ .
\end{aligned}$$

The above problem has a unique numerical solution. However, if one omit the zero-slope boundary conditions, i.e. $\partial_x u^3|_{(x,z)=(\pm x_0,0)}=0$, then one can impose an arbitrary boundary moment as $\partial_{xx}u^3|_{(x,z)=(\pm x_0,0)}=2E^{-1}\eta_0$, where $\eta_0\in\mathbb{R}$ is a constant external moments density. However, if one numerically models this problem with the boundary moments, i.e. without the zero-slope boundary conditions, then the numerical scheme fails to converge. Hint: consider the change of variables $(w^1(x),w^3(x))_{\mathsf{E}}=(\partial_{xx}u^1(x,z),\partial_{xx}u^3(x,z))_{\mathsf{E}}|_\omega$ for the numerical scheme.

It is unclear that if are making a mistake in the proof of theorem 3 or we are not correctly numerically modelling the problem. If it is the proof, then the problem must lie in the rigid displacement result from Section 3.4, or, if it is the numerical modelling, then the problem must lie in the boundary updating approach in the finite-difference scheme. Unfortunately, our knowledge in weighted Sobolev spaces is not sufficient to investigate this problem further. For possible solutions a comprehensive analytical treatment of boundary conditions for higher-order elliptic equations can be found in chapters 3 and 6 of Necas *et al.* [144] and an analysis of finite-difference schemes for fourth-order elliptic differential operators can be found in section 2.7 of Jovanovic and Suli [93].

5.3 Regularity

Regularity is very important when finding numerical solutions. For example, one requires the minimiser of the energy functional to have higher regularity in order to construct finite-difference solu-

tions. But in our framework that we presented in chapters 3 and 4 only finite-element solutions can be mathematically justified. Yet, we know the existence of finite-difference solutions due to numerical analysis. Can one prove the existence of higher regularity solutions with sufficient mathematical rigour?

To investigate this matter further recall theorem 3. The set $\boldsymbol{V}_{\mathscr{S}}(\omega,\Omega)$ is a linear set as any finite linear combination of the elements in the set belongs to the set. Now, let $\bar{\boldsymbol{X}} \in C^3(\bar{\Omega};\mathbf{E}^3)$ and let $\partial\Omega$ be a uniform-$C^3(\mathbb{R}^2;\mathbb{R})$ boundary (see section 4.10 of Adams [3]). Then, a possible minimiser $\boldsymbol{u}$ of $J(\cdot)$, maybe written as $\boldsymbol{u} = \boldsymbol{u}_0 + \tilde{\boldsymbol{u}}$ where $\boldsymbol{u}_0 \in \boldsymbol{H}_0^1(\Omega)$ and $\tilde{\boldsymbol{u}} \in H^2(\Omega)\times H^2(\Omega)\times H^3(\Omega)$. Note that the latter condition follows from the boundary trace embedding theorem (see theorem 5.36 of Adams [3]) and Rellich-Kondrachov theorem (see theorem 6.3 of Adams [3]), i.e. we have the compact embeddings $H^2(\Omega) \to H^1(\omega)$ and $H^3(\Omega) \to H^2(\omega)$. Clearly, we still have $\boldsymbol{u} \in \boldsymbol{V}_{\mathscr{S}}(\omega,\Omega)$. Now, if we let $\boldsymbol{f} \in H^1(\Omega)\times H^1(\Omega)\times H^2(\Omega)$, then from theorem 3.9-4 of Ciarlet [39] (for proof see Agmon *et al.* [5] and Geymonat [75]) we obtain $\boldsymbol{u}_0 \in H^2(\Omega)\times H^2(\Omega)\times H^3(\Omega)$. This implies that $\boldsymbol{u} \in H^2(\Omega)\times H^2(\Omega)\times H^3(\Omega)$.

Note that our problem is a *displacement-traction* problem: it is displacement due to $\boldsymbol{u}|_{\partial\Omega_0} = \boldsymbol{0}$ and traction due to $\boldsymbol{\tau}_0$. Thus, we require much finer analysis on trace spaces and fractional order spaces. Luckily, comprehensive analysis of fractional order spaces can be found in chapter 7 of Adams [3] and analysis on the regularity of solutions can be found in chapter 4 of Necas *et al.* [144]. Thus, it may be possible for one to construct a proof such that $\boldsymbol{u} \in C^3(\Omega)\times C^3(\Omega)\times C^4(\Omega)$, which is sufficient for proving the existence of finite-difference solutions.

But does this mean that the every minimiser of $J(\cdot)$ has the form $\boldsymbol{u} = \boldsymbol{u}_0 + \tilde{\boldsymbol{u}}$, where $\boldsymbol{u}_0 \in \boldsymbol{H}_0^1(\Omega)$ and $\tilde{\boldsymbol{u}} \in H^2(\Omega)\times H^2(\Omega)\times H^3(\Omega)$, or that the form $\boldsymbol{u} = \boldsymbol{u}_0 + \tilde{\boldsymbol{u}}$ satisfies any minimising solution: certainly not! Without a firm proof everything we discussed regarding the higher order regularity is merely speculative. One requires more sophisticated analysis to solve this regularity problem.

5.4 Signorini's Problem

Signorini's problem describes the contact of a linearly elastic body with a rigid frictionless foundation where the solution describes the displacement field of the elastic body at the contact region as well as the range of the contact region, as the contact region is also considered as a part of the solution. On a historical note the general problem of the equilibrium of a linearly elastic body in contact with a rigid frictionless foundation is initially introduced by Signorini [178, 179].

Characterisation of Signorini's problem is as follows: consider a three-dimensional linearly elastic body, which is described by the displacement field $\boldsymbol{v}$, in contact with a rigid foundation. Let $\Gamma_C \subset \partial\Omega$ be the *candidate contact surface*. Note that the actual surface on which the body comes in contact with the foundation is not known in advance, but it is assumed that it is contained in the candidate contact surface as a proper subset. Now, let ψ be the initial relative displacement field between the

elastic body and the rigid foundation. This leads the following equations at the candidate contact surface,

$$\begin{aligned}
\left[\bar{n}_i T^i_j(\boldsymbol{v}) - \bar{n}_i \bar{n}^k T^i_k(\boldsymbol{v})\right]|_{\Gamma_C} &= 0 \,, \forall\, j \in \{1,2,3\} \,, \\
\bar{n}_i \bar{n}^k \bar{n}_l T^i_k(\boldsymbol{v})(v^l - \psi^l)|_{\Gamma_C} &= 0 \,, \\
\bar{n}_i (v^i - \psi^i)|_{\Gamma_C} &\leq 0 \,, \\
\bar{n}_i \bar{n}^k T^i_k(\boldsymbol{v})|_{\Gamma_C} &\leq 0 \,,
\end{aligned}$$

where $\bar{\boldsymbol{n}}$ is the unit outward normal to Γ_C.

To extend Signorini's problem to a shell supported by an elastic foundation consider the method for a pseudo-two-body contact problem described in section 6.8 of Kikuchi and Oden [102]. Armed with this knowledge, let $\boldsymbol{u}$ describe the displacement field of the shell. Now, assume that this shell is in contact with an elastic foundation with a frictionless boundary. We use the curvilinear coordinate system of the shell as the coordinate system of the elastic foundation, and given that the lower-surface of the shell satisfies assertion 1, we asserts that the foundation is located beneath the lower-surface of the shell. Now, let $\boldsymbol{v}$ be the displacement field of the foundation and let $\boldsymbol{\psi}$ be the initial relative displacement field between shell and the foundation, which is a known field in advance. Thus, the energy functional of a shell with a thickness h on a frictionless elastic foundation may have the form

$$\begin{aligned}
J(\boldsymbol{u},\boldsymbol{v}) = &\int_\Omega \left[\frac{1}{2} A^{ijkl} E_{ij}(\boldsymbol{v}) E_{kl}(\boldsymbol{v}) - f^i v_i\right] d\Omega \\
&+ \int_\omega \left[\frac{1}{2} B^{\alpha\beta\gamma\delta}\left(h\epsilon_{\alpha\beta}(\boldsymbol{u})\epsilon_{\gamma\delta}(\boldsymbol{u}) + \frac{1}{3}h^3 \rho_{\alpha\beta}(\boldsymbol{u})\rho_{\gamma\delta}(\boldsymbol{u})\right) - h f^i_0 u_i\right] d\omega \\
&- \int_{\partial\omega\setminus\partial\omega_0} \left[h\tau^i_0 u_i + \frac{1}{3}h^3 \eta^\alpha_0 \nabla_\alpha u^3\right] d(\partial\omega) \;,\; \forall\, (\boldsymbol{u},\boldsymbol{v}) \in \boldsymbol{V}_{\text{Signorini}}(\omega,\Omega) \;,
\end{aligned}$$

where

$$\begin{aligned}
\boldsymbol{V}_{\text{Signorini}}(\omega,\Omega) &= \{\boldsymbol{u} \in \boldsymbol{V}_{\text{Shell}}(\omega), \boldsymbol{v} \in \boldsymbol{V}_{\text{Foundation}}(\Omega) \mid \bar{n}_i(v^i - u^i - \psi^i)|_{\Gamma_C} \leq 0\} \;, \\
\boldsymbol{V}_{\text{Shell}}(\omega) &= \{\boldsymbol{u} \in H^1(\omega)\times H^1(\omega)\times H^2(\omega) \mid \boldsymbol{u}|_{\partial\omega_0} = \boldsymbol{0},\; n^\alpha \partial_\alpha u^3|_{\partial\omega_0} = 0\} \;, \\
\boldsymbol{V}_{\text{Foundation}}(\Omega) &= \{\boldsymbol{v} \in \boldsymbol{H}^1(\Omega) \mid \boldsymbol{v}|_{\partial\Omega_0} = \boldsymbol{0}\} \;,
\end{aligned}$$

$\bar{\boldsymbol{n}}$ is the unit outward normal to the boundary $\partial\Omega$ and $\boldsymbol{n}$ is the unit outward normal to the boundary $\partial\omega$ in curvilinear coordinates. Note that $\Omega \subset \mathbb{R}^3$ is a connected open bounded domain with a sufficiently smooth boundary $\partial\Omega$ such that $\Gamma_C, \partial\Omega_0 \subset \partial\Omega$, where $\bar{\Gamma}_C \cap \partial\bar{\Omega}_0 = \emptyset$ with $\text{meas}(\partial\Omega_0;\mathbb{R}^2) > 0$. Also, $\omega \subset \mathbb{R}^2$ is a connected open bounded plane with a sufficiently smooth boundary $\partial\omega$ such that $\partial\omega_0 \subset \partial\omega$ with $\text{meas}(\partial\omega_0;\mathbb{R}) > 0$. Furthermore, $\boldsymbol{f} \in \boldsymbol{L}^2(\Omega)$, $\boldsymbol{f}_0 \in \boldsymbol{L}^2(\omega)$, $\boldsymbol{\tau}_0 \in \boldsymbol{L}^2(\partial\omega)$ and $\boldsymbol{\eta}_0 \in \boldsymbol{L}^2(\partial\omega)$ where $\boldsymbol{\eta}_0$ is a external moments density field.

For Signorini's case we fix the displacement field of the shell in a proper subset of its boundary, i.e. $\boldsymbol{u}|_{\partial\omega_0} = \boldsymbol{0}$ and $n^\alpha \partial_\alpha u^3|_{\partial\omega_0} = 0$. With our previous analysis, we do not consider this condition as we treated the shell as a boundary form. But, now the shell is a separate body, and thus, we must assert the current condition to keep the problem static and to avoid a pure-traction problem.

Thus far we only considered smooth contact surfaces. But, what if the contact surface is no longer smooth? To extend to above problem to include friction consider Signorini's problem with Coulomb's law of static friction that is described in section 10.2 of Kikuchi and Oden [102]. Using Kikuchi and Oden's model as inspiration, we extend hypothesis 3 by considering the relative displacements between the shell and the elastic foundation. Thus, the energy functional of a shell with a thickness h on a elastic foundation with a displacement-based friction condition may have the form

$$\begin{aligned} J(\boldsymbol{u},\boldsymbol{v}) = &\int_\Omega \left[\frac{1}{2}A^{ijkl}E_{ij}(\boldsymbol{v})E_{kl}(\boldsymbol{v}) - f^i v_i\right] d\Omega \\ &+ \int_\omega \left[\frac{1}{2}B^{\alpha\beta\gamma\delta}\left(h\epsilon_{\alpha\beta}(\boldsymbol{u})\epsilon_{\gamma\delta}(\boldsymbol{u}) + \frac{1}{3}h^3\rho_{\alpha\beta}(\boldsymbol{u})\rho_{\gamma\delta}(\boldsymbol{u})\right) - hf_0^i u_i\right] d\omega \\ &- \int_{\partial\omega\setminus\partial\omega_0}\left[h\tau_0^i u_i + \frac{1}{3}h^3\eta_0^\alpha\nabla_\alpha u^3\right] d(\partial\omega)\ ,\ \forall\ (\boldsymbol{u},\boldsymbol{v}) \in \boldsymbol{V}_{\text{Friction}}(\omega,\Omega)\ , \end{aligned}$$

where

$$\boldsymbol{V}_{\text{Friction}}(\omega,\Omega) = \{(\boldsymbol{u},\boldsymbol{v}) \in \boldsymbol{V}_{\text{Signorini}}(\omega,\Omega)\ |\ \left[2\nu_F\bar{\boldsymbol{n}}\cdot(\boldsymbol{v}-\boldsymbol{u}-\boldsymbol{\psi}) + |(\boldsymbol{v}-\boldsymbol{u}-\boldsymbol{\psi}) - \bar{\boldsymbol{n}}\cdot(\boldsymbol{v}-\boldsymbol{u}-\boldsymbol{\psi})|\right]|_{\Gamma_C} \leq 0\}\ ,$$

and ν_F is the coefficient of friction between the elastic foundation and the shell. Note that $\boldsymbol{u}\cdot\boldsymbol{v} = u_i v^i$ and $|\boldsymbol{v}| = (v_i v^i)^{\frac{1}{2}}$ for any vectors $\boldsymbol{u},\boldsymbol{v}$ in the curvilinear space.

Can we guarantee that the above problems even have solutions? Certainly not. Even Kikuchi and Oden's [102] (frictionless) two-body problem is not necessarily a two-body problem. It is a much simpler problem where a single elastic body folded in on itself so one only needs to deal with a single displacement field (see section 6.8 of [102]). However, even the single body case is given as a hypothetical model as the existence and the uniqueness of solutions are not proven by the authors. The problems that we present may have solutions, but without proving the existence of solutions with rigorous mathematics this remains a merely an interesting hypothetical model.

For further information on the subject we direct the reader to chapter 6 of Kikuchi and Oden [102] for rigorous analysis of Signorini's problem, where the authors meticulously present the mathematical framework for a variational statement of Signorini's problem, and prove the existence and the uniqueness of solutions. Just let $g = n_i\psi^i$ to be consistent with Kikuchi and Oden's [102] terminology. Among other finer analyses the authors also present a finite-element approximation that is developed for the exterior penalty formulation of Signorini's problem using 9-node isoparametric quadrilateral elements, and give many solved examples with the use of the finite-element penalty method. Furthermore, extensions to Signorini's problem, such as the elastic pseudo-two-body contact problem, can be found in section 6.8 of the publication and Signorini's problem with Coulomb's law with static friction can be found in section 10.2 of the publication.

5.5 Nonlinear Elasticity

Nonlinear elastic problems are an immensely important branch in the field of mathematical elasticity. For example, large deformation of elastic bodies cannot accurately be modelled by linear elasticity as the latter method is only valid for infinitesimal deformations. Nonlinear elasticity models require

finite deformation modelling, also it is sometimes the case in mathematical elasticity that certain results in linear elasticity cannot be mathematically justified as it can be with hyperelasticity (see section 2 subsection 7.7 of Morassi and Paroni [139] for the examples of convexity and policonvexity). Furthermore, certain forcings of the elastic body may depend on the displacement field, and thus, making the force density a function of the displacement field (for examples of such problems, please see chapter 2 section 4 Lions [123]). For such problems analysis in linear elasticity is insufficient, and thus, one must extend the work to nonlinear mathematical elasticity.

Now, recall theorem 3 or 4 and consider the field $\boldsymbol{f}$ for an example. Thus far we only considered the case $\boldsymbol{f} = \boldsymbol{f}(x^1, x^2, x^3)$, but not $\boldsymbol{f} = \boldsymbol{f}(\boldsymbol{u})$. But, what if the latter is the problem in question? If this the case, then we are dealing with a semi-linear problem. For example, assume that there exists a constant C that depends on Ω and $\bar{\boldsymbol{X}}$ such that $\int_\Omega |\boldsymbol{f}(\boldsymbol{u})| \, d\Omega \leq C||\boldsymbol{u}||_{\boldsymbol{L}^2(\Omega)}$. Given that C is sufficiently small, one may show the existence of solutions with slight modification of the proof for theorem 3. However, it is unclear how this new term will affect Korn's inequality, and thus, we do not assert any strong claims regarding existence of minimisers with any certainty. Instead, we refer the reader to the publication by Badiale and Serra [13] for an in-depth study of existence results for semi-linear elliptic equations using the variational approach.

To study finite deformations, or even to study Signorini's problem that we present in Section 5.4 accurately, one must move to the realm of fully nonlinear problems. To examine this further consider the map

$$\bar{\boldsymbol{r}}(\boldsymbol{v}) = \bar{\boldsymbol{X}} + v^i \partial_i \bar{\boldsymbol{X}} \ ,$$

where $\boldsymbol{v} = \boldsymbol{v}(x^1, x^2, x^3)$ is the displacement field of the foundation. Thus, nonlinear Green-St Venant strain tensor components can be expressed as

$$E_{ij}(\boldsymbol{v}) = \frac{1}{2}\left(\partial_i \bar{r}_k(\boldsymbol{v}) \partial_j \bar{r}^k(\boldsymbol{v}) - \partial_i \bar{X}_k \partial_j \bar{X}^k\right) \ .$$

Armed with this knowledge, one can express the *stored energy density* as

$$W(\boldsymbol{v}) = \frac{1}{2} A^{ijkl} E_{ij}(\boldsymbol{v}) E_{kl}(\boldsymbol{v}) \ .$$

As the stored energy density $W(\cdot)$ is a scalar, any change of coordinates to the Euclidean coordinate system will not affect the energy density. Thus, if one make this transformation, then one can easily show that the stored energy density is *policonvex*, i.e. there exists a convex functional

$$Z : \mathbb{M}^{3\times 3} \times \mathbb{M}^{3\times 3} \times \mathbb{R} \to \mathbb{R} \ ,$$

such that

$$W(\boldsymbol{v}) = Z(\bar{\boldsymbol{\nabla}}_{\mathsf{E}} \boldsymbol{v}_{\mathsf{E}}, \operatorname{cof}(\bar{\boldsymbol{\nabla}}_{\mathsf{E}} \boldsymbol{v}_{\mathsf{E}}), \det(\bar{\boldsymbol{\nabla}}_{\mathsf{E}} \boldsymbol{v}_{\mathsf{E}})) \ ,$$

where $\bar{\boldsymbol{\nabla}}_{\mathsf{E}}$ is the differential operator in the Euclidean space, $\boldsymbol{v}_{\mathsf{E}} = v^i \partial_i \bar{\boldsymbol{X}}$ is a Euclidean displacement field, and $\operatorname{cof}(\boldsymbol{M}) = (\det \boldsymbol{M}) \boldsymbol{M}^{-T}$, $\forall \ \boldsymbol{M} \in \mathbb{M}^{3\times 3}$, is the cofactor of a matrix and $\mathbb{M}^{3\times 3}$ is the space of 3×3 matrices. For more on policonvexity please consult section 2 of Morassi and Paroni

[139].

Existence of a minimiser can be shown using the techniques from the study of hyperelasticity. The first ever successful proof is derived by Ball [17], where the author also proves the existence of minimisers for displacement-traction problems and pure-traction problems. If the reader wishes to see the proof of the existence of minimisers for a unilateral boundary condition of place problem, problems of self-contact without friction and of non-interpenetration matter, then please consult chapter 7 of Ciarlet [36].

Now, consider the map

$$\boldsymbol{r}(\boldsymbol{w}) = \boldsymbol{R}(\boldsymbol{w}) + x^3 \frac{\partial_1 \boldsymbol{R}(\boldsymbol{w}) \times \partial_2 \boldsymbol{R}(\boldsymbol{w})}{||\partial_1 \boldsymbol{R}(\boldsymbol{w}) \times \partial_2 \boldsymbol{R}(\boldsymbol{w})||} \ ,$$

where $\boldsymbol{R}(\boldsymbol{w}) = \boldsymbol{\sigma} + w^\alpha \partial_\alpha \boldsymbol{\sigma} + w^3 \boldsymbol{N}$ and $\boldsymbol{w} = \boldsymbol{w}(x^1, x^2)$ is the displacement field with respect to the mid-surface of the shell. Thus, the nonzero nonlinear strain tensor components can be expressed as

$$e_{\alpha\beta}(\boldsymbol{w}) = \frac{1}{2} \left(\partial_\alpha r_i(\boldsymbol{w}) \partial_\beta r^i(\boldsymbol{w}) - \partial_\alpha (\sigma_i + x^3 N_i) \partial_\beta (\sigma^i + x^3 N^i) \right) \ .$$

With some further calculations, one can show that

$$\boldsymbol{e}(\boldsymbol{w}) = \boldsymbol{\epsilon}(\boldsymbol{w}) - x^3 \boldsymbol{\rho}(\boldsymbol{w}) \ ,$$

where

$$\begin{aligned} \epsilon_{\alpha\beta}(\boldsymbol{w}) &= \frac{1}{2} \left(\partial_\alpha R_i(\boldsymbol{w}) \partial_\beta R^i(\boldsymbol{w}) - \partial_\alpha \sigma_i \partial_\beta \sigma^i \right) \ , \\ \rho_{\alpha\beta}(\boldsymbol{w}) &= \left(\partial_{\alpha\beta} R_i(\boldsymbol{w}) \frac{(\partial_1 \boldsymbol{R}(\boldsymbol{w}) \times \partial_2 \boldsymbol{R}(\boldsymbol{w}))^i}{||\partial_1 \boldsymbol{R}(\boldsymbol{w}) \times \partial_2 \boldsymbol{R}(\boldsymbol{w})||} - N_i \partial_{\alpha\beta} \sigma^i \right) \ , \end{aligned}$$

(see chapter 4 of Ciarlet [39]). Armed with this knowledge, one can express the *stored energy density of a nonlinear shell* with a thickness $2h$ as

$$w_{2h}^{\text{mid}}(\boldsymbol{w}) = \frac{1}{2h} \int_{-h}^{h} \frac{1}{2} B^{\alpha\beta\gamma\delta} \left(\epsilon_{\alpha\beta}(\boldsymbol{w}) - x^3 \rho_{\alpha\beta}(\boldsymbol{w}) \right) \left(\epsilon_{\gamma\delta}(\boldsymbol{w}) - x^3 \rho_{\gamma\delta}(\boldsymbol{w}) \right) dx^3 \ .$$

Thus, for an overlying nonlinear shell with a thickness h (see hypothesis 2) the stored energy density is

$$w_h^{\text{low}}(\boldsymbol{u}) = \frac{1}{2} B^{\alpha\beta\gamma\delta} \left(\epsilon_{\alpha\beta}(\boldsymbol{u}) \epsilon_{\gamma\delta}(\boldsymbol{u}) + \frac{1}{3} h^2 \rho_{\alpha\beta}(\boldsymbol{u}) \rho_{\gamma\delta}(\boldsymbol{u}) \right) \ ,$$

i.e. $w_h^{\text{low}}(\boldsymbol{u}) = w_{2h}^{\text{mid}}(\boldsymbol{w})$, where $\boldsymbol{u} = \boldsymbol{u}(x^1, x^2)$ is the displacement field with respect to the lower-surface. It can be proven by Γ-convergence that the three-dimensional hyperelastic body tends to the nonlinear shell problem as the thickness approaches zero. As the existence of a minimiser can be proven for three-dimensional hyperelastic bodies, Γ-convergence automatically provides the existence of a minimiser for nonlinear shells. For the proof please consult section 2.5 of Ciarlet and Mardare [40]. Note that the first rigorous proof of this approach is presented by Dret ans Raoult [114], and Friesecke *et al.* [66]. For more on Γ-convergence please consult section 3 of Morassi and Paroni [139].

Separately we can prove the existence of weak solutions for nonlinear shells and three-dimensional hyperelastic bodies. But the question is: can we prove the existence of a weak solution for a nonlinear shell supported by a hyperelastic foundation, either as a two-body problem as in Signorini's problem case (see Section 5.4) or as the nonlinear shell as a boundary form of the hyperelastic foundation case (analogous to chapters 3 and 4)? The answer is no. This problem requires more sophisticated analysis, and thus, we leave it as future work.

5.6 Dynamic Case

In this section we discuss the evolution equations of shells supported by elastic foundations. Consider a real-life scenario where one applies an unbalanced force and or a moment to an overlying shell on an elastic foundation. How will it behave?

For our framework we assumed that our shell and the elastic body in question are isotropic and homogeneous, and thus, there exist two positive constants ϱ and $\bar{\varrho}$ such that they are the mass densities of the respective bodies. Now, assume that our problem in question evolves within the time interval $[0,T]$, where $T>0$. Now, let $\Omega_T=\Omega\times(0,T)$, $\omega_T=\omega\times(0,T)$ and $\partial\omega_T=\partial\omega\times(0,T)$. Given that we are considering Signorini's problem (so no boundary forms), let $\boldsymbol{u}=\boldsymbol{u}(x^1,x^2,t)$ be the displacement of the shell and $\boldsymbol{v}=\boldsymbol{v}(x^1,x^2,x^3,t)$ be the displacement of the elastic foundation. For convenience, assume that the initial and the final first-order partial derivatives of the displacement field with respect to time of both bodies are zero, i.e. $(\partial_t v^1,\partial_t v^2,\partial_t v^3)|_{t\in\{0,T\}}=\mathbf{0}$ and $(\partial_t u^1,\partial_t u^2,\partial_t u^3)|_{t\in\{0,T\}}=\mathbf{0}$. Thus, one can express the *action functional* of a shell with a thickness h on an elastic foundation as

$$
\begin{aligned}
S(\boldsymbol{u},\boldsymbol{v})=&\int_{\Omega_T}\left[\frac{1}{2}A^{ijkl}E_{ij}(\boldsymbol{v})E_{kl}(\boldsymbol{v})-f^iv_i-\frac{1}{2}\bar{\varrho}\partial_t v_i\partial_t v^i\right]d\Omega_T\\
&+\int_{\omega_T}\left[\frac{1}{2}B^{\alpha\beta\gamma\delta}\left(h\epsilon_{\alpha\beta}(\boldsymbol{u})\epsilon_{\gamma\delta}(\boldsymbol{u})+\frac{1}{3}h^3\rho_{\alpha\beta}(\boldsymbol{u})\rho_{\gamma\delta}(\boldsymbol{u})\right)-hf_0^iu_i\right.\\
&\qquad\left.-\frac{1}{2}\varrho\left(h\partial_t u_i\partial_t u^i-\frac{1}{3}h^3\rho^\alpha_\alpha(\partial_t\boldsymbol{u})\partial_t u^3\right)\right]d\omega_T\\
&-\int_{\partial\omega_T}\left[h\tau_0^iu_i-\frac{1}{3}h^3\eta_0^\alpha\left(\partial_\alpha\boldsymbol{\sigma}\right)\cdot\left(\frac{\partial_1\boldsymbol{R}(\boldsymbol{u})\times\partial_2\boldsymbol{R}(\boldsymbol{u})}{||\partial_1\boldsymbol{R}(\boldsymbol{u})\times\partial_2\boldsymbol{R}(\boldsymbol{u})||}\right)\right]d(\partial\omega_T)\,,
\end{aligned}
$$

with the displacement fields satisfying the conditions

$$
\begin{aligned}
\boldsymbol{v}|_{\partial\Omega_0}&=\mathbf{0}\ \text{(Zero displacement condition)}\,,\\
\boldsymbol{v}|_{\Omega\times\{0\}}&=\mathbf{0}\ \text{(Initial condition of the foundation)}\,,\\
\boldsymbol{u}|_{\omega\times\{0\}}&=\mathbf{0}\ \text{(Initial condition of the shell)}\,,\\
\bar{\boldsymbol{n}}\cdot(\boldsymbol{v}-\boldsymbol{u}-\boldsymbol{\psi})|_{\Gamma_C}&\leq 0\ \text{(Signorini's condition)}\,,\\
\left[2\nu_F\bar{\boldsymbol{n}}\cdot(\boldsymbol{v}-\boldsymbol{u}-\boldsymbol{\psi})+|(\boldsymbol{v}-\boldsymbol{u}-\boldsymbol{\psi})-\bar{\boldsymbol{n}}\cdot(\boldsymbol{v}-\boldsymbol{u}-\boldsymbol{\psi})|\right]|_{\Gamma_C}&\leq 0\ \text{(Displacement-based friction condition)}\,,
\end{aligned}
$$

where ∂_t is the partial derivative with respect to time. Note that $\partial_t\bar{\boldsymbol{r}}(\boldsymbol{v})\cdot\partial_t\bar{\boldsymbol{r}}(\boldsymbol{v})=\partial_t v_i\partial_t v^i$ and

$$
\begin{aligned}
\frac{1}{2h}\int_{-h}^{h}\partial_t\boldsymbol{r}(\boldsymbol{u})\cdot\partial_t\boldsymbol{r}(\boldsymbol{u})\,dx^3&=||\partial_t\left(u^\alpha\partial_\alpha\boldsymbol{\sigma}+u^3\boldsymbol{N}\right)||^2+\frac{1}{3}h^2\left|\left|\partial_t\left(\frac{\partial_1\boldsymbol{R}(\boldsymbol{u})\times\partial_2\boldsymbol{R}(\boldsymbol{u})}{||\partial_1\boldsymbol{R}(\boldsymbol{u})\times\partial_2\boldsymbol{R}(\boldsymbol{u})||}\right)\right|\right|^2\,,\\
&=\partial_t u_\alpha\partial_t u^\alpha+\partial_t u_3\partial_t u^3-\frac{1}{3}h^2\rho^\alpha_\alpha(\partial_t\boldsymbol{u})\partial_t u^3\,.
\end{aligned}
$$

As we are dealing with curvilinear coordinates, integrating by parts with respect to the time variable leads the appearance of Christoffel symbols, despite that both the diffeomorphism and the injective immersion are independent of time, i.e. $\bar{\boldsymbol{X}}(x^1, x^2, x^3) \neq \bar{\boldsymbol{X}}(x^1, x^2, x^3, t)$ and $\boldsymbol{\sigma}(x^1, x^2) \neq \boldsymbol{\sigma}(x^1, x^2, t)$ (see section 7.6 of Kay [101]). Armed with this knowledge, and the fact that we are assuming that the initial and the final first-order partial derivatives of the displacement fields with respect to time of both bodies are zero, we get the following relation in the foundation,

$$\int_{\Omega_T} \partial_t v_i \partial_t v^i \, d\Omega_T = - \int_{\Omega_T} \left(\partial_{tt} v^i + \bar{\Gamma}^i_{kl} \partial_t v^k \partial_t v^l \right) v_i \, d\Omega_T \, ,$$

and the following relation in the shell,

$$\begin{aligned} \int_{\omega_T} \left[\partial_t u_\alpha \partial_t u^\alpha + \partial_t u_3 \partial_t u^3 \right] d\omega_T = - \int_{\omega_T} \Big[& \left(\partial_{tt} u^\alpha + \Gamma^\alpha_{\gamma\delta} \partial_t u^\gamma \partial_t u^\delta - 2 F_{[\mathrm{II}]\gamma}^{\ \ \alpha} \partial_t u^\gamma \partial_t u^3 \right) u_\alpha \\ & + \left(\partial_{tt} u^3 + F_{[\mathrm{II}]\alpha\gamma} \partial_t u^\alpha \partial_t u^\gamma \right) u_3 \Big] d\omega_T \, . \end{aligned}$$

As one can see that to accurately model this problem, one needs to consider the nonlinear case. Also, notice that for the dynamic case one do not assert zero-Dirichlet and the zero-slope of the displacement field of the shell in a proper subset of its boundary, as now one may allow the shell to move freely without any mathematical restrictions due its dynamic nature.

The crucial question is that can we prove the existence of solutions to the dynamic problem? The answer is no. Fortunately, a comprehensive analysis on vibration of shells can be found in Leissa [115] and Soedel [181]. For shell-membranes, an asymptotic justification for the equations of dynamic shell-membranes can be found in Xiao [212]. Furthermore, there is a vast number of publications in the study of dynamic elastic problems in Euclidean coordinates, particularly in plate theory. For example, a thorough numerical analysis of the dynamical rectangular plates can be found in section 9 of Reddy [163]. Note that, if we consider the linear case, then the dynamic problem we present in this section is a *hyperbolic* problem. For elementary analysis on hyperbolic equations can be found in section 7.2 and section 11.1.2 of Evans [63]. But, for a more in-depth analysis of evolution problems please consult Lions [123].

5.7 Conclusions

In this chapter we presented possible future research topics as open questions. These open questions are areas that we did not study with mathematical rigour due to time constraints and lack of pre-existing research material. Above, we described a fundamental issue concerning the well-posedness of our overlying shell model. We also explored: (i) means to extend the regularity of the weak solutions of the theorem 3 to higher regularity, (ii) means to extend Signorini's problem to overlying shells on elastic foundations with friction, (iii) means to extend the problem to either semi-linear case or nonlinear case or both, and (iv) means to extend the problem to the dynamic case. Although, we did not prove the existence of solutions for any of the cases that we presented or, at least, give any numerical solutions, we did meticulously document the necessary literature to consult so that the reader may prove or disprove the given formulations.

6 Modelling Skin Abrasion

Abstract

In this chapter we derive a belt-friction model for a membrane over a rigid obstacle of positive mean-curvature. Also, we derive a static friction model for a shell-membrane supported by an elastic foundation. Then, we use the models to process experimental data that we gathered from human subjects to see which mechanical, elastic and geometrical factors can affect the coefficient of friction between skin and fabrics, and the deformation field and the stress profile at the contact area.

6.1 Introduction

In this chapter we attempt to mathematically model and experimentally investigate skin abrasion. We begin, in Sections 6.1.1, 6.1.2 and 6.1.3, by describing various types of skin abrasion documented in the current literature. Then, we begin our mathematical modelling in Section 6.2 where we take Kikuchi and Oden's [102] model for Coulomb's law of static friction for the slip case and apply it to a membrane supported by a rigid foundation to derive a belt-friction model. Then, in Section 6.3, we use this mathematical model to examine which mechanical, elastic and geometrical factors lead to a smaller coefficient of friction in a belt-friction setting. In Section 6.4 we examine the data that we gathered from experiments conducted on human subjects and use regression analysis to determine the implication of using belt-friction models to calculate the coefficient of friction between in-vivo skin and fabrics. We conclude our analysis of the experimental results by highlighting which physical factors can significantly affect the experimental results.

In Section 6.5 we use theorem 4 and Ciarlet's [38] theory of linear shell-membranes (see chapter 4 and 5 of Ciarlet [38]) to derive a theory for frictionally coupled static shell-membranes on elastic foundations. Then, in Section 6.6, we use this theory to conduct numerical simulations to identify which elastic and geometrical factors can lead to a lower shear generation at the contact area of the overlying shell-membrane model. In Section 6.7 we examine the data that we gathered from further experiments conducted on human subjects and compare the data against the numerical solutions of the overlying shell-membrane model to investigate the stress profile between the fabric and each subject's skin. We conclude our analysis of the shell-membrane model by documenting which elastic and geometric factors can lead to a lower shear between human skin and fabrics. The ultimate goal is to identify which elastic and geometric factors can minimise mechanical abrasion due to repetitive movement of fabrics over human skin, so that we may present our findings to healthcare providers to encourage and facilitate the development of products and practices that are less damaging to human skin.

6.1.1 Pressure Ulcers

Pressure ulcers are an area of localised cutaneous damage that is typically associated with pressure from bony protuberances on aged skin. Pressure ulcers can develop when a large amount of pressure is applied to an area of skin over a short period of time or when less pressure is applied

over a prolong period of time. When pressure is applied to soft tissue, it results in completely or partially obstructed blood flow to the soft tissue, starving the tissue of oxygen and nutrients, which eventually leads to necrosis in the affected area, and thus, an ulcer. Shear (i.e. constant and prolonged static friction) is also a cause, as it can pull on blood vessels that feed the skin, and thus, restricting the blood flow. Pressure ulcers often occur in very sedentary individuals such as those with impaired mobility, bedridden and wheelchair bound [132]. If the reader is interested in this subject, then please consult publication by Maklebust and Sieggreen [132].

It is given that friction contributes to skin damage by stripping of the epidermal layer of the skin: creating an environment conducive to further skin damage due to friction. An alteration in the coefficient of friction increases skin's adherence to the outside surface, which can eventually leads to wounds and infections. Note that this does not result in pressure ulcers, but it is observed in the same settings. Also, note that the language used by authors who specialised in the study of pressure ulcers is different to mathematicians' language. What they referrer to as shear appears to be a force related to static friction, and friction appears to be a force related to dynamic friction. By the definitions of shear and friction given by Bergstrom [25], this is the only logical conclusion.

Murray *et al.* [142] give many preventive measures for pressure ulcers. For example, to eliminate shear and friction, the authors states that to protect the exposed skin by protective dressings, padding or sheepskin, and for those who are bedridden elevating the foot of bed to 20 degrees when sitting to prevent sliding and maintaining the head of the bed at the lowest possible elevation, consistent with individual's medical condition and comfort.

It is estimated that over $400,000$ individuals will develop a new pressure ulcer annually in the UK (mainly the elderly) and approximately $51,000$ of them will be admitted to a hospital [64]. A study conducted in 1993 [197] shows that the cost to the NHS of treating pressure ulcers is around $£180$ - $£321$ million, which is approximately 0.4% - 0.8% of the total health spending. This figure is considered to be substantial underestimate, even allowing for inflation [22].

In 2003 Bennett *et al.* [22] find the cost of treating pressure ulcers in UK (excluding MRSA, surgical interventions and litigation costs) ranges between $£1.4$ to $£2.1$ billion annually, which is over 4% of gross NHS expenditure. The cost is deduced by estimating the daily cost of the resources required to deliver protocols of care reflecting good clinical practice. It is estimated that each episode cost from $£1,064$ for a grade-1 ulcer (i.e. non-blanchable erythema of intact skin, include discolouration of the skin, warmth, oedema, indurations or hardness may also be used as indicators, particularly on individuals with darker skin) to $£10,551$ for a grade-4 ulcer (i.e. extensive destruction, tissue necrosis, damage to muscle, bone, supporting structures with or without full thickness skin loss, with expected cost of treating critical colonisation, cellulitis and osteomyelitis). In a severe case, such as in the case of osteomyelitis, treatment can cost on average of $£16,500$ per episode per individual patient. In cases of MRSA the costs maybe significantly higher. Due to the lack of literature it is difficult to estimate litigation costs to the NHS related to pressure ulcer care, but one must assume

it be a substantial amount. For example, in the USA, The Omnibus Budget Reconciliation Act in 1987 made it easier for claimants to prove that a provider is negligent following the development of pressure damage. Thus, between 1992 and 1996 the median settlement value following successful litigation for negligence regarding a pressure ulcer is $\$279,000$ [193]. Again, this evidence strongly indicates the fact that preventive measures are immensely important. Lowering the probability of causing pressure ulcers leads to fewer resources are spent on treating pressure ulcers, and thus, reducing spending in the NHS.

6.1.2 Sport Related Trauma to the Skin Due to Friction

Due to excessive movement athletes are subject to repeated mechanical trauma to the skin, which in turn often leads to observable, documented, often painful (but never fatal) skin trauma [24]. The following conditions are documented sports related conditions and trauma to the skin caused by friction.

Fissure of the nipple, often referred as jogger's nipple, is a result from repeated irritation and friction of the nipples against a top (garment) during a prolonged period of exercise or a sporting activity. It is often experienced by runners and bicycle riders as they are exposed to the friction on the nipple for the greatest periods of time. Once affected bleeding is common, often associated with pain. Coating the nipples with petrolatum before running is said to be helpful. Also, it is advisable to use talcum powder, wearing a swim suit to reduce friction or, best of all, wearing a sports-bra [116]. Note that Powell [158] states that bicyclist's nipple is viewed more as a thermal injury in cold weather rather than an injury from friction.

Friction blisters are a skin condition that may occur at sites of combined pressure and friction, and maybe enhanced by heat, moisture, or cotton socks [79]. It is often observed on weight-bearing surfaces, and affects the feet when partaking running sports such as track, basketball and football. It is caused by shearing frictional forces, primarily horizontal, and increased heat due to physical exertion and humidity due to perspiration can further promotes blisters [44]. Common affected areas are joints, the tips of fingers and toes, and the heel of the foot. Preventive measures include hardening of the skin with 10% tannic acid soaks, wearing two pairs of powdered socks, use of protective hand and foot gear, and, above all, the use of correctly fitting sport-shoes. The use of padding with various types of polymeric materials is discussed by Muller [141]. One of the treatments presented by Scher [173] consists of draining the blister with a sterile needle and covering it with an occlusive pressure dressing such as adhesive tape. Topical antimicrobials are advisable to assist in preventing any secondary infection.

Traction alopecia (hair loss due to abrasion) is caused primarily by pulling force being applied to the hair or the scalp area. Copperman [43] observes traction alopecia in a women who jogged daily with a tight-banded wide-stripped heavy headphones. Switching to a lighter headpiece reportedly stopped the hair loss. The author also describes alopecia in two young male break-dancers, where constant spinning on top of the head eroded the hair shafts down to the scalp. Ely [61] observes

traction alopecia in a young female gymnast. The gymnast lost her hair from frontal scalp to the occiput (the back of the head) due to constant head stands and rollovers performed on the balance beam.

Calcaneal Petechiae, often referred as the black heal, are trauma-induced darkening lesions (acral) of the posterior or posterolateral aspect of the heel that occurs primarily in young adult athletes [196]. It is often observed on the feet of athletes engaged in sports such as tennis, basketball and other sporting activities that require repetitive and rapid acceleration and deceleration [171]. It is caused by blood being deposited in the thick stratum corneum of the edge of the heel, just above the thick plantar skin at places where blood vessels are minimally protected by fatty tissue, due to repeated lateral shearing forces on the epidermis (the upper most part of the skin) sliding over the rete pegs (epithelial extensions that project into the underlying connective tissue in both skin and mucous membranes) of the papillary dermis (uppermost layer of the dermis) [88]. These types of lesions are also observed on the edges of the palms of weight lifters and on the balls of the thumb of golfers. Black heel is first documented by Crissey and Peachy [51] on a group of basketball players in 1961. Rufli [171] found black heal (referred as hyperkeratosis hemorrhagica in the publication) in 2.85% of 596 nineteen-year-old Swiss military recruits who were subjected to military drills. Duprey [20] found an 18% prevalence in young people at a regional athletic training facility (25% males, 6% females). Black heel is often is asymptomatic (harmless); however, the diagnosis is clinically significant as it may easily be confused with nevus (mole) or malignant melanoma, where the latter condition can be life threatening [94].

Callus is a toughened area of skin which has become relatively thick and hard in response to repeated friction and or pressure. It is often occurs near bony prominences (where bones are close to the surface) [76, 85]. Formation of calluses represents a protective response of the skin to protect itself against further damage due to friction. However, exposure to more aggressive frictional forces to the skin cause blisters rather than allow calluses to form. Calluses are often observed in the hands of a gymnasts, archers, tennis players, golfers and bowlers, and on the feet of a dancers, runners and basketball players [168].

If the reader is more interested the subject please consult Bergfeld [24]. In fact, all the conditions described above are from Bergfeld's [24] publication. Other conditions that Bergfeld [24] present are tennis toe, subungual hematomas, abrasions, dermal nodules, subcutaneous nodules, striae distensae, contact dermatitis, cutaneous infections, and dermatitis due to physical and climatic factors.

6.1.3 Other Types Trauma to the Skin Due to Friction

It is documented that friction plays a role in the development of dermatitis in other settings. In many cases, it is observed that friction damages the stratum corneum and the stratum basale to varying degrees [209].

It is believed that friction plays a significant role in incontinence associated dermatitis as many authors publish literature on the coefficient of friction (measuring techniques and actual measurements) between human skin and fabrics in incontinence related publications [23, 48, 45, 46]. Incontinence is caused by involuntary leakage of urine or loss of voluntary control of the bowels. Causes include Polyuria (excessive urine production), muscle or nerve damage and pelvic floor dysfunction. The NHS estimates that between 3 and 6 million adults in the UK have some degree of urinary incontinence [200], and the prevalence is set to increase due to an aging population. It is documented that wearing of incontinence pads over prolong periods are the very cause of the problems in incontinence associated dermatitis. Despite the fact that pads absorb moisture, in many cases, the pads acts as a barrier that prevents water from escaping. This leads to an over hydration of the stratum corneum in the epidermis. Scheuplein and Blank [174] find an increase in skin hydration leads to increase in the thickness of the stratum corneum, and thus, the weakening of the cell structure. Tests conducted on adults and on infants show that over-hydration of the stratum corneum is responsible for a threefold increase in the coefficient of friction. Berg [23] states that prolong wearing of pads leads to weakening of the cell structure and an increase in the coefficient of friction that may cause mechanical abrasion, and thus, eventually leading to dermatitis. The author shows that an increase in skin hydration (due to pads) with the presence of urine and faecal enzymes lead to an increase in skin permeability, skin pH (from acidity to neutral) and increase in microbial count, and this can lead to higher aberration damage. Furthermore, Wilkinson [209] states that ill-fitting diapers cause chafing in actively kicking infants.

Frictionally-induced fissured lesions are observed below the ears or at the side of the nose in wearers of ill-fitting spectacle frames [62]. Epstein [62] documents cases of two patients diagnosed with clinically basal-cell epithelioma-like lesions (epithelial tumour) on the ear, which was later revealed, upon further examination, as a fissured lesion caused by rubbing ear-piece from the eyeglasses.

Contact dermatitis from clothing and attire, especially from synthetics fibber shirt collars and polo neck jumpers, is observed, and the neck area is considered to be specifically susceptible [209]. Angelini [8] studies the contact allergy in a series of 165 patients with eczematous dermatitis of the feet correlated clinically with shoe contact and found that friction is a contributor of contact dermatitis.

Dermatitis due to friction is also observed in individuals who do manual labour. White [208] states that in those who are handling turpentine it is necessary to have friction to develop and bring out blebs and pustules. The author also documents dermatitis intertriginous areas (areas where two skins may touch) affecting colliers (workers on ships that are design to carry coal) and fraying of the skin of the forearms and thighs of coal miners due to coal and stone dust. The author further documents that cotton workers developing excoriated dermatitis (wounds), even infections of the webs of the palms from moisture and friction. Similar lesions are observed in farmers as a result of constant irritation from the hairs on cow udders: due to milking.

In skin already affected by medical conditions friction may worsen the problem and may lead to new

lesions. For example, juvenile plantar dermatitis, which is a condition with the symptoms of glazed, shiny, and broken lamellar like scales on the skin, is often found on the frictional areas of the sides and under surfaces of the toes and forefeet of children between 3 and 14 years of age. There is a higher prevalence in the summer months and for those who wears synthetic socks or shoes [176]. Cowen [49] reports a case in which the lesions improved when the individual began to wear cotton socks, which may have contributed to lowering the frictional forces experienced on the skin.

6.2 Belt-Friction model

In this section we derive a pure-traction belt-friction model to describe the behaviour of dynamic true-membranes supported by static rigid foundations.

Let $\omega \subset \mathbb{R}^2$ be a simply connected open bounded domain with the sufficiently smooth boundary $\partial\omega$ and let $\boldsymbol{\sigma} \in C^2(\omega; \mathbf{E}^3)$ be an injective immersion. Now, assume that an isotropic elastic true-membrane is in contact with a rigid non-hyperbolic surface of positive mean-curvature such that in the stress-free configuration of the true-membrane the contact area can be parameterised by the immersion $\boldsymbol{\sigma}$. Now, assert that the true-membrane is dynamic, but the contact area remains static and constant as ω. Now, invoke the governing equations that is derived in chapter 2, the terminology from Section 1.5 and the time-dependence from Section 5.6 to find

$$\nabla_\alpha \tau^{\alpha\beta}(\boldsymbol{w}) + f_r^\beta(\boldsymbol{w}) + g_r^\beta = \varrho \left(\partial_{tt} w^\beta + \Gamma^\beta_{\alpha\gamma} \partial_t w^\alpha \partial_t w^\gamma\right) \ , \tag{76}$$

$$F_{[\mathrm{II}]\alpha\gamma} \tau^{\alpha\gamma}(\boldsymbol{w}) + f_r^3(\boldsymbol{w}) + g_r^3 = \varrho F_{[\mathrm{II}]\alpha\gamma} \partial_t w^\alpha \partial_t w^\gamma \ , \tag{77}$$

with the boundary conditions

$$n_\alpha \tau^{\alpha\beta}(\boldsymbol{w})|_{\partial\omega} = \tau_0^\beta \ , \ \forall \ \beta \in \{1, 2\} \ , \tag{78}$$

where $\boldsymbol{w} \in C^2(\omega; \mathbb{R}^2)$ is the displacement field and ϱ is the mass density of the true-membrane, $\boldsymbol{g} \in C^0(\omega; \mathbb{R}^3)$ is an external force density field, $f_r^\beta(\boldsymbol{w})$ are the shear force densities, $f_r^3(\boldsymbol{w})$ is the normal reaction density, $\boldsymbol{n} \in C^0(\omega; \mathbb{R}^2)$ is the unit outward normal to the boundary and $\boldsymbol{\tau}_0 \in C^0(\omega; \mathbb{R}^2)$ is a traction field.

Note that this pure-traction problem, and thus, the boundary traction field $\boldsymbol{\tau}_0$ cannot be arbitrary chosen. To proceed, assume that the velocity, the acceleration and the force density fields are known and fixed prior to the problem, and invoke the *compatibility condition for pure-traction problems* (see section 1.3.4 of Necas *et al.* [144] or section 1.8 of Ciarlet [38]) to find

$$\int_{\partial\omega} \tau_0^\beta u_\beta \, d(\partial\omega) + \int_\omega \left(f_r^\beta(\boldsymbol{w}) + g_r^\beta - \varrho \left(\partial_{tt} w^\beta + \Gamma^\beta_{\alpha\gamma} \partial_t w^\alpha \partial_t w^\gamma\right)\right) u_\beta \, d\omega = 0 \ ,$$
$$\forall \ \boldsymbol{u} \in \{\boldsymbol{v} \in \boldsymbol{H}^1(\omega) \mid \boldsymbol{\epsilon}(\boldsymbol{v}) = \boldsymbol{0}\} \ ,$$

where $\boldsymbol{\epsilon}(\cdot)$ is the strain tensor of the true-membrane. Note that the compatibility condition implies that the internal forces are balanced by all the applied external forces.

Now, assert that the contact area is rough and the friction law governing this region is governed by Kikuchi and Oden's [102] model for Coulomb's law of static friction for the slip case. Adapting this friction law to model membranes, with the techniques introduced in Section 2.2, one finds

$$f_r^\beta(\boldsymbol{w}) + \nu_F(w_\alpha w^\alpha)^{-\frac{1}{2}} w^\beta f_r^3(\boldsymbol{w}) = 0 \ , \tag{79}$$

where ν_F is the coefficient of friction with respect to Coulomb's law of friction. Now, one may rearrange the compatibility condition and use the modified Coulomb's law of friction (79) to find a relationship between the coefficient of friction and the external loadings as

$$\begin{aligned} \nu_F \int_\omega (w_\gamma w^\gamma)^{-\frac{1}{2}} f_r^3(\boldsymbol{w}) w^\alpha u_\alpha \, d\omega = & \int_{\partial\omega} \tau_0^\alpha u_\alpha \, d(\partial\omega) \\ & + \int_\omega \left(g_r^\alpha - \varrho \left(\partial_{tt} w^\alpha + \Gamma^\alpha_{\gamma\delta} \partial_t w^\gamma \partial_t w^\delta \right) \right) u_\alpha \, d\omega \ , \\ & \forall \ \boldsymbol{u} \in \{ \boldsymbol{v} \in \boldsymbol{H}^1(\omega) \mid \boldsymbol{\epsilon}(\boldsymbol{v}) = \boldsymbol{0} \} \ . \end{aligned} \tag{80}$$

Given that the fields $(\partial_t w^1, \partial_t w^2)$ and $(\partial_{tt} w^1, \partial_{tt} w^2)$ are known quantities prior to the problem, w^β and $f_r^j(\boldsymbol{w})$ give one five unknowns and equations (76), (77) and (79) provide one with five equations. Thus, the system is fully determined with respect to the boundary conditions (78). Furthermore, condition (80) provides one with a stronger system as, if the coefficient of friction is an unknown, then a known traction can close the system and vice versa. But does it mean that this model is valid? The answer is no. This belt-friction model is derived from a friction law that is design to model static bodies. We asserted that velocity and acceleration fields, $(\partial_t w^1, \partial_t w^2)$ and $(\partial_{tt} w^1, \partial_{tt} w^2)$ respectively, are known quantities prior to the problem, but speed and the acceleration may change during a given time interval. Finally, with our limited knowledge we cannot prove the existence of solution for this model. The problem of proving the existence of solutions arises from the function $f_r^\beta(\boldsymbol{w})$, as it is a function of both $\boldsymbol{w}$ and $\boldsymbol{\nabla w}$. If $f_r^\beta(\boldsymbol{w})$ is a purely a function of $\boldsymbol{w}$, then the existence of solutions maybe proved by variational methods for semi-linear elliptic equations (see Badiale and Serra [13]), but with the $\boldsymbol{\nabla w}$ dependence, our model is not even a variational problem. Closed system it maybe, but this model is flawed, and thus, any result that maybe generated from this model is merely speculative.

6.3 Numerical Analysis

To conduct numerical experiments assume a surface of revolution case, where the both contact surface and the unstressed true-membrane parameterised by the same immersion (i.e. an aximembrane case). Let this immersion be $\boldsymbol{\sigma}(x^1, x^2) = (x^1, \varphi(x^1)\sin(x^2), \varphi(x^1)\cos(x^2))_{\mathsf{E}}$, where $x^1 \in (0, l)$ and $x^2 \in (-\frac{1}{2}\pi, 0)$. To keep the contact area as a surface of positive mean-curvature, assert that $\varphi(x^1) = r_0 - 16c(l^{-1}x^1 - \frac{1}{2})^4$, where $c < r_0$. Note that l, c and r_0 are some positive constants that one can specify later. With some calculations, one finds that the first fundamental form tensor is $\boldsymbol{F}_{[\mathsf{I}]} = \mathrm{diag}((\psi_1)^2, (\psi_2)^2)$, where $\psi_1 = (1+(\varphi'(x^1))^2)^{\frac{1}{2}}$ and $\psi_2 = \varphi(x^1)$. With a few more calculations, one finds

$$\begin{aligned} \Gamma^1_{11} &= (\psi_1)^{-1}\partial_1\psi_1 \ , & F_{[\mathsf{II}]1}{}^1 &= (\psi_1)^{-1}\varphi''(x^1)\left(1+(\varphi'(x^1))^2\right)^{-1} \ , \\ \Gamma^2_{21} &= (\psi_2)^{-1}\partial_1\psi_2 \ , & F_{[\mathsf{II}]2}{}^2 &= -(\psi_2)^{-1}\left(1+(\varphi'(x^1))^2\right)^{-\frac{1}{2}} \ , \end{aligned}$$

where $\Gamma^{\gamma}_{\alpha\beta}$ are Christoffel symbols of the second kind and $\boldsymbol{F}_{[\mathrm{II}]}$ is the second fundamental form tensor. Now, given that $\boldsymbol{w} = (w^1(x^1, x^2), w^2(x^1, x^2))$ is the displacement field, one finds that the covariant derivatives are

$$\begin{aligned}
\nabla_1 w^1 &= \partial_1 w^1 + \Gamma^1_{11} w^1 \ , \\
\nabla_1 w^2 &= \partial_1 w^2 + \Gamma^2_{21} w^2 \ , \\
\nabla_2 w^1 &= \partial_2 w^1 - (\psi_1)^{-2} (\psi_2)^2 \Gamma^2_{21} w^2 \ , \\
\nabla_2 w^2 &= \partial_2 w^2 + \Gamma^2_{22} w^2 \ .
\end{aligned}$$

Now, assume that the membrane is subjected to the acceleration of gravity. i.e. subject to the field $(0, 0, -g)_{\mathsf{E}}$. With a coordinate transform, from Euclidean to curvilinear, one may re-expresses acceleration due to gravity in curvilinear coordinates as $g\boldsymbol{J}$, where

$$\boldsymbol{J} = \left(-\varphi'(x^1)(\psi_1)^{-2} \cos(x^2), (\varphi(x^1))^{-1} \sin(x^2), -(\psi_1)^{-1} \cos(x^2) \right) \ ,$$

and x^2 is the acute angle that the vector $(0, 0, 1)_{\mathsf{E}}$ makes with the vector $(0, \psi_2, 0)$.

Now, given that ϱ is the mass density, $(0, 0, 0)$ is the acceleration field and $(0, (\psi_2)^{-1} V, 0)$ is the velocity field of the membrane, one can express the governing equations of the membrane as

$$\begin{aligned}
(\Lambda - \mu)\partial^1 \left(\nabla_\alpha w^\alpha \right) + \mu \Delta w^1 + \varrho g J^1 + f^1_r(\boldsymbol{w}) &= -\varrho (\psi_1)^{-2} \Gamma^2_{21} V^2 \ , \\
(\Lambda - \mu)\partial^2 \left(\nabla_\alpha w^\alpha \right) + \mu \Delta w^2 + \varrho g J^2 + f^2_r(\boldsymbol{w}) &= 0 \ ,
\end{aligned}$$

and

$$\begin{aligned}
&\left(\Lambda \left(\partial_1 w^1 + \Gamma^1_{11} w^1 \right) + (\Lambda - 2\mu) \left(\partial_2 w^2 + \Gamma^2_{21} w^1 \right) \right) F_{[\mathrm{II}]}{}^1_1 \\
&\quad + \left((\Lambda - 2\mu) \left(\partial_1 w^1 + \Gamma^1_{11} w^1 \right) + \Lambda \left(\partial_2 w^2 + \Gamma^2_{21} w^1 \right) \right) F_{[\mathrm{II}]}{}^2_2 + \varrho g J^3 + f^3_r(\boldsymbol{w}) = \varrho F_{[\mathrm{II}]}{}^2_2 V^2 \ ,
\end{aligned}$$

where $\Lambda = 4(\lambda + 2\mu)^{-1} \mu(\lambda + \mu)$ and λ and μ are first and second Lamé's parameters respectively.

Assume that the contact area is rough, and thus, one obtains a final governing equation to solve the problem, which is

$$f^\beta_r(\boldsymbol{w}) + \nu_F (w_\alpha w^\alpha)^{-\frac{1}{2}} w^\beta f^3_r(\boldsymbol{w}) = 0 \ ,$$

where the coefficient of friction, ν_F, is considered to be an unknown. Now, divide the boundary into sub-boundaries as

$$\begin{aligned}
\partial\omega_f &= \{\{0\} \times (-\frac{1}{2}\pi, 0)\} \cup \{\{l\} \times (-\frac{1}{2}\pi, 0)\} \\
\partial\omega_{T_0} &= \{[0, l] \times \{-\frac{1}{2}\pi\}\} \ , \\
\partial\omega_{T_{\mathsf{max}}} &= \{\{[0, l] \times \{0\}\} \ ,
\end{aligned}$$

and assert that the boundary conditions are

$$\begin{aligned}
\left[(\Lambda - 2\mu) \left(\partial_1 w^1 + \Gamma^1_{11} w^1 \right) + \Lambda \left(\partial_2 w^2 + \Gamma^2_{21} w^1 \right) \right] |_{\partial\omega_{T_0}} &= \tau_0 \text{ (traction)} \ , \\
\left[(\Lambda - 2\mu) \left(\partial_1 w^1 + \Gamma^1_{11} w^1 \right) + \Lambda \left(\partial_2 w^2 + \Gamma^2_{21} w^1 \right) \right] |_{\partial\omega_{T_{\mathsf{max}}}} &= \tau_{\mathsf{max}} \text{ (traction)} \ ,
\end{aligned}$$

$$\left[\Lambda\left(\partial_1 w^1 + \Gamma^1_{11} w^1\right) + (\Lambda - 2\mu)\left(\partial_2 w^2 + \Gamma^2_{21} w^1\right)\right]|_{\partial\omega_f} = 0 \text{ (zero-Robin)} ,$$
$$\left[(\psi_1)^2 \partial_2 w^1 + (\psi_2)^2 \partial_1 w^2\right]|_{\partial\omega} = 0 \text{ (zero-Robin)} ,$$

where $\tau_{\mathsf{max}} > \tau_0$ are positive constants.

Now, take condition (80), where $\boldsymbol{u} \in \{\boldsymbol{v} \in \boldsymbol{H}^1(\omega) \mid \boldsymbol{\epsilon}(\boldsymbol{v}) = \boldsymbol{0}\}$, and modify it slightly to make it easier to numerically model by assuming $\boldsymbol{u} = (\psi_1, \psi_2)$ and $(w_\gamma w^\gamma)^{-\frac{1}{2}} w^\alpha u_\alpha = (u_\gamma u^\gamma)^{-\frac{1}{2}} u^\alpha u_\alpha$ to obtain

$$\sqrt{2}\,\nu_F \int_\omega f_r^3(\boldsymbol{w}) \psi_1 \psi_2 \, dx^1 dx^2 = (\tau_{\mathsf{max}} - \tau_0) \int_0^l \psi_1 \psi_2 \, dx^1 + \varrho \int_\omega \left(g J^\alpha \psi_\alpha + (\psi_1)^{-1} \Gamma^2_{21} V^2\right) \psi_1 \psi_2 \, dx^1 dx^2 . \tag{81}$$

Now, we are ready to conduct some numerical experiments. Our goal in this section is to investigate how variables such as the Gaussian curvature, Young's modulus, Poisson's ratio, speed and the mass density of the membrane, and tractions may affect the value coefficient of friction. Note that for our experiments we keep the values $\tau_0 = 1$, $l = 1$, $r_0 = 1$ and $g = 9.81$ fixed.

To conduct numerical experiments we employ the second-order-accurate finite-difference method in conjunction with Newton's method for nonlinear systems as in Section 2.6. Another issue we must tackle is the discretisation of the domain. As we are dealing with curvilinear coordinates, there is a inherit grid dependence. To be precise, it is approximately $\Delta x^2 \leq \psi_0 \Delta x^1$, $\forall\ \psi_0 \in \{(\psi_2)^{-1}\psi_1 \mid x^1 \in [0, l]\}$, where Δx^β is a small increment in x^β direction. For our purposes we use $\Delta x^2 = \frac{1}{N-1}$ and $\psi_0 = (\psi_2)^{-1}\psi_1|_{x^1 = \frac{1}{2}l}$, where $N = 250$. Finally, we must define a terminating condition. For this, we choose to terminate our iterating process once the condition $|1 - (\nu_{Fm})^{-1}\nu_{Fm+1}| < 10^{-8}$ is satisfied, where ν_{Fm} is the m^{th} iterative solution for the coefficient of friction. Note that to numerically model equation (81), we use the prismoidal formula [136]. Also, as this is a pure-traction problem, the solution is highly unstable. By construction we have $w^2|_{\partial\omega_{T_0}} \leq 0$, and thus, whenever this condition is violated we enforce the condition $w^2|_{\partial\omega_{T_0}} = 0$ to keep the solution from diverging out of control.

Now, recall the capstan equation with gravity from Section 2.5.2 and the dynamic case from Section 5.6. When adapted for our particular problem for the $c = 0$ and zero-Poisson's ratio case, the modified capstan equation has the form

$$\tau_{\mathsf{max}} = \tau_0 \exp\left(\frac{1}{2}\pi\mu_F\right) + \varrho\frac{V^2}{r_0}\left(1 - \exp\left(\frac{1}{2}\pi\mu_F\right)\right) + \varrho g\left(\frac{1-\mu_F^2}{1+\mu_F^2} + \frac{2\mu_F}{1+\mu_F^2}\exp\left(\frac{1}{2}\pi\mu_F\right)\right) . \tag{82}$$

We use this modified capstan equation (82) to calculate the capstan coefficient of friction to compare our data against. The reader must understand that the extended capstan equation from theorem 1 is only valid for when both Poisson's ratio and the Gaussian curvature are both zero, yet we use this value as a base line to compare Coulomb's coefficient of friction that we obtain from our belt-friction model.

Figure 61 is calculated with the values of $\tau_{\mathsf{max}} = \frac{3}{2}$, $c = 0$, $E = 10^3$, $\nu = \frac{1}{4}$, $V = 0.01$, $\varrho = 0.01$ and with a grid of 160×250 points. Figure 61 shows the axial (i.e. w^1) and the azimuthal (i.e. w^2) displacements, where width is l (i.e. the magnitude of x^1) and θ is the contact angle (i.e. x^2). The

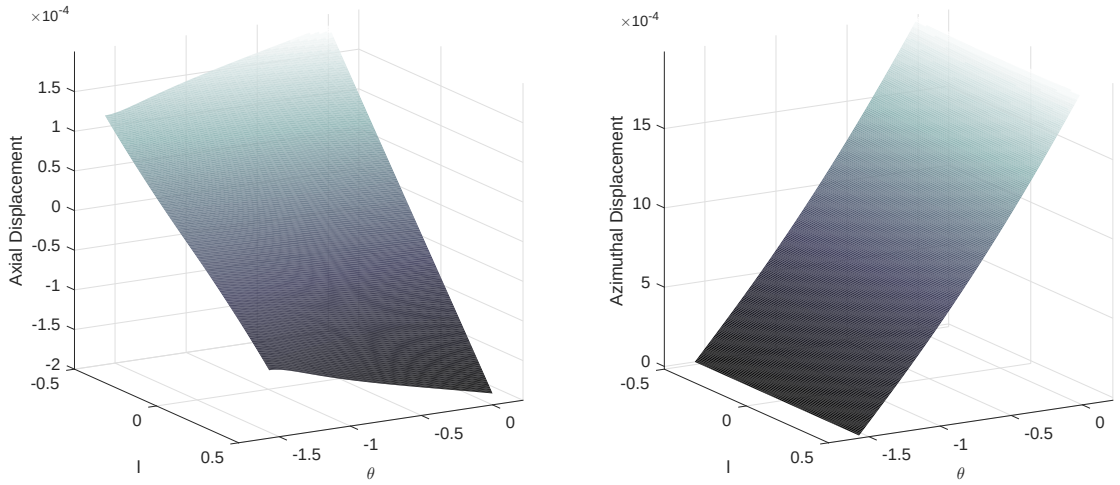

Figure 61: Displacement field of the membrane predicted by the belt-friction model.

maximum axial displacement is observed at $x^2 = 0$ with an axial displacement of $w^1 = 1.86 \times 10^{-3}$. The maximum azimuthal displacement is observed at $x^2 = 0$ with an azimuthal displacement of $w^2 = 1.96 \times 10^{-4}$. Coulomb's coefficient of friction calculated in this case is $\nu_F = 0.195$. If one approximate this problem with the modified capstan equation, by assuming $c = 0$ and $\nu = 0$, then one gets the value $\mu_F = 0.195$ for the capstan coefficient of friction.

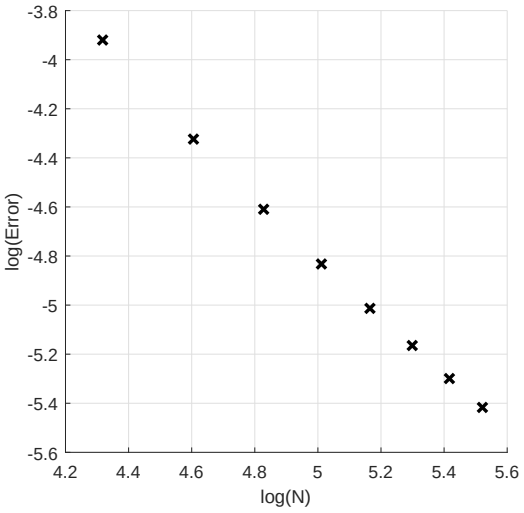

Figure 62: Grid dependence of the belt-friction model.

Another necessary numerical analysis we must perform is the grid dependence analysis for our numerical solution. As the reader can see from figure 62, as N increases, the difference between the numerical solution N and $N + 1$ decreases. For our experiments we found that the azimuthal grid points and the error share the relation $N \propto \text{Error}^{-0.808}$, where $\text{Error} = |1 - ||\boldsymbol{w}_{N-1}||_{\ell^2}^{-1} ||\boldsymbol{w}_N||_{\ell^2}|$. Note that figure 62 is calculated with the values of $\tau_{\text{max}} = \frac{3}{2}$, $c = 0$, $E = 10^3$, $\nu = \frac{1}{4}$, $V = 0.01$ and $\varrho = 0.01$.

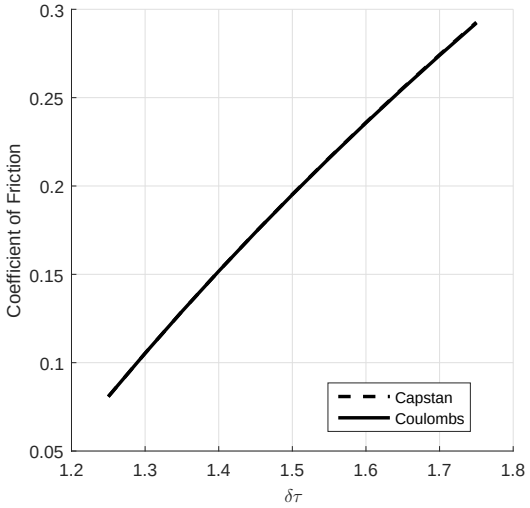

Figure 63: Coefficient of friction relative to $\delta\tau = \tau_{\max}/\tau_0$.

Figure 63 is calculated with the values $\delta\tau \in \{0, \frac{1}{20}, \frac{2}{20}, \frac{3}{20}, \frac{4}{20}, \frac{5}{20}, \frac{6}{20}, \frac{7}{20}, \frac{8}{20}, \frac{9}{20}\}$, $c = 0$, $E = 10^3$, $\nu = \frac{1}{4}$, $V = 0.01$ and $\varrho = 0.01$. It shows that as the tension ratio increases, the coefficient of friction also increases. This is intuitive as the maximum applied-tension increases, the coefficient of friction must increases to maintain a constant speed, and thus, a strong correlation between the tension ratio, and both capstan and Coulomb's coefficient of friction.

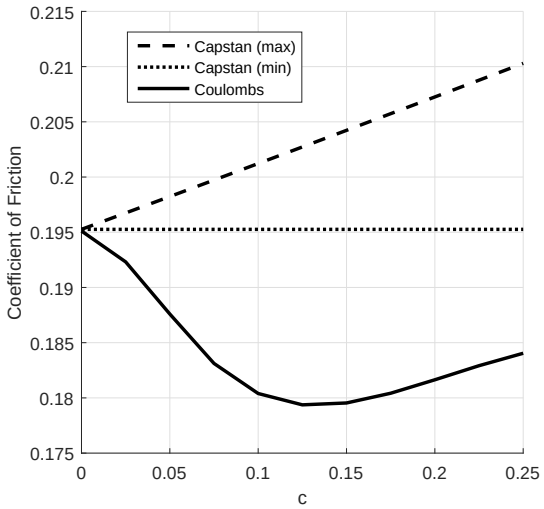

Figure 64: Coefficient of friction relative to c.

Now, let us examine what effect varying Gaussian curvature, $K = F_{[\mathrm{II}]1}{}^1 F_{[\mathrm{II}]2}{}^2$, has on the coefficient of friction. Note that K is a function of x^1, and thus, it varies across the contact surface. Let $x^1 \approx 0$ or $x^1 \approx 1$, then, if $c \approx 0$, then $K \approx 0$ and, if $c \approx 1$, then $K \approx (1-c)^{-1}$. This implies that there exists a positive correlation between c and K, i.e. as c increases so does K. Thus, we investigate how c related to ν_F. Figure 64 is calculated with the values $\delta\tau = \frac{3}{2}$, $c \in \{0, \frac{1}{40}, \frac{2}{40}, \frac{3}{40}, \frac{4}{40}, \frac{5}{40}, \frac{6}{40}, \frac{7}{40}, \frac{8}{40}, \frac{9}{40}\}$, $E = 10^3$, $\nu = \frac{1}{4}$, $V = 0.01$ and $\varrho = 0.01$. Figures 64 shows that as c increases (i.e. Gaussian curvature increases) coefficient of friction decreases and there exists an optimum value of c where the

coefficient of friction is a minimum. For our experiments this value is observed at $c = \frac{1}{8}$. The former part of the previous statement is intuitive. To illustrate this consider a membrane being pulled over a surface with high a Gaussian curvature. The higher curvature leads to a higher normal reaction force, which in turn results in a higher frictional force and finally a higher maximum applied-tension. Also, inclusion of a nonzero lateral curvature (note that we are considering a case with two positive principal curvatures) means that higher maximum applied-tension is required to support the strains in the lateral planer direction. Thus, for even a relatively small coefficient of friction a higher maximum applied-tension can be observed. Thus, one expects to see a low coefficient of friction for a high Gaussian curvature. However, the latter part of the former statement is a surprising outcome i.e. the existence of an optimum Gaussian curvature where the coefficient of friction a minimum. Furthermore, we observe that the capstan coefficient of friction is a gross over estimate of Coulomb's coefficient of friction and tends to contradicts the correlation for the values $c < \frac{1}{8}$. This overestimate is a result of Poisson's ratio, which we observe later.

Another set of numerical experiments that we conduct for is to examine the behaviour of the coefficient of friction relative to Young's modulus. For this, we use the values $\delta\tau = \frac{3}{2}$, $c = 0$, $1 \leq E \leq 10^{10}$, $\nu = \frac{1}{4}$, $V = 0.01$ and $\varrho = 0.01$. From our numerical experiments we find that the coefficient of friction is constant with the value $\nu_F = 0.195$. This result is intuitive as whatever the value of Young's modulus is (given that is not zero or infinite), one rescale the displacement field, $\boldsymbol{w}$, without affecting coefficient of friction. This result is also analogous to the capstan equation case as the capstan equation is also independent of Young's modulus of the membrane.

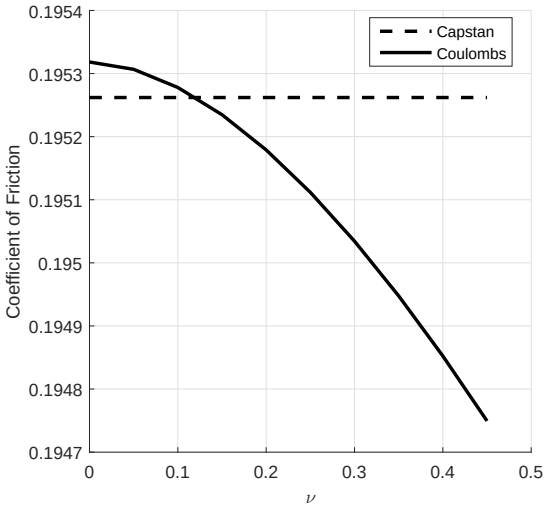

Figure 65: Coefficient of friction relative to ν.

Figure 65 is calculated with the values $\delta\tau = \frac{3}{2}$, $c = 0$, $E = 10^3$, $\nu \in \{0, \frac{1}{20}, \frac{2}{20}, \frac{3}{20}, \frac{4}{20}, \frac{5}{20}, \frac{6}{20}, \frac{7}{20}, \frac{8}{20}, \frac{9}{20}\}$, $V = 0.01$ and $\varrho = 0.01$. It shows that as Poisson's ratio decreases, the coefficient of friction also decreases. This is intuitive as tension in one direction leads to a tension in the lateral planer direction due to nonzero Poisson's ratio, and thus, one requires a larger maximum applied-tension to overcome friction relative to zero-Poisson's ratio case, which is a documented phenomenon in

the literature [96]. Thus, one expects to see coefficient of friction to decrease as Poisson's ratio increases. Furthermore, the figure also shows that when Poisson's ratio is zero, the capstan coefficient of friction it is an underestimate of Coulomb's coefficient of friction.

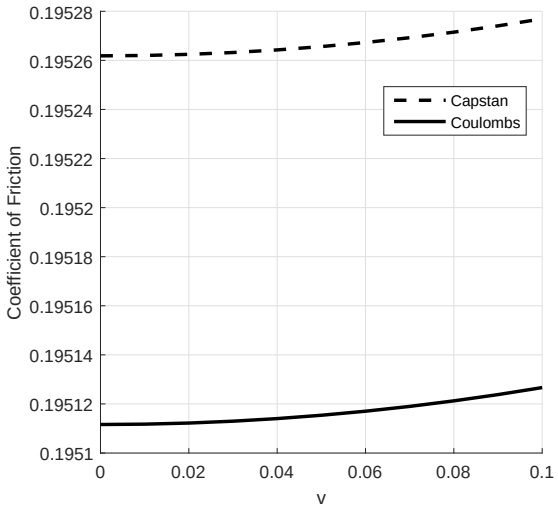

Figure 66: Coefficient of friction relative to V.

Figure 66 is calculated with the values $\delta\tau = \frac{3}{2}$, $c = 0$, $E = 10^3$, $\nu = \frac{1}{4}$, $V \in \{0, \frac{1}{100}, \frac{2}{100}, \frac{3}{10}, \frac{4}{10}, \frac{5}{10}, \frac{6}{10}, \frac{7}{10}, \frac{8}{10}, \frac{9}{10}, 1\}$ and $\varrho = 0.01$. It shows that as the speed in which the membrane is being pulled increases, the coefficient of friction also increases. This may seems counter intuitive, but consider following fact: a centripetal force is required to keep a body on a curved path, and higher the speed of the body is then higher (higher in magnitude) the centripetal force is required to keep the body in the given curved orbit. Thus, for our case a higher speed implies a lower normal reaction force, which in turn implies a lower frictional force. This means that one requires a lower maximum applied-tension, and this is also a result implied by the modified capstan equation. Thus, as the speed in which the membrane is being pulled increases, the coefficient of friction also increases.

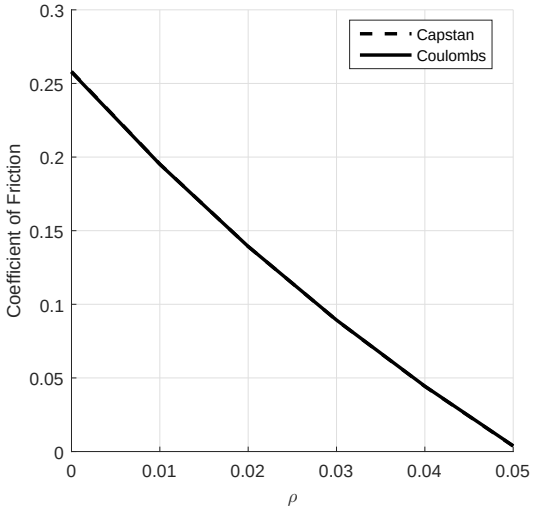

Figure 67: Coefficient of friction relative to ρ.

Figure 67 is calculated with the values of $\delta\tau = \frac{3}{2}$, $c = 0$, $E = 10^3$, $\nu = \frac{1}{4}$, $V = 0.01$ and $\varrho \in \{0, \frac{1}{10}\frac{2}{10}, \frac{3}{10}, \frac{4}{10}, \frac{5}{10}, \frac{6}{10}, \frac{7}{10}, \frac{8}{10}, \frac{9}{10}, 1\}$. This shows as the mass density (with respect to the volume) of the membrane increases, both capstan and Coulomb's coefficient of friction decreases significantly. Out of all the numerical experiments this has is the most significant result as for a relatively small decrease in mass density leads to such an enormous increase in the coefficient of friction, for both capstan and Coulomb's. Thus, for a given membrane mass density appears to be the most significant variable that affects the value of the coefficient of friction.

6.4 Experimental Data: June 2015 Trial

In this section we analyse the data obtained from experiments that we conducted on human subjects based on Cottenden *et al.* [45], Cottenden *et al.* [46] and Cottenden *et al.*'s [48] experimental methodology. We recruit 10 subjects, 5 males and 5 females, all between the ages of 18 to 60, and we obtained the approval to do so from the UCL Research Ethics Committee: UCL Ethics Project ID number 5876/001. Experimentee data is found in table 2 if the reader wishes to reproduce any results, where BMI is the body mass index, Radius is the radius of the mid upper arm and δl is a measure of how *flaccid* subject's tissue is. For more comprehensive set of raw data please consult Dr N. Ovenden of UCL at n.ovenden@ucl.ac.uk.

Subject	Gender	Age (Years)	BMI	Radius (cm)	δl
F19	Female	19	21.0	3.98	0.994
F34	Female	34	22.0	4.22	0.991
F40	Female	40	23.4	3.82	1.01
F53	Female	53	27.3	4.54	1.02
F60	Female	60	22.5	4.46	1.02
M18	Male	18	17.5	3.50	0.98
M23	Male	23	24.7	4.77	1.04
M25	Male	25	22.6	4.22	1.01
M26	Male	26	22.8	4.50	0.988
M54	Male	54	26.2	5.09	1.00

Table 2: Experimentee data 2015.

Our experimental configuration is as follows. We first record subject's gender, age, height, weight and the dimension of their upper arm. Then, we place their upper arm horizontally, bicep facing upwards, on an armrest that is designed for subject's comfortability during the experiments. The armrest acts also as a restraint to limit subject's movement, and thus, to reduce the chance of skewed data. Then, we place a fabric (a nonwoven fabric) over their bicep and attach one end to the tensometer (Dia-Stron MTT170 provided by Dr S. Falloon of UCL). The dimensions of the fabric is 4cm$\times 50$cm, and from our measurements, the fabric has an approximate thickness of 0.5mm and an approximate mass of 0.6g. It is given to us that the fabric is 95% polypropylene and 5%

cotton, but no further information (Young's modulus, Poisson's ratio, manufacturer's details) is given to us. Finally, we mark the skin with a 3cm$\times 5$cm grid with 1cm$\times 1$cm grid spacing, 0.5cm away from either side of the fabric and starting from the highest part (of the horizontal axis) of the arm, then placing semi-hemispherical markers with a radius of 2mm. See figure 68 for a visual representation.

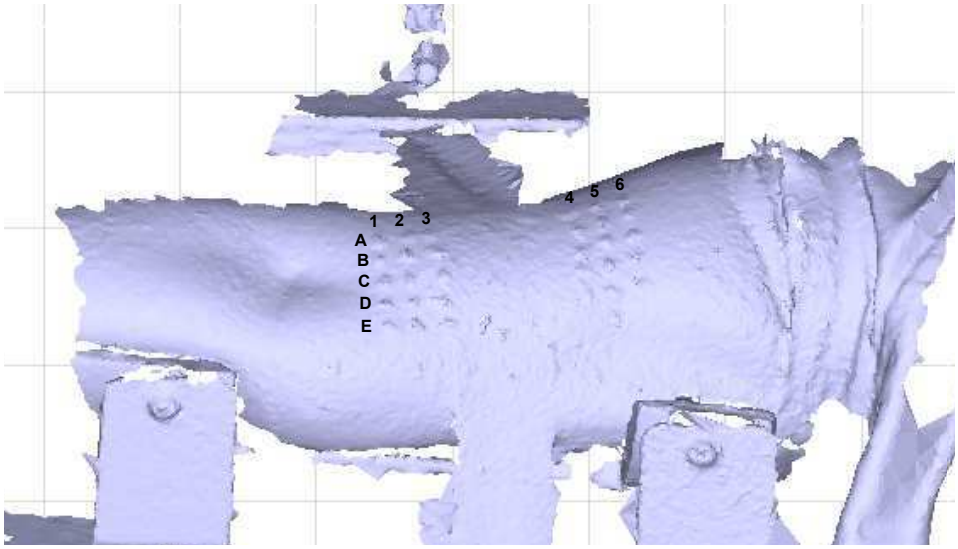

Figure 68: Experimental configuration on subject F53 (.stl file).

Our experimental methodology is as follows. We attach the free end of the fabric to various masses that are included in the set $\{40\text{g}, 60\text{g}, 80\text{g}, 100\text{g}, 120\text{g}, 140\text{g}\}$ and we pull the fabric with a constant speed of $\frac{1}{6}$cms^{-1}. We use the tensometer to record the tension needed to pull the fabric, we use a static-3D scanner (3dMD Photogrammetric System[13] provided by Mr C. Ruff of UCLH) to record the before and after deformation of the upper arm, and we use a video camera to record everything in real time as well as to record any other phenomena. We repeat experiment for each applied mass at least twice and take 3D scanning data at least six times per each experiment, recording two undeformed scans and four deformed scans. Thus, in sum, we obtain a minimum of 120 tensometer readings and a minimum of 720 3D scans. Each of the $21,600$ grid-point marker-locations are located manually by calculating each marker position on the .stl files that is generated by the 3D scanner. Note that most experiments are repeated, in the cases of obvious undesirable events, to get the most consistent results. Also, a new fabric (same type and dimensions) is used per each subject for health and safety reasons, and a very specific side of the fabric is chosen to face subjects' skin as the coefficient of friction between different sides fabric and subjects' skin may skew the experimental results.

The justification for why we chosen to conduct the experiments on the upper arm in the vicinity of the bicep is that the surface has two degrees of approximate symmetry. Also, as the bicep is a single muscle, one may argue that this area is locally homogeneous and approximately isotropic. Thus, from a modelling perspective this is a very convenient body part to numerically model.

[13] http://3dmd.com

One of the biggest problems we faced with these experiments is the difficulty in obtaining accurate data. The contributing factors that reduce the reliability of data are: (i) The markers that we use must to be large enough so that there are visible in the .stl files, which are generated by the 3D scanner, but this inherently introduces a very large error in the region of 2mm$\times 4$mm$\times 4$mm, as every time we select a marker, we cannot guarantee on the exact location on the marker that we are selecting. This margin of error is relatively high as most marker displacements from the unstrained position is less than 4mm; (ii) Due to the obscure angle of the 3D scanner some of the markers cannot be identified on the .stl files. Very often the unidentifiable markers are **A1** to **A3**; (iii) The tensometer uses Windows 98 operating system to function, and thus, it is often prone to crashes, leading to much data loss; (iv) Subjects' inability remain stationary during the course of the experiment have skewed the data significantly. Note that duration of each experimental run is approximately 3 minutes. Even with constant breaks no subject is capable of staying perfectly stationary for 3 minutes at a time for at least 12 times; (v) Stick and slip behaviour. The error introduced by selecting marker positions can be minimised if we use much larger masses, but with larger masses we often observe stick and slip behaviour (see section 13.2 of Kikuchi and Oden [102] for more on stick and slip behaviour) with an approximate frequency of 1Hz. This is huge problem and it is mostly observed in younger subjects, especially in F19, M18 and M23. In fact, for F19 this phenomenon is observed for the lowest of masses. The reason why stick and slip phenomenon is a problem is that the 3D scanner takes an instant scan, i.e. a snapshot like an ordinary camera, and thus, if the snapshot is taken in the stick period, then the scanner can record the true deformation, but, if the snap shot is taken during the slip period, then the scanner cannot record the true deformation as the skin of the subject is relaxed and it is now in between a state of full and zero deformation; (vi) The perspiration of the subject during the experiment. In the literature, hydration of the skin shown to significantly increase the coefficient of friction between skin and fabrics [55, 170]. During the course of the experiment the level of a subject's perspiration may change and this may significantly skew the data. In our experiments heavy perspiration is observed in the subjects M23 and M26; (vii) We cannot measure the physical and elastic properties (Young's modulus, Poisson's ratio, internal biological structure and dimensions) of subject' upper arm. Thus, we are deprived of vital data that are required for a three-dimensional numerical model.

Table 3 shows the tension ratio, $\delta\tau = T_{\text{max}}/T_0$, for each subject with respect to each applied mass, where T_{max} are the tensometer readings, $T_0 =$ Mass $\times\, g$ are the weight of the applied mass and $g = 9.81$ is the acceleration due to gravity. Note that the tensometer data of F34 for 60g, M25 for 140g and M54 for 40g are corrupted.

Cottenden *et al.* [45], Cottenden *et al.* [46] and Cottenden *et al.*'s [48] experimental methodology implies that belt-friction modes, capstan equation in particular, can be used to accurately calculate the coefficient of friction between in-vivo skin and fabrics. However, belt-friction models assume that the foundation is rigid, and thus, it is now unsuitable to apply a belt-friction model to calculate the coefficient friction as now the foundation is not rigid, i.e. as subjects' tissue is elastic. If belt-friction models are applicable to model coefficient of friction as the authors assert, then we expect to see a

Subject	$\delta\tau$					
	40g	60g	80g	100g	120g	140g
F19	2.19	1.70	1.52	1.92	1.88	1.86
F34	2.08	$\cdots$	1.93	1.89	1.83	1.83
F40	1.99	1.96	1.92	1.89	1.88	1.79
F53	2.13	2.31	2.23	2.15	1.84	1.70
F60	2.29	2.20	2.06	1.99	1.96	1.95
M18	1.99	1.90	1.88	1.84	1.68	1.76
M23	2.46	2.28	2.24	2.19	2.33	1.99
M25	2.14	1.98	1.81	1.80	1.98	$\cdots$
M26	2.41	2.31	2.26	2.18	2.31	1.99
M54	$\cdots$	2.12	2.03	1.77	1.91	1.96

Table 3: Experimental data 2015.

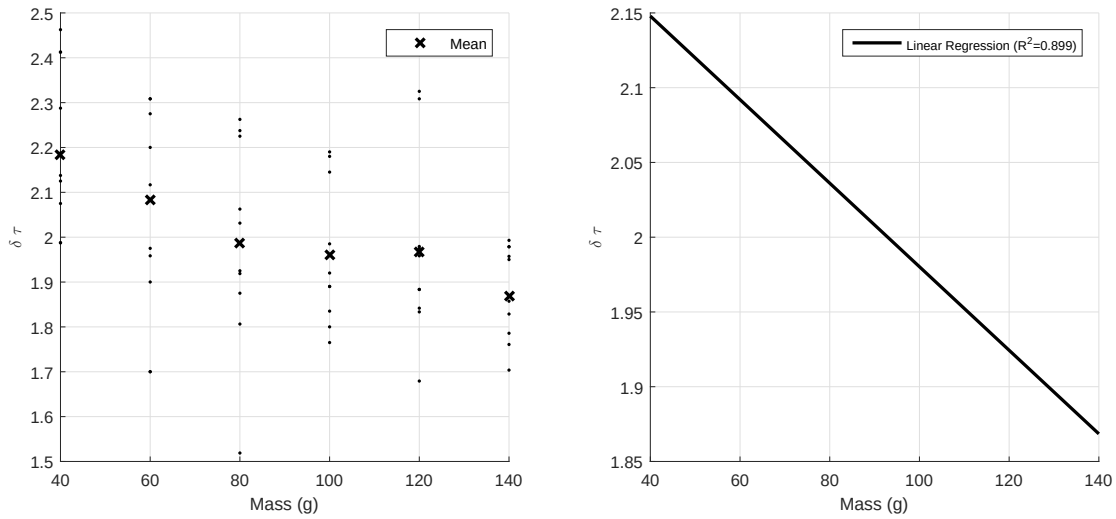

Figure 69: Tension ratio against applied mass (in grams).

constant relationship between tension ratios and the applied masses. But, if one consult figure 69, one can see the how the tension ratio vary with the applied mass. In fact, if one calculates the mean coefficients friction between the fabric and subjects' skin, a non-constant relationship between the coefficients of friction and the applied mass is evident (see figure 70). This offers clear evidence that belt-friction models are not suitable for measuring the coefficient of friction when the foundation is no longer rigid. Note that the mean values of Coulomb's coefficient of friction is calculated with the belt-friction model for $E = 10^3$, $\nu = \frac{1}{4}$ and a terminating error of 10^{-8}. Also, mean values capstan coefficient of friction is calculated with the extended capstan equation (82) with Matlab fsolve function.

Cottenden *et al.* [45], Cottenden *et al.* [47] and Karavokyros [100] do acknowledge this problem and assert that the there exists a c_0 such that $T_{\text{max}} = c_0 + T_0 \exp(\mu_F \theta_0)$, where c_0 is the inter-

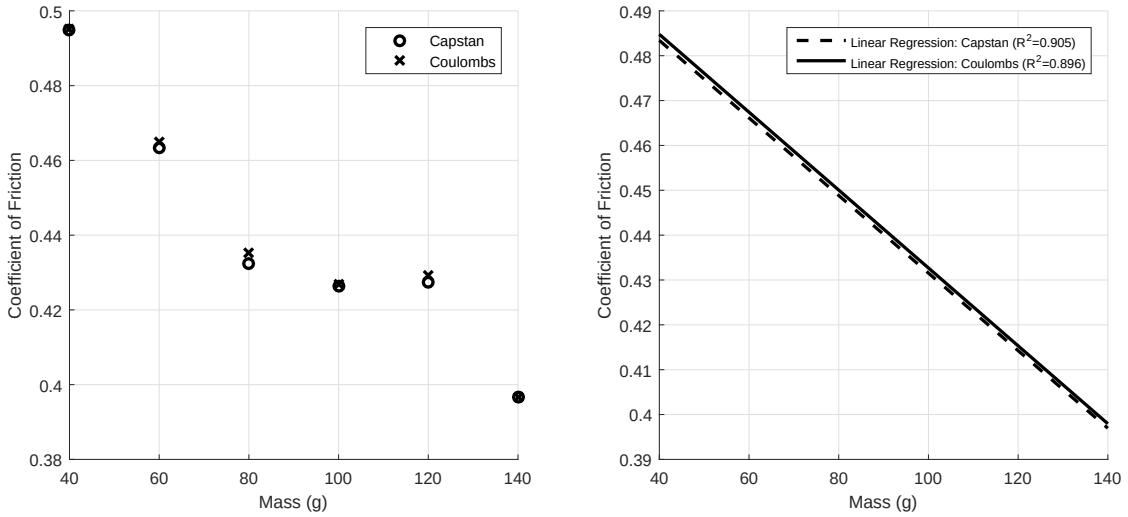

Figure 70: Coefficient of fiction against the applied mass (in grams).

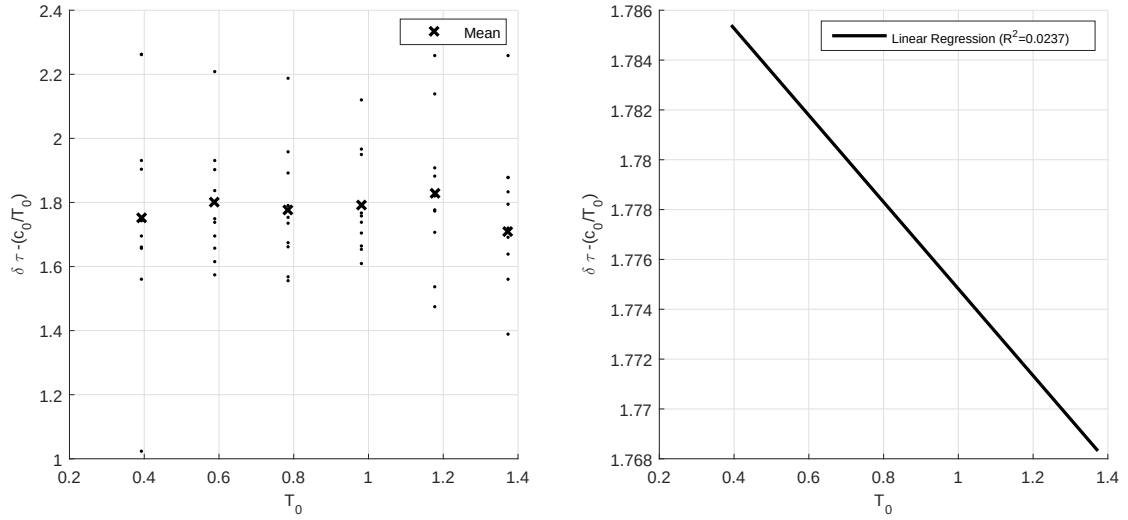

Figure 71: $\delta\tau - (c_0/T_0)$ against T_0.

cept of the linear regression line of T_{max} on T_0, which the authors define as the offset. Thus, the authors imply that $\delta\tau - (c_0/T_0)$ is a constant for all T_0 as $\exp(\mu_F\theta_0)$ is a constant, where θ_0 is a fixed contact angle. Now, assuming a linear relationship between T_{max} and T_0 is possible (linear in a sense of regression); if one calculates this offset of each subject F19, F34, F40, F53, F60, M18, M23, M25, M26 and M54 with linear regression, then one respectively gets the values $-0.0290, 0.149, 0.130, 0.432, 0.214, 0.168, 0.219, 0.187, 0.0589,$ and 0.109 for c_0. Now, if one plots $\delta\tau - (c_0/T_0)$ against T_0, then one gets figure 71. As the reader can see that $\delta\tau - (c_0/T_0)$ is not constant with respect to T_0 as the authors asserted, i.e. we get $\delta\tau - (c_0/T_0) = -0.0174T_0 + 1.79$ with $\text{R}^2 = 0.0237$, where R^2 is the coefficient of determination. In fact, logarithmic regression implies that the mean maximum applied-tension is related to the mean minimum applied-tension by $0.396T_{\text{max}} + 1 = 2.34\log(0.396T_0 + 1) + 0.997$ with a residual sum of squares of rss $= 1.00 \times 10^{-3}$ and a coefficient of determination of $\text{R}^2 = 0.997$, while authors' data analysis methodology implies that $T_{\text{max}} = 0.196 + 1.74T_0$ with a higher residual sum of squares of rss $= 9.85 \times 10^{-3}$ and a lower coefficient of determination of $\text{R}^2 = 0.995$. Furthermore, calculating the coefficient of friction with

authors' linear regression method leads to a positive correlation between the coefficient of friction and the radius of subjects' upper arm, which is not a desirable result and we explain why this is so in later analysis. Now, this is direct evidence that one must not use linear regression models to model friction between fabrics and in-vivo skin. Note that all regression results are calculated with Regression Tools at Xuru's Website [214].

The above numerical and regression analysis motivates one to make the following hypothesis:

Hypothesis 4. *Consider a rectangular membrane over a rough elastic prism whose unstrained contact region parameterised by the map* $(x, f(\theta), g(\theta))_E$*, where* $f(\cdot)$ *and* $g(\cdot)$ *are* $C^1([\theta_0, \theta_{max}])$ 2π*-periodic functions,* $|x| \leq \infty$*, and the contact interval* $[\theta_0, \theta_{max}]$ *is chosen such that* $g'f'' - f'g'' > 0$*,* $\forall\ x^2 \in [\theta_0, \theta_{max}]$*. If* T_{max} *is the maximum applied-tension at* θ_{max} *and* T_0 *is the minimum applied-tension at* θ_0*, then there exists a regression curve* $Y(\cdot)$ *of the form* $\varepsilon T_{max} + \xi = Y(\varepsilon T_0 + \xi)$*, such that* $Y'(\xi)$ *is positive and invariant with respect to the quantity*

$$r_0 = \left(\arctan\left(\frac{g'(\theta_0)}{f'(\theta_0)}\right) - \arctan\left(\frac{g'(\theta_{max})}{f'(\theta_{max})}\right)\right)^{-1} \int_{\theta_0}^{\theta_{max}} \left((f')^2 + (g')^2\right)^{\frac{1}{2}}\ d\theta\ ,$$

where the normalising constant ε *is chosen such that* $\varepsilon \leq 1/max(T_{max})$ *and the translating constant* ξ *is chosen such that* $Y'(\xi)$ *is not singular. Furthermore, given such a regression curve* $Y(\cdot)$*, the coefficient of friction* μ_F *has the following relation,*

$$\mu_F = \left(\arctan\left(\frac{g'(\theta_0)}{f'(\theta_0)}\right) - \arctan\left(\frac{g'(\theta_{max})}{f'(\theta_{max})}\right)\right)^{-1} \log\left(Y'(\xi)\right)\ ,$$

and, in particular, μ_F *is independent of* r_0*.*

Given a rectangular membrane with a zero-Poisson's ratio over a rigid cylinder, in our experimental configuration the solution for the tension across the membrane takes the form described by equation (82) (see Section 6.3 for more detail). Thus, the regression curve of T_{max} on T_0 can be expressed as $T_{\text{max}} = c_0 + c_1 T_0$, where

$$c_0 = \varrho l h \frac{V^2}{r_0}\left(1 - \exp\left(\frac{1}{2}\pi\mu_F\right)\right) + \varrho l h g\left(\frac{1-\mu_F^2}{1+\mu_F^2} + \frac{2\mu_F}{1+\mu_F^2}\exp\left(\frac{1}{2}\pi\mu_F\right)\right)\ ,$$
$$c_1 = \exp\left(\frac{1}{2}\pi\mu_F\right)\ ,$$

and where l is the width and h is the thickness of the membrane, and thus, $\mu_F = 2\pi^{-1}\log(c_1)$. However, if one consider a membrane of nonzero Poisson's ratio or an elastic prism, then this linear regression line of T_{max} on T_0 will no longer hold. Thus, hypothesis 4 is a simple extension of this observation with the use of theorem 1. Note that Doonmez and Marmarali [59] used multiple regression analysis to study the coefficient of friction, and thus, further justifying the necessity for hypothesis 4.

Due to the finite deformation of both the membrane and the foundation under stress we predict that the regression curve has the form $Y(\varepsilon T_0 + 1) = a + b(\varepsilon T_0 + 1) + c\log(\varepsilon T_0 + 1)$, where a, b and c are constants to be determined by a given experiment and the $\log(\cdot)$ term is implied by the true strain (for more on true strain please consult Rees [167]). Thus, in our experimental configuration we have $\mu_F = 2\pi^{-1}\log(b + c)$. Unfortunately, our experimental data is not comprehensive enough and

our understanding in regression analysis is not extensive enough to test this hypothesis or more generally to test hypothesis 4.

As we cannot calculate the coefficient of friction with a good degree of accuracy, let us use the tension ratio, $\delta\tau$, to find some useful information regarding the frictional interaction between in-vivo skin and fabrics. Note that figure 63 from our numerical analysis implies that there exists a strong positive correlation between the tension ratio and the coefficient of friction. Thus, the tension ratio from our experiments maybe used to infer the nature of the coefficient of friction between subjects' skin and the fabric.

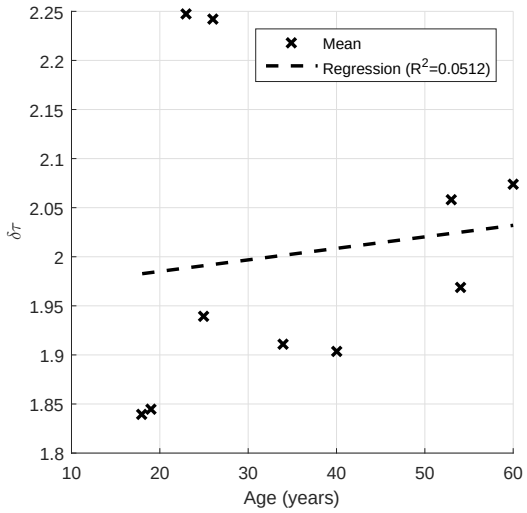

Figure 72: Coefficient of fiction against the age (in years).

Figure 72 shows the tension ratio against subjects' age, where the linear regression line is $\delta\tau = 0.00117 \times$ Age $+ 1.96$ and the age is in years ($R^2 = 0.0512$). As the reader can see there is no obvious relationship between the age of the subject and the tension ratio. In fact, the highest tension ratios are observed in M23 and M26 (two of the youngest subjects) who were excessively perspiring during the course of the experiments.

Figure 73 shows the tension ratio against the body mass index (BMI), where the linear regression line is $\delta\tau = 0.0169 \times$ BMI $+ 1.61$ ($R^2 = 0.0961$). Note that the BMI is calculated with the use of the NHS BMI calculator [199]. As the reader can see that there is a vague positive correlation between the BMI and the tension ratio. However, this does neither imply nor does not imply that those who are with a higher BMI have a greater risk of skin abrasion, i.e *correlation does not imply causation* [6]. The reason we observe this correlation is because that those who have a higher BMI tend to have a greater fat content, i.e. higher volume of flaccid tissue. Thus, during the experiments a higher tension needs to be applied to the fabric as the as a portion of the tension is expended on deforming the flaccid tissue of the subject. If this higher tension is fed in to a belt-friction model, then what one gets in return is a higher coefficient of friction. This is a perfect example of *garbage in, garbage out* [177], where a logical numerical model outputting nonsensical gibberish due to flawed

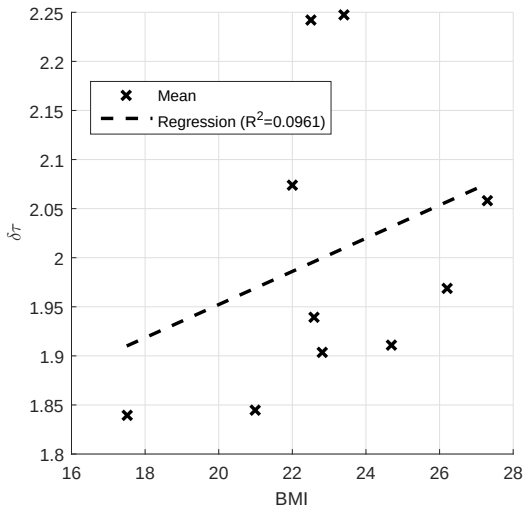

Figure 73: Coefficient of fiction against the BMI.

input data.

To see if this is indeed the case let us examine how flaccid subjects' tissue are and what effect the flaccidity has on the tension ratio, and thus, on the coefficient of friction. Recall figure 68. From experiments we found that the marker that is most prone to displacement is **A4** and the least prone to displacement is **E6**. Thus, if we define relative distance ratio δl to be the Euclidean distance between the point **A4** and **E6** after deformation divided by the distance between the point **A4** and **E6** before deformation, i.e.

$$\delta l = \frac{\sum_{10\text{g},\ldots,140\text{g}} ||\text{deformed}(\mathbf{A4} - \mathbf{E6})||}{\sum_{10\text{g},\ldots,140\text{g}} ||\text{undeformed}(\mathbf{A4} - \mathbf{E6})||} \,,$$

(see table 2), then this be a good quantity to measure how flaccid subject's tissue is (inspired by the spring modules).

The reasoning for defining δl as above is as follows: (i) it utilises the marker that is most prone to displacement, and thus, reducing the error introduced by selecting position of the marker as we discussed previously, (ii) the subjects tend to move during the experiments, and thus, the results can be significantly skewed with respect to a fixed point, yet the relative distance between the points **A4** and **E6** due to rigid transformations should remain fairly constant, (iii) the 3D scanner chooses a reference point arbitrarily after each calibration, but the relative distance between two points in space always remain constant, and (iv) δl is a ratio, and thus, it is not dependent on subjects' physical dimensions.

Figure 74 shows the tension ratio against δl, where the linear regression line is $\delta\tau = 4.39 \times \delta l - 2.41$ ($R^2 = 0.282$). As the reader can see that there is a positive correlation between δl and the tension ratio. This further supports our hypothesis that more flaccid tissue leads to the appearance of a higher coefficient of friction as a portion of the maximum applied-tension is expended on deforming subject's tissue.

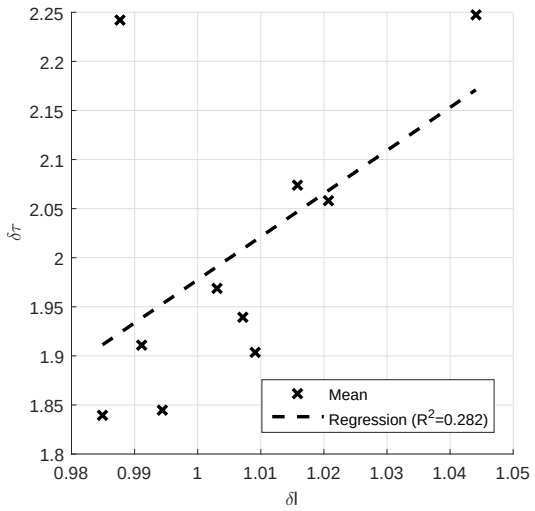

Figure 74: Coefficient of fiction against the δl.

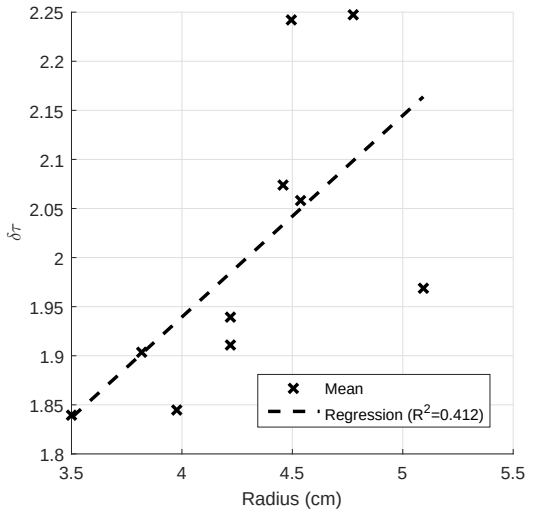

Figure 75: Coefficient of fiction against the radius of the upper arm (in cm).

Figure 75 shows the tension ratio against the radius of the mid part of the upper arm, where the linear regression line is $\delta\tau = 0.205 \times$ Radius $+ 1.12$ and the radius is in centimetres ($R^2 = 0.412$). Note that the Radius is calculated by measuring the girth around the bicep when the arm is held horizontally, but relaxed, while the palm is facing up, and then then dividing to measurement by 2π. As the reader can see that see there is a strong positive correlation between the radius and the tension ratio. However, this does neither imply nor does not imply that those who have larger biceps have a greater risk of skin abrasion. The reason why we observe this correlation is exactly same as the cases before. The larger the radius is, the larger the volume of tissue that needs to be deformed, and thus, a larger maximum applied-tension. This, in turn, leads to a larger coefficient of friction predicted by belt-friction models.

From figures 73, 75 and 74, one can clearly see that the very presence of an elastic foundation

leads to a nonlinear relationship between T_0 and T_{max}, which in turn can significantly skew ones experimental results if one uses a belt-friction model to calculate the coefficient of friction.

6.4.1 Remark

A possible technique that maybe used to measure the coefficient of friction of human skin is by a method proposed by Asserin *et al.* [9]. The authors construct a device that is capable of measuring the coefficient of friction between a reference material and in-vivo human skin. They state that the device is accurate enough to discern the arithmetic mean of roughness between the values 0.4μm–50μm, where μm is the units for micrometers. The in-vivo experiments are conducted on three human subjects. They is all female with each having the ages 20, 42 and 50. The authors calculate the coefficient of friction of the 42 year old female's lower arm which is 0.7, but the coefficient of friction with respect to what reference material is not specified. With their device the authors hope to investigate the change in texture of the skin due to the application of cosmetic products.

6.5 Shell-Membranes Supported by Elastic Foundations with Static Friction

In this section we derive a shell-membrane model to describe the behaviour of overlying membranes on elastic foundations subjected to static friction. Recall our shell model with friction from chapter4, but now assume that the thickness of the shell is so thin and the bending moments are so small that the overlying body can further be approximated by a shell-membrane. Thus, we obtain:

Corollary 5. *Let $\Omega \subset \mathbb{R}^3$ be a connected open bounded domain that satisfies the segment condition with a uniform-$C^1(\mathbb{R}^3;\mathbb{R}^2)$ boundary $\partial\Omega$ such that $\omega, \partial\Omega_0 \subset \partial\Omega$, where $\bar{\omega} \cap \partial\bar{\Omega}_0 = \emptyset$ with $\operatorname{meas}(\partial\Omega_0;\mathbb{R}^2) > 0$, and let $\omega \subset \mathbb{R}^2$ be a connected open bounded plane that satisfies the segment condition with a uniform-$C^1(\mathbb{R}^2;\mathbb{R})$ boundary $\partial\omega$. Let $\bar{\boldsymbol{X}} \in C^1(\bar{\Omega};\boldsymbol{E}^3)$ be a diffeomorphism and be $\boldsymbol{\sigma} \in C^2(\bar{\omega};\boldsymbol{E}^3)$ be injective an immersion. Let $\boldsymbol{f} \in \boldsymbol{L}^2(\Omega)$, $\boldsymbol{f}_0 \in \boldsymbol{L}^2(\omega)$ and $\boldsymbol{\tau}_0 \in \boldsymbol{L}^2(\partial\omega)$. Then there exists a unique field $\boldsymbol{u} \in \boldsymbol{V}_{\mathscr{M}}(\omega,\Omega)$ such that $\boldsymbol{u}$ is the solution to the minimisation problem*

$$J(\boldsymbol{u}) = \min_{\boldsymbol{v}\in\boldsymbol{V}_{\mathscr{M}}(\omega,\Omega)} J(\boldsymbol{v}) \ ,$$

where

$$\boldsymbol{V}_{\mathscr{M}}(\omega,\Omega) = \{\boldsymbol{v} \in \boldsymbol{H}^1(\Omega) \mid \boldsymbol{v}|_\omega \in H^1(\omega)\times H^1(\omega)\times L^2(\omega), \boldsymbol{v}|_{\partial\Omega_0} = \boldsymbol{0}, \left[2\nu_F v^3 + (v_\alpha v^\alpha)^{\frac{1}{2}}\right]|_\omega \leq 0 \text{ a.e.}\} \ ,$$

$$\begin{aligned} J(\boldsymbol{u}) = &\int_\Omega \left[\frac{1}{2}A^{ijkl}E_{ij}(\boldsymbol{u})E_{kl}(\boldsymbol{u}) - f^i u_i\right] d\Omega \\ &+ h\int_\omega \left[\frac{1}{2}B^{\alpha\beta\gamma\delta}\epsilon_{\alpha\beta}(\boldsymbol{u})\epsilon_{\gamma\delta}(\boldsymbol{u}) - f_0^i u_i\right] d\omega - h\int_{\partial\omega} \tau_0^\alpha u_\alpha \ d(\partial\omega) \ , \end{aligned}$$

h is the thickness of the shell-membrane and ν_F is the coefficient of friction between the foundation and the shell-membrane.

Proof. Follows from theorem 4 for the $h^2\rho_\alpha^\gamma(\boldsymbol{u})\rho_\gamma^\alpha(\boldsymbol{u}) \ll \epsilon_\alpha^\gamma(\boldsymbol{u})\epsilon_\gamma^\alpha(\boldsymbol{u})$ case and the results on shell-membranes from chapters 4 and 5 of Ciarlet [38]. □

6.6 Numerical Analysis

To conduct numerical experiments assume a shell-membrane with a thickness h, supported by an elastic foundation, where the unstrained configuration of the foundation is an annular cylindrical which is characterised by the diffeomorphism $\bar{X}(x,\theta,r) = (x, r\sin(\theta),\ r\cos(\theta))_{\mathsf{E}}$, where $(x^1,x^2,x^3) = (x,\theta,r)$, $x \in (-L,L)$, $\theta \in (-\pi,\pi]$ and $r \in (a_0,a)$, and assume that the contact region is defined by $x \in (-\ell,\ell)$, $\theta \in (-\frac{1}{2}\pi,0)$, where $0 < \ell < L$. Let the sufficiently smooth field $\boldsymbol{u} = (u^1(x,\theta,r), u^2(x,\theta,r), u^3(x,\theta,r))$ be the displacement field of the foundation. With some calculations one finds that the metric tensor is $\boldsymbol{g} = \operatorname{diag}(1,r^2,1)$ and the covariant derivatives are

$$
\begin{aligned}
&\bar{\nabla}_1 u^1 = \partial_1 u^1 \,, && \bar{\nabla}_1 u^2 = \partial_1 u^2 \,, && \bar{\nabla}_1 u^3 = \partial_1 u^3 \,,\\
&\bar{\nabla}_2 u^1 = \partial_2 u^1 \,, && \bar{\nabla}_2 u^2 = \partial_2 u^2 + r^{-1} u^3 \,, && \bar{\nabla}_2 u^3 = \partial_2 u^3 - r u^2 \,,\\
&\bar{\nabla}_3 u^1 = \partial_3 u^1 \,, && \bar{\nabla}_3 u^2 = \partial_3 u^2 + r^{-1} u^2 \,, && \bar{\nabla}_3 u^3 = \partial_3 u^3 \,.
\end{aligned}
$$

With further calculations, one can express the governing equations of the foundation as

$$
\begin{aligned}
(\bar{\lambda}+\bar{\mu})\partial^1(\bar{\nabla}_i u^i) + \bar{\mu}\bar{\Delta} u^1 = 0 \,,\\
(\bar{\lambda}+\bar{\mu})\partial^2(\bar{\nabla}_i u^i) + \bar{\mu}\bar{\Delta} u^2 = 0 \,,\\
(\bar{\lambda}+\bar{\mu})\partial^3(\bar{\nabla}_i u^i) + \bar{\mu}\bar{\Delta} u^3 = 0 \,.
\end{aligned}
$$

The boundary of the foundation can be decomposed into sub-boundaries as

$$
\begin{aligned}
\partial\Omega &= \bar{\omega} \cup \partial\Omega_0 \cup \partial\Omega_f \,,\\
\omega &= \{a\} \times (-\frac{1}{2}\pi, 0) \times (-\ell,\ell) \,,\\
\partial\Omega_0 &= \{\{a_0\} \times (-\pi,\pi] \times [-L,L]\} \cup \{(a_0,a] \times (-\pi,\pi] \times \{\{-L\} \cup \{L\}\}\} \,,\\
\partial\Omega_f &= \{\{a\} \times (-\pi,\pi] \times (-L,L)\} \setminus \bar{\omega} \,.
\end{aligned}
$$

Thus, one can express the boundary conditions of the foundation as

$$
\begin{aligned}
\boldsymbol{u}|_{\partial\Omega_0} &= \boldsymbol{0} \text{ (zero-Dirichlet)} \,,\\
\big[\partial_3 u^1 + \partial_1 u^3\big]|_{\partial\Omega_f} &= 0 \text{ (zero-Robin)} \,,\\
\big[r^2\partial_3 u^2 + \partial_2 u^3\big]|_{\partial\Omega_f} &= 0 \text{ (zero-Robin)} \,,\\
\big[\bar{\lambda}(\partial_1 u^1 + \partial_2 u^2 + r^{-1}u^3) + (\bar{\lambda}+2\bar{\mu})\partial_3 u^3\big]|_{\partial\Omega_f} &= 0 \text{ (zero-Robin)} \,.
\end{aligned}
$$

Let $\boldsymbol{u}|_\omega = (u^1(x,\theta,a), u^2(x,\theta,a), u^3(x,\theta,a))$ be the displacement field of the shell-membrane. With some calculations, one finds that the first fundamental form tensor is $\boldsymbol{I\!I}_{[\mathrm{I}]} = \operatorname{diag}(1,a^2)$ and the covariant derivatives are

$$
\begin{aligned}
&\nabla_1 u^1 = \partial_1 u^1 \,, && \nabla_1 u^2 = \partial_1 u^2 \,,\\
&\nabla_2 u^1 = \partial_2 u^1 \,, && \nabla_2 u^2 = \partial_2 u^2 \,.
\end{aligned}
$$

With further calculations (see Section 4.3.3 and considering the case $h^2\rho^\gamma_\alpha(\boldsymbol{u})\rho^\alpha_\gamma(\boldsymbol{u}) \ll \epsilon^\gamma_\alpha(\boldsymbol{u})\epsilon^\alpha_\gamma(\boldsymbol{u})$), one can express the governing equations of the shell-membrane as:

If $[2\nu_F u^3 + (u^1u^1 + r^2u^2u^2)^{\frac{1}{2}}]|_\omega < 0$, then

$$
\begin{aligned}
(\Lambda-\mu)\partial^1(\nabla_\alpha u^\alpha) + \mu\Delta u^1 + \frac{1}{a}(\Lambda-2\mu)\partial^1 u^3 - \frac{1}{h}\mathrm{Tr}(T_3^1(\boldsymbol{u})) = 0\ ,\\
(\Lambda-\mu)\partial^2(\nabla_\alpha u^\alpha) + \mu\Delta u^2 + \frac{1}{a}\Lambda\partial^2 u^3 - \frac{1}{h}\mathrm{Tr}(T_3^2(\boldsymbol{u})) = 0\ ,\\
(\Lambda-2\mu)\partial_1 u^1 + \Lambda\left(\partial_2 u^2 + \frac{1}{a}u^3\right) + \frac{a}{h}\mathrm{Tr}(T_3^3(\boldsymbol{u})) = 0\ ,
\end{aligned}
$$

where $\Lambda = 2\lambda\mu(\lambda+2\mu)^{-1}$;

If $[2\nu_F u^3 + (u^1u^1 + r^2u^2u^2)^{\frac{1}{2}}]|_\omega = 0$, then

$$
\begin{aligned}
&(\Lambda-\mu)\partial^1(\nabla_\alpha u^\alpha) + \mu\Delta u^1 - \frac{(\Lambda-2\mu)}{2a\nu_F}\partial^1(u^1u^1+a^2u^2u^2)^{\frac{1}{2}} - \frac{1}{h}\mathrm{Tr}(T_3^1(\boldsymbol{u})) - \frac{(\Lambda-\mu)}{4a\nu_F^2}u^1 - \frac{(\bar\lambda+\bar\mu)}{4h\nu_F^2}u^1\\
&\quad + \frac{1}{2\nu_F}\frac{u^1}{(u^1u^1+a^2u^2u^2)^{\frac{1}{2}}}\left((\Lambda-2\mu)\partial_1u^1 + \Lambda\partial_2u^2 + \frac{a}{h}\left(\bar\lambda(\partial_1u^1+\partial_2u^2) + (\bar\lambda+2\bar\mu)\partial_3u^3\right)\right) = 0\ ,\\
&(\Lambda-\mu)\partial^2(\nabla_\alpha u^\alpha) + \mu\Delta u^2 - \frac{\Lambda}{2a\nu_F}\partial^2(u^1u^1+a^2u^2u^2)^{\frac{1}{2}} - \frac{1}{h}\mathrm{Tr}(T_3^2(\boldsymbol{u})) - \frac{(\Lambda-\mu)}{4a\nu_F^2}u^2 - \frac{(\bar\lambda+\bar\mu)}{4h\nu_F^2}u^2\\
&\quad + \frac{1}{2\nu_F}\frac{u^2}{(u^1u^1+a^2u^2u^2)^{\frac{1}{2}}}\left((\Lambda-2\mu)\partial_1u^1 + \Lambda\partial_2u^2 + \frac{a}{h}\left(\bar\lambda(\partial_1u^1+\partial_2u^2) + (\bar\lambda+2\bar\mu)\partial_3u^3\right)\right) = 0\ .
\end{aligned}
$$

The boundary of the shell-membrane can be decomposed into sub-boundaries as

$$
\begin{aligned}
\partial\omega &= \partial\omega_{T_0}\cup\partial\omega_{T_{\mathsf{max}}}\cup\partial\omega_f\ ,\\
\partial\omega_{T_0} &= [-\ell,\ell]\times\{-\frac{1}{2}\pi\}\ ,\\
\partial\omega_{T_{\mathsf{max}}} &= [-\ell,\ell]\times\{0\}\ ,\\
\partial\omega_f &= \{\{-\ell\}\cup\{\ell\}\}\cup(-\frac{1}{2}\pi,0)\ .
\end{aligned}
$$

Thus, one can express the boundary conditions of the shell-membranes as

$$
\begin{aligned}
\left[(\Lambda-2\mu)\partial_1u^1 + \Lambda(\partial_2u^2 + a^{-1}u^3)\right]|_{\partial\omega_{T_0}} &= \tau_0\ \text{(traction)}\ ,\\
\left[(\Lambda-2\mu)\partial_1u^1 + \Lambda(\partial_2u^2 + a^{-1}u^3)\right]|_{\partial\omega_{T_{\mathsf{max}}}} &= \tau_{\mathsf{max}}\ \text{(traction)}\ ,\\
\left[\Lambda\partial_1u^1 + (\Lambda-2\mu)(\partial_2u^2 + a^{-1}u^3)\right]|_{\partial\omega_f} &= 0\ \text{(zero-Robin)}\ ,\\
\left[\partial_2u^1 + a^2\partial_1u^2\right]|_{\partial\omega_f} &= 0\ \text{(zero-Robin)}\ .
\end{aligned}
$$

To conduct numerical experiments we employ the second-order-accurate finite-difference method in conjunction with Newton's method for nonlinear systems as in Section 2.6. Another issue we must tackle is the discretisation of the domain. As we are dealing with curvilinear coordinates, there is a inherit grid dependence. To be precise, it is approximately $r\Delta x^2 \leq \Delta x^1$ and $r\Delta x^2 \leq \Delta x^2$, for all $a_0 \leq r \leq a$, where Δx^j is a small increment in x^j direction. For our purposes we use $\Delta x^2 = \frac{1}{N-1}$ and $r = a$, where $N = 250$. Finally, we must define a terminating condition. For this we choose to terminate our iterating process given that the condition $|1 - ||\boldsymbol{u}_m||_{\ell^2}^{-1}||\boldsymbol{u}_{m+1}||_{\ell^2}| < 10^{-10}$ is satisfied.

We model a stiff shell-membrane on a relatively flaccid foundation with a large coefficient of friction. To do so, we keep the values $\nu_F = 1$, $h = 0.001$, $a = 1$, $\ell = \frac{1}{4}$, $L = \frac{1}{2}$, $E = 10^3$, $\nu = \frac{1}{4}$, $\bar\nu = 0$, $\tau_0 = 1$ and $\tau_{\mathsf{max}} = 2$ fixed for all experiments.

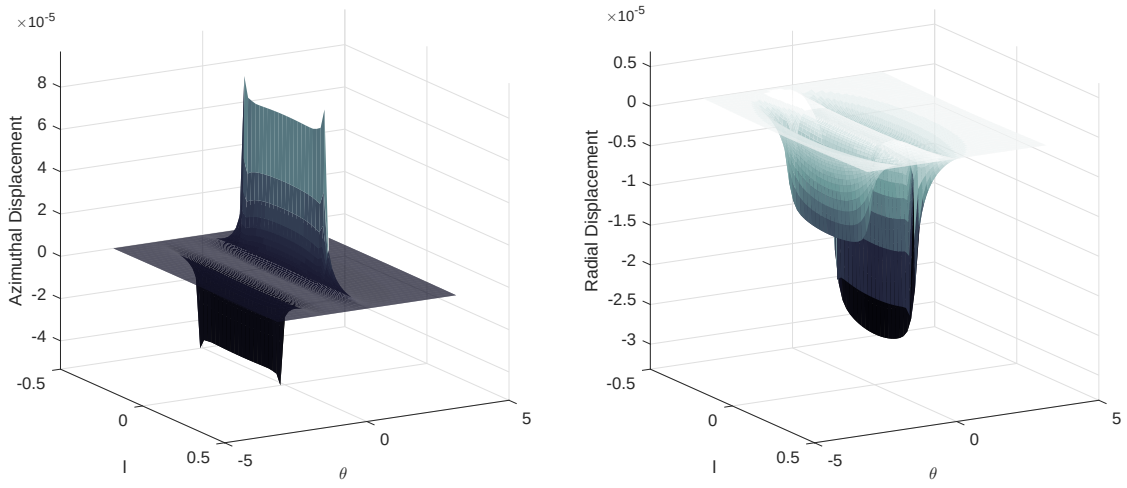

Figure 76: Displacement field in the outer surface of the foundation.

Figure 76 is calculated with the values of $a_0 = \frac{1}{4}$, $\bar{E} = 10$ and with a grid of 44×252 points. Figure 76 shows the azimuthal (i.e. u^2) and the radial (i.e. u^3) displacements. The maximum azimuthal displacement is observed at $(\pm\frac{1}{4}, 0, 1)$ with an azimuthal displacement of $u^2 = 8.53 \times 10^{-5}$. The maximum radial displacement is observed at $(0, 0, 1)$ with a radial displacement of $u^3 = -2.68 \times 10^{-5}$. Also, (not displayed) the maximum axial displacements are observed at $(\pm\frac{1}{4}, 0, 1)$ with respective axial displacements of $u^1 = \pm 3.69 \times 10^{-5}$. This maximum in the displacement field is observed on the boundary with the highest traction, i.e. on the boundary with τ_{max} acting on it.

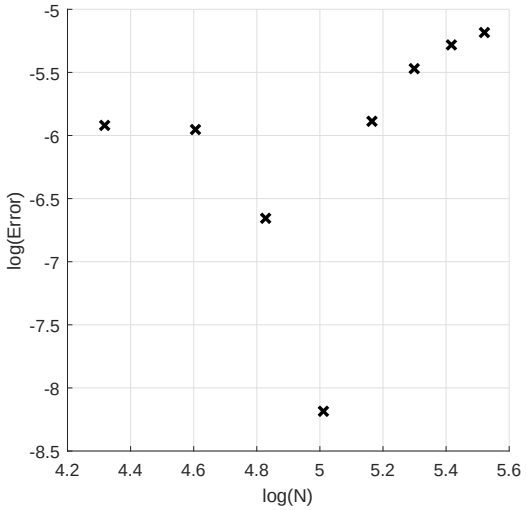

Figure 77: Grid dependence of the shell-membrane model.

Another numerical analysis we must perform is the grid dependence analysis for the numerical solution. As the reader can see from figure 77, as N increases, the difference between the numerical solution N and $N+1$ initially decreases, but after $N = 150$ the error between the solutions inexplicably increases, where $\text{Error} = |1 - ||\boldsymbol{u}_{N-1}||_{\ell^2}^{-1}||\boldsymbol{u}_N||_{\ell^2}|$. It is unclear why this is the case. Perhaps it is due to the nonlinear nature of the problem. But for all of our experiments we use $N = 250$. Note

that figure 77 is calculated with the values of $a_0 = \frac{1}{4}$ and $\bar{E} = 10$.

Now, to investigate the displacement and the shear at the contact region we calculate the following:

$$\text{Displacement} = \left(\Sigma_{\{\Delta x^1, \Delta x^2\}} u_i u^i|_\omega\right)^{\frac{1}{2}} \ ;$$
$$\text{Shear} = \left(\Sigma_{\{\Delta x^1, \Delta x^2\}} T^3_\alpha(\boldsymbol{u}) T^\alpha_3(\boldsymbol{u})|_\omega\right)^{\frac{1}{2}} \ .$$

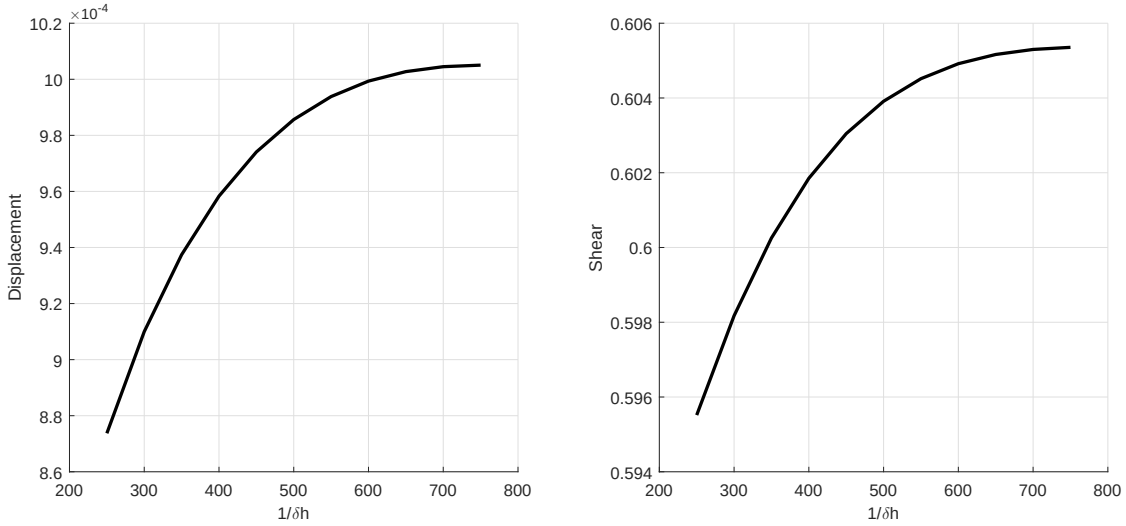

Figure 78: Displacement and the shear at the contact region for $1/\delta h = (a - a_0)/h$.

Figure 78 shows the total displacement and the total shear of the outer boundary of the foundation for a_0. For these experiments we assert that $a_0 \in \{\frac{5}{20}, \frac{6}{20}, \frac{7}{20}, \frac{8}{20}, \frac{9}{20}, \frac{10}{20}, \frac{11}{20}, \frac{12}{20}, \frac{13}{20}, \frac{14}{20}, \frac{15}{20}\}$ and $\bar{E} = 10$. From figure 78, one can see that as the thickness of the foundation increases, both the total displacement of the body and the shearing stress on the body increases. The increase in displacement as the thickness of the foundation increases is a logical result as the thickness increases, more matter is available to be displaced. Also, the increase in shear stress as the thickness of the foundation increases is a logical result as the thickness increases, more force is expended on the foundation to deform the ever increasing volume.

Figure 79 shows the total displacement and the total shear of the outer boundary of the foundation for $\bar{E}$. For these experiments we assert that $a_0 = \frac{1}{4}$ and $\bar{E} = \{10, 20, 30, 40, 50, 60, 70, 80, 90, 100\}$. From figure 79 one can see that as Young's modulus of the foundation increases, the shear stress experienced on the body increases, but the total displacement of the body decreases. Only the decrease in displacement as Young's modulus of the foundation increases is logical, as Young's modulus increases, one needs to increase the amount of force applied to achieve the same amount of displacement. Thus, higher Young's modulus results in a lower displacement. However, the change in shear profile eludes a valid physical interpretation.

From our experimental results, we make the following predictions. Given a shell-membrane supported by an elastic foundation subjected to static friction, then: A-(i) as the thickness of the elastic body increases, the displacement of the body increases, A-(ii) as the thickness of the elastic body

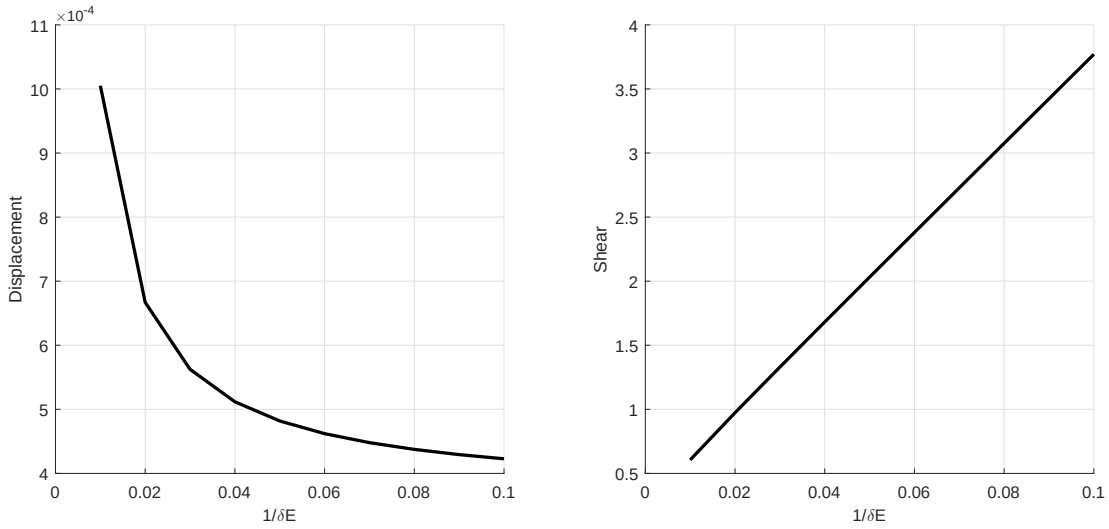

Figure 79: Displacement and the shear at the contact region for $1/\delta E = \bar{E}/E$.

increases, the shear stress acting on the body increases, A-(iii) as Young's modulus of the elastic body increases, the displacement of the body decreases, and A-(iv) as Young's modulus of the elastic body increases, the shear stress acting on the body increases.

6.7 Experimental Data: February 2016 Trial

In this section we analyse the data obtained from further experiments conducted on human subjects. We keep the same experimental setup as in Section 6.4, but with minor modifications, and with the help from the numerical analysis from Section 6.6 we attempt to investigate the behaviour of human tissue due to movement of fabrics.

Subject	$\delta\tau$					Radius (cm)	δl	Displacement (cm)
	40g	80g	120g	160g	200g			
F34	1.10	1.11	1.02	0.969	0.765	4.22	0.269	0.679
F35	0.975	1.03	$\cdots$	1.75	1.28	4.30	0.268	0.664
F53	1.28	1.56	1.38	1.04	1.66	4.38	0.275	1.02
F59	0.975	1.25	1.10	1.30	1.13	4.14	0.269	0.797
F60	1.73	1.29	0.858	1.18	1.50	4.34	0.281	1.04
M18	0.650	$\cdots$	1.31	0.819	0.940	3.58	0.269	0.652
M23	1.20	0.975	1.22	0.963	1.14	4.46	0.269	0.641
M26	2.15	0.775	2.08	1.29	1.29	4.50	0.266	0.731

Table 4: Experimentee and experimental data 2016.

For this trial we recruit 8 participants, 3 males and 5 females, all are between the ages of 18 to 60. Experimental data is found in the table 4 if the reader wishes to reproduce ant results. Note that $\delta\tau = T_{\text{max}}/T_0$ is the tension ratio, where $T_0 =$ mass $\times\, g$ and $g = 9.81$ is the acceleration due

to gravity, and Radius is the radius of the mid part of the upper arm. Unfortunately F35-120g and M18-80g data are unavailable due to corrupt files.

As we are attempting to investigate the deformation of tissue, we use greater masses than the 2015 trial. Also, now with the software 3dMDvultus we can select points directly on a .tsb file instead of using .stl files. Thus, unlike in Section 6.4, we omitted the use of 3D markers that is responsible for producing significant errors in the displacements.

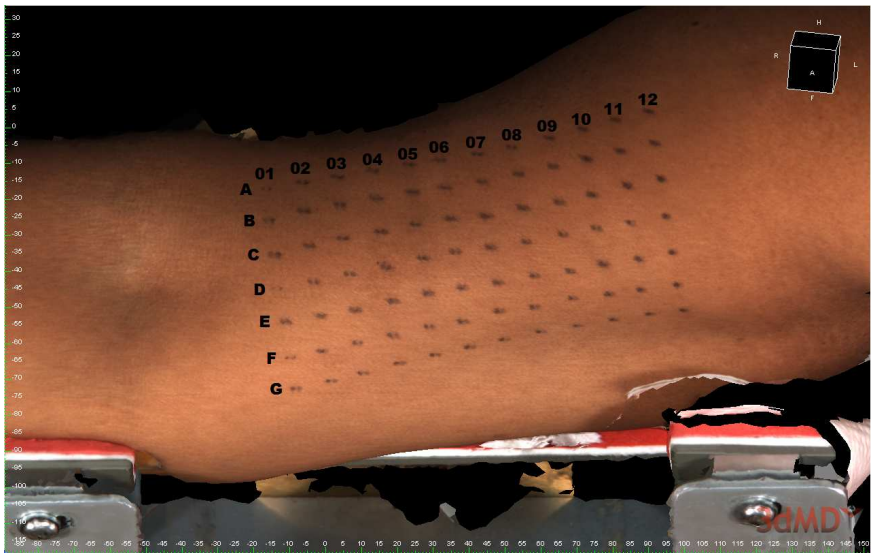

Figure 80: Experimental configuration on subject F53 (.tsb file).

Figure 80 shows a .tsb figure of the subject F53 unstrained. It appears that often two markers are occupying the same space. This is a result of two .png files inadequately overlapping, which is the case for every scan. This problem is inherited by 3dMDvultus and we remedy this by taking the mean value, of what appears to be two different markers, as the true marker location.

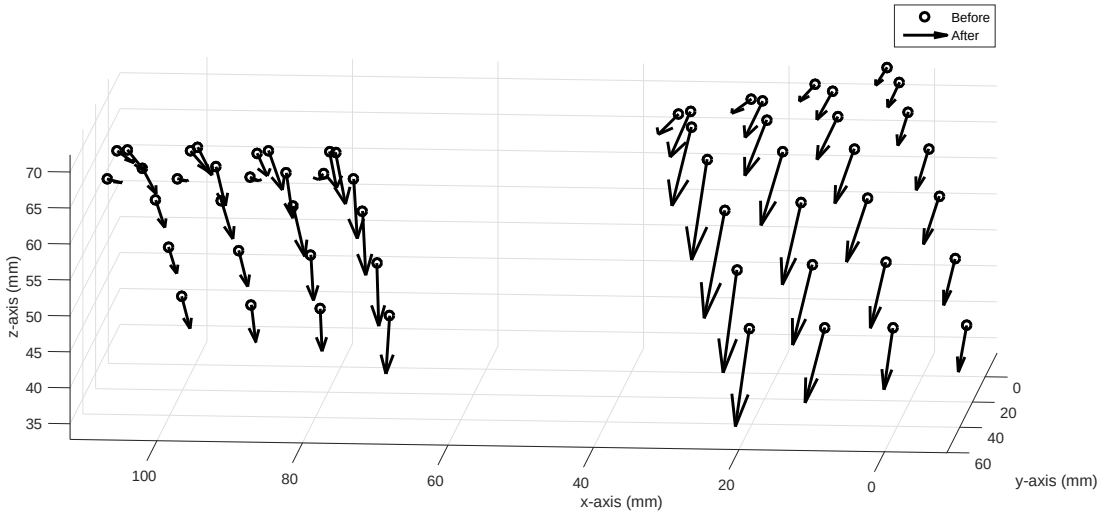

Figure 81: Marker displacement on F53 for 200g.

Figure 81 shows graphical representation of the displacement of the markers of F53 for the 200g case. The circles show the unstrained configuration markers prior to the tensometer run and the tips of the arrows show the stained configuration of the markers during the tensometer run. Clearly, we omit the markers **A05**, ..., **A08**, ..., **G08** as they are hidden beneath the fabric. Unfortunately, due to the movement of subjects during the experiments it is unclear to conclusively say that the final configuration of the markers is a result of the experiments or as a result of subject's movements, and this is the case with all the subjects. Also, we are unable to replicate the deformation in Section 6.6 as our models assume linear elasticity, and thus, to model finite deformation we must consider nonlinear elasticity. However, even if we did numerically model finite strains, we are still unable to model the experimental deformations due to the fact that our numerical models assume static friction, but our experiments are conducted for the dynamic friction case. Despite these difficulties, some interesting results can be expected from the data, which are discussed below.

As heavier hanging masses lead to larger deformations, and thus, we mainly consider the case 200g for the following numerical analysis. During our experiments we saw that the only legible markers that experience the largest displacements are the markers **A04**, **A09**, ..., **G09**. Thus, we restrict our attention to these markers, with using the markers **A03**, **A10**, ..., **G10** as reference points. Note that in rare occasions the markers **A04**, ..., **G04** become hidden due to shifting of the fabric. For these cases we restrict our attention to the markers **A03**, **A08**, ..., **G08** and **A02**, **A09**, ..., **G09**.

As described in Section 6.4, relative displacements are assumed to be independent to the movement of the subject. Thus, we calculate the relative displacements by following equation

$$\begin{aligned}\text{Displacement} = \frac{1}{14}\big|&(||\text{deformed}(\mathbf{A04}-\mathbf{A03})||^2 - ||\text{undeformed}(\mathbf{A04}-\mathbf{A03})||^2)\\ &+\dots\\ &+(||\text{deformed}(\mathbf{G10}-\mathbf{G09})||^2 - ||\text{undeformed}(\mathbf{G10}-\mathbf{G09})||^2)\big|^{\frac{1}{2}}\,.\end{aligned}$$

As we require some elastic property of subjects' tissue, we calculate δl by

$$\delta l = \left(\frac{||\text{deformed}(\mathbf{A04}-\mathbf{A03})||^2+\dots+||\text{deformed}(\mathbf{G10}-\mathbf{G09})||^2}{||\text{undeformed}(\mathbf{A04}-\mathbf{A03})||^2+\dots+||\text{undeformed}(\mathbf{G10}-\mathbf{G09})||^2}\right)^{\frac{1}{2}},$$

to measure how flaccidity of subject's tissue. We further assume that $\delta l \sim \delta E$. See table 4 for all the calculated values of relative displacements and δl.

Figure 82 shows the relative displacement and the tension ratio, $\delta\tau$, for 200g with respect to varying radius of the mid part of the upper arm. It clearly shows that as the radius increases, so is the maximum applied-tension. We encountered and investigated this phenomenon in Section 6.4 and predicted it in Section 6.6. Furthermore, this correlation holds for all masses, i.e. for all $\delta\tau$, and thus, further validating our prediction from Section 6.6, i.e. A-(ii). A vague correlation can be visible for the relative displacement and the radius, and thus, our prediction regarding radius of the body and the displacement from Section 6.6, i.e. A-(i), maybe justified.

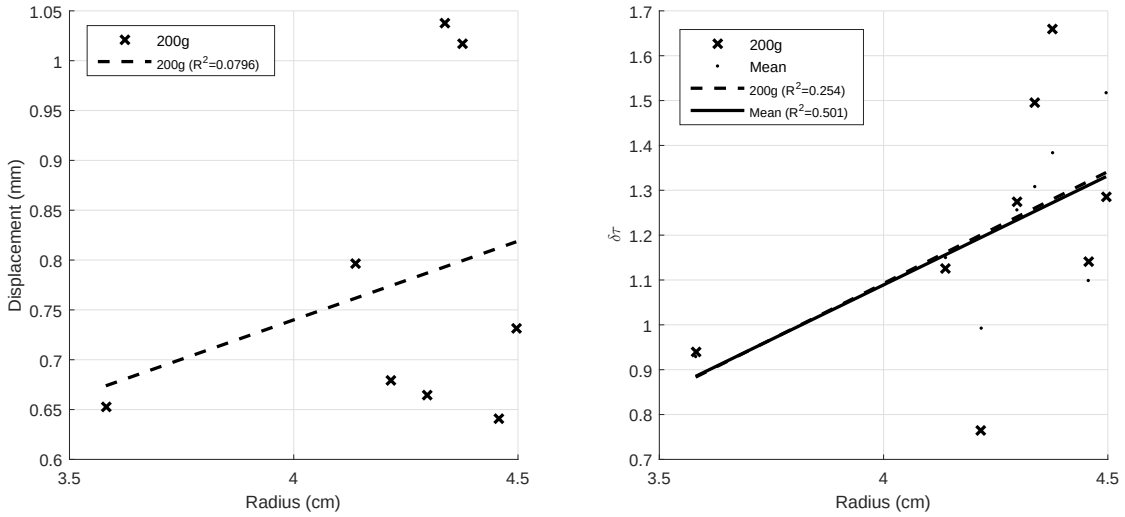

Figure 82: Displacement and tension ratio for varying radius (in cm).

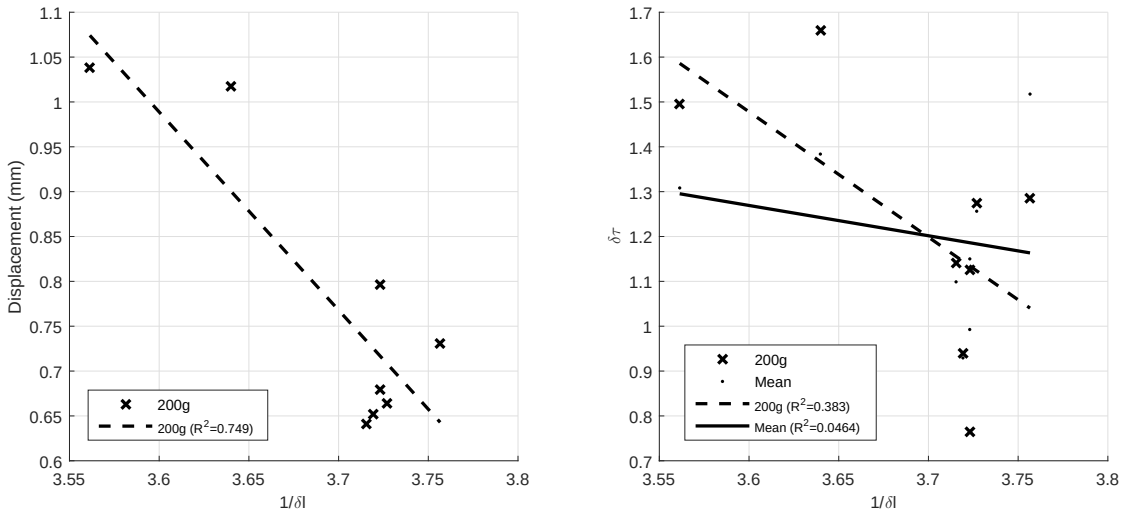

Figure 83: Displacement and tension ratio for varying δl.

Figure 83 shows the relative displacement and the tension ratio, $\delta\tau$, for 200g with respect to varying $1/\delta l$. It clearly shows that as subject's tissue become less flaccid, the magnitude of the tissue deformation becomes less pronounced, i.e. as subject's tissue becomes stiffer, it gets harder to deform. We encountered and investigated this phenomenon in Section 6.4 and predicted it in Section 6.6. Furthermore, this is the strongest correlation (i.e. with the highest correlation coefficient) that we observed, and thus, further validating our prediction from Section 6.6, i.e. A-(iii). We also observe a weak positive correlation between the stiffness of subject's tissue (i.e. $1/\delta l$) and the tension ratio. This correlation is logical as stiffer the foundation gets, we expect less force to get transfered from the membrane in to the foundation (visualise the difference between membrane on an elastic foundation and membrane on a rigid foundation). Furthermore, this effect is previously observed in Section 6.4 (see figure 74). Unfortunately, this correlation contradicts what is predicted by our numerical modelling from Section 6.6, i.e. figure 79-right, and thus, our prediction regarding the foundation stiffness and the shear, i.e. A-(iv), cannot be corroborated.

6.7.1 Remark

A possible technique that maybe used to measure the elastic properties of subject's tissue, to be use in our numerical models, is the shearwave dispersion ultrasound vibrometry (SDUV). This is an ultrasound based method that is used in measuring the shear elasticity and viscosity in various types of soft tissues with the use of dispersion of shear wave velocities, which arise from the inherent viscoelastic nature of soft tissue. Urban *et al.* [202] use SDUV in both ex-vivo (exorcised muscle samples of porcine and bovine) and in-vivo (a liver and a heart of a porcine) tissues. The authors state that SDUV gave high temporal and spatial resolution material property measurements of soft tissue that can be integrated with B-mode imaging (medical ultrasound that displays the acoustic impedance of a two-dimensional cross-section of tissue) to provide a new tool for clinicians to use for diagnosis and monitoring of therapies.

6.8 Conclusions

In this chapter we investigated aspects of mathematically modelling skin damage due to friction. In Section 6.2 we derived a belt-friction model, for a true-membrane over a non-hyperbolic rigid obstacle with a positive mean-curvature, with the use of Kikuchi and Oden's [102] model for Coulombs law of static friction for the slip case. This belt-friction model is derived with a very hypothetical approach. Thus, we are unable to conduct finer analysis, including the existence of solutions, due to the fact that it is not possible to express the governing equations in a variational form. Therefore, we remind the reader that what we derived is not a mathematical theory. By conducting numerical experiments, in Section 6.3, we found that (given that we keep all other variables fixed): (i) there exists a strong positive correlation between the maximum applied-tension and the coefficient of friction, (ii) there exists an initial negative correlation between the Gaussian curvature of the rigid foundation and the coefficient of friction, and there exists an optimum Gaussian curvature where the coefficient of friction is a minimum, (iii) there exists a negative correlation between Poisson's ratio of the membrane and the coefficient of friction, (iv) there exists a negative correlation between the speed in which the membrane is being pulled and the coefficient of friction, (v) there exists a positive correlation between the mass density of the membrane and the coefficient of friction, where the mass density of the membrane is responsible for significantly increasing the coefficient of friction relative to other variables, and (vi) the coefficient of friction is not affected by Young's modulus of the membrane, which coincide with the capstan equation as it is also independent of Young's modulus of the membrane, given that Young's modulus is neither zero nor infinite. All the results we found are intuitive, but the existence of an optimum Gaussian curvature where the coefficient of friction is a minimum is a surprising result.

In Section 6.4, with experiments conducted on human subjects and with elementary regression analysis, we show that it is unwise to use belt-friction models to calculate the friction between in-vivo skin and fabrics as the existence of an elastic foundation can significantly influence one's experimental results. We found that, if one uses a belt-friction model to calculate the coefficient of friction between in-vivo skin and fabrics, then there exists a weak, but a positive correlation between

the tension ratio and the following: body mass index and flaccidity of subject's tissue. Also, there exists a very strong positive correlation between the tension ratio and radius of the mid part of the upper arm. Thus, if one uses a belt-fiction model to calculate the coefficient of friction, then one gets a positive correlations between the coefficient of friction and: the body mass index, flaccidity of subject's tissue and the radius of subject's upper arm. These results may or may not mean that of those with a higher body mass index or very flaccid tissue or larger biceps are more susceptible to skin abrasion. This correlation is simply due to the fact that belt-friction models (capstan equation or otherwise) assume that the foundation is rigid, and thus, a greater proportionality between the magnitude of the coefficient of friction and the magnitude of the tension ratio. In our experiments some of the tension is expended on deforming subjects' tissue, and thus, making the magnitude of the tension ratio much greater, which in turn leads to the illusion of a higher coefficient of friction.

In Section 6.5 we derived a model for an overlying shell-membrane supported by an elastic foundation subjected to static friction. By conducting numerical experiments, in Section 6.6, we found that: (i) as the thickness of the elastic body increases, the displacement of the body increases, (ii) as the thickness of the elastic body increases, the shear stress acting on the body increases, (iii) as Young's modulus of the elastic body increases, the displacement of the body decreases, and (iv) as Young's modulus of the elastic body increases, the shear stress acting on the body increases (which defies a realistic physical interpretation). These results imply that for thick rigid shell-membranes we can expect to see a lower shear generation on the contact region between the shell and the foundation.

In Section 6.7 we attempted to use our shell-membrane model to process experimental data that we obtained from human subjects in an attempt to investigate the deformation of the human tissue due to movement of fabrics. We discovered that there exists a positive correlation between: B-(i) the displacement of subject's tissue and the radius of subject's arm, B-(ii) the tension ratio and radius of subject's arm, B-(iii) the displacement of the subject's tissue and the flaccidity of subject's tissue, and B-(iv) the tension ratio and the flaccidity of subject's tissue. Observations B-(i), B-(ii) and B-(iii) are all predicted in Section 6.5 and previously observed in Section 6.4. Note that the result B-(iv) is also previously observed in the experiments from Section 6.4; it is also very intuitive. However, this effect could not be predicted by our numerical modellings from Section 6.5.

Unfortunately, in Section 6.6, we failed to accurately model the problem as our numerical models assume static friction and infinitesimal deformations, while the experiments are conducted for dynamic friction and finite deformation settings. Fortunately, we laid the groundwork for modelling the above problem with some mathematical rigour and for further discussions on Signorini's problem, nonlinear elasticity and dynamic pure-traction cases please consult chapter 5.

7 Conclusions

In this thesis we presented a general theory for static linearly elastic isotropic shells supported by static linearly elastic isotropic foundations, for both the bonded and frictionally coupled cases in curvilinear coordinates.

We began in chapter 1 where we introduced the critical definitions, the fundamental theorems and the most notable applications relating to the study of shell and membrane theory, and contact conditions governing elastic bodies, in particular, friction. There, we critically analysed the existing literature on the study of thin objects such as films, plates, membranes and shells, and we highlighted their limitations, flaws and given correct formulations when possible. In particular, we meticulously documented the erroneous mathematical work of Howell *et al.* [84] (see Section 1.4), Cottenden *et al.* [48] (see Section 1.8), Efrati *et al.* [60] (see Section 1.9) and Baldelli and Bourdin [16] (see Section 1.10). The flaws of the given authors' work are revealed by a combination of correct mathematical proofs and or counterexamples. Furthermore, we offered corrections to their work whenever possible, again with meticulous detail.

In chapter 2 we examined the behaviour of membranes of zero-Poisson's ratio (or strings) supported by rigid foundations of positive mean-curvature and zero-Gaussian curvature, where the contact region is governed by the common friction-law. To be more precise, we extended the capstan equation to general geometries and gave closed-form solutions for all the cases.

Then, in Section 2.6, we extended Kikuchi and Oden's [102] model for Coulomb's law of static friction to curvilinear coordinates. There, we conducted numerical experiments to see how close the modified Kikuchi and Oden's model resembles the modified capstan equation. Our numerical results imply that the capstan coefficient of friction is an underestimate of Coulomb's coefficient of friction, i.e. $\mu_F \leq \nu_F$. Also, for a fixed coefficient of friction, as the critical parametric-latitude of the contact region increases, as the thickness of the body decreases or as Poisson's ratio of the body increases, one requires a larger force to debond the body. In addition, Young's modulus of the body does not affect the governing equation at the contact region.

The work presented in chapter 2 has real life applications in cable drive devices, particularly in the field of robotics. Please consult Section 1.6 for more detail.

In chapter 3 we begin the study of shells that are supported by elastic foundations. To begin, we considered the case where the shell is bonded to the foundation. We derived the equations for the overlying shell with the mathematical techniques for Koiter's linear shell theory and linear elasticity theory in curvilinear coordinates put forward by Ciarlet [38], and a technique that is used in the derivation of surface Cauchy-Bourne model [89]. Then, we treated the overlying bonded shell as a boundary form of the elastic foundation, which is analogous to the work of Necas *et al.* [144], and we used the mathematical techniques put forward by Ciarlet [38], and Badiale and Serra [13]

to mathematically, and thus, conclusively, prove the existence and the uniqueness of solutions for the proposed model. Thus, concluding that what we derived is a mathematical theory.

To check the physical validity of our work we extended Baldelli and Bourdin's [16] model for stiff films on elastic foundations to curvilinear coordinates via asymptotic analysis. Then, in Section 3.5, we numerically modelled the displacement field at the contact region with a bonded two-body elastic problem and compared the solution against our bonded shell model and extend Baldelli and Bourdin's model, for a set of variable which Baldelli and Bourdin's [16] model is mostly accurate for. Numerical results show that the error between the bonded two-body solution and extend Baldelli and Bourdin's model is always several magnitudes greater than the error between the bonded two-body solution and our bonded shell solution, and this is the case for all the input variables. This implies that our shell model is far superior model in comparison when approximating contact region of thin bodies that are bonded to elastic foundations.

To conclude our numerical analysis for the bonded case, in Section 3.7, we modelled the displacement field of the foundation of the bonded two-body elastic problem and compared the solutions against our bonded shell solutions. Our analysis showed that our bonded shell on an elastic foundation model can approximate two-body elastic model's foundation with a significant degree of accuracy given that Young's modulus of the shell is significantly higher than Young's modulus of the foundation. Now, this result coincides with what is documented in the literature [4]. We also observe other factors can equally affect the accuracy of our bonded shell model, such as Poisson's ratio and the thickness of the shell, and the critical parametric-latitude of the contact region. However, one cannot arbitrarily increase or decrease elastic and geometrical properties (e.g. cannot arbitrarily increase Young's modulus of the shell in the hope of gaining accuracy), as we often observe optimal values for elastic and geometric properties where the error is a minimum.

Chapter 3 is the strongest chapter of the thesis as we have a definitive model (classical three-dimensional elasticity equations) and a relatively pre-existing model (extended Baldelli and Bourdin's model) to compare our bonded shell model against to determined the validity of our work. Also, these types of models have a wide range of applications, particularly in the field of flexible and stretchable electronics (see Section 1.7), and they may possibly be applied to model gyrification (see Section 3.8.1).

In chapter 4 we concluded our study on shells that are supported by elastic foundations by asserting that the contact region is governed by a displacement-based friction condition that is analogous to Coulomb's law of static friction. We treated this displacement-based frictional condition as a constraint, which is analogous to the work of Kinderlehrer and Stampacchia [107], and with the mathematical techniques put forward by Evans [63], and Kinderlehrer and Stampacchia [107], we mathematically proved the existence and the uniqueness of solutions, and thus, concluding that what we derived a mathematical theory.

Then, in Section 4.6, we extended Kikuchi and Oden's model for Coulomb's law of static friction in the curvilinear space that we originally derived in Section 2.6 to model a two-body contact problem, i.e. an overlying elastic body on an elastic foundation subjected to Coulomb's law of static friction in curvilinear coordinates. We used extended Kikuchi and Oden's model to numerically simulate an overlying thin, but still three-dimensional body on an elastic foundation, i.e. two-body elastic problem with friction, and compared it to our shell model with friction to see how close the solutions are. The numerical analysis shows that, if the shell is thick (within reasons), shell is very stiff, shell is close to incompressible, the contact region has a very high coefficient of friction or the contact region has a low critical parametric-latitude, then the displacement of the foundation predicted by both models are in better agreement.

Unlike in Chapter 3, in Chapter 4 we do not have a definitive model to compare our model against, i.e. there exists no definitive mathematical theory that describes the behaviour between two bodies that are in contact with friction. Thus, all we do to further this section is analysing how the solutions obtained by each modelling approach vary over the parameter space. As a result of this we cannot make an assertion on how physically valid each model is. For example, in Section 2.6 we saw that first modified Kikuchi and Oden's model for Coulomb's law of static friction behave slightly differently to the capstan equation under certain conditions, and, yet these are two models that supposedly model the same physical phenomena with common roots stretching back to Amontons' laws of friction.

In chapter 5 we presented few interesting areas where the question of the existence of solutions and the physical validity are still remaining unsolved. There, we described a fundamental issue concerning the well-posedness of our overlying shell model. Then, we meticulously presented a way of extending the regularity of the weak solutions of our work, a way to include Signorini's problem, a way to extend the problem to either the semi-linear case or to the nonlinear case or both, and an approach to extend the problem to model the dynamic case. The work in this section may seems speculative, but the reader must understand that we gone to great lengths to present the most mathematically logical formulations and to compile all the necessary publications to justify our assertions.

In chapter 6 we studied several methods to mathematically model skin abrasion. With our belt-friction model, shell-membranes on elastic foundations with friction model and experiments conducted on human subjects, we found that the stress that is expended on deforming the elastic foundation is positively correlated with the thickness and the flaccidity of the elastic foundation. With numerical and regression analysis, we show that the effects due mechanical and geometrical properties, most notably the thickness of the elastic foundation and the mass density of the overlying membrane, can significantly affect the results of experiments that are conducted on in-vivo skin, in particular, if one's goal is to measure the coefficient of friction.

Thus, we conclude our mathematical study of overlying shells on elastic foundations.

References

[1] M. Abramowitz, I. A. Stegun, et al. *Handbook of mathematical functions*, volume 1046. Dover New York, 1965.

[2] A. Acharya. On compatibility conditions for the left cauchy–green deformation field in three dimensions. *Journal of elasticity*, 56(2):95–105, 1999.

[3] R. A. Adams and J. J. F. Fournier. *Sobolev spaces*, volume 140. Academic press, 2003.

[4] L. Aghalovyan and D. Prikazchikov. *Asymptotic theory of anisotropic plates and shells*. World Scientific, 2015.

[5] S. Agmon, A. Douglis, and L. Nirenberg. Estimates near the boundary for solutions of elliptic partial differential equations satisfying general boundary conditions ii. *Communications on pure and applied mathematics*, 17(1):35–92, 1964.

[6] J. Aldrich. Correlations genuine and spurious in pearson and yule. *Statistical science*, pages 364–376, 1995.

[7] H. G. Allen. *Analysis and Design of Structural Sandwich Panels: The Commonwealth and International Library: Structures and Solid Body Mechanics Division*. Elsevier, 2013.

[8] G. Angelini, G. A. Vena, and C. L. Meneghini. Shoe contact dermatitis. *Contact Dermatitis*, 6(4):279–283, 1980.

[9] J. Asserin, H. Zahouani, P. Humbert, V. Couturaud, and D. Mougin. Measurement of the friction coefficient of the human skin in vivo: quantification of the cutaneous smoothness. *Colloids and surfaces B: Biointerfaces*, 19(1):1–12, 2000.

[10] B. Audoly and A. Boudaoud. Buckling of a stiff film bound to a compliant substrate—part i:: Formulation, linear stability of cylindrical patterns, secondary bifurcations. *Journal of the Mechanics and Physics of Solids*, 56(7):2401–2421, 2008.

[11] B. Audoly and A. Boudaoud. Buckling of a stiff film bound to a compliant substrate—part ii:: A global scenario for the formation of herringbone pattern. *Journal of the Mechanics and Physics of Solids*, 56(7):2422–2443, 2008.

[12] B. Audoly and A. Boudaoud. Buckling of a stiff film bound to a compliant substrate—part iii:: Herringbone solutions at large buckling parameter. *Journal of the Mechanics and Physics of Solids*, 56(7):2444–2458, 2008.

[13] M. Badiale and E. Serra. *Semilinear Elliptic Equations for Beginners: Existence Results via the Variational Approach*. Springer Science & Business Media, 2010.

[14] J. H. Baek, Y. K. Kwak, and S. H. Kim. On the frequency bandwidth change of a servo system with a gear reducer due to backlash and motor input voltage. *Archive of Applied Mechanics*, 73(5-6):367–376, 2003.

[15] A. A. L. Baldelli. *On Fracture of Thin Films: a Variational Approach*. PhD thesis, Citeseer, 2013.

[16] A. A. L. Baldelli and B. Bourdin. On the asymptotic derivation of winkler-type energies from 3d elasticity. *Journal of Elasticity*, pages 1–27, 2015.

[17] J. M. Ball. Convexity conditions and existence theorems in nonlinear elasticity. *Archive for rational mechanics and Analysis*, 63(4):337–403, 1976.

[18] S. J. Ball, I. E. Brown, and S. H. Scott. A planar 3dof robotic exoskeleton for rehabilitation and assessment. In *Engineering in Medicine and Biology Society, 2007. EMBS 2007. 29th Annual International Conference of the IEEE*, pages 4024–4027. IEEE, 2007.

[19] O. Baser and E. I. Konukseven. Theoretical and experimental determination of capstan drive slip error. *Mechanism and Machine Theory*, 45(6):815–827, 2010.

[20] R. Basex A., Salvador and A. Dupre. Pseudo-chromidrose plantaire. *Bull Soc Franc Dermatol Syph*, 69:489–490, 1962.

[21] S. Behzadipour and A. Khajepour. *Cable-based robot manipulators with translational degrees of freedom*. INTECH Open Access Publisher, 2006.

[22] G. Bennett, C. Dealey, J. Posnett, et al. The cost of pressure ulcers in the uk. *Age and ageing*, 33(3):230–235, 2004.

[23] R. W. Berg. Etiologic factors in diaper dermatitis: a model for development of improved diapers. *Pediatrician*, 14:27, 1987.

[24] W. F. Bergfeld and J. S. Taylor. Trauma, sports, and the skin. *American journal of industrial medicine*, 8(4-5):403–413, 1985.

[25] N. Bergstrom. *Treatment of Pressure Ulcers*. AHCPR pub. Diane Publishing Company, 1994.

[26] S. R. Bodner, J. Singer, A. Solan, and Z. Hashin. *Theoretical and Applied Mechanics 1992*. Elsevier Science, 2012.

[27] E. Bonderover and S. Wagner. A woven inverter circuit for e-textile applications. *Electron Device Letters, IEEE*, 25(5):295–297, 2004.

[28] F. P. Bowden and D. Tabor. *The friction and lubrication of solids*, volume 2. Wiley Online Library, 1964.

[29] A. Brooks, G. Dickins, A. Zelinsky, J. Kieffer, and S. Abdallah. A high-performance camera platform for real-time active vision. In *Field and Service Robotics*, pages 527–532. Springer, 1998.

[30] R. Burden, J. Faires, and A. Burden. *Numerical analysis*. Nelson Education, 2015.

[31] L. T. Campos, J. T. Oden, and N. Kikuchi. A numerical analysis of a class of contact problems with friction in elastostatics. *Computer Methods in Applied Mechanics and Engineering*, 34(1):821–845, 1982.

[32] M. C. Carrozza, G. Cappiello, S. Micera, B. B. Edin, L. Beccai, and C. Cipriani. Design of a cybernetic hand for perception and action. *Biological cybernetics*, 95(6):629–644, 2006.

[33] M. C. Choi, Y. Kim, and C. S. Ha. Polymers for flexible displays: From material selection to device applications. *Progress in Polymer Science*, 33(6):581–630, 2008.

[34] R. Christensen. *Log-linear models and logistic regression*. Springer Science & Business Media, 2006.

[35] J. U. Chu, D. H. Jeong, I. Youn, K. Choi, and Y. J. Lee. Myoelectric hand prosthesis with novel adaptive grasping and self-locking. *International Journal of Precision Engineering and Manufacturing*, 12(6):1095–1103, 2011.

[36] P. G. Ciarlet. Mathematical elasticity. vol. i, volume 20 of studies in mathematics and its applications, 1988.

[37] P. G. Ciarlet. *Theory of Plates*. Mathematical Elasticity. Elsevier Science, 1997.

[38] P. G. Ciarlet. *Theory of Shells*. Mathematical Elasticity. Elsevier Science, 2000.

[39] P. G. Ciarlet. An introduction to differential geometry with applications to elasticity. *Journal of Elasticity*, 78(1-3):1–215, 2005.

[40] P. G. Ciarlet and C. Mardare. An introduction to shell theory. *Differential Geometry: Theory and Applications*, 9:94–184, 2008.

[41] S. K. Clark. *Mechanics of pneumatic tires*. US Department of Transportation, National Highway Traffic Safety Administration, 1981.

[42] M. Controzzi, C. Cipriani, and M. C. Carrozza. Miniaturized non-back-drivable mechanism for robotic applications. *Mechanism and Machine Theory*, 45(10):1395–1406, 2010.

[43] S. M. Copperman. Two new causes of alopecia. *JAMA*, 252(24):3367–3367, 1984.

[44] T. A. Cortese, K. Fukuyama, W. Epstein, and M. B. Sulzberger. Treatment of friction blisters: an experimental study. *Archives of dermatology*, 97(6):717–721, 1968.

[45] A. M. Cottenden, D. J. Cottenden, S. Karavokiros, and W. K. R. Wong. Development and experimental validation of a mathematical model for friction between fabrics and a volar forearm phantom. *Proceedings of the Institution of Mechanical Engineers, Part H: Journal of Engineering in Medicine*, 222(7):1097–1106, 2008.

[46] A. M. Cottenden, W. K. Wong, D. J. Cottenden, and A. Farbrot. Development and validation of a new method for measuring friction between skin and nonwoven materials. *Proceedings of the Institution of Mechanical Engineers, Part H: Journal of Engineering in Medicine*, 222(5):791–803, 2008.

[47] D. J. Cottenden. *A multiscale analysis of frictional interaction between human skin and nonwoven fabrics*. PhD thesis, UCL (University College London), 2011.

[48] D. J. Cottenden and A. M. Cottenden. An analytical model of the motion of a conformable sheet over a general convex surface in the presence of frictional coupling. *The Quarterly Journal of Mechanics and Applied Mathematics*, page hbp012, 2009.

[49] P. S. Cowen et al. Juvenile plantar dermatosis in an adult. *British Journal of Dermatology*, 104(5):599–599, 1981.

[50] G. Crawford. *Flexible flat panel displays*. John Wiley & Sons, 2005.

[51] J. Crissey and J. Peachy. Calcaneal petechiae. *Arch Dermatol*, 83:501, 1961.

[52] S. Cuenot, C. Frétigny, S. Demoustier-Champagne, and Be. Nysten. Surface tension effect on the mechanical properties of nanomaterials measured by atomic force microscopy. *Physical Review B*, 69(16):165410, 2004.

[53] A. S. Demidov. *Generalized functions in mathematical physics: main ideas and concepts*, volume 237. Nova Publishers, 2001.

[54] L. Demkowicz and J. T. Oden. On some existence and uniqueness results in contact problems with nonlocal friction. *Nonlinear Analysis: Theory, Methods & Applications*, 6(10):1075–1093, 1982.

[55] S. Derler and L. C. Gerhardt. Tribology of skin: review and analysis of experimental results for the friction coefficient of human skin. *Tribology Letters*, 45(1):1–27, 2012.

[56] D. A. Dillard, J. A. Hinkley, W. S. Johnson, and T. L. St. Clair. Spiral tunneling cracks induced by environmental stress cracking in larc^{TM}-tpi adhesives. *The Journal of Adhesion*, 44(1-2):51–67, 1994.

[57] H. Ding, W. Chen, and L. Zhang. *Elasticity of transversely isotropic materials*, volume 126. Springer Science & Business Media, 2006.

[58] M. P. do Carmo. *Differential Geometry of Curves and Surfaces*. Pearson Education Taiwan Limited, 2009.

[59] S. Döonmez and A. Marmarali. A model for predicting a yarn's knittability. *Textile research journal*, 74(12):1049–1054, 2004.

[60] E. Efrati, E. Sharon, and R. Kupferman. Elastic theory of unconstrained non-euclidean plates. *Journal of the Mechanics and Physics of Solids*, 57(4):762–775, 2009.

[61] P. H. Ely. Balance beam alopecia. *Archives of dermatology*, 114(6):968, 1978.

[62] E. Epstein. Granuloma fissuratum of the ears. *Archives of dermatology*, 91(6):621–622, 1965.

[63] L. C. Evans. *Partial Differential Equations*. Graduate studies in mathematics. American Mathematical Society, 2010.

[64] M. A. Farage, K. W. Miller, E. Berardesca, and H. I. Maibach. Incontinence in the aged: contact dermatitis and other cutaneous consequences. *Contact Dermatitis*, 57(4):211–217, 2007.

[65] S. R. Forrest. The path to ubiquitous and low-cost organic electronic appliances on plastic. *Nature*, 428(6986):911–918, 2004.

[66] G. Friesecke, R. D. James, M. G. Mora, and S. Müller. Derivation of nonlinear bending theory for shells from three-dimensional nonlinear elasticity by gamma-convergence. *Comptes Rendus Mathematique*, 336(8):697–702, 2003.

[67] G. Friesecke, R. D. James, and S. Müller. The föppl–von kármán plate theory as a low energy γ-limit of nonlinear elasticity. *Comptes Rendus Mathematique*, 335(2):201–206, 2002.

[68] G. Friesecke, R. D. James, and S. Müller. A hierarchy of plate models derived from nonlinear elasticity by gamma-convergence. *Archive for rational mechanics and analysis*, 180(2):183–236, 2006.

[69] G. Friesecke, R. D. James, S. Müller, et al. A theorem on geometric rigidity and the derivation of nonlinear plate theory from three dimensional elasticity. 2002.

[70] D. Y. Gao. Duality theory in nonlinear buckling analysis for von kámán equations. *Studies in applied mathematics*, 94(4):423–444, 1995.

[71] D. Y. Gao. Nonlinear elastic beam theory with application in contact problems and variational approaches. *Mechanics Research Communications*, 23(1):11–17, 1996.

[72] D. Y. Gao. Finite deformation beam models and triality theory in dynamical post-buckling analysis. *International journal of non-linear mechanics*, 35(1):103–131, 2000.

[73] I. Gelfand. Shilov, generalized functions, vol. 2. *Spaces of fundamental and generalized functions, Acad. Press, London*, 1968.

[74] A. N. Gent and P. B. Lindley. The compression of bonded rubber blocks. *Proceedings of the Institution of Mechanical Engineers*, 173(1):111–122, 1959.

[75] G. Geymonat. Sui problemi ai limiti per i sistemi lineari ellittici. *Annali di Matematica Pura ed Applicata*, 69(1):207–284, 1965.

[76] R. C. Gibbs and M. C. Boxer. Abnormal biomechanics of feet and their cause of hyperkeratoses. *Journal of the American Academy of Dermatology*, 6(6):1061–1069, 1982.

[77] J. B. Griffiths and J. Podolskỳ. *Exact Space-Times in Einstein's General Relativity*. Cambridge Monographs on Mathematical Physics. Cambridge University Press, 2009.

[78] P. Grosberg and D. E. A. Plate. 19—capstan friction for polymer monofilaments with rigidity. *Journal of the Textile Institute*, 60(7):268–283, 1969.

[79] K. M. Herring and D. H. Richie Jr. Friction blisters and sock fiber composition. a double-blind study. *Journal of the American podiatric medical association*, 80(2):63–71, 1990.

[80] M. Hetényi. *Beams on elastic foundation: theory with applications in the fields of civil and mechanical engineering*. University of Michigan, 1971.

[81] D. H. Hodges, R. A. Ormiston, and D. A. Peters. On the nonlinear deformation geometry of euler-bernoulli beams. Technical report, DTIC Document, 1980.

[82] H. G. Howell. 24—the general case of friction of a string round a cylinder. *Journal of the Textile Institute Transactions*, 44(8-9):T359–T362, 1953.

[83] H. G. Howell. 35—the friction of a fibre round a cylinder and its dependence upon cylinder radius. *Journal of the Textile Institute Transactions*, 45(8):T575–T579, 1954.

[84] P. Howell, G. Kozyreff, and J. Ockendon. *Applied solid mechanics*. Number 43. Cambridge University Press, 2009.

[85] J. Howse. Disorders of the great toe in dancers. *Clinics in sports medicine*, 2(3):499–505, 1983.

[86] H. In, K. J. Cho, K. Kim, and B. Lee. Jointless structure and under-actuation mechanism for compact hand exoskeleton. In *Rehabilitation Robotics (ICORR), 2011 IEEE International Conference on*, pages 1–6. IEEE, 2011.

[87] H. In, S. Kang, and K. J. Cho. Capstan brake: Passive brake for tendon-driven mechanism. In *Intelligent Robots and Systems (IROS), 2012 IEEE/RSJ International Conference on*, pages 2301–2306. IEEE, 2012.

[88] A. K. Izumi. Pigmented palmar petechiae (black palm). *Archives of dermatology*, 109(2):261–261, 1974.

[89] K. Jayawardana, C. Mordacq, C. Ortner, and H. S. Park. An analysis of the boundary layer in the 1d surface cauchy–born model. *ESAIM: Mathematical Modelling and Numerical Analysis*, 47(01):109–123, 2013.

[90] D. U. Jin, J. S. Lee, T. W. Kim, S. G. An, D. Straykhilev, Y. S. Pyo, H. S. Kim, D. B. Lee, Y. G. Mo, H. D. Kim, et al. 65.2: Distinguished paper: World-largest (6.5”) flexible full color top emission amoled display on plastic film and its bending properties. In *SID Symposium Digest of Technical Papers*, volume 40, pages 983–985. Wiley Online Library, 2009.

[91] J. Johnson. Free space laser communications advanced technology demonstration. In *AIAA, Space Programs and Technologies Conference, Huntsville, AL*, 1993.

[92] K. L. Johnson and K. L. Johnson. *Contact mechanics*. Cambridge university press, 1987.

[93] B. S. Jovanović and E. Süli. *Analysis of finite difference schemes: for linear partial differential equations with generalized solutions*, volume 46. Springer Science & Business Media, 2013.

[94] L. Juhlin and B. Ponten. Plantar pseudochromohidrosis simulating malignant melanoma. *Acta dermato-venereologica*, 47(4):255, 1967.

[95] J. H. Jung, T. J. Kang, and J. R. Youn. Effect of bending rigidity on the capstan equation. *Textile research journal*, 74(12):1085–1096, 2004.

[96] J. H. Jung, N. Pan, and T. J. K. Generalized capstan problem: Bending rigidity, nonlinear friction, and extensibility effect. *Tribology International*, 41(6):524–534, 2008.

[97] J. H. Jung, N. Pan, and T. J.in Kang. Capstan equation including bending rigidity and non-linear frictional behavior. *Mechanism and Machine Theory*, 43(6):661–675, 2008.

[98] D. Kalman. *Uncommon Mathematical Excursions: Polynomia and Related Realms*. Number 35. MAA, 2009.

[99] S. Kang, H. In, and K. J. Cho. Design of a passive brake mechanism for tendon driven devices. *International Journal of Precision Engineering and Manufacturing*, 13(8):1487–1490, 2012.

[100] S. E. S. Karavokyros. Skin friction - validating a mathematical model with a simple laboratory model. Project report for msc bemi, University College London, Department of Medical Physics and Bioengineering, 2006.

[101] D. Kay. *Schaum's Outline of Tensor Calculus*. McGraw Hill Professional, 1988.

[102] N. Kikuchi and J.T. Oden. *Contact Problems in Elasticity: A Study of Variational Inequalities and Finite Element Methods*. Studies in Applied Mathematics. Society for Industrial and Applied Mathematics, 1988.

[103] E. H. Kim, S. W. Lee, and Y. K. Lee. A dexterous robot hand with a bio-mimetic mechanism. *International Journal of Precision Engineering and Manufacturing*, 12(2):227–235, 2011.

[104] S. H. Kim. Portable display device having an expandable screen, July 17 2001. US Patent 6,262,785.

[105] Y. S. Kim, M. K. Jain, and D. R. Metzger. A finite element study of capstan friction test. In *AIP Conference Proceedings*, volume 712, pages 2264–2269. IOP INSTITUTE OF PHYSICS PUBLISHING LTD, 2004.

[106] Y. S. Kim and J. S. Park. Folder-type portable communication device having flexible display unit, July 24 2012. US Patent 8,229,522.

[107] D. Kinderlehrer and G. Stampacchia. *An introduction to variational inequalities and their applications*, volume 31. Siam, 1980.

[108] H. C. Ko, G. Shin, S. Wang, M. P. Stoykovich, J. W. Lee, D. H. Kim, J. S. Ha, Y. Huang, K. C. Hwang, and J. A. Rogers. Curvilinear electronics formed using silicon membrane circuits and elastomeric transfer elements. *Small*, 5(23):2703–2709, 2009.

[109] W. T. Koiter. On the nonlinear theory of thin elastic shells. i- introductory sections. ii- basic shell equations. iii- simplified shell equations(nonlinear theory of thin elastic shells, discussing surface geometry and deformation, equations of equilibrium and boundary conditions and stress functions). *Koninklijke Nederlandse Akademie van Wetenschappen, Proceedings, Series B*, 69(1):1–54, 1966.

[110] W. T. Koiter. Comment on: The linear and non-linear equilibrium equations for thin elastic shells according to the kirchhoff-love hypotheses: Lj hart-smith, int. j. mech. sci. 12, 1 (1970). *International Journal of Mechanical Sciences*, 12(7):663, 1970.

[111] A. N. Kolmogorov, S. V. Fomin, N. A. Brunswick, and A. Jeffrey. *Measure, Lebesgue integrals and Hilbert space*, volume 2. Academic Press New York, 1961.

[112] P. J. Kyberd, M. Evans, and S. Te Winkel. An intelligent anthropomorphic hand, with automatic grasp. *Robotica*, 16(05):531–536, 1998.

[113] L. D. Landau and E. M. Lifshitz. *Course of Theoretical Physics Vol 7: Theory and Elasticity*. Pergamon Press, 1959.

[114] H. Le Dret and A. Raoult. The membrane shell model in nonlinear elasticity: a variational asymptotic derivation. *Journal of Nonlinear Science*, 6(1):59–84, 1996.

[115] A. W. Leissa. *Vibration of shells*. Acoustical Society of America New York, 1993.

[116] F. Levit. Jogger's nipples. *The New England journal of medicine*, 297(20):1127, 1977.

[117] J. Lewis. Material challenge for flexible organic devices. *Materials today*, 9(4):38–45, 2006.

[118] T. Li, Z. Huang, Z. Suo, Stéphanie P. Lacour, and S. Wagner. Stretchability of thin metal films on elastomer substrates. *Applied Physics Letters*, 85(16):3435–3437, 2004.

[119] T. Li, Z. Y. Huang, Z. C. Xi, S. P. Lacour, S. Wagner, and Z. Suo. Delocalizing strain in a thin metal film on a polymer substrate. *Mechanics of Materials*, 37(2):261–273, 2005.

[120] W. Liang, M. Zhou, and F. Ke. Shape memory effect in cu nanowires. *Nano Letters*, 5(10):2039–2043, 2005.

[121] A. Libai and J. G. Simmonds. *The nonlinear theory of elastic shells*. Cambridge university press, 2005.

[122] C. M. Light and P. H. Chappell. Development of a lightweight and adaptable multiple-axis hand prosthesis. *Medical engineering & physics*, 22(10):679–684, 2000.

[123] J. L. Lions. *Quelques méthodes de résolution des problemes aux limites non linéaires*, volume 31. Dunod Paris, 1969.

[124] M. M. Lipschutz. *Schaum's Outline of Theory and Problems of Differential Geometry*. Schaum's outline series : theory and problem. McGraw-Hill, 1969.

[125] S. Logothetidis. *Handbook of Flexible Organic Electronics: Materials, Manufacturing and Applications*. Woodhead Publishing Series in Electronic and Optical Materials. Elsevier Science, 2014.

[126] A. E. H. Love. The small free vibrations and deformation of a thin elastic shell. *Philosophical Transactions of the Royal Society of London. A*, pages 491–546, 1888.

[127] N. Lu, Z. Suo, and J. J. Vlassak. The effect of film thickness on the failure strain of polymer-supported metal films. *Acta Materialia*, 58(5):1679–1687, 2010.

[128] N. Lu, X. Wang, Z. Suo, and J. Vlassak. Metal films on polymer substrates stretched beyond 50%. *Applied Physics Letters*, 91(22):221909, 2007.

[129] N. Lu, X. Wang, Z. Suo, and J. Vlassak. Failure by simultaneous grain growth, strain localization, and interface debonding in metal films on polymer substrates. *Journal of Materials Research*, 24(02):379–385, 2009.

[130] Y. Lu and D. Fan. Transmission backlash of precise cable drive system. *Proceedings of the Institution of Mechanical Engineers, Part C: Journal of Mechanical Engineering Science*, 227(10):2256–2267, 2013.

[131] E. Magenes and G. Stampacchia. I problemi al contorno per le equazioni differenziali di tipo ellittico. *Annali della Scuola Normale Superiore di Pisa-Classe di Scienze*, 12(3):247–358, 1958.

[132] J. Maklebust and M. Sieggreen. *Pressure ulcers: Guidelines for prevention and management*. Lippincott Williams & Wilkins, 2001.

[133] P. R. Manger, M. Prowse, M. Haagensen, and J. Hemingway. Quantitative analysis of neocortical gyrencephaly in african elephants (loxodonta africana) and six species of cetaceans: comparison with other mammals. *Journal of Comparative Neurology*, 520(11):2430–2439, 2012.

[134] A. J. P. Martin and R. Mittelmann. 18—some measurements of the friction of wool and mohair. *Journal of the Textile Institute Transactions*, 37(12):T269–T280, 1946.

[135] R. Merzouki, J. A. Davila, L. Fridman, and J. C. Cadiou. Backlash phenomenon observation and identification in electromechanical system. *Control Engineering Practice*, 15(4):447–457, 2007.

[136] B. E. Meserve and R. E. Pingry. Some notes on the prismoidal formula. *The Mathematics Teacher*, 45(4):257–263, 1952.

[137] R. D. Mindlin. Influence of rotary inertia and shear on flexural motions of isotropic elastic plates. 1951.

[138] P. Moon and D. E. Spencer. *Field theory handbook: including coordinate systems, differential equations and their solutions*. Springer, 2012.

[139] A. Morassi and R. Paroni. *Classical and Advanced Theories of Thin Structures: Mechanical and Mathematical Aspects*. CISM International Centre for Mechanical Sciences. Springer Vienna, 2009.

[140] P. M. Morse. Diatomic molecules according to the wave mechanics. ii. vibrational levels. *Physical Review*, 34(1):57, 1929.

[141] S. A. Muller. Dermatologic disorders in athletes. *The Journal of the Kentucky Medical Association*, 74(5):225, 1976.

[142] L. D. Murray, N. Magazinovic, M. C. Stacey, et al. Clinical practice guidelines for the prediction and prevention of pressure ulcers. 2001.

[143] S. K. Mustafa, G. Yang, S. H. Yeo, and W. Lin. Kinematic calibration of a 7-dof self-calibrated modular cable-driven robotic arm. In *Robotics and Automation, 2008. ICRA 2008. IEEE International Conference on*, pages 1288–1293. IEEE, 2008.

[144] J. Necas, C. G. Simader, Š. Necasová, G. Tronel, and A. Kufner. *Direct Methods in the Theory of Elliptic Equations*. Springer Monographs in Mathematics. Springer Berlin Heidelberg, 2011.

[145] P. Osborne. *The Mercator Projections*. doi:10.5281/zenodo.35392, 2013.

[146] R. M. Overney. Introduction to tribology – friction. http://depts.washington.edu/nanolab/ChemE554/Summaries%20ChemE%20554/Introduction%20Tribology.htm, 2007.

[147] M. Pagliaro, R. Ciriminna, and G. Palmisano. Flexible solar cells. *ChemSusChem*, 1(11):880–891, 2008.

[148] I. P. D. Panagiotopoulos. A nonlinear programming approach to the unilateral contact-, and friction-boundary value problem in the theory of elasticity. *Ingenieur-Archiv*, 44(6):421–432, 1975.

[149] P. D. Panagiotopoulos. Ungleichungsprobleme und differentialinklusionen in der analytischen mechanik. *Annual Public. School of Technology*, pages 100–139, 1982.

[150] H. S. Park. Quantifying the size-dependent effect of the residual surface stress on the resonant frequencies of silicon nanowires if finite deformation kinematics are considered. *Nanotechnology*, 20(11):115701, 2009.

[151] H. S. Park, W. Cai, H. D. Espinosa, and H. Huang. Mechanics of crystalline nanowires. *MRS bulletin*, 34(03):178–183, 2009.

[152] H. S. Park, M. Devel, and Z. Wang. A new multiscale formulation for the electromechanical behavior of nanomaterials. *Computer methods in applied mechanics and Engineering*, 200(29):2447–2457, 2011.

[153] H. S. Park and P. A. Klein. Surface cauchy-born analysis of surface stress effects on metallic nanowires. *Physical Review B*, 75(8):085408, 2007.

[154] H. S. Park and P. A. Klein. A surface cauchy-born model for silicon nanostructures. *Computer methods in applied mechanics and engineering*, 197(41):3249–3260, 2008.

[155] H. S. Park, P. A. Klein, and G. J. Wagner. A surface cauchy–born model for nanoscale materials. *International Journal for Numerical Methods in Engineering*, 68(10):1072–1095, 2006.

[156] J. C. Perry and J. Rosen. Design of a 7 degree-of-freedom upper-limb powered exoskeleton. In *Biomedical Robotics and Biomechatronics, 2006. BioRob 2006. The First IEEE/RAS-EMBS International Conference on*, pages 805–810. IEEE, 2006.

[157] J. L. Pons, E. Rocon, R. Ceres, D. Reynaerts, B. Saro, S. Levin, and W. Van Moorleghem. The manus-hand dextrous robotics upper limb prosthesis: mechanical and manipulation aspects. *Autonomous Robots*, 16(2):143–163, 2004.

[158] B. Powell. Bicyclist's nipples. *JAMA*, 249(18):2457–2457, 1983.

[159] A. N. Pressley. *Elementary differential geometry*. Springer Science & Business Media, 2010.

[160] S. Qiao and N. Lu. Analytical solutions for bonded elastically compressible layers. *International Journal of Solids and Structures*, 58:353–365, 2015.

[161] D. Quadling. *Mechanics 1*. Cambridge Advanced Level Mathematics. Cambridge University Press, 2004.

[162] C. L. Rao, J. Lakshinarashiman, R. Sethuraman, and S. M. Sivakumar. *Engineering Mechanics: Statics and Dynamics*. PHI Learning Pvt. Ltd., 2003.

[163] J. N. Reddy. *Theory and analysis of elastic plates and shells*. CRC press, 2006.

[164] J. N. Reddy. *An Introduction to Nonlinear Finite Element Analysis: with applications to heat transfer, fluid mechanics, and solid mechanics*. OUP Oxford, 2014.

[165] J. N. Reddy and C. M. Wang. Deflection relationships between classical and third-order plate theories. *Acta Mechanica*, 130(3-4):199–208, 1998.

[166] J. N. Reddy and C. M. Wang. On shear deformation plate solutions: Relationship to the classical solutions. In *Advances in the Mechanics of Plates and Shells*, pages 259–276. Springer, 2002.

[167] D. Rees. *Basic engineering plasticity: an introduction with engineering and manufacturing applications*. Butterworth-heinemann, 2012.

[168] F. Ronchese. *Occupational marks and other physical signs: a guide to personal identification*. Grune & Stratton, 1948.

[169] P. Rosakis. Continuum surface energy from a lattice model. *NETWORKS AND HETEROGENEOUS MEDIA*, 9(3):453–476, 2014.

[170] G. M. Rotaru, D. Pille, F. K. Lehmeier, R. Stämpfli, A. Scheel-Sailer, R. M. Rossi, and S. Derler. Friction between human skin and medical textiles for decubitus prevention. *Tribology International*, 65:91–96, 2013.

[171] T. Rufli. [hyperkeratosis haemorrhagica]. *Der Hautarzt; Zeitschrift fur Dermatologie, Venerologie, und verwandte Gebiete*, 31(11):606–609, 1980.

[172] P. K. Saha and W. R. D. Wilson. Influence of plastic strain on friction in sheet metal forming. *Wear*, 172(2):167–173, 1994.

[173] R. K. Scher. Jogger's toe. *International journal of dermatology*, 17(9):719–720, 1978.

[174] R. J. Scheuplein and I. H. Blank. Permeability of the skin. *Physiol Rev*, 51(4):702–747, 1971.

[175] R. L. Schilling. *Measures, integrals and martingales*, volume 13. Cambridge University Press, 2005.

[176] A. B. Shank. The aetiology of juvenile plantar dermatosis. *British Journal of Dermatology*, 100(6):641–648, 1979.

[177] G. B. Shelly and M. E. Vermaat. *Discovering Computers 2011: Brief*. Cengage Learning, 2010.

[178] A. Signorini. Sopra alcune questioni di statica dei sistemi continui. *Annali della Scuola Normale Superiore di Pisa-Classe di Scienze*, 2(2):231–251, 1933.

[179] A. Signorini. *Questioni di elasticità non linearizzata*. Edizioni Cremonese, 1960.

[180] C. Siyu, T. Jinyuan, L. Caiwang, and W. Qibo. Nonlinear dynamic characteristics of geared rotor bearing systems with dynamic backlash and friction. *Mechanism and Machine Theory*, 46(4):466–478, 2011.

[181] W. Soedel. *Vibrations of shells and plates*. CRC Press, 2004.

[182] A. Sokal. Functional analysis mathematics 3103. http://www.ucl.ac.uk/ ucahad0/, 2013. University College London.

[183] M. B. Song. Electronic paper display device, manufacturing method and driving method thereof, July 6 2010. US Patent 7,751,115.

[184] M. Spivak. *Calculus on manifolds*, volume 1. WA Benjamin New York, 1965.

[185] G.i Stellin, G. Cappiello, S. Roccella, M. C. Carrozza, P. Dario, G. Metta, G. Sandini, and F. Becchi. Preliminary design of an anthropomorphic dexterous hand for a 2-years-old humanoid: towards cognition. *Hand*, 20:9, 2006.

[186] H. Stephani, D. Kramer, M. MacCallum, C. Hoenselaers, and E. Herlt. *Exact Solutions of Einstein's Field Equations*. Cambridge Monographs on Mathematical Physics. Cambridge University Press, 2003.

[187] I. M. Stuart. Capstan equation for strings with rigidity. *British Journal of Applied Physics*, 12(10):559, 1961.

[188] Y. Sumi. *Mathematical and Computational Analyses of Cracking Formation: Fracture Morphology and Its Evolution in Engineering Materials and Structures*, volume 2. Springer, 2014.

[189] O. Sutherland, S. Rougeaux, S. Abdallah, and A. Zelinsky. Tracking with hybrid-drive active vision. 2000.

[190] H. W. Swift. Plastic instability under plane stress. *Journal of the Mechanics and Physics of Solids*, 1(1):1–18, 1952.

[191] T. Tallinen, J. Y. Chung, J. S. Biggins, and L. Mahadevan. Gyrification from constrained cortical expansion. *Proceedings of the National Academy of Sciences*, 111(35):12667–12672, 2014.

[192] T. Tallinen, J. Y. Chung, F. Rousseau, N. Girard, J. Lefèvre, and L. Mahadevan. On the growth and form of cortical convolutions. *Nature Physics*, 2016.

[193] J. S. Thomson and R. G. Brooks. The economics of preventing and treating pressure ulcers: a pilot study. *Journal of Wound Care*, 8(6):312–316, 1999.

[194] S. P. Timoshenko. X. on the transverse vibrations of bars of uniform cross-section. *The London, Edinburgh, and Dublin Philosophical Magazine and Journal of Science*, 43(253):125–131, 1922.

[195] S. P. Timoshenko. History of strength of materialsmcgraw-hill. *New York*, 1953.

[196] B. E. Tlougan, A. J. Mancini, J. A. Mandell, D. E. Cohen, and M. R. Sanchez. Skin conditions in figure skaters, ice-hockey players and speed skaters. *Sports medicine*, 41(11):967–984, 2011.

[197] R. Touche. The cost of pressure sores. *Reports to the Department of Health. Department of Health, London, UK*, 1993.

[198] Unknown. http://www.brainmuseum.org.

[199] Unknown. Bmi healthy weight calculator. http://www.nhs.uk/Tools/Pages/Healthyweightcalculator.aspx, 10 2013.

[200] Unknown. Urinary incontinence, nhs direct online health encyclopaedia. http://www.nhsdirect.wales.nhs.uk/encyclopaedia/i/article/incontinence,urinary, 12 2014.

[201] Unknown. Matlab. https://uk.mathworks.com/help/matlab/ref/norm.html, 2016. 2-Norm of Matrix.

[202] M. W. Urban, S. Chen, and M. Fatemi. A review of shearwave dispersion ultrasound vibrometry (sduv) and its applications. *Current medical imaging reviews*, 8(1):27, 2012.

[203] S. Wagner, Stéphanie P. Lacour, J. Jones, I. H. Pai-hui, J. C. Sturm, and Z. Li, T.and Suo. Electronic skin: architecture and components. *Physica E: Low-dimensional Systems and Nanostructures*, 25(2):326–334, 2004.

[204] R. M. Wald. *General Relativity*. University of Chicago Press, 2010.

[205] C. M. Wang and W. A. M. Alwis. Simply supported polygonal mindlin plate deflections using kirchhoff plates. *Journal of engineering mechanics*, 121(12):1383–1385, 1995.

[206] K. Washizu. *Variational methods in elasticity and plasticity*. Pergamon press, 1975.

[207] M. Wei and R. Chen. An improved capstan equation for nonflexible fibers and yarns. *Textile research journal*, 68(7):487–492, 1998.

[208] R. P. White. The dermatoses or occiupation7al affections of the skin. *Lewis, London*, 1934.

[209] D. S. Wilkinson. Dermatitis from repeated trauma to the skin. *American journal of industrial medicine*, 8(4-5):307–317, 1985.

[210] T. J. Willmore and T. J. Willmore. *Riemannian geometry*. Oxford University Press, 1996.

[211] Z. C. Xia and J. W. Hutchinson. Crack patterns in thin films. *Journal of the Mechanics and Physics of Solids*, 48(6):1107–1131, 2000.

[212] L. M. Xiao. Asymptotic analysis of dynamic problems for linearly elastic shells–justification of equations for dynamic membrane shells. *Asymptotic Analysis*, 17(2):121–134, 1998.

[213] X. Xu, H. Subbaraman, S. Chakravarty, A. Hosseini, J. Covey, Y. Yu, D. Kwong, Y. Zhang, W. C. Lai, Y. Zou, et al. Flexible single-crystal silicon nanomembrane photonic crystal cavity. *ACS nano*, 8(12):12265–12271, 2014.

[214] Xuru. Xuru's website. http://www.xuru.org, 03 2016. Regression Tools.

[215] M. S. Yang. Liquid crystal display device and method for manufacturing the same, August 11 1998. US Patent 5,793,460.

[216] G. Yun and H. S. Park. A multiscale, finite deformation formulation for surface stress effects on the coupled thermomechanical behavior of nanomaterials. *Computer Methods in Applied Mechanics and Engineering*, 197(41):3337–3350, 2008.

[217] G. Yun and H. S. Park. Surface stress effects on the bending properties of fcc metal nanowires. *Physical Review B*, 79(19):195421, 2009.